

Syracuse University

## SURFACE at Syracuse University

---

Dissertations - ALL

SURFACE at Syracuse University

---

Summer 7-16-2021

# Peptide Corination for the Mitigation of Nausea and Emesis in the Treatment of Type 2 Diabetes

Ian Tinsley  
Syracuse University

Follow this and additional works at: <https://surface.syr.edu/etd>

 Part of the [Chemistry Commons](#)

---

### Recommended Citation

Tinsley, Ian, "Peptide Corination for the Mitigation of Nausea and Emesis in the Treatment of Type 2 Diabetes" (2021). *Dissertations - ALL*. 1432.  
<https://surface.syr.edu/etd/1432>

This Dissertation is brought to you for free and open access by the SURFACE at Syracuse University at SURFACE at Syracuse University. It has been accepted for inclusion in Dissertations - ALL by an authorized administrator of SURFACE at Syracuse University. For more information, please contact [surface@syr.edu](mailto:surface@syr.edu).

## Abstract

This thesis addresses several questions focused on the activation of receptors expressed within the area postrema (AP) and the nucleus tractus solitarius (NTS), regions known to influence nausea and emesis. Prevention of such effects were achieved via corination, covalent attachment to vitamin B12 (B12) or other corrin constructs, of GLP glucagon-like peptide-one (GLP-1) receptor (GLP-1R) agonists or via the use of GRASP a growth differentiation factor 15 (GDF15) glial derived neurotropic family receptor  $\alpha$ -like (GFRAL) complex antagonist.

**Q1:** (Chapter 2) Can a B12 bound Ex4 (B12-Ex4) reduce central nervous system penetrance while maintaining peripheral gluco-regulation in Goto-Kakizaki (GK) rats and the musk shrew?

Goal: Perform *in vivo* analysis of glucose levels, feeding behavior, and presence of emesis following administration of B12-Ex4.

**Q2:** (Chapter 3) Can covalent attachment of Ex4 to B12 biosynthetic precursor dicyanocobinamide (Cbi) (Cbi-Ex4) mitigate nausea and emesis in the musk shrew?

Goal: Perform *in vivo* analysis of glucose levels, feeding behavior, and presence of emesis following administration of Cbi-Ex4.

**Q3:** (Chapter 3) Can a Cbi-Ex4 conjugate prevent brain penetrance while maintaining equipotent agonism and binding to the GLP-1R and retained pharmacodynamic profile on pancreatic GLP-1R populations?

Goal: Design and synthesis a library of Cbi-Ex4 conjugates with the goal of designing a construct with equipotent binding and agonism of the GLP-1R.

**Q4:** (Chapter 4) Can antagonism of the growth differentiation factor 15 (GDF15) glial derived neurotrophic family receptor  $\alpha$ -like (GFRAL) complex mitigate nausea?

Goal: Design peptide antagonists for the antagonism of the GDF15:GFRAL complex for the mitigation of nausea and emesis.

**Q5:** (Chapter 5) Can functional fluorescent probes be utilized in the identification of new receptor populations and elucidation of their function?

Goal: Design functional fluorescent probes of leptin, Ex4, and oxytocin to investigate receptor location and function *in vivo*.

**Peptide Corination for the Mitigation of Nausea and Emesis in  
the Treatment of Type 2 Diabetes**

by

Ian Chandler Tinsley

B.S., University of Illinois Springfield, 2015

M.S., Eastern Illinois University, 2017

DISSERTATION

Submitted in partial fulfillment of the requirements for the degree of  
Doctor of Philosophy in Chemistry

Syracuse University

July 2021



Copyright 2021 © Ian Chandler Tinsley

All rights reserved

# Table of Contents

<b>Chapter 1: Introduction</b>	<b>Page #</b>
1.1 Glucose Homeostasis	1
1.1.1 Type I and II Diabetes mellitus Effect on Glucoregulation	2
1.1.1.1 Impact of T2DM and Comorbid Obesity	3
1.1.1.1.1 Treatment of T2DM	4
1.1.1.1.2 Glucagon-like peptide-one (GLP-1) and its Receptor (GLP-1R)	7
1.1.1.1.2.1 Exendin-4 (Ex4)	7
1.1.2 Distribution and Activation of the GLP-1R	9
1.1.2.1 Unwarranted Side Effects Associated with GLP-1R Activation in the CNS	9
1.2 Vitamin B12 (B12)	10
1.2.1 History of B12	10
1.2.2 Structure of B12 and Corrinoids	13
1.2.2.1 Biosynthetic Precursors and Structural Derivatives of B12	15
1.2.2.1.1 Dicyanocobinamide (Cbi)	17
1.2.3 Metabolism of B12	18
1.2.4 Dietary Uptake of B12 in Humans	19
1.2.4.1 Transport Proteins of B12	22
1.2.4.1.1 Haptocorrin (HC)	22
1.2.4.1.2 Intrinsic Factor (IF)	23
1.2.4.1.3 Transcobalamin (TC)	24

1.2.5 Distribution of B12 Transport Proteins and Investigations of B12 Conjugates in Various Lab Animal Models	25
1.2.5.1. Zebrafish	25
1.2.5.2 Mammalian Vertebrates	27
1.2.6 B12/ Corrin Binding Capacity	32
1.2.7 Chemical Modifications of B12 and Cbi	33
1.2.8 Developing a GLP-1R Agonist Devoid of Nausea, Emesis, and Weight loss	34
1.3 Glial cell-derived neurotrophic factor (GDNF) Family and the GDNF Family Ligands (GFLs)	37
1.3.1 Growth/Differentiation Factor 15 (GDF15)	39
1.3.2 The receptors of GFL, GDNF Receptor- $\alpha$ (GFR $\alpha$ )	39
1.3.2.1 GDNF Family Receptor- $\alpha$ Like (GFRAL)	40
1.3.2.2 GFL Signaling Receptor RET	41
1.3.2.3 Signaling Through the GFR $\alpha$ /GFRAL:RET Complex	41
1.3.3 Targeting the GDF15:GFRAL Complex (Agonism and Antagonism)	42
1.4 H188 FRET Assays and Fluorescent Probes of Neuroendocrine Hormones	42
1.5 References	45
<b>Chapter 2: A Second-generation Glucagon-like Peptide-1 Receptor Agonist Mitigates Vomiting and Anorexia While Retaining Glucoregulatory Potency in Lean Diabetic and Emetic Mammalian Models</b>	<b>78</b>
2.1 Introduction	79
2.2 Design and Synthesis of B12-Ex4	80

2.3 In Vivo Effects of Ex4 and B12-Ex4 in <u>Shrews</u>	81
2.3.1 Systemically Delivered B12-Ex4 Enhances Glucose Clearance Relative to Ex4	81
2.3.2 Systemically Delivered B12-Ex4 Co-localizes with Insulin in Pancreatic $\beta$ -cells	83
2.3.3 B12-Ex4 does not alter food intake or body weight, dissimilar to administration of Ex4	84
2.3.4 B12-Ex4 treatment produces slight emesis compared with the emetic effects of Ex4	86
2.3.5 Systemic Administration of B12-Ex4 does not induce c-Fos in the AP or NTS	89
2.3.6 Central Administration of B12-Ex4 and Ex4 Similarly Produce Emesis	90
2.4 In Vivo Effects of Ex4 and B12-Ex4 in Lean Diabetic <u>Goto-Kakazaki (GK) Rats</u>	91
2.4.1 B12-Ex4 enhances glucose clearance during an OGTT without inducing anorexia and bodyweight loss	91
2.5 Outcomes and Conclusions	93
2.6 References	98
<b>Chapter 3: Corination of a GLP-1 Receptor Agonist for Glycemic Control without Emesis</b>	105
3.1 Introduction	107
3.2. Synthesis of Dicyanocobinamide (Cbi)	110
3.3 Design and Synthesis of Cbi-Ex4	112
3.3.1 Synthesis of Cbi-Aminobutyne (Cbi-AB)	112
3.3.2 Synthesis and Characterization of Cbi-Ex4	114
3.4 Agonism and Function at the GLP-1R	116

3.5 Cobalamin Binding Capacity in Shrew Blood	117
3.6 Binding Affinity for Cbi Transport Proteins	118
3.7 In Vivo Investigations of Ex4 versus Cbi-Ex4 in Shrews	119
3.7.1 Ex4 versus Cbi-Ex4 in Intraperitoneal (I.P.) Glucose Tolerance Test (IPGTT)	119
3.7.2 Ex4 versus Cbi-Ex4 in Delayed IPGTT	121
3.7.3 Ex4 versus Cbi-Ex4 effect on Feeding Behavior	122
3.7.4 Conjugation to Cbi Improves the Pharmacokinetic Properties of Ex4	124
3.7.5 Prevalence of Emesis in Shrews Following Administration of Ex4 versus Cbi-Ex4	126
3.7.6 C-Fos Staining of AP/NTS	131
3.8 Prebinding Cbi-Ex4 to Haptocorrin (HC)	132
3.9 Outcomes and Conclusions	132
3.10 Optimization of Cbi-Ex4 Construct	134
3.11 Selection of Linkers for New Library of Cbi-Ex4/40 Constructs	135
3.12 Synthesis and Characterization of New Cbi-Ex4/40 Constructs	136
3.13 The Effect of Corination on the Secondary Structure of Ex4	137
3.14 <i>In Vitro</i> Optimization of Cbi-Ex4	138
3.14.1 Agonism at GLP-1R	138
3.14.2 Competitive Binding at GLP-1R	140
3.15 Identification of New Lead Candidate	141
3.16 Glucose-Stimulated Insulin Secretion (GSIS) in Rat Pancreatic Islets	142
3.17 <i>In Vivo</i> Functional Experiments	143
3.17.1 22 versus 1 and Ex4 in IPGTT	143

3.17.2 22 Effects on Food Intake and Body Weight Change versus 1 and Ex4	145
3.17.3 22 Prevalence of Emetic Episodes Following Administration of 1, 22, and Ex4	145
3.18 Outcomes and Conclusions	147
3.19 References	149
<b>Chapter 4: Peptide Ligands of the GDNF Family Receptor <math>\alpha</math>-like (GFRAL)</b>	165
4.1 Introduction	166
4.2 Design of a GFRAL Antagonist	167
4.3 <i>In Vivo</i> screening of GFANT peptides	168
4.4 Fluorescent tagging of GRASP-05	170
4.4.1 Design and Synthesis of GRASP-555	170
4.4.2 <i>In vivo</i> Injection of GRASP-555 in Rats	173
4.5 In-solution Structure of GRASP-05 Utilizing Nuclear Magnetic Resonance (NMR)	173
4.6 Microsomal Stability Assays of GRASP-05	175
4.7 Lipidation of GRASP-05	176
4.7.1 Design and Synthesis of Lipidated GRASP-05 (Lip-GRASP-05)	177
4.8 Developing an ELISA for monitoring GRASP	178
4.9 Outcomes and Conclusions	179
4.10 References	180
<b>Chapter 5: Fluorescent Probes of Neuroendocrine Hormones for the Identification of Receptor Distribution and Function</b>	185
5.1 Introduction	186
5.2 Leptin	186

5.2.1 Design, Synthesis, and Characterization of a Fluorescent Leptin (Cy5-Leptin)	187
5.3 Function of Exendin-4 (Ex4) at the Glucagon-like Peptide-1 (GLP-1) Receptor (GLP-1R)	191
5.3.1 Design, Synthesis, and Characterization of AF546-Ex4 (REX)	192
5.4 Signaling of Oxytocin at the Oxytocin Receptor	195
5.4.1 Design, Synthesis, and Characterization of AF546-Oxytocin (ROxy)	196
5.5 Conclusions	198
5.6 References	200
<b>Chapter 6: Experimental</b>	203
6.1 General Methods	203
6.2 Materials	204
6.3 Ethics Statement	205
6.4 RP-HPLC Methods	205
<b>6.5 Experimental-Chapter 2</b>	205
6.5.1 Synthesis of B12-Ex4	205
6.5.1.1 Synthesis of B12-Carboxylic Acid (B12-CA)	205
6.5.1.2 Synthesis of B12-Aminobutyne (B12-AB)	205
6.5.1.3 Synthesis of B12-Ex4	206
6.5.1.4 Synthesis of B12-Ex4-Cy5	206
	206

## 6.6 Experimental-Chapter 3

**Note: Numbering Corresponds to that used in Chapter 3**

6.6.1 Synthesis of Dicyanocobinamide (Cbi) (2)	206
6.6.2 Synthesis of Cbi-Ex4/40	211
6.6.2.1 Synthesis of Cbi-Propargylamine (Cbi-Pro) (4)	211
6.6.2.2 Synthesis of Cbi-Butyne (Cbi-But) (5)	215
6.6.2.3 Synthesis of Cbi-Pentyne (Cbi-Pent) (6)	219
6.6.2.4 Synthesis of Cbi-Hexyne (Cbi-Hex) (7)	223
6.6.2.5 Synthesis of Cbi-PEG2 (8)	227
6.6.2.6 Synthesis of Cbi-PEG4 (9)	231
6.6.2.7 Synthesis of Cbi-4EPMA (10)	235
6.6.2.8 Synthesis of Cbi-3EPMA (11)	239
6.6.2.9 Synthesis of Cbi-Pro-Ex4 (12)	243
6.6.2.10 Synthesis of Cbi-But-Ex4 (13)	244
6.6.2.11 Synthesis of Cbi-Pent-Ex4 (14)	246
6.6.2.12 Synthesis of Cbi-Hex-Ex4 (15)	248
6.6.2.13 Synthesis of Cbi-PEG2-Ex4 (16)	250
6.6.2.14 Synthesis of Cbi-PEG4-Ex4 (17)	252
6.6.2.15 Synthesis of Cbi-4EPMA-Ex4 (18)	254
6.6.2.16 Synthesis of Cbi-3EPMA-Ex4 (19)	256
6.6.2.17 Synthesis of Cbi-Pro-Ex40 (20)	258
6.6.2.18 Synthesis of Cbi-But-Ex40 (21)	260



6.6.2.19 Synthesis of Cbi-Pent-Ex40 (22)	262
6.6.2.20 Synthesis of Cbi-Hex-Ex40 (23)	264
6.6.2.21 Synthesis of Cbi-PEG2-Ex40 (24)	266
6.6.2.22 Synthesis of Cbi-PEG4-Ex40 (25)	268
6.6.2.23 Synthesis of Cbi-4EPMA-Ex40 (26)	270
6.6.2.24 Synthesis of Cbi-3EPMA-Ex40 (27)	272
6.6.3 Agonism (EC50) at Human GLP-1R	274
6.6.4 Competitive Binding Assay (IC50) at Human GLP-1R	275
6.6.5 Ex4 and Cbi-Ex4 ELISA	275
6.6.6 Structural Studies Using Circular Dichroism (CD)	275
<b>6.7 Experimental of Chapter 4</b>	276
6.7.1 Determining Structure of GRASP-05 Utilizing 2D NMR	276
6.7.2 Synthesis of AF546-GRASP-05	277
6.7.3 Development by this author of an in-house ELISA for GDF15 Binding	278
<b>6.8 Experimental-Chapter 5</b>	281
6.8.1 Synthesis of Fluorescent Probes	281
6.8.1.1 Synthesis of AF546-Ex4 (Rex)	281
6.8.1.2 Synthesis of Cy5-Leptin (Cy5-Leptin)	281
6.8.1.3 Synthesis of AF546-Oxytocin (ROxy)	282
<b>6.9 Experimental-Chapter 7</b>	282
6.9.1 Synthesis of Linear Oxytocin	282
6.9.2 Cyclic Oxytocin - Disulfide Bridge Formation in Oxytocin	283

6.9.3 Synthesis of Oxytocin Conjugates	283
6.9.3.1 Synthesis of B12-DBCO (B12-DBCO)	283
6.9.3.2 Synthesis of B12-Oxytocin (B12-Oxy)	284
6.10 References	285
<b>7. Ongoing and Future Work</b>	<b>286</b>
7.1 Building on lead candidate 22 (Chapter 3)	286
7.2 Prebinding of Corrinated Conjugates to Human Haptocorrin for Improved Pharmacokinetics	287
7.3 The Future of Corrination	288
7.3.1 Satiating Signaling via Vagal Oxytocin Receptors	288
7.3.1.1 Design, Synthesis, and Characterization of B12-Oxytocin (B12-Oxy)	289
7.3.1.2 Synthesis of B12-DBCO Linker	289
7.3.1.3 Synthesis of B12-Oxytocin (B12-Oxy)	291
7.3.1.4 In Vivo investigations of B12-Oxy in Male and Female Rats	293
7.4 References	295
<b>8. Appendix</b>	<b>299</b>
Appendix A: Publications	299
Appendix B: Curriculum Vitae	299

## Abbreviations

3EPMA	(3-ethynylphenyl)methanamine
4EPMA	(4-ethynylphenyl)methanamine
<sup>57</sup> Co	<sup>57</sup> Cobalt
AF	AlexaFluor®
AUC	Area Under the Curve
AMN	Amnionless
AP	Area Postrema
B12	Vitamin B12, Cyanocobalamin
B12-AB	B12-aminobutyne
B12-Ex4	B12-Exendin-4
BG	Blood Glucose
BSA	Bovine Serum Albumin
cAMP	Cyclic Adenosine Monophosphate
Cbi	Dicyanocobinamide
CD	Circular Dichroism
CD320	Cluster of differentiation 320
CDT	1,1-carbonyl-di-(1,2,4-triazole)
CNS	Central Nervous System
CuAAC	Copper(I) catalyzed Azide-Alkyne cycloaddition
CUBAM	Cubilin-amnionless

CUB	Cubilin
Cy5	Cyanine5
DMEM	Dulbecco's Modified Eagle Medium
DMF	Dimethylformamide
DMSO	Dimethylsulfoxide
DPP-IV	Dipeptidyl peptidase IV
DVC	Dorsal Vagal Complex
EAS	Electronic Absorption Spectra
EC <sub>50</sub>	Half-maximal Effective Concentration
EDC	1-Ethyl-3-(3-dimethylaminopropyl)carbodiimide
ELISA	Enzyme Linked Immunosorbent Assay
EPAC	Exchange Protein directly Activated by cAMP
Ex4	Exendin-4 with K12 azido modification
Ex40	Exendin-4 with an azido-lysine added as residue 40
FBS	Fetal Bovine Serum
FRET	Forster Resonance Energy Transfer
GLP-1	Glucagon-like Peptide-1
GLP-1R	Glucagon-like Peptide-1 Receptor
GPCR	G-protein Coupled Receptor
GSIS	Glucose-Stimulated Insulin Secretion
GTT	Glucose Tolerance Test
HC	Haptocorrin

HEK-293	Human Embryonic Kidney Cells
HObt	Hydroxybenzotriazole
IC <sub>50</sub>	Half-maximal Inhibitory Concentration
IBX	2-iodoxybenzoic acid
ICV	Intracerebroventricular Injection
IF	Intrinsic Factor
IHC	Immunohistochemistry
IP	Intraperitoneal Injection
IPGTT	Intraperitoneal Glucose Tolerance Test
ISR	Insulin Secretion Rate
LC-MS	Liquid chromatography-mass spectrometry
nEx4	Native Exendin-4
NMP	1-methyl-2-pyrrolidinone
NMR	Nuclear Magnetic Resonance
OGTT	Oral Glucose Tolerance Test
PNS	Peripheral Nervous System
RIA	Radioimmunoassay
RP-HPLC	Reversed-Phase High-Performance Liquid Chromatography
SC	Subcutaneous Injections
SD	Sprague–Dawley rat
SEM	Standard Error of the Mean
SES	Standard Extracellular Saline

SPAAC	Strained Promoted Azide-Alkyne Cycloaddition
T2DM	Type 2 Diabetes Mellitus
TBTA	tris(benzyltriazolylmethyl)amine
TC	Transcobalamin
TEA	Triethylamine
$t_R$	Retention Time

## List of Tables and Figures

<b>Chapter 1: Introduction</b>	<b>Page #</b>
<b>Figure 1.</b> Glucose homeostasis is controlled through the hormones, glucagon and insulin.	2
<b>Table 1.</b> Properties of Some Glucose-Lowering Agents Used in the Treatment of Type 2 Diabetes Mellitus.	6
<b>Figure 2.</b> Structure of Ex4. PDB code 1JRJ. Image generated by the author using PyMol.	8
<b>Figure 3.</b> Chemical Structure of B12 as cyanocobalamin, with corrin ring highlighted in red.	14
<b>Figure 4.</b> Biosynthetic pathways of adenosylcobalamin. Used with permission of publisher under the Creative Commons license.	16
<b>Figure 5.</b> Chemical structures of cobinamide phosphate, cobinamide, and cobyrinic acid. All structures are truncated forms of B12.	17
<b>Figure 6.</b> B12 functions as a co-factor for the enzymes methionine synthase and methylmalonyl-CoA Mutase within the cytosol and mitochondria, respectively.	19
<b>Figure 7.</b> Human Dietary Uptake Pathway of B12. Abbreviations used: HC: Haptocorrin; Cbl: cobalamin/B12; P: Protein; IF: Intrinsic Factor; TC: Transcobalamin.	21
<b>Figure 8.</b> B12 bound to haptocorrin. PDB code 4KKI. Image generated by the author using PyMol.	23
<b>Figure 9.</b> B12 bound to intrinsic factor. PDB code 2PMV. Image generated by the author using PyMol.	24

**Figure 10.** B12 bound to transcobalamin. PDB code 2BB5. Image generated by the author using PyMol. 25

**Table 2.** Unsaturated Binding Capacity (UBC) of Serum and Gastric Juice in Various Lab Animal Models. 33

**Figure 11.** Corriation of Ex4 (Cbi-Ex4) does not prevent GLP-1R agonism in the pancreas but does mitigate agonism in the CNS as tracked by emesis and anorexia. Ex4 alone agonizes GLP-1R populations in both the pancreas and CNS. 36

**Figure 12.** Monomer of GDF15 a Member of the GFL. PDB code 5VZ4. Image generated by the author using PyMol. 38

**Figure 13.** Dimer of GDF15 a Member of the GFL. PDB code 5VT2. Image generated by the author using PyMol. 38

**Figure 14.** Domain structures of the H88 adenovirus. Used with permission of author. 43

## **Chapter 2: A Second-generation Glucagon-like Peptide-1 Receptor Agonist**

### **Mitigates Vomiting and Anorexia While Retaining Glucoregulatory Potency in Lean Diabetic and Emetic Mammalian Models**

**Figure 1.** Systemically delivered B12-Ex4 enhances glucose clearance during an intraperitoneal glucose tolerance test (IPGTT). In an IPGTT, Ex4 (5 nmol/kg, i.e., ≈20 μg/kg) and B12-Ex4 (5 nmol/kg) showed a similar potency in suppressing BG levels after intraperitoneal (IP) glucose administration (2 g/kg, IP) compared with saline; saline versus B12-Ex4: \*\*\* P < .001; saline versus Ex4: ### P < .001. AUC analysis from 0 (i.e., post-glucose bolus) to 120 minutes; B12-Ex4 and Ex4 similarly reduced AUCs 81



compared with saline. All data are expressed as mean  $\pm$  standard error of mean (SEM). IPGTT data was analyzed with repeated measurements two-way ANOVA followed by Tukey's post hoc test. AUC data was analyzed with repeated measurements one-way ANOVA followed by Tukey's post hoc test. Means with different letters are significantly different ( $P < .05$ ). In IPGTT,  $n = 13$ , within subject design; AUC,  $n = 5$ , within subject design).

**Figure 2.** Equimolar dosing of Ex4 (5 nmol/kg, i.e.,  $\approx 20 \mu\text{g}/\text{kg}$ ), B12-Ex4 (5 nmol/kg) or saline were administered without subsequent glucose administration. Both Ex4 and B12-Ex4 treatments were no longer effective in reducing BG levels and had no effect on AUC. All data are expressed as mean  $\pm$  SEM. Blood glucose data was analyzed with repeated measurements two-way ANOVA followed by Tukey's post hoc test. AUC data was analyzed with repeated measurements one-way ANOVA followed by Tukey's post hoc test. Means with different letters are significantly different ( $P < .05$ ). In IPGTT,  $n = 13$ , within subject design; AUC,  $n = 5$ , within subject design. 82

**Figure 3.** Systemically injected fluorophore-labelled B12-Ex4 (Cy5-B12-Ex4, 5 nmol/kg) co-localized with insulin in shrew pancreatic tissue supporting the hypothesis that B12-Ex4 acts at the pancreas to improve glycemic control. 83

**Figure 4.** Pharmacological doses of B12-Ex4 do not affect feeding and body weight in shrews. Ex4 (5 nmol/kg, i.e.  $\approx 20 \mu\text{g}/\text{kg}$ ) suppressed feeding at 3, 6, 12 and 24 hours, whereas equimolar doses of B12-Ex4 (5 nmol/kg) had no effect on food intake. Ex4-induced anorexia was accompanied by body weight loss. No significant changes in body weight were observed after B12-Ex4 administration compared with controls. All 84

data are expressed as mean  $\pm$  SEM. Data was analyzed with repeated measurements one-way ANOVA followed by Tukey's post hoc test. Means with different letters are significantly different ( $P < .05$ ). In food intake studies,  $n = 8$ , within subject design; in body weight change studies,  $n = 6$ , within subject design.

**Figure 5.** Supra-pharmacological doses of B12-Ex4 do not affect feeding and body weight in shrews. Ex4 (50 nmol/kg, i.e.  $\approx 200 \mu\text{g}/\text{kg}$ ) suppressed eating at all measured time points. By strict contrast, supra-pharmacological equimolar doses of B12-Ex4 did not show any effects. While severe body weight loss occurred following supra-pharmacological doses of Ex4, no significant changes occurred in the B12-Ex4-treated animals. All data are expressed as mean  $\pm$  SEM. Data was analyzed with repeated measurements one-way ANOVA followed by Tukey's post hoc test. Means with different letters are significantly different ( $P < .05$ ). In food intake studies,  $n = 8$ , within subject design; in body weight change studies,  $n = 6$ , within subject design. 85

**Figure 1.** Emesis in shrews is significantly reduced following pharmacological B12-Ex4 (5 nmol/kg) treatment compared with native Ex4 (5 nmol/kg, i.e.  $\approx 20 \mu\text{g}/\text{kg}$ ), denoting improved tolerance. The percentage of shrews experiencing emesis was significantly different between Ex4 and equimolar B12-Ex4 (\*\*\*) ( $P < .001$ ). None of the animals experienced emesis following saline administration (data not shown). The number of single emetic episodes following Ex4 (5 nmol/kg, i.e.  $\approx 20 \mu\text{g}/\text{kg}$ ), equimolar B12-Ex4 (5 nmol/kg) or saline systemic administration was recorded for 90 minutes. Ex4 induced robust emetic responses that were not observed after B12-Ex4 or saline injections. The number of emetic bouts was also lower after B12-Ex4 treatment 86

compared with Ex4 and it did not differ from saline controls. Latency to the first emetic episode in Ex4 animals that exhibited emesis. Heatmap showing the emetic latency and intensity, as well as the number of emetic episodes induced by Ex4 or B12-Ex4 for each animal across time. Evidence of emesis was analyzed with Fisher's exact test. Emetic episodes and bouts were analyzed with repeated measurements one-way ANOVA followed by Tukey's post hoc test. Emesis studies, n = 16, within subject design. Means with different letters are significantly different (P < .05).

**Figure 7.** Emesis in shrews is significantly reduced following supra-pharmacological B12-Ex4 (50 nmol/kg) treatment compared with native Ex4 (50 nmol/kg, i.e. ≈200 μg/kg), denoting improved tolerance. Astonishingly, no emesis occurred after B12-Ex4 administration. The percentage of shrews experiencing emesis was completely reversed between Ex4 and equimolar B12-Ex4 (\*\*\* P < .001). No animal experienced emesis following saline injection (data not shown). The number of emetic episodes and bouts following Ex4, equimolar B12-Ex4 or saline administration was analyzed over 90 minutes. Also, at this dosage Ex4 induced robust emetic responses. Latency to the first emetic episode in Ex4 shrews that exhibited emesis. Heatmap showing the emetic latency and intensity, as well as the number of emetic episodes for each animal across time. All data are expressed as mean ± SEM. Emetic episodes and bouts were analyzed with repeated measurements one-way ANOVA followed by Tukey's post hoc test. Emesis studies, n = 8, within subject design. Means with different letters are significantly different (P < .05).

88

**Figure 8.** Systemic administered B12-Ex4 does not activate the area postrema (AP) or the nucleus tractus solitarius (NTS) in shrew. Representative immunostainings of the AP/NTS region showing the c-Fos response following saline (n = 4), Ex4 (5 nmol/kg, n = 4) and equimolar B12-Ex4 (n = 5) systemic treatment. Peripheral Ex4 administration significantly increased the number of c-Fos immunoreactive (IR) cells in the AP/NTS of shrews 3 hours after injection. The number of c-Fos–positive cells in the AP/NTS was significantly lower in B12-Ex4–treated animals and it did not differ from saline-treated shrews. Data was analyzed with one-way ANOVA followed by Tukey post hoc test. Means with different letters are significantly different from each other (P < .05). Values are expressed as mean ± SEM. Scale bar 100 μm.

89

**Figure 9.** Systemic administration of B12-Ex4 does not result in emesis but does when delivered centrally. Ex4 (0.24 nmol, i.e., 1 μg), equimolar B12-Ex4 or vehicle was infused into the lateral ventricle. The percentage of shrews showing emesis was similar between Ex4 and B12-Ex4. The number of single emetic episodes or bouts following Ex4, B12-Ex4 or saline was recorded for 120 minutes. Both Ex4 and B12-Ex4 induced comparable emetic responses, while none of the animals experienced emesis following vehicle delivery (data not shown). Latency to the first emetic episode in Ex4- and B12-Ex4–treated animals that exhibited emesis did not differ. Evidence of emesis was analyzed with Fisher's exact test. Emetic episodes and bouts were analyzed with Student t-test (n=8, within subject design). Values are expressed as mean ± SEM.

90

**Figure 10.** B12-Ex4 enhances glucose clearance during an oral glucose tolerance test (OGTT) without inducing anorexia and body weight loss in the Goto-Kakizaki lean

92

diabetic rat model. In an OGTT, liraglutide (100 µg/kg, i.e., 26.6 nmol/kg) and 5 nmol/kg B12-Ex4 suppressed blood glucose levels after intraperitoneal (IP) glucose administration (1 g/kg, per os (PO)) compared with 5 nmol/kg Ex4 (i.e.; ≈20 µg/kg) and saline. \* saline versus others; #: Ex4 versus others; \$: liraglutide versus others. \*, #, \$: P < .05; \*\*, ##, \$\$: P < .01; \*\*\*, ###, \$\$\$: P < .001. Liraglutide and Ex4 induced a strong anorectic effect, which was not observed after B12-Ex4 treatment. Hypophagia was accompanied by body weight loss in liraglutide- and Ex4-treated animals, while no significant body weight change was observed following B12-Ex4. Data were analyzed with repeated measure two-way ANOVA or one-way ANOVA followed by Tukey post hoc test; n = 21, within subject design. All data are expressed as mean ± SEM. Means with different letters are significantly different from each other (P < .05).

### **Chapter 3: Corination of a GLP-1 Receptor Agonist for Glycemic Control without**

#### **Emesis**

**Figure 1.** Synthetic scheme for Cbi. Cbi was formed via microwave from B12. 111

**Figure 2.** RP-HPLC Trace (Shimadzu Prominence HPLC using a C18 column (Eclipse XDB-C18 5µm, 4.6 x 150 mm) (RP-HPLC, from 1% CH<sub>3</sub>OH/H<sub>2</sub>O + 0.1% TFA to 70% CH<sub>3</sub>OH/H<sub>2</sub>O + 0.1% TFA in 15 min)) showing the α- and β-isomer products at 5.2 and 6.7 minutes. Purity 98%. 111

**Figure 3.** ESI-MS (Shimadzu LCMS-8040) of Cbi, expected  $m/z = 1042$ , observed  $m/z = 1016$  [M-CN]<sup>+1</sup>. 112

- Figure 4.** Synthetic scheme for Cbi-AB synthesis, 1-amino-3-butyne was coupled to Cbi through secondary alcohol to create carbamate linkage utilizing 1,1'-carbonyl-di-(1,2,4-triazole) (CDT), priming the Cbi for conjugation to Ex4. 113
- Figure 5.** RP-HPLC Trace (Shimadzu Prominence HPLC using a C18 column (Eclipse XDB-C18 5 $\mu$ m, 4.6 x 150 mm) (RP-HPLC, from 1% CH<sub>3</sub>OH/H<sub>2</sub>O + 0.1% TFA to 70% CH<sub>3</sub>OH/H<sub>2</sub>O + 0.1% TFA in 15 min)) showing the  $\alpha$ - and  $\beta$ - isomers of the Cbi-AB Product at 7.4 and 7.9 minutes. Purity 97%. 114
- Figure 6.** ESI-MS (Shimadzu LCMS-8040) of Cbi-Alkyne, expected  $m/z = 1129$ , observed  $m/z = 1111 [M^+ - H_2O]^+$ . 114
- Figure 7.** Synthetic scheme for Cbi-Ex4, Cbi-AB was clicked onto an azido Exendin-4 utilized CuAAC. 115
- Figure 8.** RP-HPLC Trace (Shimadzu Prominence HPLC using a C18 column (Eclipse XDB-C18 5 $\mu$ m, 4.6 x 150 mm) (RP-HPLC, from 1% CH<sub>3</sub>CN/H<sub>2</sub>O + 0.1% TFA to 70% CH<sub>3</sub>CN/H<sub>2</sub>O + 0.1% TFA in 15 min)) showing the Cbi-Ex4 Product at 11.7 min. Purity 98%. 115
- Figure 9.** ESI-MS (Shimadzu LCMS-8040) of Cbi-Ex4, expected  $m/z = 5354$ , observed  $m/z = 1339 [M^+ + 3H^+]^{+4}$ ,  $1071 [M^+ + 4H^+]^{+5}$ . 116
- Figure 10.** Dose-dependent Cbi-Ex4 agonism at the human GLP-1 receptor, as monitored in FRET assays using the cAMP biosensor H188<sup>69</sup> expressed in HEK293 cells.<sup>70</sup> EC<sub>50</sub> value for Cbi-Ex4 was determined to be  $200 \pm 0.09$  pM (mean  $\pm$  SEM). 117

**Table 1.** B12 and its binding proteins, transcobalamin (TC) and haptocorrin (HC) as measured in shrew serum, and their inhibition by increasing concentration of Cbi-Ex4. The sum of Apo TC + Apo HC ~equals B12 binding capacity. \* Conducted by Dr. Ebba Nexo at University of Aarhus, Denmark. 118

**Figure 11.** Binding affinity plots of Cbi ((CN)<sub>2</sub>Cbi) and Cbi-Ex4 by the B12 binding proteins transcobalamin (TC) and haptocorrin (HC). Figure 11 shows the binding affinity (K<sub>a</sub>) of B12 binding proteins transcobalamin and haptocorrin to endogenously occurring Cbi and the Cbi conjugated Ex4 (Cbi-Ex4). HC is known to be the only physiologically relevant binder of Cbi and this is reflected in the binding constant of HC with Cbi (K<sub>a</sub> 0.036 nM). HC also binds Cbi-Ex4 (K<sub>a</sub> 0.456), albeit with ~ 10-fold lower affinity. Consistent with the known binding profile of TC, only weak binding occurs for TC with Cbi or Cbi-Ex4 (K<sub>a</sub> > 2 μM). \* Conducted by Dr. Ebba Nexo at University of Aarhus, Denmark. 118

**Figure 12.** Ex4 (1.25, 5, and 50 nmol/kg, i.p.; i.e., ≈5, 20, and 200 mg/kg; respectively) dose-dependently suppressed blood glucose (BG) levels following glucose administration (2 g/kg, i.p.). Saline versus 5 nmol/kg Ex4: \*\*p < 0.01, \*\*\*p < 0.001; saline versus 50 nmol/kg Ex4: ###p < 0.001; saline versus 1.25 nmol/kg Ex4: §§p < 0.01; 1.25 nmol/kg Ex4 versus 50 nmol/kg Ex4: @@@p < 0.001; 1.25 nmol/kg Ex4 versus 5 nmol/kg Ex4: Φp < 0.05, ΦΦp < 0.01, ΦΦΦp < 0.001. Area under the curve (AUC) from 0 (i.e., post-glucose bolus) to 120 min after Ex4. In an IPGTT Cbi-Ex4 dose-dependently reduced BG levels comparably to equimolar doses of Ex4. Saline versus 5-nmol/kg Cbi-Ex4: \*\*p < 0.01, \*\*\*p < 0.001; saline versus 50 nmol/kg Cbi-Ex4: ###p 120

< 0.001; saline versus 1.25 nmol/kg Cbi-Ex4: §p < 0.05; 1.25 nmol/kg Cbi-Ex4 versus 50 nmol/kg Cbi-Ex4: @@@ p < 0.001. AUC from 0 to 120 min following Cbi-Ex4. All data expressed as mean ± SEM. Data in IPGTT was analyzed with repeated-measurements two-way ANOVA followed by Tukey's post hoc test. AUC data in was analyzed with repeated-measurements one-way ANOVA followed by Tukey's post hoc test. Means with different letters are significantly different (p < 0.05).

**Figure 13.** In an IPGTT, Ex4 (5 nmol/kg, i.e. 20 µg/kg) and equimolar doses of Cbi-Ex4 121 suppressed blood glucose (BG) levels after IP glucose administration (2 g/kg, IP) compared to saline; vehicle vs Cbi-Ex4: \*\*\* P < 0.001; vehicle vs Ex4: ### P < 0.001; Ex4 vs Cbi-Ex4: §§ P < 0.01). Area under the curve (AUC) analyses from 0 (i.e., post-glucose bolus) to 60 and 0 to 120 min; respectively. Cbi-Ex4 and Ex4 similarly reduced AUCs compared to vehicle. All data expressed as mean ± SEM. IPGTT data in was analyzed with repeated measurements two-way ANOVA followed by Tukey's post-hoc test. All other data was analyzed with repeated measurements one-way ANOVA followed by Tukey's post hoc test. Means with different letters are significantly different (P < 0.05).

**Figure 14.** In a delayed glucose load IPGTT, Ex4, Cbi-Ex4 (5 nmol/kg) or vehicle were 122 injected 6 h before glucose load. While Ex4-treatment was no longer effective in reducing BG levels, Cbi-Ex4 retained its BG lowering properties; saline versus Cbi-Ex4: \*\*p < 0.01, \*\*\*p < 0.001; Ex4 versus Cbi-Ex4: §§p < 0.01), §§§p < 0.001. AUC analyses from 0 to 60 min and 0 to 120 min, respectively. Cbi-Ex4-treated animals had lower AUC 0-120 compared to Ex4-treated animals and a lower AUC 0–60



compared to Ex4-treated animals and controls. All data expressed as mean  $\pm$  SEM.

Data in IPGTT was analyzed with repeated-measurements two-way ANOVA followed by Tukey's post hoc test. AUC data in was analyzed with repeated-measurements one-way ANOVA followed by Tukey's post hoc test. Means with different letters are significantly different ( $p < 0.05$ ).

**Figure 15.** Ex4 dose-dependently induced anorexia leading to weight loss. (J and K) 123

Equimolar doses of Cbi-Ex4 had no effect on food intake or body weight. All data expressed as mean  $\pm$  SEM. Data was analyzed with repeated-measurements two-way ANOVA followed by Tukey's post hoc test.

**Figure 16.** Ex4 (5 nmol/kg) induced anorexia at 3h, 6h, 12h and 24h post injection, 124

whereas Cbi-Ex4 had no effect on food intake. Latency to eat was increased only in Ex4-treated animals. All data expressed as mean  $\pm$  SEM. Food intake was analyzed with repeated measurements two-way ANOVA followed by Tukey's post-hoc test. All other data were analyzed with repeated measurements one-way ANOVA followed by Tukey's post hoc test. Means with different letters are significantly different ( $P < 0.05$ ).

**Figure 17.** Pharmacokinetic profile of two equimolar doses (25 nmol/kg and 50 126 nmol/kg) of Ex4 and Cbi-Ex4. Data expressed as mean  $\pm$  SEM. Full PK parameters are given in Table 2.

**Table 2.** Pharmacokinetic parameters measured for Ex4 and Cbi-Ex4 in *S. murinus*. 126

AUC indicates area under the curve between 0 and 360 or 0-1440 minutes;  $C_{Max}$  is the maximum measured concentration;  $T_{1/2}$  is the elimination half-life;  $V_d$  is volume of distribution, Cl is clearance and  $K_e$  is elimination rate constant.

**Figure 18.** Ex4 (1.25, 5, and 50 nmol/kg) induced emesis during 120 min after injection 129

in a dose-related fashion. The number of animals exhibiting emesis, expressed as a fraction of the total number of animals tested, is indicated above each treatment group. Latency to the first emetic episode of shrews that exhibited emesis after Ex4 treatment. Number of shrews experiencing emesis following Cbi-Ex4 (1.25, 5, and 50 nmol/kg) during 120 min after injection. The ratio of animals exhibiting emesis is indicated above each treatment group. Latency to the first emetic episode of shrews that experienced emesis after Cbi-Ex4 treatment. Heatmaps showing latency, number, and intensity of emesis following Ex4 and Cbi-Ex4 dosing for each individual animal across time. All data expressed as mean  $\pm$  SEM. Means with different letters are significantly different ( $p < 0.05$ ). Emetic episode data was analyzed with repeated-measurements one-way ANOVA followed by Tukey's post hoc test.

**Figure 19.** Cbi-Ex4 vs. Ex4 direct comparison on emesis. The number of single emetic 130

episodes following, Ex4 (5 nmol/kg, i.e. 20  $\mu$ g/kg), Cbi-Ex4 or saline administration was recorded for 120 min. Ex4 induced robust emetic responses that were not observed after Cbi-Ex4 or saline injections. The number of emetic bouts was also lower in Cbi-Ex4-treated animals compared to Ex4 and it did not differ from controls. Graphical representation of latency to the first emetic episode between Ex4 and Cbi-

Ex4-treated animals that exhibited emesis. The percentage of shrews experiencing emesis was significantly different between Ex4 and Cbi-Ex4. Heatmap showing latency, number and intensity of emesis for each animal across time. All data expressed as mean  $\pm$  SEM. Means with different letters are significantly different ( $P < 0.05$ ). Emetic episode and bout data was analyzed with repeated measurements one-way ANOVA followed by Tukey's post hoc test. Frequency of emesis in animals was analyzed with Fisher's exact test.

**Figure 20.** Quantification of c-Fos positive neurons in the rostral, medial, and caudal NTS and medial AP. Peripheral Ex4 administration significantly increased the number of c-Fos immunoreactive cells in the AP/NTS of shrews 3 h after injection. The number of c-Fos positive cells in the AP/NTS was significantly lower in Cbi-Ex4 treated animals. All data expressed as mean  $\pm$  SEM. Data was analyzed with one-way ANOVA followed by Tukey's post hoc test. Scale bar, 100  $\mu$ m. 131

**Figure 21.** Dose response and regression plot for HC-Cbi-Ex4 agonism at the GLP-1R. 132

**Figure 22.** (Left) Structure of the Cbi ((CN)<sub>2</sub>Cbi) starting material, a purple solid prepared via microwave chemistry from B12, with the hydroxyl group boxed used as a site of conjugation to linker series. (Right) Library of linkers used in the conjugation of Cbi to Ex4 peptides. The library of linkers chosen in this study included short hydrophobic alkane chains, amphiphilic PEG, and rigid substituted ethynyl phenyl methanamines, which were coupled to the Cbi hydroxyl group via CDT-mediated amide formation, resulting in Cbi compounds (**4–11**) with an available alkyne group 135

for subsequent reaction with azido-modified Ex4 peptides via copper-mediated alkyne-azide click chemistry (Figure 23).

**Figure 23.** Synthetic Scheme of Cbi Linkers (**4–11**) and Cbi-Peptide Conjugates (**12–27**). 136

**Figure 24.** Effect of Cbi conjugation on the secondary structure of Ex4 or Ex40. CD spectra were collected with a sample concentration of 40  $\mu$ M at pH 7 between 200 and 250 nm. % helicity was measured at 222 nm. 138

**Figure 25.** Conjugation of Cbi to Ex4 or Ex40 peptides maintains agonism at the GLP-1R. Nonlinear regression analysis was performed with GraphPad Prism 8. All compounds were assayed at least as triplicate independent runs. Data are shown as mean  $\pm$  SEM. 139

**Figure 26.** *In vitro* dose escalation competition binding studies of 12-27 compared with Ex4 and Ex40 controls against fluorescent GLP-1red. \* Conducted by EuroscreenFast. 141

**Table 3.** EC<sub>50</sub> and IC<sub>50</sub> Values with Hill Slopes and % Helicity of Cbi Conjugates **12–27**. 142

<sup>a</sup>Data represents EC<sub>50</sub> obtained using nonlinear regression analysis of data from highest FRET values obtained for each data point. Experiments were performed as three independent runs. <sup>b</sup>Data represents the Hill slope obtained using nonlinear regression analysis of data from highest FRET values obtained for each data point. Experiments were performed as three independent runs. <sup>c</sup>Data represents mean residue ellipticity [ $\theta$ ]<sub>222</sub> determined from the CD spectra of a 40  $\mu$ M solution of peptide in H<sub>2</sub>O at RT pH 7.0. Average [ $\theta$ ]<sub>222</sub> values utilized to calculate percent helicity were obtained by performing the experiment in triplicate. Percent helicity was calculated using  $100 \times ([\theta]_{222}/^{\max}[\theta]_{222})$ .  $^{\max}[\theta]_{222} = -40,000 [1 - (2.5/n)]$ , where n is the residue number. Experiments were performed as three independent runs.

<sup>d</sup>Data represents IC<sub>50</sub> values obtained from competitive binding assays against red fluorescent GLP-1 using nonlinear regression analysis from highest values obtained for each data point. Experiments were performed as two independent runs. <sup>e</sup>Hill slopes were obtained using nonlinear regression analysis from highest values obtained for each data point. Results are expressed as mean  $\pm$  SEM.

**Figure 27.** **22** increases glucose-stimulated insulin secretion in rat islets relative to glucose controls. Insulin secretion rate from static cultures of Sprague–Dawley rat islets incubated in media containing glucose (10 mM) and Ex4 (10 or 50 nM) or **22** (10 or 50 nM).<sup>104</sup> Data was calculated from three independent experiments and analyzed with repeated-measurements two-way ANOVA followed by Tukey’s post hoc test. 143

Results are expressed as mean  $\pm$  SEM, \*\*\*\*  $p < 0.0001$ . \* Conducted by Varun Kamat under the guidance of Dr. Ian R. Sweet at University of Washington.

**Figure 28.** Cbi-Ex4 enhances glucose clearance without inducing emesis or body weight loss. (A) In an IPGTT, Ex4, **1**, and **22** (50 nmol/kg, IP) showed similar potency in suppressing BG levels after glucose administration (2 g/kg, IP) compared to saline; vehicle vs **1**: \*\*\*  $P < 0.001$ ; vehicle vs **22**: ###  $P < 0.001$ ; vehicle vs Ex4: §§§  $P < 0.001$ ; **1** vs **22**:  $\Phi\Phi$   $P < 0.01$  ( $n = 12$  shrews). Area under the curve (AUC) analysis from 0 (i.e., post-glucose bolus) to 60 min following **1**, **22**, and Ex4. AUC analysis from 0 to 120 min; **22** and Ex4 similarly reduced AUCs compared to vehicle ( $P < 0.05$ ). All data expressed as mean  $\pm$  SEM ( $n = 10$ ). IPGTT data was analyzed with repeated-measurements two-way ANOVA followed by Tukey's posthoc test. AUC data was analyzed with repeated measurements one-way ANOVA followed by Tukey's posthoc test. Means with different letters are significantly different ( $P < 0.05$ ). 144

**Figure 29.** Ex4 and **22** (5 nmol/kg, IP) induced anorexia at 6, 24, and 48 h (and at 72 h for Ex4 only), whereas **1** had no effect on food intake ( $n = 10$ ). Ex4-induced anorexia was accompanied by significant body weight loss at 24 h. No significant changes in body weight occurred after **1** and **22** administration compared to controls. All data expressed as mean  $\pm$  SEM ( $n = 10$ ). Data was analyzed with repeated-measurements two-way ANOVA followed by Tukey's post hoc test. Means with different letters are significantly different ( $P < 0.05$ ). 145

**Figure 30.** The number of single emetic episodes following Ex4, **1**, **22**, or saline systemic administration was recorded for 120 min. The number of animals 147

exhibiting emesis, expressed as a fraction of the total number of animals tested, is indicated above each treatment group. Ex4 induced robust emetic responses that were not observed after **1** or saline injections. **22** induced emesis in two of the animals tested; however, the number of emetic episodes was significantly lower than that of Ex4 and did not differ from animals treated with vehicle or **1** (n = 10). Heatmaps showing latency, number, and intensity of emesis following Ex4, **1**, and **22** dosing for each individual animal across time. All data expressed as mean  $\pm$  SEM (n = 10). Emetic episode data was analyzed with repeated measurements one-way ANOVA followed by Tukey's post hoc test. Means with different letters are significantly different (P < 0.05).

#### **Chapter 4: Peptide Ligands of the GDNF Family Receptor $\alpha$ -like (GFRAL)**

**Table 1.** Designed GFRAL antagonists. Sequences were designed using amino acids of native ligand, GDF15, known to interact with GFRAL receptor. Note: Sequences are confidential (Office of Technology Transfer, Syracuse University). 168

**Figure 1.** The AP lies at the caudal end of the fourth ventricle adjacent to the NTS. 169  
Direct injection via the fourth ventricle allows for activation of neurons found in the AP and NTS.

**Figure 2.** GRASP-05 reduces GDF15-induced kaolin intake. 4<sup>th</sup> ICV GRASP-05 (300 pmol) significantly reduces 4<sup>th</sup> ICV GDF15 (30 pmol)-induced kaolin intake in the rat (n=9/group, within-subject design) Data expressed as mean  $\pm$  SEM. Means with different letters are significantly different (P < 0.05). 169

- Figure 3.** Synthetic scheme for GRASP-555. DBCO AF-546 was successfully “clicked” to GRASP-05 utilizing SPAAC. 171
- Figure 4.** RP-HPLC Trace (Shimadzu Prominence HPLC using a C18 column (Eclipse XDB-C18 5 $\mu$ m, 4.6 x 150 mm) (RP-HPLC, from 1% CH<sub>3</sub>OH/H<sub>2</sub>O + 0.1% TFA to 90% CH<sub>3</sub>OH/H<sub>2</sub>O + 0.1% TFA in 25 min)) showing GRASP-555 product at 10.9 min. Purity 99%. 171
- Figure 5.** ESI-MS (Shimadzu LCMS-8040) of GRASP-555, expected m/z = 4386, observed m/z = [M+2H<sup>+</sup>+Na<sup>+</sup>]<sup>+3</sup>: 1487, [M+3H]<sup>+3</sup>: 1463, [M+4H<sup>+</sup>+H<sub>2</sub>O]<sup>+4</sup>: 1116, [M+4H]<sup>+4</sup>: 1097, [M+5H]<sup>+5</sup>: 878. 172
- Figure 6.** GRASP-555 electronic absorption spectra were obtained on a Varian Cary 50 Bio spectrophotometer in a 2mL quartz cuvette between 400 nm – 700 nm in aqueous acetonitrile. 172
- Figure 7.** GRASP-555 10 mg/kg; IP shows co-localization with GFRAL-expressing neurons in the AP and NTS of rats. 173
- Figure 8.** Solution state structure of GRASP solved by NMR revealing secondary ‘Hairpin-like’ structure with GDF15 like ‘loop’. Structure solved by Dr. Deborah Kerwood, Syracuse University. 174
- Figure 9.** GDF15 (green) binding to GFRAL (blue/purple) (PDB 5VZ4) with bound GRASP (Red) simulated using HADDOCK 2.2. A close-up rendering shows GRASP ‘blocking’ the region of GDF15 (W32) known to be vital for RET recruitment. 175



**Figure 10.** Microsomal stability assay in rats. The half-life was calculated to be: 104.43 min. Reaction velocity (V) was calculated to be 511  $\mu\text{L}/\text{mg}$ . Intrinsic clearance ( $\text{Cl}_{\text{int}}$ ) was determined to be 339  $\mu\text{L}/\text{min}/\text{mg}$  protein. 176

**Figure 11.** Synthetic scheme for Lip-GRASP-05. DBCO AF-546 was successfully “clicked” to GRASP-05 utilizing SPAAC. 177

**Figure 12.** ESI-MS (Shimadzu LCMS-8040) of Lip-GRASP-05, expected  $m/z = 4258$ , observed  $m/z = [\text{M}+3\text{H}^+]^{+3}: 1420, [\text{M}+4\text{H}^+]^{+4}: 1065, [\text{M}+5\text{H}^+]^{+5}: 852$ . 177

**Figure 13.** ELISA assay of GDF15 binding to human recombinant GFRAL (0.1  $\mu\text{g}/\text{mL}$ ). 178

**Figure 14.** GenScript Generated Primary Antibody. 178

## **Chapter 5: Fluorescent Probes of Neuroendocrine Hormones for the Identification of Receptor Distribution and Function**

**Figure 1.** Structure of leptin. PDB code 1AX8. Image generated by the author using PyMol. 187

**Figure 2.** RP-HPLC Trace (Shimadzu Prominence HPLC using a C18 column (Eclipse XDB-C18 5 $\mu\text{m}$ , 4.6 x 150 mm) (RP-HPLC, from 1%  $\text{CH}_3\text{OH}/\text{H}_2\text{O}$  + 0.1% TFA to 90%  $\text{CH}_3\text{OH}/\text{H}_2\text{O}$  + 0.1% TFA in 25 min)) showing Cy5-Leptin product at 9.9 min. Purity 98%. 188

**Figure 3.** Cy5-Leptin mass was found to be between 15-20 kDa and confirmed utilizing 12.5% SDS-PAGE. 189

**Figure 4.** Cy5-Leptin electronic absorption spectra were obtained on a Varian Cary 50 Bio spectrophotometer in a 2mL quartz cuvette between 500 nm – 800 nm in aqueous acetonitrile. 190

<b>Figure 5.</b> Immunohistochemical visualization of Cy5-Lep colocalized to DVC astrocytes. Used with permission of publisher under the Creative Commons license.	191
<b>Figure 6.</b> Synthetic scheme for REX.	193
<b>Figure 7.</b> RP-HPLC Trace (Shimadzu Prominence HPLC using a C18 column (Eclipse XDB-C18 5 $\mu$ m, 4.6 x 150 mm) (RP-HPLC, from 1% CH <sub>3</sub> OH/H <sub>2</sub> O + 0.1% TFA to 90% CH <sub>3</sub> OH/H <sub>2</sub> O + 0.1% TFA in 25 min)) showing REX product at 14.1 min. Purity 97%.	193
<b>Figure 8.</b> ESI-MS (Shimadzu LCMS-8040) of REX, expected m/z = 5319, observed m/z = [M+3H <sup>+</sup> ] <sup>+3</sup> : 1773, [M+4H <sup>+</sup> ] <sup>+4</sup> : 1331.	194
<b>Figure 9.</b> REX electronic absorption spectra were obtained on a Varian Cary 50 Bio spectrophotometer in a 2mL quartz cuvette between 400 nm – 700 nm in aqueous acetonitrile.	194
<b>Figure 10.</b> <i>In vitro</i> dose escalation study of REX showing increase in cAMP levels in GLP-1R stably transfected HEK-293-H188 c20 cells.	195
<b>Figure 11.</b> Synthetic scheme for ROxy. B12-DBCO was successfully “clicked” to OTaz utilizing SPAAC.	197
<b>Figure 12.</b> RP-HPLC Trace (Shimadzu Prominence HPLC using a C18 column (Eclipse XDB-C18 5 $\mu$ m, 4.6 x 150 mm) (RP-HPLC, from 1% CH <sub>3</sub> OH/H <sub>2</sub> O + 0.1% TFA to 90% CH <sub>3</sub> OH/H <sub>2</sub> O + 0.1% TFA in 25 min) showing ROxy product at 12.0 min. Purity 99%.	197
<b>Figure 13.</b> ESI-MS (Shimadzu LCMS-8040) of B12-Oxy, expected m/z = 2154, observed m/z = [M+H <sub>2</sub> O+2H <sup>+</sup> ] <sup>+2</sup> : 1097, [M+2H <sup>+</sup> ] <sup>+2</sup> : 1078.	198

**Figure 14.** ROxy electronic absorption spectra was obtained on a Varian Cary 50 Bio 198  
spectrophotometer in a 2mL quartz cuvette between 400 nm – 700 nm in aqueous  
acetonitrile.

## Chapter 6: Experimental

**Figure 1.** RP-HPLC trace showing the  $\alpha$ - and  $\beta$ -isomer products of **2** at 5.2 and 6.7 207  
min.

**Figure 2.** ESI-MS of **2**, expected  $m/z = 1042$ , observed  $m/z = [M-CN]^{+1} 1016$ . 207

**Figure 3.** Electronic absorption spectroscopy of **2**. 208

**Figure 4.** H NMR of **2** (400 MHz, 298K, D<sub>2</sub>O). 209

**Figure 5.** <sup>13</sup>C NMR of **2** (400 MHz, 298K, D<sub>2</sub>O). 210

**Figure 6.** RP-HPLC trace showing the  $\alpha$ - and  $\beta$ -isomer products of **4** at 8.8 and 9.5 211  
min.

**Figure 7.** ESI-MS of **4**, expected  $m/z = 1115$ , observed  $m/z = [M^+-H_2O]^{+1}: 1096$ ,  $[M^+-$  212  
 $H_2O+H^+]^{+2}: 549$ .

**Figure 8.** Electronic absorption spectroscopy of **4**. 212

**Figure 9.** <sup>1</sup>H NMR of **4** (400 MHz, 298K, D<sub>2</sub>O). 213

**Figure 10.** <sup>1</sup>H NMR of **4** (400 MHz, 298K, D<sub>2</sub>O) (Aromatic). Characteristic signals 214  
(H19) of  $\beta$ - (6.50) and  $\alpha$ - (6.42) aquo-isomers of **4** are observed.

**Figure 11.** RP-HPLC trace showing the  $\alpha$ - and  $\beta$ -isomer products of **5** at 7.4 and 7.9 215  
min.

**Figure 12.** ESI-MS of **5**, expected  $m/z = 1129$ , observed  $m/z = [M^+-H_2O]^{+1}: 1111$ ,  $[M^+-$  216  
 $H_2O+H^+]^{+2}: 556$ .

<b>Figure 13.</b> Electronic absorption spectroscopy of <b>5</b> .	216
<b>Figure 14.</b> $^1\text{H}$ NMR of <b>5</b> (400 MHz, 298K, $\text{D}_2\text{O}$ ).	217
<b>Figure 15.</b> $^1\text{H}$ NMR of <b>5</b> (400 MHz, 298K, $\text{D}_2\text{O}$ ) (Aromatic). Characteristic signals (H19) of $\beta$ -(6.49) and $\alpha$ - (6.42) aquo-isomers of <b>5</b> are observed.	218
<b>Figure 16.</b> RP-HPLC trace showing the $\alpha$ - and $\beta$ -isomer products of <b>6</b> at 10.4 and 11.0 min.	219
<b>Figure 17.</b> ESI-MS of <b>6</b> , expected $m/z = 1143$ , observed $m/z = [\text{M}^+ - \text{H}_2\text{O}]^{+1}$ : 1124, $[\text{M}^+ - \text{H}_2\text{O} + \text{H}^+]^{+2}$ : 563.	220
<b>Figure 18.</b> Electronic absorption spectra of <b>6</b> .	220
<b>Figure 19.</b> $^1\text{H}$ NMR of <b>6</b> (400 MHz, 298K, $\text{D}_2\text{O}$ ).	221
<b>Figure 20.</b> $^1\text{H}$ NMR of <b>6</b> (400 MHz, 298K, $\text{D}_2\text{O}$ ) (Aromatic). Characteristic signals (H19) of $\beta$ - (6.50) and $\alpha$ - (6.43) aquo-isomers of <b>6</b> are observed.	222
<b>Figure 21.</b> RP-HPLC trace showing the $\alpha$ - and $\beta$ -isomer products of <b>7</b> 11.3 and 11.8 min.	223
<b>Figure 22.</b> ESI-MS of <b>7</b> , expected $m/z = 1157$ , observed $m/z = [\text{M}^+ - \text{H}_2\text{O}]^{+1}$ : 1139, $[\text{M}^+ - \text{H}_2\text{O} + \text{H}^+]^{+2}$ : 570.	224
<b>Figure 23.</b> Electronic absorption spectra of <b>7</b> .	224
<b>Figure 24.</b> $^1\text{H}$ NMR of <b>7</b> (400 MHz, 298K, $\text{D}_2\text{O}$ ).	225
<b>Figure 25.</b> $^1\text{H}$ NMR of <b>7</b> (400 MHz, 298K, $\text{D}_2\text{O}$ ) (Aromatic). Characteristic signals (H19) of $\beta$ - (6.49) and $\alpha$ - (6.42) aquo-isomers of <b>7</b> are observed.	226
<b>Figure 26.</b> RP-HPLC trace showing the $\alpha$ - and $\beta$ -isomer products of <b>8</b> at 18.4 and 19.3 min.	227

<b>Figure 27.</b> ESI-MS of <b>8</b> , expected $m/z = 1204$ , observed $m/z = [M^+-H_2O]^{+1}$ : 1185, $[M^+-H_2O+H^+]^{+2}$ : 593.	228
<b>Figure 28.</b> Electronic absorption spectra of <b>8</b> .	228
<b>Figure 29.</b> $^1H$ NMR of <b>8</b> (400 MHz, 298K, $D_2O$ ).	229
<b>Figure 30.</b> $^1H$ NMR of <b>8</b> (400 MHz, 298K, $D_2O$ ) (Aromatic). Characteristic signals (H19) of $\beta$ - (6.50) and $\alpha$ - (6.43) aquo-isomers of <b>8</b> are observed.	230
<b>Figure 31.</b> RP-HPLC trace showing the $\alpha$ - and $\beta$ -isomer products of <b>9</b> at 20.0 and 21.8 min.	231
<b>Figure 32.</b> ESI-MS of <b>9</b> , expected $m/z = 1292$ , observed $m/z = [M^+-H_2O]^{+1}$ : 1273, $[M^+-H_2O+H^+]^{+2}$ : 637.	232
<b>Figure 33.</b> Electronic absorption spectra of <b>9</b> .	232
<b>Figure 34.</b> $^1H$ NMR of <b>9</b> (400 MHz, 298K, $D_2O$ ).	233
<b>Figure 35.</b> $^1H$ NMR of <b>9</b> (400 MHz, 298K, $D_2O$ ) (Aromatic). Characteristic signals (H19) of $\beta$ - (6.50) and $\alpha$ - (6.43) aquo-isomers of <b>9</b> are observed.	234
<b>Figure 36.</b> RP-HPLC trace showing the $\alpha$ - and $\beta$ - isomer products of <b>10</b> at 12.4 and 12.8 min.	235
<b>Figure 37.</b> ESI-MS of <b>10</b> , expected $m/z = 1191$ , observed $m/z = [M^+-H_2O]^{+1}$ : 1173.	236
<b>Figure 38.</b> Electronic absorption spectra of <b>10</b> .	236
<b>Figure 39.</b> $^1H$ NMR of <b>10</b> (400 MHz, 298K, $D_2O$ ).	237
<b>Figure 40.</b> $^1H$ NMR of <b>10</b> (400 MHz, 298K, $D_2O$ ) (Aromatic). Characteristic Signals (H19) of and $\beta$ - (6.49) and $\alpha$ - (6.43) aquo-isomers of <b>10</b> are observed. Additional	238

peak groupings between 7.56-7.51 and 7.35-7.28 are indicative of the phenyl ring linker.

**Figure 41.** RP-HPLC trace showing the  $\alpha$ - and  $\beta$ - isomer products of **11** at 12.6 and 13.0 min. 239

**Figure 42.** ESI-MS of **11**, expected  $m/z = 1191$ , observed  $m/z = [M^+ - H_2O]^{+1}$ : 1172,  $[M^+ - H_2O + H^+]^{+2}$ : 587. 240

**Figure 43.** Electronic absorption spectra of **11**. 240

**Figure 44.**  $^1H$  NMR of **11**. (400 MHz, 298K,  $D_2O$ ). 241

**Figure 45.**  $^1H$  NMR of **11**. (400 MHz, 298K,  $D_2O$ ) (Aromatic). Characteristic signals (H19) of  $\beta$ - (6.49) and  $\alpha$ - (6.42) aquo-isomers of **11** are observed. Additional peak groupings between 7.48-7.37 are indicative of the phenyl ring linker. 242

**Figure 46.** RP-HPLC trace showing product **12** at 11.7 min. 243

**Figure 47.** ESI-MS of **12**, expected  $m/z = 5327$ , observed  $m/z = [M^+ - H_2O + 2H^+]^{+3}$ : 1771,  $[M^+ - H_2O + 3H^+]^{+4}$ : 1328. 243

**Figure 48.** *In vitro* dose escalation study of **12** showing increase in cAMP levels in GLP-1R stably transfected HEK-293-H188 c20 cells. 244

**Figure 49.** RP-HPLC trace showing product **13** at 12.0 min. 245

**Figure 50.** ESI-MS of **13**, expected  $m/z = 5341$ , observed  $m/z = [M^+ - H_2O + 2H^+]^{+3}$ : 1775,  $[M^+ - H_2O + 3H^+ + CH_3OH]^{+4}$ : 1364,  $[M^+ - H_2O + 3H^+]^{+4}$ : 1332. 245

**Figure 51.** *In vitro* dose escalation study of **13** showing increase in cAMP levels in GLP-1R stably transfected HEK-293-H188 c20 cells. 246

**Figure 52.** RP-HPLC trace showing product **14** at 12.0 min. 247

<b>Figure 53.</b> ESI-MS of <b>14</b> , expected $m/z = 5355$ , observed $m/z = [M^+-H_2O+2H^+]^{+3}$ : 1780, [ $M^+-H_2O+3H^+$ ] $^{+4}$ : 1335.	247
<b>Figure 54.</b> <i>In vitro</i> dose escalation study of <b>14</b> showing increase in cAMP levels in GLP-1R stably transfected HEK-293-H188 c20 cells.	248
<b>Figure 55.</b> RP-HPLC trace showing product <b>15</b> at 12.0 min.	249
<b>Figure 56.</b> ESI-MS of <b>15</b> , expected $m/z = 5369$ , observed $m/z = [M^+-H_2O+2H^+]^{+3}$ : 1784, [ $M^+-H_2O+3H^+$ ] $^{+4}$ : 1339.	249
<b>Figure 57.</b> <i>In vitro</i> dose escalation study of <b>15</b> showing increase in cAMP levels in GLP-1R stably transfected HEK-293-H188 c20 cells.	250
<b>Figure 58.</b> RP-HPLC trace showing product <b>16</b> at 11.7 min.	251
<b>Figure 59.</b> ESI-MS of <b>16</b> , expected $m/z = 5416$ , observed $m/z = [M^+-H_2O+2H^+]^{+3}$ : 1800, [ $M^+-H_2O+3H^+$ ] $^{+4}$ : 1350.	251
<b>Figure 60.</b> <i>In vitro</i> dose escalation study of <b>16</b> showing increase in cAMP levels in GLP- 1R stably transfected HEK-293-H188 c20 cells.	252
<b>Figure 61.</b> RP-HPLC trace showing product <b>17</b> at 12.3 min.	253
<b>Figure 62.</b> ESI-MS of <b>17</b> , expected $m/z = 5504$ , observed $m/z = [M^+-$ $H_2O+2H^++CH_3CN]^{+3}$ : 1870, [ $M^+-H_2O+3H^++CH_3OH]^{+4}$ : 1404, [ $M^+-H_2O+4H^+$ ] $^{+5}$ : 1098.	253
<b>Figure 63.</b> <i>In vitro</i> dose escalation study of <b>17</b> showing increase in cAMP levels in GLP- 1R stably transfected HEK-293-H188 c20 cells.	254
<b>Figure 64.</b> RP-HPLC trace showing product <b>18</b> at 12.2 min.	255
<b>Figure 65.</b> ESI-MS of <b>18</b> , expected $m/z = 5403$ , observed $m/z = [M^+-H_2O+2H^+]^{+3}$ : 1796, [ $M^+-H_2O+CH_3OH+3H^+$ ] $^{+4}$ : 1379, [ $M^+-H_2O+3H^+$ ] $^{+4}$ : 1347.	255

<b>Figure 66.</b> <i>In vitro</i> dose escalation study of <b>18</b> showing increase in cAMP levels in GLP-1R stably transfected HEK-293-H188 c20 cells.	256
<b>Figure 67.</b> RP-HPLC trace showing product <b>19</b> at 12.6 min.	257
<b>Figure 68.</b> ESI-MS of <b>19</b> , expected $m/z = 5403$ , observed $m/z = [M^+-H_2O+2H^+]^{+3}: 1796$ , $[M^+-H_2O+CH_3OH+3H^+]^{+4}: 1379$ , $[M^+-H_2O+3H^+]^{+4}: 1347$ .	257
<b>Figure 69.</b> <i>In vitro</i> dose escalation study of <b>19</b> showing increase in cAMP levels in GLP-1R stably transfected HEK-293-H188 c20 cells.	258
<b>Figure 70.</b> RP-HPLC trace showing product <b>20</b> at 11.8 min.	259
<b>Figure 71.</b> ESI-MS of <b>20</b> , expected $m/z = 5456$ , observed $m/z = [M^+-H_2O+2H^+]^{+3}: 1813$ , $[M^+-H_2O+3H^+]^{+4}: 1360$ , $[M^+-H_2O+4H^+]^{+5}: 1088$ , $[M^+-H_2O+5H^+]^{+6}: 907$ , $[M^+-H_2O+6H^+]^{+7}: 777$ .	259
<b>Figure 72.</b> <i>In vitro</i> dose escalation study of <b>20</b> showing increase in cAMP levels in GLP-1R stably transfected HEK-293-H188 c20 cells.	260
<b>Figure 73.</b> RP-HPLC trace showing product <b>21</b> at 11.8 min.	261
<b>Figure 74.</b> ESI-MS of <b>21</b> , expected $m/z = 5469$ , observed $m/z = [M^+-H_2O+2H^++CH_3CN]^{+3}: 1859$ , $[M^+-H_2O+2H^+]^{+3}: 1819$ , $[M^+-H_2O+3H^++CH_3OH]^{+4}: 1395$ , $[M^+-H_2O+3H^+]^{+4}: 1364$ $[M^+-H_2O+4H^+]^{+5}: 1091$ .	261
<b>Figure 75.</b> <i>In vitro</i> dose escalation study of <b>21</b> showing increase in cAMP levels in GLP-1R stably transfected HEK-293-H188 c20 cells.	262
<b>Figure 76.</b> RP-HPLC trace showing product <b>22</b> at 11.8 min.	263
<b>Figure 77.</b> ESI-MS of <b>22</b> , expected $m/z = 5483$ , observed $m/z = [M^+-H_2O+2H^+]^{+3}: 1822$ , $[M^+-H_2O+3H^+]^{+4}: 1367$ , $[M^+-H_2O+5H^+]^{+6}: 912$ , $[M^+-H_2O+6H^+]^{+7}: 781$ .	263



<b>Figure 78.</b> <i>In vitro</i> dose escalation study of <b>22</b> showing increase in cAMP levels in GLP-1R stably transfected HEK-293-H188 c20 cells.	264
<b>Figure 79.</b> RP-HPLC trace showing product <b>23</b> at 11.8 min.	265
<b>Figure 80.</b> ESI-MS of <b>23</b> , expected $m/z = 5497$ , observed $m/z = [M^+-H_2O+2H^+]^{+3}$ : 1827, $[M^+-H_2O+3H^+]^{+4}$ : 1371, $[M^+-H_2O+5H^+]^{+6}$ : 914, $[M^+-H_2O+6H^+]^{+7}$ : 784, $[M^+-H_2O+7H^+]^{+8}$ : 685.	265
<b>Figure 81.</b> <i>In vitro</i> dose escalation study of <b>23</b> showing increase in cAMP levels in GLP-1R stably transfected HEK-293-H188 c20 cells.	266
<b>Figure 82.</b> RP-HPLC trace showing product <b>24</b> at 11.6 min.	267
<b>Figure 83.</b> ESI-MS of <b>24</b> , expected $m/z = 5544$ , observed $m/z = [M^+-H_2O+2H^++CH_3CN]^{+3}$ : 1884, $[M^+-H_2O+3H^++CH_3OH]^{+4}$ : 1414, $[M^+-H_2O+3H^+]^{+4}$ : 1382.	267
<b>Figure 84.</b> <i>In vitro</i> dose escalation study of <b>24</b> showing increase in cAMP levels in GLP-1R stably transfected HEK-293-H188 c20 cells.	268
<b>Figure 85.</b> RP-HPLC trace showing product <b>25</b> at 12.0 min.	269
<b>Figure 86.</b> ESI-MS of <b>25</b> , expected $m/z = 5632$ , observed $m/z = [M^+-H_2O+2H^++CH_3CN]^{+3}$ : 1914, $[M^+-H_2O+3H^++CH_3OH]^{+4}$ : 1436.	269
<b>Figure 87.</b> <i>In vitro</i> dose escalation study of <b>25</b> showing increase in cAMP levels in GLP-1R stably transfected HEK-293-H188 c20 cells.	270
<b>Figure 88.</b> RP-HPLC trace showing product <b>26</b> at 11.9 min.	271
<b>Figure 89.</b> ESI-MS of <b>26</b> , expected $m/z = 5531$ , observed $m/z = [M^+-H_2O+CH_3OH+3H^+]^{+4}$ : 1411, $[M^+-H_2O+3H^+]^{+4}$ : 1379, $[M^+-H_2O+4H^+-CN]^{+4}$ : 1353, $[M^+-H_2O+4H^+]^{+5}$ : 1104.	271

<b>Figure 90.</b> <i>In vitro</i> dose escalation study of <b>26</b> showing increase in cAMP levels in GLP-1R stably transfected HEK-293-H188 c20 cells.	272
<b>Figure 91.</b> RP-HPLC trace showing product <b>27</b> at 11.9 min.	273
<b>Figure 92.</b> ESI-MS of <b>27</b> , expected $m/z = 5531$ , observed $m/z = [M^+ - H_2O + CH_3CN + 2H^+]^{+3}$ : 1880, $[M^+ - H_2O + 2H^+]^{+3}$ : 1838, $[M^+ - H_2O + CH_3OH + 3H^+]^{+4}$ : 1410, $[M^+ - H_2O + 3H^+]^{+4}$ : 1379, $[M^+ - H_2O + 4H^+]^{+5}$ : 1103.	273
<b>Figure 93.</b> <i>In vitro</i> dose escalation study of <b>27</b> showing increase in cAMP levels in GLP-1R stably transfected HEK-293-H188 c20 cells.	274
<b>Chapter 7. Ongoing and Future Work</b>	
<b>Figure 1.</b> Synthetic scheme for B12-DBCO. B12 was functionalized with a DBCO linker through CDT activation of the 5'-alcohol of the f-sidechain.	290
<b>Figure 2.</b> RP-HPLC Trace (Shimadzu Prominence HPLC using a C18 column (Eclipse XDB-C18 5 $\mu$ m, 4.6 x 150 mm) (RP-HPLC, from 1% CH <sub>3</sub> OH/H <sub>2</sub> O + 0.1% TFA to 90% CH <sub>3</sub> OH/H <sub>2</sub> O + 0.1% TFA in 25 min)) showing B12-DBCO linker product at 10.5 min. Purity 92%.	290
<b>Figure 3.</b> ESI-MS (Shimadzu LCMS-8040) of B12-DBCO, expected $m/z = 1808$ , observed $m/z = [M + 2H]^{2+}$ : 905.	291
<b>Figure 4.</b> Synthetic scheme for B12-Oxy. B12-DBCO was successfully "clicked" to OTaz utilizing SPAAC.	292
<b>Figure 5.</b> RP-HPLC Trace (Shimadzu Prominence HPLC using a C18 column (Eclipse XDB-C18 5 $\mu$ m, 4.6 x 150 mm) (RP-HPLC, from 1% CH <sub>3</sub> OH/H <sub>2</sub> O + 0.1% TFA to 90%	292

CH<sub>3</sub>OH/H<sub>2</sub>O + 0.1% TFA in 25 min)) showing B12-Oxy product at 11.2 min. Purity 99%.

**Figure 6.** ESI-MS (Shimadzu LCMS-8040) of B12-Oxy, expected m/z = 2856, observed m/z = [M+2H<sup>+</sup>]<sup>+2</sup>: 1429, [M+3H<sup>+</sup>]<sup>+3</sup>: 953. 293

**Figure 7.** Peripherally administered, IP, oxytocin reduces food intake in male and female rats. 293

**Figure 8.** CNS penetrance is not required for the hypophagic effect of oxy. All rats receiving B12-Oxy reduced food intake compared to their intake on vehicle (saline). Equimolar dose of oxy also reduced food intake, with preliminary indication of a more potent and longer-lasting feeding behavior impact of B12-OT. 294

## Chapter 1: Introduction

### 1.1 Glucose Homeostasis

Carbohydrates are one of the four major classes of biological macromolecules and performs various functions including energy supply, energy storage, and structural support in humans, animals, and plants.<sup>1</sup> One of the simplest, most common, and critically important sugars is glucose. This six-carbon monosaccharide is the most preferred source of energy in mammalian cells.<sup>2</sup> The high demand for glucose by most tissues and organs, including the brain, requires a constant available supply. Despite the high requirements for glucose, its concentration must be finely regulated within a narrow window.<sup>3,4</sup> In humans, an accepted value of fasting blood glucose (BG) levels ranges between 70 mg/dL and 100 mg/dL.<sup>5</sup> Deviations from this concentration can have profound effects ranging from disease to death. In cases of high BG levels (hyperglycemia; defined BG levels >125 mg/dL when fasting or greater than 200mg/dL two hours following a meal), individuals may suffer from blindness, renal failure, or vascular disease. Individuals with low BG levels (hypoglycemia; defined as BG levels  $\leq$ 70 mg/dL), could lose consciousness, experience seizures, or death.<sup>5</sup>

Glucose homeostasis is controlled through the hormones glucagon and insulin produced by the  $\alpha$ - and  $\beta$ -cells of the pancreatic islets of Langerhans.<sup>3,4,6-8</sup> Following energy consumption glucose levels increase resulting in increased secretion of insulin. Secretion of insulin results in a decrease in blood glucose concentrations by promoting cellular uptake of glucose while also stimulating glycogen formation (Figure 1).<sup>9-12</sup> In fasted states, blood glucose concentration decreases promoting the release of glucagon. The secretion of glucagon promotes the breakdown of glycogen and increases glucose release from the liver (Figure 1).<sup>6,10-12</sup>

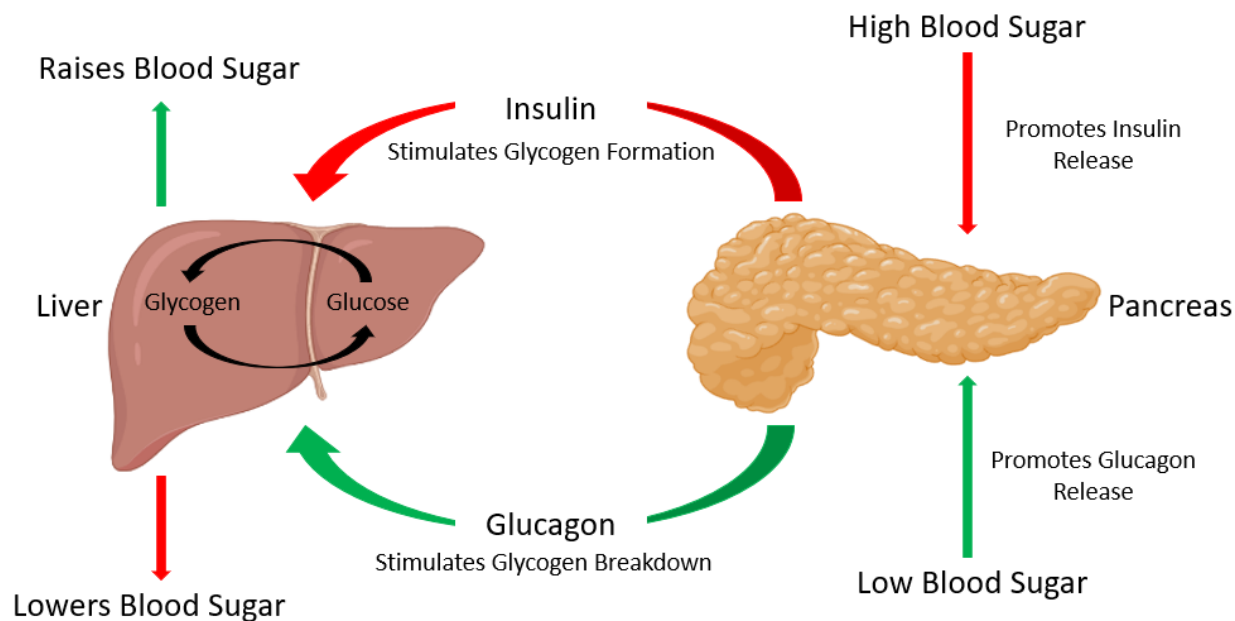


**Figure 1.** Glucose homeostasis is controlled through the hormones, glucagon and insulin.

### 1.1.1 Type I and II Diabetes mellitus Effect on Glucoregulation

One of the largest global public health concerns and leading causes of mortality and reduced life expectancy is diabetes mellitus (DM).<sup>13-16</sup> Diabetes, meaning “siphon” and mellitus meaning “honey”, was first described by the ancient Greek physician Aretaeus, due to the sweet taste of urine from affected individuals.<sup>17</sup> Characterized by chronic hyperglycemia, DM is a metabolic disease resulting in diminished glucoregulation due to defects in insulin secretion, insulin action, or both.<sup>17,18</sup> There are two predominant forms of the disease, type 1 (T1DM) and type 2 (T2DM), but additional forms exist.<sup>18</sup> Typically identified before the age of 30, T1DM is an autoimmune disease defined by the destruction of the  $\beta$ -islets of the pancreas and comprises approximately 5-10% of all diabetic cases but is the most prevalent form (80-90%) in children and adolescents.<sup>18</sup> The absence of  $\beta$ -islets results in an inability to produce insulin with concomitant

elevated blood glucose concentrations. Treatment for T1DM necessitates the use of insulin injections.<sup>18</sup>

T2DM is the most prevalent form of the disease making up 90-95% of all cases across the entire population. T2DM is defined by insulin *resistance*. Individuals suffering from T2DM are capable of producing insulin, but the body is incapable of utilizing it to perform its proper function.<sup>18</sup> The increased demand for insulin due to diminished function can result in damage to the pancreatic  $\beta$ -islets resulting in similar outcomes as observed in individuals with T1DM.<sup>18</sup>

#### **1.1.1.1 Impact of T2DM and Comorbid Obesity**

There is currently a major increase in co-morbid obesity and T2DM.<sup>14-16</sup> Worldwide, there are 1.9 billion people who are overweight of which 600 million are obese. In addition, 387 million people have been diagnosed with diabetes, 95% of which are T2DM.<sup>14,19-21</sup> In 2017, the World Health Organization (WHO) estimated there were 476 million cases of T2DM and project cases to reach 571 million by 2025.<sup>13</sup> Similar estimates and values have been proposed by the International Diabetes Federation (IDF). The IDF estimates 451 million current cases and increasing to 693 million cases by 2045.<sup>13</sup> The estimations of current cases can be difficult as many cases go undiagnosed. Individuals suffering from diabetes are at higher risk for mortality as it is currently a top-10 cause of death.<sup>13</sup> These co-morbidities are costly, and their dramatic rise in prevalence has caused a substantial increase in health cost.<sup>14,19-21</sup> In 2007, the direct medical cost of diabetes was estimated at \$116 billion, but that value has dramatically risen to \$237 billion in 2017.<sup>22,23</sup> These values account for 1 in every 4 health care dollars spent in the United States.<sup>22,23</sup> The financial burden of treating/managing diabetes is largely due to the lifelong need for pharmaceutical intervention.<sup>24,25</sup>

#### 1.1.1.1.1 Treatment of T2DM

Given individuals suffering from T2DM can produce insulin their treatment does not require insulin injections, as observed in individuals suffering from T1DM. The first attempts to maintain a blood sugar levels should be through a change in diet and implementation of an exercise program.<sup>18,26</sup> If an individual is unable to maintain glucose levels via exercise and diet, a clinician may prescribe one of various medications. One of the most widely and generally first prescribed drugs for the treatment of T2DM is metformin.<sup>26-29</sup> The primary function of metformin is to increase an individual's sensitivity to insulin and thus allowing the insulin produced to be used more efficiently.<sup>27,28</sup> In addition to influencing insulin function, metformin also lowers glucose production in the liver. The use of metformin as a therapeutic is limited by the fact that it is only effective for a few years, Kahn *et al.* identified that metformin fails in 21% of prescribed patients within five years,<sup>30</sup> and is coupled with side effects including nausea, abdominal pain, and diarrhea.<sup>26-29</sup> As the efficacy of metformin declines sulfonylureas are often added to the treatment regimen.<sup>26,29,31-33</sup> Sulfonylureas act directly by stimulating insulin secretion. While potent and effective in stimulating insulin secretion, the use of this pharmacotherapy can facilitate hypoglycemia.<sup>31-33</sup> An alternative to sulfonylureas is the use of glinides.<sup>26,29</sup> Much like sulfonylureas, glinides stimulate the pancreas to secrete more insulin. While faster acting than sulfonylureas, glinides function is much shorter. Side effects caused using glinides include hypoglycemia and weight gain.<sup>26,29</sup> Additional therapeutic options that do not aim to increase insulin secretion including thiazolidinediones and dipeptidyl peptidase IV (DPP-IV) inhibitors.<sup>26,29</sup> Thiazolidinediones, like metformin, increase body tissues sensitivity to insulin.<sup>34-36</sup> DPP-IV inhibitors prevent the degradation of endogenous peptide hormones capable of increasing

insulin levels (*e.g.* glucagon-like peptide-one (GLP-1)).<sup>37,38</sup> Metformin, sulfonylureas, glinides, thiazolidinediones, and DPP-IV inhibitors are all oral medications and are considered first and second line therapeutics. Third- and fourth-line medications are injectable medications, many of which target the GLP-1 receptor (GLP-1R), *e.g.* Exenatide.<sup>39-43</sup> Table 1 provides a list of current approved therapeutics for the treatment of glucoregulation. These medications regulate gastric emptying and food intake while increasing insulin secretion and decreasing glucagon secretion.<sup>26,29</sup> A final treatment option, if none of the previously described options are effective, is direct use of insulin itself. Administration of insulin injections must be precisely monitored as too frequent injections may lead to excessive drop in blood sugar.<sup>44</sup>



**Table 1.** Properties of Some Glucose-Lowering Agents Used in the Treatment of Type 2 Diabetes Mellitus.<sup>26,29</sup>

<b>Class</b>	<b>Compounds</b>	<b>Route of Administration</b>	<b>Physiological Function</b>	<b>Cost</b>	<b>Advantages</b>	<b>Disadvantages</b>
Biguanides	<ul style="list-style-type: none"> <li>• Metformin</li> </ul>	Oral	<ul style="list-style-type: none"> <li>• Increase insulin sensitivity</li> <li>• Decrease glucose production</li> </ul>	Low	<ul style="list-style-type: none"> <li>• Experience</li> <li>• No weight gain</li> </ul>	<ul style="list-style-type: none"> <li>• GIT side effects</li> <li>• Vitamin B12 deficiency</li> </ul>
Sulfonylureas	<ul style="list-style-type: none"> <li>• Glyburide</li> <li>• Glipizide</li> <li>• Glimepiride</li> </ul>	Oral	<ul style="list-style-type: none"> <li>• Increase insulin secretion</li> </ul>	Low	<ul style="list-style-type: none"> <li>• Experience</li> <li>• No weight gain</li> </ul>	<ul style="list-style-type: none"> <li>• Hypoglycemia</li> <li>• Weight gain</li> </ul>
Glinides	<ul style="list-style-type: none"> <li>• Repaglinide</li> <li>• Nateglinide</li> </ul>	Oral	<ul style="list-style-type: none"> <li>• Increase insulin secretion</li> </ul>	High	<ul style="list-style-type: none"> <li>• Dosing flexibility</li> </ul>	<ul style="list-style-type: none"> <li>• Hypoglycemia</li> <li>• Weight gain</li> </ul>
Thiazolidinediones	<ul style="list-style-type: none"> <li>• Pioglitazone</li> </ul>	Oral	<ul style="list-style-type: none"> <li>• Increase insulin sensitivity</li> </ul>	Low	<ul style="list-style-type: none"> <li>• No hypoglycemia</li> <li>• Durability</li> </ul>	<ul style="list-style-type: none"> <li>• Weight gain</li> <li>• Bone fractures</li> </ul>
DPP-IV Inhibitors	<ul style="list-style-type: none"> <li>• Sitagliptin</li> <li>• Saxagliptin</li> <li>• Linagliptin</li> </ul>	Oral	<ul style="list-style-type: none"> <li>• Inhibits DPP-IV activity</li> </ul>	High	<ul style="list-style-type: none"> <li>• Well tolerated</li> </ul>	<ul style="list-style-type: none"> <li>• Pancreatitis</li> </ul>
GLP-1R Agonists	<ul style="list-style-type: none"> <li>• Exenatide</li> <li>• Liraglutide</li> <li>• Semaglutide</li> </ul>	Injection and Oral	<ul style="list-style-type: none"> <li>• Increase insulin secretion</li> <li>• Satiety</li> </ul>	High	<ul style="list-style-type: none"> <li>• No hypoglycemia</li> <li>• Weight reduction</li> </ul>	<ul style="list-style-type: none"> <li>• GIT side effects</li> <li>• Patient compliance</li> </ul>

#### **1.1.1.1.2 Glucagon-like peptide-one (GLP-1) and its Receptor (GLP-1R)**

Produced by the  $\alpha$ -cells of the pancreas and the intestinal L-cells, proglucagon is a protein and precursor to glicentin, glicentin-related pancreatic polypeptide, glucagon, oxyntomodulin, major proglucagon fragment, glucagon-like peptide-1 (GLP-1) and -2 (GLP-2).<sup>45</sup> Each of these smaller proglucagon fragments play roles in metabolic functions including food intake and satiety, fluid homeostasis, thermogenesis, and gastrointestinal motility.<sup>45</sup> Three forms of GLP-1 may be processed from proglucagon including a single full form, GLP-1 (1-37), and two truncated forms: amidated GLP-1 (7-36amide) and glycine extended GLP-1 (7-37).<sup>45</sup> The primary function of GLP-1 is to control insulin levels in response to a rise in blood glucose concentrations, typically post prandially. Nearly all GLP-1 found in humans is in one of the truncated forms, 80% of which is 7-36amide and 20% 7-37. While both the truncated forms are equally potent in stimulating insulin secretion the full form has a much lower effect.<sup>45</sup> The ability for GLP-1 stimulate insulin secretion is dependent on its intact form. DPP-IV quickly degrades GLP-1 ( $t_{1/2}$  = 1-2 min) resulting in the production of GLP-1 (9-36amide) or GLP-1 (9-37), which are rapidly cleared by the kidneys.<sup>37,45</sup> Fasting levels of GLP-1 in humans are found to be 5-10 pM and increase upon addition of glucose.<sup>46</sup> GLP-1 function is dependent upon binding and activation of its receptor GLP-1R.

##### **1.1.1.1.2.1 Exendin-4 (Ex4)**

The glucagon superfamily consists of various biologically active peptides, many of which contain a characteristic n-terminal histidine residue and a phenylalanine residue in their sixth position.<sup>47</sup> Investigations in *Heloderma* lizards, specifically *Heloderma horridum* and *Heloderma suspectum*, have identified numerous peptides all fitting this characteristic and capable of acting

at the GLP-1R.<sup>48</sup> The venom of these lizards was shown to have a secretory effect on pancreatic acini of guinea pigs.<sup>49,50</sup> Initial investigations in to these lizards found two biologically active peptides: helospectin (exendin-1 (Ex1))<sup>51</sup> and helodermin (exendin-2(Ex2)).<sup>52</sup> Further investigations into *Heloderma horridum* by Eng *et al.* identified a third Exendin, Exendin-3 (Ex3).<sup>47</sup> A fourth exendin, exendin-4 (Ex4) (Figure 2), was found exclusively in the saliva of *Heloderma suspectum*.<sup>53</sup> While structurally similar to Ex3, Ex4 contains amino acid substitutions at the second (S2G) and third (D3E) residues.<sup>53</sup> Ex4 and GLP-1 only share 53% sequence similarity, but Ex4 is able to fully agonize the GLP-1R (EC<sub>50</sub> 33 pM) resulting in dose-dependent glucose-induced insulin secretion.<sup>54</sup> Structural differences observed in Ex4 include various amino acid substitutions and a c-terminal extension to the sequence. One key amino acid substitution is observed in the second position (A2G) resulting in resistance to DPP-IV leading to a half-life of 2.4 hours. The protection from DPP-IV provided by this substitution does not translate to other proteases and as such must be administered subcutaneously.<sup>54</sup> A synthetic variant of Ex4, Byetta (Exenatide), was approved by the FDA for the treatment of T2DM in 2005.<sup>54</sup>

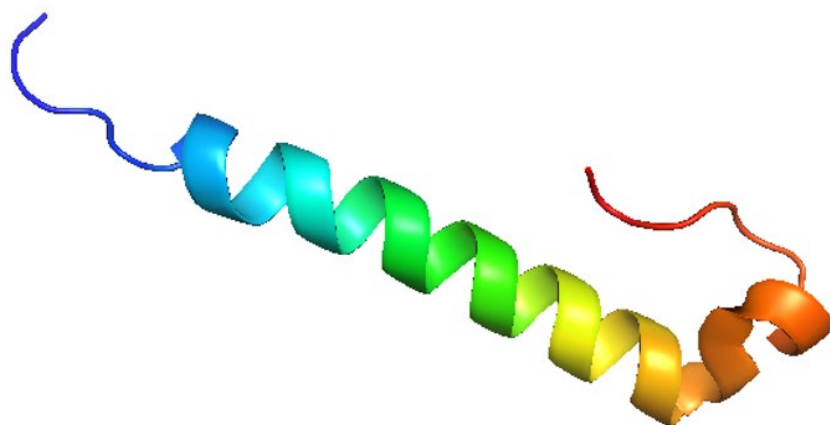


**Figure 2.** Structure of Ex4. PDB code 1JRJ.<sup>55</sup> Image generated by the author using PyMol.

### **1.1.2 Distribution and Activation of the GLP-1R**

The actions of GLP-1 are mediated through its receptor GLP-1R. The GLP-1R is a class B G-protein coupled receptor (GPCR) and a member of the glucagon receptor superfamily.<sup>45</sup> Activation of this receptor occurs via endocrine hormones and stimulates the G<sub>s</sub> pathway resulting in an increase in cyclic adenosine monophosphate (cAMP).<sup>45</sup> The human GLP-1R is distributed in both the central nervous system (CNS) and the peripheral nervous system (PNS).<sup>45,56-61</sup> Within the CNS the receptor may be found in regions of the hindbrain, hypothalamus (HYP), and subfornical organ (SFO); specifically: paraventricular nucleus (PVN), dorsal medial nucleus, arcuate nucleus (ARC), area postrema (AP), and nucleus of the solitary tract (NTS).<sup>61</sup> Activation of the GLP-1R in the CNS is not limited to glucoregulation but is also largely attributed to the anorectic effects observed following administration of a GLP-1R agonist.<sup>62</sup> The GLP-1R is distributed throughout the PNS including: the vagus nerve, pancreatic  $\beta$ -cells, stomach, and adipose tissue.<sup>56-59</sup> Distinct activation of the GLP-1R in the PNS has been shown to maintain glucoregulation without anorectic effects observed when activation populations in the CNS.<sup>46,63-66</sup>

#### **1.1.2.1 Unwarranted Side Effects Associated with GLP-1R Activation in the CNS**

Activation of the GLP-1R population in AP and NTS is the cause of many negative side effects, hypophagia and nausea/malaise, of current GLP-1R agonists as this is the vomiting control center of the CNS.<sup>67-69</sup> The hypophagic effects of all known GLP-1R agonists are accompanied by nausea, vomiting, and malaise. In fact, ~20-50% of T2DM patients prescribed GLP-1R agonists experience nausea and/or vomiting, leading to discontinuation of drug treatment in ~6-10% and

reduced dose tolerance in another ~15%.<sup>70-77</sup> Thus, ~1 in 4 T2DM patients (~7 million US citizens) are not able to fully benefit from current FDA-approved GLP-1-based drugs.

## **1.2 Vitamin B12 (B12)**

Vitamin B12 (B12) is a naturally occurring water soluble organometallic compound that is essential for normal physiological functioning.<sup>78,79</sup> As only bacteria are capable of producing this essential vitamin, humans must obtain it through their diet.<sup>78,80</sup> High concentrations of B12 ( $\mu\text{g}/100\text{ g}$ ) can be consumed via red meats including: liver (26-58), beef and lamb (1-3); other sources are found in assorted dairy foods (0.3-2.4).<sup>79</sup> The average human consumes 5-30  $\mu\text{g}$  of B12<sup>80</sup> despite the recommended daily requirement being 2.4  $\mu\text{g}$ .<sup>78,81,82</sup> B12, unlike other essential vitamins, can be stored for prolonged periods of time in the liver (2-3 mg).<sup>80</sup> While a lack of B12 intake can lead to pernicious anemia as well as other diseases and disorders, identification can take years due to such large storage in the liver. There are no reported effects from an overconsumption or intake of B12.<sup>78,79</sup> The cellular uptake of B12 is highly dependent on the binding and transport of B12 through the gastrointestinal tract (GIT) utilizing a system of proteins and receptors.<sup>80-85</sup>

### **1.2.1 History of B12**

The discovery, isolation, and characterization of the largest and most complex vitamin<sup>86</sup> and “nature’s most beautiful cofactor”<sup>87</sup> took more than 100 years and warranted the receipt of two Nobel Prizes.<sup>88</sup> Published in 1824, The first documented description of pernicious anemia, a B12 deficiency disease, took place in 1824 when James Scarth Combe described the symptoms of a 47 year old patient with previously excellent health whom died within one year.<sup>89</sup> Published under the title “History of a Case of Anemia”, Combe’s description lacked evidence and detail

leading scientists to be unconvinced this was the condition the patient suffered from. Despite evidence for the first description of pernicious anemia Combe is not credited with its original description.<sup>88</sup> In 1855, Thomas Addison describes what is accepted at the first description of pernicious anemia in his work titled "On the Constitutional and Local effects of Disease of the Suprarenal Capsules". In this work, Addison described an idiopathic anemia that occurred in both sexes and resulted in failed appetite and waxy appearance and was ultimately fatal.<sup>90</sup> In a 1872 article entitled "Progressive Pernicious Anemia", Anton Biermer provided a detailed account of 15 cases of fatal anemia in which he later designated pernicious anemia.<sup>90</sup> Identifying the cause of pernicious anemia and the symptoms associated with the disease were investigated for years to come with little progress in identifying the cause of the condition. In 1860, Austin Flint hypothesized that the disease was degenerative to the glandular tubuli of the stomach. Building on this hypothesis, Samuel Fenwick analyzed stomach tissue postmortem from patients suffering from pernicious anemia. In 1877 Fenwick reported the presence of atrophy and glandular lesions in this tissue.<sup>88</sup> Additional postmortem investigations performed by James Russell and coworkers identified degeneration of the spinal cord in patients that suffered from pernicious anemia.<sup>91</sup> After nearly two decades no progress had been made for the clinical treatment of pernicious anemia until work by George Whipple identified that diet could influence blood formation in dogs made anemic by repeated phlebotomy. Whipple also found raw liver and extracts were more effective at stimulating blood cell production than cooked liver.<sup>88</sup> In 1926, Minot and Murphy showed patients suffering from pernicious anemia could be treated utilizing a specific diet. Their diet suggested the consumption of 120-240 gm of cooked calf, beef liver, or lamb kidney and ≥ 120 gm of mutton muscle meat. The diet was completed with high amounts of fruits and

vegetables due to high iron content and limited amounts of fat due to the belief it contained blood destroying properties.<sup>92</sup> Minot and Murphy's study encompassed 45 patients and all showed rapid improvement with the exception of one patient whom discontinued the diet.<sup>92</sup> The investigative work on pernicious anemia by Whipple, Minot, and Murphy awarded them the Nobel Prize in 1934.<sup>88</sup>

In related investigations William Castle was investigating achlorhydria, an absence of hydrochloric acid in gastric juices, a condition nearly always found in patients suffering from pernicious anemia. Castle believed pernicious anemia was caused by malnourishment or a lack of dietary consumption, but was caused by a missing component in dietary uptake leading to a decrease in uptake.<sup>88</sup> Through experimentation Castle was able to identify that the lack of hydrochloric acid did not affect the patient, but that the patients lacked an ability to respond to specific component found in beef muscle. This component was believed to prevent pernicious anemia from occurring. Castle identified this component as "extrinsic factor" and the stomach component responsible for activity "intrinsic factor".<sup>93,94</sup>

The identification of an "extrinsic factor" by Castle led to increased research to identify this factor. The successful isolation of this factor occurred in 1948 simultaneously by a research group led by Folkers of Merck Sharpe and Dohme and a group led by Smith and Parker of Glaxo Laboratories. Both groups were able to successfully isolate small red needle B12 crystals.<sup>95-100</sup> Given the isolation of B12 crystals the composition and structure was able to be determined. Both groups were able to identify that the compound contained cobalt. Utilizing elemental analysis Brink et al. and several other groups were able to identify the composition of B12.<sup>101,102</sup> Once the composition of the compound had been solved, Dorothy Hodgkin utilized X-ray

crystallography to solve its structure.<sup>103,104</sup> Hodgkin's work utilizing X-ray crystallography awarded her the Nobel Prize in 1964.<sup>88</sup> The total synthesis of B12 took more than a decade following the identification of its structure. Woodward and his team of over 100 scientists reported the first total synthesis in 1971.<sup>105</sup>

### 1.2.2 Structure of B12 and Corrinoids

The determination of B12 composition to be  $C_{61-64}H_{86-92}N_{14}O_{13}PCo$  and the presence of cyanide paved the way for determining the structure of B12.<sup>101,102</sup> Initial crystallographic investigations identified the planar groups of the molecule before ultimately determining the final structure.<sup>103</sup> At the core of the vitamin is a macrocyclic, corrin, ring composed of four reduced pyrrole rings coordinated around a cobalt atom ( $Co^{3+}$ ) (Figure 3).<sup>106</sup> While similar to the porphyrin ring, the corrin contains key structural differences to distinguish the two structures. Porphyrins are completely saturated and composed of 20 carbons, whereas corrins, due to the loss of a methylene spacer, have a lower degree of saturation resulting an asymmetric 19 carbon construct (Figure 3).<sup>107</sup> Methylene spacers are found between pyrroles A-B, B-C, and C-D while a direct bond is formed between pyrroles A and D. The corrin ring contains seven amide side chains composed of three acetamides (side chains *a*, *c*, and *g*) and four propionamides (side chains *b*, *d*, *e*, and *f*) (Figure 3).<sup>103,108</sup> Given the electronic configuration of  $Co^{3+}$  ( $d^6$ , low spin) there is a preferred 6-coordinate octahedral geometry.<sup>82</sup> While the corrin occupies the four planar coordination sites, the two additional axial coordination sites, on the  $\alpha$ - and  $\beta$ -faces of the corrin, remain available.<sup>103,106,107</sup> In "base-on" forms, predominant at physiological pH, of B12 the  $\alpha$ -axial ligand is occupied by a 5,6-dimethylbenzamidazole (DMB) base and coordinated to the cobalt through a nitrogen atom. DMB is linked to the corrin ring through the D pyrrole via a ribose ring,



a phosphate, and propanolamine and propionic acid residues (Figure 3).<sup>103</sup> Protonation of the DMB ligand results in a “base-off” variant of B12 with altered properties.<sup>108,109</sup> The ligands of the  $\beta$ -axial position may be occupied by various anions including:  $\text{CN}^-$ ,  $\text{CH}_3^-$ ,  $\text{Ado}^-$ ,  $\text{NO}_2^-$ ,  $\text{SCN}^-$ ,  $\text{SeCN}^-$ ,  $\text{SO}_3^-$ , and thiourea.<sup>83</sup> Despite the extensive library of ligands that may occupy the  $\beta$ -axial site, only two are biologically active: methylcobalamin (MeCbl) and adenosylcobalamin (AdoCbl).<sup>82,110–112</sup> Additional constructs, including B12 biosynthetic precursors, containing the corrin moiety are deemed corrinoids.<sup>106</sup>

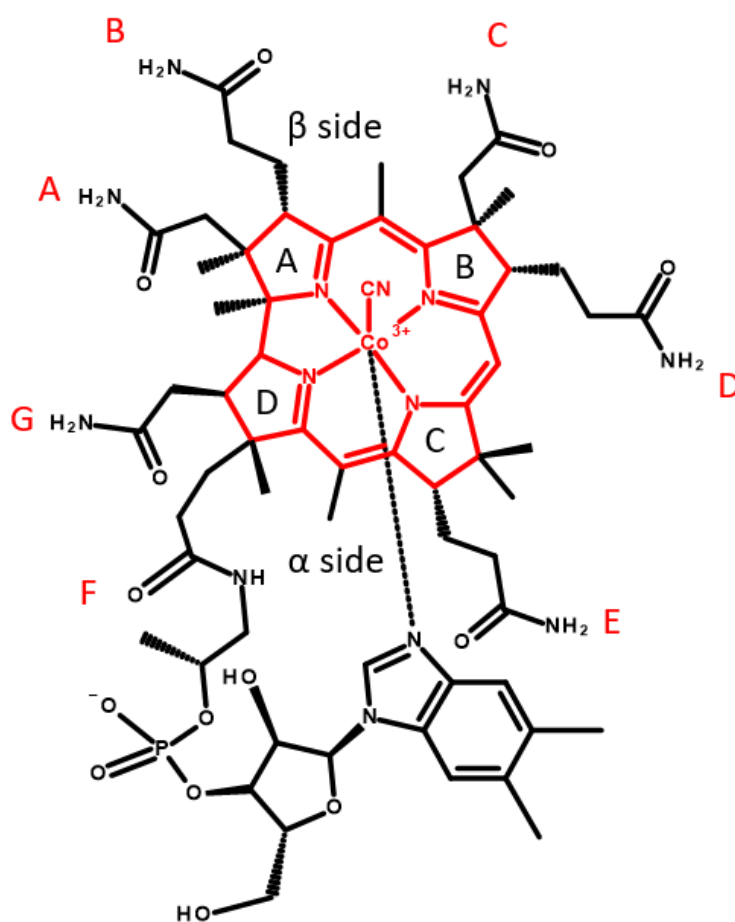


**Figure 3.** Chemical Structure of B12 as cyanocobalamin, with corrin ring highlighted in red.

### 1.2.2.1 Biosynthetic Precursors and Structural Derivatives of B12

The biosynthesis of B12 requires microbial fermentation and is limited to few bacteria and archaea.<sup>113</sup> There are two primary routes of synthesis; an aerobic pathway carried out by bacteria and an anaerobic pathway performed by archaea (Figure 4). A third alternative pathway capable of being utilized by some strains of bacteria and archaea is a salvage pathway (Figure 4).<sup>113</sup> The two primary routes of synthesis are differentiated from one another based upon the timing of insertion of the cobalt ion and the oxygen requirements.<sup>113</sup> The aerobic pathway utilizes precorrin-2 as its precursor while the anaerobic pathway utilized sirohydrochlorin (Figure 4).<sup>113</sup> Both precorrin-2 and sirohydrochlorin are derived from uroporphyrinogen III, a porphyrin precursor derived from  $\delta$ -aminolevulinate (ALA). The synthetic pathways reconverge at coby(II)rinic acid a, c-diamide (Figure 4).<sup>113</sup> In bacteria and archaea capable of utilizing the salvage pathway, exogenous corrinoids are shipped into the cell through an ATP-binding cassette transport system.<sup>113</sup> One such corrinoid utilized in this pathway is cobinamide, the penultimate biosynthetic precursor of B12 (Figure 5). Other potential corrinoids include, but are not limited to, cobyric acid and cobinamide phosphate (Figure 5).<sup>114</sup>

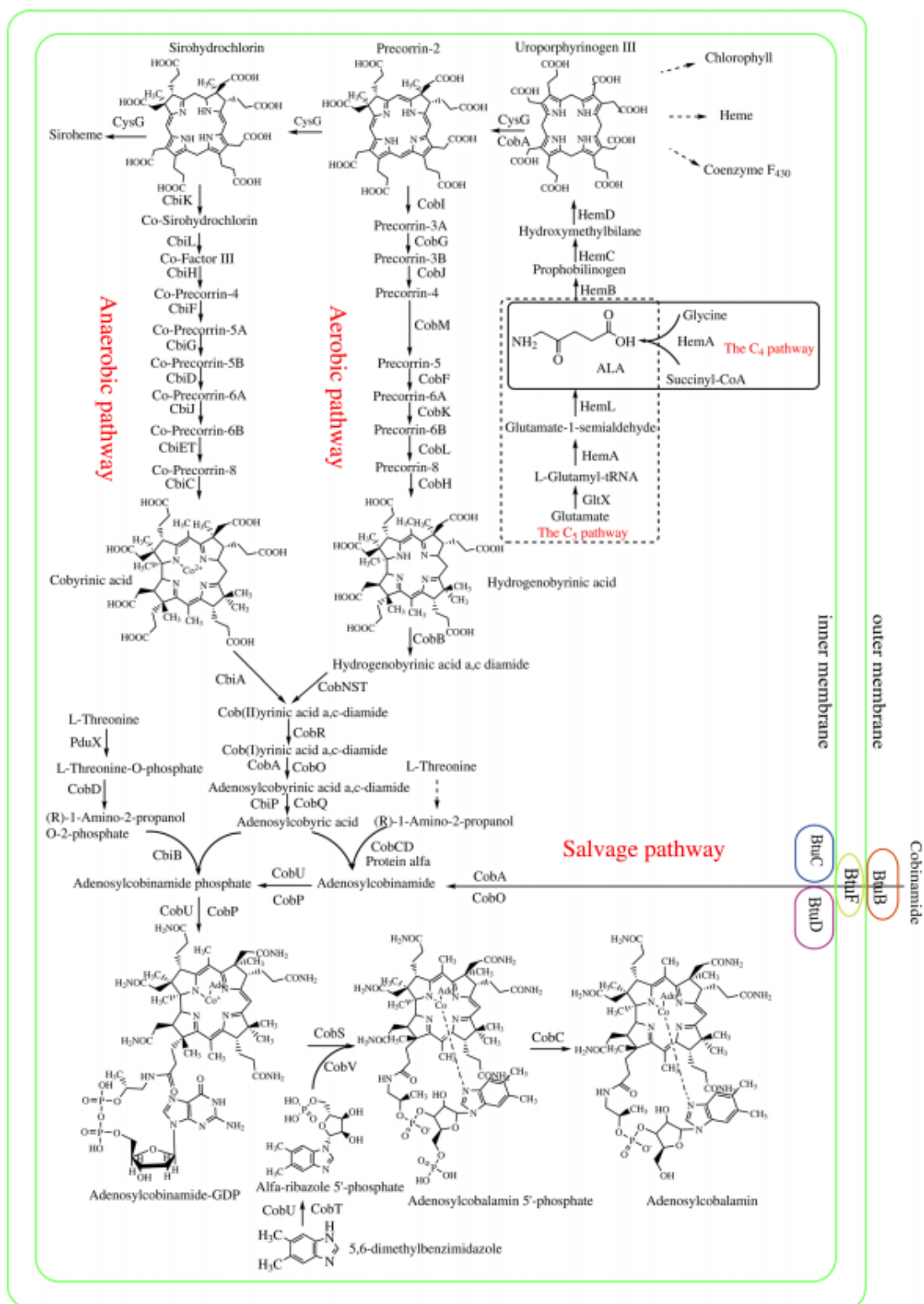


**Figure 4.** Biosynthetic pathways of adenosylcobalamin. Used with permission of publisher under the Creative Commons license (<http://creativecommons.org/licenses/by/4.0/>).<sup>113</sup>

### 1.2.2.1.1 Dicyanocobinamide (Cbi)

Of particular interest for this research program is the B12 precursor dicyanocobinamide (Cbi).<sup>109,115–119</sup> Cbi is a “base-off” precursor and lacks the pseudo-nucleotide moiety observed in B12 (Figure 5).<sup>109,120</sup> Both the  $\alpha$ - and  $\beta$ -axial ligands are occupied by  $\text{CN}^-$  ion in Cbi (Figure 5), but in acidic aqueous environments one or both ions may be replaced by water.<sup>109</sup> If only one of the axial ligands are replaced, isomers may form as substitution could occur at either the  $\alpha$ - or  $\beta$ -axial position.<sup>109</sup> If both are replaced by water the resulting construct is deemed diaquocobinamide.<sup>121</sup> At elevated pH levels the axial ligands may be replaced by hydroxide ions resulting in the formation of dihydroxocobinamide.<sup>122</sup> At neutral pH cobinamide may also form isomers of aquohydroxocobinamide.<sup>122</sup> To date there is limited synthetic cobinamide chemistry in the literature, mostly focusing on the novel cobinamides to treat hydrogen sulfide<sup>123,124</sup> or cyanide poisoning<sup>115,118,125–130</sup>. Cbi is of particular interest in this program since it has no known biological function in humans and has no effect on B12 physiology, is highly water soluble, and its uptake into the CNS would be limited.<sup>116,131</sup> This compound also contains a readily modifiable primary alcohol in its structure allowing for chemical transformation.

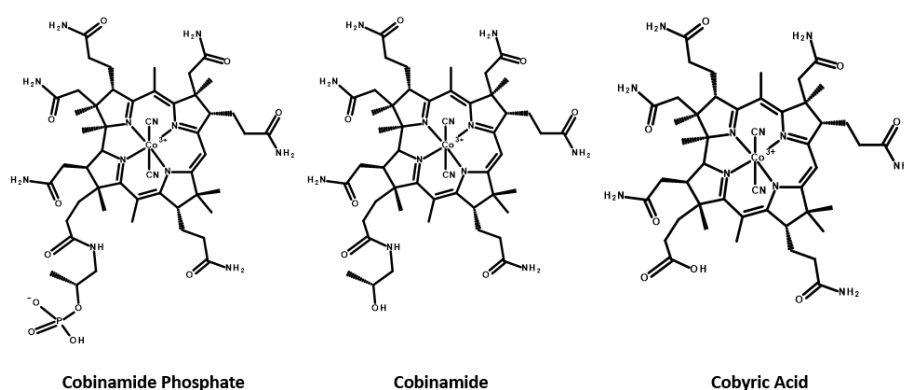


**Figure 5.** Chemical structures of cobinamide phosphate, cobinamide, and cobyric acid. All structures are truncated form of B12.

### 1.2.3 Metabolism of B12

The ability of B12 to act as a coenzyme in the body is highly dependent on the  $\beta$ -face axial ligand and the oxidation state of the central cobalt atom. While only the alkyl cobalamins methyl cobalamin and adenosylcobalamin are biologically functional, both cyanocobalamin and hydroxocobalamin can be readily converted *in vivo* to the biological active forms.<sup>132,133</sup> The central cobalt atom is capable of existing as Co(I), Co(II), and Co(III) at physiological conditions. The oxidation state of the cobalt atom influences the coordination number. Co(I) prefers four coordinate square planar geometry while Co(II) and Co(III) prefer five coordinate square pyramidal and six coordinate octahedral geometry, respectively.<sup>82,86</sup> The carbon cobalt bonds observed in alkyl cobalamins, specifically in MeCbl and AdoCbl, is characteristically weak and is essential in the ability for B12 to act as a cofactor.<sup>82</sup> Both MeCbl and AdoCbl work as coenzymes in the cytoplasm and mitochondria, respectively.<sup>82,85</sup> Upon binding to their respective enzymes, both MeCbl and AdoCbl exist in the “base-off” conformation with the  $\alpha$ -axial ligand occupied by histidine found in the enzyme.<sup>82</sup> In the cytoplasm, methionine synthase – a methyltransferase – utilizes MeCbl for the formation of methionine from homocysteine (Figure 6).<sup>82</sup> The formation of methionine and reformation of MeCbl occurs over a two-step process. First, the carbon cobalt bond in MeCbl is heterolytically cleaved and transferred to homocysteine resulting in the formation of methionine and cob(I)alamin. Secondly, the reformation of the cofactor occurs via the removal a methyl group from 5-methyltetrahydrofolate (5-methyl-THF) to produce MeCbl and tetrahydrofolate (THF).<sup>82,85,134,135</sup> In the mitochondria, methylmalonyl-CoA-mutase (MCM) – an isomerase – utilizes AdoCbl for the formation of succinyl-CoA from methylmalonyl-CoA (Figure 6). During the catalytic formation of succinyl-CoA AdoCbl is homolytically cleaved resulting in the

formation of cob(II)alamin and the initiation of the 5'-deoxyadenosyl radical. Propagation of the 5'-deoxyadenosyl radical initiates the rearrangement of methylmalonyl-CoA to succinyl-CoA. Termination of the radical species occurs at the end of each catalytic cycle when cob(II)alamin and the 5'-deoxyadenosyl radical recombine.<sup>82,85,136,137</sup>

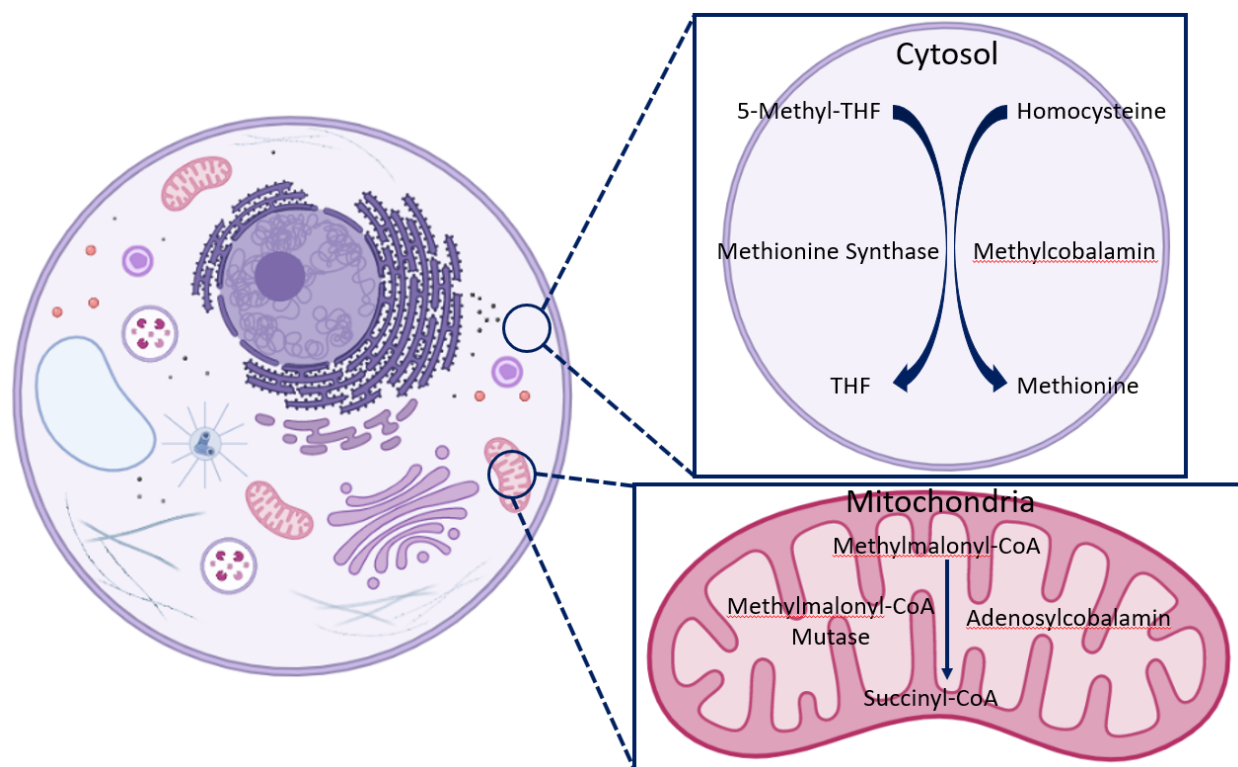


**Figure 6.** B12 functions as a co-factor for the enzymes methionine synthase and methylmalonyl-CoA Mutase within the cytosol and mitochondria, respectively.

#### 1.2.4 Dietary Uptake of B12 in Humans

The entrance of B12 into the cell is reliant upon its uptake and transportation through the GIT utilizing three transport proteins: haptocorrin (HC), intrinsic factor (IF), and transcobalamin (TC) as well as two receptors: CD320 and the cubilin (CUB) and amnionless (AMN) complex

CUBAM (Figure 7).<sup>82,85,138,139</sup> Following the consumption of food, B12 is released through the action of peptic enzymes and the acidic environment of the GIT.<sup>82,83,116,138</sup> The now free vitamin is bound by HC, forming a new HC:B12 complex that travels from the stomach to the duodenum where increased pH levels lead to the degradation of the HC:B12 complex (Figure 7).<sup>82,83,116,138</sup> Following the dissociation from HC, B12 freely binds to IF. The IF:B12 complex allows for the transport of B12 across the intestinal enterocyte site via receptor mediated endocytosis at the CUBAM receptor (Figure 7).<sup>82,83,116,138</sup> Within the enterocyte IF is broken down in the lysosome leading to the release of B12 into the bloodstream. Within the bloodstream B12 is capable of binding to TC and HC. Following the binding of B12 to TC, TC:B12, it is transported across cellular membranes through the TC:B12 CD320 receptor (Figure 7).<sup>82,83,116,138</sup> Once internalized the vitamin is released and via the breakdown of TC in the lysosome where B12 undergoes further chemical modification in order to perform its function as a cofactor in the previously stated enzymes (Figure 7).<sup>82,85,138,140</sup>

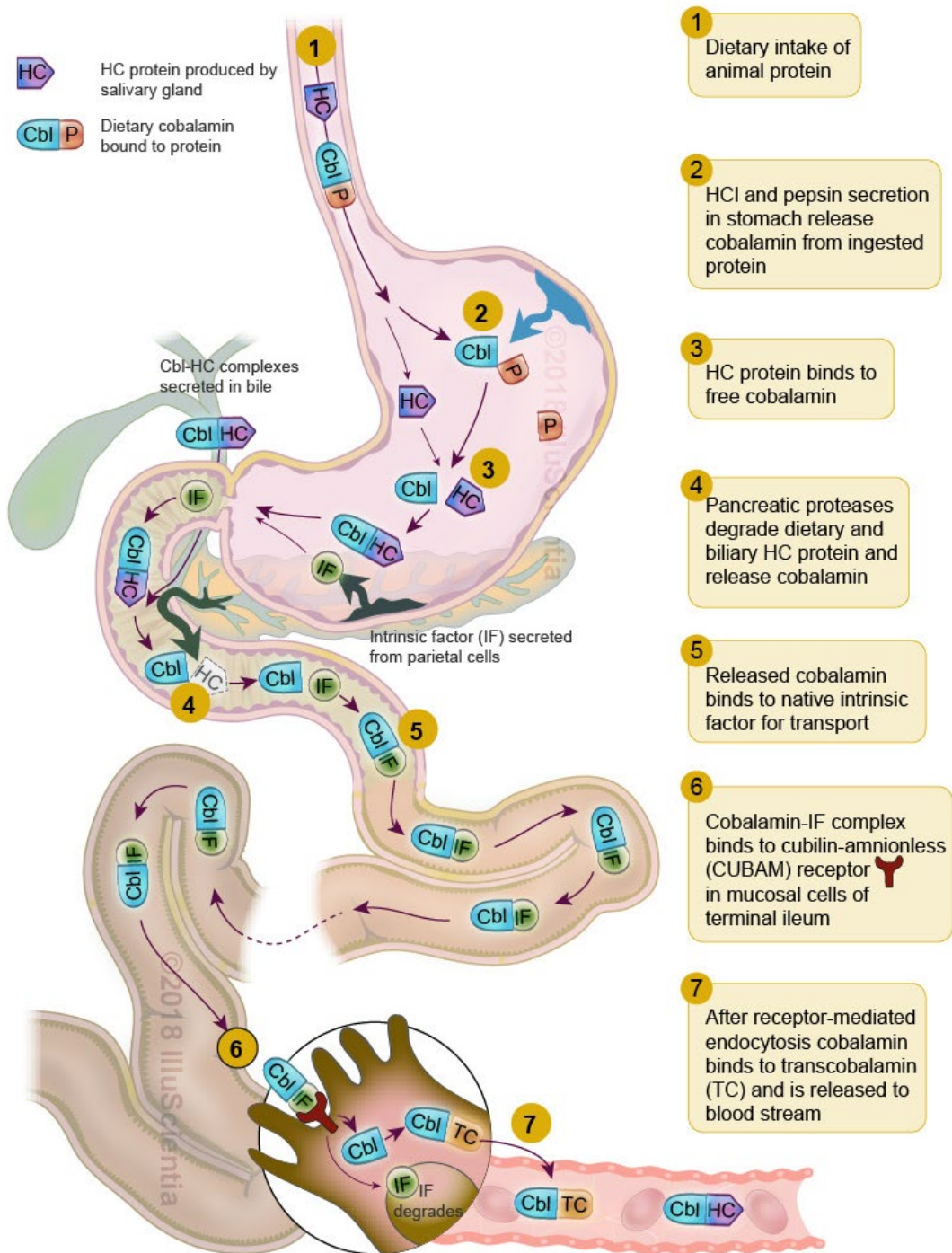


**Figure 7.** Human Dietary Uptake Pathway of B12. Abbreviations used: HC: Haptocorrin; Cbl: cobalamin/B12; P: Protein; IF: Intrinsic Factor; TC: Transcobalamin.



### 1.2.4.1 Transport Proteins of B12

The successful uptake and delivery of B12 to the cell is vastly dependent on the three transport proteins HC, IF, and TC. Despite their low sequence similarity, approximately 25%, these proteins have evolved from a single common ancestor. TC is the oldest transport protein followed by IF and lastly HC.<sup>82,141</sup> The age of these various transport proteins is reflected in their distribution of species other than homo sapiens. The structural scaffold of each of these proteins is highly conserved and allows each protein to bind and transport a single molecule of B12.<sup>85</sup> Each of these carrier proteins have a high affinity for B12 and provide protection from the highly acidic environment of the GIT. Protection of B12 by the transport proteins begins immediately upon consumption. B12 is highly susceptible to degradation<sup>142,143</sup> and hydrolysis<sup>108,144,145</sup> and must be protected to ensure proper delivery and function in the cell.

#### 1.2.4.1.1 Haptocorrin (HC)

The first protein found in the human B12 uptake pathway is HC (Figure 8). Found in both the saliva as well as the bloodstream,<sup>82</sup> HC is a heavily glycosylated 65 kDa protein with high affinity ( $K_d = 0.01$  pM) for B12 under acidic conditions ( $\text{pH} \leq 3$ ).<sup>85,138,146,147</sup> Given HC's stability under highly acidic conditions it is able to protect B12 from degradation via acid hydrolysis.<sup>108,144,145</sup> HC's binding affinity for B12 decreases as it enters the duodenum due to increased pH and the presence of pancreatic enzymes. This high stability to acidic conditions is highlighted by its 9-10 day half-life.<sup>148</sup> The binding specificity of HC to B12 is lower than both TC and IF as it can bind not only B12, but also incomplete B12 and other corrinoids.<sup>116,139</sup> While the specific function of HC in the B12 pathway is understood its function in plasma has yet to be identified. Its ability to bind other corrin rings suggests a roll as a scavenger preventing inactive

corrinoids from entering the cell.<sup>82,149,150</sup> Upon the binding of an inactive corrin it could be recycled through the hepatobiliary pathway.<sup>82</sup>

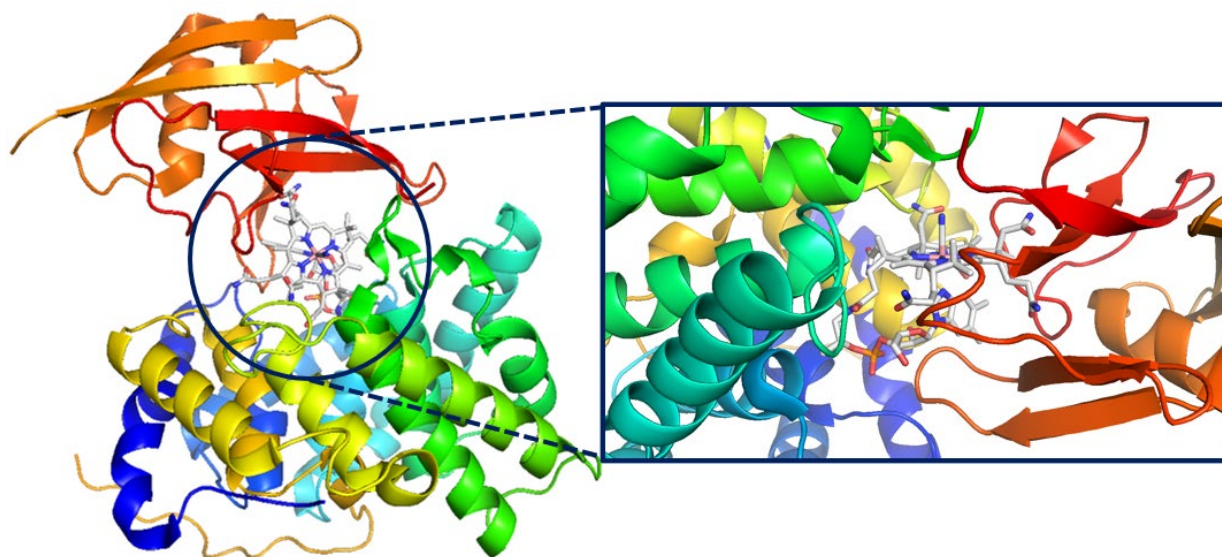


**Figure 8.** B12 bound to haptocorrin. PDB code 4KKI.<sup>147</sup> Image generated by the author using PyMol.

#### 1.2.4.1.2 Intrinsic Factor (IF)

IF, the second transport protein, like HC, is a glycoprotein with a molecular weight 50 kDa (Figure 9).<sup>82,85,151</sup> IF has both a high binding affinity ( $K_d = 1.0 \text{ pM}$ ) and binding specificity for B12.<sup>82,83,85</sup> IF is produced by gastric mucosa and is resistant to proteolytic degradation.<sup>138</sup> The primary function of intrinsic factor is to facilitate the transport of B12 across the intestinal enterocyte via the CUBAM receptor.<sup>82,85</sup> IF is broken down in the ileal enterocyte via lysosomal enzymes.<sup>152</sup> IF is only capable of binding intact B12.<sup>139</sup>

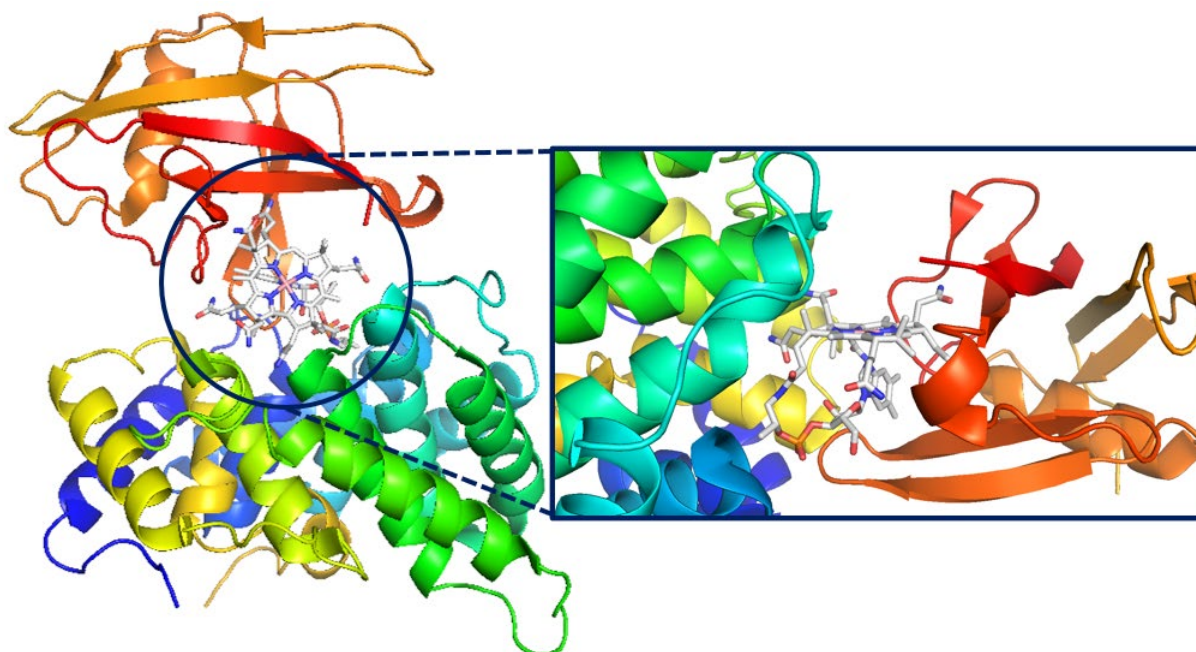


**Figure 9.** B12 bound to intrinsic factor. PDB code 2PMV.<sup>151</sup> Image generated by the author using PyMol.

#### 1.2.4.1.3 Transcobalamin (TC)

The final transport protein TC is a non-glycosylated protein with a molecular weight of 45.5 kDa (Figure 10).<sup>82,85,153–155</sup> TC has both a high binding affinity ( $K_d = 0.005$  pM) and binding specificity for B12.<sup>82,83,85,139</sup> Produced by endothelial cells, the primary function of TC is to bind and transport newly absorbed B12 in the bloodstream to cells.<sup>82,83,85</sup> Internalization of the TC:B12 complex occurs via the CD320 receptor.<sup>82,83,85,156</sup> Once internalized TC is degraded by the lysosome.<sup>82,83</sup> Like intrinsic factor, TC will only bind intact B12.<sup>139</sup>

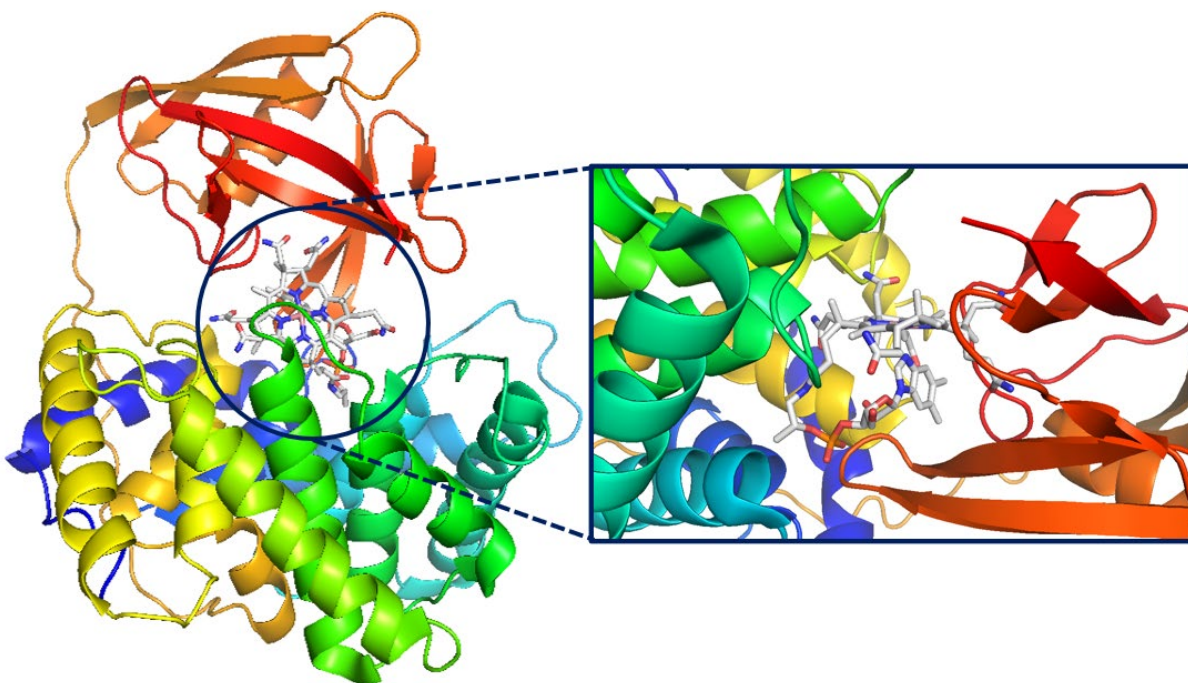


**Figure 10.** B12 bound to transcobalamin. PDB code 2BB5.<sup>153</sup> Image generated by the author using PyMol.

### 1.2.5 Distribution of B12 Transport Proteins and Investigations of B12 Conjugates in Various Lab Animal Models

Given the evolution and specialization of the B12 uptake pathway the distribution of binding proteins varies in animal species. To date, the transition, of a corrinated conjugate, from benchtop to in vivo investigation has frequently culminated with in vitro experiments. Despite the lack of progression to in vivo investigation, several corrin conjugates have been investigated in vivo. Nearly all corrin conjugates tested in vivo to date consist of peptide B12conjugates.

#### 1.2.5.1. Zebrafish

Zebrafish are an ideal animal model due to their ability to rapidly breed and their low cost of housing.<sup>141,157</sup> Dating back to 1930, zebrafish were used as a developmental and embryological

model.<sup>158</sup> By 1990, the successful use of zebrafish mutants made it a mainstream model in developmental biology.<sup>158</sup> The successful use of this animal as a developmental model have increased its use in the study of human disease.<sup>158</sup> The integration of zebrafish into small molecule screening has helped in the identification of new therapeutic compounds.<sup>159,160</sup> Despite the positive benefits of working with a small animal model like zebrafish there are limitations in their use as a model for investigating a corrinated conjugate. Although this animal model may be used for preliminary investigations it would not readily translate to that of a human due to the large differences in their uptake pathways. Investigations by Greibe *et al.*<sup>141</sup> have identified that zebrafish do not contain the three transport proteins found in humans but contain one transport protein resembling structure and function to that of the three proteins found in humans.<sup>141</sup>

The single protein isolated from the zebrafish experiment was termed HIT,<sup>141</sup> given its likeness to specific portions of the B12 binding proteins HC,<sup>147</sup> IF,<sup>151</sup> and TC.<sup>153</sup> This protein had properties similar to that of IF, resistance towards degradation by enzymes,<sup>138</sup> while also being similar to TC, in that no carbohydrates were observed.<sup>141</sup> The HIT protein was found to be similar in size to TC (~46 kDa), but the cobalamin binding site contained the highest sequence similarity with that of IF.<sup>141</sup> Despite similar structure and function to the transport proteins found in humans the binding affinities of HIT for cobalamin and its analogues differed compared to humans. Specifically, HIT showed decreased binding of Cbi compared to that of human HC, but also showed improved binding of AdoCbl compared to that of human TC. HIT was capable of binding B12 with equal potency to that of human HC, IF, and TC while also having the capacity to bind additional corrinoids.<sup>141</sup> The available amount of HIT protein to be targeted with a

therapeutic requires further investigation as a large portion of the protein is secreted into water much like the secretion of HC to extracellular fluids in mammals.<sup>141,161</sup>

Given the differences found in B12 transport between the zebrafish and the human it would not be an ideal animal model for studying a corrinated conjugate. Given the presence of only a single protein performing all known functions of transport proteins found in humans, the ability to specifically target a single transport protein is lost. Although, it could provide some preliminary insight and be coupled with other investigations a higher order species such as a mammalian vertebrate should be used if translation to human studies is to occur.

Despite the potential limitations associated with studying corrinated conjugates in zebrafish, work by Wang *et al.*<sup>162</sup> utilized this model to assess the cytotoxic effects of a B12 conjugated chitosan derivative used in the delivery of scutellarin (Scu) for the treatment of type 2 diabetes mellitus (T2DM) induced retinopathy.<sup>162</sup> The B12-conjugate was assessed for both acute toxic effects and the presence of developmental defects in zebrafish embryos. 72 hours post incubation no embryonic developmental defects were observed at concentrations up to 250  $\mu\text{g}/\text{mL}$ .<sup>162</sup>

#### **1.2.5.2 Mammalian Vertebrates**

Rats and mice have long been used as animal models due to their similarity to humans in regard to anatomy, physiology, and genome.<sup>163</sup> Depending on the diseased state being studied either of these two species could be utilized and are often the chosen species for pre-clinical trials.<sup>164</sup> Depending on the diseased state being investigated a preference for mice over rats or vice versa may occur.<sup>164</sup> In application and investigation of corrinated conjugates both mice and rats have slightly different uptake pathways than humans much like that of the zebrafish. While

human transport of B12 consists of three transport proteins<sup>82,85,116</sup> rats and mice utilize two transport proteins.<sup>165,166</sup> Like that of the zebrafish both mice and rats lack HC that is found in humans.<sup>82,85,116</sup> Unlike that of the zebrafish both rats and mice contain IF and TC. Despite the lack of HC in these rodents the TC found in serum acts similarly to that of human HC and TC.<sup>165,166</sup> This TC, like a zebrafish,<sup>141</sup> lacks the presence of carbohydrates and is similar to human TC in both sequence and size.<sup>165,166</sup> In addition to its structural similarity to that of human TC its function is also similar to that of human HC based on its ability to bind additional corrin rings, specifically Cbi.<sup>165</sup>

Due to the presence of only two transport proteins in the rat and the mouse there are limitations to its application in studying a corrinated conjugate. Specifically, the ability to specifically target HC and TC is lost due to the presence of a single protein capable of performing both functions in this species.<sup>165</sup> If a designed conjugate aimed to target IF specifically, this model could still be utilized. While both rats and mice are an ideal animal for studying a human disease,<sup>163,164</sup> limitations exist in their ability to properly investigate a corrinated conjugate.

Although both rats and mice lack the same B12 uptake pathway observed in humans they both are a standard for preliminary in vivo screening. Building on the results obtained in zebrafish Wang *et al.*<sup>162</sup> also investigated the pharmacokinetic enhancement of Scu, a compound limited by poor oral bioavailability and water solubility, through their B12 chitosan derivative conjugate for the delivery of sculetarin in male Sprague-Dawley rats. Rats were administered (40mg/kg) doses of Scu, Scu loaded chitosan derivative (Chit-DC-Scu), and Scu loaded B12-conjugated chitosan derivative (Chit-DC-VB12-Scu).<sup>162</sup> Both Chit-DC-Scu and Chit-DC-VB12-Scu showed improved bioavailability compared to that of free SCU. Additional experiments in rats

investigating retinal damage and blood flow performed by Wang *et al.* found scutellarin to be effective in attenuating retinal damage in diabetic Sprague-Dawley rats, but Chi-DC-Scu and Chi-DC-VB12-Scu were more effective than the compound alone.<sup>162</sup> Wang *et al.*, concluded that Chi-DC-VB12-Scu shows promising preliminary in vivo results and has therapeutic application in the treatment of retinopathy induced by diabetes.<sup>162</sup>

The improvement of the pharmacodynamic properties of bioavailability and water solubility is a hallmark of corination.<sup>167,168</sup> Given the poor oral bioavailability of luteinizing hormone releasing hormone (LHRH) antagonists' patients require frequent injection or nasal inhalation of the therapeutic.<sup>169</sup> To circumvent such drawbacks and the limitations associated with peptide delivery, Russell-Jones *et al.*<sup>169</sup> exploited the B12 uptake pathway for the delivery of LHRH antagonists. Specifically, Russel-Jones and coworkers used covalently linked ANTIDE, one of the most potent antagonists described to date, and its derivatives to B12 with the aim to improve oral bioavailability of LHRH antagonists.<sup>169</sup> Direct conjugation of B12 to ANTIDE and derivatives resulted in decreased potency in vitro and in vivo in castrated Sprague-Dawley rats.<sup>169</sup> It was presumed the presence of B12 resulted in a steric effect limiting binding of the antagonists to its receptor. In attempts to restore the in vivo function of the B12-ANTIDE conjugate, Russell-Jones and coworkers utilized a biodegradable disulfide linkage.<sup>169</sup> The employment of such a link caused a slight decrease in in vitro potency but improved the ability to inhibit the release of luteinizing hormone castrated Sprague-Dawley rats. All conjugates synthesized regardless of function showed improved solubility compared to that of the free ANTIDE.<sup>169</sup>

Another investigation utilizing B12 to improve bioavailability of a protein was performed by Petrus *et al.*<sup>170</sup> The delivery of insulin for glycemic control has been limited by a variety of



factors including poor bioavailability, possibility of contaminant pathogen uptake, compromised function of lungs as a result of prolonged usage, trouble dispensing exact dose.<sup>171</sup> Glycemic control is often regulated using oral delivery for long or intermediate acting insulin while short acting insulin is utilized through injection. The use of frequent injection commonly leads to a decrease in patient compliance.<sup>170,171</sup> In order to develop a non-invasive delivery system of insulin Petrus *et al.* utilized a vitamin B12 conjugated for the delivery of insulin.<sup>170</sup> To determine the efficacy of the newly designed conjugate, Petrus *et al.* utilized a STZ-induced diabetic rat model. Results of this investigation showed a 4.7-fold increase in area under the blood glucose curve. An additional study delivered the B12-insulin conjugate in the presence of excess free B12. The area under the blood glucose curve showed no effect at maintaining blood glucose confirming the hypothesis that the construct was mediated by the B12 uptake pathway. In addition to its ability to maintain glucoregulation the B12-insulin construct showed prolonged hypoglycemic activity compared to that of free insulin.<sup>170</sup>

The most commonly correlated peptides are those of neuroendocrine hormones, including both PYY3-36 (PYY)<sup>172</sup> and Exendin-4 (Ex4).<sup>138,167,168,173</sup> Limitations of PYY as a therapeutic include short half-life and initiation of nausea upon administration.<sup>172,174</sup> To potentially increase peptide activity through protection, B12 has been utilized as a potential bioconjugate by Henry *et al.* In investigations using Sprague Dawley rats as an *in vivo* model B12-PYY and PYY were delivered as subcutaneous pulses and resulted in B12-PYY having a stronger reduction in daily food intake and weight gain compared to that of a free PYY.<sup>172</sup>

Another neuroendocrine hormone used in the treatment of T2DM is Ex4, but like PYY, is commonly accompanied by nausea and malaise.<sup>138,167,168,173</sup> Mietlicki-Baase *et al.* utilized a B12-

Ex4 conjugate to improve glucose tolerance without producing anorexia and malaise.<sup>168</sup> Mietlicki-Baase and coworkers investigated the effects of this construct in male rats and mice. Using male Sprague Dawley rats B12-Ex4 did not suppress food intake, reduce body weight, nor induce conditioned taste avoidance (CTA) as observed in matching studies utilizing Ex4.<sup>168</sup> To further investigate the potential beneficial effects of conjugating Ex4 to B12, glycemic control was measured using C57BL/6J mice. In an IPGTT the administration of B12-Ex4 had a hypoglycemic response similar to that of free Ex4.<sup>168</sup>

Corrin-conjugates have also been utilized outside of drug delivery and the improvement of bioavailability. Investigations by Ikotun *et al.* utilized a copper<sup>64</sup> labeled B12-NOTA construct to explore the nutritional demand of proliferating cells in preclinical tumor models.<sup>175</sup> This construct was the first B12 conjugate utilized for positron emission tomography (PET) imaging. The effectiveness of this B12-en-Bn-NOTA-<sup>64</sup>Cu was investigated in various murine tumor models. This conjugate was effective and resulted in high tracer accumulation in various animal models.<sup>175</sup>

Given the limitations observed in the use of both rats and mice, lower ordered mammals, additional higher ordered mammals provide opportunities for investigations of cobalamin conjugates and ultimately translation into human studies. The musk shrew (*Suncus murinus*) is a well-established model of emesis and feeding behavior and is suitable for examination of the GLP-1 system as this species exhibits glucoregulatory, hypophagic and emetic responsivity following administration of current Food and Drug Administration-approved GLP-1R agonists.<sup>176,177</sup>

### **1.2.6 B12/ Corrin Binding Capacity**

The ability to design effective cobalamin conjugates for the treatment of a variety of diseases has been hindered by the inability to translate successful in vitro screening to an appropriate in vivo model. The ability to identify and select an animal model for in vivo investigation has been hindered by the lack of readily useable data regarding the uptake pathways of various laboratory animal models. A compilation of the available data regarding the cobalamin uptake pathway in various laboratory models including the presence of transport proteins and their saturated binding capacities was compiled by the author and is detailed in Table 2.<sup>141,167,178-184</sup>

**Table 2.** Unsaturated Binding Capacity (UBC) of Serum and Gastric Juice in Various Lab Animal Models.

Species	Total Serum UCBC (nmol/L)	Haptocorrin UCBC (nmol/L)	Transcobalamin UCBC (nmol/L)	Total Gastric UCBC (nmol/L)
Homosapien	0.735-1.710 <sup>178-183</sup>	0.075-0.350 <sup>182,183</sup>	0.300-1.165 <sup>182,183</sup>	30-51 <sup>178,179</sup>
Rhesus Monkey	1.5-30 <sup>178,181</sup>	NF	NF	NF
Porcine (Hog)	1.1-7.1 <sup>178-181</sup>	NF	NF	NF
Dog	1.7-2.3 <sup>178,181</sup>	NF	NF	180 <sup>178</sup>
Cat	12-23 <sup>178,180,181</sup>	NF	NF	NF
Shrew	12.38 <sup>167</sup>	4.63 <sup>167</sup>	8.04 <sup>167</sup>	NF
Rabbit	13-18 <sup>178-181</sup>	NF	NF	NF
Hamster	30 <sup>178</sup>	NF	NF	NF
Guinea Pig	2.0-6.8 <sup>178,178,181</sup>	NF	NF	NF
Rat	1.7-2.9 <sup>178-181</sup>	NA	2.3 <sup>178</sup>	7.5 <sup>178</sup>
Mouse	28-32 <sup>178,181</sup>	NA	28 <sup>178</sup>	NF
Rainbow Trout	2500 <sup>184</sup>	NA	NA	NF
Zebrafish	8.2 <sup>141</sup>	NA	NA	NF

### 1.2.7 Chemical Modifications of B12 and Cbi

While bound to each protein in its uptake pathway B12 maintains a solvent exposed surface. The solvent exposed surface of B12 while bound to HC is 3.2% ( $\approx 39 \text{ \AA}^2$ ) (Figure 8),<sup>147</sup> this value is doubled when bound to TC, 6.6% ( $\approx 80 \text{ \AA}^2$ ) (Figure 9),<sup>153</sup> and doubles again to 13.2% ( $\approx 163 \text{ \AA}^2$ ) when bound to IF (Figure 10).<sup>151</sup> Given the complex structure of the compound there are multiple functional groups that can be readily modified. These modifiable functional groups

are ideal locations for conjugation to small molecules or peptides.<sup>83</sup> While multiple sites can be easily chemically modified few locations can be chosen while maintaining recognition by all three transport proteins. The ability to modify at multiple locations allows for specific targeting of one of the three transport proteins.

The B12 structure contains five different regions which may be chemically modified while maintaining recognition by all transport proteins: 1) the peripheral corrin ring  $\epsilon$ -propionamide, 2) the peripheral corrin ring  $\beta$ -propionamide, 3) the 5'-hydroxyl group found in the ribose unit of the  $\alpha$ -tail, 4) the 2'-hydroxyl group found in the ribose unit of the  $\alpha$ -tail, 5) the phosphate moiety of the  $\alpha$ -tail, 6) the cobalt cation (Figure 3).<sup>83,117,185</sup> The B12 molecule contains multiple other functional groups that are capable of being modified, but modifications at these locations can affect the binding of the conjugate to individual or all transport proteins. While this may be of interest depending on the conjugate being designed those modifications are not discussed herein and the reader is directed to Wierzba *et al.*<sup>117</sup> and o'Proinsias *et al.*<sup>185</sup> for further discussion.

### **1.2.8 Developing a GLP-1R Agonist Devoid of Nausea, Emesis, and Weight loss**

The dramatic rise of type 2 diabetes (T2D) and obesity as comorbidities has driven a concomitant rise in new pharmaceutical interventions to treat such disorders, either together or individually.<sup>24,25,186-190</sup> One extremely successful family of pharmaceuticals in this field has been that of glucagon-like peptide-1 receptor agonists (GLP-1RAs),<sup>46,64,65,191-193</sup> such as exenatide (i.e., Exendin-4; Ex4),<sup>54,138</sup> liraglutide,<sup>194-197</sup> and semaglutide.<sup>196-198</sup> Exenatide and liraglutide confer glucoregulation in tandem with a body weight reduction of 5-6% over ~1 year,<sup>196,197</sup> while semaglutide can produce a weight loss of 10- 12% over the same time period.<sup>196,197</sup> The hypophagic effects of all GLP-1RAs are however accompanied by nausea and vomiting (emesis)

in upward of 25% of patients,<sup>70–76</sup> the result of penetrance and direct action of the GLP-1RA in the CNS, particularly in the nucleus tractus solitarius and area postrema of the hind-brain.<sup>62,199–</sup>  
<sup>201</sup> Thus, the development of a GLP-1RA that does not access the CNS would be expected then to mitigate the side effects of nausea and emesis and reduce the hypophagic effects. The reasons for removing the side effects are obvious, but less clear is the fact that there is a current unmet clinical need to broaden pharmacopoeia for certain subpopulations of T2D patients, including lean individuals, those in a state of cachexia (wasting of body tissues/chronic weight loss), or those who must avoid weight loss from other life-threatening diseases such as chronic obstructive pulmonary disease, cystic fibrosis, cancer, and HIV.<sup>202–206</sup> Indeed, the prevalence of T2DM in COPD patients is  $\approx 20\%$  with an incidence for COPD of  $\approx 10\%$  in the overall diabetic population.<sup>207–209</sup> Further, depending on the tumor type, between 8% and 18% of the cancer patients at the time of diagnosis also suffer from T2DM,<sup>204,210</sup> and 30%–40% of hospitalized heart failure patients are diabetic.<sup>211</sup> This subgroup of T2DM patients is already at increased risk for cachexia, nausea/malaise, and unintended weight loss.<sup>212,213</sup> In these T2DM patients, as well as overweight/obese T2DM patients that cannot effectively tolerate the nausea/emesis of existing GLP-1-based therapeutics. the data provided here support the hypothesis that the a corrinated Ex4 construct can improve glycemic control without producing anorexia and drug-treatment-induced malaise.

Reduced caloric intake and body weight may be viewed as positive therapeutic outcomes in many T2DM patients prescribed existing GLP-1-based therapeutics (i.e., in those patients with accompanying obesity); however, there is a substantial number of T2DM patients that require glycemic control without weight loss. Thus, we set out to create GLP-1RAs with reduced brain

penetrance but with retained, comparable pharmacodynamic profiles on pancreatic GLP-1R populations.<sup>138,167,168,172,173</sup> Recently, we have taken the approach of utilizing components of the vitamin B12 (B12) dietary uptake pathway including that of the corrin ring containing B12<sup>138,168,172,173,214</sup> itself as well as B12 precursors such as Cbi (Figure 11)<sup>167</sup> in a process we have coined “corrination”. The benefits of corrination over other conjugation modes lie in the ability to specifically target select corrin binding proteins such as intrinsic factor, transcobalamin, or haptocorrin for use in targeting or to affect pharmacokinetics, modify solubility, and alter drug localization, all without having to reverse the process to allow for maintained drug function pending suitable design.

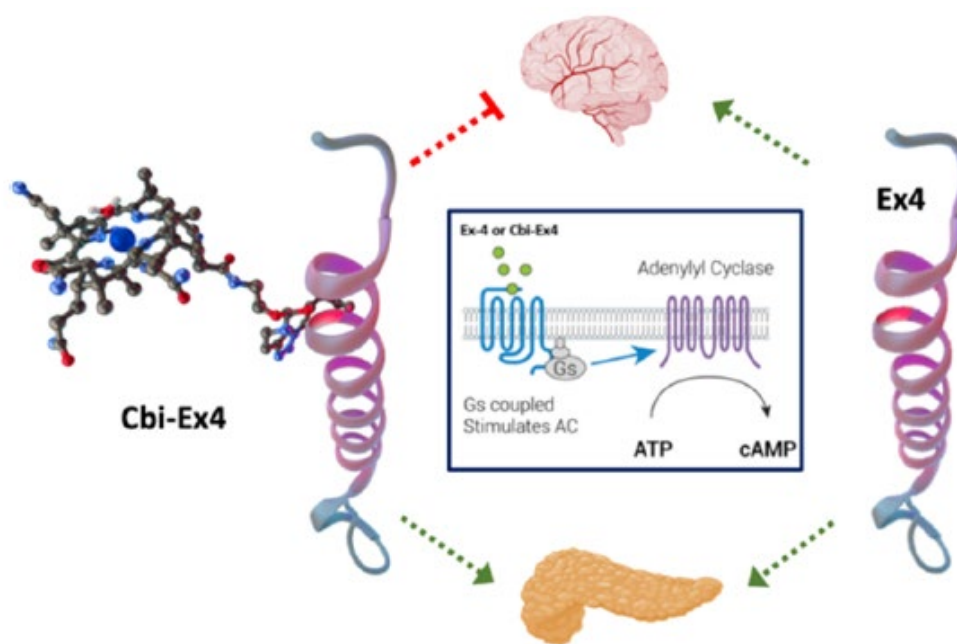


**Figure 11.** Corrination of Ex4 (Cbi-Ex4) does not prevent GLP-1R agonism in the pancreas but does mitigate agonism in the CNS as tracked by emesis and anorexia. Ex4 alone agonizes GLP-1R populations in both the pancreas and CNS.

### 1.3 Glial cell-derived neurotrophic factor (GDNF) Family and the GDNF Family Ligands (GFLs)

The transforming growth factor- $\beta$  (TGF- $\beta$ ) superfamily is a constantly expanding family of peptides and proteins involved in the proliferation, growth, and differentiation of cells. The superfamily consists of bone morphogenetic proteins, growth and differentiation factors, activins, inhibins, and glial-derived neurotrophic factors (GDNFs). Additional proteins and peptides are also part of this superfamily, but are not further separated into their own subfamily.<sup>215–219</sup> Due to their various roles in cell signaling they are heavily involved in development and disease. The dysregulation of the TGF- $\beta$  superfamily signaling has been identified in cancer, cardiovascular, fibrotic, and skeletal diseases.<sup>217</sup> Some of the most distant members of the TGF- $\beta$  superfamily are the members of the GDNF family.<sup>220</sup> There are four members of the GDNF family including: GDNF, artemin (ARTN), persephin (PSPN) and neurturin (NRTN).<sup>221–227</sup> The ligands of this family are considered distant members of the TGF- $\beta$  superfamily due to their conserved pattern of cysteine residues in their primary sequence and structural similarity observed with other members of the family.<sup>228</sup> Monomers of the GFL are composed of an  $\alpha$ -helical heel region, a cysteine-knot motif, and a finger region composed of two fingers formed by anti-parallel  $\beta$ -strands connected by loops (Figure 12). In circulation the GFLs are found as homodimers in which the monomers are coupled in a head-to-tail conformation (Figure 13).<sup>228</sup>



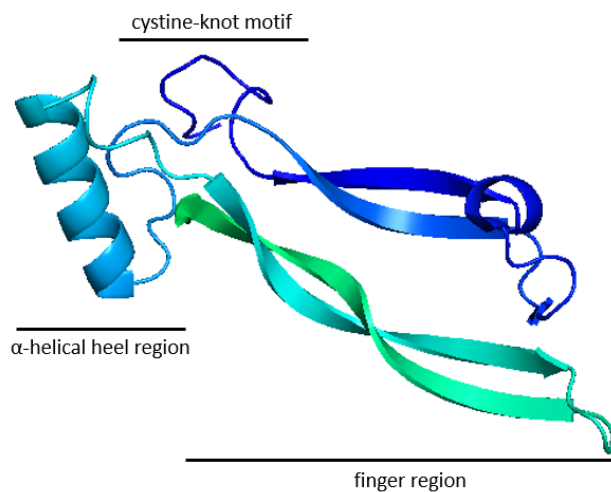


**Figure 12.** Monomer of GDF15 a Member of the GFL. PDB code 5VZ4.<sup>229</sup> Image generated by the author using PyMol.

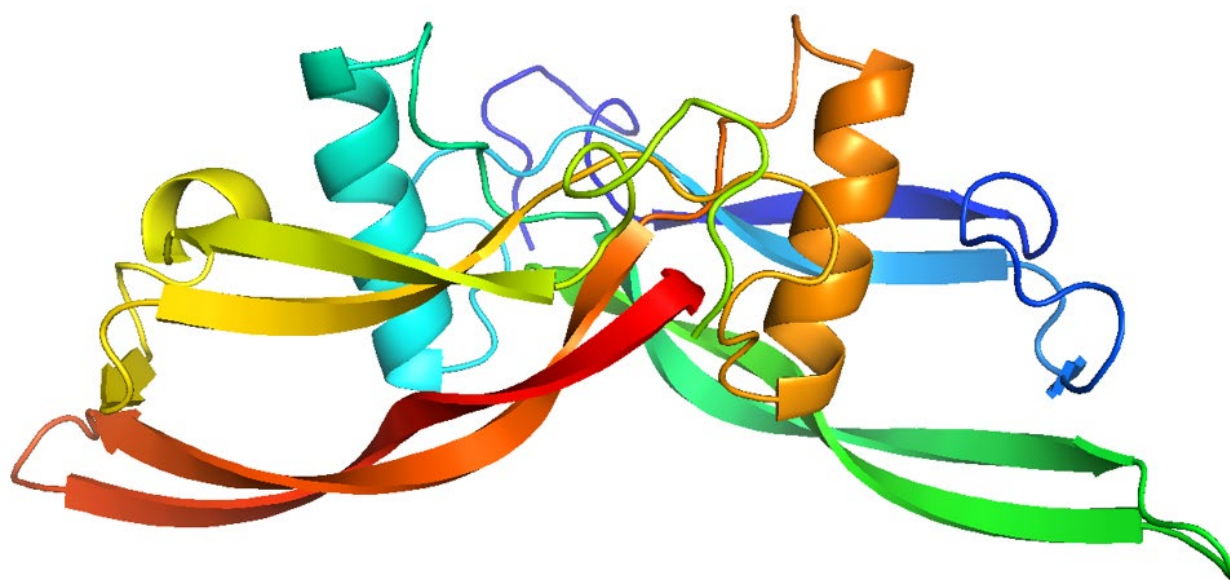


**Figure 13.** Dimer of GDF15 a Member of the GFL. PDB code 5VT2.<sup>222</sup> Image generated by the author using PyMol.

### 1.3.1 Growth/Differentiation Factor 15 (GDF15)

Growth differentiation factor 15 (GDF15), previously known as macrophage inhibitory cytokine 1 (MIC-1), NAG1, PLAB, and PDF, here on referred to as GDF15, is a stress response cytokine and a distant member of the TGF- $\beta$  superfamily.<sup>220,230–232</sup> Unlike the other GFLs, GDF15, has high specificity for its receptor and is in capable of binding to other receptors found in the GDNF family.<sup>220</sup> GDF15 is found in all individuals and circulates as a mature dimer with a molecular weight of approximately 25 KDa.<sup>220</sup> Serum concentrations vary with individuals with basal levels ranging from 200-1,200 pg/mL.<sup>233</sup> Concentrations of GDF15 increase in states of inflammation including exercise, smoking, obesity, pregnancy, and cancer.<sup>220–222,234–237</sup> In cases of pregnancy In advanced cancers GDF15 influences anorexia/cachexia syndrome and has been shown to induce weight loss and appetite suppression.<sup>220,230,238</sup> Tumor bearing mice engineered to increase GDF15 expression resulted in increased weight loss due to a loss in both fat and lean mass due to decreased energy intake. Loss of mass was able to be mitigated through antibody treatment targeting GDF15.<sup>238</sup> The overexpression of GDF15 in transgenic mice lead to lean phenotypes, decreased energy consumption, and resistance to obesity.<sup>238</sup> The overexpression of GDF15 improved glucose tolerance in both normal and high fat diets.<sup>239</sup> In an inverse study, it was shown that mice with a deletion of GDF15 resulted in an obese phenotype which could be corrected with injections of GDF15.<sup>240</sup>

### 1.3.2 The receptors of GFL, GDNF Receptor- $\alpha$ (GFR $\alpha$ )

The binding receptors of the GFLs are of the GDNF family receptors, GFR $\alpha$ . Each of the GFLs have unique binding affinities to their own GFR $\alpha$ .<sup>241</sup> GDNF specifically binds to GFR $\alpha$ 1, NRTN binds to GFR $\alpha$ 2, ARTN to GFR $\alpha$ 3, and PSPN GFR $\alpha$ 4.<sup>225–228,241</sup> While each ligand of the GFL contains

their own receptor, there is some promiscuity in binding and GFLs have been shown to activate other GFR $\alpha$  receptors.<sup>225,229,242</sup> These receptors are anchored to the cell surface via a glycosylphosphatidylinositol (GPI).<sup>225,226,228,230,241,243</sup> Given that the GFR $\alpha$ s are GPI anchored they are commonly localized in lipid rafts.<sup>241</sup> In addition to GPI anchored receptors, the GFR $\alpha$  receptors are capable of existing in soluble forms.<sup>223,244</sup> Transmembrane forms of the GFR $\alpha$ 1 exist but are unable to transport RET to the lipid rafts despite activating RET phosphorylation.<sup>244</sup>

### 1.3.2.1 GDNF Family Receptor- $\alpha$ Like (GFRAL)

The receptor for GDF15 remained unclear until 2017 when four independent laboratories identified its receptor, GFRAL.<sup>20,224,229,245,246</sup> Highly expressed in the CNS, specifically in the AP and NTS, GFRAL is a distant member of the GFR $\alpha$  family.<sup>20,220,224,229,245,246</sup> While the individual isoforms found in the GFR $\alpha$  family are capable of binding more than one ligand, GFRAL is highly specific in its binding only for GDF15.<sup>220</sup> While the members of the GFR $\alpha$  family are GPI anchored, GFRAL is a transmembrane protein.<sup>220,230</sup> An additional isoform of GFRAL exists in which exon 6 has been removed. The resulting receptor maintains binding sites for GDF15, but eliminates the transmembrane sequence and thus producing a soluble receptor.<sup>220,247</sup> To date the expression and function of this receptor is still being investigated.<sup>220</sup> Deletion of the GFRAL receptor in mice resulted in no response following GDF15 injection, but predisposed the mice to obesity when fed a high fat diet.<sup>20,229</sup> In experiments performed by Tsai *et al.*, it was found that the AP and NTS had to be intact in order for effects of GDF15 to be observed and that animals were unresponsive to treatments following lesion of the AP and NTS.<sup>248</sup>

### 1.3.2.2 GFL Signaling Receptor RET

Rearranged during transformation (RET),<sup>225,228</sup> is a single-pass transmembrane receptor tyrosine kinase (RTK).<sup>228</sup> The extra cellular region of RET is composed of four cadherin like domains (CLD<sub>1-4</sub>) and a cysteine-rich domain proximal to the cellular membrane.<sup>228</sup> Given the presence of the repeating CLD and calcium binding site RET is defined as a distant member of the cadherin superfamily.<sup>225,228</sup> Between CLD<sub>2</sub> and CLD<sub>3</sub> is a calcium binding site. The binding of calcium is required for proper folding and function of RET.<sup>228</sup> The intracellular region of RET is composed of a juxtamembrane domain, a tyrosine kinase domain, and a C-terminal tail.<sup>228</sup> All members of the GFLs including GDF15 share a common signaling receptor, RET.<sup>220,228,230,241,249,250</sup> While RET is the signaling receptor for the GFLs they are not able to stimulate signaling via the receptor alone.<sup>228</sup> The GFR $\alpha$ /GFRAL:RET complex is unique as it is the only known RTK requiring separate ligand binding components.<sup>228,243</sup> While the GFR $\alpha$  receptors are found in lipid rafts, RET is not and must be recruited in order for signaling to occur.<sup>241</sup>

### 1.3.2.3 Signaling Through the GFR $\alpha$ /GFRAL:RET Complex

Following the binding of a GFL to its unique GPI anchored binding receptor, GFR $\alpha$ , the GFL-GFR $\alpha$  complex then recruits RET to the lipid raft containing GFR $\alpha$ . This new ternary complex leads to dimerization, autophosphorylation, and intracellular signaling.<sup>241</sup> The final signaling assembly is composed of a 2:2:2 stoichiometry containing two GFL: two GFR $\alpha$ : and two RET.<sup>228,249,250</sup> The proper function and ability to signal requires intact lipid rafts as cholesterol depletion has been shown to decrease GDNF stimulated intracellular effects.<sup>244</sup> Various models have been proposed for how the complex formation takes place. The first proposed model suggests a circulating homodimer of the GFL symmetrically binds to two of its GFR $\alpha$

simultaneously and then recruits RET and thus activating kinase domains. An alternative model suggests a stepwise approach in which a circulating homodimer GFL binds to a single GFR $\alpha$  receptor at which time RET is recruited and then additional molecules of GFR $\alpha$  and RET dimerize in the lipid raft.<sup>251</sup> In the case of signaling through the soluble receptor one of the GFLs bind to their native GFR $\alpha$  at which time the GFL: GFR $\alpha$  complex then binds to ret and the ternary complex is recruited to a lipid raft.<sup>223</sup> The activation of RET and its signaling plays roles in cell survival, differentiation, proliferation, and migration.<sup>241,249,250</sup> Given the possibility of separate function by the soluble GFRAL receptor additional functions of this complex may exist.<sup>220</sup>

### **1.3.3 Targeting the GDF15:GFRAL Complex (Agonism and Antagonism)**

Given the complex role the GDF15:GFRAL pathway plays in energy homeostasis it is an ideal target for the treatment of various diseased states. The pathways resistance to obesity and glucose intolerance highlights its application in the treatment of comorbid disease obesity and diabetes. The pathways influence on anorexia and cachexia in states of high GDF15 serum levels provides another avenue for pharmaceutical development. Approximately 50-90% of all pregnant women experience nausea and vomiting as a result of the pregnancy itself. Nearly 1/5<sup>th</sup> of this population require medication to treat such side effects. Hyperemesis gravidarum (HG) is a severe case that occurs in 0.3-2.0% of pregnancies. In a genome wide study GDF15 was found to be upregulated suggesting a role in the condition.<sup>252</sup>

### **1.4 H188 FRET Assays and Fluorescent Probes of Neuroendocrine Hormones**

To determine the agonism of Corrin-Ex4 conjugates at the GLP-1R, HEK293 cells stably transfected with the receptor were utilized. The cells were infected with the H188 adenovirus, the most sensitive exchange protein directly activated by cAMP (EPAC) fluorescence resonance

energy transfer (FRET) reporter.<sup>253</sup> This reporter consists of a cAMP binding domain flanked by a mTurquoise2 $\Delta$  FRET donor chromophore at the N-terminus and a tandem cp173 Venus-Venus FRET acceptor chromophore at the C-terminus of fluorescent proteins (Figure 14). When cAMP binds the EPAC, a conformational change occurs, causing the two chromophores to move closer, creating an increase in FRET response.<sup>254</sup> This EPAC was chosen based on its higher sensitivity (~70%) than other FRET assays such as AKAR3 (~20%).<sup>254</sup>

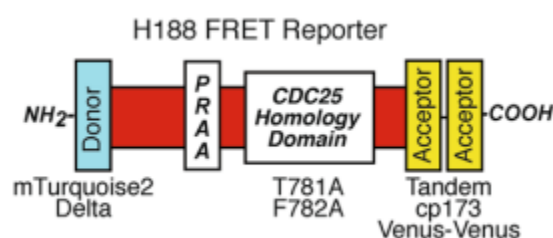


**Figure 14.** Domain structures of the H88 adenovirus. Used with permission of author.<sup>254</sup>

Currently there is an unmet need for the development of fluorescent probes to better understand the neurocircuitry involved in the suppression of reward circuits. While it is known that the GIT generates a number of signals to trigger satiation, the mechanisms behind and underpinning such signaling is complicated by a lack of tools to track where and when certain pathways are activated or inhibited. The development of a library of different fluorescent Ex4s, for example, offers an opportunity to explore whether, and when, this peptide binds to its cognate receptor as a monomer or dimer.

In the case of leptin, a hormone produced by adipose tissue that helps to prevent food consumption there continues to be debate on leptin receptor distribution, especially in cells in the brain not typically associated with leptin signaling.

Another relevant example to this work is that of oxytocin, well known for its role in childbirth and 'bonding', but much less explored in terms of a role in energy homeostasis. The design of a fluorescent, functional, oxytocin would allow for the further investigation of this multifunctional peptide, especially given oxytocin antibody have failed to provide adequate data from *ex vivo* studies. The design and synthesis of fluorescent probes of these three peptide hormones is discussed herein (Chapter 5).

## 1.5 References

- (1) Cummings, J. H.; Stephen, A. M. Carbohydrate Terminology and Classification. *Eur. J. Clin. Nutr.* **2007**, *61*, S5–S18.
- (2) Mergenthaler, P.; Lindauer, U.; Dienel, G. A.; Meisel, A. Sugar for the Brain: The Role of Glucose in Physiological and Pathological Brain Function. *Trends Neurosci.* **2013**, *36* (10), 587–597.
- (3) Szablewski, L. Glucose Homeostasis – Mechanism and Defects. In *Diabetes - Damages and Treatments*; Rigobelo, E., Ed.; InTech: Rijeka, Croatia, 2011; pp 227–256.
- (4) Szablewski, L. Glucose Homeostasis. In *Glucogenesis*; Zheng, W., Ed.; InTech: Rijeka, Croatia, 2017; pp 5–20.
- (5) Guemes, M.; Rahman, S. A.; Hussain, K. What Is a Normal Blood Glucose? *Arch. Dis. Child.* **2016**, *101* (6), 569–574.
- (6) Qaid, M. M.; Abdelrahman, M. M. Role of Insulin and Other Related Hormones in Energy Metabolism-A Review. *Cogent Food Agric.* **2016**, *2* (1), 1267691.
- (7) Ojha, A.; Ojha, U.; Mohammed, R.; Chandrashekar, A.; Ojha, H. Current Perspective on the Role of Insulin and Glucagon in the Pathogenesis and Treatment of Type 2 Diabetes Mellitus. *Clin. Pharmacol. Adv. Appl.* **2019**, *11*, 57–65.
- (8) Kazafeos, K. Incretin Effect: GLP-1, GIP, DPP4. *Diabetes Res. Clin. Pract.* **2011**, *93S*, S32–S36.
- (9) Kim, W.; Egan, J. M. The Role of Incretins in Glucose Homeostasis and Diabetes Treatment. *Pharmacol. Rev.* **2008**, *60* (4), 470–512.
- (10) Nauck, M. A.; Meier, J. J. The Incretin Effect in Healthy Individuals and Those with Type 2



- Diabetes: Physiology, Pathophysiology, and Response to Therapeutic Interventions. *Lancet Diabetes Endocrinol.* **2016**, *4*, 525–536.
- (11) Aronoff, S. L.; Berkowitz, K.; Shreiner, B.; Want, L. Glucose Metabolism and Regulation: Beyond Insulin and Glucagon. *Diabetes Spectr.* **2004**, *17* (3), 183–190.
- (12) Röder, P. V.; Wu, B.; Liu, Y.; Han, W. Pancreatic Regulation of Glucose Homeostasis. *Exp. Mol. Med.* **2016**, *48*, e219.
- (13) Lin, X.; Xu, Y.; Pan, X.; Xu, J.; Ding, Y.; Sun, X.; Song, X.; Ren, Y.; Shan, P. F. Global, Regional, and National Burden and Trend of Diabetes in 195 Countries and Territories: An Analysis from 1990 to 2025. *Sci. Rep.* **2020**, *10* (1), 14790.
- (14) Evers, A.; Haack, T.; Lorenz, M.; Bossart, M.; Elvert, R.; Henkel, B.; Stengelin, S.; Kurz, M.; Glien, M.; Dudda, A.; Lorenz, K.; Kadereit, D.; Wagner, M. Design of Novel Exendin-Based Dual Glucagon-like Peptide 1 (GLP-1)/Glucagon Receptor Agonists. *J. Med. Chem.* **2017**, *60* (10), 4293–4303.
- (15) DeFronzo, R. A.; Ferrannini, E.; Groop, L.; Henry, R. R.; Herman, W. H.; Holst, J. J.; Hu, F. B.; Kahn, C. R.; Raz, I.; Shulman, G. I.; Simonson, D. C.; Testa, M. A.; Weiss, R. Type 2 Diabetes Mellitus. *Nat. Rev. Dis. Prim.* **2015**, *1* (July), 15019.
- (16) Khera, R.; Murad, M. H.; Chandar, A. K.; Dulai, P. S.; Wang, Z.; Prokop, L. J.; Loomba, R.; Camilleri, M.; Singh, S. Association of Pharmacological Treatments for Obesity With Weight Loss and Adverse Events. *J. Am. Med. Assoc.* **2016**, *315* (22), 2424–2434.
- (17) Blaslov, K.; Naranđa, F. S.; Kruljac, I.; Renar, I. P. Treatment Approach to Type 2 Diabetes: Past, Present and Future. *World J. Diabetes* **2018**, *9* (12), 209–219.
- (18) Kharroubi, A. T. Diabetes Mellitus: The Epidemic of the Century. *World J. Diabetes* **2015**, *6*

- (6), 850.
- (19) Knowler, W. C.; Barrett-Connor, E.; Fowler, S. E.; Hamman, R. F.; Lachin, J. M.; Walker, E. A.; Nathan, D. M. Reduction of the Incidence of Type 2 Diabetes with Lifestyle Intervention or Metformin. *Int. Urol. Nephrol.* **2002**, *346* (6), 393–403.
- (20) Mullican, S. E.; Lin-Schmidt, X.; Chin, C. N.; Chavez, J. A.; Furman, J. L.; Armstrong, A. A.; Beck, S. C.; South, V. J.; Dinh, T. Q.; Cash-Mason, T. D.; Cavanaugh, C. R.; Nelson, S.; Huang, C.; Hunter, M. J.; Rangwala, S. M. GFRAL Is the Receptor for GDF15 and the Ligand Promotes Weight Loss in Mice and Nonhuman Primates. *Nat. Med.* **2017**, *23* (10), 1150–1157.
- (21) Lee, S.; Lee, D. Y. Glucagon-like Peptide-1 and Glucagon-like Peptide-1 Receptor Agonists in the Treatment of Type 2 Diabetes. *Ann. Pediatr. Endocrinol. Metab.* **2017**, *1012*, 15–26.
- (22) Riddle, M. C.; Herman, W. H. The Cost of Diabetes Cared an Elephant in the Room. *Diabetes Care* **2018**, *41* (5), 929–932.
- (23) Yang, W.; Dall, T. M.; Beronjia, K.; Lin, J.; Semilla, A. P.; Chakrabarti, R.; Hogan, P. F.; Petersen, M. P. Economic Costs of Diabetes in the U.S. in 2017. *Diabetes Care* **2018**, *41* (5), 917–928.
- (24) Sadry, S. A.; Drucker, D. J. Emerging Combinatorial Hormone Therapies for the Treatment of Obesity and T2DM. *Nat. Rev. Endocrinol.* **2013**, *9* (7), 425–433.
- (25) Drucker, D. J.; Sherman, S. I.; Bergenstal, R. M.; Buse, J. B. The Safety of Incretin-Based Therapies - Review of the Scientific Evidence. *J. Clin. Endocrinol. Metab.* **2011**, *96* (7), 2027–2031.
- (26) Inzucchi, S. E.; Bergenstal, R. M.; Buse, J. B.; Diamant, M.; Ferrannini, E.; Nauck, M.; Peters,

- A. L.; Tsapas, A.; Wender, R.; Matthews, D. R. Management of Hyperglycemia in Type 2 Diabetes: A Patient-Centered Approach. *Diabetes Care* **2012**, *35* (6), 1364–1379.
- (27) Gong, L.; Goswami, S.; Giacomini, K. M.; Altman, R. B.; Klein, T. E. Metformin Pathways: Pharmacokinetics and Pharmacodynamics. *Pharmacogenet Genomics* **2012**, *22* (11), 820–827.
- (28) Schlender, L.; Martinez, Y. V.; Adeniji, C.; Reeves, D.; Faller, B.; Sommerauer, C.; Al Qur'An, T.; Woodham, A.; Kunnamo, I.; Sönnichsen, A.; Renom-Guiteras, A. Efficacy and Safety of Metformin in the Management of Type 2 Diabetes Mellitus in Older Adults: A Systematic Review for the Development of Recommendations to Reduce Potentially Inappropriate Prescribing. *BMC Geriatr.* **2017**, *17* (Suppl 1).
- (29) Thrasher, J. Pharmacologic Management of Type 2 Diabetes Mellitus: Available Therapies. *Am. J. Med.* **2017**, *130* (6), S4–S17.
- (30) Kahn, S. E.; Haffner, S. M.; Heise, M. A.; Herman, W. H.; Holman, R. R.; Jones, N. P.; Kravitz, B. G.; Lachin, J. M.; O'Neill, M. C.; Zinman, B.; Viberti, G. Glycemic Durability of Rosiglitazone, Metformin, or Glyburide Monotherapy. *N. Engl. J. Med.* **2006**, *355* (23), 2427–2443.
- (31) Aquilante, C. L. Sulfonylurea Pharmacogenomics in Type 2 Diabetes: The Influence of Drug Target and Diabetes Risk Polymorphisms. *Expert Rev. Cardiovasc. Ther.* **2020**, *8* (3), 359–372.
- (32) Genuth, S. Should Sulfonylureas Remain an Acceptable First-Line Add-On to Metformin Therapy in Patients with Type 2 Diabetes? No, It's Time to Move On! *Diabetes Care* **2015**, *38* (1), 170–175.

- (33) Rendell, M. The Role of Sulphonylureas in the Management of Type 2 Diabetes Mellitus. *Drugs* **2004**, *64* (12), 1339–1358.
- (34) Lebovitz, H. E. Thiazolidinediones: The Forgotten Diabetes Medications. *Curr. Diab. Rep.* **2019**, *19* (12), 1–13.
- (35) Soccio, R. E.; Chen, E. R.; Lazar, M. A. Thiazolidinediones and the Promise of Insulin Sensitization in Type 2 Diabetes. *Cell Metab.* **2014**, *20* (4), 573–591.
- (36) Glazer, n. B.; Cheatham, W. W.; Benbow, A.; Stewart, M.; Yeoman, G. Thiazolidinediones for Type 2 Diabetes. *BMJ* **2001**, *321*, 252–253.
- (37) Green, B. D.; Flatt, P. R.; Bailey, C. J. Dipeptidyl Peptidase IV (DPP IV) Inhibitors: A Newly Emerging Drug Class for the Treatment of Type 2 Diabetes. *Diabetes Vasc. Dis. Res.* **2006**, *3* (3), 159–165.
- (38) Drucker, D. J. Therapeutic Potential of Dipeptidyl Peptidase IV Inhibitors for the Treatment of Type 2 Diabetes. *Expert Opin. Investig. Drugs* **2003**, *12* (1), 87–100.
- (39) Nauck, M. A.; Meier, J. J. Are All GLP-1 Agonists Equal in the Treatment of Type 2 Diabetes? *Eur. J. Endocrinol.* **2019**, *181* (6), R211–R234.
- (40) Yang, C. Y.; Chen, Y. R.; Ou, H. T.; Kuo, S. Cost-Effectiveness of GLP-1 Receptor Agonists versus Insulin for the Treatment of Type 2 Diabetes: A Real-World Study and Systematic Review. *Cardiovasc. Diabetol.* **2021**, *20* (1), 1–10.
- (41) Nauck, M. A.; Quast, D. R.; Wefers, J.; Meier, J. J. GLP-1 Receptor Agonists in the Treatment of Type 2 Diabetes – State-of-the-Art. *Mol. Metab.* **2020**, *46*, 101102.
- (42) Brunton, S. A.; Wysham, C. H. GLP-1 Receptor Agonists in the Treatment of Type 2 Diabetes: Role and Clinical Experience to Date. *Postgrad. Med.* **2020**, *132* (sup2), 3–14.

- (43) Galstyan, G. R.; Karataeva, E. A.; Yudovich, E. A. Evolution of Glucagon-like Peptide-1 Receptor Agonists for the Treatment of Type 2 Diabetes. *Diabetes Mellit.* **2017**, *20* (4), 286–298.
- (44) McCall, A. L. Insulin Therapy and Hypoglycemia. *Insul. Ther.* **2002**, *41* (1), 193–222.
- (45) Müller, T. D.; Finan, B.; Bloom, S. R.; D'Alessio, D.; Drucker, D. J.; Flatt, P. R.; Fritsche, A.; Gribble, F.; Grill, H. J.; Habener, J. F.; Holst, J. J.; Langhans, W.; Meier, J. J.; Nauck, M. A.; Perez-Tilve, D.; Pocai, A.; Reimann, F.; Sandoval, D. A.; Schwartz, T. W.; Seeley, R. J.; Stemmer, K.; Tang-Christensen, M.; Woods, S. C.; DiMarchi, R. D.; Tschöp, M. H. Glucagon-like Peptide 1 (GLP-1). *Mol. Metab.* **2019**, *30* (September), 72–130.
- (46) Baggio, L. L.; Drucker, D. J. Biology of Incretins: GLP-1 and GIP. *Gastroenterology* **2007**, *132*, 2131–2157.
- (47) Eng, J.; Andrews, P. C.; Kleinman, W. A.; Singh, L.; Raufman, J. P. Purification and Structure of Exendin-3, a New Pancreatic Secretagogue Isolated from *Heloderma Horridum* Venom. *J. Biol. Chem.* **1990**, *265* (33), 20259–20262.
- (48) Holz, G. G.; Leech, C. A.; Habener, J. F. Insulinotropic Toxins as Molecular Probes for Analysis of Glucagon-like Peptide-1 Receptor-Mediated Signal Transduction in Pancreatic  $\beta$ -Cells. *Biochimie* **2000**, *82* (9–10), 915–926.
- (49) Vandermeers, A.; Vandermeers-Piret, M. C.; Robberecht, P.; Waelbroeck, M.; Dehaye, J. P.; Winand, J.; Christophe, J. Purification of a Novel Pancreatic Secretory Factor (PSF) and a Novel Peptide with VIP- and Secretin-like Properties (Helodermin) from Gila Monster Venom. *FEBS Lett.* **1984**, *166* (2), 273–276.
- (50) Raufman, J. P.; Jensen, R. T.; Sutliff, V. E.; Pisano, J. J.; Gardner, J. D. Actions of Gila Monster

- Venom on Dispersed Acini from Guinea Pig Pancreas. *Am. J. Physiol.* **1982**, 242 (5), G470–G474.
- (51) Parker, D. S.; Raufman, J. P.; O'Donohue, T. L.; Bledsoe, M.; Yoshida, H.; Pisano, J. J. Amino Acid Sequences of Helospectins, New Members of the Glucagon Superfamily, Found in Gila Monster Venom. *J. Biol. Chem.* **1984**, 259 (19), 11751–11755.
- (52) Hoshino, M.; Yanaihara, C.; Hong, Y. M.; Kishida, S.; Katsumaru, Y.; Vandermeers, A.; Vandermeers-Piret, M. C.; Robberecht, P.; Christophe, J.; Yanaihara, N. Primary Structure of Helodermin, a VIP-Secretin-like Peptide Isolated from Gila Monster Venom. *FEBS Lett.* **1984**, 178 (2), 233–239.
- (53) Eng, J.; Kleinman, W. A.; Singh, L.; Singh, G.; Raufman, J. P. Isolation and Characterization of Exendin-4, an Exendin-3 Analogue, from *Heloderma Suspectum* Venom. Further Evidence for an Exendin Receptor on Dispersed Acini from Guinea Pig Pancreas. *J. Biol. Chem.* **1992**, 267 (11), 7402–7405.
- (54) Yap, M. K. K.; Misuan, N. Exendin-4 from *Heloderma Suspectum* Venom: From Discovery to Its Latest Application as Type II Diabetes Combatant. *Basic Clin. Pharmacol. Toxicol.* **2019**, 124 (5), 513–527.
- (55) Neidigh, J. W.; Fesinmeyer, R. M.; Prickett, K. S.; Andersen, N. H. Exendin-4 and Glucagon-like-Peptide-1: NMR Structural Comparisons in the Solution and Micelle-Associated States. *Biochemistry* **2001**, 40 (44), 13188–13200.
- (56) Horsch, D.; Goke, R.; Eissele, R.; Michael, B.; Goke, B. Reciprocal Cellular Distribution of Glucagon-like Peptide-1 (GLP-1) Immunoreactivity and GLP-1 Receptor mRNA in Pancreatic Islets of Rat. *Pancreas* **1997**, 14 (3), 290–294.

- (57) Goke, R.; Larsen, P. J.; Mikkelsen, J. D.; Sheikh, S. P. Distribution of GLP-1 Binding Sites in the Rat Brain: Evidence That Exendin-4 Is a Ligand of Brain GLP-1 Binding Sites. *Eur. J. Neurosci.* **1995**, *7* (11), 2294–2300.
- (58) Uttenthal, L. O.; Blázquez, E. Characterization of High-Affinity Receptors for Truncated Glucagon-like Peptide-1 in Rat Gastric Glands. *FEBS Lett.* **1990**, *262* (1), 139–141.
- (59) Valverde, I.; Merida, E.; Delgado, E.; Trapote, M.; Villanueva-Penacarrillo, M. Presence and Characterization of Glucagon-like Peptide-1(7-36) Amide Receptors in Solubilized Membranes of Rat Adipose Tissue. *Endocrinology* **1993**, *132* (1), 75–79.
- (60) Muscogiuri, G.; DeFronzo, R. A.; Gastaldelli, A.; Holst, J. J. Glucagon-like Peptide-1 and the Central/Peripheral Nervous System: Crosstalk in Diabetes. *Trends Endocrinol. Metab.* **2017**, *28* (2), 88–103.
- (61) Baggio, L. L.; Drucker, D. J. Glucagon-like Peptide-1 Receptors in the Brain: Controlling Food Intake and Body Weight. *J. Clin. Invest.* **2014**, *124* (10), 4223–4226.
- (62) Kanoski, S. E.; Fortin, S. M.; Arnold, M.; Grill, H. J.; Hayes, M. R. Peripheral and Central GLP-1 Receptor Populations Mediate the Anorectic Effects of Peripherally Administered GLP-1 Receptor Agonists, Liraglutide and Exendin-4. *Endocrinology* **2011**, *152* (8), 3103–3112.
- (63) Hayes, M. R.; De Jonghe, B. C.; Kanoski, S. E. Role of the Glucagon-like-Peptide-1 Receptor in the Control of Energy Balance. *Physiol. Behav.* **2010**, *100* (5), 503–510.
- (64) Hayes, M. R.; Mietlicki-Baase, E. G.; Kanoski, S. E.; De Jonghe, B. C. Incretins and Amylin: Neuroendocrine Communication between the Gut, Pancreas, and Brain in Control of Food Intake and Blood Glucose. *Annu. Rev. Nutr.* **2014**, *34*, 237–260.
- (65) Kanoski, S. E.; Hayes, M. R.; Skibicka, K. P. GLP-1 and Weight Loss: Unraveling the Diverse

- Neural Circuitry. *Am. J. Physiol. - Regul. Integr. Comp. Physiol.* **2016**, *310* (10), R885–R895.
- (66) Drucker, D. J. The Biology of Incretin Hormones. *Cell Metab.* **2006**, *3* (3), 153–165.
- (67) Miller, A. D.; Leslie, R. A. The Area Postrema and Vomiting. *Frontiers in Neuroendocrinology.* **1994**, *15* (4), 301–320.
- (68) B.J., Y.; M.F., C.; D.J., M.; A.A., M. Integration of Vestibular and Emetic Gastrointestinal Signals That Produce Nausea and Vomiting: Potential Contributions to Motion Sickness Bill. *Exp. Brain Res.* **2014**, *27* (4), 1–19.
- (69) Babic, T.; Browning, K. N. The Role of Vagal Neurocircuits in the Regulation of Nausea and Vomiting. *Eur. J. Pharmacol.* **2014**, *722*, 38–47.
- (70) Bergenstal, R. M.; Wysham, C.; MacConell, L.; Malloy, J.; Walsh, B.; Yan, P.; Wilhelm, K.; Malone, J.; Porter, L. E. Efficacy and Safety of Exenatide Once Weekly versus Sitagliptin or Pioglitazone as an Adjunct to Metformin for Treatment of Type 2 Diabetes (DURATION-2): A Randomised Trial. *Lancet* **2010**, *376* (9739), 431–439.
- (71) Buse, J. B.; Henry, R. R.; Han, J.; Kim, D. D.; Fineman, M. S.; Baron, A. D. Effects of Exenatide (Exendin-4) on Glycemic Control over 30 Weeks in Sulfonylurea-Treated Patients with Type 2 Diabetes. *Diabetes Care* **2004**, *27* (11), 2628–2635.
- (72) DeFronzo, R. A.; Ratner, R. E.; Han, J.; Kim, D. D.; Fineman, M. S.; Baron, A. D. Effects of Exenatide (Exendin-4) on Glycemic Control and Weight over 30 Weeks in Metformin-Treated Patients with Type 2 Diabetes. *Diabetes Care* **2005**, *28* (5), 1092–1100.
- (73) John, L. E.; Kane, M. P.; Busch, R. S.; Hamilton, R. A. Expanded Use of Exenatide in the Management of Type 2 Diabetes. *Diabetes Spectr.* **2007**, *20* (1), 59–63.
- (74) Kendall, D. M.; Riddle, M. C.; Rosenstock, J.; Zhuang, D.; Kim, D. D.; Fineman, M. S.; Baron,



- A. D. Effects of Exenatide (Exendin-4) on Glycemic Control over 30 Weeks in Patients with Type 2 Diabetes Treated with Metformin and a Sulfonylurea. *Diabetes Care* **2005**, *28* (5), 1083–1091.
- (75) Weinstock, R. S.; Guerci, B.; Umpierrez, G.; Nauck, M. A.; Skrivanek, Z.; Milicevic, Z. Safety and Efficacy of Once-Weekly Dulaglutide versus Sitagliptin after 2years in Metformin-Treated Patients with Type 2 Diabetes (AWARD-5): A Randomized, Phase III Study. *Diabetes, Obes. Metab.* **2015**, *17* (9), 849–858.
- (76) Wang, T.; Gou, Z.; Wang, F.; Nling, M.; Zhai, S. Di. Comparison of GLP-1 Analogues versus Sitagliptin in the Management of Type 2 Diabetes: Systematic Review and Meta-Analysis of Head-to-Head Studies. *PLoS One* **2014**, *9* (8).
- (77) Bettge, K.; Kahle, M.; Abd El Aziz, M. S.; Meier, J. J.; Nauck, M. A. Occurrence of Nausea, Vomiting and Diarrhoea Reported as Adverse Events in Clinical Trials Studying Glucagon-like Peptide-1 Receptor Agonists: A Systematic Analysis of Published Clinical Trials. *Diabetes, Obes. Metab.* **2017**, *19* (3), 336–347.
- (78) Kennedy, D. O. B Vitamins and the Brain : Mechanisms , Dose and Efficacy - A Review. *Nutrients* **2016**, *8* (2), 68.
- (79) Leary, F. O.; Samman, S. Vitamin B12 in Health and Disease. *Nutrients* **2010**, *2* (3), 299–316.
- (80) Petrus, A. K.; Fairchild, T. J.; Doyle, R. P. Traveling the Vitamin B12 Pathway: Oral Delivery of Protein and Peptide Drugs. *Angew. Chemie - Int. Ed.* **2009**, *48* (6), 1022–1028.
- (81) Shipton, M. J.; Thachil, J. Vitamin B12 Deficiency - A 21st Century Perspective. *Clin. Med. J. R. Coll. Physicians London* **2015**, *15* (2), 145–150.

- (82) Gherasim, C.; Lofgren, M.; Banerjee, R. Navigating the B12 Road: Assimilation, Delivery, and Disorders of Cobalamin. *J. Biol. Chem.* **2013**, *288* (19), 13186–13193.
- (83) Clardy, S. M.; Allis, D. G.; Fairchild, T. J.; Doyle, R. P. Vitamin B12 in Drug Delivery: Breaking through the Barriers to a B12 Bioconjugate Pharmaceutical. *Expert Opin. Drug Deliv.* **2011**, *8* (1), 127–140.
- (84) Stupperich, E.; Nexø, E. Effect of the Cobalt-N Coordination on the Cobamide Recognition by the Human Vitamin B Binding Proteins Intrinsic Factor, Transcobalamin and Haptocorrin. *Eur. J. Biochem.* **1991**, *199* (2), 299–303.
- (85) Nielsen, M. J.; Rasmussen, M. R.; Andersen, C. B. F.; Nexø, E.; Moestrup, S. K. Vitamin B 12 Transport from Food to the Body's Cells - A Sophisticated, Multistep Pathway. *Nat. Rev. Gastroenterol. Hepatol.* **2012**, *9* (6), 345–354.
- (86) Randaccio, L.; Geremia, S.; Demitri, N.; Wuerges, J. Vitamin B12: Unique Metalorganic Compounds and the Most Complex Vitamins. *Molecules* **2010**, *15*, 3228–3259.
- (87) Stubbe, J. Binding Site Revealed of Nature's Most Beautiful Cofactor. *Science* **1994**, *266* (5191), 1663–1664.
- (88) Scott, J. M.; Molloy, M. The Discovery of Vitamin B 12. *Ann. Nutr. Metab.* **2012**, *61* (3), 239–245.
- (89) Combe, J. S. History of a Case of Anemia. *Trans. Medico-Chirurgical Soc. Edinburgh* **1824**, 194–204.
- (90) Whitby, S. L. The Evolution of the Treatment of Addisonian Anaemia. *Br. Med. J.* **1955**, *1*, 1401–1406.
- (91) Russell, J. S.; Batten, F. E.; Collier, J. Subacute Combined Degeneration of the Spinal Cord.

- Brain* **1900**, 23, 39–100.
- (92) Minot, G. R.; Murphy, W. P. Treatment of Pernicious Anemia by a Special Diet. *J. Am. Med. Assoc.* **1926**, 87 (20), 470–476.
- (93) Castle, W. B. On The Etiological Relationship of Achylia Gastrica To Pernicious Anemia. *Am. J. Med. Sci.* **1929**, 178 (6), 748–763.
- (94) Castle, W. B.; Ham, T. H. OBSERVATIONS ON THE ETIOLOGIC RELATIONSHIP OF ACHYLIA GASTRICA TO PERNICIOUS ANEMIA: V. FURTHER EVIDENCE FOR THE ESSENTIAL PARTICIPATION OF EXTRINSIC FACTOR IN HEMATOPOIETIC RESPONSES TO MIXTURES OF BEEF MUSCLE AND GASTRIC JUICE AND TO HOG STOMACH MUCOSA. *J. Am. Med. Assoc.* **1936**, 107 (18), 1456–1463.
- (95) Smith, E. L. Purification of Anti-Pernicious Anaemia Factors from Liver. *Nature* **1948**, 161, 638–639.
- (96) Smith, E. L.; Parker, L. F. J. Purification of Anti-Pernicious Anaemia Factor. *Biochem. J.* **1948**, 43 (1), viii.
- (97) Shorb, M. S. Activity of Vitamin B12 for the Growth of *Lactobacillus Lactis*. *Science* **1948**, 107 (2781), 397–398.
- (98) Rickes, E. L.; Brink, N. G.; Koniuszy, F. R.; Wood, T. R.; Folkers, K. Crystalline Vitamin B12. *Science* **1948**, 107 (2781), 396–397.
- (99) Smith, E. L. Presence of Cobalt in the Anti-Pernicious Anemia Factor. *Nature* **1948**, 162, 144–145.
- (100) Rickes, E. L.; Brink, N. G.; Koniuszy, F. R.; Wood, T. R.; Folkers, K. Vitamin B12, A Cobalt Complex. *Science* **1948**, 108 (2797), 134.

- (101) Brink, C.; WHITE, J. G.; HODGKIN, D. C.; LINDSEY, J.; PICKWORTH, J.; ROBERTSON, J. H. X-Ray Crystallographic Evidence on the Structure of Vitamin B12. *Nature* **1954**, *174* (4443), 1169–1171.
- (102) Brink, N. G.; Kuehl, F. A.; Folkers, K. Vitamin B12: The Identification of Vitamin B12 as a Cyano-Cobalt Coordination Complex. *Science* **1950**, *112* (2909), 354.
- (103) Hodgkin, D. C.; Kamoer, J.; Mackay, M.; Pickworth, J. Structure of Vitamin B12. *Nature* **1956**, *178*, 64–66.
- (104) Howard, J. A. K. Dorothy Hodgkin and Her Contributions To Biochemistry. *Nat. Rev. Mol. Cell Biol.* **2003**, *4*, 891–896.
- (105) Woodward, R. B. The Total Synthesis of Vitamin B12. *Pure Appl. Chem.* **1973**, *33* (1), 145–178.
- (106) IUPAC-IUB Commission on Biochemical Nomenclature. The Nomenclature of Corrinoids. *Biochemistry* **1974**, *13* (7), 1555–1560.
- (107) Shemin, D.; Bray, R. C. THE BIOSYNTHESIS OF THE CORRIN STRUCTURE OF VITAMIN B12. *Ann. N. Y. Acad. Sci.* **1964**, *112* (2), 615–621.
- (108) Fedosov, S. N.; Ruetz, M.; Gruber, K.; Fedosova, N. U.; Kräutler, B. A Blue Corrinoid from Partial Degradation of Vitamin B 12 in Aqueous Bicarbonate: Spectra, Structure, and Interaction with Proteins of B 12 Transport. *Biochemistry* **2011**, *50* (37), 8090–8101.
- (109) Zhou, K.; Zelder, F. Identification of Diastereomeric Cyano - Aqua Cobinamides with a Backbone-Modified Vitamin B12 Derivative and with <sup>1</sup>H NMR Spectroscopy. *Eur. J. Inorg. Chem.* **2011**, No. 1, 53–57.
- (110) Paul, C.; Brady, D. M. Comparative Bioavailability and Utilization of Particular Forms of B12

- Supplements with Potential to Mitigate B12-Related Genetic Polymorphisms. *Integr. Med.* **2017**, *16* (1), 42–49.
- (111) Banerjee, R.; Ragsdale, S. W. The Many Faces of Vitamin B12: Catalysis by Cobalamin-Dependent Enzymes. *Annu. Rev. Biochem.* **2003**, *72*, 209–247.
- (112) Krautler, B. Vitamin B 12 : Chemistry and Biochemistry. *Biochem. Soc. Trans.* **2005**, *33*, 806–810.
- (113) Fang, H.; Kang, J.; Zhang, D. Microbial Production of Vitamin B12: A Review and Future Perspectives. *Microb. Cell Fact.* **2017**, *16* (1), 1–14.
- (114) Hassan, S.; Jackowska, A.; Gryko, D. Truncated Vitamin B12 Derivative with the Phosphate Group Retained. *J. Porphyr. Phthalocyanines* **2019**, *23*, 555–560.
- (115) Broderick, K. E.; Potluri, P.; Zhuang, S.; Scheffler, I. E.; Sharma, V. S.; Pilz, R. B.; Boss, G. R. Cyanide Detoxification by the Cobalamin Precursor Cobinamide. *Exp. Biol. Medicin* **2006**, *231* (5), 641–649.
- (116) Green, R.; Allen, L. H.; Bjørke-Monsen, A. L.; Brito, A.; Guéant, J. L.; Miller, J. W.; Molloy, A. M.; Nexø, E.; Stabler, S.; Toh, B. H.; Ueland, P. M.; Yajnik, C. Vitamin B12 Deficiency. *Nat. Rev. Dis. Prim.* **2017**, *3*.
- (117) Wierzba, A. J.; Hassan, S.; Gryko, D. Synthetic Approaches toward Vitamin B12 Conjugates. *Asian J. Org. Chem.* **2019**, *8* (1), 6–24.
- (118) Ma, J.; Dasgupta, P. K.; Zelder, F. H.; Boss, G. R. Cobinamide Chemistries for Photometric Cyanide Determination. A Merging Zone Liquid Core Waveguide Cyanide Analyzer Using Cyanoaquacobinamide. *Anal. Chim. Acta* **2012**, *736*, 78–84.
- (119) Ó Proinsias, K.; Karczewski, M.; Zieleniewska, A.; Gryko, D. Microwave-Assisted

- Cobinamide Synthesis. *J. Org. Chem.* **2014**, *79* (16), 7752–7757.
- (120) Wedemeyer-Exl, C.; Darbre, T.; Keese, R. Preparation of Dicyano- and Methylcobinamide from Vitamin B12a. *Synthesis (Stuttg.)* **2008**, No. 21, 3429–3432.
- (121) Fanchiang, Y. T.; Bratt, G. T.; Hogenkamp, H. P. Methyl Transfer from Methylcobalamin to Diaquocobinamide. *Proc. Natl. Acad. Sci. U. S. A.* **1984**, *81* (9), 2698–2702.
- (122) Marques, H. M.; Kenneth, C. B.; Brooks, H. The Ligand-Substitution Reactions of Aqua Hydroxocobinamide Proceed through a Dissociative Interchange Mechanism. *J. Am. Chem. Soc. Dalt. Trans.* **1993**, 3475–3478.
- (123) Anantharam, P.; Whitley, E. M.; Mahama, B.; Kim, D. S.; Sarkar, S.; Santana, C.; Chan, A.; Kanthasamy, A. G.; Kanthasamy, A.; Boss, G. R.; Rumbleiha, W. K. Cobinamide Is Effective for Treatment of Hydrogen Sulfide-Induced Neurological Sequelae in a Mouse Model. *Ann. N. Y. Acad. Sci.* **2017**, *1408* (1), 61–78.
- (124) Hendry-Hofer, T. B.; Ng, P. C.; McGrath, A. M.; Mukai, D.; Brenner, M.; Mahon, S.; Maddry, J. K.; Boss, G. R.; Bebartha, V. S. Intramuscular Aminotetrazole Cobinamide as a Treatment for Inhaled Hydrogen Sulfide Poisoning in a Large Swine Model. *Ann. N. Y. Acad. Sci.* **2020**, *1479* (1), 159–167.
- (125) Männel-Croisé, C.; Probst, B.; Zelder, F. A Straightforward Method for the Colorimetric Detection of Endogenous Biological Cyanide. *Anal. Chem.* **2009**, *81* (22), 9493–9498.
- (126) Chan, A.; Jiang, J.; Fridman, A.; Guo, L. T.; Shelton, G. D.; Liu, M. T.; Green, C.; Haushalter, K. J.; Patel, H. H.; Lee, J.; Yoon, D.; Burney, T.; Mukai, D.; Mahon, S. B.; Brenner, M.; Pilz, R. B.; Boss, G. R. Nitrocobinamide, a New Cyanide Antidote That Can Be Administered by Intramuscular Injection. *J. Med. Chem.* **2015**, *58* (4), 1750–1759.

- (127) Chan, A.; Balasubramanian, M.; Blackledge, W.; Mohammad, O. M.; Alvarez, L.; Boss, G. R.; Bigby, T. D. Cobinamide Is Superior to Other Treatments in a Mouse Model of Cyanide Poisoning. *Clin. Toxicol.* **2010**, *48* (7), 709–717.
- (128) Lee, J.; Mahon, S. B.; Mukai, D.; Burney, T.; Katebian, B. S.; Chan, A.; Bebarta, V. S.; Yoon, D.; Boss, G. R.; Brenner, M. The Vitamin B12 Analog Cobinamide Is an Effective Antidote for Oral Cyanide Poisoning. *J. Med. Toxicol.* **2016**, *12* (4), 370–379.
- (129) Greenawald, L. A.; Snyder, J. L.; Fry, N. L.; Sailor, M. J.; Boss, G. R.; Finklea, H. O.; Bell, S. Development of a Cobinamide-Based End-of-Service-Life Indicator for Detection of Hydrogen Cyanide Gas. *Sensors ad actuators. B, Chem.* **2015**, *221*, 379–385.
- (130) Brenner, M.; Mahon, S. B.; Lee, J.; Kim, J.; Mukai, D.; Goodman, S.; Kreuter, K. A.; Ahdout, R.; Mohammad, O.; Sharma, V. S.; Blackledge; Boss, G. R. Comparison of Cobinamide to Hydroxocobalamin in Reversing Cyanide Physiologic Effects in Rabbits Using Diffuse Optical Spectroscopy Monitoring. *J. Biomed. Opt.* **2010**, *15* (1), 017001.
- (131) Hardlei, T. F.; Nexo, E. A New Principle for Measurement of Cobalamin and Corrinoids, Used for Studies of Cobalamin Analogs on Serum Haptocorrin. *Clin. Chem.* **2009**, *55* (5), 1002–1010.
- (132) Uchino, H.; Yagiri, Y.; Yoshino, T.; Kondo, M.; Wakisaka, G. Conversion of Cyano- and Hydroxo-Cobalamin in Vivo into Co-Enzyme Form of Vitamin B12 in the Rat. *Nature* **1965**, *205*, 176–177.
- (133) Obeid, R.; Fedosov, S. N.; Nexo, E. Cobalamin Coenzyme Forms Are Not Likely to Be Superior to Cyano- and Hydroxyl-Cobalamin in Prevention or Treatment of Cobalamin Deficiency. *Mol. Nutr. Food Res.* **2015**, *59* (7), 1364–1372.

- (134) Chen, L. H.; Liu, M. L.; Hwang, H. Y.; Chen, L. S.; Korenberg, J.; Shanet, B. Human Methionine Synthase: CDBA Cloning, Gene Localization, and Expression. *J. Biol. Chem.* **1997**, *272* (6), 3628–3634.
- (135) Banerjee, R. V.; Matthews, R. G. Cobalamin-dependent Methionine Synthase. *FASEB J.* **1990**, *4* (5), 1450–1459.
- (136) Padmakumar, R.; Taoka, S.; Padmakumar, R.; Baneijee, R. Coenzyme B12 Is Coordinated by Histidine and Not Dimethylbenzimidazole on Methylmalonyl-CoA Mutase. *J. Am. Chem. Soc.* **1995**, *117*, 7033–7034.
- (137) Takahashi-Iñiguez, T.; García-Hernandez, E.; Arreguín-Espinosa, R.; Flores, M. E. Role of Vitamin B12 on Methylmalonyl-CoA Mutase Activity. *J. Zhejiang Univ. Sci. B* **2012**, *13* (6), 423–437.
- (138) Bonaccorso, R. L.; Chepurny, O. G.; Becker-Paully, C.; Holz, G. G.; Doyle, R. P. Enhanced Peptide Stability Against Protease Digestion Induced by Intrinsic Factor Binding of a Vitamin B12 Conjugate of Exendin-4. *Mol. Pharm.* **2015**, *12* (9), 3502–3506.
- (139) Fedosov, S. N.; Fedosova, N. U.; Kräutler, B.; Nexø, E.; Petersen, T. E. Mechanisms of Discrimination between Cobalamins and Their Natural Analogues during Their Binding to the Specific B12-Transporting Proteins. *Biochemistry* **2007**, *46* (21), 6446–6458.
- (140) Clardy-James, S.; Chepurny, O. G.; Leech, C. A.; Holz, G. G.; Doyle, R. P. Synthesis, Characterization and Pharmacodynamics of Vitamin-B12-Conjugated Glucagon-Like Peptide-1. *ChemMedChem* **2013**, *8* (4), 582–586.
- (141) Greibe, E.; Fedosov, S.; Nexø, E. The Cobalamin-Binding Protein in Zebrafish Is an Intermediate between the Three Cobalamin-Binding Proteins in Human. *PLoS One* **2012**, *7*



- (4), e35660.
- (142) Abu-Soud, H. M.; Maitra, D.; Byun, J.; Souza, C. E. A.; Banerjee, J.; Saed, G. M.; Diamond, M. P.; Andreana, P. R.; Pennathur, S. The Reaction of HOCl and Cyanocobalamin: Corrin Destruction and the Liberation of Cyanogen Chloride. *Free Radic. Biol. Med.* **2012**, *52* (3), 616–625.
- (143) Ahmad, I.; Qadeer, K.; Zahid, S.; Sheraz, M. A.; Ismail, T.; Hussain, W.; Ansari, I. A. Effect of Ascorbic Acid on the Degradation of Cyanocobalamin and Hydroxocobalamin in Aqueous Solution: A Kinetic Study. *AAPS PharmSciTech* **2014**, *15* (5), 1324–1333.
- (144) Dion, H. W.; Calkins, D. G.; Piffner, J. J. Hydrolysis Products of Pseudovitamin B12. *J. Am. Chem. Soc.* **1952**, *74* (4), 1108.
- (145) Bonnett, R.; Raleigh, J. A.; Redman, D. G. The Hydrolysis of Vitamin B12. Studies with Model Amides. *J. Am. Chem. Soc.* **1965**, *87* (7), 1600–1607.
- (146) Fedosov, S. N.; Berglund, L.; Fedosova, N. U.; Nexø, E.; Petersen, T. E. Comparative Analysis of Cobalamin Binding Kinetics and Ligand Protection for Intrinsic Factor, Transcobalamin, and Haptocorrin. *J. Biol. Chem.* **2002**, *277* (12), 9989–9996.
- (147) Furger, E.; Frei, D. C.; Schibli, R.; Fischer, E.; Protá, A. E. Structural Basis for Universal Corrinoid Recognition by the Cobalamin Transport Protein Haptocorrin. *J. Biol. Chem.* **2013**, *288* (35), 25466–25476.
- (148) Burger, R. L.; Schneider, R. J.; Mehlman, C. S.; Allen, R. H. Human Plasma R Type Vitamin B12 Binding Proteins. II. The Role of Transcobalamin I, Transcobalamin III, and the Normal Granulocyte Vitamin B12 Binding Protein in the Plasma Transport of Vitamin B12. *J. Biol. Chem.* **1975**, *250* (19), 7707–7713.

- (149) Jensen, H. R.; Laursen, M. F.; Lildballe, D. L.; Andersen, J. B.; Nexø, E.; Licht, T. R. Effect of the Vitamin B12-Binding Protein Haptocorrin Present in Human Milk on a Panel of Commensal and Pathogenic Bacteria. *BMC Res. Notes* **2011**, *4*, 2–7.
- (150) Samson, R. R.; Mirtle, C.; McClelland, D. B. L. Secretory IgA Does Not Enhance the Bacteriostatic Effects of Iron-Binding or Vitamin B12-Binding Proteins in Human Colostrum. *Immunology* **1979**, *38* (2), 367–36773.
- (151) Mathews, F. S.; Gordon, M. M.; Chen, Z.; Rajashankar, K. R.; Ealick, S. E.; Alpers, D. H.; Sukumar, N. Crystal Structure of Human Intrinsic Factor: Cobalamin Complex at 2.6-Å Resolution. *Proc. Natl. Acad. Sci. U. S. A.* **2007**, *104* (44), 17311–17316.
- (152) Gordon, M. M.; Howard, T.; Becich, M. J.; Alpers, D. H. Cathepsin L Mediates Intracellular Ileal Digestion of Gastric Intrinsic Factor. *Am. J. Physiol.* **1995**, *268* (1), G33–G40.
- (153) Wuerges, J.; Garau, G.; Geremia, S.; Fedosov, S. N.; Petersen, T. E.; Randaccio, L. Structural Basis for Mammalian Vitamin B12 Transport by Transcobalamin. *Proc. Natl. Acad. Sci. U. S. A.* **2006**, *103* (12), 4386–4391.
- (154) Christensen, P. A.; Brynskov, J.; Gimsing, P.; Petersen, J. Vitamin B12 Binding Proteins (Transcobalamin and Haptocorrin) in Serum and Synovial Fluid of Patients with Rheumatoid Arthritis and Traumatic Synovitis. *Scand. J. Rheumatol.* **1983**, *12* (3), 268–272.
- (155) Savage, C. R.; Green, P. D. Biosynthesis of Transcobalamin II by Adult Rat Liver Parenchymal Cells in Culture. *Arch. Biochem. Biophys.* **1976**, *173* (2), 691–702.
- (156) Quadros, E. V.; Sequeira, J. M. Cellular Uptake of Cobalamin: Transcobalamin and the TCbIR/CD320 Receptor. *Biochimie* **2013**, *95* (5), 1008–1018.
- (157) Chakraborty, C.; Hsu, C.; Wen, Z.; Lin, C.; Agoramoorthy, G. Zebrafish: A Complete Animal

- Model for In Vivo Drug Discovery and Development. *Curr. Drug Metab.* **2009**, *10* (2), 116–124.
- (158) Lieschke, G. J.; Currie, P. D. Animal Models of Human Disease: Zebrafish Swim into View. *Nat. Rev. Genet.* **2007**, *8* (5), 353–367.
- (159) Murphey, R. D.; Zon, L. I. Small Molecule Screening in the Zebrafish. *Methods* **2006**, *39* (3), 255–261.
- (160) Richter, S.; Schulze, U.; Tomancák, P.; Oates, A. C. Small Molecule Screen in Embryonic Zebrafish Using Modular Variations to Target Segmentation. *Nat. Commun.* **2017**, *8* (1).
- (161) Morkbak, A. L.; Poulsen, S. S.; Nexø, E. Haptocorrin in Humans. *Clin. Chem. Lab. Med.* **2007**, *45* (12), 1751–1759.
- (162) Wang, J.; Tan, J.; Luo, J.; Huang, P.; Zhou, W.; Chen, L.; Long, L.; Zhang, L. ming; Zhu, B.; Yang, L.; Deng, D. Y. B. Enhancement of Scutellarin Oral Delivery Efficacy by Vitamin B12-Modified Amphiphilic Chitosan Derivatives to Treat Type II Diabetes Induced-Retinopathy. *J. Nanobiotechnology* **2017**, *15* (1), 1–17.
- (163) Bryda, E. C. Science of Medicine. *Mo. Med.* **203AD**, *110* (3), 207–277.
- (164) Ellenbroek, B.; Youn, J. Rodent Models in Neuroscience Research: Is It a Rat Race? *Dis. Model. Mech.* **2016**, *9* (10), 1079–1087.
- (165) Hygum, K.; Lildballe, D. L.; Greibe, E. H.; Morkbak, A. L.; Poulsen, S. S.; Sorensen, B. S.; Petersen, T. E.; Nexø, E. Mouse Transcobalamin Has Features Resembling Both Human Transcobalamin and Haptocorrin. *PLoS One* **2011**, *6* (5).
- (166) Kalra, S.; Seetharam, S.; Yammani, R. R.; Seetharam, B. Rat Transcobalamin: Cloning and Regulation of mRNA Expression. *J. Physiol.* **2004**, *556* (2), 623–635.

- (167) Borner, T.; Workinger, J. L.; Tinsley, I. C.; Fortin, S. M.; Stein, L. M.; Chepurny, O. G.; Holz, G. G.; Wierzba, A. J.; Gryko, D.; Nexø, E.; Shaulson, E. D.; Bamezai, A.; Da Silva, V. A. R.; De Jonghe, B. C.; Hayes, M. R.; Doyle, R. P. Corination of a GLP-1 Receptor Agonist for Glycemic Control without Emesis. *Cell Rep.* **2020**, *31* (11), 107768.
- (168) Mietlicki-Baase, E. G.; Liberini, C. G.; Workinger, J. L.; Bonaccorso, R. L.; Borner, T.; Reiner, D. J.; Koch-Laskowski, K.; McGrath, L. E.; Lhamo, R.; Stein, L. M.; De Jonghe, B. C.; Holz, G. G.; Roth, C. L.; Doyle, R. P.; Hayes, M. R. A Vitamin B12 Conjugate of Exendin-4 Improves Glucose Tolerance without Associated Nausea or Hypophagia in Rodents. *Diabetes, Obes. Metab.* **2018**, *20* (5), 1223–1234.
- (169) Russell-Jones, G. J.; Westwood, S. W.; Farnworth, P. G.; Findlay, J. K.; Burger, H. G. Synthesis of LHRH Antagonists Suitable for Oral Administration via the Vitamin B12 Uptake System. *Bioconjug. Chem.* **1995**, *6* (1), 34–42.
- (170) Petrus, A. K.; Vortherms, A. R.; Fairchild, T. J.; Doyle, R. P. Vitamin B12 as a Carrier for the Oral Delivery of Insulin. *ChemMedChem* **2007**, *2* (12), 1717–1721.
- (171) Shah, R. B.; Patel, M.; Maahs, D. M.; Shah, V. N. Insulin Delivery Methods: Past, Present and Future. *Int. J. Pharm. Investig.* **2016**, *6* (1), 1–9.
- (172) Henry, K. E.; Elfers, C. T.; Burke, R. M.; Chepurny, O. G.; Holz, G. G.; Blevins, J. E.; Roth, C. L.; Doyle, R. P. Vitamin B12 Conjugation of Peptide-YY3-36 Decreases Food Intake Compared to Native Peptide-YY3-36 upon Subcutaneous Administration in Male Rats. *Endocrinology* **2015**, *156* (5), 1739–1749.
- (173) Borner, T.; Shaulson, E. D.; Tinsley, I. C.; Stein, L. M.; Horn, C. C.; Hayes, M. R.; Doyle, R. P.; De Jonghe, B. C. A Second-Generation Glucagon-like Peptide-1 Receptor Agonist Mitigates

- Vomiting and Anorexia While Retaining Glucoregulatory Potency in Lean Diabetic and Emetic Mammalian Models. *Diabetes, Obes. Metab.* **2020**, *22* (10), 1729–1741.
- (174) Toräng, S.; Veedfald, S.; Rosenkilde, M. M.; Hartmann, B.; Holst, J. J. The Anorexic Hormone Peptide Yy3-36 Is Rapidly Metabolized to Inactive Peptide Yy3-34 in Vivo. *Physiol. Rep.* **2015**, *3* (7), 1–8.
- (175) Ikotun, O. F.; Marquez, B. V.; Fazen, C. H.; Kahkoska, A. R.; Doyle, R. P.; Lapi, S. E. Investigation of a Vitamin B12 Conjugate as a PET Imaging Probe. *ChemMedChem* **2014**, *9* (6), 1244–1251.
- (176) Chan, S. W.; Lin, G.; Yew, D. T. W.; Yeung, C. K.; Rudd, J. A. Separation of Emetic and Anorexic Responses of Exendin-4, a GLP-1 Receptor Agonist in *Suncus Murinus* (House Musk Shrew). *Neuropharmacology* **2013**, *70* (5–6), 141–147.
- (177) Chan, S. W.; Lin, G.; Yew, D. T. W.; Rudd, J. A. A Physiological Role of Glucagon-like Peptide-1 Receptors in the Central Nervous System of *Suncus Murinus* (House Musk Shrew). *Eur. J. Pharmacol.* **2011**, *668* (1–2), 340–346.
- (178) Hippe, E.; Jorgensen, F. S.; Olesen, H. Cobalamin and Binding Proteins in Stomach and Serum from Various Animal Species Data for B12 Binding Capacities and Molecular Sizes of the Binding Proteins. *Comp. Biochem. Physiol. Part B Comp. Biochem.* **1977**, *56* (3), 305–309.
- (179) Gregory, M. E.; Holdsworth, E. S. A Study of Protein-Binding in the Metabolism of Vitamin B12. *Biochem. J.* **1959**, *72* (4), 549–556.
- (180) Rosenthal, H. L.; Austin, S. Vitamin B12 Unsaturated Binding Capacity of Sera from Various Animals. *Proc. Soc. Exp. Biol. Med.* **1962**, *109*, 179–181.

- (181) Tan, C. H.; Blaisdell, S. J. Characteristics of the Serum Vitamin B12 Binding Substances of Selected Vertebrates. *Comp. Biochem. Physiol. Part B Comp. Biochem.* **1975**, *50* (4), 541–548.
- (182) Gimsing, P.; Nexø, E. Cobalamin-Binding Capacity of Haptocorrin and Transcobalamin: Age-Related Reference Intervals and Values from Patients. *Clin. Chem.* **1989**, *35* (7), 1447–1451.
- (183) Hansen, M.; Brynskov, J.; Christensen, P. A.; Krintel, J. J.; Gimsing, P. Cobalamin Binding Proteins (Haptocorrin and Transcobalamin) in Human Cerebrospinal Fluid. *Scand. J. Haematol.* **1985**, *34* (3), 209–212.
- (184) Greibe, E.; Fedosov, S.; Sørensen, B. S.; Højrup, P.; Poulsen, S. S.; Nexø, E. A Single Rainbow Trout Cobalamin-Binding Protein Stands in for Three Human Binders. *J. Biol. Chem.* **2012**, *287* (40), 33917–33925.
- (185) Proinsias, K.; Giedyk, M.; Gryko, D. Vitamin B12: Chemical Modifications. *Chem. Soc. Rev.* **2013**, *42* (16), 6605–6619.
- (186) Chen, L.; Magliano, D. J.; Zimmet, P. Z. The Worldwide Epidemiology of Type 2 Diabetes Mellitus - Present and Future Perspectives. *Nat. Rev. Endocrinol.* **2012**, *8* (4), 228–236.
- (187) Flegal, K. M.; Carroll, M. D.; Ogden, C. L.; Curtin, L. R. CLINICIAN ' S CORNER Among US Adults , 1999-2008. *J. Am. Med. Assoc.* **2013**, *303* (3), 235–241.
- (188) Sherwin, R.; Jastreboff, A. M. Year in Diabetes 2012: The Diabetes Tsunami. *J. Clin. Endocrinol. Metab.* **2012**, *97* (12), 4293–4301.
- (189) Franks, P. W.; McCarthy, M. I. Exposing the Exposures Responsible for Type 2 Diabetes and Obesity. *Science* **2016**, *354* (6308), 69–73.

- (190) Upadhyay, J.; Polyzos, S. A.; Perakakis, N.; Thakkar, B.; Paschou, S. A.; Katsiki, N.; Underwood, P.; Park, K. H.; Seufert, J.; Kang, E. S.; Sternthal, E.; Karagiannis, A.; Mantzoros, C. S. Pharmacotherapy of Type 2 Diabetes: An Update. *Metabolism*. **2018**, *78*, 13–42.
- (191) Holst, J. J. The Physiology of Glucagon-like Peptide 1. *Physiol. Rev.* **2007**, *87* (4), 1409–1439.
- (192) Lovshin, J. A.; Drucker, D. J. Incretin-Based Therapies for Type 2 Diabetes Mellitus. *Nat. Rev. Endocrinol.* **2009**, *5* (5), 262–269.
- (193) Hayes, M. R.; Schmidt, H. D. GLP-1 Influences Food and Drug Reward. *Curr. Opin. Behav. Sci.* **2016**, *9*, 66–70.
- (194) Madsen, K.; Knudsen, L. B.; Agersøe, H.; Nielsen, P. F.; Thøgersen, H.; Wilken, M.; Johansen, N. L. Structure-Activity and Protraction Relationship of Long-Acting Glucagon-like Peptide-1 Derivatives: Importance of Fatty Acid Length, Polarity, and Bulkiness. *J. Med. Chem.* **2007**, *50* (24), 6126–6132.
- (195) Knudsen, L. B.; Nielsen, P. F.; Huusfeldt, P. O.; Johansen, N. L.; Madsen, K.; Pedersen, F. Z.; Thøgersen, H.; Wilken, M.; Agersø, H. Potent Derivatives of Glucagon-like Peptide-1 with Pharmacokinetic Properties Suitable for Once Daily Administration. *J. Med. Chem.* **2000**, *43* (9), 1664–1669.
- (196) Knudsen, L. B.; Lau, J. The Discovery and Development of Liraglutide and Semaglutide. *Front. Endocrinol. (Lausanne)*. **2019**, *10* (APR), 155.
- (197) O’Neil, P. M.; Birkenfeld, A. L.; McGowan, B.; Mosenzon, O.; Pedersen, S. D.; Wharton, S.; Carson, C. G.; Jepsen, C. H.; Kabisch, M.; Wilding, J. P. H. Efficacy and Safety of Semaglutide Compared with Liraglutide and Placebo for Weight Loss in Patients with Obesity: A Randomised, Double-Blind, Placebo and Active Controlled, Dose-Ranging, Phase 2 Trial.

- Lancet* **2018**, 392 (10148), 637–649.
- (198) Lau, J.; Bloch, P.; Schäffer, L.; Pettersson, I.; Spetzler, J.; Kofoed, J.; Madsen, K.; Knudsen, L. B.; McGuire, J.; Steensgaard, D. B.; Strauss, H. M.; Gram, D. X.; Knudsen, S. M.; Nielsen, F. S.; Thygesen, P.; Reedtz-Runge, S.; Kruse, T. Discovery of the Once-Weekly Glucagon-Like Peptide-1 (GLP-1) Analogue Semaglutide. *J. Med. Chem.* **2015**, 58 (18), 7370–7380.
- (199) Sisley, S.; Gutierrez-Aguilar, R.; Scott, M.; D'Alessio, D.; Sandoval, D.; Seeley, R. Neuronal GLP1R Mediates Liraglutide's Anorectic but Not Glucose-Lowering Effect. *J. Clin. Invest.* **2014**, 124 (6), 2456–2463.
- (200) Secher, A.; Jelsing, J.; Baquero, A. F.; Hecksher-Sørensen, J.; Cowley, M. A.; Dalbøge, L. S.; Hansen, G.; Grove, K. L.; Pyke, C.; Raun, K.; Schäfer, L.; Tang-Christensen, M.; Verma, S.; Witgen, B. M.; Vrang, N.; Knudsen, L. B. The Arcuate Nucleus Mediates GLP-1 Receptor Agonist Liraglutide-Dependent Weight Loss. *J. Clin. Invest.* **2014**, 124 (10), 4473–4488.
- (201) Kanoski, S. E.; Rupprecht, L. E.; Fortin, S. M.; De Jonghe, B. C.; Hayes, M. R. The Role of Nausea in Food Intake and Body Weight Suppression by Peripheral GLP-1 Receptor Agonists, Exendin-4 and Liraglutide. *Neuropharmacology* **2012**, 62 (5–6), 1916–1927.
- (202) Moheet, A.; Moran, A. CF-Related Diabetes: Containing the Metabolic Miscreant of Cystic Fibrosis. *Pediatr. Pulmonol.* **2017**, 52, S37–S43.
- (203) Husain, N. E.; Noor, S. K.; Elmadhoun, W. M.; Almobarak, A. O.; Awadalla, H.; Woodward, C. L.; Mital, D.; Ahmed, M. H. Diabetes, Metabolic Syndrome and Dyslipidemia in People Living with HIV in Africa: Re-Emerging Challenges Not to Be Forgotten. *HIV/AIDS - Res. Palliat. Care* **2017**, 9, 193–202.
- (204) Gallo, M.; Muscogiuri, G.; Felicetti, F.; Faggiano, A.; Trimarchi, F.; Arvat, E.; Vigneri, R.;



- Colao, A. Adverse Glycaemic Effects of Cancer Therapy: Indications for a Rational Approach to Cancer Patients with Diabetes. *Metabolism*. **2018**, *78*, 141–154.
- (205) Ho, T. W.; Huang, C. T.; Ruan, S. Y.; Tsai, Y. J.; Lai, F.; Yu, C. J. Diabetes Mellitus in Patients with Chronic Obstructive Pulmonary Disease-The Impact on Mortality. *PLoS One* **2017**, *12* (4), 1–15.
- (206) Honors, M. A.; Kinzig, K. P. The Role of Insulin Resistance in the Development of Muscle Wasting during Cancer Cachexia. *J. Cachexia. Sarcopenia Muscle* **2012**, *3* (1), 5–11.
- (207) Caughey, G. E.; Roughead, E. E.; Vitry, A. I.; McDermott, R. A.; Shakib, S.; Gilbert, A. L. Comorbidity in the Elderly with Diabetes: Identification of Areas of Potential Treatment Conflicts. *Diabetes Res. Clin. Pract.* **2010**, *87* (3), 385–393.
- (208) Kerr, E. A.; Heisler, M.; Krein, S. L.; Kabeto, M.; Langa, K. M.; Weir, D.; Piette, J. D. Beyond Comorbidity Counts: How Do Comorbidity Type and Severity Influence Diabetes Patients' Treatment Priorities and Self-Management? *J. Gen. Intern. Med.* **2007**, *22* (12), 1635–1640.
- (209) Mannino, D. M.; Thorn, D.; Swensen, A.; Holguin, F. Prevalence and Outcomes of Diabetes, Hypertension and Cardiovascular Disease in COPD. *Eur. Respir. J.* **2008**, *32* (4), 962–969.
- (210) Van De Poll-Franse, L. V.; Houterman, S.; Janssen-Heijnen, M. L. G.; Dercksen, M. W.; Coebergh, J. W. W.; Haak, H. R. Less Aggressive Treatment and Worse Overall Survival in Cancer Patients with Diabetes: A Large Population Based Analysis. *Int. J. Cancer* **2007**, *120* (9), 1986–1992.
- (211) Echouffo-Tcheugui, J. B.; Xu, H.; DeVore, A. D.; Schulte, P. J.; Butler, J.; Yancy, C. W.; Bhatt, D. L.; Hernandez, A. F.; Heidenreich, P. A.; Fonarow, G. C. Temporal Trends and Factors Associated with Diabetes Mellitus among Patients Hospitalized with Heart Failure: Findings

- from Get With The Guidelines—Heart Failure Registry. *Am. Heart J.* **2016**, *182*, 9–20.
- (212) von Haehling, S.; Anker, S. D. Prevalence, Incidence and Clinical Impact of Cachexia: Facts and Numbers—Update 2014. *J. Cachexia. Sarcopenia Muscle* **2014**, *5* (4), 261–263.
- (213) von Haehling, S.; Anker, M. S.; Anker, S. D. Prevalence and Clinical Impact of Cachexia in Chronic Illness in Europe, USA, and Japan: Facts and Numbers Update 2016. *J. Cachexia. Sarcopenia Muscle* **2016**, *7* (5), 507–509.
- (214) Workinger, J. L.; Kuda-Wedagedara, A. N. W.; Julin, M. M.; White, J. M.; Nexø, E.; Viola, N. T.; Doyle, R. P. Systemically Administered Plant Recombinant Holo-Intrinsic Factor Targets the Liver and Is Not Affected by Endogenous B12 Levels. *Sci. Rep.* **2019**, *9* (1), 1–8.
- (215) Poniatowski, L. A.; Wojdasiewicz, P.; Gasik, R.; Szukiewicz, D. Transforming Growth Factor Beta Family: Insight into the Role of Growth Factors in Regulation of Fracture Healing Biology and Potential Clinical Applications. *Mediators Inflamm.* **2015**, *2015*.
- (216) Luo, J.; Chen, X. Q.; Li, P. The Role of TGF- $\beta$  and Its Receptors in Gastrointestinal Cancers. *Transl. Oncol.* **2019**, *12* (3), 475–484.
- (217) Horbelt, D.; Denkis, A.; Knaus, P. A Portrait of Transforming Growth Factor  $\beta$  Superfamily Signalling: Background Matters. *Int. J. Biochem. Cell Biol.* **2012**, *44* (3), 469–474.
- (218) Weiskirchen, R.; Meurer, S. K.; Gressner, O. A.; Herrmann, J.; Borkham-Kamphorst, E.; Gressner, A. M. BMP-7 as Antagonist of Organ Fibrosis. *Front. Biosci.* **2009**, *14* (13), 4992–5012.
- (219) Burt, D. W.; Law, A. S. Evolution of the Transforming Growth Factor-Beta Superfamily. *Prog. Growth Factor Res.* **1994**, *5* (1), 99–118.
- (220) Tsai, V. W. W.; Husaini, Y.; Sainsbury, A.; Brown, D. A.; Breit, S. N. The MIC-1/GDF15-GFRAL

- Pathway in Energy Homeostasis: Implications for Obesity, Cachexia, and Other Associated Diseases. *Cell Metab.* **2018**, *28* (3), 353–368.
- (221) Brown, D. A.; Lindmark, F.; Stattin, P.; Bälter, K.; Adami, H. O.; Zheng, S. L.; Xu, J.; Isaacs, W. B.; Grönberg, H.; Breit, S. N.; Wiklund, F. E. Macrophage Inhibitory Cytokine 1: A New Prognostic Marker in Prostate Cancer. *Clin. Cancer Res.* **2009**, *15* (21), 6658–6664.
- (222) Xiong, Y.; Walker, K.; Min, X.; Hale, C.; Tran, T.; Komorowski, R.; Yang, J.; Davda, J.; Nuanmanee, N.; Kemp, D.; Wang, X.; Liu, H.; Miller, S.; Lee, K. J.; Wang, Z.; Véniant, M. M. Long-Acting MIC-1/GDF15 Molecules to Treat Obesity: Evidence from Mice to Monkeys. *Sci. Transl. Med.* **2017**, *9* (412), 1–12.
- (223) Paratcha, G.; Ledda, F.; Baars, L.; Couplier, M.; Besset, V.; Anders, J.; Scott, R.; Ibáñez, C. F. Released GFR $\alpha$ 1 Potentiates Downstream Signaling, Neuronal Survival, and Differentiation via a Novel Mechanism of Recruitment of c-Ret to Lipid Rafts. *Neuron* **2001**, *29* (1), 171–184.
- (224) Emmerson, P. J.; Wang, F.; Du, Y.; Liu, Q.; Pickard, R. T.; Gonciarz, M. D.; Coskun, T.; Hamang, M. J.; Sindelar, D. K.; Ballman, K. K.; Foltz, L. A.; Muppidi, A.; Alsina-Fernandez, J.; Barnard, G. C.; Tang, J. X.; Liu, X.; Mao, X.; Siegel, R.; Sloan, J. H.; Mitchell, P. J.; Zhang, B. B.; Gimeno, R. E.; Shan, B.; Wu, X. The Metabolic Effects of GDF15 Are Mediated by the Orphan Receptor GFRAL. *Nat. Med.* **2017**, *23* (10), 1215–1219.
- (225) Airaksinen, M. S.; Titievsky, A.; Saarma, M. GDNF Family Neurotrophic Factor Signaling: Four Masters, One Servant. *Mol. Cell. Neurosci.* **1999**, *13* (5), 313–325.
- (226) Plaza-Menacho, I.; Mologni, L.; McDonald, N. Q. Mechanisms of RET Signaling in Cancer: Current and Future Implications for Targeted Therapy. *Cell. Signal.* **2014**, *26* (8), 1743–

1752.

- (227) Airaksinen, M. S.; Saarma, M. THE GDNF FAMILY : SIGNALLING , BIOLOGICAL FUNCTIONS AND THERAPEUTIC VALUE. *Nat. Rev. Neurosci.* **2002**, *3*, 383–394.
- (228) Wang, X. Structural Studies of GDNF Family Ligands with Their Receptors - Insights into Ligand Recognition and Activation of Receptor Tyrosine Kinase RET. *Biochim. Biophys. Acta - Proteins Proteomics* **2013**, *1834* (10), 2205–2212.
- (229) Hsu, J. Y.; Crawley, S.; Chen, M.; Ayupova, D. A.; Lindhout, D. A.; Higbee, J.; Kutach, A.; Joo, W.; Gao, Z.; Fu, D.; To, C.; Mondal, K.; Li, B.; Kekatpure, A.; Wang, M.; Laird, T.; Horner, G.; Chan, J.; Mcentee, M.; Lopez, M.; Lakshminarasimhan, D.; White, A.; Wang, S. P.; Yao, J.; Yie, J.; Matern, H.; Solloway, M.; Haldankar, R.; Parsons, T.; Tang, J.; Shen, W. D.; Chen, Y. A.; Tian, H.; Allan, B. B. Non-Homeostatic Body Weight Regulation through a Brainstem-Restricted Receptor for GDF15. *Nature* **2017**, *550* (7675), 255–259.
- (230) Breit, S. N.; Tsai, V. W. W.; Brown, D. A. Targeting Obesity and Cachexia: Identification of the GFRAL Receptor–MIC-1/GDF15 Pathway. *Trends Mol. Med.* **2017**, *23* (12), 1065–1067.
- (231) Bootcov, M. R.; Bauskin, A. R.; Valenzuela, S. M.; Moore, A. G.; Bansal, M.; He, X. Y.; Zhang, H. P.; Donnellan, M.; Mahler, S.; Pryor, K.; Walsh, B. J.; Nicholson, R. C.; Fairlie, W. D.; Por, S. B.; Robbins, J. M.; Breit, S. N. MIC-1, a Novel Macrophage Inhibitory Cytokine, Is a Divergent Member of the TGF- $\beta$  Superfamily. *Proc. Natl. Acad. Sci. U. S. A.* **1997**, *94* (21), 11514–11519.
- (232) Bauskin, A. R.; Zhang, H. P.; Fairlie, W. D.; He, X. Y.; Russell, P. K.; Moore, A. G.; Brown, D. A.; Stanley, K. K.; Breit, S. N. The Propeptide of Macrophage Inhibitory Cytokine (MIC-1), a TGF- $\beta$  Superfamily Member, Acts as a Quality Control Determinant for Correctly Folded

- MIC-1. *EMBO J.* **2000**, *19* (10), 2212–2220.
- (233) Brown, D. A.; Bauskin, A. R.; Fairlie, W. D.; Smith, M. D.; Liu, T.; Xu, N.; Breit, S. N. Antibody-Based Approach to High-Volume Genotyping for MIC-1 Polymorphism. *Biotechniques* **2002**, *33* (1).
- (234) Kleinert, M.; Clemmensen, C.; Sjøberg, K. A.; Carl, C. S.; Jeppesen, J. F.; Wojtaszewski, J. F. P.; Kiens, B.; Richter, E. A. Exercise Increases Circulating GDF15 in Humans. *Mol. Metab.* **2018**, *9* (January), 187–191.
- (235) Moore, A. G.; Brown, D. A.; Fairlie, W. D.; Bauskin, A. R.; Brown, P. K.; Munier, M. L. C.; Russell, P. K.; Salamonsen, L. A.; Wallace, E. M.; Breit, S. N. The Transforming Growth Factor- $\beta$  Superfamily Cytokine Macrophage Inhibitory Cytokine-1 Is Present in High Concentrations in the Serum of Pregnant Women. *J. Clin. Endocrinol. Metab.* **2000**, *85* (12), 4781–4788.
- (236) Boyle, G. M.; Pedley, J.; Martyn, A. C.; Banducci, K. J.; Strutton, G. M.; Brown, D. A.; Breit, S. N.; Parsons, P. G. Macrophage Inhibitory Cytokine-1 Is Overexpressed in Malignant Melanoma and Is Associated with Tumorigenicity. *J. Invest. Dermatol.* **2009**, *129* (2), 383–391.
- (237) Breit, S. N.; Carrero, J. J.; Tsai, V. W. W.; Yagoutifam, N.; Luo, W.; Kuffner, T.; Bauskin, A. R.; Wu, L.; Jiang, L.; Barany, P.; Heimbürger, O.; Murikami, M. A.; Apple, F. S.; Marquis, C. P.; Macla, L.; Lin, S.; Sainsbury, A.; Herzog, H.; Law, M.; Stenvinkel, P.; Brown, D. A. Macrophage Inhibitory Cytokine-1 (MIC-1/GDF15) and Mortality in End-Stage Renal Disease. *Nephrol. Dial. Transplant.* **2012**, *27* (1), 70–75.
- (238) Johnen, H.; Lin, S.; Kuffner, T.; Brown, D. A.; Tsai, V. W. W.; Bauskin, A. R.; Wu, L.;

- Pankhurst, G.; Jiang, L.; Junankar, S.; Hunter, M.; Fairlie, W. D.; Lee, N. J.; Enriquez, R. F.; Baldock, P. A.; Corey, E.; Apple, F. S.; Murakami, M. M.; Lin, E. J.; Wang, C.; During, M. J.; Sainsbury, A.; Herzog, H.; Breit, S. N. Tumor-Induced Anorexia and Weight Loss Are Mediated by the TGF- $\beta$  Superfamily Cytokine MIC-1. *Nat. Med.* **2007**, *13* (11), 1333–1340.
- (239) Macia, L.; Tsai, V. W. W.; Nguyen, A. D.; Johnen, H.; Kuffner, T.; Shi, Y. C.; Lin, S.; Herzog, H.; Brown, D. A.; Breit, S. N.; Sainsbury, A. Macrophage Inhibitory Cytokine 1 (MIC-1/GDF15) Decreases Food Intake, Body Weight and Improves Glucose Tolerance in Mice on Normal & Obesogenic Diets. *PLoS One* **2012**, *7* (4), e34868.
- (240) Tsai, V. W. W.; Macia, L.; Johnen, H.; Kuffner, T.; Manadhar, R.; Jørgensen, S. B.; Lee-Ng, K. K. M.; Zhang, H. P.; Wu, L.; Marquis, C. P.; Jiang, L.; Husaini, Y.; Lin, S.; Herzog, H.; Brown, D. A.; Sainsbury, A.; Breit, S. N. TGF- $\beta$  Superfamily Cytokine MIC-1/GDF15 Is a Physiological Appetite and Body Weight Regulator. *PLoS One* **2013**, *8* (2), e55174.
- (241) Saarma, M. GDNF Recruits the Signaling Crew into Lipid Rafts. *Trends Neurosci.* **2001**, *24* (8), 427–429.
- (242) Fielder, G. C.; Yang, T. W.; Razdan, M.; Li, Y.; Lu, J. The GDNF Family : A Role in Cancer ? *Neoplasia* **2018**, *20* (1), 99–117.
- (243) Jing, S.; Wen, D.; Yu, Y.; Holst, P. L.; Luo, Y.; Fang, M.; Tamir, R.; Antonio, L.; Hu, Z.; Cupples, R.; Louis, J. C.; Hu, S.; Altrock, B. W.; Fox, G. M. GDNF-Induced Activation of the Ret Protein Tyrosine Kinase Is Mediated by GDNFR- $\alpha$ , a Novel Receptor for GDNF. *Cell* **1996**, *85* (7), 1113–1124.
- (244) Tansey, M. G.; Baloh, R. H.; Milbrandt, J.; Johnson, E. M. GFR $\alpha$ -Mediated Localization of RET to Lipid Rafts Is Required for Effective Downstream Signaling, Differentiation, and

- Neuronal Survival. *Neuron*. **2000**, 25 (3), 611–623.
- (245) Cimino, I.; Coll, A. P.; Yeo, G. S. H. GDF15 and Energy Balance: Homing in on a Mechanism. *Nat. Med.* **2017**, 23 (10), 1119–1120.
- (246) Yang, L.; Chang, C. C.; Sun, Z.; Madsen, D.; Zhu, H.; Padkjær, S. B.; Wu, X.; Huang, T.; Hultman, K.; Paulsen, S. J.; Wang, J.; Bugge, A.; Frantzen, J. B.; Nørgaard, P.; Jeppesen, J. F.; Yang, Z.; Secher, A.; Chen, H.; Li, X.; John, L. M.; Shan, B.; He, Z.; Gao, X.; Su, J.; Hansen, K. T.; Yang, W.; Jørgensen, S. B. GFRAL Is the Receptor for GDF15 and Is Required for the Anti-Obesity Effects of the Ligand. *Nat. Med.* **2017**, 23 (10), 1158–1166.
- (247) Li, Z.; Wang, B.; Wu, X.; Cheng, S. Y.; Paraoan, L.; Zhou, J. Identification, Expression and Functional Characterization of the GRAL Gene. *J. Neurochem.* **2005**, 95 (2), 361–376.
- (248) Tsai, V. W.; Manandhar, R.; Jørgensen, S. B.; Lee-ng, K. K. M.; Zhang, P.; Marquis, C. P.; Jiang, L.; Husaini, Y.; Lin, S.; Sainsbury, A.; Sawchenko, P. E.; Brown, D. A.; Breit, S. N. The Anorectic Actions of the TGF b Cytokine MIC-1 / GDF15 Require an Intact Brainstem Area Postrema and Nucleus of the Solitary Tract. *PLoS One* **2014**, 9 (6), e100370.
- (249) Mulligan, L. M. GDNF and the RET Receptor in Cancer: New Insights and Therapeutic Potential. *Front. Physiol.* **2019**, 10 (JAN), 1–13.
- (250) Mulligan, L. M. RET Revisited: Expanding the Oncogenic Portfolio. *Nat. Rev. Cancer* **2014**, 14 (3), 173–186.
- (251) Schlee, S.; Carmillo, P.; Whitty, A. Quantitative Analysis of the Activation Mechanism of the Multicomponent Growth-Factor Receptor Ret. *Nat. Chem. Biol.* **2006**, 2 (11), 636–644.
- (252) Fejzo, M. S.; Sazonova, O. V; Sathirapongsasuti, J. F.; Hallgrímsdóttir, I. B.; Vacic, V.; Macgibbon, K. W.; Schoenberg, F. P.; Mancuso, N.; Slamon, D. J.; Mullin, P. M. Placenta

and Appetite Genes GDF15 and IGFBP7 Are Associated with Hyperemesis Gravidarum. *Nat. Commun.* **2018**, *9*, 1178.

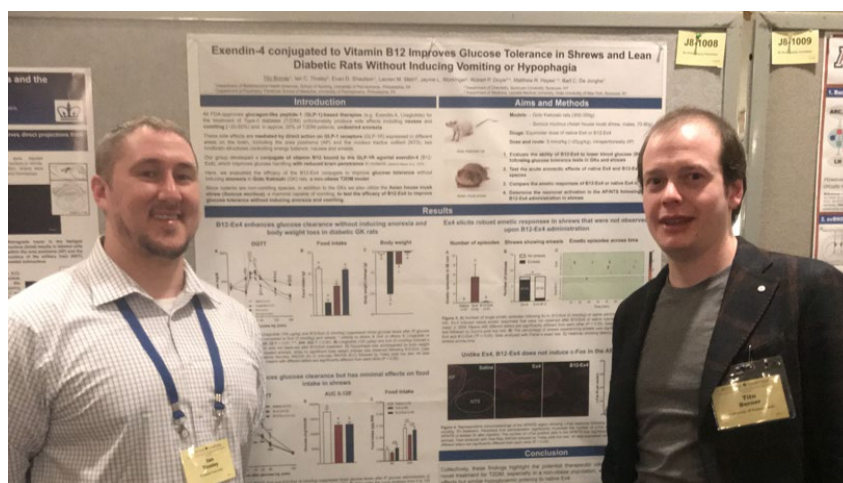
- (253) Klarenbeek, J.; Goedhart, J.; Van Batenburg, A.; Groenewald, D.; Jalink, K. Fourth-Generation Epac-Based FRET Sensors for CAMP Feature Exceptional Brightness, Photostability and Dynamic Range: Characterization of Dedicated Sensors for FLIM, for Ratiometry and with High Affinity. *PLoS One* **2015**, *10* (4), e0122513.
- (254) Chepurny, O. G.; Bonaccorso, R. L.; Leech, C. A.; Wöllert, T.; Langford, G. M.; Schwede, F.; Roth, C. L.; Doyle, R. P.; Holz, G. G. Chimeric Peptide EP45 as a Dual Agonist at GLP-1 and NPY2R Receptors. *Sci. Rep.* **2018**, *8*, 3749.



## Chapter 2: A Second-generation Glucagon-like Peptide-1 Receptor Agonist Mitigates Vomiting and Anorexia While Retaining Glucoregulatory Potency in Lean Diabetic and Emetic Mammalian Models

The work reported in this chapter resulted in a peer-reviewed research paper: Tito Borner, Evan D. Shaulson, **Ian C. Tinsley**, Lauren Stein, Charles C. Horn, Matthew R. Hayes, Robert P. Doyle,\* and Bart C. De Jonghe\*. A second-generation glucagon-like peptide-1 receptor agonist mitigates vomiting and anorexia while retaining glucoregulatory potency in lean diabetic and emetic mammalian models. *Diabetes, Obesity, and Metabolism* **2020**, *22* (10), 1729-1741

All synthetic work, including synthesis of all tested compounds and the fluorescent analog, their purification, chemical and *in vitro* biochemical characterization, and preparation for *in vivo* testing was conducted by the author. In addition, the author assisted in *in vivo* data collection specifically included in Figures 4 and 5, and conducted with Dr. Tito Borner of the University of Pennsylvania.



This work was presented by the author (Left) and Dr. Tito Borner (Right; University of Pennsylvania) at the Keystone Symposia on Molecular and Cellular Biology, Banff, Alberta, Canada, February 2019.

## 2.1 Introduction

Nausea and vomiting are omnipresent side effects of human diseases and pharmacotherapies that have spawned significant drug discovery efforts to combat their many causes.<sup>1</sup> Glucagon-like peptide-1 receptor (GLP-1R)-based therapies for the treatment of type 2 diabetes mellitus (T2DM), such as Exendin-4 (Ex4) and liraglutide, are no exception,<sup>2</sup> causing nausea and vomiting in  $\approx$ 25% to 50% of patients prescribed these drugs.<sup>3-7</sup>

A recently reported vitamin B12 (B12) conjugate of Ex4 (hereafter called 'B12-Ex4') reported by the Doyle group<sup>8,9</sup> showed retention of glucoregulation comparable with native Ex4 without producing Ex4-associated anorexia or conditioned taste avoidance (CTA) in lean, healthy rats.<sup>8</sup> Furthermore, B12-Ex4 co-localized with insulin-containing  $\beta$ -cells within the pancreas, while brain penetrance of a fluorescently tagged B12-Ex4 was not detected within the hypothalamus, area postrema (AP), or nucleus tractus solitarius (NTS) of the brain stem.<sup>8</sup> These results corroborated prior *in vitro*, *ex vivo* and functional *in vivo* observations that the incretin action on the pancreas<sup>10-12</sup> and hypoglycemic effects of Ex4 remained intact when bound to B12, while central sites of Ex4 action controlling energy homeostasis and nausea/malaise (e.g. the brainstem AP and NTS, as well as hypothalamic nuclei)<sup>13-15</sup> were putatively not agonized following B12-Ex4 treatment. The B12-Ex4 construct may be of considerable clinical utility given the potential for retained glycemic control in combination with improved tolerability and associated patient compliance through a mechanism of action that simultaneously limits central nervous system (CNS) penetrance and retains peripheral (i.e., pancreatic) pharmacodynamics.

Weight loss is considered desirable for many patients with T2DM considered overweight or obese, as they may benefit from improvements in insulin signaling and overall health with

concomitant adipose tissue loss.<sup>16,17</sup> However, patients with T2DM who also suffer from comorbidities associated with cachexia (e.g. cancer,<sup>18</sup> cystic fibrosis,<sup>19</sup> HIV,<sup>20</sup> chronic obstructive pulmonary disease,<sup>21</sup> and sarcopenia<sup>22</sup>), would also benefit from use of the front-line treatments for T2DM in the form of GLP1-R agonists, without affecting their body weight. In addition, ≈10% of patients with T2DM, such as those potentially with polygenic/inherited T2DM, are not overweight/obese,<sup>23</sup> and weight loss below normal weight status is undesirable. To this end, given previously reported work in healthy, lean rats, showing comparable glycemic control without anorexia/weight loss following acute B12-Ex4 treatment compared with native Ex4,<sup>8</sup> we sought to employ the use of the Goto-Kakizaki (GK) rat, a model of spontaneous insulin resistance and T2DM.<sup>24</sup> These animals develop T2DM early in life and maintain a lean phenotype (see Ostenson and Efendic<sup>25</sup> for a discussion/review), making this strain ideal to model T2D without concomitant obesity.

The musk shrew (*Suncus murinus*) is a well-established model of emesis<sup>26</sup> and feeding behavior<sup>27</sup> and is suitable for examination of the GLP-1 system as this species exhibits glucoregulatory, hypophagic and emetic responsivity following administration of current Food and Drug Administration-approved GLP-1R agonists such as Ex4.<sup>14,15</sup> Immunohistochemical and pharmacological analyses were performed to examine the effects of B12-Ex4 versus Ex4 administration on glycemic control, emesis and feeding behavior in shrews.

## **2.2 Design and Synthesis of B12-Ex4**

B12-Ex4 was synthesized, characterized, and screened for receptor agonism as previously described.<sup>9</sup> Briefly, the 5' hydroxyl group of B12 was selectively oxidized to a carboxylic acid (B12CA) using 2-iodoxybenzoic acid, as previously described.<sup>28</sup> Subsequent coupling of 1-amino-

3-butyne to B12CA with 1-ethyl-3-(3-(dimethylamino)propyl)carbodiimide (EDC) and 1-hydroxybenzo-triazole (HOBt) produced B12 with a terminal alkyne at the ribose 5'-position (B12AB). A K12 azido modified Ex4 was conjugated to B12AB utilizing Huisgens/Sharpless<sup>29-31</sup> click chemistry to produce B12-Ex4.

## 2.3 *In Vivo* Effects of Ex4 and B12-Ex4 in Shrews

### 2.3.1 Systemically Delivered B12-Ex4 Enhances Glucose Clearance Relative to Ex4

I first tested whether B12-Ex4 reduces blood glucose (BG) following an IPGTT in shrews. I observed that shrews treated with equimolar (5 nmol/kg) B12-Ex4 and native Ex4 (5 nmol/kg, i.e.  $\approx 20 \mu\text{g}/\text{kg}$ ) display similar improvements in glucose clearance following glucose load compared with saline controls (Figure 1). Post hoc analyses showed that both compounds significantly suppressed BG at 20, 40 and 60 minutes after glucose administration compared with saline treatment (all  $P < .001$ ). Furthermore, the area under the curve (AUC) for B12-Ex4 did not differ from native Ex4 following glucose administration (Figure 1).

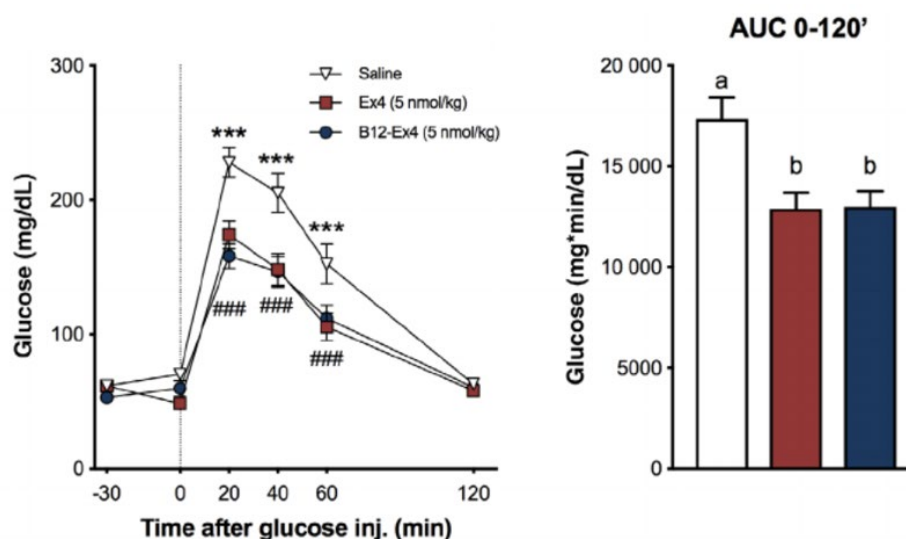


**Figure 1.** Systemically delivered B12-Ex4 enhances glucose clearance during an intraperitoneal glucose tolerance test (IPGTT). In an IPGTT, Ex4 (5 nmol/kg, i.e.,  $\approx 20 \mu\text{g}/\text{kg}$ ) and B12-Ex4 (5

nmol/kg) showed a similar potency in suppressing BG levels after intraperitoneal (IP) glucose administration (2 g/kg, IP) compared with saline; saline versus B12-Ex4: \*\*\*  $P < .001$ ; saline versus Ex4: ###  $P < .001$ . AUC analysis from 0 (i.e., post-glucose bolus) to 120 minutes; B12-Ex4 and Ex4 similarly reduced AUCs compared with saline. All data are expressed as mean  $\pm$  standard error of mean (SEM). IPGTT data was analyzed with repeated measurements two-way ANOVA followed by Tukey's post hoc test. AUC data was analyzed with repeated measurements one-way ANOVA followed by Tukey's post hoc test. Means with different letters are significantly different ( $P < .05$ ). In IPGTT,  $n = 13$ , within subject design; AUC,  $n = 5$ , within subject design).

To investigate the effects of B12-Ex4 and Ex4 on baseline glucose homeostasis, equimolar Ex4, B12-Ex4 or saline were administered without subsequent glucose injection and observed that both Ex4 and B12-Ex4 did not produce basal BG change or impact the glucose AUC (Figure 2).

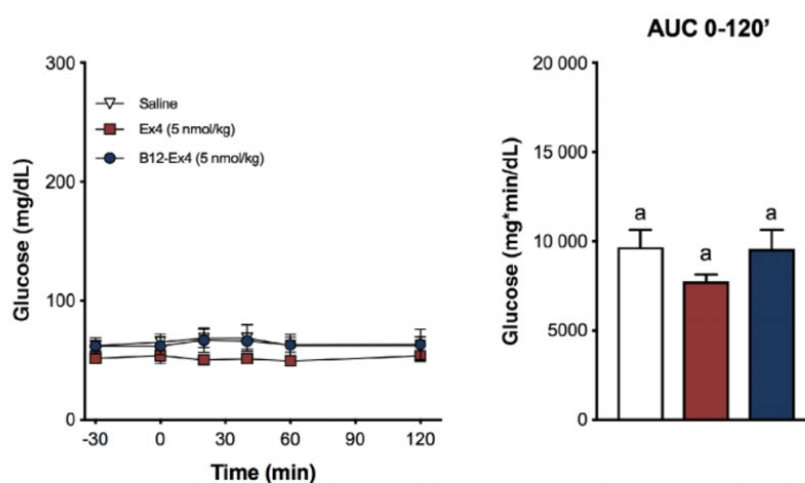


**Figure 2.** Equimolar dosing of Ex4 (5 nmol/kg, i.e.,  $\approx 20 \mu\text{g}/\text{kg}$ ), B12-Ex4 (5 nmol/kg) or saline were administered without subsequent glucose administration. Both Ex4 and B12-Ex4 treatments

were no longer effective in reducing BG levels and had no effect on AUC. All data are expressed as mean  $\pm$  SEM. Blood glucose data was analyzed with repeated measurements two-way ANOVA followed by Tukey's post hoc test. AUC data was analyzed with repeated measurements one-way ANOVA followed by Tukey's post hoc test. Means with different letters are significantly different ( $P < .05$ ). In IPGTT,  $n = 13$ , within subject design; AUC,  $n = 5$ , within subject design.

### 2.3.2 Systemically Delivered B12-Ex4 Co-localizes with Insulin in Pancreatic $\beta$ -cells

To assess whether B12-Ex4 is taken up by insulin-producing cells in the pancreas, shrews were injected IP with a fluorescently labelled version of B12-Ex4 (Cy5-B12-Ex4, 5 nmol/kg) and sacrificed 3 hours after delivery. Results show that upon systemic administration, Cy5-B12-Ex4 co-localized with insulin in pancreatic  $\beta$ -cells (Figure 3).

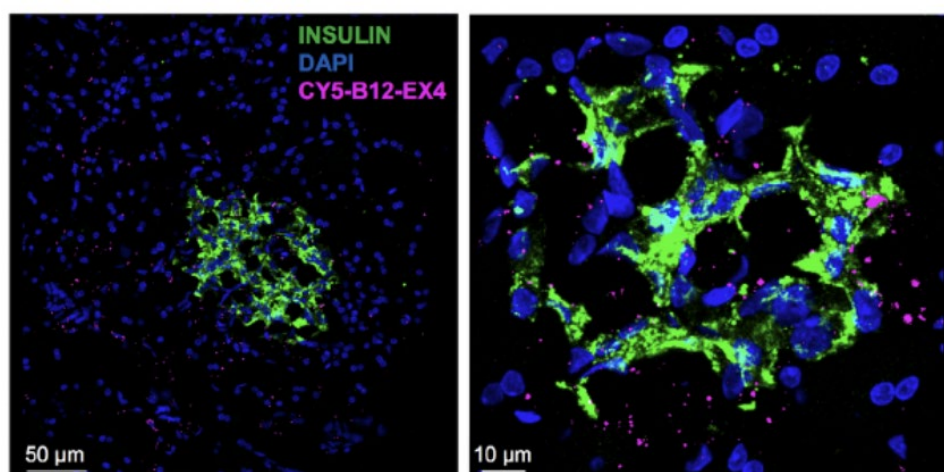


**Figure 3.** Systemically injected fluorophore-labelled B12-Ex4 (Cy5-B12-Ex4, 5 nmol/kg) co-localized with insulin in shrew pancreatic tissue supporting the hypothesis that B12-Ex4 acts at the pancreas to improve glycemic control.

### 2.3.3 B12-Ex4 does not alter food intake or body weight, dissimilar to administration of Ex4

Shrews received an IP injection of Ex4 (5 nmol/kg, i.e.,  $\approx 20 \mu\text{g}/\text{kg}$ ), B12-Ex4(5 nmol/kg) or saline, to test whether B12-Ex4 administration alters food intake or body weight in this species. In line with previous reports, systemic administration of Ex4 produced hypophagia in shrews at all measured time points and bodyweight loss 24 hours after injection (Figure 4). By contrast, no significant effects on food intake or body weight were observed following B12-Ex4 treatment (Figure 4).

#### Doses: 5 nmol/kg

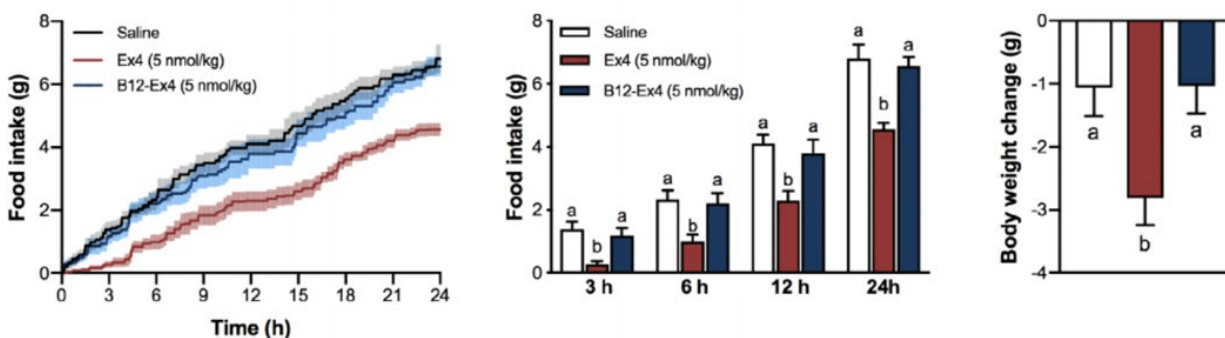


**Figure 4.** Pharmacological doses of B12-Ex4 do not affect feeding and body weight in shrews. Ex4 (5 nmol/kg, i.e.  $\approx 20 \mu\text{g}/\text{kg}$ ) suppressed feeding at 3, 6, 12 and 24 hours, whereas equimolar doses of B12-Ex4 (5 nmol/kg) had no effect on food intake. Ex4-induced anorexia was accompanied by body weight loss. No significant changes in body weight were observed after B12-Ex4 administration compared with controls. All data are expressed as mean  $\pm$  SEM. Data was analyzed with repeated measurements one-way ANOVA followed by Tukey's post hoc test. Means with different letters are significantly different ( $P < .05$ ). In food intake studies,  $n = 8$ , within subject design; in body weight change studies,  $n = 6$ , within subject design.

In a second experiment, shrews were injected IP with a supra-pharmacological dose of Ex4 (50 nmol/kg, i.e.,  $\approx 200 \mu\text{g}/\text{kg}$ ), B12-Ex4 (50 nmol/kg) or saline. Ex4 induced anorexia at all measured time points, and 24 hours body weight loss (Figure 5). By contrast, administration of equimolar doses of B12-Ex4 did not induce hypophagia or body weight loss compared with saline-treated animals (Figure 5).

#### Doses: 50 nmol/kg

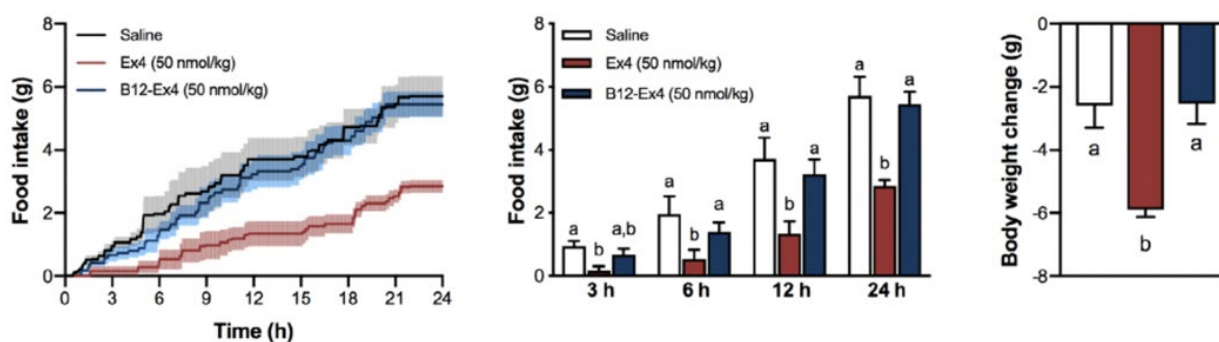


**Figure 5.** Supra-pharmacological doses of B12-Ex4 do not affect feeding and body weight in shrews. Ex4 (50 nmol/kg, i.e.  $\approx 200 \mu\text{g}/\text{kg}$ ) suppressed eating at all measured time points. By strict contrast, supra-pharmacological equimolar doses of B12-Ex4 did not show any effects. While severe body weight loss occurred following supra-pharmacological doses of Ex4, no significant changes occurred in the B12-Ex4-treated animals. All data are expressed as mean  $\pm$  SEM. Data was analyzed with repeated measurements one-way ANOVA followed by Tukey's post hoc test. Means with different letters are significantly different ( $P < .05$ ). In food intake studies,  $n = 8$ , within subject design; in body weight change studies,  $n = 6$ , within subject design.



### 2.3.4 B12-Ex4 treatment produces slight emesis compared with the emetic effects of Ex4

Ex4 (5 nmol/kg, i.e.,  $\approx 20 \mu\text{g}/\text{kg}$ ) induced emesis in most of the shrews tested (Figure 6). By contrast, only one shrew experienced emesis after equimolar B12-Ex4 (5 nmol/kg) administration ( $P < .001$ ). The number of single emetic episodes and emetic bouts in the 90 minutes window after drug administration were also significantly reduced after B12-Ex4 compared with Ex4 and did not differ from the control condition (Figure 6). Ex4 triggered emesis with an average latency of  $19 \pm 5$  minutes (Figure 6). A heat map representation of the Ex4 and B12-Ex4 effects on emetic intensity and latency for each individual animal across time can be seen in Figure 6.

Doses: 5 nmol/kg

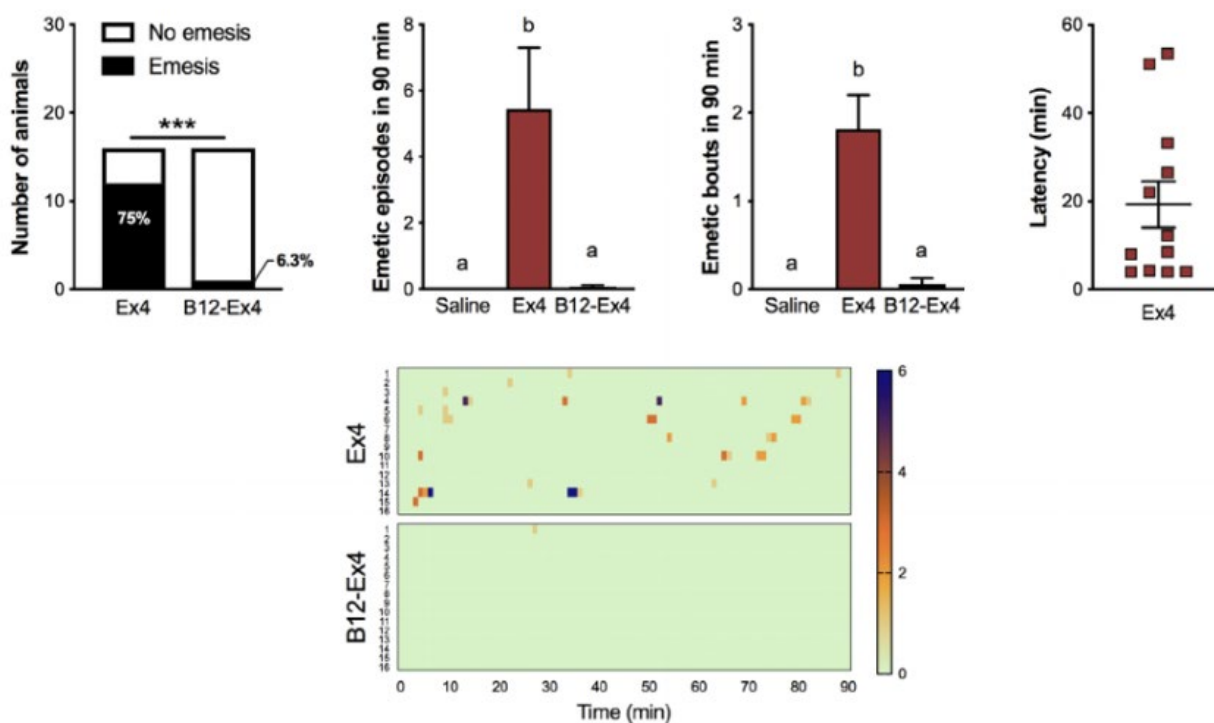


**Figure 6.** Emesis in shrews is significantly reduced following pharmacological B12-Ex4 (5 nmol/kg) treatment compared with native Ex4 (5 nmol/kg, i.e.  $\approx 20 \mu\text{g}/\text{kg}$ ), denoting improved tolerance. The percentage of shrews experiencing emesis was significantly different between Ex4 and

equimolar B12-Ex4 (\*\*\*)  $P < .001$ ). None of the animals experienced emesis following saline administration (data not shown). The number of single emetic episodes following Ex4 (5 nmol/kg, i.e.  $\approx 20 \mu\text{g}/\text{kg}$ ), equimolar B12-Ex4 (5 nmol/kg) or saline systemic administration was recorded for 90 minutes. Ex4 induced robust emetic responses that were not observed after B12-Ex4 or saline injections. The number of emetic bouts was also lower after B12-Ex4 treatment compared with Ex4 and it did not differ from saline controls. Latency to the first emetic episode in Ex4 animals that exhibited emesis. Heatmap showing the emetic latency and intensity, as well as the number of emetic episodes induced by Ex4 or B12-Ex4 for each animal across time. Evidence of emesis was analyzed with Fisher's exact test. Emetic episodes and bouts were analyzed with repeated measurements one-way ANOVA followed by Tukey's post hoc test. Emesis studies,  $n = 16$ , within subject design. Means with different letters are significantly different ( $P < .05$ )

Next, we tested a supra-pharmacological dose of Ex4 (50 nmol/kg, i.e.  $\approx 200 \mu\text{g}/\text{kg}$ ) and B12-Ex4 (50 nmol/kg) and observed that Ex4 induced profound emesis, reflected by both the number and severity of emetic episodes, in 100 % (i.e. 8/8,  $P < .001$ ) of the shrews tested, while an equimolar dose of B12-Ex4 did not induce emesis in shrews. The average latency to first emetic episode induced by Ex4 was  $52 \pm 8$  minutes (Figure 7). The emetic profiles of each animal following B12-Ex4 or Ex4 administration are represented in Figure 7.

Doses: 50 nmol/kg

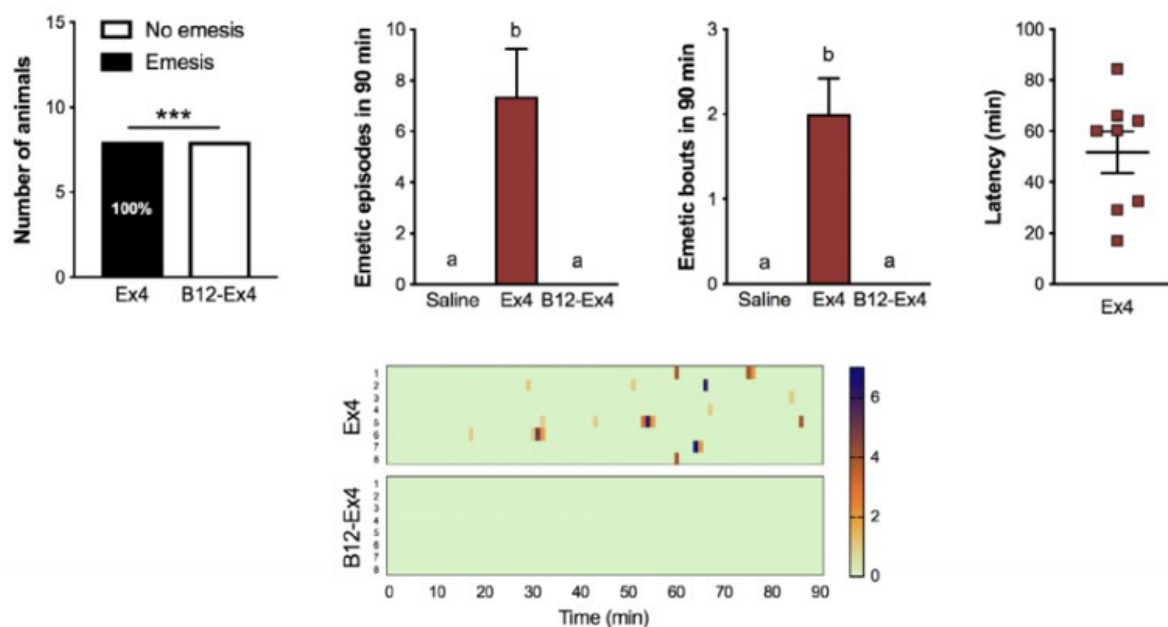


**Figure 7.** Emesis in shrews is significantly reduced following supra-pharmacological B12-Ex4 (50 nmol/kg) treatment compared with native Ex4 (50 nmol/kg, i.e.  $\approx 200 \mu\text{g}/\text{kg}$ ), denoting improved tolerance. Astonishingly, no emesis occurred after B12-Ex4 administration. The percentage of shrews experiencing emesis was completely reversed between Ex4 and equimolar B12-Ex4 (\*\*\*)  $P < .001$ ). No animal experienced emesis following saline injection (data not shown). The number of emetic episodes and bouts following Ex4, equimolar B12-Ex4 or saline administration was analyzed over 90 minutes. Also, at this dosage Ex4 induced robust emetic responses. Latency to the first emetic episode in Ex4 shrews that exhibited emesis. Heatmap showing the emetic latency and intensity, as well as the number of emetic episodes for each animal across time. All data are expressed as mean  $\pm$  SEM. Emetic episodes and bouts were analyzed with repeated measurements one-way ANOVA followed by Tukey's post hoc test. Emesis studies,  $n = 8$ , within subject design. Means with different letters are significantly different ( $P < .05$ ).

### 2.3.5 Systemic Administration of B12-Ex4 does not induce c-Fos in the AP or NTS

Ex4, but not B12-Ex4, induced c-Fos immunofluorescence compared with saline-treated controls within the NTS and AP (Figure 8). This data supports our hypothesis that conjugation of Ex4 to B12 results in diminished access to CNS GLP-1Rs. The reduced penetrance of the CNS is an explanation for the lack of B12-Ex4-induced emesis in the shrew. C-Fos activation following administration of Ex4 is consistent with previously reported results.<sup>13,32–35</sup>

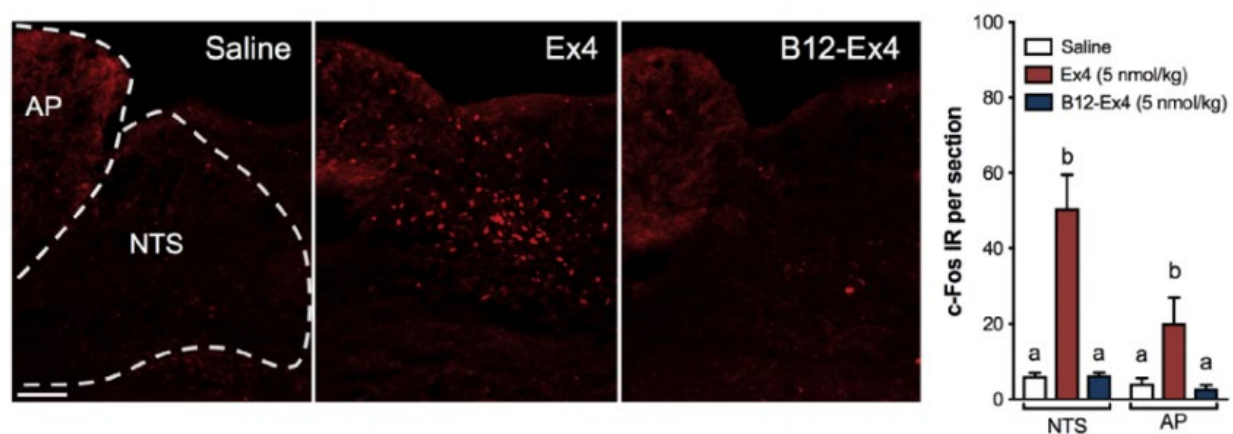


**Figure 8.** Systemic administered B12-Ex4 does not activate the area postrema (AP) or the nucleus tractus solitarius (NTS) in shrew. Representative immunostainings of the AP/NTS region showing the c-Fos response following saline (n = 4), Ex4 (5 nmol/kg, n = 4) and equimolar B12-Ex4 (n = 5) systemic treatment. Peripheral Ex4 administration significantly increased the number of c-Fos immunoreactive (IR) cells in the AP/NTS of shrews 3 hours after injection. The number of c-Fos-positive cells in the AP/NTS was significantly lower in B12-Ex4-treated animals and it did not differ from saline-treated shrews. Data was analyzed with one-way ANOVA followed by Tukey post hoc test. Means with different letters are significantly different from each other (P < .05). Values are expressed as mean  $\pm$  SEM. Scale bar 100  $\mu$ m.

### 2.3.6 Central Administration of B12-Ex4 and Ex4 Similarly Produce Emesis

Direct intracerebroventricular injection (ICV) administration of Ex4 (0.24 nmol) and B12-Ex4 (0.24 nmol) induced emesis with similar emetogenic profiles. We observed no difference in the percentage of shrews experiencing emesis following central B12-Ex4 or Ex4 administration (Figure 9). Furthermore, the number of single emetic episodes, the number of emetic bouts, as well as the latency to the first emetic response (Figure 9), were not statistically different between B12-Ex4 and Ex4. ICV administration of artificial cerebrospinal fluid did not induce any emesis in shrews (data not shown).

Doses: 0.24 nmol (~ 1  $\mu$ g Ex4) ICV

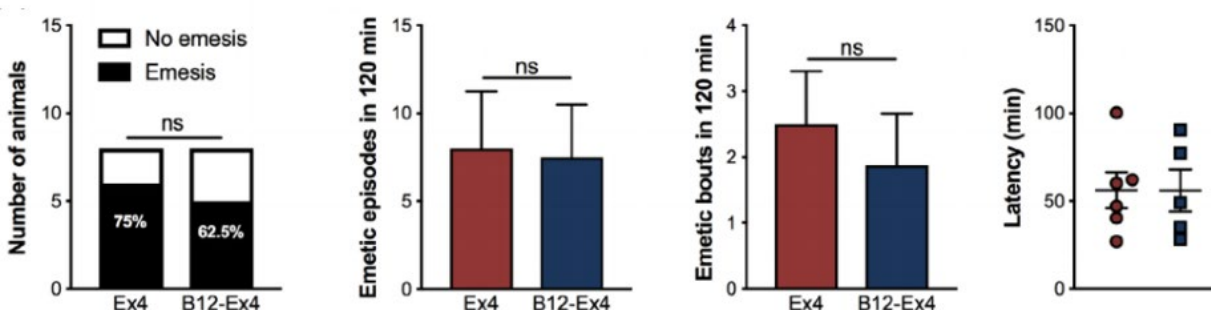


**Figure 9.** Systemic administration of B12-Ex4 does not result in emesis but does when delivered centrally. Ex4 (0.24 nmol, i.e., 1  $\mu$ g), equimolar B12-Ex4 or vehicle was infused into the lateral ventricle. The percentage of shrews showing emesis was similar between Ex4 and B12-Ex4. The number of single emetic episodes or bouts following Ex4, B12-Ex4 or saline was recorded for 120 minutes. Both Ex4 and B12-Ex4 induced comparable emetic responses, while none of the animals experienced emesis following vehicle delivery (data not shown). Latency to the first emetic episode in Ex4- and B12-Ex4-treated animals that exhibited emesis did not differ. Evidence of

emesis was analyzed with Fisher's exact test. Emetic episodes and bouts were analyzed with Student t-test (n=8, within subject design). Values are expressed as mean  $\pm$  SEM.

## **2.4 *In Vivo* Effects of Ex4 and B12-Ex4 in Lean Diabetic Goto-Kakazaki (GK) Rats**

### **2.4.1 B12-Ex4 enhances glucose clearance during an OGTT without inducing anorexia and bodyweight loss**

We tested the effects of Ex4, B12-Ex4 and liraglutide on oral glucose tolerance, food intake and body weight in GK rats. Like the effects of liraglutide (100  $\mu$ g/kg), B12-Ex4 reduced the glucose level following an OGTT compared with saline at 20 and 40 minutes after glucose load, and to native Ex4 (5 nmol/kg) at 120 and 180 minutes after glucose load (Figure 10). However, while both liraglutide and native Ex4 suppressed 24 hours food intake leading to 24 hours body weight loss (all  $P < .05$ ), no hypohagic or body weight suppressive effects were observed after B12-Ex4 administration in this lean diabetic model (Figure 10).

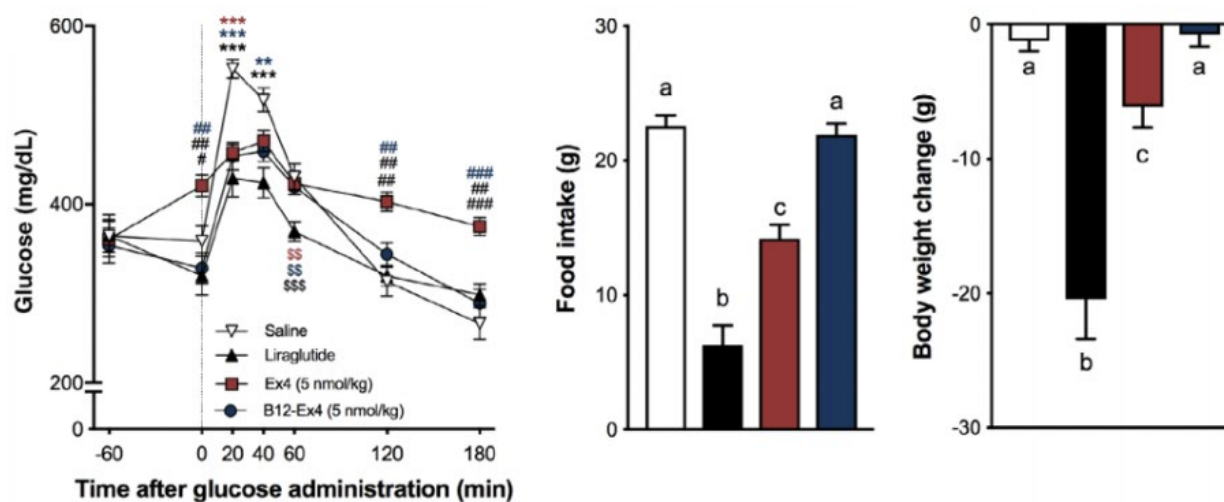


**Figure 10.** B12-Ex4 enhances glucose clearance during an oral glucose tolerance test (OGTT) without inducing anorexia and body weight loss in the Goto-Kakizaki lean diabetic rat model. In an OGTT, liraglutide (100  $\mu\text{g}/\text{kg}$ , i.e., 26.6 nmol/kg) and 5 nmol/kg B12-Ex4 suppressed blood glucose levels after intraperitoneal (IP) glucose administration (1 g/kg, per os (PO)) compared with 5 nmol/kg Ex4 (i.e.,  $\approx 20 \mu\text{g}/\text{kg}$ ) and saline. \* saline versus others; #: Ex4 versus others; \$: liraglutide versus others. \*, #, \$:  $P < .05$ ; \*\*, ##, \$\$:  $P < .01$ ; \*\*\*, ###, \$\$\$:  $P < .001$ . Liraglutide and Ex4 induced a strong anorectic effect, which was not observed after B12-Ex4 treatment. Hypophagia was accompanied by body weight loss in liraglutide- and Ex4-treated animals, while no significant body weight change was observed following B12-Ex4. Data were analyzed with repeated measure two-way ANOVA or one-way ANOVA followed by Tukey post hoc test;  $n = 21$ , within subject design. All data are expressed as mean  $\pm$  SEM. Means with different letters are significantly different from each other ( $P < .05$ ).

## 2.5 Outcomes and Conclusions

Existing GLP-1-based pharmacotherapies are excellent glucoregulatory drugs for treating hyperglycaemia in most patients with T2D despite reported nausea and vomiting. These phenomena, however, are gaining notoriety as overlooked major side effects in many patients, which reduce patient compliance and make current GLP-1R agonists 'suboptimal'.<sup>3-7,36,37</sup> Designing and testing second-generation GLP-1-based drugs aimed at improving patient tolerance while preserving or enhancing glucoregulatory control therefore provides clear clinical value. B12-Ex4 produced comparable glycemic control, and better tolerance, in an emetic mammalian species and in a lean polygenetic rat model of T2DM than Ex4.

In line with previous reports in lean, non-diabetic rats and shrews,<sup>8,14,36,37</sup> both native Ex4 doses (5 and 50 nmol/kg) tested here induced anorexia and body weight loss over 24 hours in shrews. By contrast, no such effects occurred after B12-Ex4 treatments, even at supra-pharmacological doses (i.e., 50 nmol/kg). The lack of short-term effects on feeding was unexpected given reports of a role of vagal afferent signaling in the mediation of the early-phase anorexia induced by both GLP-1 and native Ex4 in rats.<sup>38,39</sup> Previous reports also observed this effect in lean, healthy rats treated with the highest dose of B12-Ex4.<sup>8</sup> This incongruity, however, could be explained by broad species differences in metabolism between rats and shrews, rather than by the direct action of the drug.

Furthermore, B12-Ex4 administration resulted in a near complete absence of emesis compared with potent emetic effects of Ex4 in the shrew. In fact, we observed that  $\approx 10$ -fold the threshold concentration necessary for glucoregulation did not cause emesis with B12-Ex4, while all animals tested with this dose of Ex4 experienced emesis. Together, these findings show that



it is possible to both physiologically and pharmacologically separate the emetic potential of GLP-1R agonists like Ex4 from their glucoregulatory role, and that a wide range of B12-Ex4 doses produce limited anorectic or emetic side effects. This data suggests that a B12-Ex4 conjugate could improve T2DM medication adherence compared with existing GLP-1 mimetic drugs. This is particularly relevant given the pleiotropic nature of GLP-1, with a myriad of effects, mainly beneficial, which render GLP-1 analogues as one of the best current treatments for T2DM. Indeed, alternative therapies approved for the treatment of T2DM (e.g., dipeptidyl peptidase-4 inhibitors, metformin and sulfonylureas) do not achieve the same overall positive outcome on glucose handling compared with GLP-1R agonists.<sup>40,41</sup> Importantly, these alternative strategies also lead to modest but significant body weight reductions.<sup>40,41</sup>

Preventing access to CNS GLP-1Rs is the probable explanation for the lack of B12-Ex4–induced emesis in the shrew. Our immune-histological evidence supports this notion as we observed sparse c-Fos activation following systemic B12-Ex4 administration in the AP and NTS, two hindbrain nuclei known to mediate feeding behavior and emesis,<sup>13,32–35</sup> while native Ex4 produced robust activation of these nuclei. To provide functional evidence that B12 conjugation itself does not impact the emetic nature of Ex4, we centrally administered B12-Ex4 directly into the lateral ventricle of the shrew, which produced a comparable emetic profile with that of native Ex4 (e.g. the number of emetic episodes, latency to vomit, and the proportion of treated animals experiencing emesis). This data suggests that when centrally delivered, and thus bypassing the blood–brain barrier, B12-Ex4 is a stimulus that can produce an emetic profile consistent with Ex4 alone.

To speculate how conjugation to B12 reduces CNS penetrance of Ex4, increased polarity may be an important variable rather than the increased molecular size alone, given that GLP-1R agonists with greater molecular masses, such as liraglutide, have been shown to penetrate the hindbrain and to stimulate direct GLP-1R activation.<sup>42-44</sup> It is also possible that the binding of B12-Ex4 to the B12 carrier proteins transcobalamin (TC) or haptocorrin (HC) in serum, previously confirmed for this construct,<sup>8</sup> further reduces brain penetrance because its size (now >60 KDa) either actively transports the conjugate to systemic targets (via TC), maintains the conjugate in serum (via HC), or protects the conjugate from proteolytic degradation (via TC or HC),<sup>9</sup> as is typical for dietary B12 alone.<sup>45</sup> As noted, however, the shrew has both TC and HC, unlike rodents, which have only TC. In comparison with studies performed for B12-Ex4 in rodents,<sup>8</sup> we see comparable pharmacodynamics (in terms of illness behaviors and glucoregulation), suggesting that the presence of both TC and HC is not specifically necessary for the conjugate. It may be that the benefits of conjugation lie solely with the B12 molecule itself, or simply through the effects of binding to any B12 binding protein in terms of protection and/or mitigation of hindbrain access. This data suggests that it is the unique structure of B12-Ex4, rather than simply mass, which drives its unique pharmacodynamic profile and underlying properties.

Pancreatic  $\beta$ -cells expressing the GLP-1R represent the probable cellular substrate mediating the hypoglycemic effects of B12-Ex4 in shrews. A previously reported fluorescently tagged B12-Ex4 conjugate (Cy5-B12-Ex4) was shown to co-localize with insulin in the shrew pancreatic  $\beta$ -cells.<sup>8</sup> By employing fluorescently tagged Ex4 in combination with Cy5-B12-Ex4, further investigations are warranted to examine the binding specificity of B12-Ex4 in the pancreas. Nevertheless, the current data supports previous work shown in rodents<sup>8</sup> and

strengthens the notion that the incretin effect occurring after GLP-1 analogue administration is mediated by direct activation of GLP-1Rs expressed on pancreatic  $\beta$ -cells, mimicking the paracrine actions of pancreatic-derived GLP-1.<sup>10-12</sup>

It is also possible that GLP-1Rs expressed in other peripheral tissues may be engaged by B12-Ex4 and thus contribute to its beneficial effects on glucose homeostasis. For instance, it has been shown that low doses of Ex4 that mimic endogenous GLP-1 release can modulate glycaemia and gastric emptying via vagal afferent signaling.<sup>39</sup> Further, GLP-1Rs are also abundantly expressed on enteric neurons, and emerging evidence suggests a role of the enteric nervous system in the mediation of effects induced by GLP-1 analogues.<sup>46-49</sup> Whether B12-Ex4 acts on GLP-1Rs expressed in the periphery beyond the pancreas, possibly within the peripheral and enteric nervous system, and to what degree these hypothetical actions contribute to the observed augmented glucoregulation, requires further investigation.

I also report that B12-Ex4 improves glucose clearance relative to Ex4 in a lean, polygenetic model of T2DM, the GK rat. Like liraglutide, B12-Ex4 does not produce the transient stress-induced hyperglycemic response in the GK rat commonly observed from Ex4 across rat models (lean, obese or GK),<sup>50,51</sup> a phenomenon tied to the high CNS penetrance of Ex4. Consistent with the lack of a CNS stress-mediated hyperglycaemia reported for Ex4,<sup>50,51</sup> B12-Ex4 did not produce the documented CNS-dependent outcomes of anorexia and body weight loss in this lean model of T2DM.

In summary, I report both the preservation of hypoglycemic responses and superior tolerance of B12-Ex4 over native Ex4 in musk shrews and the GK rat. The data presented here in shrews and GK rats support our hypothesis that limiting or blocking Ex4 entry into the brain

dramatically reduces the side effects of the Ex4 drug (i.e. prevents anorexia and emesis), while maintaining the glucoregulatory efficacy of the compound without influencing energy balance in shrews. The overall outcomes of this work highlight the translational potential of B12-Ex4–based pharmacotherapies for use in lean T2D patients where weight loss is an undesirable outcome, although chronic studies are needed to elucidate the efficacy, tolerability, and pharmacodynamics of B12-Ex4 in long-term treatment. Albeit small, there is the possibility that B12-Ex4 chronic exposure would interfere with normal B12 physiology, potentially reducing the amount of dietary B12 available in the body.<sup>52</sup> Further, while I do not predict tachyphylaxis, the extent to which the observed positive effects will be maintained requires future empirical testing. Nonetheless, the presented data underlie the potential use of B12-Ex4 for patients with T2DM who either do not tolerate current GLP-1 agonists or suffer from co-morbidities associated with an anorectic/cachectic state, for which the body weight-suppressing effects of a standard GLP-1R agonist are an unwanted side effect, with the loss of nausea/emesis an additional benefit.

## 2.6 References

- (1) Sanger, G. J.; Andrews, P. L. R. A History of Drug Discovery for Treatment of Nausea and Vomiting and the Implications for Future Research. *Front. Pharmacol.* **2018**, *9* (SEP), 1–35.
- (2) Htike, Z. Z.; Zaccardi, F.; Papamargaritis, D.; Webb, D. R.; Khunti, K.; Davies, M. J. Efficacy and Safety of Glucagon-like Peptide-1 Receptor Agonists in Type 2 Diabetes: A Systematic Review and Mixed-Treatment Comparison Analysis. *Diabetes, Obes. Metab.* **2017**, *19* (4), 524–536.
- (3) Bergenstal, R. M.; Wysham, C.; MacConell, L.; Malloy, J.; Walsh, B.; Yan, P.; Wilhelm, K.; Malone, J.; Porter, L. E. Efficacy and Safety of Exenatide Once Weekly versus Sitagliptin or Pioglitazone as an Adjunct to Metformin for Treatment of Type 2 Diabetes (DURATION-2): A Randomised Trial. *Lancet* **2010**, *376* (9739), 431–439.
- (4) Buse, J. B.; Henry, R. R.; Han, J.; Kim, D. D.; Fineman, M. S.; Baron, A. D. Effects of Exenatide (Exendin-4) on Glycemic Control over 30 Weeks in Sulfonylurea-Treated Patients with Type 2 Diabetes. *Diabetes Care* **2004**, *27* (11), 2628–2635.
- (5) DeFronzo, R. A.; Ratner, R. E.; Han, J.; Kim, D. D.; Fineman, M. S.; Baron, A. D. Effects of Exenatide (Exendin-4) on Glycemic Control and Weight over 30 Weeks in Metformin-Treated Patients with Type 2 Diabetes. *Diabetes Care* **2005**, *28* (5), 1092–1100.
- (6) John, L. E.; Kane, M. P.; Busch, R. S.; Hamilton, R. A. Expanded Use of Exenatide in the Management of Type 2 Diabetes. *Diabetes Spectr.* **2007**, *20* (1), 59–63.
- (7) Kendall, D. M.; Riddle, M. C.; Rosenstock, J.; Zhuang, D.; Kim, D. D.; Fineman, M. S.; Baron, A. D. Effects of Exenatide (Exendin-4) on Glycemic Control over 30 Weeks in Patients with Type 2 Diabetes Treated with Metformin and a Sulfonylurea. *Diabetes Care* **2005**, *28* (5),

- 1083–1091.
- (8) Mietlicki-Baase, E. G.; Liberini, C. G.; Workinger, J. L.; Bonaccorso, R. L.; Borner, T.; Reiner, D. J.; Koch-Laskowski, K.; McGrath, L. E.; Lhamo, R.; Stein, L. M.; De Jonghe, B. C.; Holz, G. G.; Roth, C. L.; Doyle, R. P.; Hayes, M. R. A Vitamin B12 Conjugate of Exendin-4 Improves Glucose Tolerance without Associated Nausea or Hypophagia in Rodents. *Diabetes, Obes. Metab.* **2018**, *20* (5), 1223–1234.
- (9) Bonaccorso, R. L.; Chepurny, O. G.; Becker-Pauly, C.; Holz, G. G.; Doyle, R. P. Enhanced Peptide Stability Against Protease Digestion Induced by Intrinsic Factor Binding of a Vitamin B12 Conjugate of Exendin-4. *Mol. Pharm.* **2015**, *12* (9), 3502–3506.
- (10) Lamont, B. J.; Li, Y.; Kwan, E.; Brown, T. J.; Gaisano, H.; Drucker, D. J. Pancreatic GLP-1 Receptor Activation Is Sufficient for Incretin Control of Glucose Metabolism in Mice. *J. Clin. Invest.* **2012**, *122* (1), 388–402.
- (11) Smith, E. P.; An, Z.; Wagner, C.; Lewis, A. G.; Cohen, E. B.; Li, B.; Mahbod, P.; Sandoval, D.; Perez-Tilve, D.; Tamarina, N.; Philipson, L. H.; Stoffers, D. A.; Seeley, R. J.; D'Alessio, D. A. The Role of  $\beta$  Cell Glucagon-like Peptide-1 Signaling in Glucose Regulation and Response to Diabetes Drugs. *Cell Metab.* **2014**, *19* (6), 1050–1057.
- (12) Chambers, A. P.; Sorrell, J. E.; Haller, A.; Roelofs, K.; Hutch, C. R.; Kim, K. S.; Gutierrez-Aguilar, R.; Li, B.; Drucker, D. J.; D'Alessio, D. A.; Seeley, R. J.; Sandoval, D. A. The Role of Pancreatic Preproglucagon in Glucose Homeostasis in Mice. *Cell Metab.* **2017**, *25* (4), 927–934.
- (13) Kanoski, S. E.; Rupprecht, L. E.; Fortin, S. M.; De Jonghe, B. C.; Hayes, M. R. The Role of Nausea in Food Intake and Body Weight Suppression by Peripheral GLP-1 Receptor

- Agonists, Exendin-4 and Liraglutide. *Neuropharmacology* **2012**, *62* (5–6), 1916–1927.
- (14) Chan, S. W.; Lin, G.; Yew, D. T. W.; Yeung, C. K.; Rudd, J. A. Separation of Emetic and Anorexic Responses of Exendin-4, a GLP-1 Receptor Agonist in *Suncus Murinus* (House Musk Shrew). *Neuropharmacology* **2013**, *70* (5–6), 141–147.
- (15) Chan, S. W.; Lin, G.; Yew, D. T. W.; Rudd, J. A. A Physiological Role of Glucagon-like Peptide-1 Receptors in the Central Nervous System of *Suncus Murinus* (House Musk Shrew). *Eur. J. Pharmacol.* **2011**, *668* (1–2), 340–346.
- (16) Andersen, A.; Lund, A.; Knop, F. K.; Vilsbøll, T. Glucagon-like Peptide 1 in Health and Disease. *Nat. Rev. Endocrinol.* **2018**, *14* (7), 390–403.
- (17) Bray, G. A.; Frühbeck, G.; Ryan, D. H.; Wilding, J. P. H. Management of Obesity. *Lancet* **2016**, *387* (10031), 1947–1956.
- (18) Gallo, M.; Muscogiuri, G.; Felicetti, F.; Faggiano, A.; Trimarchi, F.; Arvat, E.; Vigneri, R.; Colao, A. Adverse Glycaemic Effects of Cancer Therapy: Indications for a Rational Approach to Cancer Patients with Diabetes. *Metabolism.* **2018**, *78*, 141–154.
- (19) Moheet, A.; Moran, A. CF-Related Diabetes: Containing the Metabolic Miscreant of Cystic Fibrosis. *Pediatr. Pulmonol.* **2017**, *52*, S37–S43.
- (20) Noubissi, E. C.; Katte, J. C.; Sobngwi, E. Diabetes and HIV. *Curr. Diab. Rep.* **2018**, *18* (11).
- (21) Gläser, S.; Krüger, S.; Merkel, M.; Bramlage, P.; Herth, F. J. F. Chronic Obstructive Pulmonary Disease and Diabetes Mellitus: A Systematic Review of the Literature. *Respiration* **2015**, *89* (3), 253–264.
- (22) Mesinovic, J.; Zengin, A.; De Courten, B.; Ebeling, P. R.; Scott, D. Sarcopenia and Type 2 Diabetes Mellitus: A Bidirectional Relationship. *Diabetes, Metab. Syndr. Obes. Targets*

- Ther.* **2019**, *12*, 1057–1072.
- (23) Caspard, H.; Jabbour, S.; Hammar, N.; Fenici, P.; Sheehan, J. J.; Kosiborod, M. Recent Trends in the Prevalence of Type 2 Diabetes and the Association with Abdominal Obesity Lead to Growing Health Disparities in the USA: An Analysis of the NHANES Surveys from 1999 to 2014. *Diabetes, Obes. Metab.* **2018**, *20* (3), 667–671.
- (24) Goto, Y.; Kakizaki, M.; Masaki, N. Production of Spontaneous Diabetic Rats by Repetition of Selective Breeding. *Tohoku J. Exp. Med.* **1976**, *119* (1), 85–90.
- (25) Östenson, C. G.; Efendic, S. Islet Gene Expression and Function in Type 2 Diabetes; Studies in the Goto-Kakizaki Rat and Humans. *Diabetes, Obes. Metab.* **2007**, *9* (SUPPL. 2), 180–186.
- (26) Ueno, S.; Matsuki, N.; Saito, H. Suncus Murinus: A New Experimental Model In Emesis Research. *Life Sci.* **1987**, *41* (4), 513–518.
- (27) Andrews, P. L. R.; Friedman, M. I.; Liu, Y. L.; Smith, J. E.; Sims, D. W. Potential Energetic Implications of Emesis in the House Musk Shrew (*Suncus Murinus*). *Physiol. Behav.* **2005**, *84* (4), 519–524.
- (28) Clardy-James, S.; Bernstein, J. L.; Kerwood, D. J.; Doyle, R. P. Site-Selective Oxidation of Vitamin B12 Using 2-Iodoxybenzoic Acid. *Synlett* **2012**, *23* (16), 2363–2366.
- (29) Kolb, H. C.; Finn, M. G.; Sharpless, K. B. Click Chemistry: Diverse Chemical Function from a Few Good Reactions. *Angew. Chemie - Int. Ed.* **2001**, *40* (11), 2004–2021.
- (30) Huisgen, R. 1,3-Dipolar Cycloadditions. *Proc. Chem. Soc.* **1961**, *144* (5), 357–396.
- (31) Kolb, H.; Sharpless, K. B. The Growing Impact of Click Chemistry on Drug Discovery. *Drug Discov. Today* **2003**, *8* (24), 1128–1137.
- (32) Hornby, P. J. Central Neurocircuitry Associated with Emesis. *Am. J. Med.* **2001**, *111* (8



- SUPPL. 1), 106–112.
- (33) Miller, A. D.; Leslie, R. A. The Area Postrema and Vomiting. *Frontiers in Neuroendocrinology*. **1994**, *15* (4), 301–320.
- (34) Grill, H. J.; Hayes, M. R. The Nucleus Tractus Solitarius: A Portal for Visceral Afferent Signal Processing, Energy Status Assessment and Integration of Their Combined Effects on Food Intake. *Int. J. Obes.* **2009**, *33* (SUPPL. 1), S11–S15.
- (35) Price, C. J.; Hoyda, T. D.; Ferguson, A. V. The Area Postrema: A Brain Monitor and Integrator of Systemic Autonomic State. *Neuroscientist* **2008**, *14* (2), 182–194.
- (36) Zhao, P.; Liang, Y. L.; Belousoff, M. J.; Deganutti, G.; Fletcher, M. M.; Willard, F. S.; Bell, M. G.; Christe, M. E.; Sloop, K. W.; Inoue, A.; Truong, T. T.; Clydesdale, L.; Furness, S. G. B.; Christopoulos, A.; Wang, M. W.; Miller, L. J.; Reynolds, C. A.; Danev, R.; Sexton, P. M.; Wootten, D. Activation of the GLP-1 Receptor by a Non-Peptidic Agonist. *Nature* **2020**, *577* (7790), 432–436.
- (37) Aroda, V. R.; Rosenstock, J.; Terauchi, Y.; Altuntas, Y.; Lalic, N. M.; Villegas, E. C. M.; Jeppesen, O. K.; Christiansen, E.; Hertz, C. L.; Haluzík, M. PIONEER 1: Randomized Clinical Trial of the Efficacy and Safety of Oral Semaglutide Monotherapy in Comparison with Placebo in Patients with Type 2 Diabetes. *Diabetes Care* **2019**, *42* (9), 1724–1732.
- (38) Labouesse, M. A.; Stadlbauer, U.; Weber, E.; Arnold, M.; Langhans, W.; Pacheco-López, G. Vagal Afferents Mediate Early Satiety and Prevent Flavour Avoidance Learning in Response to Intraperitoneally Infused Exendin-4. *J. Neuroendocrinol.* **2012**, *24* (12), 1505–1516.
- (39) Krieger, J. P.; Arnold, M.; Pettersen, K. G.; Lossel, P.; Langhans, W.; Lee, S. J. Knockdown of

- GLP-1 Receptors in Vagal Afferents Affects Normal Food Intake and Glycemia. *Diabetes* **2016**, *65* (1), 34–43.
- (40) Brunton, S. GLP-1 Receptor Agonists vs. DPP-4 Inhibitors for Type 2 Diabetes: Is One Approach More Successful or Preferable than the Other? *Int. J. Clin. Pract.* **2014**, *68* (5), 557–567.
- (41) Liu, J.; Hu, Y.; Xu, Y.; Jia, Y.; Miao, L.; Wang, G. Comparison of Exenatide and Metformin Monotherapy in Overweight/Obese Patients with Newly Diagnosed Type 2 Diabetes. *Int. J. Endocrinol.* **2017**, *2017*, 9401606.
- (42) Kanoski, S. E.; Fortin, S. M.; Arnold, M.; Grill, H. J.; Hayes, M. R. Peripheral and Central GLP-1 Receptor Populations Mediate the Anorectic Effects of Peripherally Administered GLP-1 Receptor Agonists, Liraglutide and Exendin-4. *Endocrinology* **2011**, *152* (8), 3103–3112.
- (43) Sisley, S.; Gutierrez-Aguilar, R.; Scott, M.; D'Alessio, D.; Sandoval, D.; Seeley, R. Neuronal GLP1R Mediates Liraglutide's Anorectic but Not Glucose-Lowering Effect. *J. Clin. Invest.* **2014**, *124* (6), 2456–2463.
- (44) Secher, A.; Jelsing, J.; Baquero, A. F.; Hecksher-Sørensen, J.; Cowley, M. A.; Dalbøge, L. S.; Hansen, G.; Grove, K. L.; Pyke, C.; Raun, K.; Schäfer, L.; Tang-Christensen, M.; Verma, S.; Witgen, B. M.; Vrang, N.; Knudsen, L. B. The Arcuate Nucleus Mediates GLP-1 Receptor Agonist Liraglutide-Dependent Weight Loss. *J. Clin. Invest.* **2014**, *124* (10), 4473–4488.
- (45) Green, R.; Allen, L. H.; Bjørke-Monsen, A. L.; Brito, A.; Guéant, J. L.; Miller, J. W.; Molloy, A. M.; Nexø, E.; Stabler, S.; Toh, B. H.; Ueland, P. M.; Yajnik, C. Vitamin B12 Deficiency. *Nat. Rev. Dis. Prim.* **2017**, *3*, 17040.
- (46) Richards, P.; Parker, H. E.; Adriaenssens, A. E.; Hodgson, J. M.; Simon, C.; Trapp, S.; Gribble,

- F. M.; Reimann, F. Identification and Characterisation of Glucagon-like Peptide-1 Receptor Expressing Cells Using a New Transgenic Mouse Model. *Diabetes* **2014**, *63* (4), 1224–1233.
- (47) Varin, E. M.; Mulvihill, E. E.; Baggio, L. L.; Koehler, J. A.; Cao, X.; Seeley, R. J.; Drucker, D. J. Distinct Neural Sites of GLP-1R Expression Mediate Physiological versus Pharmacological Control of Incretin Action. *Cell Rep.* **2019**, *27* (11), 3371–3384.
- (48) Drucker, D. J. Mechanisms of Action and Therapeutic Application of Glucagon-like Peptide-1. *Cell Metab.* **2018**, *27* (4), 740–756.
- (49) Washington, M. C.; Raboin, S. J.; Thompson, W.; Larsen, C. J.; Sayegh, A. I. Exenatide Reduces Food Intake and Activates the Enteric Nervous System of the Gastrointestinal Tract and the Dorsal Vagal Complex of the Hindbrain in the Rat by a GLP-1 Receptor. *Brain Res.* **2010**, *1344*, 124–133.
- (50) Gao, W.; Jusko, W. J. Pharmacokinetic and Pharmacodynamic Modeling of Exendin-4 in Type 2 Diabetic Goto-Kakizaki Rats. *J. Pharmacol. Exp. Ther.* **2011**, *336* (3), 881–890.
- (51) Pérez-Tilve, D.; González-Matías, L.; Aulinger, B. A.; Alvarez-Crespo, M.; Gil-Lozano, M.; Alvarez, E.; Andrade-Olivie, A. M.; Tschöp, M. H.; D’Alessio, D. A.; Mallo, F. Exendin-4 Increases Blood Glucose Levels Acutely in Rats by Activation of the Sympathetic Nervous System. *Am. J. Physiol. - Endocrinol. Metab.* **2010**, *298* (5), 1088–1096.
- (52) Lildballe, D. L.; Mutti, E.; Birn, H.; Nexø, E. Maximal Load of the Vitamin B12 Transport System: A Study on Mice Treated for Four Weeks with High-Dose Vitamin B12 or Cobinamide. *PLoS One* **2012**, *7* (10), e46657.

### Chapter 3: Corination of a GLP-1 Receptor Agonist for Glycemic Control without Emesis

The work reported in this chapter resulted in two peer-reviewed research papers:

(1) **Ian C. Tinsley**, Tito Borner, Jayme L. Workinger, Samantha M. Fortin, Lauren M. Stein, Oleg G. Chepurny, George G. Holz, Aleksandra J. Wierzba, Dorota Gryko, Ebba Nexo, Evan D. Shaulson, Ankur Bamezai, Valentina A. Rodriguez Da Silva, Bart C. De Jonghe, Matthew R. Hayes, Robert P. Doyle\*. Corination of a GLP-1 Receptor Agonist for Glycemic Control without Emesis.

*Cell Reports*. **2020**, *31* (11), 107768.

(2) **Ian C. Tinsley**, Tito Borner, MacKenzie L. Swanson, Oleg G. Chepurny, Sarah A. Doble, Varun Kamat, Ian R. Sweet, George G. Holz, Matthew R. Hayes, Bart C. De Jonghe, Robert P. Doyle\*. Synthesis, Optimization, and Biological Evaluation of Corinated Conjugates of the GLP-1R Agonist Exendin-4. *J. Med. Chem.* **2021**, *64* (6), 3479-3492.

The author was co-first author (with Dr. Tito Borner) on both papers and performed all synthetic work including synthesis of all tested compounds and their purification, chemical and *in vitro* biochemical characterization, and preparation for *in vivo* testing. In addition, the author assisted in all *in vivo* data collected in collaboration with Dr. Tito Borner of the University of Pennsylvania. Along with RPD, this author was also the lead author of the *J. Med. Chem* paper.



The paper published in the *Journal of Medicinal Chemistry* (Tinsley et al., **2021**, 64 (6), 3479-3492) was selected as issue cover.

### 3.1 Introduction

The dramatic rise of type 2 diabetes mellitus (T2DM) and obesity as comorbidities has driven a concomitant rise in new pharmaceutical interventions to treat such disorders, either together or individually.<sup>1-7</sup> Type 2 diabetes mellitus (T2DM) management involves lifelong pharmaceutical interventions,<sup>6,7</sup> including those based on glucagon-like peptide-1 (GLP-1), an incretin hormone produced in the intestine and brainstem.<sup>8,9</sup> One extremely successful family of pharmaceuticals in this field has been that of glucagon-like peptide-1 receptor agonists (GLP-1RAs),<sup>8-13</sup> such as exenatide (i.e., Exendin-4; Ex4), liraglutide,<sup>14-16</sup> and semaglutide.<sup>14,17,18</sup> Existing US Food and Drug Administration (FDA)-approved GLP-1 receptor (GLP-1R) agonists enhance postprandial insulin secretion and reduce food intake.<sup>8,12,13</sup> Exenatide and liraglutide confer glucoregulation in tandem with a body weight reduction of 5–6% over ~1 year,<sup>14,18</sup> while semaglutide can produce a weight loss of 10–12% over the same time period.<sup>14,18</sup> While weight loss is attractive when considering GLP-1R agonists for obesity treatment, the hypophagic effects of all known GLP-1R agonists are accompanied by nausea and vomiting, which affects ~20%–50% of patients and leads to discontinuation of drug treatment in ~6%–10% and reduced dose tolerance in another ~15% of patients.<sup>19-25</sup> Evidence-based medical reports are now clear that nausea and emesis are the principal side effects of existing GLP-1 therapeutics as a result of central nervous system (CNS) penetrance.<sup>26-30</sup> Even with common approaches to mitigate side effects such as slow-dose escalation or titration, a recent report from GlaxoSmithKline concluded that patients reported GI-related issues that “made me feel sick” (64.4%) and “made me throw up” (45.4%) as their major reasons for treatment discontinuation.<sup>31</sup> Importantly, such adverse gastrointestinal events of GLP-1R agonists are persistent in the profile of current second-

generation GLP-1R-based drugs such as dulaglutide, semaglutide, and albiglutide.<sup>32-34</sup> Importantly, for some diabetic patients with comorbidities such as cancer, cystic fibrosis, HIV, or general disease-cachexia, any further weight loss and malaise are unacceptable side effects that necessitate the creation of a new class of GLP-1 therapeutic.<sup>35-39</sup>

There is convincing evidence that a significant portion of the increase in glucose-stimulated insulin secretion following administration of current exogenous GLP-1R ligands is mediated by direct activation of GLP-1R expressed on pancreatic  $\beta$ -cells,<sup>8,13,40,41</sup> mimicking the paracrine effects of pancreatic derived GLP-1 that may not occur with endogenous L-cell derived GLP-1.<sup>42-44</sup> In contrast, GLP-1Rs expressed in the central nervous system (CNS), in particular those in the hindbrain,<sup>45,46</sup> mediate the food intake- and body weight-suppressive effects of GLP-1R agonists, such as liraglutide and exenatide (synthetic Ex4).<sup>27-29,47</sup> This CNS site-of-action, and not a vagally mediated effect, is also responsible for mediating the illness-like behaviors (e.g., nausea, conditioned taste avoidance, emesis) of systemically delivered GLP-1R agonists.<sup>30</sup> Thus, from a therapeutic standpoint aimed at normalizing the chronic hyperglycemia of diabetic patients, designing a GLP-1R agonist that does not penetrate readily into the CNS (or at least the hindbrain), but retains enhanced pharmacological action on  $\beta$ -cells, would theoretically provide an improved tool for glycemic control without eliciting unwanted nausea/malaise.

Taking advantage of the highly controlled transport and trafficking of vitamin B12 (B12) that occurs in mammalian physiology,<sup>48-52</sup> together with bioconjugate technology involving peptide-based conjugation to B12 and B12 fragments, Ex4 was covalently attached to dicyanocobinamide (Cbi), a corrin-ring containing precursor of B12, to create the compound Cbi-Ex4. The theoretical advantage of this construct was 3-fold. First, there is no known biological

function of Cbi in humans and Cbi does not affect intact B12 physiology.<sup>53</sup> Second, Cbi is highly water soluble and the uptake of Cbi-Ex4 through the blood brain barrier and into the CNS would putatively be extremely low.<sup>53</sup> Indeed, evidence collected postmortem from human brain and liver clearly demonstrated negligible amounts of B12 (11.3 pmol/g) and an  $\approx$ 10-fold lower relative concentration of corrinoid-type analogs (1.3 pmol/g; including cobinamide) in the brain, with the liver being the main site of concentration for both B12 and corrinoid analogs (total >600 pmol/g).<sup>54</sup> These first two advantages of Cbi-Ex4 provide support for the third and most important hypothesized benefit—namely that Cbi-Ex4 should theoretically be a GLP-1R agonist that retains a peripheral site of action when systemically administered, providing a pancreatic-mediated mechanism for Cbi-Ex4 to improve hyperglycemia, without producing any CNS-mediated illness-like behaviors.

Cbi has been identified in humans,<sup>55</sup> but has no influence on normal B12 homeostasis<sup>53</sup> since it is *not* recognized by the B12 blood transporting protein transcobalamin (TC), critical for blood-brain barrier penetrance and cell entry via the CD320 receptor.<sup>53</sup> Instead, Cbi is recognized in blood *only* by the B12 binding protein haptocorrin (HC). The function of circulating HC is unknown and no known specific receptor for the Cbi-HC complex has been identified.<sup>56</sup> Indeed, congenital defects in plasma HC are asymptomatic, suggesting that HC and Cbi are not physiologically relevant in humans.<sup>57</sup> Further, the plasma-binding capacity of HC for molecular forms of B12, including Cbi, in humans is very limited (reference interval 90–270 pM).<sup>58</sup> Thus, using Cbi (in a conjugate process we coin here “corrination”) as a pharmacodynamic/pharmacokinetic modifier of a target peptide pharmaceutical, we have created an “inert” carrier in terms of affecting B12 homeostasis, but one that would have the advantage of putatively



reducing/avoiding CNS permeability/localization while improving the general proteolytic survival and/or reduce clearance of the bound peptide. Unfortunately, rodents do not represent ideal models to test Cbi-Ex4 as (1) they lack the separate HC and TC proteins as found in human blood<sup>59</sup> and (2) they lack the emetic reflex.<sup>60</sup> The musk shrew (*Suncus murinus*) was therefore chosen as the model system to evaluate the *in vivo* efficacy and tolerability of Cbi-Ex4, as shrews are capable of emesis and were believed, through bioinformatics, to have the same B12 binding profile in blood as humans (*vide infra*). Importantly, in the context of modeling the GLP-1 system, the shrew also shows hypoglycemia, anorexia, and emetic sensitivity to existing GLP-1R agonists.<sup>61,62</sup>

### 3.2. Synthesis of Dicyanocobinamide (Cbi)

Synthesis of Dicyanocobinamide (Cbi) (**2**). The synthesis of dicyanocobinamide (Cbi) was performed according to previously reported methods.<sup>63</sup> Briefly, to a 10 mL microwave reaction vessel containing a magnetic stir bar were added B12 (cyanocobalamin) (303.8 mg, 0.225 mmol), sodium cyanide (NaCN) (36.9 mg, 0.7096 mmol), and 5 mL of EtOH, and the vessel was sealed. The reaction was heated to 120 °C for 10 min. Following completion of the microwave reaction, the remaining solution was transferred and diluted using isopropyl alcohol (iPrOH). The reaction was purified utilizing a normal-phase silica column. The reaction was eluted using 100% methanol (MeOH). The product eluted as a purple product. The isolated product was precipitated utilizing diethyl ether (Et<sub>2</sub>O) and allowed to dry producing a solid, purple product, **2**, in 80% yield (187.4 mg, 0.1795 mmol) (Figure 1). Solubility was measured to be 400 mg/mL in deionized water. **2** was purified by RP-HPLC as described for method A1, to 98%; t<sub>R</sub>: 5.2 and 6.7 min (Figure 2); ESI-MS expected *m/z* = 1042, observed *m/z* = 1016 [M-CN]<sup>+1</sup> (Figure 3).

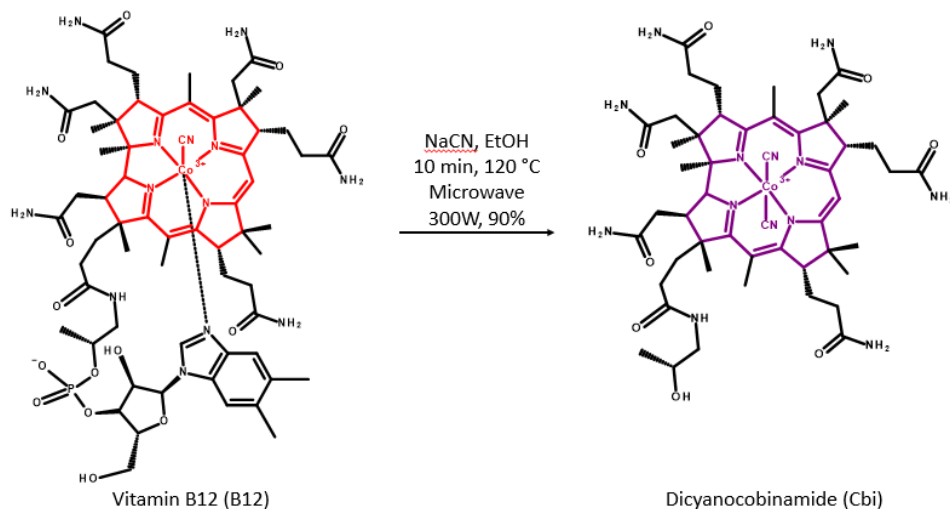


**Figure 1.** Synthetic scheme for Cbi. Cbi was formed via microwave from B12.

mV

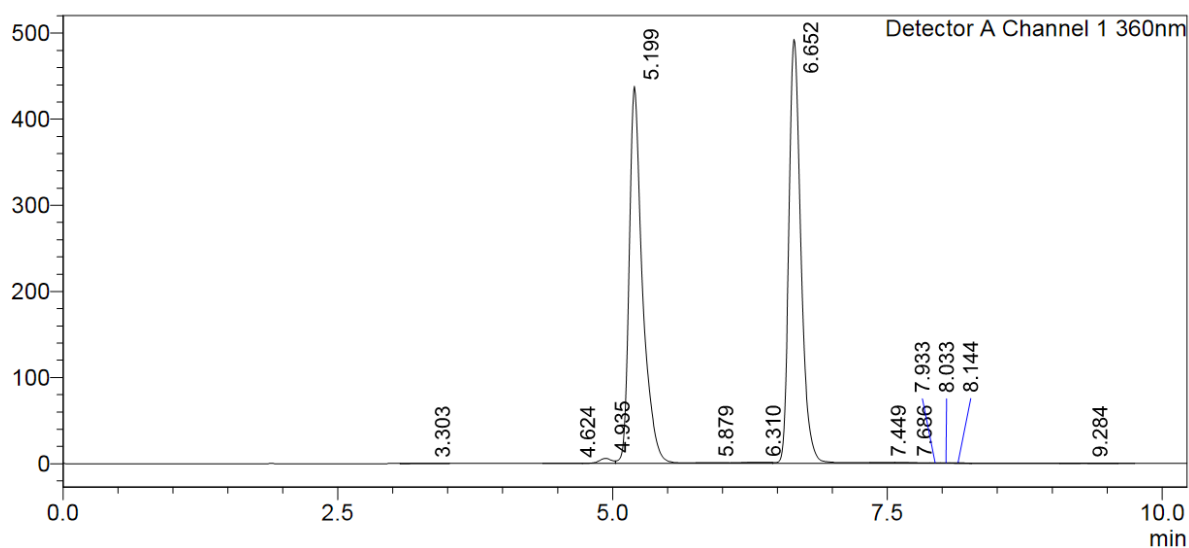


**Figure 2.** RP-HPLC Trace (Shimadzu Prominence HPLC using a C18 column (Eclipse XDB-C18 5 $\mu$ m, 4.6 x 150 mm) (RP-HPLC, from 1% CH<sub>3</sub>OH/H<sub>2</sub>O + 0.1% TFA to 70% CH<sub>3</sub>OH/H<sub>2</sub>O + 0.1% TFA in 15 min)) showing the  $\alpha$ - and  $\beta$ -isomer products at 5.2 and 6.7 minutes. Purity 98%.

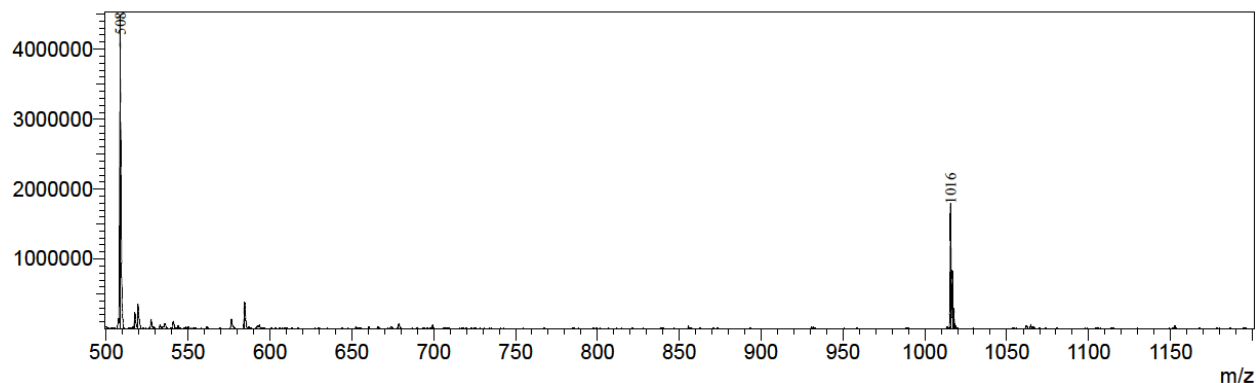


**Figure 3.** ESI-MS (Shimadzu LCMS-8040) of Cbi, expected  $m/z = 1042$ , observed  $m/z = 1016$  [M-CN]<sup>+1</sup>.

### 3.3 Design and Synthesis of Cbi-Ex4

Corrination of Ex4 with the Cbi compound dicyanocobinamide was successfully synthesized to produce a GLP-1R agonist, namely, Cbi-Ex4. The conjugate is linked between the K12 residue of Ex4 and the terminal *f*-branch of Cbi. These two positions were previously reported by us<sup>49</sup> and others<sup>64,65</sup> to support high-efficiency conjugation. While no spacer optimization was conducted, we utilized a spacer length that was already established by us to yield a high-potency B12-Ex4 conjugate.<sup>48,66</sup>

#### 3.3.1 Synthesis of Cbi-Aminobutyne (Cbi-AB)

The purple Cbi produced was activated with an excess of 1,1'-carbonyl-di-(1,2,4-triazole) (CDT) in dry N-methyl-2-pyrrolidone (NMP) and heating at 40 °C under argon for ~10 min or until complete dissolution was observed. Upon dissolution, 1-amino-3-butyne was added in large excess (20×) relative to the activated Cbi along with triethylamine (TEA), and the reaction was allowed to proceed for 1 h, again at 40 °C under argon with stirring. Initially, it was observed via RP-HPLC tracking on a C18 column (data not shown) that the reaction proceeded slowly, so in subsequent experiments, a second equivalent of linker (20×) and TEA were added at the 1 h time

point, and the reaction was allowed to proceed, as before, for an additional hour. Based on the additional step, yields for Cbi-AB was 53% with facile purification to produce the Cbi-AB (Figure 4) with purities at, or in excess of, 97% (as tracked by RP-HPLC) (Figure 5). ESI-MS analysis showed expected  $m/z = 1129$ , observed  $m/z = 1111 [M^+ - H_2O]^+$  (Figure 6). It should also be noted that a color change was observed upon formation of the Cbi-linkers, going from purple to orange upon purification of the Cbi-AB in water. This color change was previously reported by Zhou and Zelder<sup>67</sup> and assigned to the formation of isomers, namely,  $\alpha$ -cyano- $\beta$ -aqua- and  $\alpha$ -aqua- $\beta$ -cyano-Cbi (as indicated in Figure 4). This suggestion of isomer formation was supported by the HPLC traces of Cbi-AB (Figure 5), which clearly showed the presence of both isomers. Given the fact that such isomers were not expected to negatively affect the subsequent chemistry or biology, isomers were combined prior to peptide coupling.

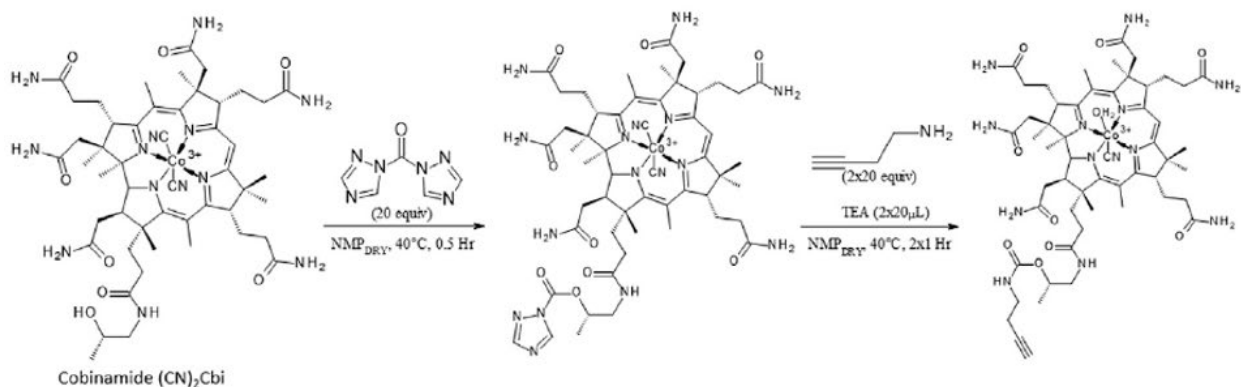


**Figure 4.** Synthetic scheme for Cbi-AB synthesis, 1-amino-3-butyne was coupled to Cbi through secondary alcohol to create carbamate linkage utilizing 1,1'-carbonyl-di-(1,2,4-triazole) (CDT), priming the Cbi for conjugation to Ex4.

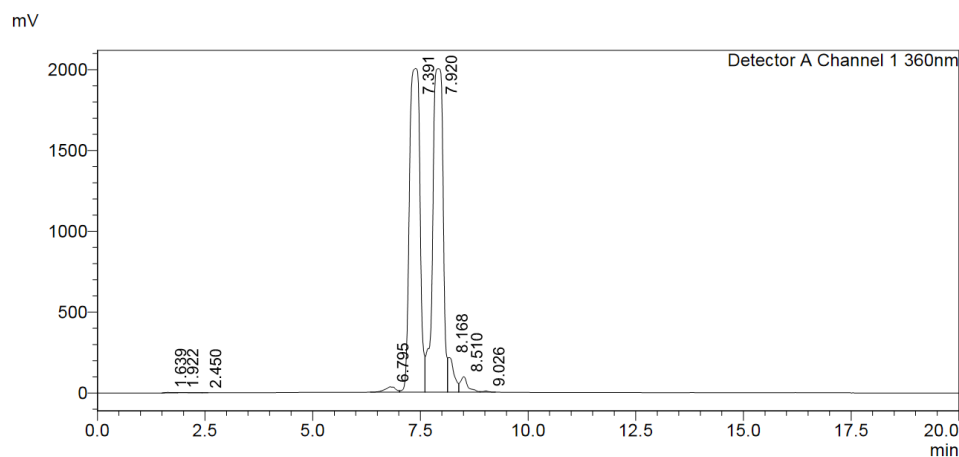


**Figure 5.** RP-HPLC Trace (Shimadzu Prominence HPLC using a C18 column (Eclipse XDB-C18 5 $\mu$ m, 4.6 x 150 mm) (RP-HPLC, from 1% CH<sub>3</sub>OH/H<sub>2</sub>O + 0.1% TFA to 70% CH<sub>3</sub>OH/H<sub>2</sub>O + 0.1% TFA in 15 min)) showing the  $\alpha$ - and  $\beta$ - isomers of the Cbi-AB Product at 7.4 and 7.9 minutes. Purity 97%..

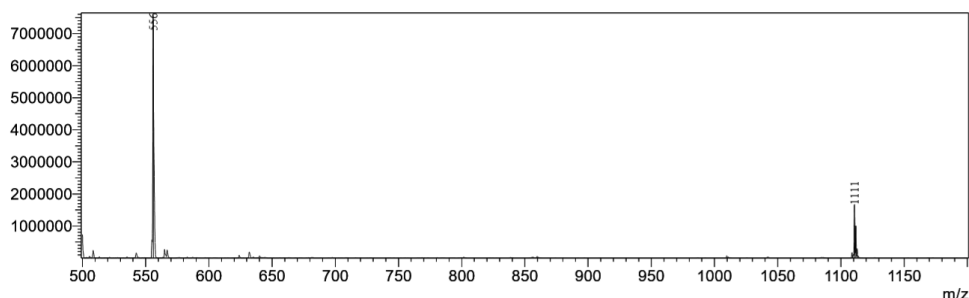


**Figure 6.** ESI-MS (Shimadzu LCMS-8040) of Cbi-Alkyne, expected  $m/z = 1129$ , observed  $m/z = 1111$  [ $M^+ - H_2O$ ]<sup>+</sup>.

### 3.3.2 Synthesis and Characterization of Cbi-Ex4

Coupling of K12-azido-modified Ex4 (noted throughout here simply as Ex4 ) to produce conjugate Cbi-Ex4 was achieved via copper(I)- mediated alkyne-azide cycloaddition (CuAAC) over 16 h at room temperature in a 4:1 dimethylformamide (DMF)/H<sub>2</sub>O solvent system in the presence of the tertiary amine tris((1-benzyl-4- triazolyl)methyl)amine (TBTA) to stabilize copper(I) (Figure 7).<sup>68</sup> Yield obtained were quantitative based on the starting peptide, and Cbi-Ex4 were produced

to at least 97% purity prior to biological or in vivo evaluation (as tracked by RP-HPLC) (Figure 8). ESI-MS analysis showed expected  $m/z = 5354$ , observed  $m/z = 1339 [M^{+}+3H^{+}]^{+4}$ ,  $1071 [M^{+}+4H^{+}]^{+5}$  (Figure 9).

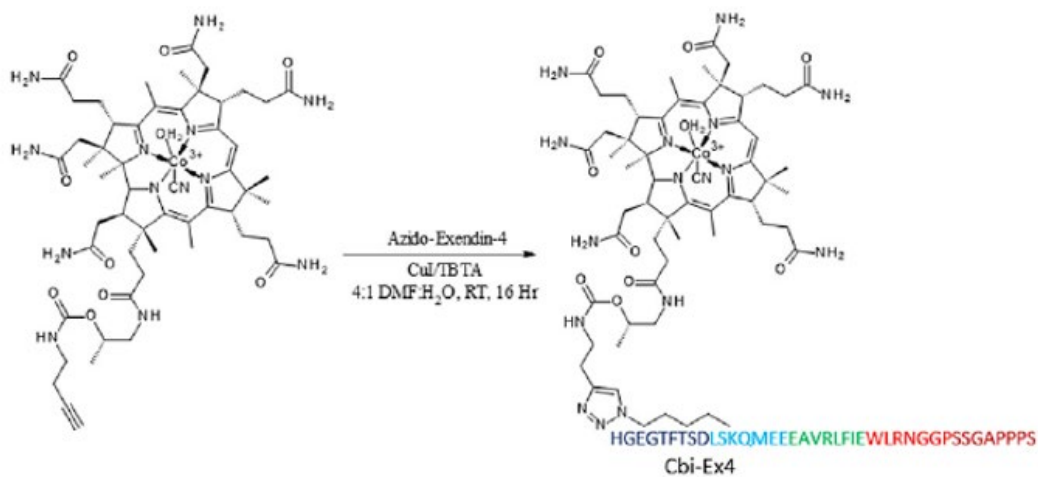


**Figure 7.** Synthetic scheme for Cbi-Ex4, Cbi-AB was clicked onto an azido Exendin-4 utilized CuAAC.

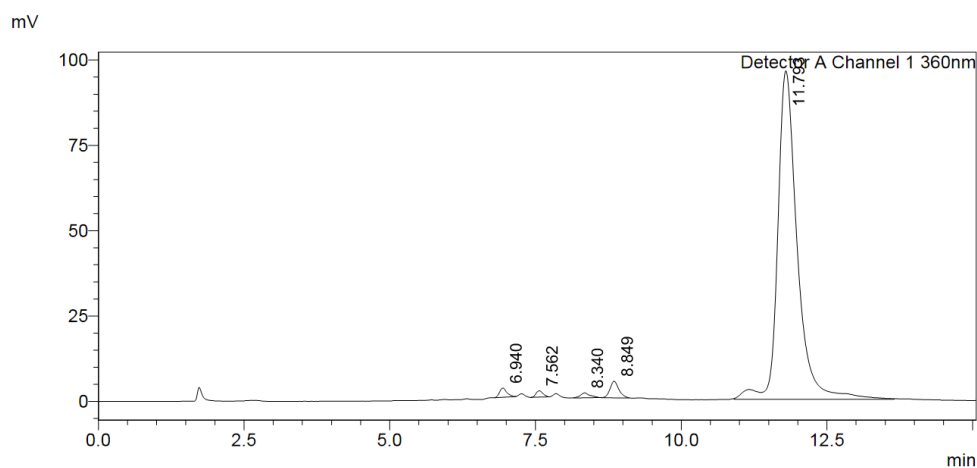


**Figure 8.** RP-HPLC Trace (Shimadzu Prominence HPLC using a C18 column (Eclipse XDB-C18 5 $\mu$ m, 4.6 x 150 mm) (RP-HPLC, from 1% CH<sub>3</sub>CN/H<sub>2</sub>O + 0.1% TFA to 70% CH<sub>3</sub>CN/H<sub>2</sub>O + 0.1% TFA in 15 min)) showing the Cbi-Ex4 Product at 11.7 min. Purity 98%.

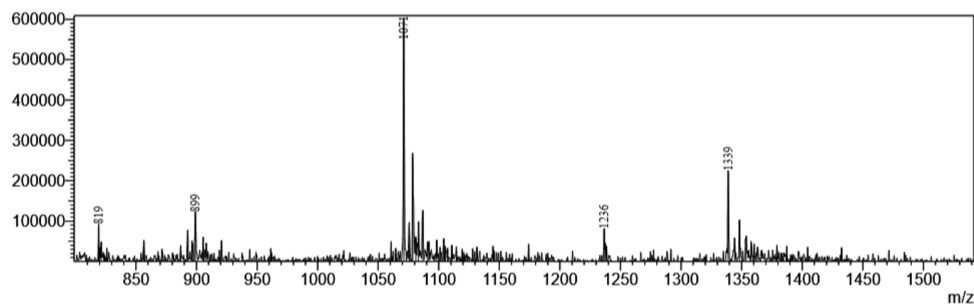


**Figure 9.** ESI-MS (Shimadzu LCMS-8040) of Cbi-Ex4, expected  $m/z = 5354$ , observed  $m/z = 1339$

$[M^{+}+3H^{+}]^{+4}$ , 1071  $[M^{+}+4H^{+}]^{+5}$ .

### 3.4 Agonism and Function at the GLP-1R

Cbi-Ex4 produces half maximal effective concentration ( $EC_{50}$ ) of  $\approx 200$  pM in fluorescence resonance energy transfer (FRET) assays that monitor levels of cAMP in HEK-239 cells stably transfected with the human GLP-1R (Figure 10).

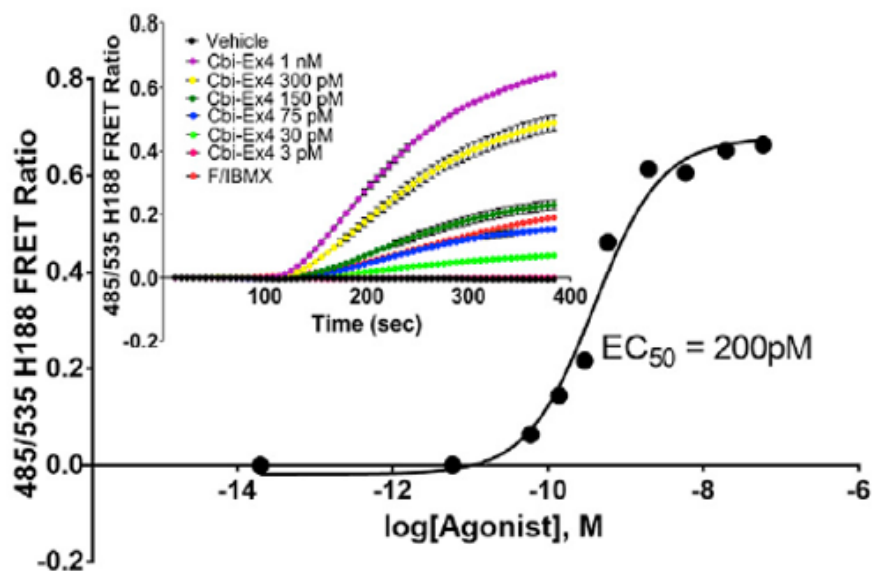


**Figure 10.** Dose-dependent Cbi-Ex4 agonism at the human GLP-1 receptor, as monitored in FRET assays using the cAMP biosensor H188<sup>69</sup> expressed in HEK293 cells.<sup>70</sup> EC<sub>50</sub> value for Cbi-Ex4 was determined to be  $200 \pm 0.09$  pM (mean  $\pm$  SEM).

### 3.5 Cobalamin Binding Capacity in Shrew Blood

Initially, we confirmed the presence of both HC and TC in shrew blood by performing radio-<sup>57</sup>Co-B12 binding assays and serum B12 protein isolation and identification. In addition to confirming the presence of HC (and separately TC, the profile found in humans, but not rodents,<sup>71</sup> we showed that the total blood B12 binding in *S. murinus* was  $\approx 12$  nM, of which  $\approx 4.5$  nM was due to apo-HC (Table 1).

**Table 1.** B12 and its binding proteins, transcobalamin (TC) and haptocorrin (HC) as measured in shrew serum, and their inhibition by increasing concentration of Cbi-Ex4. The sum of Apo TC +



Apo HC ~equals B12 binding capacity. \* Conducted by Dr. Ebba Nexø at University of Aarhus, Denmark.

	Shrew Serum	+ Cbi-Ex4, nmol/L, final concentration	
		25	50
Total B12 (nmol/L)	6.51		
B12 Binding capacity (nmol/L)	12.38	6.53	4.74
Apo – TC (nmol/L)	8.04	5.89	4.37
Apo – HC (nmol/L)	4.63	0.640	0.630

### 3.6 Binding Affinity for Cbi Transport Proteins

We also demonstrate that, as hypothesized, only HC ( $K_a$  0.45 nM Cbi-Ex4 versus 0.036 nM for Cbi), not TC ( $K_a$  for Cbi-Ex4 > 0.2 mM), binds Cbi-Ex4, and that such binding to HC was  $\approx$ 10-fold lower in affinity than for Cbi alone (Figure 11).

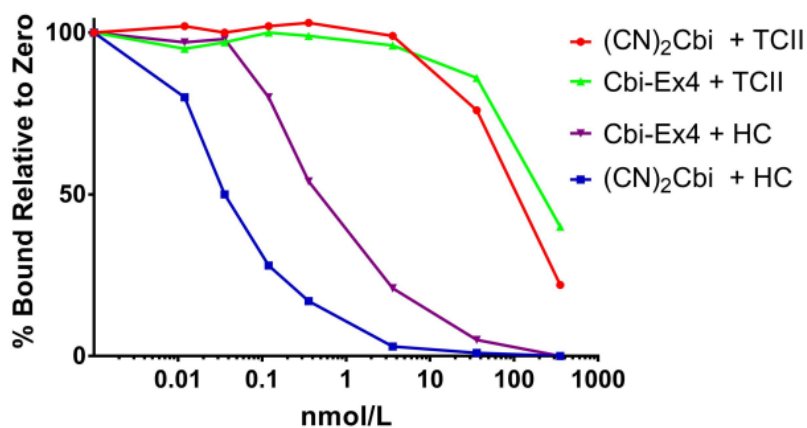


**Figure 11.** Binding affinity plots of Cbi ((CN)<sub>2</sub>Cbi) and Cbi-Ex4 by the B12 binding proteins transcobalamin (TC) and haptocorrin (HC). Figure 11 shows the binding affinity ( $K_a$ ) of B12 binding proteins transcobalamin and haptocorrin to endogenously occurring Cbi and the Cbi conjugated Ex4 (Cbi-Ex4). HC is known to be the only physiologically relevant binder of Cbi and

this is reflected in the binding constant of HC with Cbi ( $K_a$  0.036 nM). HC also binds Cbi-Ex4 ( $K_a$  0.456), albeit with  $\sim$  10-fold lower affinity. Consistent with the known binding profile of TC, only weak binding occurs for TC with Cbi or Cbi-Ex4 ( $K_a > 2 \mu\text{M}$ ). \* Conducted by Dr. Ebba Nexø at University of Aarhus, Denmark.

### **3.7 *In Vivo* Investigations of Ex4 versus Cbi-Ex4 in Shrews**

#### **3.7.1 Ex4 versus Cbi-Ex4 in Intraperitoneal (I.P.) Glucose Tolerance Test (IPGTT)**

Glucose-stimulated insulin secretion following administration of a GLP-1 analog is mediated principally by activation of GLP-1Rs expressed on pancreatic  $\beta$ -cells.<sup>42–44</sup> Therefore, as a proof of concept, we first tested whether Cbi-Ex4 retains its *in vivo* ability to reduce blood glucose following an intraperitoneal (i.p.) glucose tolerance test (IPGTT) across different doses compared to equimolar doses of native Ex4. We observed that shrews treated with Cbi-Ex4 and native Ex4 display improved glucose clearance following i.p. glucose administration compared to vehicle injections (Figure 12). Furthermore, the plasma glucose clearing rate of Cbi-Ex4 did not differ from the relative equimolar dose of native Ex4 following acute administration, which is indicative of a retained glucoregulatory potency (Figure 12, 13).

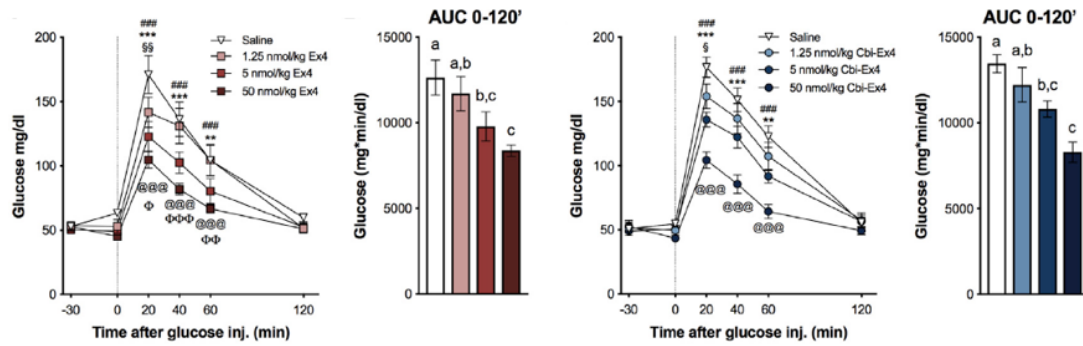


**Figure 12.** Ex4 (1.25, 5, and 50 nmol/kg, i.p.; i.e.,  $\approx$ 5, 20, and 200 mg/kg; respectively) dose-dependently suppressed blood glucose (BG) levels following glucose administration (2 g/kg, i.p.). Saline versus 5 nmol/kg Ex4: \*\*p < 0.01, \*\*\*p < 0.001; saline versus 50 nmol/kg Ex4: ###p < 0.001; saline versus 1.25 nmol/kg Ex4:  $\S\S$ p < 0.01; 1.25 nmol/kg Ex4 versus 50 nmol/kg Ex4: @@@p < 0.001; 1.25 nmol/kg Ex4 versus 5 nmol/kg Ex4:  $\Phi$ p < 0.05,  $\Phi\Phi$ p < 0.01,  $\Phi\Phi\Phi$ p < 0.001. Area under the curve (AUC) from 0 (i.e., post-glucose bolus) to 120 min after Ex4. In an IPGTT Cbi-Ex4 dose-dependently reduced BG levels comparably to equimolar doses of Ex4. Saline versus 5-nmol/kg Cbi-Ex4: \*\*p < 0.01, \*\*\*p < 0.001; saline versus 50 nmol/kg Cbi-Ex4: ###p < 0.001; saline versus 1.25 nmol/kg Cbi-Ex4:  $\S$ p < 0.05; 1.25 nmol/kg Cbi-Ex4 versus 50 nmol/kg Cbi-Ex4: @@@p < 0.001. AUC from 0 to 120 min following Cbi-Ex4. All data expressed as mean  $\pm$  SEM. Data in IPGTT was analyzed with repeated-measurements two-way ANOVA followed by Tukey's post hoc test. AUC data in was analyzed with repeated-measurements one-way ANOVA followed by Tukey's post hoc test. Means with different letters are significantly different (p < 0.05).

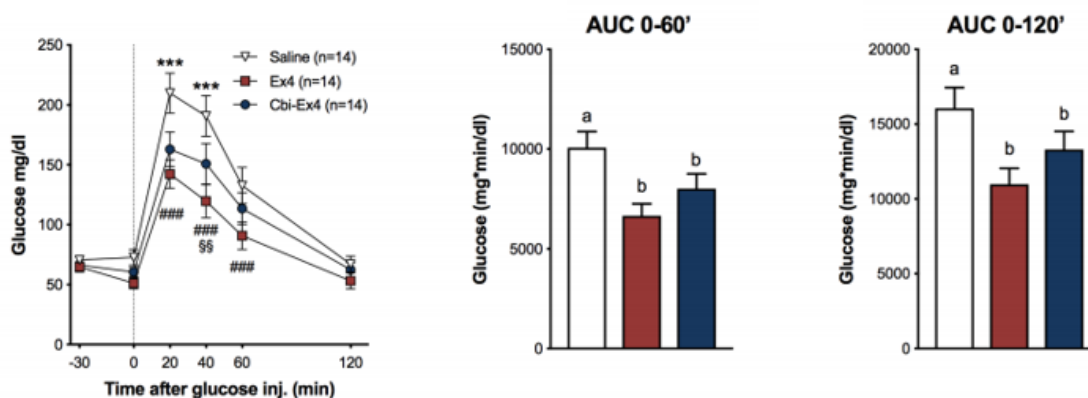


**Figure 13.** In an IPGTT, Ex4 (5 nmol/kg, i.e. 20  $\mu$ g/kg) and equimolar doses of Cbi-Ex4 suppressed blood glucose (BG) levels after IP glucose administration (2 g/kg, IP) compared to saline; vehicle vs Cbi-Ex4: \*\*\*  $P < 0.001$ ; vehicle vs Ex4: ###  $P < 0.001$ ; Ex4 vs Cbi-Ex4: §§  $P < 0.01$ ). Area under the curve (AUC) analyses from 0 (i.e., post-glucose bolus) to 60 and 0 to 120 min; respectively. Cbi-Ex4 and Ex4 similarly reduced AUCs compared to vehicle. All data expressed as mean  $\pm$  SEM. IPGTT data in was analyzed with repeated measurements two-way ANOVA followed by Tukey's post-hoc test. All other data was analyzed with repeated measurements one-way ANOVA followed by Tukey's post hoc test. Means with different letters are significantly different ( $P < 0.05$ ).

### 3.7.2 Ex4 versus Cbi-Ex4 in Delayed IPGTT

Based on these observations, we then further hypothesized that Cbi-Ex4 may also retain a plasma glucose-lowering action for a longer duration compared to native Ex4. Therefore, a “delayed” IPGTT was performed, in which an i.p. glucose bolus was administered 360 min *after* drug administration to determine whether a longer time window exists for Cbi-Ex4 to facilitate glucose clearance relative to native Ex4. Results show a significant suppression in plasma glucose

concentrations 6 h following Cbi-Ex4 administration in an IPGTT, with no effect on plasma glucose tolerance being observed after a 6h time delay of native Ex4 administration (Figure 14).

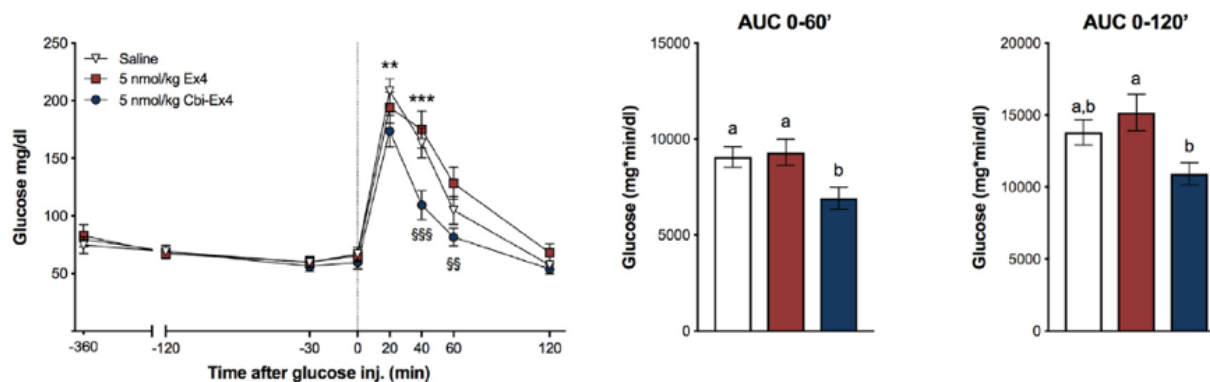


**Figure 14.** In a delayed glucose load IPGTT, Ex4, Cbi-Ex4 (5 nmol/kg) or vehicle were injected 6 h before glucose load. While Ex4-treatment was no longer effective in reducing BG levels, Cbi-Ex4 retained its BG lowering properties; saline versus Cbi-Ex4: \*\* $p < 0.01$ , \*\*\* $p < 0.001$ ; Ex4 versus Cbi-Ex4: §§ $p < 0.01$ ), §§§ $p < 0.001$ . AUC analyses from 0 to 60 min and 0 to 120 min, respectively. Cbi-Ex4-treated animals had lower AUC 0-120 compared to Ex4-treated animals and a lower AUC 0-60 compared to Ex4-treated animals and controls. All data expressed as mean  $\pm$  SEM. Data in IPGTT was analyzed with repeated-measurements two-way ANOVA followed by Tukey's post hoc test. AUC data in was analyzed with repeated-measurements one-way ANOVA followed by Tukey's post hoc test. Means with different letters are significantly different ( $p < 0.05$ ).

### 3.7.3 Ex4 versus Cbi-Ex4 effect on Feeding Behavior

Direct activation of GLP-1R expressed in various nuclei of the CNS (including, but not limited to those of the hypothalamus and dorsal vagal complex [DVC]), contributes to the body weight and food intake suppressive effects of exogenously administered first-generation GLP-1R

agonists.<sup>27–29,49</sup> Indeed, both liraglutide and Ex4 penetrate into the CNS and activate GLP-1R-expressing nuclei to induce hypophagia and body weight loss.<sup>27,42,49</sup> In line with previous reports,<sup>62</sup> systemic administration of native Ex4 produced a strong hypophagic response in the shrew, leading to body-weight loss in a dose-dependent fashion (Figure 15). This effect is due in part to the ability of native Ex4 to significantly increase the latency of the shrew to initiate feeding compared to vehicle injections (Figure 16). In contrast, Cbi-Ex4 did not significantly affect 24 h food intake or latency to eat, suggesting a lack of neural activation within the CNS (Figure 15).

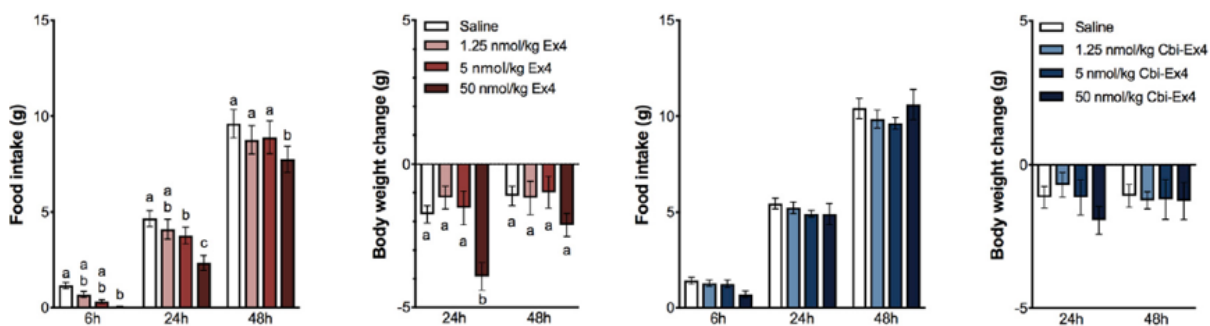


**Figure 15.** Ex4 dose-dependently induced anorexia leading to weight loss. (J and K) Equimolar doses of Cbi-Ex4 had no effect on food intake or body weight. All data expressed as mean  $\pm$  SEM. Data was analyzed with repeated-measurements two-way ANOVA followed by Tukey's post hoc test.

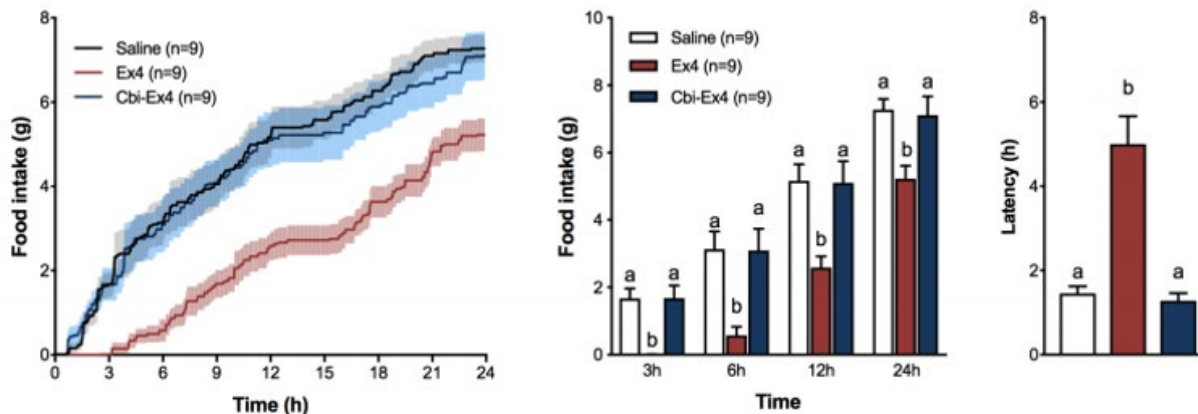


**Figure 16.** Ex4 (5 nmol/kg) induced anorexia at 3h, 6h, 12h and 24h post injection, whereas Cbi-Ex4 had no effect on food intake. Latency to eat was increased only in Ex4-treated animals. All data expressed as mean  $\pm$  SEM. Food intake was analyzed with repeated measurements two-way ANOVA followed by Tukey's post-hoc test. All other data were analyzed with repeated measurements one-way ANOVA followed by Tukey's post hoc test. Means with different letters are significantly different ( $P < 0.05$ ).

### 3.7.4 Conjugation to Cbi Improves the Pharmacokinetic Properties of Ex4

Cbi-Ex4 exhibited reduced plasma clearance (as evidenced by the area under the curve [AUC] and elimination constants) relative to native Ex4 (Figure 17, Table 2). This finding is likely due, at least in part, to improved stability of the conjugate to proteolytic activity, as has been demonstrated previously for full B12 conjugates,<sup>48</sup> and/or reduced renal clearance, both major routes of Ex4 clearance *in vivo*.<sup>72,73</sup> ELISA-based pharmacokinetic studies demonstrated that Cbi-Ex4 had a reduced rate of elimination as evidenced by the elimination constants ( $K_e$ ) of  $0.034 \text{ h}^{-1}$  for Cbi-Ex4 versus  $0.047 \text{ h}^{-1}$  for Ex4, and reduced clearance ( $0.0044 \text{ L/h}$  for Cbi-Ex4 versus  $0.0056 \text{ L/h}$  for Ex4) with no significant difference in volume of distribution between either drug (Table

2). Overall, Cbi-Ex4 provided greater drug exposure over time, as evidenced by the greater  $AUC_{0-360}$  (2.82 mg\*h/L for Ex4 versus 4.55 mg\*h/L for Cbi-Ex4), all above the values reported for the 50 nmol/kg dose (Figure 17, Table 2) . We noted also that the  $C_{max}$  values for both the 25 nmol/Kg and 50 nmol/Kg doses of Cbi-Ex4 were 17.25 and 30.96 nmol/L (4- to 7-fold greater than the maximum apo-HC levels measured and recorded above [Table 1]), suggesting that the effects of corrination are due to the Cbi itself, and are not primarily dependent on binding to HC (the only known binder of Cbi) *in vivo*. At this point it is interesting to note that Herbert and Herzlich<sup>74</sup> first suggested that HC may play a role in *removing* corrinoids from the human brain, an idea supported by subsequent work by Hansen *et al.*,<sup>75</sup> who showed HC was found in human colony stimulating factor (CSF; CSF-HC) at concentrations ranging from 10 to 41 pmol/L (median 21 pmol/L)<sup>75</sup> with plasma/ CSF ratios suggesting such HC was produced in the CNS directly. Overall, these results may be a consequence of naturally less penetrance of Cbi-Ex4 due to the presence of the highly polar Cbi group, a lack of facilitated transport into the brain for Cbi-Ex4, and/or binding by CSF-HC and subsequent removal or deactivation of Cbi-Ex4 in the CNS.



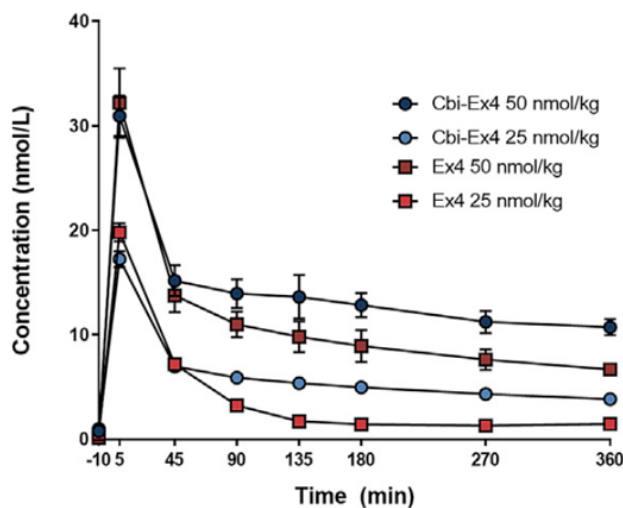


**Figure 17.** Pharmacokinetic profile of two equimolar doses (25 nmol/kg and 50 nmol/kg) of Ex4 and Cbi-Ex4. Data expressed as mean  $\pm$  SEM. Full PK parameters are given in Table 2.

**Table 2.** Pharmacokinetic parameters measured for Ex4 and Cbi-Ex4 in *S. murinus*. AUC indicates area under the curve between 0 and 360 or 0-1440 minutes;  $C_{Max}$  is the maximum measured concentration;  $T_{1/2}$  is the elimination half-life;  $V_d$  is volume of distribution, Cl is clearance and  $K_e$  is elimination rate constant.

Dose (nmol/kg)	AUC <sub>0-360</sub> (mg*H/L)	AUC <sub>0-1440</sub> (mg*H/L)	$C_{Max}$ (nmol/L)	Elimination $T_{1/2}$ (H)	$V_d$ (L)	Cl (L/H)	$K_e$ (H <sup>-1</sup> )
50.0 Ex4	2.82/hr	1.59/hr	32.19 +/- 3.03	14.85	0.12	0.0056	0.047
25.0 Ex4	0.96/hr	0.48/hr	19.80 +/- 2.47	13.52	0.16	0.0082	0.051
50.0 Cbi-Ex4	4.55/hr	2.68/hr	30.96 +/- 2.73	20.48	0.13	0.0044	0.034
25.0 Cbi-Ex4	1.94/hr	1.19/hr	17.25 +/- 1.83	15.99	0.12	0.0052	0.043

### 3.7.5 Prevalence of Emesis in Shrews Following Administration of Ex4 versus Cbi-Ex4

The most common side effects of all existing FDA-approved GLP-1R agonists are nausea, vomiting, and malaise, with approximately 20%–50% of T2DM patients that had been prescribed GLP-1-based medication, experiencing nausea and/or vomiting.<sup>19–23</sup> These adverse events are

surprisingly under-investigated, as they limit the widespread use, efficacy, and potential ubiquitous utility of existing GLP-1R agonists for treating metabolic disease. Notably, GLP-1 mediated malaise is not caused by GLP-1-mediated vagal afferent signaling, but is rather promoted by direct central GLP-1R activation,<sup>30</sup> primarily in the brainstem. We therefore hypothesized that the conjugation of Cbi to Ex4 would modify CNS penetrance of Ex4, due to the B12-selective transport system involving TC binding (and the receptor CD320), a system that does not specifically support Cbi binding/transport in general,<sup>49</sup> and specifically not in the case of Cbi-Ex4 as measured herein (Figure 11, Table 1).

Ex4 dose-dependently induced emesis with the majority of the shrews experiencing emesis after 5- and 50-nmol/kg Ex4 dosing (Figure 18). Indeed, 29% of the animals exhibited emesis upon administration of the lowest dose of native Ex4, 79% with the intermediate one, and 93% with the highest dose tested. All doses of native Ex4 triggered emesis within minutes after administration (1.25 nmol/kg Ex4:  $21 \pm 15$ ; 5 nmol/kg Ex4:  $10 \pm 5$  min; 50 nmol/kg:  $12 \pm 5$  min) (Figure 18). In contrast to the profound emesis observed after Ex4, both the prevalence and the number of emetic episodes following equimolar injections of Cbi-Ex4 were significantly reduced (5 nmol/kg Ex4 versus Cbi-Ex4:  $p = 0.005$ , 50 nmol/kg Ex4 versus Cbi-Ex4:  $p = 0.0003$ ) (Figure 18). Only one shrew experienced emesis after 1.25 nmol/kg Cbi-Ex4 (i.e., 7%), 28% after 5 nmol/kg Cbi-Ex4, and 64% after 50 nmol/kg Cbi-Ex4. In animals that displayed emesis after Cbi-Ex4 treatment, the latency was similar to native Ex4 (Figure 18). However, the severity and occurrence of the emetic episodes was less severe, as represented by the heatmaps of Ex4 and Cbi-Ex4 depicting emetic intensity and latency for each individual animal across time (Figure 18, 19). These differences are particularly striking at the 5 nmol/kg dose of Cbi-Ex4, which shows a

virtual absence of emetic events with the concurrence of strong glycemic effects (Figure 13, 19). Thus, the conjugation of Ex4 to Cbi renders a GLP-1R agonist that, at pharmacological doses, retains glucoregulatory ability without CNS-mediated emesis.

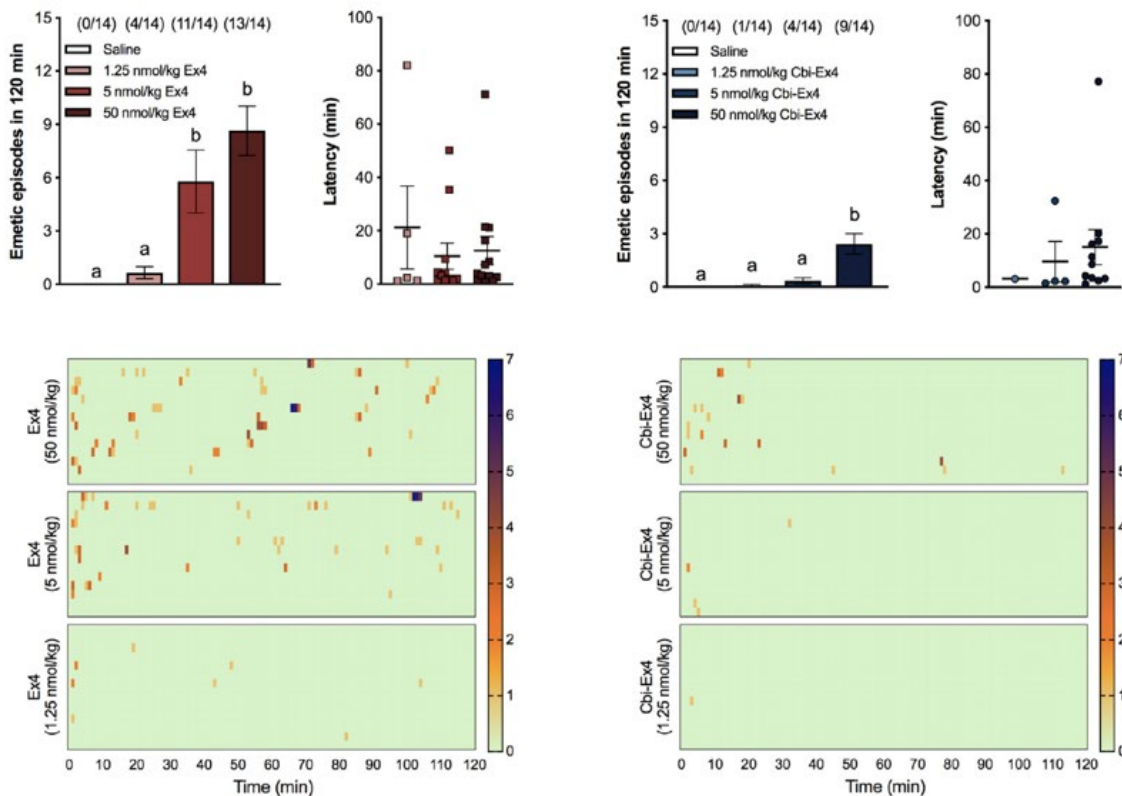


**Figure 18.** Ex4 (1.25, 5, and 50 nmol/kg) induced emesis during 120 min after injection in a dose-related fashion. The number of animals exhibiting emesis, expressed as a fraction of the total number of animals tested, is indicated above each treatment group. Latency to the first emetic episode of shrews that exhibited emesis after Ex4 treatment. Number of shrews experiencing emesis following Cbi-Ex4 (1.25, 5, and 50 nmol/kg) during 120 min after injection. The ratio of animals exhibiting emesis is indicated above each treatment group. Latency to the first emetic episode of shrews that experienced emesis after Cbi-Ex4 treatment. Heatmaps showing latency, number, and intensity of emesis following Ex4 and Cbi-Ex4 dosing for each individual animal across time. All data expressed as mean  $\pm$  SEM. Means with different letters are significantly different ( $p < 0.05$ ). Emetic episode data was analyzed with repeated-measurements one-way ANOVA followed by Tukey's post hoc test.

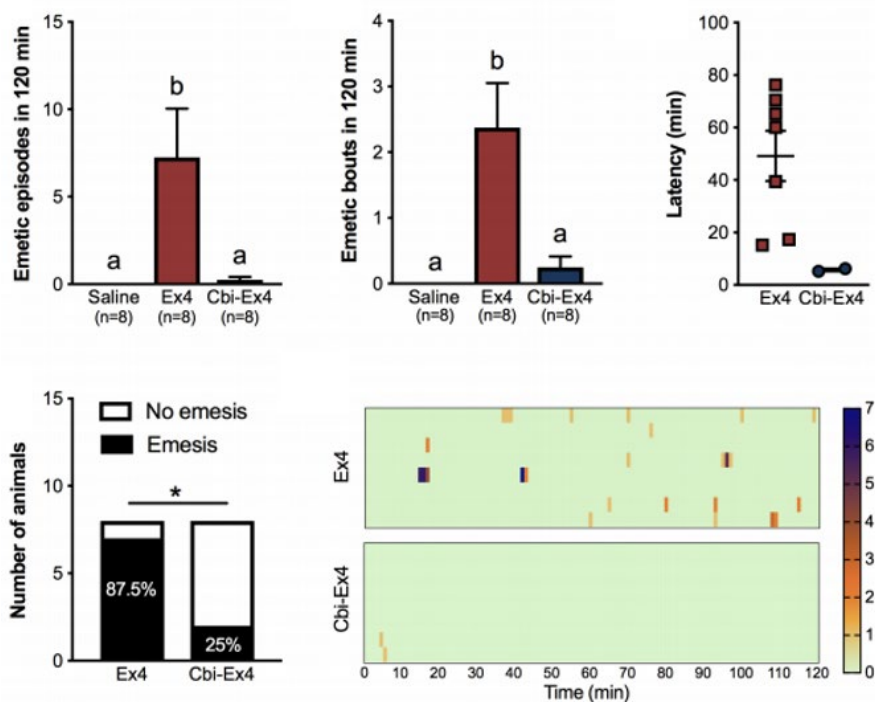


**Figure 19.** Cbi-Ex4 vs. Ex4 direct comparison on emesis. The number of single emetic episodes following, Ex4 (5 nmol/kg, i.e. 20  $\mu$ g/kg), Cbi-Ex4 or saline administration was recorded for 120 min. Ex4 induced robust emetic responses that were not observed after Cbi-Ex4 or saline injections. The number of emetic bouts was also lower in Cbi-Ex4-treated animals compared to Ex4 and it did not differ from controls. Graphical representation of latency to the first emetic episode between Ex4 and Cbi-Ex4-treated animals that exhibited emesis. The percentage of shrews experiencing emesis was significantly different between Ex4 and Cbi-Ex4. Heatmap showing latency, number and intensity of emesis for each animal across time. All data expressed as mean  $\pm$  SEM. Means with different letters are significantly different ( $P < 0.05$ ). Emetic episode and bout data was analyzed with repeated measurements one-way ANOVA followed by Tukey's post hoc test. Frequency of emesis in animals was analyzed with Fisher's exact test

### 3.7.6 C-Fos Staining of AP/NTS

Further support for this hypothesis is found by the near absence of c-Fos protein immunofluorescence (i.e., neuronal activation) in the DVC by Cbi-Ex4 compared to the robust c-Fos activation by native Ex4 (Figure 20). The DVC is a set of brainstem nuclei (comprised of the nucleus tractus solitarius [NTS], area postrema [AP], and dorsal motor nucleus of the vagus) implicated in regulation of food intake and the processing of aversive stimuli and emetic events.<sup>60,76–78</sup> Figure 20 shows that systemic native Ex4 induces robust c-Fos expression in both the NTS and AP, whereas an equimolar dose of Cbi-Ex4 did not significantly induce greater c-Fos expression compared to vehicle injections.

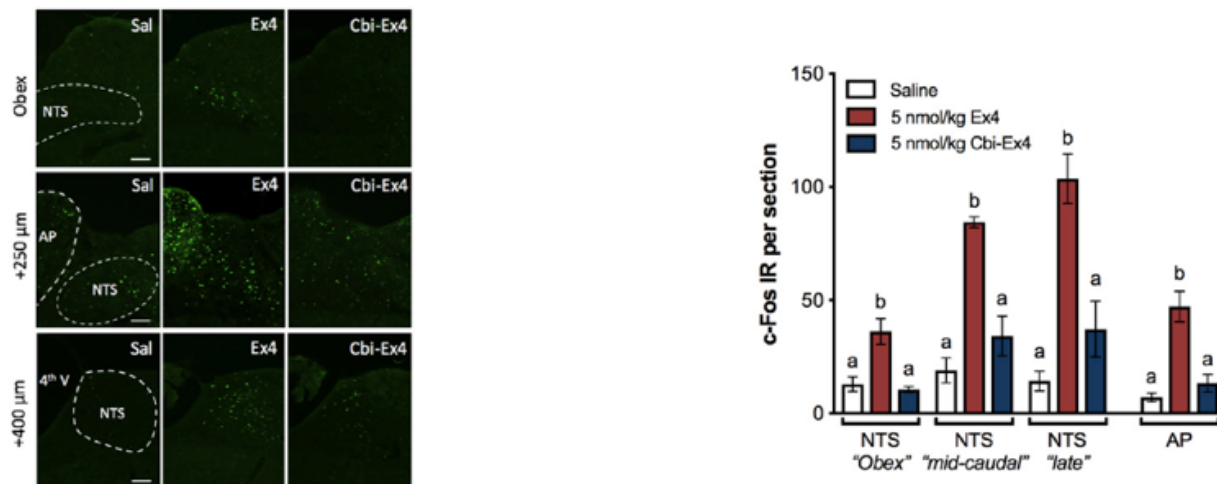


**Figure 20.** Quantification of c-Fos positive neurons in the rostral, medial, and caudal NTS and medial AP. Peripheral Ex4 administration significantly increased the number of c-Fos immunoreactive cells in the AP/NTS of shrews 3 h after injection. The number of c-Fos positive cells in the AP/NTS was significantly lower in Cbi-Ex4 treated animals. All data expressed as mean  $\pm$  SEM. Data was analyzed with one-way ANOVA followed by Tukey's post hoc test. Scale bar, 100  $\mu$ m.

### 3.8 Prebinding Cbi-Ex4 to Haptocorrin (HC)

Given the possibility of Cbi-Ex4 becoming bound by CSF-HC and subsequent removal or deactivation of the construct we sought to assay Cbi-Ex4 prebound to HC (HC-Cbi-Ex4) at the GLP-1R and noted an  $EC_{50}$  of  $\approx 3$  nM, essentially rendering a physiologically irrelevant construct.

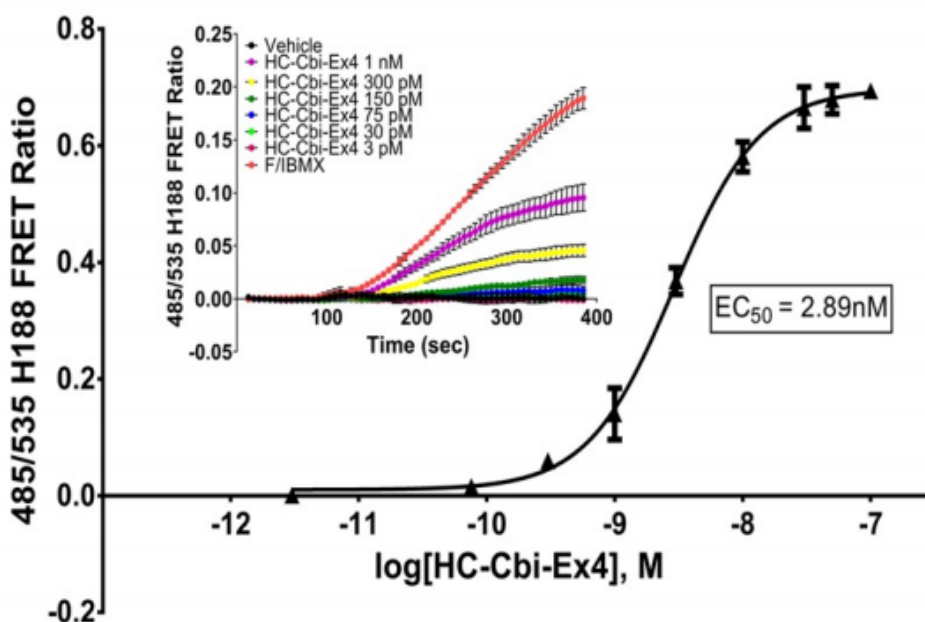


**Figure 21.** Dose response and regression plot for HC-Cbi-Ex4 agonism at the GLP-1R.

### 3.9 Outcomes and Conclusions

In summary, by exploiting a biosynthetic precursor of B12 found naturally in humans, but that is inert in the normal physiology of the vitamin, we generated a potent and metabolically stable GLP-1 receptor agonist via corrination, with enhanced and prolonged peripheral glucoregulatory actions at doses that do not affect feeding and, astonishingly, is virtually devoid of emetic responses. Chronic animal studies as well as clinical trials are required to fully elucidate

the long-term efficacy and tolerability of Cbi-Ex4. Given the high prevalence of obesity/overweight among T2DM patients, the lack of major effects on feeding and body weight could be considered a negative outcome of the corrination technology. For these patients, “classic” GLP-1R analogs, if well tolerated, may be most favorable as weight loss contributes to improved overall health. Nevertheless, our data highlights the incredible potential of corrination, exemplified herein with the development of Cbi-Ex4, as a treatment that would be most beneficial in treating lean T2DM patients, T2DM patients suffering from other comorbidities associated with an anorectic/cachectic state (cancer, COPD, and cystic fibrosis), and T2DM patients seeking glycemic control without emesis.

T2DM and cancer anorexia-cachexia syndrome show similarities in metabolic alterations.<sup>79,80</sup> Insulin resistance and reduced glucose tolerance in cancer patients are well-known phenomena. As early as the 1920s, glucose intolerance became a recognized metabolic alteration observed in cancer patients.<sup>81</sup> Data from tumor-bearing rodents, partially recapitulating the human clinical state, showed some beneficial effects of Ex4 treatment in attenuating muscle atrophy and in counteracting cancer-induced-insulin-signaling dysregulation.<sup>82</sup> However, the CNS-mediated anorectic and emetic effects induced by native Ex4 represents a substantive limitation for possible applications in humans. Cbi-Ex4 could therefore represent an interesting and new GLP-1R-based approach for future investigations into the treatment of cancer-induced insulin resistance.



### 3.10 Optimization of Cbi-Ex4 Construct

The previously discussed conjugation of Cbi with Ex4, to produce Cbi-Ex4 (**1**),<sup>83</sup> and its effects were tested *in vivo* in the musk shrew (*Suncus murinus*), a mammal capable of emesis<sup>84,85</sup> and responsive to GLP-1R targeting therapeutics.<sup>61,62,83</sup> The data showed that Cbi-Ex4 enhanced the glucoregulatory response following an intraperitoneal glucose tolerance test (IPGTT), without producing hypophagia, anorexia, body weight loss, and, more importantly, without emesis, all characteristics of classical Ex4-based therapies.<sup>83</sup> We hypothesized that these results are due to reduced drug penetrance into the CNS.<sup>48-51,83</sup> This proof-of concept corrinated Ex4 (**1**) was, however, notably less potent an agonist for the GLP-1R than Ex4 alone (200 vs 30 pM, respectively, in the same GLP-1R FRET assay).<sup>83</sup> With that in mind, we set out to optimize **1** in terms of receptor binding and agonism for the purposes of future translation. As such, we needed to synthesize and characterize a new library of Cbi-Ex4 conjugates. Of note here is that there is a dearth of synthetic cobinamide chemistry in the literature, mostly focusing on the novel cobinamides to treat hydrogen sulfide<sup>86,87</sup> or cyanide poisoning,<sup>88-95</sup> and even less so in terms of conjugation chemistry (an excellent exception being that from the Gryko group using Cbi-PNA);<sup>64,96</sup> hence, we wanted to produce Cbi-linkers that would be readily amenable to conjugation to Ex4 but indeed any targeted peptide moving forward. In these subsequent studies, we have looked to optimize **1** with a focus on agonism and binding at the GLP-1R while also expanding to the little explored chemistry pertaining to the synthesis of Cbi conjugates. As such, the structure–activity data presented in these studies integrates synthesis, receptor agonism, receptor binding, *ex vivo* insulin secretion, *in vivo* glucoregulation, emetic response, and food

intake to explore the role of the peptide conjugate site and/or the role of a specific set of spacers (linkers).

### 3.11 Selection of Linkers for New Library of Cbi-Ex4/40 Constructs

In terms of the linkers, there are three subsets that were chosen to sample space across structural features, namely, steric, hydrophobic, and amphiphilic (Figure 22). The Ex4 conjugate site was restricted to K12 and a K40 residue added to the C-terminus of Ex4 (Ex40) since both sites were proven to be amenable to modification with minimal loss of function in our hands<sup>48–51,83</sup> and in prior literature.<sup>97–99</sup>

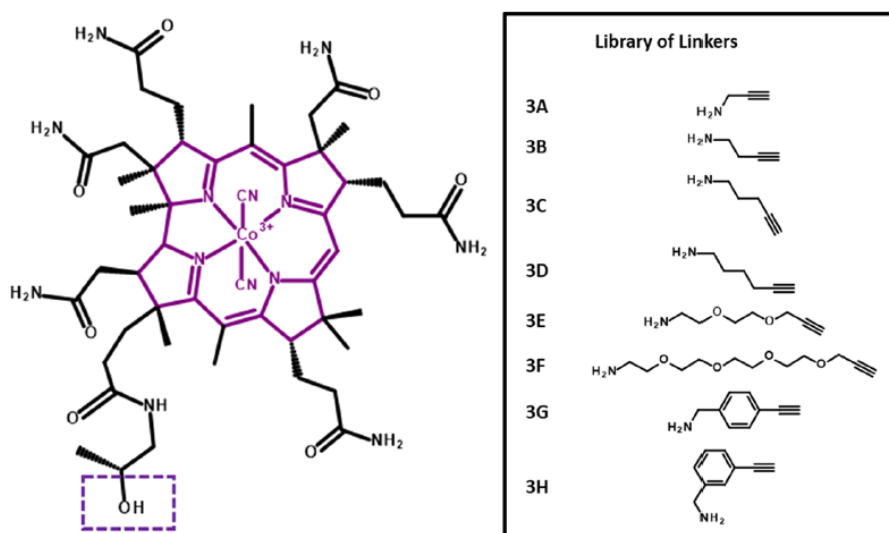


**Figure 22.** (Left) Structure of the Cbi ((CN)<sub>2</sub>Cbi) starting material, a purple solid prepared via microwave chemistry from B12, with the hydroxyl group boxed used as a site of conjugation to linker series. (Right) Library of linkers used in the conjugation of Cbi to Ex4 peptides. The library of linkers chosen in this study included short hydrophobic alkane chains, amphiphilic PEG, and rigid substituted ethynyl phenyl methanamines, which were coupled to the Cbi hydroxyl group via CDT-mediated amide formation, resulting in Cbi compounds (**4–11**) with an available alkyne

group for subsequent reaction with azido-modified Ex4 peptides via copper-mediated alkyne-azide click chemistry (Figure 23).

### 3.12 Synthesis and Characterization of New Cbi-Ex4/40 Constructs

The Cbi linker compounds (**4–11**) and Ex4 conjugates of such (**12–27**) amounted to a library of 32 compounds. These newly form compounds were synthesized as previously described above. The experimental details are shown in Figure 23, with linkers (Figure 22) indicated as R-groups.

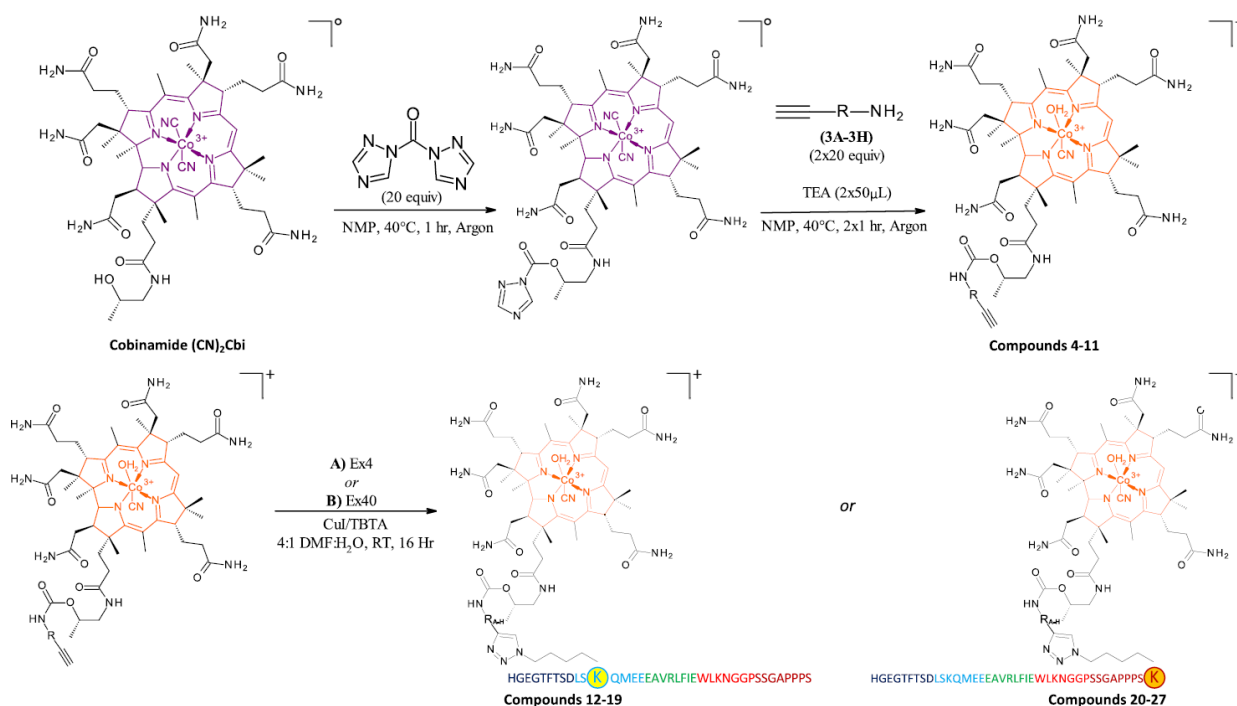


**Figure 23.** Synthetic Scheme of Cbi Linkers (**4–11**) and Cbi-Peptide Conjugates (**12–27**).

### 3.13 The Effect of Corination on the Secondary Structure of Ex4

All conjugates were investigated for the effects of corination on helicity at a concentration of 40  $\mu$ M in water at pH 7.0. Immediately, it was evident that there was minimal variation in percent helicity whereupon the Cbi was conjugated at the Ex4 C-terminal K40 (**20–27**; % helicity ranged from ~28 to 36%; Ex40 control 33.1%; Figure 24, Table 3). There was however a noticeable variation in the percent helicity for the conjugates (**12–19**) whereupon Cbi was conjugated to the K12 within the Ex4 helix (% helicity range ~20–46%; Ex4 control 24.3; Figure 24, Table 3). These results are consistent with the fact that conjugation at the C-terminus renders less consequence to the linker type or spacer distance between Cbi and the peptide, given that this region is away from the helical region of Ex4 and does not interfere with the role of this region with receptor binding/agonism. The variation noted upon conjugation at the K12 residue renders the linker critical with the highest % helicity noted as 41% with the amphiphilic PEG spacer **3F** (Figure 24, Table 3) and the lowest percent helicity noted with the small alkyl spacers **3B–3D** (Figure 24, Table 3). No overall correlation between the structure and agonism or binding was observed upon data fitting (not shown).

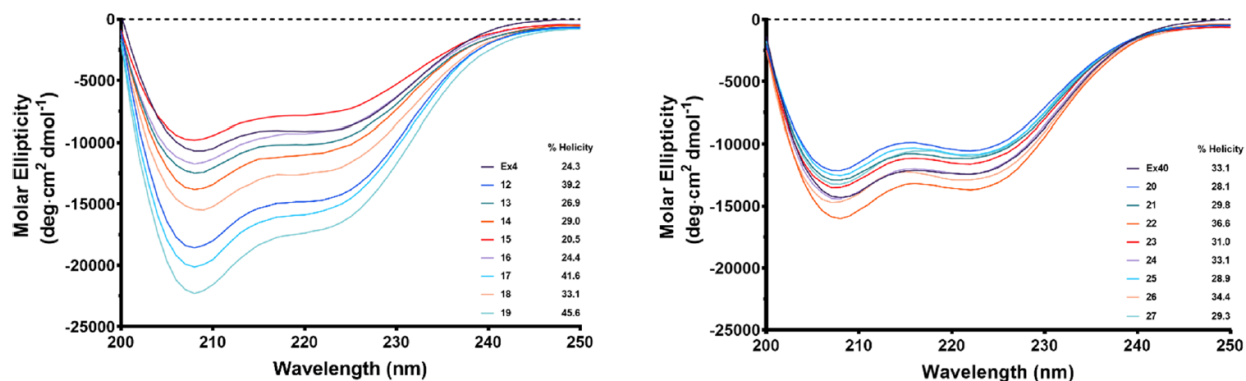


**Figure 24.** Effect of Cbi conjugation on the secondary structure of Ex4 or Ex40. CD spectra were collected with a sample concentration of 40  $\mu\text{M}$  at pH 7 between 200 and 250 nm. % helicity was measured at 222 nm.

### 3.14 *In Vitro* Optimization of Cbi-Ex4

To determine how the conjugation site of the peptide affects its function and the role linker choice plays in the attachment of the peptide to Cbi, we sought to screen **12–27** utilizing *in vitro* assays to determine potency and binding at the GLP-1R.

#### 3.14.1 Agonism at GLP-1R

Our previously discussed Cbi-Ex4 construct **1** resulted in agonism at the GLP-1R with an  $\text{EC}_{50}$  of 200 pM.<sup>83</sup> The design of the newly constructed conjugates, **12–27**, aimed to increase the potency of the original construct to that comparable of unconjugated Ex4 (<30 pM).<sup>48</sup> **12–27** were assessed utilizing *in vitro* screening in HEK C20 cells stably expressing the human GLP-1R and cAMP FRET reporter H188 produced in-house.<sup>69,100</sup> To determine if the azido modification to lysine at position K12 (Ex4) or the addition of this residue to position 40 (Ex40) had any effect on agonism at GLP-1R, they were also screened for agonism to compare with native Ex4 (nEx4; no azido modifications), resulting in  $\text{EC}_{50}$  values of 20 pM for nEx4,  $12.5 \pm 3.7$  pM for Ex4, and  $10.4 \pm 3.9$  pM for Ex40 (Table 3). All newly synthesized compounds were functional at the GLP-1R with

improved potency in all cases ( $EC_{50}$  range  $13.4 \pm 4.2$  to  $105.6 \pm 4.1$  pM) to that of our previously reported construct **1** ( $200$  pM;<sup>83</sup> Figure 25, Table 3). In general, the Ex4 conjugates **12–20** were inferior to the Ex40 conjugates (**20–27**) and displayed greater variance, with  $EC_{50}$  values ranging from  $31$  to  $106$  pM for **12–19** compared to  $13$  to  $38$  pM for **20–27**. As with the variance observed in the folded state for **12–19**, it is likely that proximity and/or interactions of the Cbi moiety to the helix interferes with receptor binding and/or interactions necessary for agonism. Conjugations performed at the C-terminal end of the peptide would be expected to place the corrin ring away from such residues as we have shown previously with B12 conjugates of the neuropeptide PYY3–36.<sup>51</sup> One Cbi-Ex4 conjugate however (**19**), which bridged Ex4 at the K12 residue with Cbi through one of the hydrophobic, rigid linkers (**3H**), was shown to be equipotent to Ex4 with an  $EC_{50}$  value of  $31.2 \pm 16.9$  pM and an  $IC_{50}$  of  $11.6 \pm 2.4$  nM (compared to  $5.98 \pm 0.94$  nM for Ex4 alone; Table 3). All Ex40-based conjugates (**20–27**) were shown to be equipotent to the unconjugated peptide. Such results are consistent with the fact that addition of, and conjugation to, the K40 residue is optimal when conjugating Cbi to Ex4.

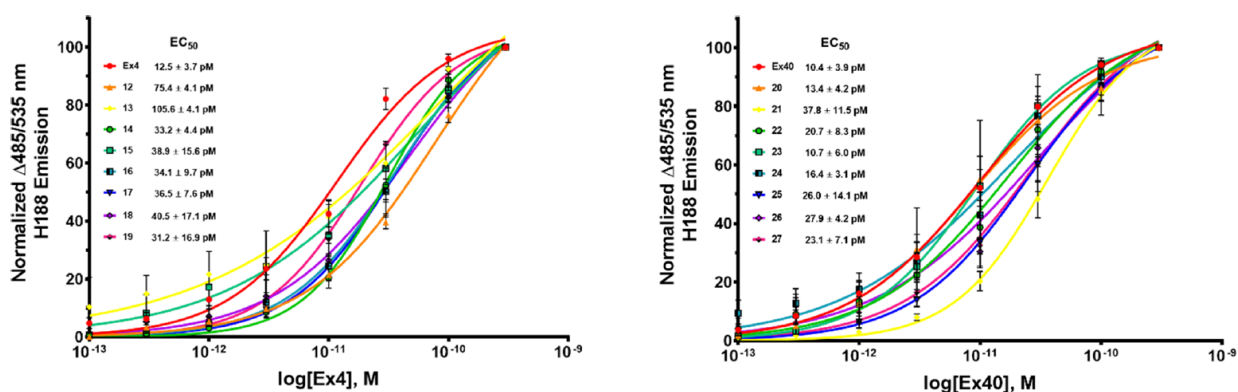


**Figure 25.** Conjugation of Cbi to Ex4 or Ex40 peptides maintains agonism at the GLP-1R. Nonlinear regression analysis was performed with GraphPad Prism 8. All compounds were assayed at least as triplicate independent runs. Data are shown as mean  $\pm$  SEM.

### 3.14.2 Competitive Binding at GLP-1R

As shown in Table 3, the presence of Cbi influences the ability of the conjugate to agonize the GLP-1R compared to that of Ex4 or Ex40. To further investigate how conjugation of Cbi affects Ex4 or Ex40, a series of competitive binding assays against GLP-1red (a red fluorescent analog of GLP-1) were conducted (Figure 26). nEx4 was utilized as a reference competitor with an  $IC_{50}$  value of 4.97 nM. We first aimed to determine if the azido modification to lysine at position K12 and the addition of this residue to position 40 had any effect on binding. It was found that both Ex4 and Ex40 had comparable binding to that of the reference compound with  $IC_{50}$  values of  $5.98 \pm 0.94$  and  $7.34 \pm 1.37$  nM, respectively (Figure 26, Table 3). All conjugates had decreased binding (12–135 nM) compared to the unconjugated peptide azido-modified Ex4 (6 nM) and Ex40 (7 nM) and nEx4 controls (5 nM). When comparing the two clusters of conjugates, **20–27** showed greater binding affinity overall compared to **12–19**. The same trend was observed when agonizing the GLP-1R (Figure 26, Table 3) in which collectively **20–27** outperformed **12–19**. Two constructs, namely, **19** and **22**, did show promising binding with  $IC_{50}$  values of  $11.6 \pm 2.4$  and  $11.9 \pm 2.5$  nM, respectively. The increased binding observed in these two conjugates was consistent with their agonism ( $31 \pm 16.9$  and  $20.7 \pm 8.3$  pM, respectively) of the GLP-1R (Figure 26, Table 3).

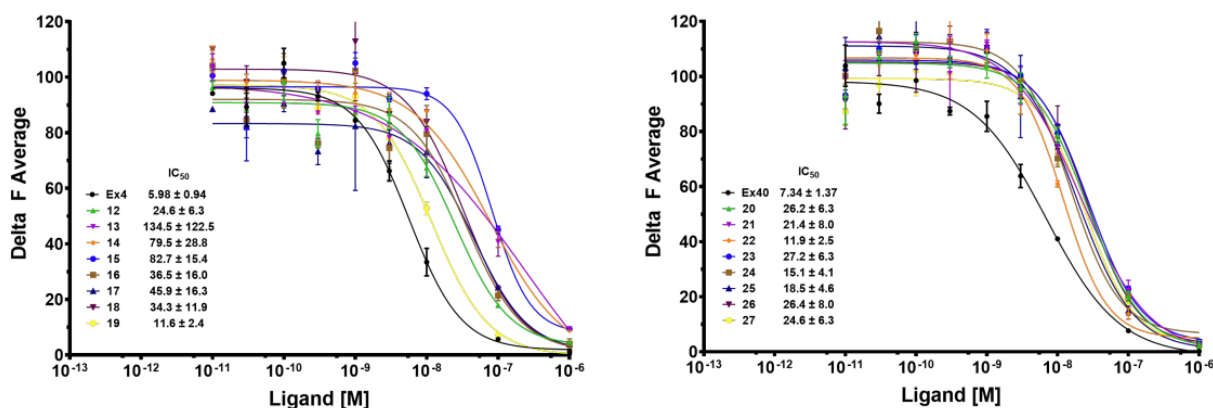


**Figure 26.** *In vitro* dose escalation competition binding studies of 12-27 compared with Ex4 and Ex40 controls against fluorescent GLP-1red. \* Conducted by EuroscreenFast.

### 3.15 Identification of New Lead Candidate

Based on overall binding potent agonism, facile synthesis, and high yield observed for **22**, especially related to those of **19**, we chose to further investigate **22** in *ex vivo* and *in vivo* experiments.

**Table 3.** EC<sub>50</sub> and IC<sub>50</sub> Values with Hill Slopes and % Helicity of Cbi Conjugates **12–27**. <sup>a</sup>Data represents EC<sub>50</sub> obtained using nonlinear regression analysis of data from highest FRET values obtained for each data point. Experiments were performed as three independent runs. <sup>b</sup>Data represents the Hill slope obtained using nonlinear regression analysis of data from highest FRET values obtained for each data point. Experiments were performed as three independent runs. <sup>c</sup>Data represents mean residue ellipticity [ $\theta$ ]<sub>222</sub> determined from the CD spectra of a 40  $\mu$ M solution of peptide in H<sub>2</sub>O at RT pH 7.0. Average [ $\theta$ ]<sub>222</sub> values utilized to calculate percent helicity were obtained by performing the experiment in triplicate. Percent helicity was calculated using



$100 \times ([\theta]_{222}/\max[\theta]_{222})$ .  $\max[\theta]_{222} = -40,000 [1 -(2.5/n)]$ , where n is the residue number.

Experiments were performed as three independent runs. <sup>d</sup>Data represents IC<sub>50</sub> values obtained from competitive binding assays against red fluorescent GLP-1 using nonlinear regression analysis from highest values obtained for each data point. Experiments were performed as two independent runs. <sup>e</sup>Hill slopes were obtained using nonlinear regression analysis from highest values obtained for each data point. Results are expressed as mean  $\pm$  SEM.

	EC <sub>50</sub> (pM) <sup>a</sup>	EC <sub>50</sub> Hill slope <sup>b</sup>	% helicity <sup>c</sup>	IC <sub>50</sub> (nM) <sup>d</sup>	IC <sub>50</sub> Hill slope <sup>e</sup>
Ex4	12.5 $\pm$ 3.7	1.1970	24.3	5.98 $\pm$ 0.94	-1.3010
12	75.4 $\pm$ 4.1	0.9110	39.2	24.6 $\pm$ 6.3	-1.1170
13	105.6 $\pm$ 4.1	1.0100	26.9	135 $\pm$ 122.5	-0.5661
14	33.2 $\pm$ 4.4	1.4170	29.0	79.5 $\pm$ 28.8	-0.7858
15	38.9 $\pm$ 15.6	1.0470	20.5	82.7 $\pm$ 15.4	-1.6990
16	34.1 $\pm$ 9.7	0.9976	24.4	36.5 $\pm$ 16.0	-1.1770
17	36.5 $\pm$ 7.6	1.0980	41.6	45.9 $\pm$ 16.3	-1.1740
18	40.5 $\pm$ 17.1	1.3030	33.1	34.3 $\pm$ 11.9	-1.1530
19	31.2 $\pm$ 16.9	1.1130	45.6	11.6 $\pm$ 2.4	-1.1270
Ex40	10.4 $\pm$ 3.9	1.1160	33.1	7.34 $\pm$ 1.37	-0.9107
20	13.4 $\pm$ 4.2	1.1890	28.1	26.2 $\pm$ 6.3	-1.1350
21	37.8 $\pm$ 11.5	1.1830	29.8	21.4 $\pm$ 8.0	-0.8940
22	20.7 $\pm$ 8.3	1.2090	36.6	11.9 $\pm$ 2.5	-1.3970
23	10.7 $\pm$ 6.0	1.0120	31.0	27.2 $\pm$ 6.3	-1.1780
24	16.4 $\pm$ 3.1	1.1370	33.1	15.1 $\pm$ 4.1	-1.2540
25	26.0 $\pm$ 14.1	0.9817	28.9	18.5 $\pm$ 4.6	-1.0840
26	27.9 $\pm$ 4.2	0.9957	34.4	26.4 $\pm$ 8.0	-1.2370
27	23.1 $\pm$ 7.1	1.2130	29.3	24.6 $\pm$ 6.3	-1.2790

### 3.16 Glucose-Stimulated Insulin Secretion (GSIS) in Rat Pancreatic Islets

The effects of **22** on GSIS were evaluated using rat pancreatic islets (Figure 27).<sup>101,102</sup> At 10 mM glucose, both **22** and nEx4 increased GSIS in a dose-responsive manner. The effect from **22** was observed to be one-third lower than that of nEx4. To investigate whether there was a difference between Ex40 and **22**, specific to the rat GLP-1R, we assayed each for functional (EC<sub>50</sub>) agonism. We observed a slight drop-off in potency with EC<sub>50</sub> values of 7.8 and 22 pM recorded for Ex40 and **22** (data not shown), respectively. nEx4 control had an EC<sub>50</sub> of 48 pM at the rat GLP-1R.<sup>103</sup>

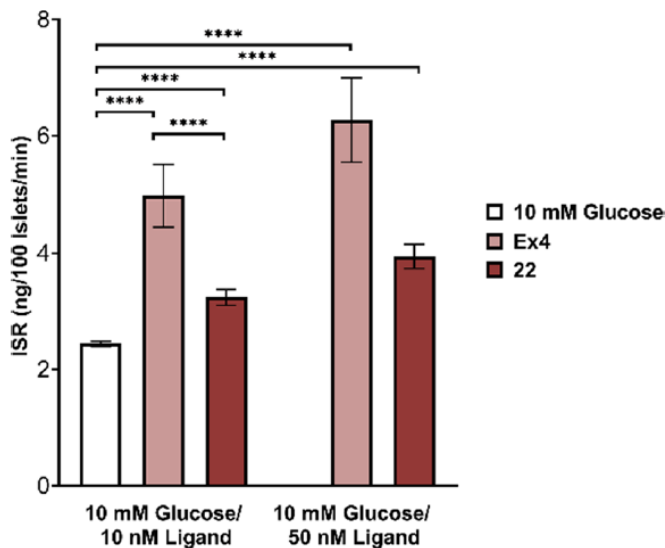


**Figure 27.** **22** increases glucose-stimulated insulin secretion in rat islets relative to glucose controls. Insulin secretion rate from static cultures of Sprague–Dawley rat islets incubated in media containing glucose (10 mM) and Ex4 (10 or 50 nM) or **22** (10 or 50 nM).<sup>104</sup> Data was calculated from three independent experiments and analyzed with repeated-measurements two-way ANOVA followed by Tukey’s post hoc test. Results are expressed as mean  $\pm$  SEM, \*\*\*\*  $p < 0.0001$ . \* Conducted by Varun Kamat under the guidance of Dr. Ian R. Sweet at University of Washington.

### 3.17 *In Vivo* Functional Experiments

#### 3.17.1 **22** versus **1** and Ex4 in IPGTT

Our first *in vivo* experiment investigated the effects of Ex4, **1** and **22** on plasma glucose levels following an IPGTT in shrews. We observed that shrews treated with **1**, **22**, or nEx4 display similar improvements in glucose handling following glucose load compared to vehicle controls (Figure 28). Post hoc analyses showed that all three compounds significantly suppressed blood glucose (BG) at 20 and at 40 min after glucose administration versus vehicle treatment (all  $p <$

0.001). Remarkably, BG values at 20 min post glucose injection in animals receiving **22** were significantly lower than those in animals treated with **1**, denoting an improved glucose tolerance/superior pharmacological efficacy ( $p < 0.01$ ). Additionally, the variation in plasma glucose concentrations, represented as area under the curves (0–60' and 0–120', respectively) for **22**, did not differ from nEx4 and were significantly lower than controls (Figure 28, all  $p < 0.05$ ).

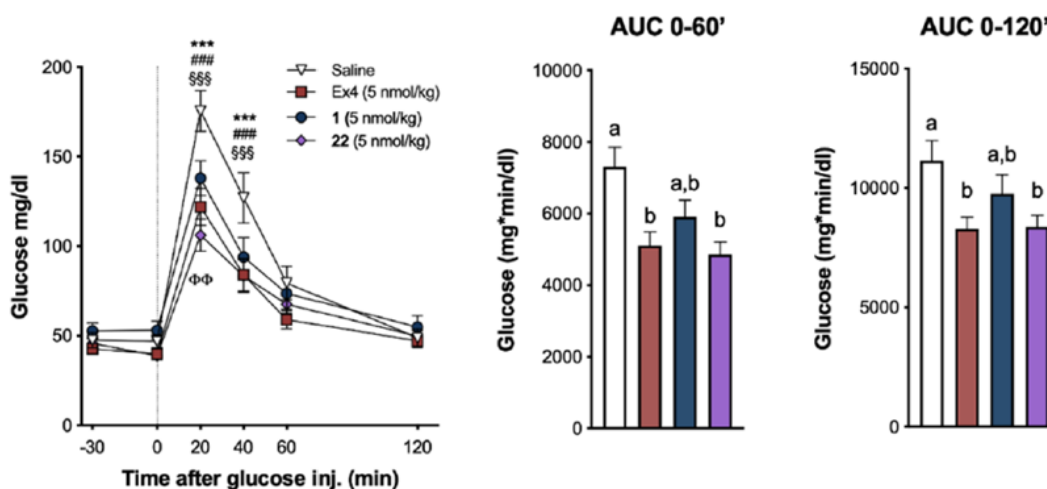


**Figure 28.** Cbi-Ex4 enhances glucose clearance without inducing emesis or body weight loss. (A) In an IPGTT, Ex4, 1, and 22 (50 nmol/kg, IP) showed similar potency in suppressing BG levels after glucose administration (2 g/kg, IP) compared to saline; vehicle vs 1: \*\*\*  $P < 0.001$ ; vehicle vs 22: ###  $P < 0.001$ ; vehicle vs Ex4: §§§  $P < 0.001$ ; 1 vs 22: ΦΦ  $P < 0.01$  ( $n = 12$  shrews). Area under the curve (AUC) analysis from 0 (i.e., post-glucose bolus) to 60 min following 1, 22, and Ex4. AUC analysis from 0 to 120 min; 22 and Ex4 similarly reduced AUCs compared to vehicle ( $P < 0.05$ ). All data expressed as mean  $\pm$  SEM ( $n = 10$ ). IPGTT data was analyzed with repeated-measurements two-way ANOVA followed by Tukey's posthoc test. AUC data was analyzed with repeated measurements one-way ANOVA followed by Tukey's posthoc test. Means with different letters are significantly different ( $P < 0.05$ ).

### 3.17.2 22 Effects on Food Intake and Body Weight Change versus 1 and Ex4

We then analyzed the effects of **1**, **22**, and Ex4 on food intake and body weight at a single, proof-of-concept, dose, in line with previous reports.<sup>48–50,83</sup> Ex4 administration produced anorexia in shrews at all measured time points (Figure 29), while **1** had no impact on feeding. **22** treatment suppressed food intake similar to Ex4 at 6, 24, and 48 h. The anorectic effect of Ex4 treatment was paralleled by a significant reduction in body weight at 24 h ( $p < 0.05$ ), which was not observed following treatment with **1** or **22** (Figure 29).

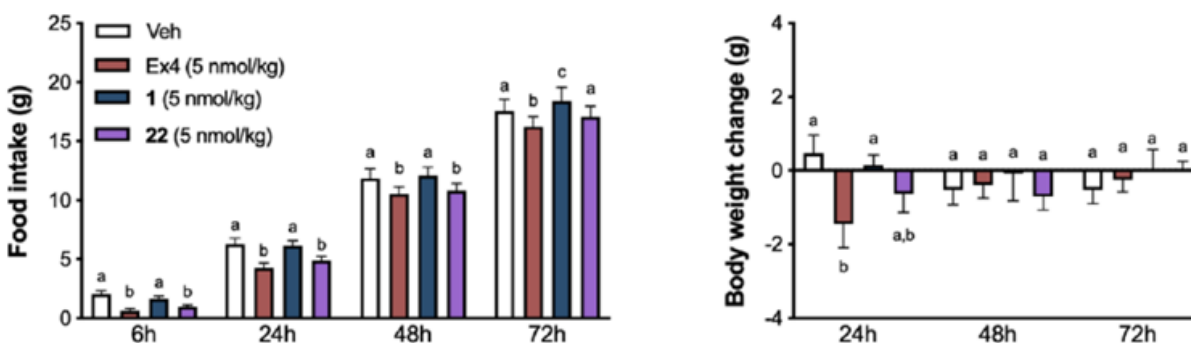


**Figure 29.** Ex4 and **22** (5 nmol/kg, IP) induced anorexia at 6, 24, and 48 h (and at 72 h for Ex4 only), whereas **1** had no effect on food intake ( $n = 10$ ). Ex4-induced anorexia was accompanied by significant body weight loss at 24 h. No significant changes in body weight occurred after **1** and **22** administration compared to controls. All data expressed as mean  $\pm$  SEM ( $n = 10$ ). Data was analyzed with repeated-measurements two-way ANOVA followed by Tukey's post hoc test. Means with different letters are significantly different ( $P < 0.05$ ).

### 3.17.3 22 Prevalence of Emetic Episodes Following Administration of 1, 22, and Ex4

To test whether **22** treatment retained the non-emetic properties of the lead conjugate **1**, indicative of an altered pharmacodynamic profile, despite its comparable potency and GLP-1R binding affinity compared to **1**, and comparable to nEx4, we compared the emetogenic properties

of **1**, **22**, and native Ex4 in shrews. Ex4 induced profound emesis in most of the shrews tested (Figure 30). Indeed, 80% of the animals exhibited emesis upon administration of native Ex4 within minutes after injection ( $29 \pm 16$  min). In line with our previous presented data, treatment with **1** did not cause emesis in any of the shrews tested. Importantly, the number of single emetic episodes occurring in the 120 min window after drug administration was also significantly reduced after **22** administration compared to Ex4 and did not differ from vehicle- or **1**-treated groups. Only two animals that received **22** experienced emesis with an average latency of  $70 \pm 29$  min. The greater emetic effect observed for **22** over **1** is likely a consequence of the greater binding and agonism of **22** at the GLP-1R, an effect that is likely to be mitigated, without loss of glucoregulation, by use of lower doses of **22** (on-going work). The difference in the emetogenic profiles of the corrinated constructs versus native Ex4 is further emphasized by the graphical visualization of emetic intensity, recurrence, and latency for each individual animal across time (Figure 30).

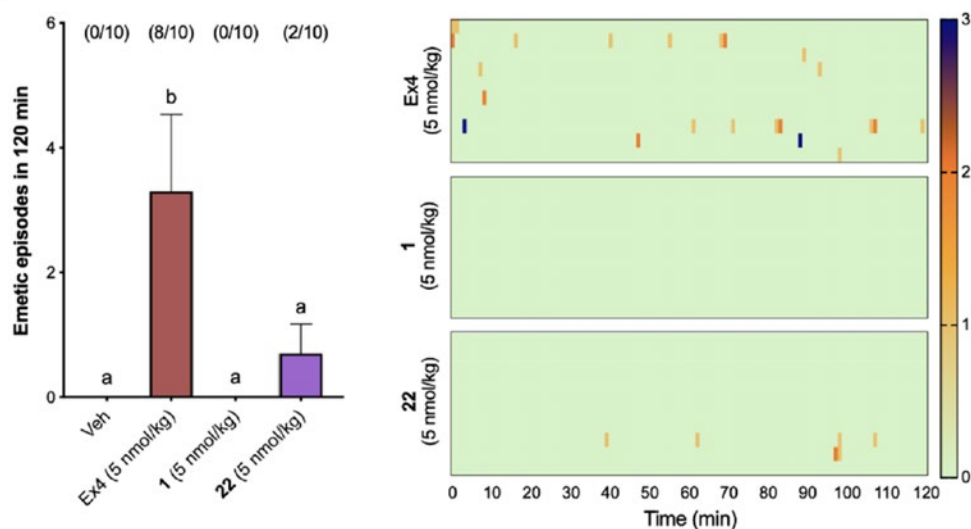


**Figure 30.** The number of single emetic episodes following Ex4, 1, 22, or saline systemic administration was recorded for 120 min. The number of animals exhibiting emesis, expressed as a fraction of the total number of animals tested, is indicated above each treatment group. Ex4 induced robust emetic responses that were not observed after 1 or saline injections. 22 induced emesis in two of the animals tested; however, the number of emetic episodes was significantly lower than that of Ex4 and did not differ from animals treated with vehicle or 1 (n = 10). Heatmaps showing latency, number, and intensity of emesis following Ex4, 1, and 22 dosing for each individual animal across time. All data expressed as mean  $\pm$  SEM (n = 10). Emetic episode data was analyzed with repeated measurements one-way ANOVA followed by Tukey's post hoc test. Means with different letters are significantly different (P < 0.05).

### 3.18 Outcomes and Conclusions

Neuroendocrine associated pharmacological side effects such as nausea and emesis are often downplayed or dismissed, left in the shadow of the overriding target, be it glucoregulation, weight loss, etc. Indeed, the weight loss gleaned from GLP-1RAs, for example, has proven to be a beneficial "side effect" of T2DM treatment due to the high comorbidity of T2DM with

obesity.<sup>105</sup> In many cases, however, such as lean T2DM patients, or patients with comorbidities where nutritional status is critical (cystic fibrosis, cancer-cachexia, sarcopenia, chronic obstructive pulmonary disease, etc.), removal of the CNS associated side effects would be greatly beneficial. Indeed, GLP-1RAs have proven to be life-altering, and the ability to expand their use, or increase patient compliance when using, should not be understated. Herein, we conceived 16 new Cbi-Ex4/Ex40 conjugates with the aim of designing a construct with equipotent binding and agonism of the GLP-1R to that of Ex4 with a view of maintaining activity at peripheral GLP-1R populations and mitigating such activity in CNS populations. We were able to successfully design several constructs with comparable binding and agonism at GLP-1R as Ex4, with one conjugate, **22** ( $IC_{50}$   $11.9 \pm 2.5$  nM,  $EC_{50}$   $20.7 \pm 8.3$  pM), translated into *ex vivo* and *in vivo* studies. **22** increased glucose secretion compared to vehicle controls in a glucose-dependent insulin secretion assay in rat islets. In an *in vivo* IPGTT, **22** provided glucoregulation comparable to Ex4. Critically, **22** showed a near absence of emesis and mild body weight lowering actions compared to profound emesis and body weight loss observed for nEx4.

While corination is poorly explored, especially as it pertains to applications that seek to prevent CNS penetration while maintaining peripheral activity of a target drug, it shows considerable promise as a platform technology, moving beyond GLP-1RAs. An additional highlight of Cbi is its water solubility (400 mg/mL), akin to glucose (450 mg/mL).<sup>106</sup> Use of Cbi conjugation with drugs with physical properties not suited to drug development, such as glucagon<sup>107–109</sup> for rescue of hypoglycemia, offers great scope for exploration.

### 3.19 References

- (1) Chen, L.; Magliano, D. J.; Zimmet, P. Z. The Worldwide Epidemiology of Type 2 Diabetes Mellitus - Present and Future Perspectives. *Nat. Rev. Endocrinol.* **2012**, *8* (4), 228–236.
- (2) Flegal, K. M.; Carroll, M. D.; Ogden, C. L.; Curtin, L. R. CLINICIAN ' S CORNER Among US Adults , 1999-2008. *J. Am. Med. Assoc.* **2013**, *303* (3), 235–241.
- (3) Sherwin, R.; Jastreboff, A. M. Year in Diabetes 2012: The Diabetes Tsunami. *J. Clin. Endocrinol. Metab.* **2012**, *97* (12), 4293–4301.
- (4) Franks, P. W.; McCarthy, M. I. Exposing the Exposures Responsible for Type 2 Diabetes and Obesity. *Science (80-. ).* **2016**, *354* (6308), 69–73.
- (5) Upadhyay, J.; Polyzos, S. A.; Perakakis, N.; Thakkar, B.; Paschou, S. A.; Katsiki, N.; Underwood, P.; Park, K. H.; Seufert, J.; Kang, E. S.; Sternthal, E.; Karagiannis, A.; Mantzoros, C. S. Pharmacotherapy of Type 2 Diabetes: An Update. *Metabolism.* **2018**, *78*, 13–42.
- (6) Sadry, S. A.; Drucker, D. J. Emerging Combinatorial Hormone Therapies for the Treatment of Obesity and T2DM. *Nat. Rev. Endocrinol.* **2013**, *9* (7), 425–433.
- (7) Drucker, D. J.; Sherman, S. I.; Bergenstal, R. M.; Buse, J. B. The Safety of Incretin-Based Therapies - Review of the Scientific Evidence. *J. Clin. Endocrinol. Metab.* **2011**, *96* (7), 2027–2031.
- (8) Hayes, M. R.; Mietlicki-Baase, E. G.; Kanoski, S. E.; De Jonghe, B. C. Incretins and Amylin: Neuroendocrine Communication between the Gut, Pancreas, and Brain in Control of Food Intake and Blood Glucose. *Annu. Rev. Nutr.* **2014**, *34*, 237–260.
- (9) Holst, J. J. The Physiology of Glucagon-like Peptide 1. *Physiol. Rev.* **2007**, *87* (4), 1409–1439.
- (10) Baggio, L. L.; Drucker, D. J. Biology of Incretins: GLP-1 and GIP. *Gastroenterology* **2007**, *132*,



2131–2157.

- (11) Lovshin, J. A.; Drucker, D. J. Incretin-Based Therapies for Type 2 Diabetes Mellitus. *Nat. Rev. Endocrinol.* **2009**, *5* (5), 262–269.
- (12) Hayes, M. R.; Schmidt, H. D. GLP-1 Influences Food and Drug Reward. *Curr. Opin. Behav. Sci.* **2016**, *9*, 66–70.
- (13) Kanoski, S. E.; Hayes, M. R.; Skibicka, K. P. GLP-1 and Weight Loss: Unraveling the Diverse Neural Circuitry. *Am. J. Physiol. - Regul. Integr. Comp. Physiol.* **2016**, *310* (10), R885–R895.
- (14) Knudsen, L. B.; Lau, J. The Discovery and Development of Liraglutide and Semaglutide. *Front. Endocrinol. (Lausanne)*. **2019**, *10*, 155.
- (15) Madsen, K.; Knudsen, L. B.; Agerso, H.; Nielsen, P. F.; Thøgersen, H.; Wilken, M.; Johansen, N. L. Structure-Activity and Protraction Relationship of Long-Acting Glucagon-like Peptide-1 Derivatives: Importance of Fatty Acid Length, Polarity, and Bulkiness. *J. Med. Chem.* **2007**, *50* (24), 6126–6132.
- (16) Knudsen, L. B.; Nielsen, P. F.; Huusfeldt, P. O.; Johansen, N. L.; Madsen, K.; Pedersen, F. Z.; Thøgersen, H.; Wilken, M.; Agersø, H. Potent Derivatives of Glucagon-like Peptide-1 with Pharmacokinetic Properties Suitable for Once Daily Administration. *J. Med. Chem.* **2000**, *43* (9), 1664–1669.
- (17) Lau, J.; Bloch, P.; Schäffer, L.; Pettersson, I.; Spetzler, J.; Kofoed, J.; Madsen, K.; Knudsen, L. B.; McGuire, J.; Steensgaard, D. B.; Strauss, H. M.; Gram, D. X.; Knudsen, S. M.; Nielsen, F. S.; Thygesen, P.; Reedtz-Runge, S.; Kruse, T. Discovery of the Once-Weekly Glucagon-Like Peptide-1 (GLP-1) Analogue Semaglutide. *J. Med. Chem.* **2015**, *58* (18), 7370–7380.

- (18) O'Neil, P. M.; Birkenfeld, A. L.; McGowan, B.; Mosenzon, O.; Pedersen, S. D.; Wharton, S.; Carson, C. G.; Jepsen, C. H.; Kabisch, M.; Wilding, J. P. H. Efficacy and Safety of Semaglutide Compared with Liraglutide and Placebo for Weight Loss in Patients with Obesity: A Randomised, Double-Blind, Placebo and Active Controlled, Dose-Ranging, Phase 2 Trial. *Lancet* **2018**, *392* (10148), 637–649.
- (19) Bergenstal, R. M.; Wysham, C.; MacConell, L.; Malloy, J.; Walsh, B.; Yan, P.; Wilhelm, K.; Malone, J.; Porter, L. E. Efficacy and Safety of Exenatide Once Weekly versus Sitagliptin or Pioglitazone as an Adjunct to Metformin for Treatment of Type 2 Diabetes (DURATION-2): A Randomised Trial. *Lancet* **2010**, *376* (9739), 431–439.
- (20) Buse, J. B.; Henry, R. R.; Han, J.; Kim, D. D.; Fineman, M. S.; Baron, A. D. Effects of Exenatide (Exendin-4) on Glycemic Control over 30 Weeks in Sulfonylurea-Treated Patients with Type 2 Diabetes. *Diabetes Care* **2004**, *27* (11), 2628–2635.
- (21) DeFronzo, R. A.; Ratner, R. E.; Han, J.; Kim, D. D.; Fineman, M. S.; Baron, A. D. Effects of Exenatide (Exendin-4) on Glycemic Control and Weight over 30 Weeks in Metformin-Treated Patients with Type 2 Diabetes. *Diabetes Care* **2005**, *28* (5), 1092–1100.
- (22) John, L. E.; Kane, M. P.; Busch, R. S.; Hamilton, R. A. Expanded Use of Exenatide in the Management of Type 2 Diabetes. *Diabetes Spectr.* **2007**, *20* (1), 59–63.
- (23) Kendall, D. M.; Riddle, M. C.; Rosenstock, J.; Zhuang, D.; Kim, D. D.; Fineman, M. S.; Baron, A. D. Effects of Exenatide (Exendin-4) on Glycemic Control over 30 Weeks in Patients with Type 2 Diabetes Treated with Metformin and a Sulfonylurea. *Diabetes Care* **2005**, *28* (5), 1083–1091.

- (24) Weinstock, R. S.; Guerci, B.; Umpierrez, G.; Nauck, M. A.; Skrivanek, Z.; Milicevic, Z. Safety and Efficacy of Once-Weekly Dulaglutide versus Sitagliptin after 2years in Metformin-Treated Patients with Type 2 Diabetes (AWARD-5): A Randomized, Phase III Study. *Diabetes, Obes. Metab.* **2015**, *17* (9), 849–858.
- (25) Wang, T.; Gou, Z.; Wang, F.; Nling, M.; Zhai, S. Di. Comparison of GLP-1 Analogues versus Sitagliptin in the Management of Type 2 Diabetes: Systematic Review and Meta-Analysis of Head-to-Head Studies. *PLoS One* **2014**, *9* (8), e103798.
- (26) Bettge, K.; Kahle, M.; Abd El Aziz, M. S.; Meier, J. J.; Nauck, M. A. Occurrence of Nausea, Vomiting and Diarrhoea Reported as Adverse Events in Clinical Trials Studying Glucagon-like Peptide-1 Receptor Agonists: A Systematic Analysis of Published Clinical Trials. *Diabetes, Obes. Metab.* **2017**, *19* (3), 336–347.
- (27) Kanoski, S. E.; Fortin, S. M.; Arnold, M.; Grill, H. J.; Hayes, M. R. Peripheral and Central GLP-1 Receptor Populations Mediate the Anorectic Effects of Peripherally Administered GLP-1 Receptor Agonists, Liraglutide and Exendin-4. *Endocrinology* **2011**, *152* (8), 3103–3112.
- (28) Sisley, S.; Gutierrez-Aguilar, R.; Scott, M.; D’Alessio, D.; Sandoval, D.; Seeley, R. Neuronal GLP1R Mediates Liraglutide’s Anorectic but Not Glucose-Lowering Effect. *J. Clin. Invest.* **2014**, *124* (6), 2456–2463.
- (29) Secher, A.; Jelsing, J.; Baquero, A. F.; Hecksher-Sørensen, J.; Cowley, M. A.; Dalbøge, L. S.; Hansen, G.; Grove, K. L.; Pyke, C.; Raun, K.; Schäfer, L.; Tang-Christensen, M.; Verma, S.; Witgen, B. M.; Vrang, N.; Knudsen, L. B. The Arcuate Nucleus Mediates GLP-1 Receptor Agonist Liraglutide-Dependent Weight Loss. *J. Clin. Invest.* **2014**, *124* (10), 4473–4488.
- (30) Kanoski, S. E.; Rupperecht, L. E.; Fortin, S. M.; De Jonghe, B. C.; Hayes, M. R. The Role of

- Nausea in Food Intake and Body Weight Suppression by Peripheral GLP-1 Receptor Agonists, Exendin-4 and Liraglutide. *Neuropharmacology* **2012**, 62 (5–6), 1916–1927.
- (31) Sikirica, M. V.; Martin, A. A.; Wood, R.; Leith, A.; Piercy, J.; Higgins, V. Reasons for Discontinuation of GLP1 Receptor Agonists: Data from a Real-World Cross-Sectional Survey of Physicians and Their Patients with Type 2 Diabetes. *Diabetes, Metab. Syndr. Obes. Targets Ther.* **2017**, 10, 403–412.
- (32) Ahrén, B.; Atkin, S. L.; Charpentier, G.; Warren, M. L.; Wilding, J. P. H.; Birch, S.; Holst, A. G.; Leiter, L. A. Semaglutide Induces Weight Loss in Subjects with Type 2 Diabetes Regardless of Baseline BMI or Gastrointestinal Adverse Events in the SUSTAIN 1 to 5 Trials. *Diabetes, Obes. Metab.* **2018**, 20 (9), 2210–2219.
- (33) Pratley, R. E.; Aroda, V. R.; Lingvay, I.; Lundemann, J.; Andreassen, C.; Navarria, A.; Viljoen, A. Emaglutide versus Dulaglutide Once Weekly in Patients with Type 2 Diabetes (SUSTAIN 7): A Randomised, Open-Label, Phase 3b Trial. *Lancet Diabetes Endocrinol.* **2018**, 6, 278–286.
- (34) Wysham, C.; Blevins, T.; Arakaki, R.; Colon, G.; Garcia, P.; Atisso, C.; Kuhstoss, D.; Lakshmanan, M. Efficacy and Safety of Dulaglutide Added onto Pioglitazone and Metformin versus Exenatide in Type 2 Diabetes in a Randomized Controlled Trial (AWARD-1). *Diabetes Care* **2014**, 37 (8), 2159–2167.
- (35) Moheet, A.; Moran, A. CF-Related Diabetes: Containing the Metabolic Miscreant of Cystic Fibrosis. *Pediatr. Pulmonol.* **2017**, 52, S37–S43.
- (36) Gallo, M.; Muscogiuri, G.; Felicetti, F.; Faggiano, A.; Trimarchi, F.; Arvat, E.; Vigneri, R.;

- Colao, A. Adverse Glycaemic Effects of Cancer Therapy: Indications for a Rational Approach to Cancer Patients with Diabetes. *Metabolism*. **2018**, *78*, 141–154.
- (37) Husain, N. E.; Noor, S. K.; Elmadhoun, W. M.; Almobarak, A. O.; Awadalla, H.; Woodward, C. L.; Mital, D.; Ahmed, M. H. Diabetes, Metabolic Syndrome and Dyslipidemia in People Living with HIV in Africa: Re-Emerging Challenges Not to Be Forgotten. *HIV/AIDS - Res. Palliat. Care* **2017**, *9*, 193–202.
- (38) Ho, T. W.; Huang, C. T.; Ruan, S. Y.; Tsai, Y. J.; Lai, F.; Yu, C. J. Diabetes Mellitus in Patients with Chronic Obstructive Pulmonary Disease-The Impact on Mortality. *PLoS One* **2017**, *12* (4), 1–15.
- (39) Honors, M. A.; Kinzig, K. P. The Role of Insulin Resistance in the Development of Muscle Wasting during Cancer Cachexia. *J. Cachexia. Sarcopenia Muscle* **2012**, *3* (1), 5–11.
- (40) Drucker, D. J. The Biology of Incretin Hormones. *Cell Metab.* **2006**, *3* (3), 153–165.
- (41) Hayes, M. R.; De Jonghe, B. C.; Kanoski, S. E. Role of the Glucagon-like-Peptide-1 Receptor in the Control of Energy Balance. *Physiol. Behav.* **2010**, *100* (5), 503–510.
- (42) Chambers, A. P.; Sorrell, J. E.; Haller, A.; Roelofs, K.; Hutch, C. R.; Kim, K. S.; Gutierrez-Aguilar, R.; Li, B.; Drucker, D. J.; D'Alessio, D. A.; Seeley, R. J.; Sandoval, D. A. The Role of Pancreatic Preproglucagon in Glucose Homeostasis in Mice. *Cell Metab.* **2017**, *25* (4), 927-934.
- (43) Lamont, B. J.; Li, Y.; Kwan, E.; Brown, T. J.; Gaisano, H.; Drucker, D. J. Pancreatic GLP-1 Receptor Activation Is Sufficient for Incretin Control of Glucose Metabolism in Mice. *J. Clin. Invest.* **2012**, *122* (1), 388–402.

- (44) Smith, E. P.; An, Z.; Wagner, C.; Lewis, A. G.; Cohen, E. B.; Li, B.; Mahbod, P.; Sandoval, D.; Perez-Tilve, D.; Tamarina, N.; Philipson, L. H.; Stoffers, D. A.; Seeley, R. J.; D'Alessio, D. A. The Role of  $\beta$  Cell Glucagon-like Peptide-1 Signaling in Glucose Regulation and Response to Diabetes Drugs. *Cell Metab.* **2014**, *19* (6), 1050–1057.
- (45) Alhadeff, A. L.; Mergler, B. D.; Zimmer, D. J.; Turner, C. A.; Reiner, D. J.; Schmidt, H. D.; Grill, H. J.; Hayes, M. R. Endogenous Glucagon-like Peptide-1 Receptor Signaling in the Nucleus Tractus Solitarius Is Required for Food Intake Control. *Neuropsychopharmacology* **2017**, *42* (7), 1471–1479.
- (46) Hayes, M. R.; Leichner, T. M.; Zhao, S.; Lee, G. S.; Zimmer, D.; Jonghe, B. C. De; Kanoski, S. E.; Grill, H. J.; Bence, K. K. Intracellular Signals Mediating the Food Intake Suppressive Effects of Hindbrain Glucagon-like-Peptide-1 Receptor Activation. *Cell Metab.* **2011**, *13* (3), 320–330.
- (47) Mietlicki-Baase, E. G.; Ortinski, P. I.; Rupprecht, L. E.; Olivos, D. R.; Alhadeff, A. L.; Christopher Pierce, R.; Hayes, M. R. The Food Intake-Suppressive Effects of Glucagon-like Peptide-1 Receptor Signaling in the Ventral Tegmental Area Are Mediated by AMPA/Kainate Receptors. *Am. J. Physiol. - Endocrinol. Metab.* **2013**, *305* (11), 1367–1374.
- (48) Bonaccorso, R. L.; Chepurny, O. G.; Becker-Pauly, C.; Holz, G. G.; Doyle, R. P. Enhanced Peptide Stability Against Protease Digestion Induced by Intrinsic Factor Binding of a Vitamin B12 Conjugate of Exendin-4. *Mol. Pharm.* **2015**, *12* (9), 3502–3506.
- (49) Mietlicki-Baase, E. G.; Liberini, C. G.; Workinger, J. L.; Bonaccorso, R. L.; Borner, T.; Reiner, D. J.; Koch-Laskowski, K.; McGrath, L. E.; Lhamo, R.; Stein, L. M.; De Jonghe, B. C.; Holz, G. G.; Roth, C. L.; Doyle, R. P.; Hayes, M. R. A Vitamin B12 Conjugate of Exendin-4 Improves

- Glucose Tolerance without Associated Nausea or Hypophagia in Rodents. *Diabetes, Obes. Metab.* **2018**, *20* (5), 1223–1234.
- (50) Borner, T.; Shaulson, E. D.; Tinsley, I. C.; Stein, L. M.; Horn, C. C.; Hayes, M. R.; Doyle, R. P.; De Jonghe, B. C. A Second-Generation Glucagon-like Peptide-1 Receptor Agonist Mitigates Vomiting and Anorexia While Retaining Glucoregulatory Potency in Lean Diabetic and Emetic Mammalian Models. *Diabetes, Obes. Metab.* **2020**, *22* (10), 1729–1741.
- (51) Henry, K. E.; Elfers, C. T.; Burke, R. M.; Chepurny, O. G.; Holz, G. G.; Blevins, J. E.; Roth, C. L.; Doyle, R. P. Vitamin B12 Conjugation of Peptide-YY3-36 Decreases Food Intake Compared to Native Peptide-YY3-36 upon Subcutaneous Administration in Male Rats. *Endocrinology* **2015**, *156* (5), 1739–1749.
- (52) Workinger, J. L.; Kuda-Wedagedara, A. N. W.; Julin, M. M.; White, J. M.; Nexo, E.; Viola, N. T.; Doyle, R. P. Systemically Administered Plant Recombinant Holo-Intrinsic Factor Targets the Liver and Is Not Affected by Endogenous B12 Levels. *Sci. Rep.* **2019**, *9* (1), 1–8.
- (53) Green, R.; Allen, L. H.; Bjørke-Monsen, A. L.; Brito, A.; Guéant, J. L.; Miller, J. W.; Molloy, A. M.; Nexo, E.; Stabler, S.; Toh, B. H.; Ueland, P. M.; Yajnik, C. Vitamin B12 Deficiency. *Nat. Rev. Dis. Prim.* **2017**, *3*, 17040.
- (54) Kanazawa, S.; Herbert, V. Noncobalamin Vitamin B12 Analogues in Human Red Cells, Liver, and Brain. *Am. J. Clin. Nutr.* **1983**, *37* (5), 774–777.
- (55) Hardlei, T. F.; Nexo, E. A New Principle for Measurement of Cobalamin and Corrinoids, Used for Studies of Cobalamin Analogs on Serum Haptocorrin. *Clin. Chem.* **2009**, *55* (5), 1002–1010.

- (56) Furger, E.; Fedosov, S. N.; Lildballe, D. L.; Waibel, R.; Schibli, R.; Nexo, E.; Fischer, E. Comparison of Recombinant Human Haptocorrin Expressed in Human Embryonic Kidney Cells and Native Haptocorrin. *PLoS One* **2012**, *7* (5), e37421.
- (57) Rosenblatt, D. S. Inherited Disorders of Folate and Cobalamin. **1997**, 61–68.
- (58) Gimsing, P.; Nexo, E. Cobalamin-Binding Capacity of Haptocorrin and Transcobalamin: Age-Related Reference Intervals and Values from Patients. *Clin. Chem.* **1989**, *35* (7), 1447–1451.
- (59) Kuda-Wedagedara, A. N. W.; Workinger, J. L.; Nexo, E.; Doyle, R. P.; Viola-Villegas, N. 89Zr-Cobalamin PET Tracer: Synthesis, Cellular Uptake, and Use for Tumor Imaging. *ACS Omega* **2017**, *2* (10), 6314–6320.
- (60) Horn, C. C.; Kimball, B. A.; Wang, H.; Kaus, J.; Diemel, S.; Nagy, A.; Gathright, G. R.; Yates, B. J.; Andrews, P. L. R. Why Can't Rodents Vomit? A Comparative Behavioral, Anatomical, and Physiological Study. *PLoS One* **2013**, *8* (4), e60537.
- (61) Chan, S. W.; Lin, G.; Yew, D. T. W.; Rudd, J. A. A Physiological Role of Glucagon-like Peptide-1 Receptors in the Central Nervous System of *Suncus Murinus* (House Musk Shrew). *Eur. J. Pharmacol.* **2011**, *668* (1–2), 340–346.
- (62) Chan, S. W.; Lin, G.; Yew, D. T. W.; Yeung, C. K.; Rudd, J. A. Separation of Emetic and Anorexic Responses of Exendin-4, a GLP-1 Receptor Agonist in *Suncus Murinus* (House Musk Shrew). *Neuropharmacology* **2013**, *70* (5–6), 141–147.
- (63) Ó Proinsias, K.; Karczewski, M.; Zieleniewska, A.; Gryko, D. Microwave-Assisted Cobinamide Synthesis. *J. Org. Chem.* **2014**, *79* (16), 7752–7757.



- (64) Równicki, M.; Wojciechowska, M.; Wierzba, A. J.; Czarnecki, J.; Bartosik, D.; Gryko, D.; Trylska, J. Vitamin B12 as a Carrier of Peptide Nucleic Acid (PNA) into Bacterial Cells. *Sci. Rep.* **2017**, *7* (1), 7644.
- (65) Wierzba, A. J.; Hassan, S.; Gryko, D. Synthetic Approaches toward Vitamin B12 Conjugates. *Asian J. Org. Chem.* **2019**, *8* (1), 6–24.
- (66) Clardy-James, S.; Chepurny, O. G.; Leech, C. A.; Holz, G. G.; Doyle, R. P. Synthesis, Characterization and Pharmacodynamics of Vitamin-B12-Conjugated Glucagon-Like Peptide-1. *ChemMedChem* **2013**, *8* (4), 582–586.
- (67) Zhou, K.; Zelder, F. Identification of Diastereomeric Cyano - Aqua Cobinamides with a Backbone-Modified Vitamin B12 Derivative and with <sup>1</sup>H NMR Spectroscopy. *Eur. J. Inorg. Chem.* **2011**, No. 1, 53–57.
- (68) Berg, R.; Straub, B. F. Advancements in the Mechanistic Understanding of the Copper-Catalyzed Azide-Alkyne Cycloaddition. *Beilstein J. Org. Chem.* **2013**, *9*, 2715–2750.
- (69) Klarenbeek, J.; Goedhart, J.; Van Batenburg, A.; Groenewald, D.; Jalink, K. Fourth-Generation Epac-Based FRET Sensors for CAMP Feature Exceptional Brightness, Photostability and Dynamic Range: Characterization of Dedicated Sensors for FLIM, for Ratiometry and with High Affinity. *PLoS One* **2015**, *10* (4), 1–11.
- (70) Chepurny, O. G.; Matsoukas, M. T.; Liapakis, G.; Leech, C. A.; Milliken, B. T.; Doyle, R. P.; Holz, G. G. Nonconventional Glucagon and GLP-1 Receptor Agonist and Antagonist Interplay at the GLP-1 Receptor Revealed in High-Throughput FRET Assays for CAMP. *J. Biol. Chem.* **2019**, *294* (10), 3514–3531.

- (71) Hygum, K.; Lildballe, D. L.; Greibe, E. H.; Morkbak, A. L.; Poulsen, S. S.; Sorensen, B. S.; Petersen, T. E.; Nexø, E. Mouse Transcobalamin Has Features Resembling Both Human Transcobalamin and Haptocorrin. *PLoS One* **2011**, *6* (5), e20638.
- (72) Copley, K.; McCowen, K.; Hiles, R.; Nielsen, L. L.; Young, A.; Parkes, D. G. Investigation of Exenatide Elimination and Its in Vivo and in Vitro Degradation. *Curr. Drug Metab.* **2006**, *7* (4), 367–374.
- (73) Simonsen, L.; Holst, J. J.; Deacon, C. F. Exendin-4, but Not Glucagon-like Peptide-1, Is Cleared Exclusively by Glomerular Filtration in Anaesthetised Pigs. *Diabetologia* **2006**, *49* (4), 706–712.
- (74) Herbert, V.; Herzlich, B. Quantitation of Intrinsic Factor. *Blood* **1983**, *61*, 819.
- (75) Hansen, M.; Brynskov, J.; Christensen, P. A.; Krintel, J. J.; Gimsing, P. Cobalamin Binding Proteins (Haptocorrin and Transcobalamin) in Human Cerebrospinal Fluid. *Scand. J. Haematol.* **1985**, *34* (3), 209–212.
- (76) Grill, H. J.; Hayes, M. R. Hindbrain Neurons as an Essential Hub in the Neuroanatomically Distributed Control of Energy Balance. *Cell Metab.* **2012**, *16* (3), 296–309.
- (77) Hesketh, P. J. Chemotherapy-Induced Nausea and Vomiting. *N. Engl. J. Med.* **2008**, *358*, 2482–2494.
- (78) Miller, A. D.; Leslie, R. A. The Area Postrema and Vomiting. *Frontiers in Neuroendocrinology.* **1994**, *15* (4), 301–320.
- (79) Chevalier, S.; Farsijani. Cancer Cachexia and Diabetes: Similarities in Metabolic Alterations and Possible Treatment. *Appl. Physiol. Nutr. Metab.* **2014**, *39* (6), 643–653.
- (80) Porporato, P. E. Understanding Cachexia as a Cancer Metabolism Syndrome. *Oncogenesis*

**2016**, 5 (2), e200.

- (81) Petruzzelli, M.; Wagner, E. F. Mechanisms of Metabolic Dysfunction in Cancer-Associated Cachexia. *Genes Dev.* **2016**, 30 (5), 489–501.
- (82) Honors, M. A.; Kinzig, K. P. Chronic Exendin-4 Treatment Prevents the Development of Cancer Cachexia Symptoms in Male Rats Bearing the Yoshida Sarcoma. *Horm. Cancer* **2012**, 5 (1), 33–41.
- (83) Borner, T.; Workinger, J. L.; Tinsley, I. C.; Fortin, S. M.; Stein, L. M.; Chepurny, O. G.; Holz, G. G.; Wierzba, A. J.; Gryko, D.; Nexø, E.; Shaulson, E. D.; Bamezai, A.; Da Silva, V. A. R.; De Jonghe, B. C.; Hayes, M. R.; Doyle, R. P. Corriation of a GLP-1 Receptor Agonist for Glycemic Control without Emesis. *Cell Rep.* **2020**, 31 (11), 107768.
- (84) De Jonghe, B. C.; Lawler, M. P.; Horn, C. C.; Tordoff, M. G. Pica as an Adaptive Response: Kaolin Consumption Helps Rats Recover from Chemotherapy-Induced Illness. *Physiol. Behav.* **2009**, 97 (1), 87–90.
- (85) Ueno, S.; Matsuki, N.; Saito, H. Suncus Murinus: A New Experimental Model In Emesis Research. *Life Sci.* **1987**, 41 (4), 513–518.
- (86) Anantharam, P.; Whitley, E. M.; Mahama, B.; Kim, D. S.; Sarkar, S.; Santana, C.; Chan, A.; Kanthasamy, A. G.; Kanthasamy, A.; Boss, G. R.; Rumbelha, W. K. Cobinamide Is Effective for Treatment of Hydrogen Sulfide-Induced Neurological Sequelae in a Mouse Model. *Ann. N. Y. Acad. Sci.* **2017**, 1408 (1), 61–78.
- (87) Hendry-Hofer, T. B.; Ng, P. C.; McGrath, A. M.; Mukai, D.; Brenner, M.; Mahon, S.; Maddry, J. K.; Boss, G. R.; Bebartha, V. S. Intramuscular Aminotetrazole Cobinamide as a Treatment

- for Inhaled Hydrogen Sulfide Poisoning in a Large Swine Model. *Ann. N. Y. Acad. Sci.* **2020**, *1479* (1), 159–167.
- (88) Männel-Croisé, C.; Probst, B.; Zelder, F. A Straightforward Method for the Colorimetric Detection of Endogenous Biological Cyanide. *Anal. Chem.* **2009**, *81* (22), 9493–9498.
- (89) Broderick, K. E.; Potluri, P.; Zhuang, S.; Scheffler, I. E.; Sharma, V. S.; Pilz, R. B.; Boss, G. R. Cyanide Detoxification by the Cobalamin Precursor Cobinamide. *Exp. Biol. Medicin* **2006**, *231* (5), 641–649.
- (90) Chan, A.; Jiang, J.; Fridman, A.; Guo, L. T.; Shelton, G. D.; Liu, M. T.; Green, C.; Haushalter, K. J.; Patel, H. H.; Lee, J.; Yoon, D.; Burney, T.; Mukai, D.; Mahon, S. B.; Brenner, M.; Pilz, R. B.; Boss, G. R. Nitrocobinamide, a New Cyanide Antidote That Can Be Administered by Intramuscular Injection. *J. Med. Chem.* **2015**, *58* (4), 1750–1759.
- (91) Chan, A.; Balasubramanian, M.; Blackledge, W.; Mohammad, O. M.; Alvarez, L.; Boss, G. R.; Bigby, T. D. Cobinamide Is Superior to Other Treatments in a Mouse Model of Cyanide Poisoning. *Clin. Toxicol.* **2010**, *48* (7), 709–717.
- (92) Lee, J.; Mahon, S. B.; Mukai, D.; Burney, T.; Katebian, B. S.; Chan, A.; Bebart, V. S.; Yoon, D.; Boss, G. R.; Brenner, M. The Vitamin B12 Analog Cobinamide Is an Effective Antidote for Oral Cyanide Poisoning. *J. Med. Toxicol.* **2016**, *12* (4), 370–379.
- (93) Greenawald, L. A.; Snyder, J. L.; Fry, N. L.; Sailor, M. J.; Boss, G. R.; Finklea, H. O.; Bell, S. Development of a Cobinamide-Based End-of-Service-Life Indicator for Detection of Hydrogen Cyanide Gas. *Sensors and Actuators, B, Chem.* **2015**, *221*, 379–385.
- (94) Brenner, M.; Mahon, S. B.; Lee, J.; Kim, J.; Mukai, D.; Goodman, S.; Kreuter, K. A.; Ahdout,

- R.; Mohammad, O.; Sharma, V. S.; Blackledge; Boss, G. R. Comparison of Cobinamide to Hydroxocobalamin in Reversing Cyanide Physiologic Effects in Rabbits Using Diffuse Optical Spectroscopy Monitoring. *J. Biomed. Opt.* **2010**, *15* (1), 017001.
- (95) Ma, J.; Dasgupta, P. K.; Zelder, F. H.; Boss, G. R. Cobinamide Chemistries for Photometric Cyanide Determination. A Merging Zone Liquid Core Waveguide Cyanide Analyzer Using Cyanoaquacobinamide. *Anal. Chim. Acta* **2012**, *736*, 78–84.
- (96) Wierzba, A. J.; Maximova, K.; Wincenciuk, A.; Równicki, M.; Wojciechowska, M.; Nexø, E.; Trylska, J.; Gryko, D. Does a Conjugation Site Affect Transport of Vitamin B12–Peptide Nucleic Acid Conjugates into Bacterial Cells? *Chem. - A Eur. J.* **2018**, *24* (70), 18772–18778.
- (97) Evers, A.; Haack, T.; Lorenz, M.; Bossart, M.; Elvert, R.; Henkel, B.; Stengelin, S.; Kurz, M.; Glien, M.; Dudda, A.; Lorenz, K.; Kadereit, D.; Wagner, M. Design of Novel Exendin-Based Dual Glucagon-like Peptide 1 (GLP-1)/Glucagon Receptor Agonists. *J. Med. Chem.* **2017**, *60* (10), 4293–4303.
- (98) Dai, S.; Liu, S.; Li, C.; Zhou, Z.; Wu, Z. Site-Selective Modification of Exendin 4 with Variable Molecular Weight Dextrans by Oxime-Ligation Chemistry for Improving Type 2 Diabetic Treatment. *Carbohydr. Polym.* **2020**, *249* (July), 116864.
- (99) Lee, J. G.; Ryu, J. H.; Kim, S. M.; Park, M. Y.; Kim, S. H.; Shin, Y. G.; Sohn, J. W.; Kim, H. H.; Park, Z. Y.; Seong, J. Y.; Kim, J. Il. Replacement of the C-Terminal Trp-Cage of Exendin-4 with a Fatty Acid Improves Therapeutic Utility. *Biochem. Pharmacol.* **2018**, *151* (January), 59–68.

- (100) Tibaduiza, E. C.; Chen, C.; Beinborn, M. A Small Molecule Ligand of the Glucagon-like Peptide 1 Receptor Targets Its Amino-Terminal Hormone Binding Domain. *J. Biol. Chem.* **2001**, *276* (41), 37787–37793.
- (101) Sweet, I. R.; Cook, D. L.; DeJulio, E.; Wallen, A. R.; Khalil, G.; Callis, J.; Reems, J. A. Regulation of ATP/ADP in Pancreatic Islets. *Diabetes* **2004**, *53* (2), 401–409.
- (102) Jung, S. R.; Reed, B. J.; Sweet, I. R. A Highly Energetic Process Couples Calcium Influx through L-Type Calcium Channels to Insulin Secretion in Pancreatic  $\beta$ -Cells. *Am. J. Physiol. - Endocrinol. Metab.* **2009**, *297* (3), 717–727.
- (103) Milliken, B.; Chepurny, O.; Doyle, R.; Holz, G. FRET Reporter Assays for cAMP and Calcium in a 96-Well Format Using Genetically Encoded Biosensors Expressed in Living Cells. *Bio-Protocol* **2020**, *10* (11).
- (104) Chen, W.; Lisowski, M.; Khalil, G.; Sweet, I. R.; Shen, A. Q. Microencapsulated 3-Dimensional Sensor for the Measurement of Oxygen in Single Isolated Pancreatic Islets. *PLoS One* **2012**, *7* (3), 1–10.
- (105) Khaodhiar, L.; McCowen, K. C.; Blackburn, G. L. Obesity and Its Comorbid Conditions. *Clin. Cornerstone* **1999**, *2* (3), 17–31.
- (106) Alves, L. A.; Ipt, P.; Biotecnologia, D. De; Engenharia, E. De; Eel, D. L. Solubility of D-Glucose in Water and Ethanol / Water Mixtures. **2007**, 2166–2170.
- (107) Mroz, P. A.; Perez-Tilve, D.; Mayer, J. P.; DiMarchi, R. D. Stereochemical Inversion as a Route to Improved Biophysical Properties of Therapeutic Peptides Exemplified by Glucagon. *Commun. Chem.* **2019**, *2*, 2.
- (108) Chabenne, J. R.; Mroz, P. A.; Mayer, J. P.; DiMarchi, R. D. Structural Refinement of Glucagon

for Therapeutic Use. *J. Med. Chem.* **2020**, *63* (7), 3447–3460.

- (109) Chabenne, J. R.; DiMarchi, M. A.; Gelfanov, V. M.; DiMarchi, R. D. Optimization of the Native Glucagon Sequence for Medicinal Purposes. *J. Diabetes Sci. Technol.* **2010**, *4* (6), 1322–1331.

#### Chapter 4: Peptide Ligands of the GDNF Family Receptor $\alpha$ -like (GFRAL)

The work in this chapter resulted in the non-provisional patent WO 2020/163502 A1: **Tinsley , I. C.**; Borner, T.; De Jonghe, B. C.; Hayes, M. R.; Doyle, R. P. Peptide Ligands of the GDNF Family Receptor A-Like (GFRAL) Receptor.

As a result of this patent a spin-out company was named Cantius Therapeutics LLC was created and is working to translate this work into clinical trials for Cachexia and Hyperemesis gravidarum.



Peptide antagonist sequences were designed by the author and Dr. Robert P. Doyle. All synthetic work, including synthesis of all tested compounds and the fluorescent analog, their purification, chemical characterization, and preparation for *in vivo* testing was conducted by the author. The in-solution NMR structure was solved by Dr. Deborah Kerwood of Syracuse University using samples produced by the author. All *in vivo* work was performed by Dr. Tito Borner of the University of Pennsylvania



## 4.1 Introduction

Growth differentiation factor 15 (GDF15), also known as macrophage inhibitory cytokine-1 (MIC-1), is a stress response cytokine expressed in a variety of tissue and secreted into circulation in response to many stimuli as part of a wide variety of disease processes, including cancer and obesity.<sup>1-4</sup> GDF15 signaling has gained significant attention in recent years with multiple simultaneous papers in 2017 identifying the GDNF family receptor  $\alpha$ -like (GFRAL) as binding GDF15 selectively and with high affinity.<sup>5-7</sup> Since then, numerous reports quickly populated the literature suggesting promise for GDF15-GFRAL signaling as a potential treatment of obesity.<sup>4,8,9</sup> Data from Hsu *et al.*<sup>6</sup> suggested that GFRAL KO mice were insensitive to long-term anorexia and cachexia/weight loss produced by the highly emetogenic chemotherapy agent cisplatin.<sup>10</sup> In this context, the reported restrictive expression of the GFRAL receptor to the area postrema (AP) and nucleus tractus solitarius (NTS) of the brainstem,<sup>7,11</sup> areas highly critical to both energy balance and emesis/nausea, suggests that GDF15-GFRAL signaling may be an important factor in body weight regulation, as well as processing of illness behaviors.

A recently published article identified that GDF15 induces anorexia through nausea and emesis.<sup>12</sup> To this end, as the GDF15 system is a clear priority targeted by Big Pharma and several academic groups as a potential treatment for metabolic diseases and clinical applications of cachexia (i.e., via GDF15 antibody development), understanding how GDF15 causes sickness and anorexia is paramount to determining the mechanism of GDF15 to induce weight loss.

Compelling evidence links GDF15 signaling with chemotherapy-induced nausea and anorexia, which remain important clinical problems despite relatively well-controlled chemotherapy-induced vomiting,<sup>13-15</sup> by showing that: 1) GDF15 signaling causes nausea and

emesis;<sup>12</sup> 2) an AP/NTS site of action is responsible for mediating the feeding effects of GDF15 signaling through binding of the GFRAL receptor complex;<sup>5-7</sup> and 3) obesity, cancer, and chemotherapy increases circulating GDF15 in rodents and humans.<sup>6,16</sup>

Neural substrates within the AP/NTS are well documented mediators of cancer anorexia-cachexia syndrome (CACCS), a condition paralleled by increased plasma GDF15.<sup>17</sup> Data from Tsai *et al.*<sup>18</sup> intriguingly show that lesions of the AP/NTS were able to block GDF15-induced anorexia and body weight loss in mice. No doubt the effects of AP lesion are due in large part to ablation of GFRAL receptors within the brainstem. Together, these reports begin to elucidate a peptide system that is a prominent contributor to treatment-induced nausea and anorexia, and/or vomiting, and weight loss. Thus, a critical question must be asked by the field: Can targeting the GDF15-GFRAL system represent a realistic treatment for obesity and co-morbid metabolic diseases without producing unwanted nausea/emesis side effects?

#### **4.2 Design of a GFRAL Antagonist**

The use of a peptide for the *antagonism* of the GFRAL receptor has several benefits compared to its antibody counterpart. Notably, low manufacturing costs, greater stability in vivo, lack of offsite interactions, better tissue penetration, especially the brain where antibodies produced to target GFRAL cannot penetrate.<sup>19</sup> Using structure-based computational design (i.e., rational design) focusing on reported<sup>6</sup> GDF15 interactions with the GFRAL receptor (binding) and subsequent RET interactions (recruitment), a small library of peptides were designed with the aim to bind GFRAL, but not recruit RET. Regions of GDF15 known to be critical for the reported GFRAL receptor specificity were incorporated in the initial library. Initial design strategies focused on interactions with GFRAL residues 201-203 [SKE]), which are unique to GFRAL and replace the

'RRR' motif critical for selectivity in other TNF- $\beta$  receptors.<sup>6</sup> In order to selectively bind to GFRAL we ensured critical residues targeting 'SKE' were included. Finally, we ensured no means to recruit RET, by both omitting important GDF15 residues (e.g. W32)<sup>6,7</sup> from the final sequences and also by placing in bulky hydrophilic residues and sequences capable of binding metal ions (particularly zinc) to further block this interaction. Azido modified lysine residues were included in the sequences to allow for future conjugation allowing for mechanistic studies (Table 1).

**Table 1.** Designed GFRAL antagonists. Sequences were designed using amino acids of native ligand, GDF15, known to interact with GFRAL receptor. Note: Sequences are confidential (Office of Technology Transfer, Syracuse University).

Peptide	Sequence
GRASP-01	EDDVSFQ <b>K(azido)</b> LDDNVRYHTLRK
GRASP-02	DDDL <b>SFQK(azido)</b> LDDNVYYHLLRK
GRASP-03	<b>K(azido)</b> LDDNVYYHLLRK
GRASP-04	<b>K(azido)</b> PMVLIQKTDGTVSLQTYD
GRASP-05	<b>TK(azido)</b> EELIHAHADPMVLIQKTDGTVSLQTYD

#### 4.3 *In Vivo* screening of GFANT peptides

The series of GRASP antagonists were tested for their ability to attenuate both anorexia and pica. The GFRAL receptor is known to be expressed in the area postrema and some evidence suggests it is also expressed in the nucleus of the solitary tract. The peptide antagonist's ability to reach this portion of the central nervous system was unknown and thus were delivered directly into the brain via intracerebroventricular (ICV) injection, specifically the fourth ventricle (Figure 1).

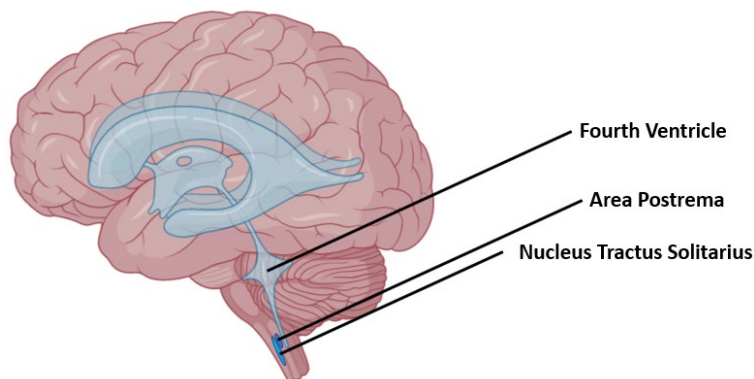


**Figure 1.** The AP lies at the caudal end of the fourth ventricle adjacent to the NTS. Direct injection via the fourth ventricle allows for activation of neurons found in the AP and NTS.

Initial testing occurred by injecting equimolar concentrations of both MIC-1/GDF15 and GFANT (30 pM). *In vivo* screening in the rat of the five designed peptides led to confirmation of GFRAL antagonism for one sequence, labelled herein as GRASP-05 (Figure 2). Initial results suggested that GRASP-01 – GRASP-04 no therapeutic effect (data not shown).

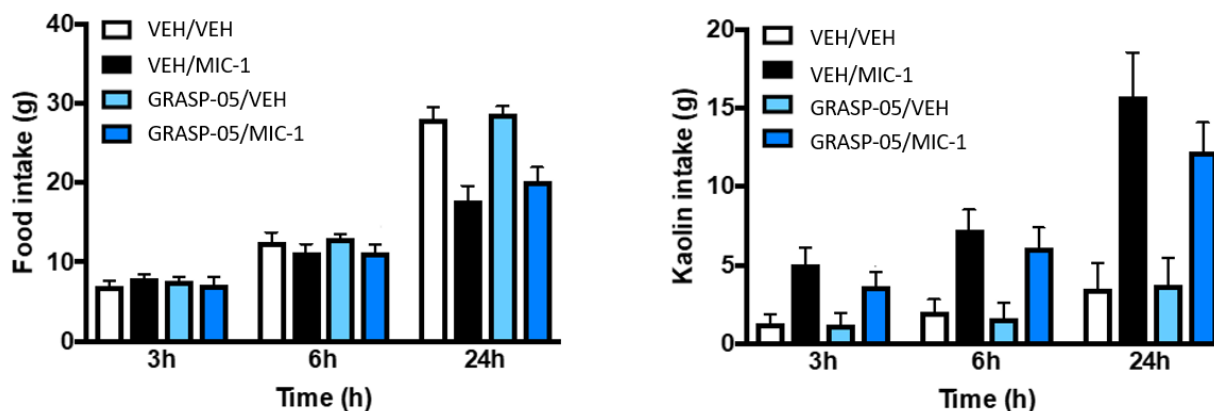


**Figure 2.** GRASP-05 reduces GDF15-induced kaolin intake. 4<sup>th</sup> ICV GRASP-05 (300 pmol) significantly reduces 4<sup>th</sup> ICV GDF15 (30 pmol)-induced kaolin intake in the rat (n=9/group, within-subject design) Data expressed as mean  $\pm$  SEM. Means with different letters are significantly different (P < 0.05).

To further investigate the ability of these peptides to work as antagonists the concentration of peptides administered was increased while maintaining 30pM concentration of MIC-1/GDF15. Injections up to 3 nM of GRASP-01 – GRASP-04 produced no antagonistic effects (data not shown).

#### 4.4 Fluorescent tagging of GRASP-05

To perform subsequent mechanistic studies a fluorescently tagged GRASP-05 construct was designed and synthesized (GRASP-555).

##### 4.4.1 Design and Synthesis of GRASP-555

Utilizing strained promoted alkyne-azide cycloaddition (SPAAC), a fluorescently labelled GRASP-05 was successfully synthesized. In short, a DBCO modified AlexaFluor®564 (DBCO-AF546) was conjugated to GRASP-05 by dissolving in 4:1 DMF: H<sub>2</sub>O and allowed to stir overnight at room temperature to produce GRASP-555 (Figure 3). GRASP-555 was purified using RP-HPLC (H<sub>2</sub>O + 0.1% TFA and MeOH from 1% CH<sub>3</sub>OH/H<sub>2</sub>O + 0.1% TFA to 90% CH<sub>3</sub>OH/H<sub>2</sub>O + 0.1% TFA in 25 min) to produce GRASP-555 in 99% purity in stoichiometric yields (Figure 4). ESI-MS expected  $m/z$  = 4386, observed  $m/z$  =  $[M+2H^++Na^+]^{+3}$ : 1487,  $[M+3H]^{+3}$ : 1463,  $[M+4H^++H_2O]^{+4}$ : 1116,  $[M+4H]^{+4}$ : 1097,  $[M+5H]^{+5}$ : 878 (Figure 5). Successfully linkage of GRASP-05 to DBCO-AF546 resulted in an excitation-maxima shift from 554 nm to 560 nm and emission maxima shift from 570 nm to 571 nm (Figure 6).

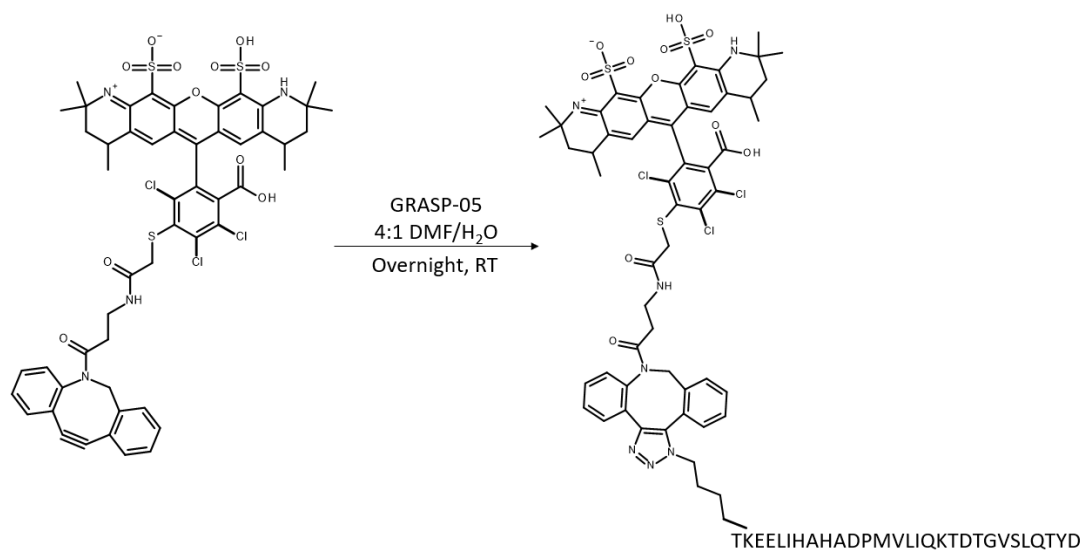


**Figure 3.** Synthetic scheme for GRASP-555. DBCO AF-546 was successfully “clicked” to GRASP-05 utilizing SPAAC.

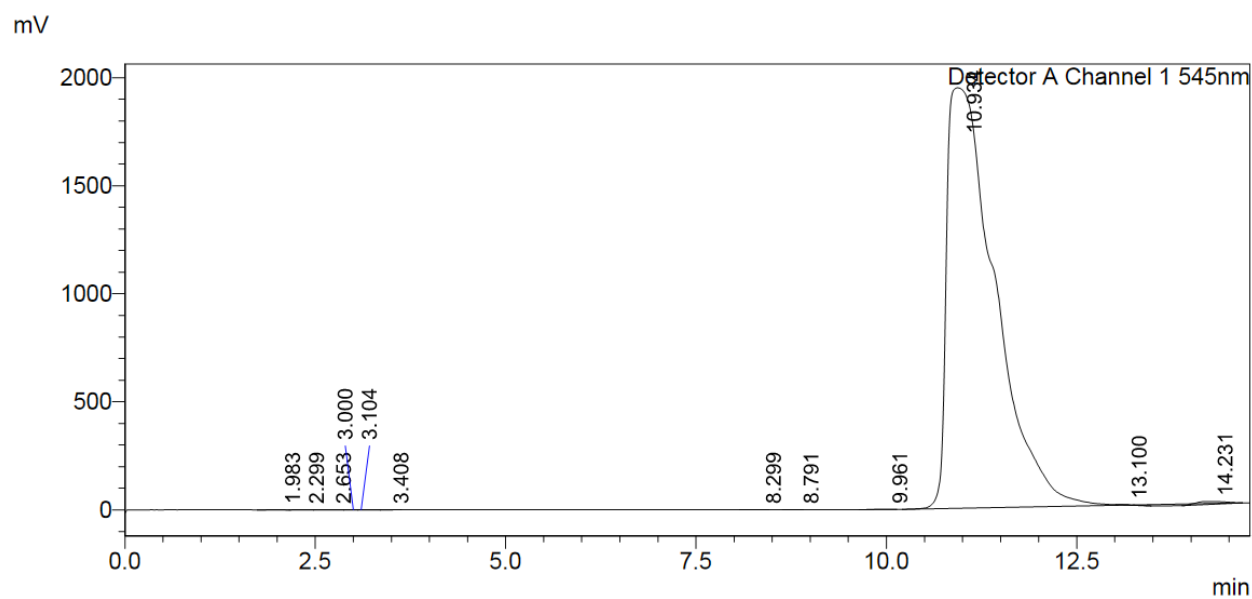


**Figure 4.** RP-HPLC Trace (Shimadzu Prominence HPLC using a C18 column (Eclipse XDB-C18 5 $\mu$ m, 4.6 x 150 mm) (RP-HPLC, from 1% CH<sub>3</sub>OH/H<sub>2</sub>O + 0.1% TFA to 90% CH<sub>3</sub>OH/H<sub>2</sub>O + 0.1% TFA in 25 min)) showing GRASP-555 product at 10.9 min. Purity 99%.

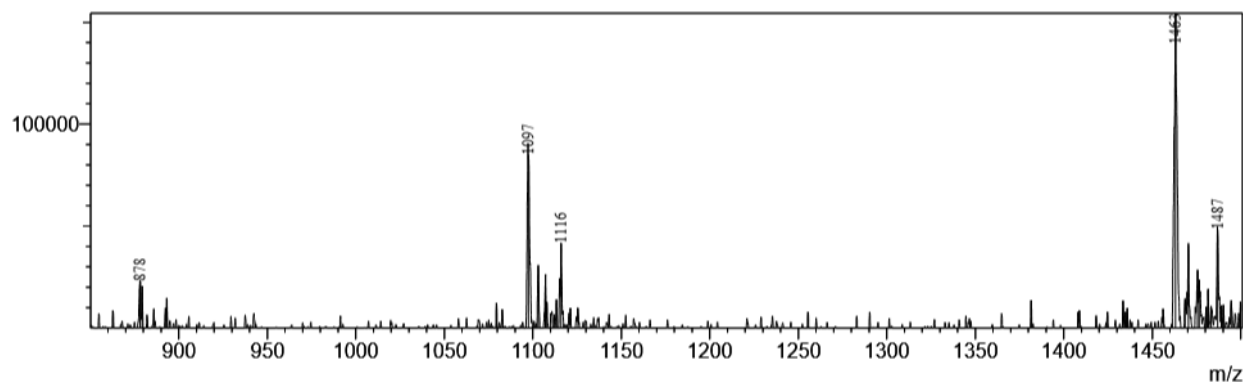


**Figure 5.** ESI-MS (Shimadzu LCMS-8040) of GRASP-555, expected  $m/z = 4386$ , observed  $m/z = [M+2H^++Na^+]^{+3}: 1487$ ,  $[M+3H]^{+3}: 1463$ ,  $[M+4H^++H_2O]^{+4}: 1116$ ,  $[M+4H]^{+4}: 1097$ ,  $[M+5H]^{+5}: 878$ .

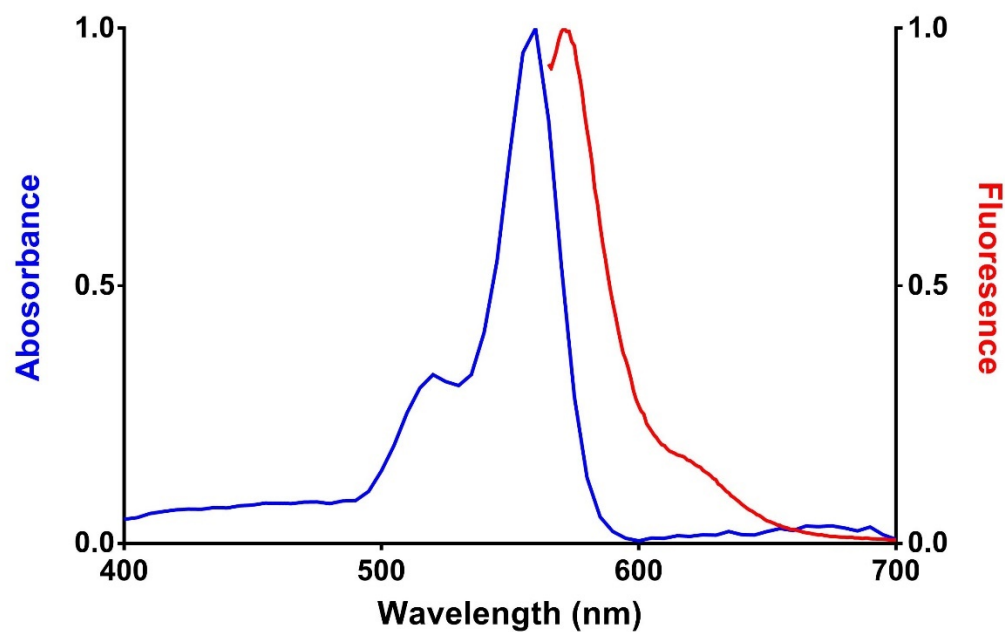


**Figure 6.** GRASP-555 electronic absorption spectra were obtained on a Varian Cary 50 Bio spectrophotometer in a 2mL quartz cuvette between 400 nm – 700 nm in aqueous acetonitrile.

#### 4.4.2 *In vivo* Injection of GRASP-555 in Rats

Successful synthesis of GRASP-555 allowed for *in vivo* mechanistic studies in rats. Following systemic administration, it was found that GRASP-555 successfully penetrated into the hindbrain (AP/NTS) and colocalized with GFRAL receptors (Figure 7).

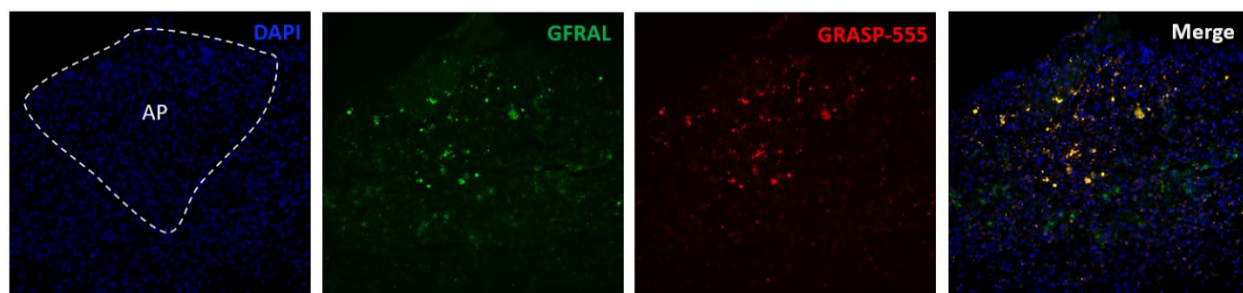


**Figure 7.** GRASP-555 10 mg/kg; IP shows co-localization with GFRAL-expressing neurons in the AP and NTS of rats.

#### 4.5 In-solution Structure of GRASP-05 Utilizing Nuclear Magnetic Resonance (NMR)

In addition to data supporting *in vivo* antagonism/ binding of GFRAL using fluorescent analog GRASP-555, the in-solution structure of GRASP was solved in collaboration with Dr. Deborah Kerwood (Syracuse University), utilizing NMR and revealed a significant secondary structure including a clear 'loop' region producing a 'hairpin-like' fold (Figure 8).





**Figure 8.** Solution state structure of GRASP solved by NMR revealing secondary ‘Hairpin-like’ structure with GDF15 like ‘loop’. Structure solved by Dr. Deborah Kerwood, Syracuse University.

The structure was the result of a 15 ns implicit solvent AMBER18 run,<sup>20,21</sup> where NMR (NOE) based distance restraints and TALOS+ based PHI and PSI angle ranges were incorporated.<sup>22</sup> Utilizing a high-ambiguity driven protein-protein docking (HADDOCK) modeling approach,<sup>23</sup> we docked GRASP into the extra-cellular binding domain of GFRAL, with and without GDF15 already bound (PDB 5VZ4).<sup>6</sup> We noted that GRASP docked proximal to GDF15 and indeed appears to block access to the W32 residue containing RET binding region of GDF15, suggesting that GRASP is a non-competitive antagonist that functions via inhibition of RET recruitment (Figure 9).

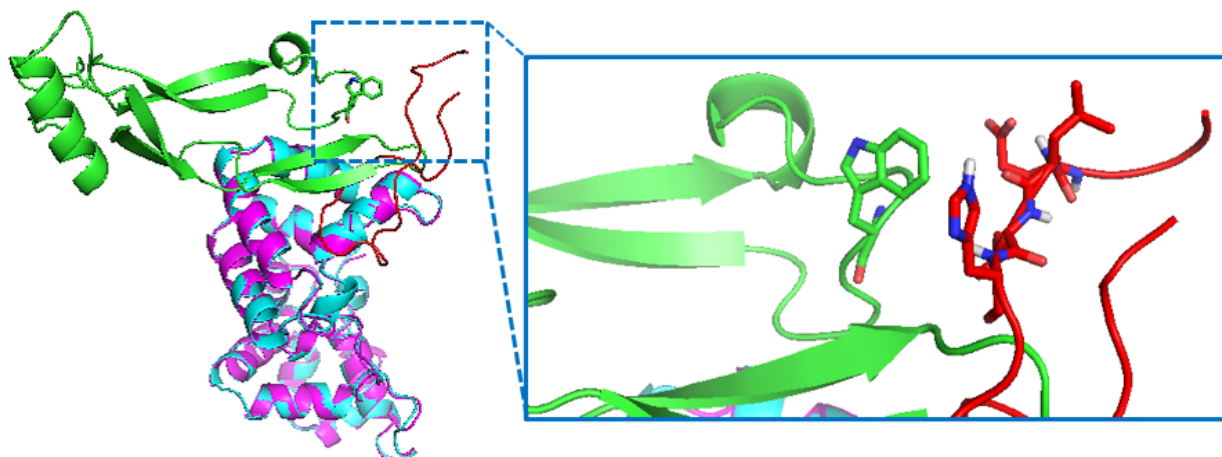


**Figure 9.** GDF15 (green) binding to GFRAL (blue/purple) (PDB 5VZ4) with bound GRASP (Red) simulated using HADDOCK 2.2. A close-up rendering shows GRASP 'blocking' the region of GDF15 (W32) known to be vital for RET recruitment.

#### 4.6 Microsomal Stability Assays of GRASP-05

An *in vitro* rat microsome (0.45 mg/mL) PK stability assay was also performed to test the pharmacokinetic (PK) properties of GRASP-05 (Figure 10).<sup>24</sup> Results of the PK stability assay on GRASP-05 determined half-life (104.4 min) and intrinsic-clearance ( $CL_{int}$ ) (3.39  $\mu\text{L}/\text{min}/\text{mg}$  protein), both suggesting an excellent PK lead peptide.

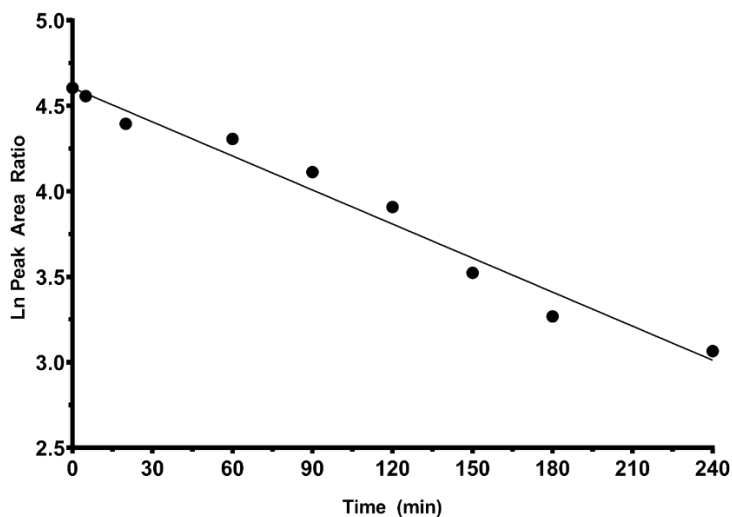


**Figure 10.** Microsomal stability assay in rats. The half-life was calculated to be: 104.43 min. Reaction velocity ( $V$ ) was calculated to be 511  $\mu\text{L}/\text{mg}$ . Intrinsic clearance ( $Cl_{\text{int}}$ ) was determined to be 339  $\mu\text{L}/\text{min}/\text{mg}$  protein.

#### 4.7 Lipidation of GRASP-05

Given the successful design approach leading to GRASP-05, validation of our computational modelling to date, solving of the solution structure of GRASP-05 via NMR, and facile reproduction of established *in vitro* assays (data not shown) we sought to further improve *in vivo* functionality. Initial *in vivo* function was monitored for 24 h, but we sought to develop a therapeutic with extended half life, beyond the already excellent PK parameters obtained, and thus designed and successfully synthesized a lipidated (dipalmitic acid) analog of GRASP (Lip-GRASP-05). Lip-GRASP-05 is predicted to have an extensively greater half-life, while not effecting

brain penetration as has been established for lipidated pharmaceutical peptides such as liraglutide.<sup>25</sup>

#### 4.7.1 Design and Synthesis of Lipidated GRASP-05 (Lip-GRASP-05)

Utilizing SPAAC, a Lip-GRASP-05 successfully synthesized. In short, a DBCO modified 16:0 dipalmitic acid (DBCO 16: PE) was conjugated to GRASP-05 by dissolving in 9:1 DMF: H<sub>2</sub>O and allowed to stir overnight at room temperature to produce Lip-GRASP-05 (Figure 11). ESI-MS expected  $m/z = 4258$ , observed  $m/z = [M+3H^+]^{+3}: 1420$ ,  $[M+4H^+]^{+4}: 1065$ ,  $[M+5H^+]^{+5}: 852$  (Figure 12).

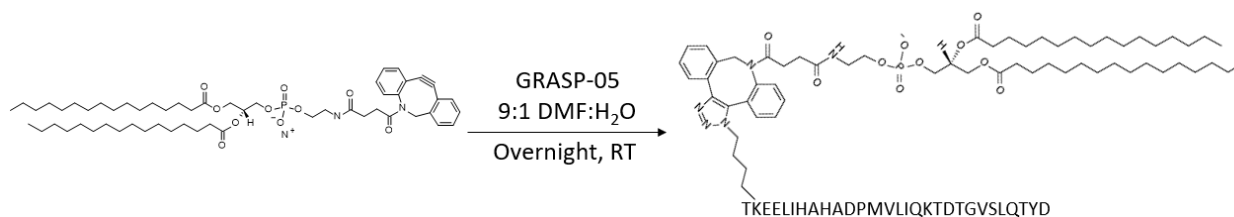


**Figure 11.** Synthetic scheme for Lip-GRASP-05. DBCO AF-546 was successfully “clicked” to GRASP-05 utilizing SPAAC.

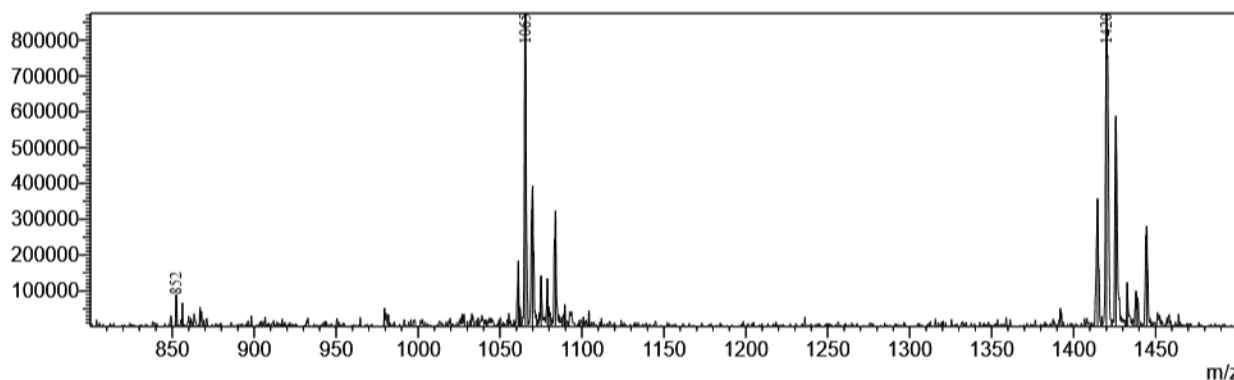


**Figure 12.** ESI-MS (Shimadzu LCMS-8040) of Lip-GRASP-05, expected  $m/z = 4258$ , observed  $m/z = [M+3H^+]^{+3}: 1420$ ,  $[M+4H^+]^{+4}: 1065$ ,  $[M+5H^+]^{+5}: 852$ .

#### 4.8 Developing an ELISA for monitoring GRASP

To successfully monitor the binding of GDF15 to the GFRAL receptor and subsequent antagonism by GRASP-05 as well as future GRASP iterations an “in house” enzyme-linked immunosorbent assay (ELISA) was developed. Specific details on the protocol can be found in the experimental chapter. Our “in-house” ELISA confirmed FDG15 binding at GFRAL with an  $ED_{50}$  of  $\approx 1$  ng/mL, consistent with previously reported values (Figure 13).<sup>5,7,11</sup>

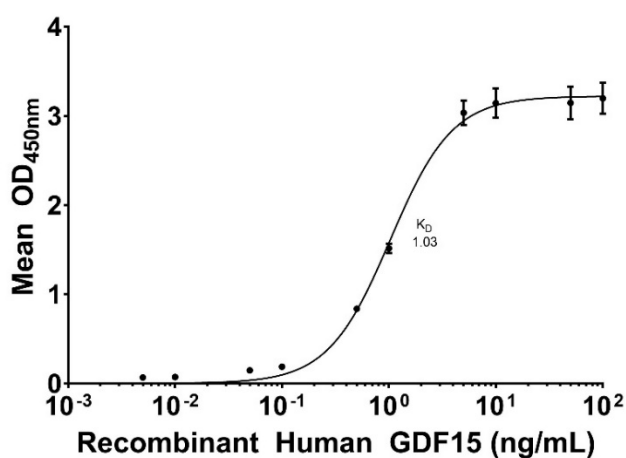


**Figure 13.** ELISA assay of GDF15 binding to human recombinant GFRAL (0.1  $\mu$ g/mL).

To directly monitor GRASP-05’s ability to bind and antagonize the GFRAL receptor a new primary antibody was developed by GenScript USA (Figure 14).



**Figure 14.** GenScript Generated Primary Antibody.

#### 4.9 Outcomes and Conclusions

The designing of an antagonist of the GFRAL receptor is a unique approach in the important and rapidly growing research area of GDF15/GFRAL signaling. GRASP-05 is currently the only peptide antagonist of its kind known to date and is promising approach to address the questions centered on blocking the GFRAL-RET complex as a means to treat nausea/emesis and sickness behaviors.

The initial work performed thus far continues to probe the fundamental understanding of how GDF15 reduces food intake. I was successfully able to design an antagonist of the GFRAL receptor what suppressed kaolin intake in an *in vivo* investigation in rats. Following fluorescent tagging of GRASP-05 it was shown that following systemic administration GRASP-05 is able to readily penetrate the blood brain barrier, a limitation by current antibody approaches. In order to improve on the pharmacokinetic profile of GRASP-05 a lipidated variant, Lip-GRASP-05, was designed and current *in vivo* analysis is ongoing. The ability to antagonize the GFRAL receptor can now be readily monitored utilizing a newly developed ELISA.

Both GRASP-05 and its future derivatives have the potential to mitigate several undesirable sickness behaviors induced by GDF15, including CNS-derived GDF15. While GRASP-05 shows potential as a standalone therapeutic it also shows promise as a pairing compound to mitigate side effects of currently approved therapeutics. Addressing this clinically unmet need will go hand-in-hand with significant advancement for the fields of ingestive behavior, obesity research, and potential tolerability of metabolic disease treatment as it pertains to the GFRAL-RET complex.

#### 4.10 References

- (1) Staff, A. C.; Bock, A. J.; Becker, C.; Kempf, T.; Wollert, K. C.; Davidson, B. Growth Differentiation Factor-15 as a Prognostic Biomarker in Ovarian Cancer. *Gynecol. Oncol.* **2010**, *118* (3), 237–243.
- (2) Bauskin, A. R.; Brown, D. A.; Kuffner, T.; Johnen, H.; Lou, X. W.; Hunter, M.; Breit, S. N. Role of Macrophage Inhibitory Cytokine-1 in Tumorigenesis and Diagnosis of Cancer. *Cancer Res.* **2006**, *66* (10), 4983–4986.
- (3) Mullican, S. E.; Rangwala, S. M. Uniting GDF15 and GFRAL: Therapeutic Opportunities in Obesity and Beyond. *Trends Endocrinol. Metab.* **2018**, *29* (8), 560–570.
- (4) Tsai, V. W. W.; Husaini, Y.; Sainsbury, A.; Brown, D. A.; Breit, S. N. The MIC-1/GDF15-GFRAL Pathway in Energy Homeostasis: Implications for Obesity, Cachexia, and Other Associated Diseases. *Cell Metab.* **2018**, *28* (3), 353–368.
- (5) Emmerson, P. J.; Wang, F.; Du, Y.; Liu, Q.; Pickard, R. T.; Gonciarz, M. D.; Coskun, T.; Hamang, M. J.; Sindelar, D. K.; Ballman, K. K.; Foltz, L. A.; Muppidi, A.; Alsina-Fernandez, J.; Barnard, G. C.; Tang, J. X.; Liu, X.; Mao, X.; Siegel, R.; Sloan, J. H.; Mitchell, P. J.; Zhang, B. B.; Gimeno, R. E.; Shan, B.; Wu, X. The Metabolic Effects of GDF15 Are Mediated by the Orphan Receptor GFRAL. *Nat. Med.* **2017**, *23* (10), 1215–1219.
- (6) Hsu, J. Y.; Crawley, S.; Chen, M.; Ayupova, D. A.; Lindhout, D. A.; Higbee, J.; Kutach, A.; Joo, W.; Gao, Z.; Fu, D.; To, C.; Mondal, K.; Li, B.; Kekatpure, A.; Wang, M.; Laird, T.; Horner, G.; Chan, J.; Mcentee, M.; Lopez, M.; Lakshminarasimhan, D.; White, A.; Wang, S. P.; Yao, J.; Yie, J.; Matern, H.; Solloway, M.; Haldankar, R.; Parsons, T.; Tang, J.; Shen, W. D.; Chen, Y. A.; Tian, H.; Allan, B. B. Non-Homeostatic Body Weight Regulation through a Brainstem-

- Restricted Receptor for GDF15. *Nature* **2017**, *550* (7675), 255–259.
- (7) Mullican, S. E.; Lin-Schmidt, X.; Chin, C. N.; Chavez, J. A.; Furman, J. L.; Armstrong, A. A.; Beck, S. C.; South, V. J.; Dinh, T. Q.; Cash-Mason, T. D.; Cavanaugh, C. R.; Nelson, S.; Huang, C.; Hunter, M. J.; Rangwala, S. M. GFRAL Is the Receptor for GDF15 and the Ligand Promotes Weight Loss in Mice and Nonhuman Primates. *Nat. Med.* **2017**, *23* (10), 1150–1157.
- (8) Patel, S.; Alvarez-Guaita, A.; Melvin, A.; Rimmington, D.; Dattilo, A.; Miedzybrodzka, E. L.; Cimino, I.; Maurin, A. C.; Roberts, G. P.; Meek, C. L.; Virtue, S.; Sparks, L. M.; Parsons, S. A.; Redman, L. M.; Bray, G. A.; Liou, A. P.; Woods, R. M.; Parry, S. A.; Jeppesen, P. B.; Kolnes, A. J.; Harding, H. P.; Ron, D.; Vidal-Puig, A.; Reimann, F.; Gribble, F. M.; Hulston, C. J.; Farooqi, I. S.; Fafournoux, P.; Smith, S. R.; Jensen, J.; Breen, D.; Wu, Z.; Zhang, B. B.; Coll, A. P.; Savage, D. B.; O’Rahilly, S. GDF15 Provides an Endocrine Signal of Nutritional Stress in Mice and Humans. *Cell Metab.* **2019**, *29* (3), 707-718.e8.
- (9) Frikke-Schmidt, H.; Hultman, K.; Galaske, J. W.; Jørgensen, S. B.; Myers, M. G.; Seeley, R. J. GDF15 Acts Synergistically with Liraglutide but Is Not Necessary for the Weight Loss Induced by Bariatric Surgery in Mice. *Mol. Metab.* **2019**, *21* (January), 13–21.
- (10) Herrstedt, J. The Latest Consensus on Antiemetics. *Curr. Opin. Oncol.* **2018**, *30* (4), 233–239.
- (11) Yang, L.; Chang, C. C.; Sun, Z.; Madsen, D.; Zhu, H.; Padkjær, S. B.; Wu, X.; Huang, T.; Hultman, K.; Paulsen, S. J.; Wang, J.; Bugge, A.; Frantzen, J. B.; Nørgaard, P.; Jeppesen, J. F.; Yang, Z.; Secher, A.; Chen, H.; Li, X.; John, L. M.; Shan, B.; He, Z.; Gao, X.; Su, J.; Hansen, K. T.; Yang, W.; Jørgensen, S. B. GFRAL Is the Receptor for GDF15 and Is Required for the



- Anti-Obesity Effects of the Ligand. *Nat. Med.* **2017**, *23* (10), 1158–1166.
- (12) Borner, T.; Shaulson, E. D.; Ghidewon, M. Y.; Barnett, A. B.; Horn, C. C.; Doyle, R. P.; Grill, H. J.; Hayes, M. R.; De Jonghe, B. C. GDF15 Induces Anorexia through Nausea and Emesis. *Cell Metab.* **2020**, *31* (2), 351–362.
- (13) Van Laar, E. S.; Desai, J. M.; Jatoi, A. Professional Educational Needs for Chemotherapy-Induced Nausea and Vomiting (CINV): Multinational Survey Results from 2,388 Health Care Providers. *Support. Care Cancer* **2015**, *23* (1), 151–157.
- (14) Cohen, L.; De Moor, C. A.; Eisenberg, P.; Ming, E. E.; Hu, H. Chemotherapy-Induced Nausea and Vomiting - Incidence and Impact on Patient Quality of Life at Community Oncology Settings. *Support. Care Cancer* **2007**, *15* (5), 497–503.
- (15) Hesketh, P. J.; Kris, M. G.; Basch, E.; Bohlke, K.; Barbour, S. Y.; Clark-Snow, R. A.; Danso, M. A.; Dennis, K.; Dupuis, L. L.; Dusetzina, S. B.; Eng, C.; Feyer, P. C.; Jordan, K.; Noonan, K.; Sparacio, D.; Somerfield, M. R.; Lyman, G. H. Antiemetics: American Society of Clinical Oncology Clinical Practice Guideline Update. *J. Clin. Oncol.* **2017**, *35* (28), 3240–3261.
- (16) Xiong, Y.; Walker, K.; Min, X.; Hale, C.; Tran, T.; Komorowski, R.; Yang, J.; Davda, J.; Nuanmanee, N.; Kemp, D.; Wang, X.; Liu, H.; Miller, S.; Lee, K. J.; Wang, Z.; Véniant, M. M. Long-Acting MIC-1/GDF15 Molecules to Treat Obesity: Evidence from Mice to Monkeys. *Sci. Transl. Med.* **2017**, *9* (412), 1–12.
- (17) Borner, T.; Arnold, M.; Ruud, J.; Breit, S. N.; Langhans, W.; Lutz, T. A.; Blomqvist, A.; Riediger, T. Anorexia-Cachexia Syndrome in Hepatoma Tumour-Bearing Rats Requires the Area Postrema but Not Vagal Afferents and Is Paralleled by Increased MIC-1/GDF15. *J. Cachexia. Sarcopenia Muscle* **2017**, *8* (3), 417–427.

- (18) Tsai, V. W.; Manandhar, R.; Jørgensen, S. B.; Lee-ng, K. K. M.; Zhang, P.; Marquis, C. P.; Jiang, L.; Husaini, Y.; Lin, S.; Sainsbury, A.; Sawchenko, P. E.; Brown, D. A.; Breit, S. N. The Anorectic Actions of the TGF  $\beta$  Cytokine MIC-1 / GDF15 Require an Intact Brainstem Area Postrema and Nucleus of the Solitary Tract. *PLoS One* **2014**, *9* (6), e100370.
- (19) Ladner, R. C.; Sato, A. K.; Gorzelany, J.; De Souza, M. Phage Display-Derived Peptides as Therapeutic Alternatives to Antibodies. *Drug Discov. Today* **2004**, *9* (12), 525–529.
- (20) Rubenstein, A. B.; Blacklock, K.; Nguyen, H.; Case, D. A.; Khare, S. D. Systematic Comparison of Amber and Rosetta Energy Functions for Protein Structure Evaluation. *J. Chem. Theory Comput.* **2018**, *14* (11), 6015–6025.
- (21) Case, D. A.; Cheatham, T. E.; Darden, T.; Gohlke, H.; Luo, R.; Merz, K. M.; Onufriev, A.; Simmerling, C.; Wang, B.; Woods, R. J. The Amber Biomolecular Simulation Programs. *J. Comput. Chem.* **2005**, *26* (16), 1668–1688.
- (22) Shen, Y.; Delaglio, F.; Cornilescu, G.; Bax, A. TALOS+: A Hybrid Method for Predicting Protein Backbone Torsion Angles from NMR Chemical Shifts. *J. Biomol. NMR* **2009**, *44* (4), 213–223.
- (23) Van Zundert, G. C. P.; Rodrigues, J. P. G. L. M.; Trellet, M.; Schmitz, C.; Kastiris, P. L.; Karaca, E.; Melquiond, A. S. J.; Van Dijk, M.; De Vries, S. J.; Bonvin, A. M. J. J. The HADDOCK2.2 Web Server: User-Friendly Integrative Modeling of Biomolecular Complexes. *J. Mol. Biol.* **2016**, *428* (4), 720–725.
- (24) Riley, R. J.; McGinnity, D. F.; Autin, R. P. A Unified Model for Predicting Human Hepatic, Metabolic Clearance from in Vitro Intrinsic Clearance Data in Hepatocytes and Microsomes. *Drug Metab. Dispos.* **2005**, *33* (9), 1304–1311.

- (25) Fortin, S. M.; Lipsky, R. K.; Lhamo, R.; Chen, J.; Kim, E.; Borner, T.; Schmidt, H. D.; Hayes, M. R. GABA Neurons in the Nucleus Tractus Solitarius Express GLP-1 Receptors and Mediate Anorectic Effects of Liraglutide in Rats. *Sci. Transl. Med.* **2020**, *12* (533), 1–12.

## Chapter 5: Fluorescent Probes of Neuroendocrine Hormones for the Identification of Receptor Distribution and Function

The work reported in this chapter resulted in a peer-reviewed research paper: Stein, L. M.; Lhamo, R.; Cao, A.; Workinger, J.; **Tinsley, I.**; Doyle, R. P.; Grill, H. J.; Hermann, G. E.; Rogers, R. C.; Hayes, M. R. Dorsal Vagal Complex and Hypothalamic Glia Differentially Respond to Leptin and Energy Balance Dysregulation. *Transl. Psychiatry* **2020**, *10* (1), 90.

All synthetic work, including syntheses of all compounds and fluorescent analogs, their purification, chemical characterization, and preparation for *in vivo* testing was conducted by the author. All *in vivo* data collection was conducted at the University of Pennsylvania (USA) or the University of Gothenburg (Sweden).



The author at the University of Pennsylvania center for neurobiology and behavior where *in vivo* experiments utilizing probes described in this chapter was, in-part, performed.

## 5.1 Introduction

Identification of target receptors, their cell populations, and cognate ligands often benefits from the use of fluorescent probes.<sup>1</sup> Key questions that can be answered include: Is the leptin receptor present on astrocytes in the brain?; Where are oxytocin receptors located in the brain?; Does ligand oligomerization occur for particular neuropeptides and if so, does this effect receptor activation? The development of specific probes to address the above questions was the aim of the work described herein. In all cases, the goal was to produce a fluorescent, functional receptor or ligand that would allow for *ex vivo* analysis of targeted brain cells in the hind-brain and brain stem. All three peptides investigated, leptin, oxytocin and exendin-4, are neuropeptides that play a role in energy metabolism via neuronal circuitry that remains opaque or not fully understood. The outcomes of this work as described in Chapter 5 identified a new population of astrocytes within the dorsal vagal complex (DVC) expressing the leptin receptor (LepR) utilizing fluorescently tagged (Cy5) leptin.<sup>2</sup> Also discussed are the design and synthesis of fluorescently tagged (AF546) oxytocin and Exendin-4 (Ex4) used in collaboration with Prof. Karolina Skibicka of the University of Gothenburg and Prof. Matthew Hayes and Dr. Lauren Stein of the University of Pennsylvania, respectively.

## 5.2 Leptin

Leptin is a neuroendocrine hormone used in energy homeostasis by inhibiting hunger and the regulation of fat stores (Figure 1).<sup>3,4</sup> Research focused on the regulation of food intake and body weight has been confined to the hypothalamus. The role of leptin signaling and agonism of the LepR within the hypothalamus has been investigated and defined, but its role within the DVC,

specifically the area postrema (AP) and nucleus tractus solitarius (NTS), regions associated with energy homeostasis, is less explored.<sup>2</sup> The DVC has been shown to suppress food intake and potentiate the intake suppressive effects of within-meal satiation signals.<sup>5-8</sup> Despite the DVCs role in energy homeostasis, the distribution and identification of the LepR within cell populations has yet to be identified. In collaboration with the group of Prof. Matthew Hayes and postdoctoral researcher Dr. Lauren Stein of the University of Pennsylvania, the expression of LepR on astrocytes in the DVC was assessed along with the role of DVC astrocytes in mediating the anorectic effects of leptin using a fluorescent leptin probe, deemed Cy5-Leptin.<sup>2</sup>

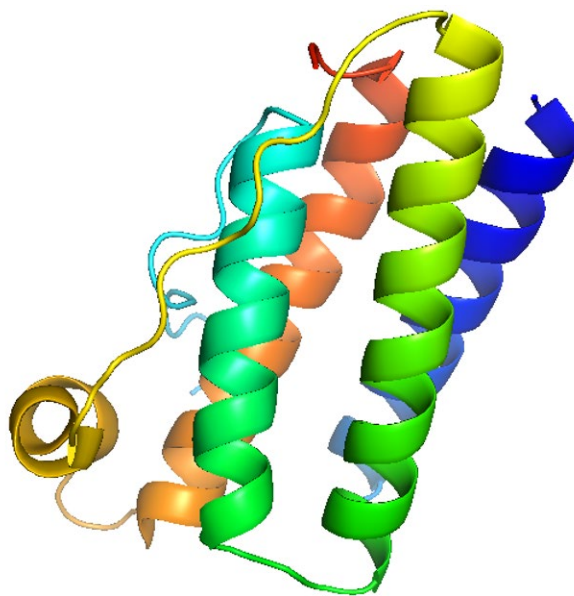


**Figure 1.** Structure of leptin. PDB code 1AX8.<sup>4</sup> Image generated by the author using PyMol.

### 5.2.1 Design, Synthesis, and Characterization of a Fluorescent Leptin (Cy5-Leptin)

Cy5-leptin was synthesized utilizing mouse recombinant leptin dissolved in pH 7.8 phosphate buffer and allowed to rock at room temperature. Cy5 labeling of the protein occurred

via NHS-Ester-Sulfo-Cy5 dissolved in 50  $\mu$ L of DMSO and added to the rocking solution in 10  $\mu$ L aliquots over one hour. Following the final addition of Cy5 the reaction rocked for an additional 2 hours to produce the final product, Cy5-Leptin. The reaction was always protected from light. Cy5-Leptin was purified using RP-HPLC (H<sub>2</sub>O + 0.1% TFA and MeOH from 1% CH<sub>3</sub>OH/H<sub>2</sub>O + 0.1% TFA to 90% CH<sub>3</sub>OH/H<sub>2</sub>O + 0.1% TFA in 20 min) (Figure 2). The mass of the Cy5-Leptin was confirmed via SDS-PAGE analysis (Figure 3). The mass observed ranged between 15-20 kDa, consistent with the addition of Cy5 to several lysine residues available for modification in the structure. Successfully linkage of Cy5 to Leptin resulted in an excitation-maxima shift from 646 nm to 650 nm and emission maxima shift from 662 nm to 669 nm (Figure 4).

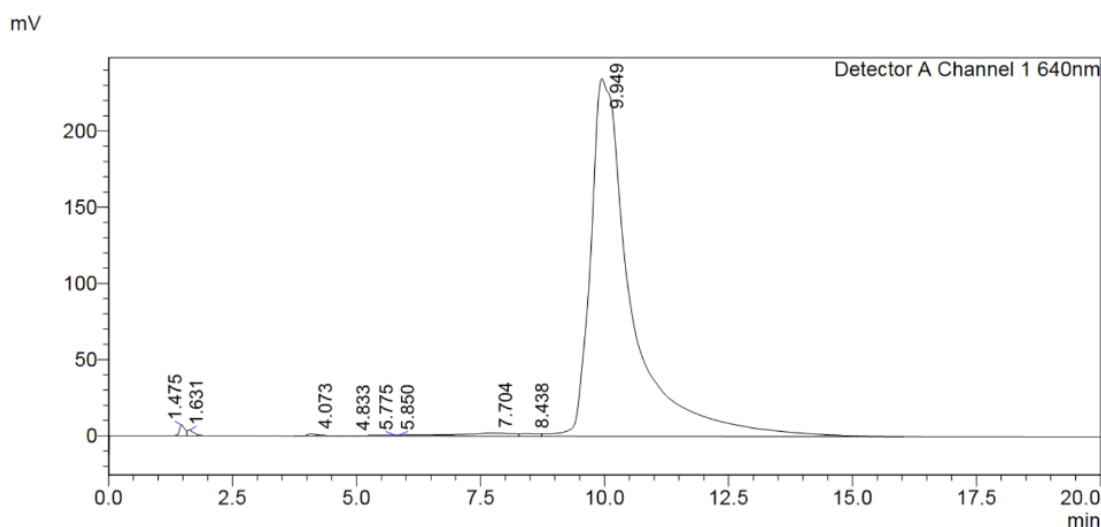


**Figure 2.** RP-HPLC Trace (Shimadzu Prominence HPLC using a C18 column (Eclipse XDB-C18 5 $\mu$ m, 4.6 x 150 mm) (RP-HPLC, from 1% CH<sub>3</sub>OH/H<sub>2</sub>O + 0.1% TFA to 90% CH<sub>3</sub>OH/H<sub>2</sub>O + 0.1% TFA in 25 min)) showing Cy5-Leptin product at 9.9 min. Purity 98%.

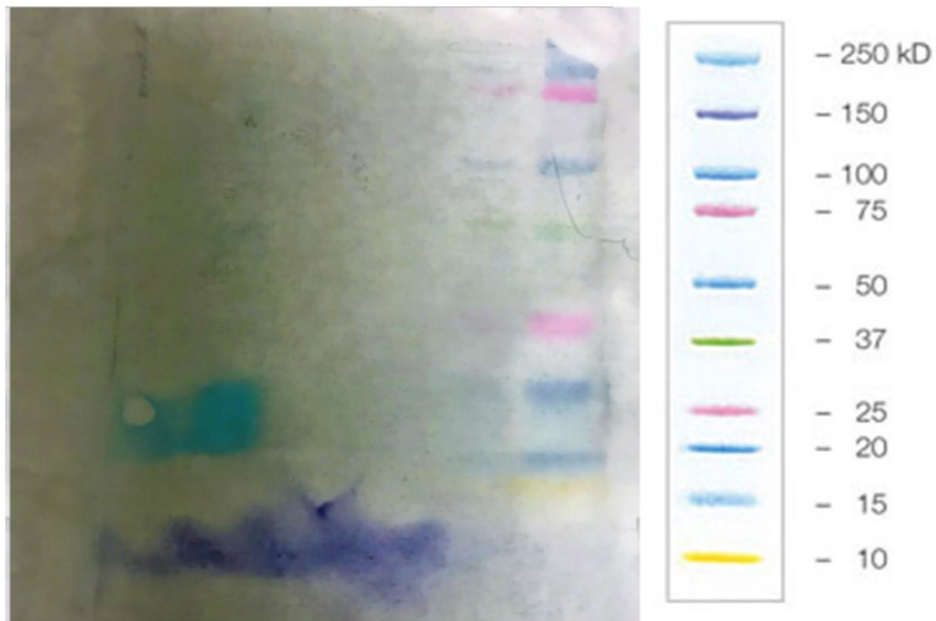


**Figure 3.** Cy5-Leptin mass was found to be between 15-20 kDa and confirmed utilizing 12.5% SDS-PAGE.



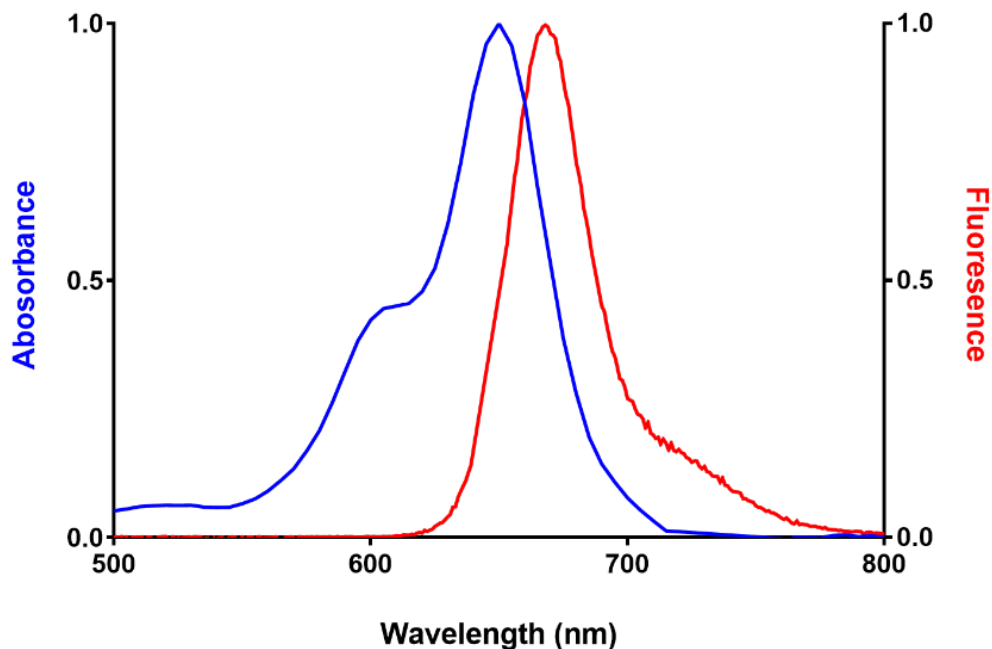


**Figure 4.** Cy5-Leptin electronic absorption spectra were obtained on a Varian Cary 50 Bio spectrophotometer in a 2mL quartz cuvette between 500 nm – 800 nm in aqueous acetonitrile.

The synthesized and characterized Cy5-leptin was successfully utilized *in vivo* and published 'Dorsal Vagal Complex and Hypothalamic Glia Differentially Respond to Leptin and Energy Balance Dysregulation' *Transl. Psychiatry* **2020**, *10* (1), 90. The use of this fluorescent probe helped to identify the expression of LepR within the DVC (Figure 5) and how its role differs from the receptor population observed within the hypothalamus.

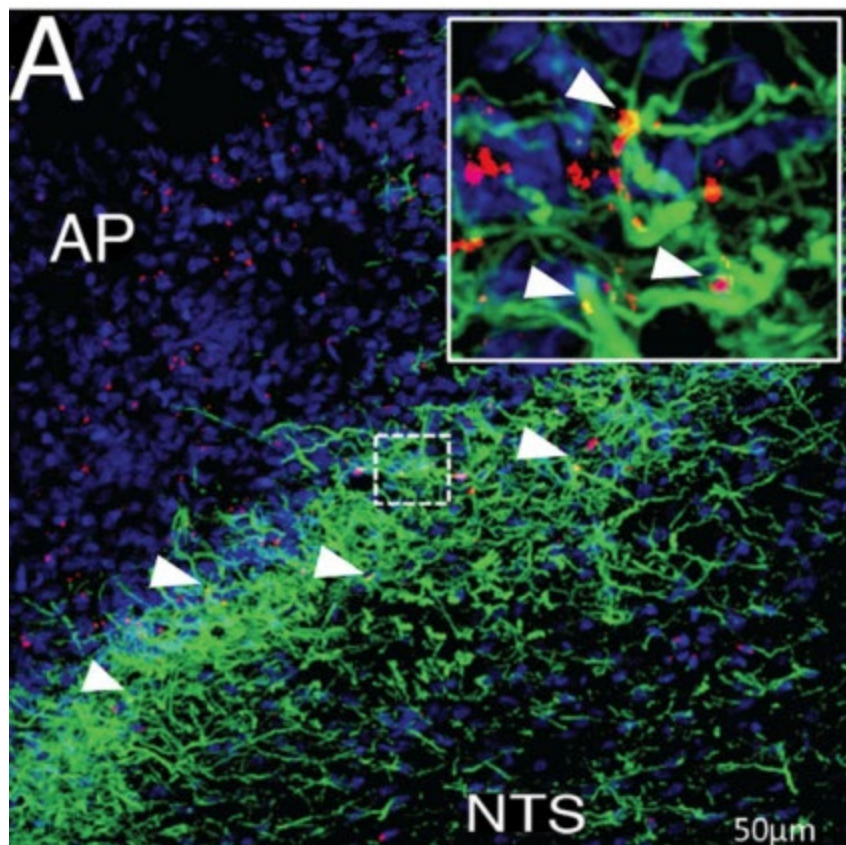


**Figure 5.** Immunohistochemical visualization of Cy5-Lep colocalized to DVC astrocytes. Used with permission of publisher under the Creative Commons license.<sup>2</sup>

### 5.3 Function of Exendin-4 (Ex4) at the Glucagon-like Peptide-1 (GLP-1) Receptor (GLP-1R)

Ex4 simulates insulin secretion through the agonism of the GLP-1R in a glucose-dependent manner.<sup>9</sup> The signaling of the GLP-1R is highly dependent on receptor dimerization.<sup>10</sup> The residence time, or length of time an agonist is bound to its receptor, influences period of action and is suggested to contribute to prolonged signaling following internalization.<sup>11</sup> Like many other G-protein coupled receptors (GPCR), the GLP-1R undergoes agonist mediated endocytosis.<sup>11</sup> Following internalization, the GLP-1R has been shown to maintain signaling with no effect on insulin secretion.<sup>12</sup> Upon endocytosis, portions of the GLP-1R are degraded in the lysosome<sup>12</sup>

while remaining portions are recycled back to the plasma membrane.<sup>13</sup> Distribution of the GLP-1R in a monomeric or dimeric state has yet to be elucidate. Of note, this property has yet to be identified in any class B GPCR.<sup>10</sup> Current work suggests that these GPCRs exist in an equilibrium of monomer and dimeric state.<sup>14-17</sup> To further investigate the residency time of Ex4 at the GLP-1R and the internalization of the receptor, a fluorescent Ex4, designated here as REX, was developed to be used in collaboration with Dr. George Holz of SUNY Upstate Medical University. Parallel investigations are occurring in collaboration with Dr. Lauren Stein of the University of Pennsylvania to monitor the distribution of the GLP-1R in both the monomeric and dimeric state.

### **5.3.1 Design, Synthesis, and Characterization of AF546-Ex4 (REX)**

Utilizing strained promoted alkyne-azide cycloaddition (SPAAC) a DBCO modified AlexaFluor®564 (DBCO-AF546) was “clicked” Ex4 where the twelfth residue, lysine, was substituted by an azido modified lysine by dissolving in 4:1 DMF: H<sub>2</sub>O (1200μL) and allowed to stir overnight at room temperature to produce AF546-Ex4 (REX) (Figure 6). REX was purified using RP-HPLC (H<sub>2</sub>O + 0.1% TFA and MeOH from 1% CH<sub>3</sub>OH/H<sub>2</sub>O + 0.1% TFA to 90% CH<sub>3</sub>OH/H<sub>2</sub>O + 0.1% TFA in 25 min) to produce REX in 97% purity in stoichiometric yields (Figure 7). ESI-MS expected  $m/z = 5319$ , observed  $m/z = [M+3H]^{+3}: 1773$ ,  $[M+4H]^{+4}: 1331$  (Figure 8). Successfully linkage of Ex4 to DBCO-AF546 resulted in an excitation-maxima shift from 554 nm to 560 nm and emission maxima shift from 570 nm to 575 nm (Figure 9).

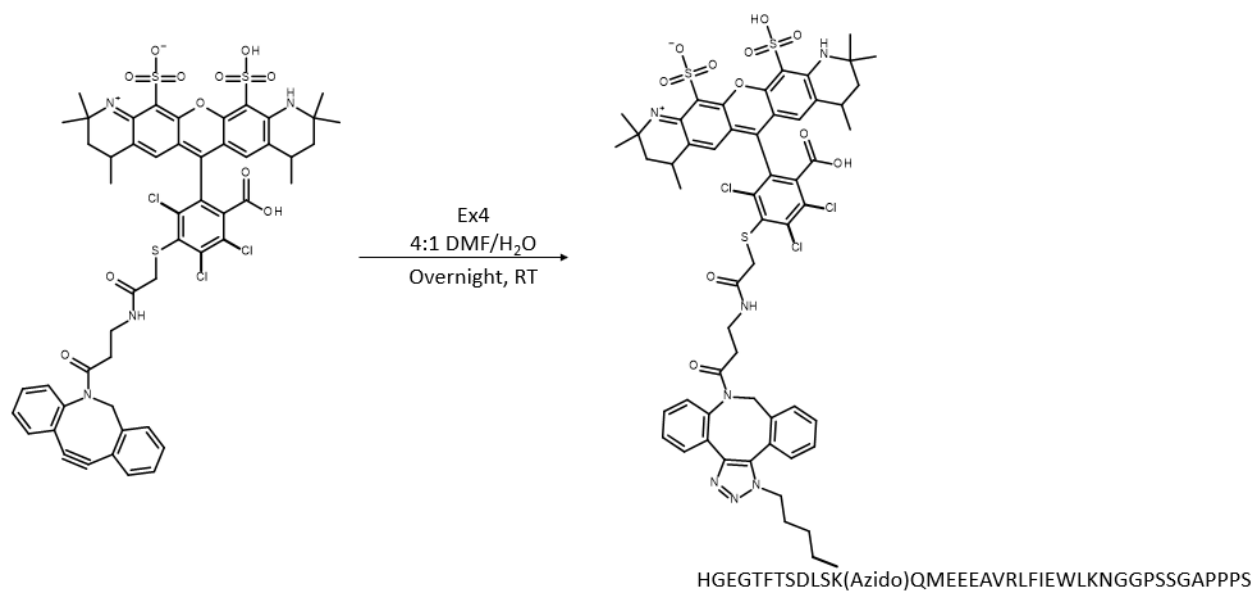


**Figure 6.** Synthetic scheme for REX.

mV

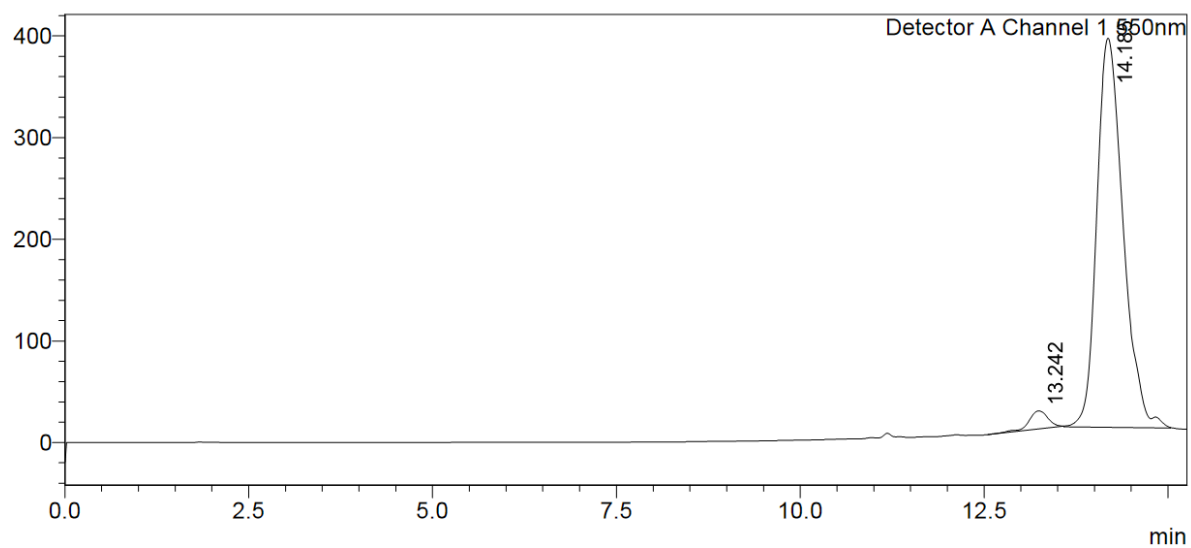


**Figure 7.** RP-HPLC Trace (Shimadzu Prominence HPLC using a C18 column (Eclipse XDB-C18 5 $\mu$ m, 4.6 x 150 mm) (RP-HPLC, from 1% CH<sub>3</sub>OH/H<sub>2</sub>O + 0.1% TFA to 90% CH<sub>3</sub>OH/H<sub>2</sub>O + 0.1% TFA in 25 min)) showing REX product at 14.1 min. Purity 97%.

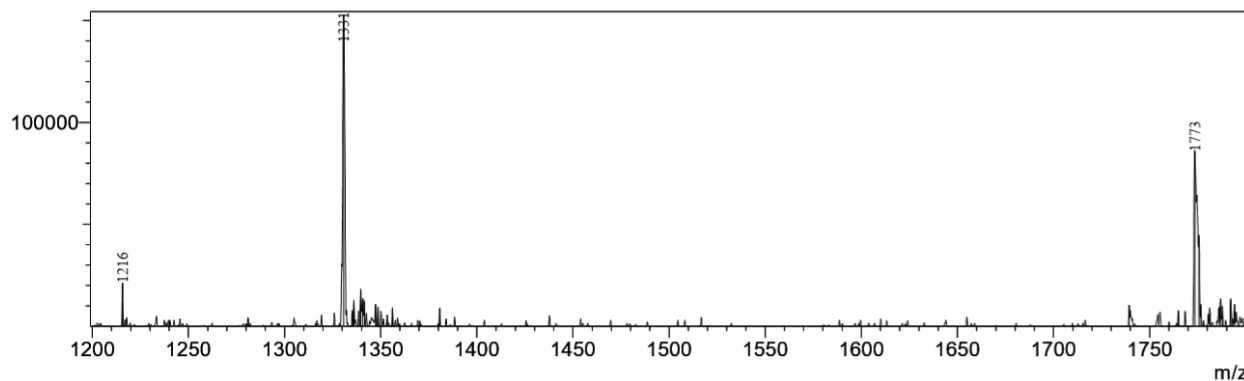


**Figure 8.** ESI-MS (Shimadzu LCMS-8040) of REX, expected  $m/z = 5319$ , observed  $m/z = [M+3H^+]^{+3}$ : 1773,  $[M+4H^+]^{+4}$ : 1331.

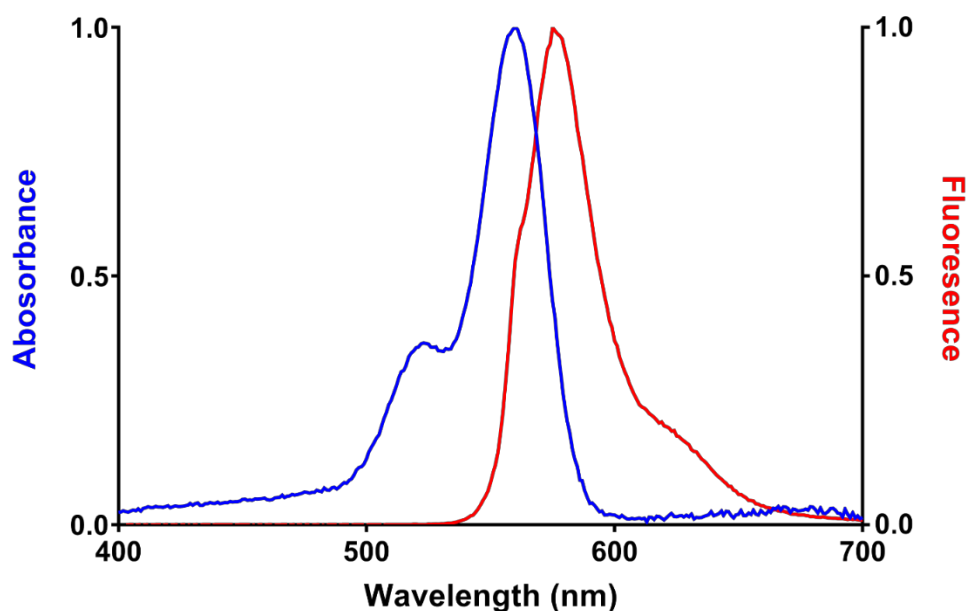


**Figure 9.** REX electronic absorption spectra were obtained on a Varian Cary 50 Bio spectrophotometer in a 2mL quartz cuvette between 400 nm – 700 nm in aqueous acetonitrile.

Upon completion and characterization of REX its ability to maintain function was tested in GLP-1R stably transfected HEK-293-H188 c20 cells. REX was shown to maintain function at the GLP-1R as shown by tracking cAMP elevation utilizing a viral H188 reporter (Figure 10).

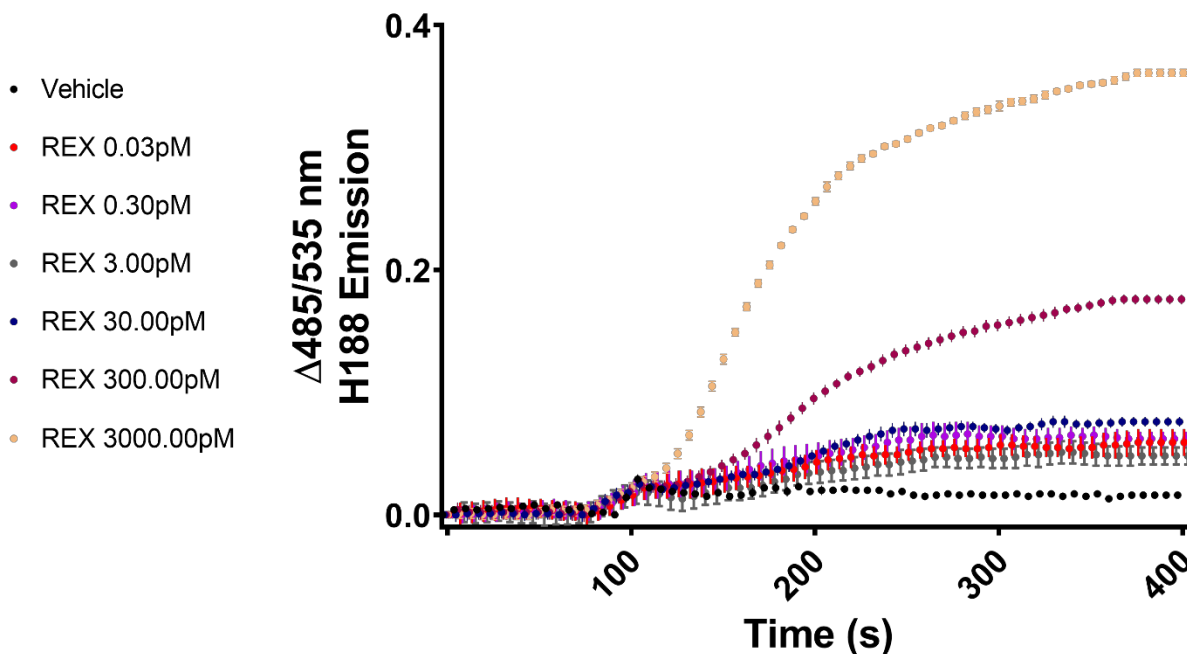


**Figure 10.** *In vitro* dose escalation study of REX showing increase in cAMP levels in GLP-1R stably transfected HEK-293-H188 c20 cells.

#### 5.4 Signaling of Oxytocin at the Oxytocin Receptor

Oxytocin (Oxy) is cyclic nine amino acid neuropeptide known for its role in reproductive and maternal behaviors.<sup>18</sup> Recently oxy has emerged as an important regulator of energy homeostasis.<sup>19</sup> The majority of studies evaluating the role of Oxy in metabolism have focused on the hypothalamus as the primary source of the peptides actions throughout the central nervous system (CNS).<sup>20</sup> However, both Oxy and its receptor (OxyR) have been found in the human gastrointestinal tract (GIT) and expressed along the vagal afferents, respectively.<sup>20,21</sup> While identified, the function of the OxyR expressed along the vagal afferents have yet to be elucidated.<sup>21</sup> Initial investigations in collaboration with Dr. Karolina Skibicka of the University of

Gothenburg have led to the hypothesis that vagal OxyR are a key relay of gut to brain satiation signaling. To investigate this hypothesis, a fluorescent oxytocin, termed ROxy, was designed and synthesized to investigate the function of this receptor sub-population. In addition, ROxy will also be utilized to identify the role of enteric Oxy. To fully elucidate the role of Oxy in the peripheral nervous system, a CNS impermeant Oxy will be developed and administered (for further discussion-see chapter 7).

#### **5.4.1 Design, Synthesis, and Characterization of AF546-Oxytocin (ROxy)**

Utilizing SPAAC, a fluorescently labelled oxytocin was successfully synthesized. In short, a DBCO modified AlexaFluor®564 (DBCO-AF546) was conjugated to an azido modified lysine in position eight of oxytocin by dissolving in 4:1 DMF: H<sub>2</sub>O and allowed to stir overnight at room temperature to produce AF546-Oxy (ROxy) (Figure 11). Roxy was purified using RP-HPLC (H<sub>2</sub>O + 0.1% TFA and MeOH from 1% CH<sub>3</sub>OH/H<sub>2</sub>O + 0.1% TFA to 90% CH<sub>3</sub>OH/H<sub>2</sub>O + 0.1% TFA in 25 min) to produce Roxy in 99% purity in stoichiometric yields (Figure 12). ESI-MS expected  $m/z = 2154$ , observed  $m/z = [M+H_2O+2H]^+2: 1097$ ,  $[M+2H]^+2: 1078$  (Figure 13). Successfully linkage of OTaz to DBCO-AF546 resulted in an excitation-maxima shift from 554 nm to 558 nm and emission maxima shift from 570 nm to 572 nm (Figure 14).

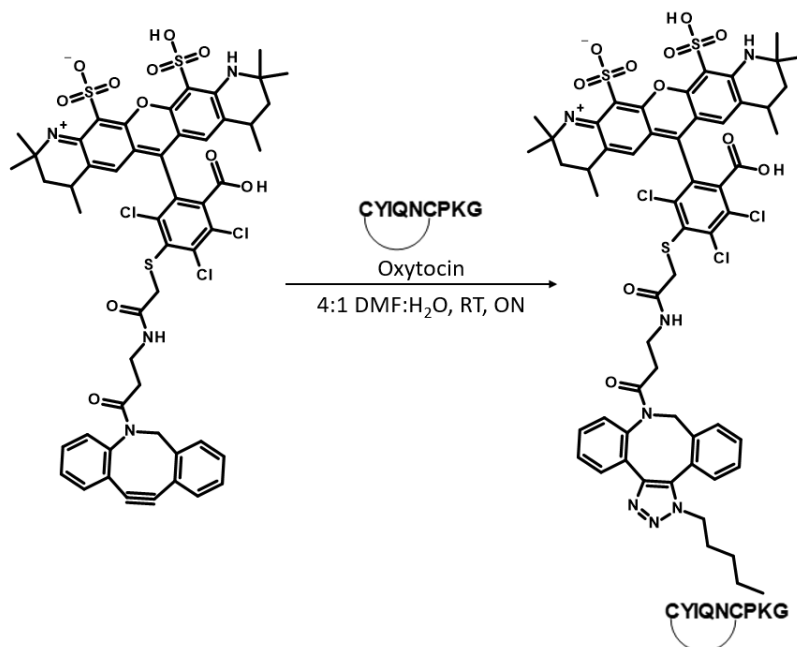


**Figure 11.** Synthetic scheme for ROxy. B12-DBCO was successfully “clicked” to OTaz utilizing SPAAC.

mV

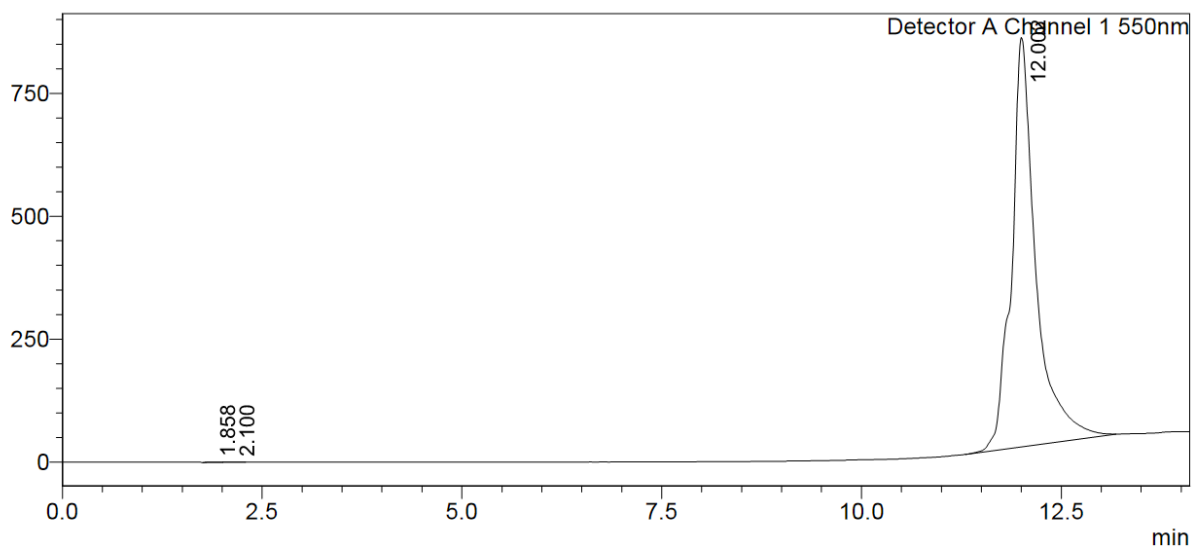


**Figure 12.** RP-HPLC Trace (Shimadzu Prominence HPLC using a C18 column (Eclipse XDB-C18 5 $\mu$ m, 4.6 x 150 mm) (RP-HPLC, from 1% CH<sub>3</sub>OH/H<sub>2</sub>O + 0.1% TFA to 90% CH<sub>3</sub>OH/H<sub>2</sub>O + 0.1% TFA in 25 min) showing ROxy product at 12.0 min. Purity 99%.



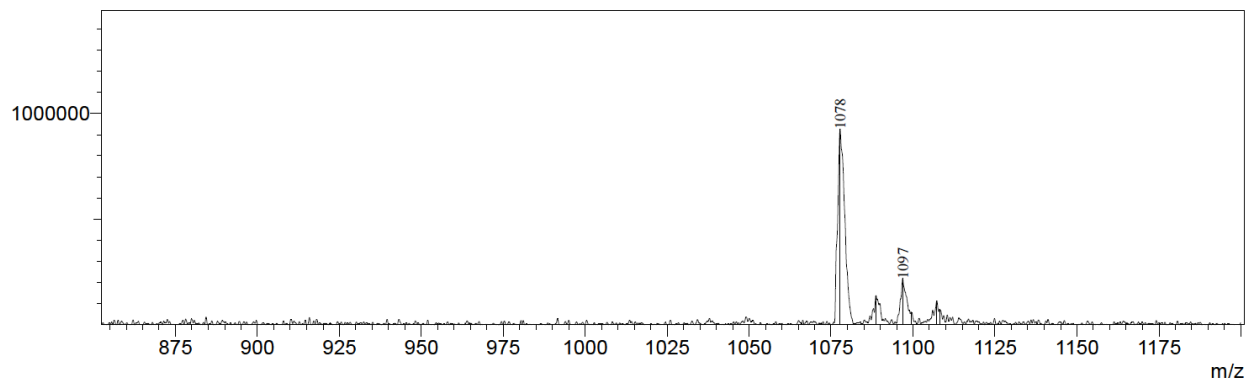


**Figure 13.** ESI-MS (Shimadzu LCMS-8040) of B12-Oxy, expected  $m/z = 2154$ , observed  $m/z = [M+H_2O+2H^+]^{+2}: 1097$ ,  $[M+2H^+]^{+2}: 1078$ .

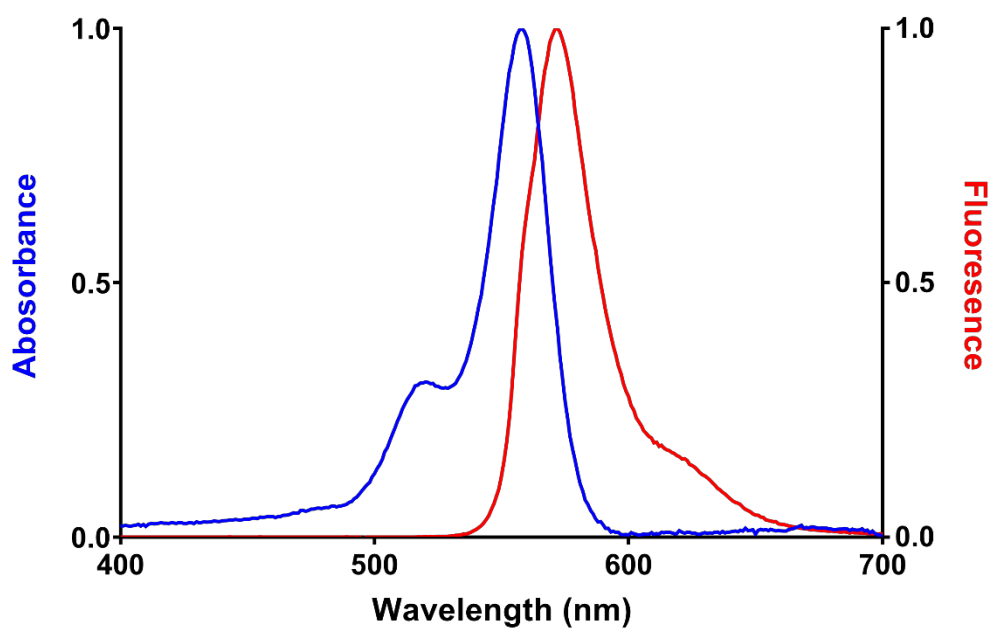


**Figure 14.** ROxy electronic absorption spectra was obtained on a Varian Cary 50 Bio spectrophotometer in a 2mL quartz cuvette between 400 nm – 700 nm in aqueous acetonitrile.

## 5.5 Conclusions

In conclusion three functional probes were successfully designed and synthesized. Cy5-leptin successfully identified a new population of astrocytes expressing LepR within the DVC

and was included in the publication: Dorsal Vagal Complex and Hypothalamic Glia Differentially Respond to Leptin and Energy Balance Dysregulation. *Transl. Psychiatry* **2020**, *10* (1), 90. The successful development of REX has led to ongoing investigations with active collaborators Dr. George Holz of SUNY Upstate Medical University and Dr. Lauren Stein of the University of Pennsylvania. ROxy continues to be used in investigation *in vivo* in Gothenburg.

## 5.6 References

- (1) Zhang, Y.; Li, S.; Zhang, H.; Xu, H. Design and Application of Receptor-Targeted Fluorescent Probes Based on Small Molecular Fluorescent Dyes. *Bioconjug. Chem.* **2021**, *32*, 4–24.
- (2) Stein, L. M.; Lhamo, R.; Cao, A.; Workinger, J.; Tinsley, I.; Doyle, R. P.; Grill, H. J.; Hermann, G. E.; Rogers, R. C.; Hayes, M. R. Dorsal Vagal Complex and Hypothalamic Glia Differentially Respond to Leptin and Energy Balance Dysregulation. *Transl. Psychiatry* **2020**, *10* (1), 90.
- (3) Park, H.-K.; Ahima, R. S. Physiology of Leptin: Energy Homeostasis, Neuroendocrine Function and Metabolism. *Metabolism* **2015**, *64* (1), 24–34.
- (4) Zhang, F.; Basinski, M. B.; Beals, J. M.; Briggs, S. L.; Churgay, L. M.; Clawson, D. K.; DiMarchi, R. D.; Furman, T. C.; Hale, J. E.; Hsiung, H. M.; Schoner, B. E.; Smith, D. P.; Zhang, X. Y.; Wery, J. P.; Schevitz, R. W. Crystal Structure of the Obese Protein Leptin-E100. *Nature* **1997**, *387* (6629), 206–209.
- (5) Kanoski, S. E.; Rupperecht, L. E.; Fortin, S. M.; De Jonghe, B. C.; Hayes, M. R. The Role of Nausea in Food Intake and Body Weight Suppression by Peripheral GLP-1 Receptor Agonists, Exendin-4 and Liraglutide. *Neuropharmacology* **2012**, *62* (5–6), 1916–1927.
- (6) Hornby, P. J. Central Neurocircuitry Associated with Emesis. *Am. J. Med.* **2001**, *111* (8 SUPPL. 1), 106–112.
- (7) Miller, A. D.; Leslie, R. A. The Area Postrema and Vomiting. *Frontiers in Neuroendocrinology*. **1994**, *15* (4), 301–320.
- (8) Grill, H. J.; Hayes, M. R. Hindbrain Neurons as an Essential Hub in the Neuroanatomically Distributed Control of Energy Balance. *Cell Metab.* **2012**, *16* (3), 296–309.
- (9) Bonaccorso, R. L.; Chepurny, O. G.; Becker-Pauly, C.; Holz, G. G.; Doyle, R. P. Enhanced

- Peptide Stability Against Protease Digestion Induced by Intrinsic Factor Binding of a Vitamin B12 Conjugate of Exendin-4. *Mol. Pharm.* **2015**, *12* (9), 3502–3506.
- (10) Harikumar, K. G.; Wootten, D.; Pinon, D. I.; Koole, C.; Ball, A. M.; Furness, S. G. B.; Graham, B.; Dong, M.; Christopoulos, A.; Miller, L. J.; Sexton, P. M. Glucagon-like Peptide-1 Receptor Dimerization Differentially Regulates Agonist Signaling but Does Not Affect Small Molecule Allostery. *Proc. Natl. Acad. Sci. U. S. A.* **2012**, *109* (45), 18607–18612.
- (11) Jones, B.; Buenaventura, T.; Kanda, N.; Chabosseu, P.; Owen, B. M.; Scott, R.; Goldin, R.; Angkathunyakul, N.; Corrêa, I. R.; Bosco, D.; Johnson, P. R.; Piemonti, L.; Marchetti, P.; Shapiro, A. M. J.; Cochran, B. J.; Hanyaloglu, A. C.; Inoue, A.; Tan, T.; Rutter, G. A.; Tomas, A.; Bloom, S. R. Targeting GLP-1 Receptor Trafficking to Improve Agonist Efficacy. *Nat. Commun.* **2018**, *9*, 1602.
- (12) Kuna, R. S.; Girada, S. B.; Asalla, S.; Vallentyne, J.; Maddika, S.; Patterson, J. T.; Smiley, D. L.; DiMarchi, R. D.; Mitra, P. Glucagon-like Peptide-1 Receptor-Mediated Endosomal CAMP Generation Promotes Glucose-Stimulated Insulin Secretion in Pancreatic  $\beta$ -Cells. *Am. J. Physiol. - Endocrinol. Metab.* **2013**, *305* (2), 161–170.
- (13) Widmann, C.; Dolci, W.; Thorens, B. Agonist-Induced Internalization and Recycling of the Glucagon-like Peptide-1 Receptor in Transfected Fibroblasts and in Insulinomas. *Biochem. J.* **1995**, *310* (1), 203–214.
- (14) Kasai, R. S.; Suzuki, K. G. N.; Prossnitz, E. R.; Koyama-Honda, I.; Nakada, C.; Fujiwara, T. K.; Kusumi, A. Full Characterization of GPCR Monomer-Dimer Dynamic Equilibrium by Single Molecule Imaging. *J. Cell Biol.* **2011**, *192* (3), 463–480.
- (15) Fonseca, J. M.; Lambert, N. A. Instability of a Class A G Protein-Coupled Receptor Oligomer

- Interface. *Mol. Pharmacol.* **2009**, *75* (6), 1296–1299.
- (16) Lambert, N. A. GPCR Dimers Fall Apart. *Sci. Signal.* **2010**, *3* (115), 1–4.
- (17) Hern, J. A.; Baig, A. H.; Mashanov, G. I.; Birdsall, B.; Corrie, J. E. T.; Lazareno, S.; Molloy, J. E.; Birdsall, N. J. M. Formation and Dissociation of M1 Muscarinic Receptor Dimers Seen by Total Internal Reflection Fluorescence Imaging of Single Molecules. *Proc. Natl. Acad. Sci. U. S. A.* **2010**, *107* (6), 2693–2698.
- (18) Lee, H.-J.; Macbeth, A. H.; Pagani, J.; Young, W. S. Oxytocin: The Great Facilitator of Life. *Prog. Neurobiol.* **2009**, *88* (2), 127–151.
- (19) Chaves, V. E.; Tilelli, C. Q.; Brito, N. A.; Brito, M. N. Role of Oxytocin in Energy Metabolism. *Peptides* **2013**, *45*, 9–14.
- (20) Zingg, H. H.; Laporte, S. A. The Oxytocin Receptor. *Trends Endocrinol. Metab.* **2003**, *14* (5), 222–227.
- (21) Iwasaki, Y.; Maejima, Y.; Suyama, S.; Yoshida, M.; Arai, T.; Katsurada, K.; Kumari, P.; Nakabayashi, H.; Kakei, M.; Yada, T. Peripheral Oxytocin Activates Vagal Afferent Neurons to Suppress Feeding in Normal and Leptin-Resistant Mice: A Route for Ameliorating Hyperphagia and Obesity. *Am. J. Physiol. - Regul. Integr. Comp. Physiol.* **2015**, *308* (5), R360–R369.

## Chapter 6: Experimental

### 6.1 General Methods

All commercial reagents and anhydrous solvents purchased were used without further purification. All reactions containing air and/or moisture sensitive reactants were performed under argon or nitrogen. Compounds were purified using a Shimadzu Prominence HPLC using a C18 column (Eclipse XDB-C18 5 $\mu$ m, 4.6 x 150 mm). All compounds were purified to or in excess of, 97% (as tracked by RP-HPLC-see supplementary materials). Products were analyzed for mass using Shimadzu LCMS-8040 or a Bruker Autoflex III Smartbeam matrix assisted laser desorption/ionization time of flight mass spectrometer (MALDI). <sup>1</sup>H NMR and <sup>13</sup>C NMR spectra were acquired on a Bruker NMR spectrometer (Avance 400 MHz) in D<sub>2</sub>O at a D1 of 3 for all compounds. EAS was collected on a Varian, Cary 50bio UV-Visible Spectrophotometer in a 1 mL quartz cuvette with baseline correction. Circular dichroism (CD) spectra were recorded with a Jasco J-715 Circular Dichroism Spectropolarimeter in 40  $\mu$ M H<sub>2</sub>O in a 0.1 cm quart cuvette. Data was analyzed and fit using GraphPad Prism 8.0. The novel HEK293 cloned cells designated as HEK293-GLP-1R-H188-C20 were obtained by G418 antibiotic resistance selection after co-transfection of cells with the human GLP-1R and the cAMP FRET reporter H188.<sup>1</sup> Cells were grown in a Memmert Incubator I (Schwabach, Germany) at 37 °C gassed with 5% CO<sub>2</sub> at ~ 95% humidity. FRET assays were conducted utilizing a Molecular Devices, FlexStation 3 Multi-Mode Microplate Reader. Data was analyzed utilizing Molecular Devices, SoftMax Pro v.5.4.6. Linear regression analyses were performed utilizing GraphPad Prism 8. All peptides were synthesized by Fmoc/tBu solid-phase peptide synthesis methodology on a CEM Liberty Blue automated microwave peptide synthesizer (CEM Corporation, Matthews, NC) starting with Fmoc-Rink Amide Protide Resin (LL)

and employing repetitive N,N'-Diisopropylcarbodiimide (DIC)/ Ethyl cyanohydroxyiminoacetate (Oxyma) activation. Peptides were cleaved from the resin and deprotected using a CEM Corporation Razor: rapid peptide cleavage system with treatment of 92.5% TFA trifluoroacetic acid (TFA) containing 2.5% triisopropylsilane (TIPS), 2.5% water, 2.5% 2,2'-(Ethylenedioxy)-diethenethiol (DODT). The obtained solution was precipitated with cold diethylether at centrifuged at 4000 rpm for 5 min. The diethylether supernatant was discarded and the remaining precipitate was redissolved in water and placed on a Labconco FreeZone 1 lyophilizer. All peptides were purified using Agilent ZORBAX 300SB-C8 (5  $\mu$ m, 9.4  $\times$  250 mm) column.

## 6.2 Materials

Purchased from Sigma Aldrich: acetonitrile (Cat # 14851), diethyl ether (Cat # 673811), ethanol (Cat # 459844), ethyl acetate (Cat # 319902), isopropyl alcohol (Cat # 34863), methanol (Cat # 34885), n-methyl-2-pyrrolidone (Cat # 328634), triethylamine (Cat # 8.08352), vitamin B<sub>12</sub> (Cat # V2876), 2-iodoxybenzoic acid (Cat #661384), sodium cyanide (Cat # 205222), 1,1'-carbonyl-di-(1,2,4-triazole) (Cat # 21863), propargylamine (Cat # P50900), 1-amino-3-butyn-1-amine (Cat # 715190), 4-pentyn-1-amine (Cat # 779407), hex-5-yn-1-amine (Cat # COM497512576), bovine serum albumin (Cat # A7030), Dulbecco's modified eagle medium (Cat # D6429), fetal bovine serum (Cat # 12303C), G-418 disulfate salt solution (Cat # G8168), HEPES (Cat # H0887). Purchased from ThermoFisher Scientific: penicillin-streptomycin (Cat # 15140122), trypsin-EDTA (Cat # 25200072). Purchased from Fisher Scientific: calcium chloride dihydrate (Cat # BP510), magnesium chloride hexahydrate (Cat # BP214), potassium chloride (Cat # BP366), sodium chloride (Cat # BP358-1). Purchased from BroadPharm: propargyl-PEG2-amine (Cat # BP22519), propargyl-PEG4-amine (Cat # BP22520). Purchased from Enamine: (4-

ethynylphenyl)methanamine (Cat # EN300-233648), (3-ethynylphenyl)methanamine (Cat # EN300-248722). Krebs-Ringer Bicarbonate (KRB) buffer was prepared as described previously. D-Glucose (Cat # G 5767) and nEx4 (Cat # E7144) were purchased from Sigma-Aldrich. Ex4 K12-azido and Ex40 K40-azido were produced by Genscript (Piscataway, New Jersey, United States). Rat insulin radioimmunoassay (RIA) kit was purchased from Millipore Sigma, Burlington, MA Cat no. RI-13K. The human GLP-1R plasmid was provided by M. Beinborn, Tufts University School of Medicine. The H188 plasmid was provided by K. Jalink, Netherlands Cancer Institute. All amino acids and activating agents were purchased from CEM Corporation (Matthews, NC, United States).

### **6.3 Ethics Statement**

All *in vivo* experiments were approved by the Institutional Care and Use Committee of the University of Pennsylvania and were conducted using the approved procedures.

### **6.4 RP-HPLC Methods**

Compounds were purified using a Shimadzu Prominence HPLC using a C18 column (Eclipse XDB-C18 5 $\mu$ m, 4.6 x 150 mm). Two differing purification methods were used: A1, H<sub>2</sub>O + 0.1% TFA and MeOH from 1% CH<sub>3</sub>OH/H<sub>2</sub>O + 0.1% TFA to 90% CH<sub>3</sub>OH/H<sub>2</sub>O + 0.1% TFA in 25 min.; A2, H<sub>2</sub>O + 0.1% TFA and CH<sub>3</sub>CN from 1% CH<sub>3</sub>CN/H<sub>2</sub>O + 0.1% TFA to 70% CH<sub>3</sub>CN/H<sub>2</sub>O + 0.1% TFA in 15 min.

## **6.5 Experimental-Chapter 2**

### **6.5.1 Synthesis of B12-Ex4**

#### **6.5.1.1 Synthesis of B12-Carboxylic Acid (B12-CA)**

B12-CA was synthesized as previously described.<sup>2</sup>

#### **6.5.1.2 Synthesis of B12-Aminobutyne (B12-AB)**

B12-AB was synthesized as previously described.<sup>2</sup>



### 6.5.1.3 Synthesis of B12-Ex4

B12-Ex4 was synthesized as previously described.<sup>2</sup>

### 6.5.1.4 Synthesis of B12-Ex4-Cy5

B12-Ex4-Cy5 was synthesized as previously described.<sup>3</sup>

## 6.6 Experimental-Chapter 3

**Note: Numbering Corresponds to that used in Chapter 3**

### 6.6.1 Synthesis of Dicyanocobinamide (Cbi) (2)

To a 10mL microwave reaction vessel containing a magnetic stir bar was added B<sub>12</sub> (cyanocobalamin) (303.8 mg, 0.225 mmol) sodium cyanide (NaCN) (36.9 mg, 0.7096 mmol) and 5 mL of EtOH and the vessel was sealed. The reaction was heated to 120°C for 10 min. Following completion of the microwave reaction the remaining solution was transferred and diluted using isopropyl alcohol (iPrOH). The reaction was purified utilizing a normal phase silica column. The reaction was eluted using 100% methanol (MeOH). The product eluted as a purple product. The isolated product was precipitated utilizing diethyl ether (Et<sub>2</sub>O) and allowed to dry producing a solid, purple product, **2**, in 80% yield (187.4mg, 0.1795 mmol). Solubility was measured as 400mg/mL in distilled water. **2** was purified by RP-HPLC as described for method A1, to 98%; t<sub>R</sub>: 5.2 and 6.7 min (Figure 1); ESI-MS expected *m/z* = 1042, observed *m/z* = [M-CN]<sup>+</sup> 1016 (Figure 2). EAS Ext Coeff<sub>354</sub> = 28,400 M<sup>-1</sup> cm<sup>-1</sup> (Figure 3). <sup>1</sup>H NMR (400 MHz, D<sub>2</sub>O): δ 5.90 (s, 1H), 3.95-3.87 (m, 1H), 3.85 (d, J= 8.4. Hz, 1H), 3.75 (d, J= 10.4 Hz, 1H), 3.41 (m, 1H), 3.36 (s, 5H), 3.30 (m, 2H), 3.25 (d, J=4.7 Hz, 1H), 3.17 (dd, J= 6.8, 6.9 Hz, 1H), 2.92-2.86 (m, 1H), 2.75-2.73 (m, 2H), 2.65-2.39 (m, 7H), 2.32-2.26 (m, 15H), 2.19-2.08 (m, 5H), 2.03-1.95 (m, 1H), 1.91-1.76 (4H), 1.69 (s, 3H), 1.54 (s, 3H), 1.50 (s, 3H), 1.44 (s, 3H), 1.32 (s, 3H), 1.19 (s, 4H), 1.16 (d, J=6.4 Hz, 4H) (Figure 4). <sup>13</sup>C NMR (400 MHz, D<sub>2</sub>O): 178.6, 178.4, 177.9, 177.5, 177.3, 176.8, 175.1, 175.0, 172.1, 163.4,

162.9, 105.1, 103.1, 91.0, 83.1, 75.0, 66.2, 64.2, 58.8, 56.3, 55.2, 53.2, 49.2, 48.9, 46.8, 46.3, 46.1, 43.7, 42.2, 39.0, 34.9, 32.5, 32.4, 31.9, 31.7, 31.5, 30.5, 26.6, 25.7, 24.9, 23.8, 21.7, 19.4, 18.7, 18.5, 17.4, 16.5, 15.1, 14.8 (Figure 5).

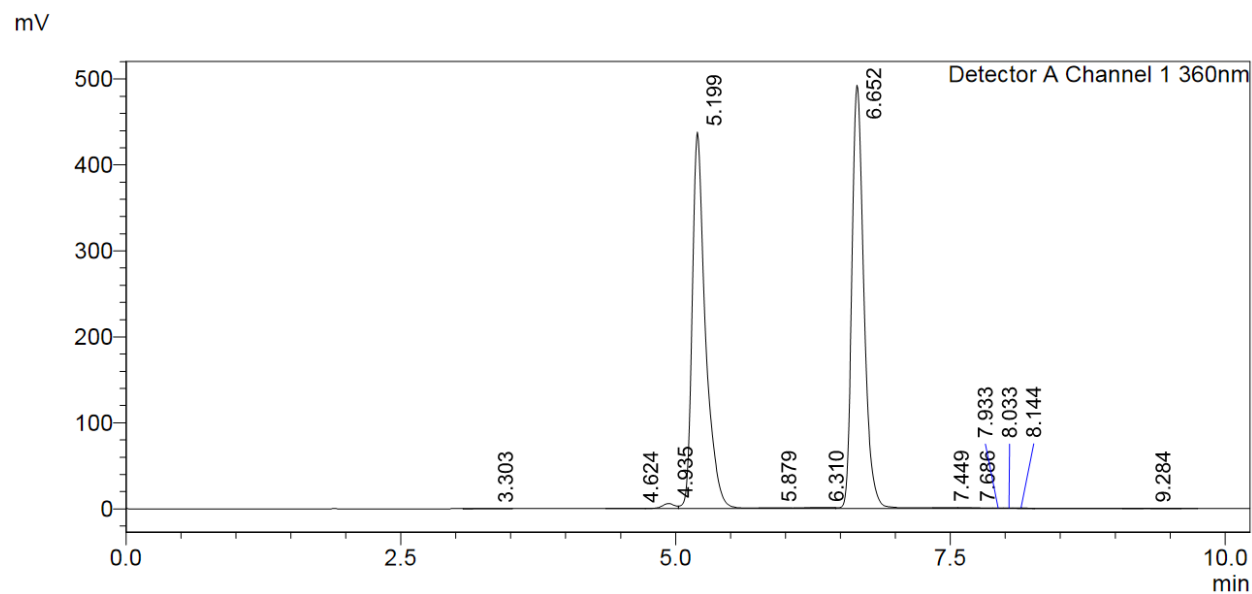


**Figure 1.** RP-HPLC trace showing the  $\alpha$ - and  $\beta$ -isomer products of **2** at 5.2 and 6.7 min.

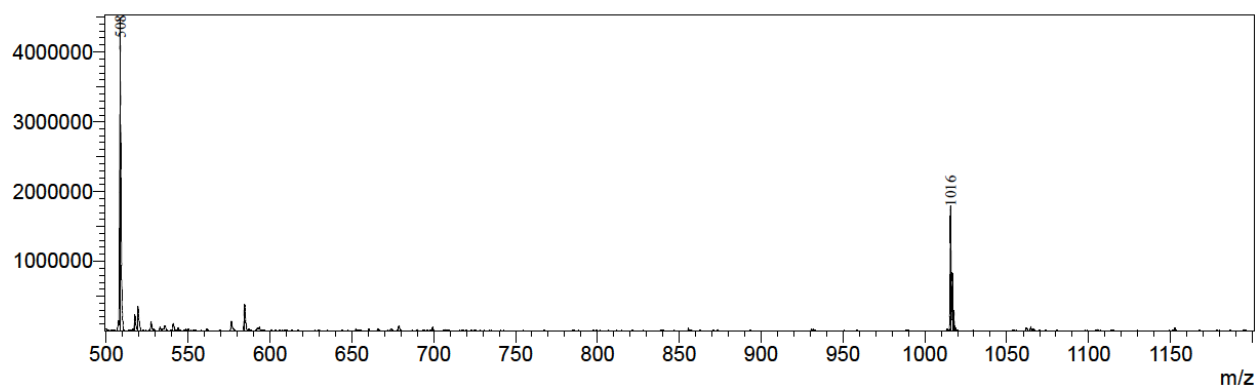


**Figure 2.** ESI-MS of **2**, expected  $m/z = 1042$ , observed  $m/z = [M-CN]^{+1} 1016$ .

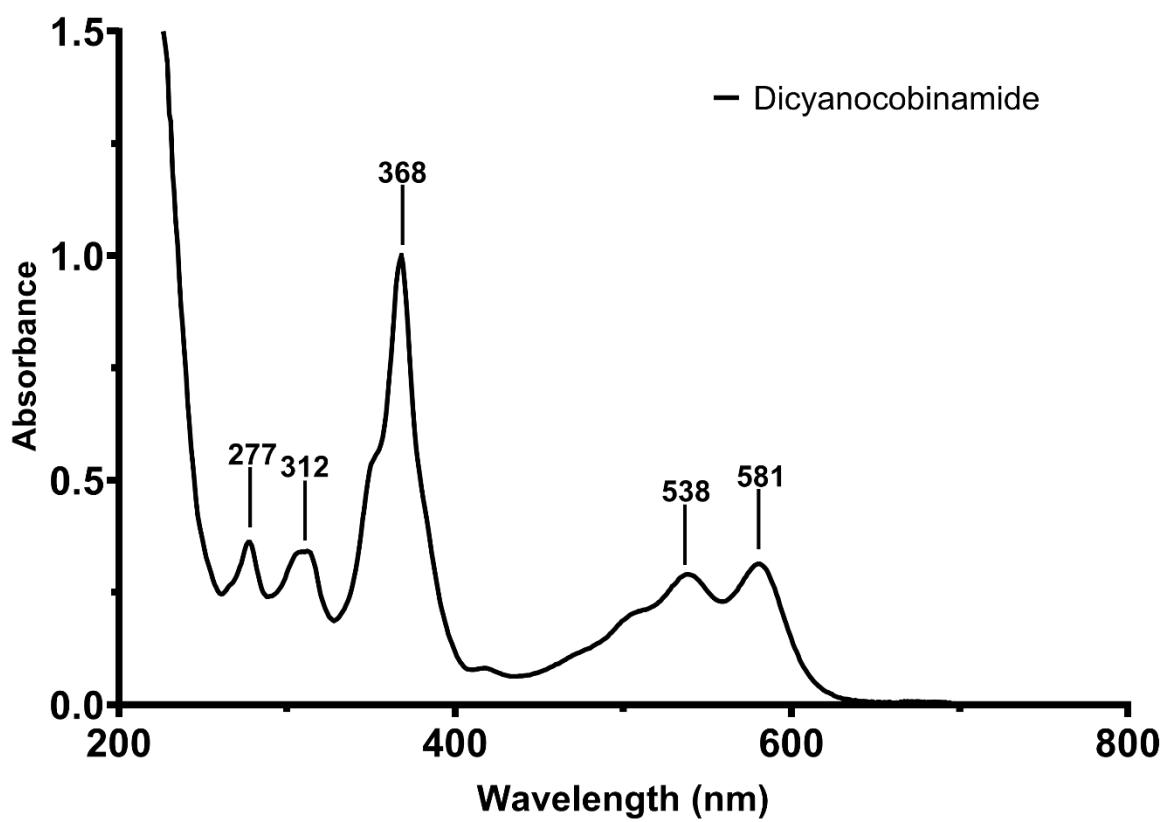


Figure 3. Electronic absorption spectroscopy of 2.

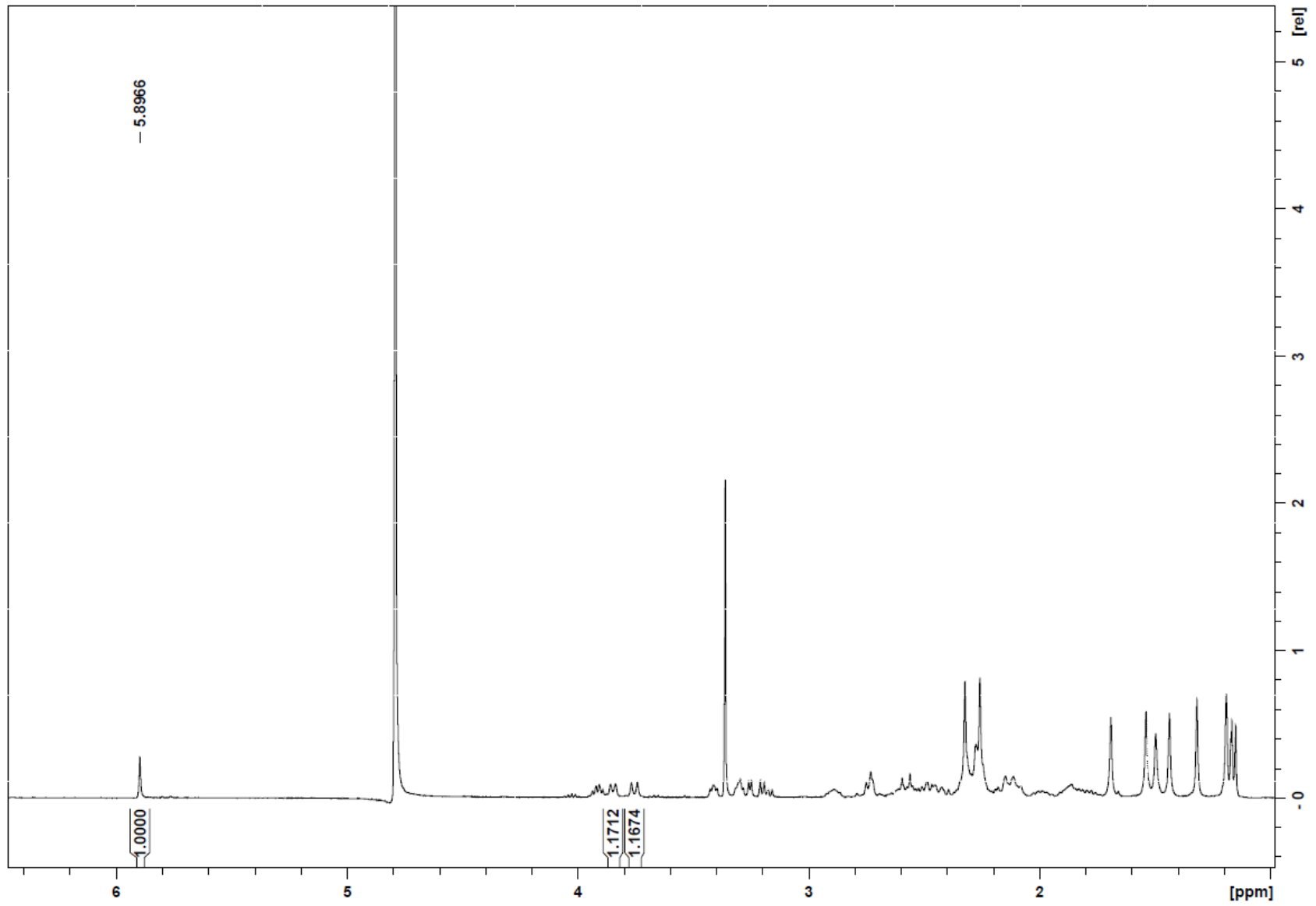


Figure 4.  $^1\text{H}$  NMR of **2** (400 MHz, 298K,  $\text{D}_2\text{O}$ ).

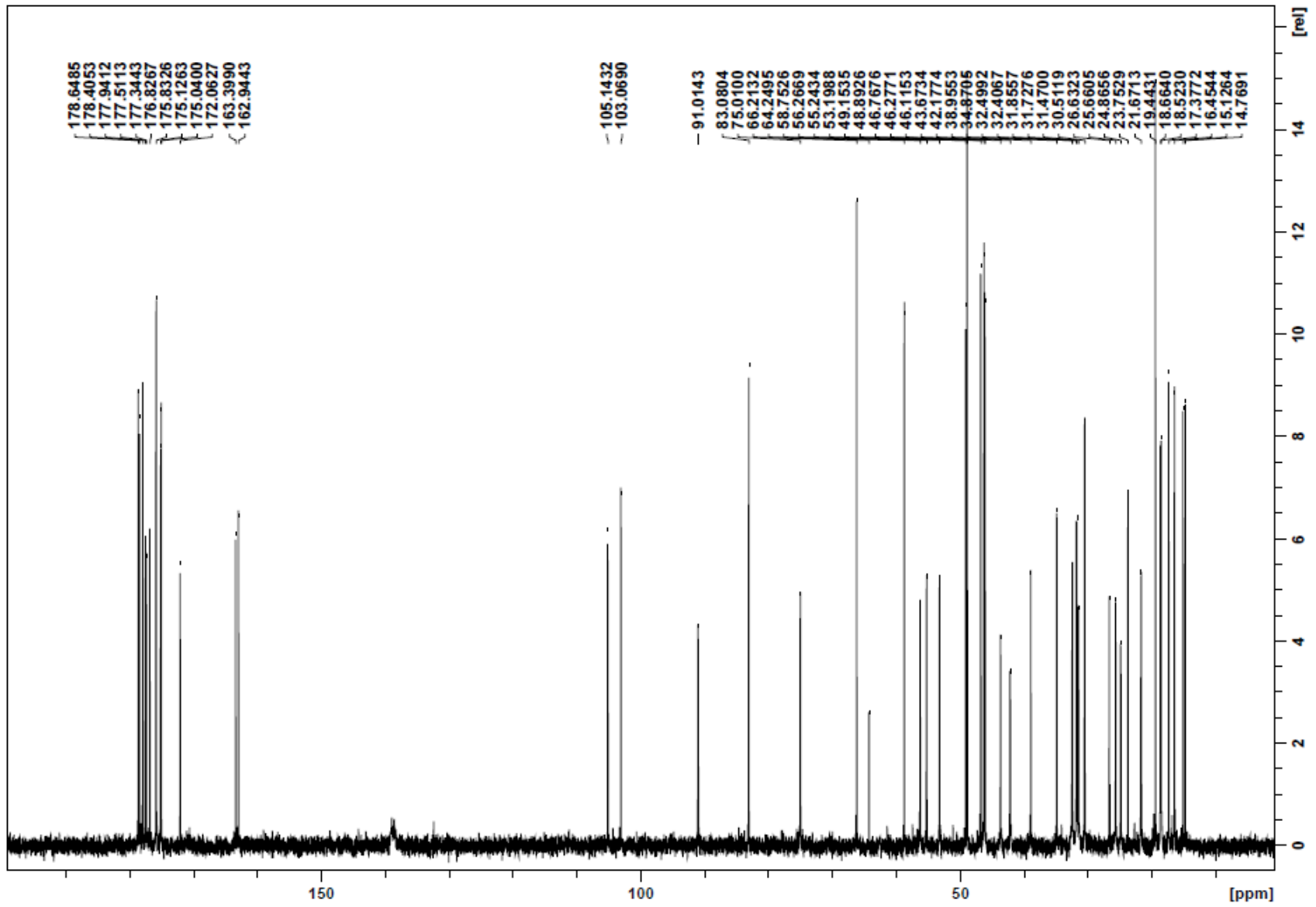


Figure 5.  $^{13}\text{C}$  NMR of **2** (400 MHz, 298K,  $\text{D}_2\text{O}$ ).

## 6.6.2 Synthesis of Cbi-Ex4/40

### 6.6.2.1 Synthesis of Cbi-Propargylamine (Cbi-Pro) (4)

**4** was prepared by combining **2** (16.8 mg, 0.0161 mmol) with CDT (51.4 mg, 0.3000 mmol) and allowed to stir for one hour at which time propargylamine (19.2  $\mu$ L, 16.5 mg, 0.300 mmol) and TEA (50  $\mu$ L) were added and stirred for one hour after which point a second equivalent amount propargylamine and TEA were added and allowed to stir for one hour to give the target compound, which was purified using RP-HPLC method A1 to produce **4** as an orange solid to 97% purity. Yield 43% (7.8 mg, 0.007 mmol). The product obtained was in the form of two different isomers with the aquo-group located on the alpha and beta positions ( $\alpha$ -cyano- $\beta$ -aqua- and  $\alpha$ -aqua- $\beta$ -cyano-).  $t_R$ : 8.8 and 9.5 min (Figure 6); ESI-MS expected  $m/z$  = 1115, observed  $m/z$  =  $[M^+ - H_2O]^{+1}$ : 1096,  $[M^+ - H_2O + H^+]^{+2}$ : 549 (Figure 7). EAS Ext Coeff<sub>354</sub> = 14,500  $M^{-1} cm^{-1}$  (Figure 8).  $^1H$  NMR (400 MHz,  $D_2O$ ):  $\delta$  6.50 (1H, s, Ar-H,  $\beta$ -aqua isomer) 6.42 (1H, s, Ar-H,  $\alpha$ -aqua isomer) (Figure 9, 10).

mV

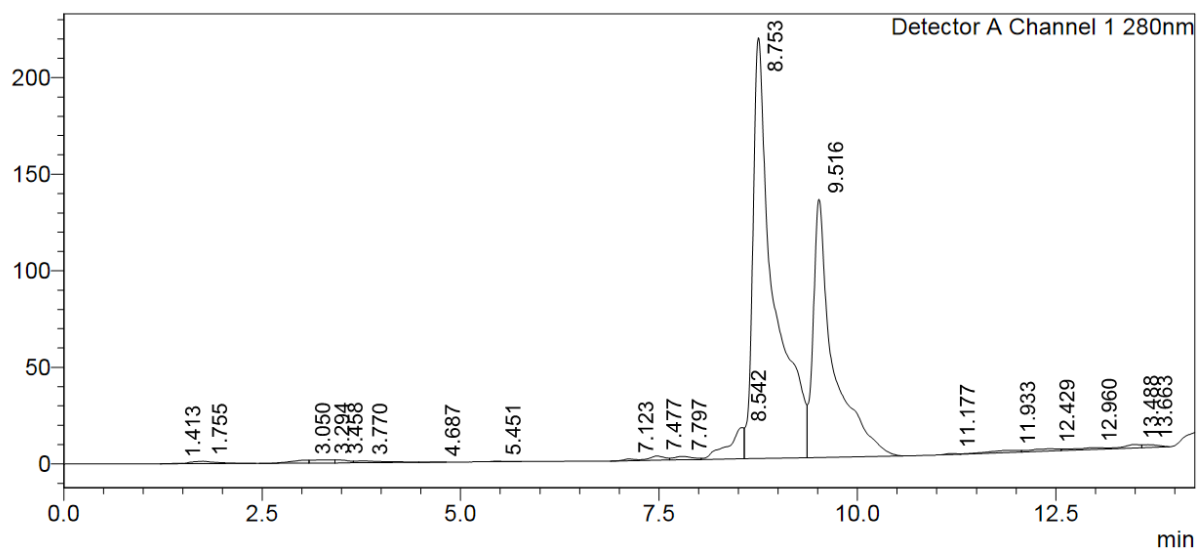


**Figure 6.** RP-HPLC trace showing the  $\alpha$ - and  $\beta$ -isomer products of **4** at 8.8 and 9.5 min.

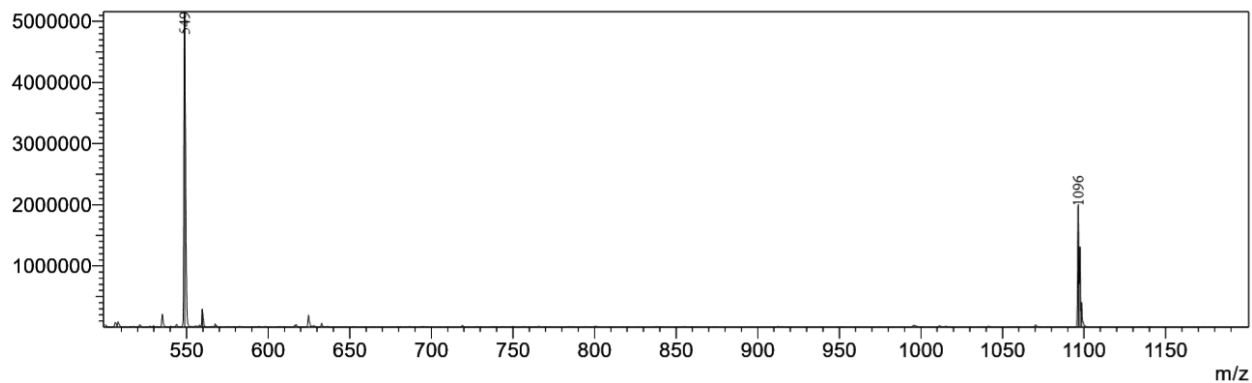


**Figure 7.** ESI-MS of **4**, expected  $m/z = 1115$ , observed  $m/z = [M^+ - H_2O]^{+1}$ : 1096,  $[M^+ - H_2O + H^+]^{+2}$ : 549.

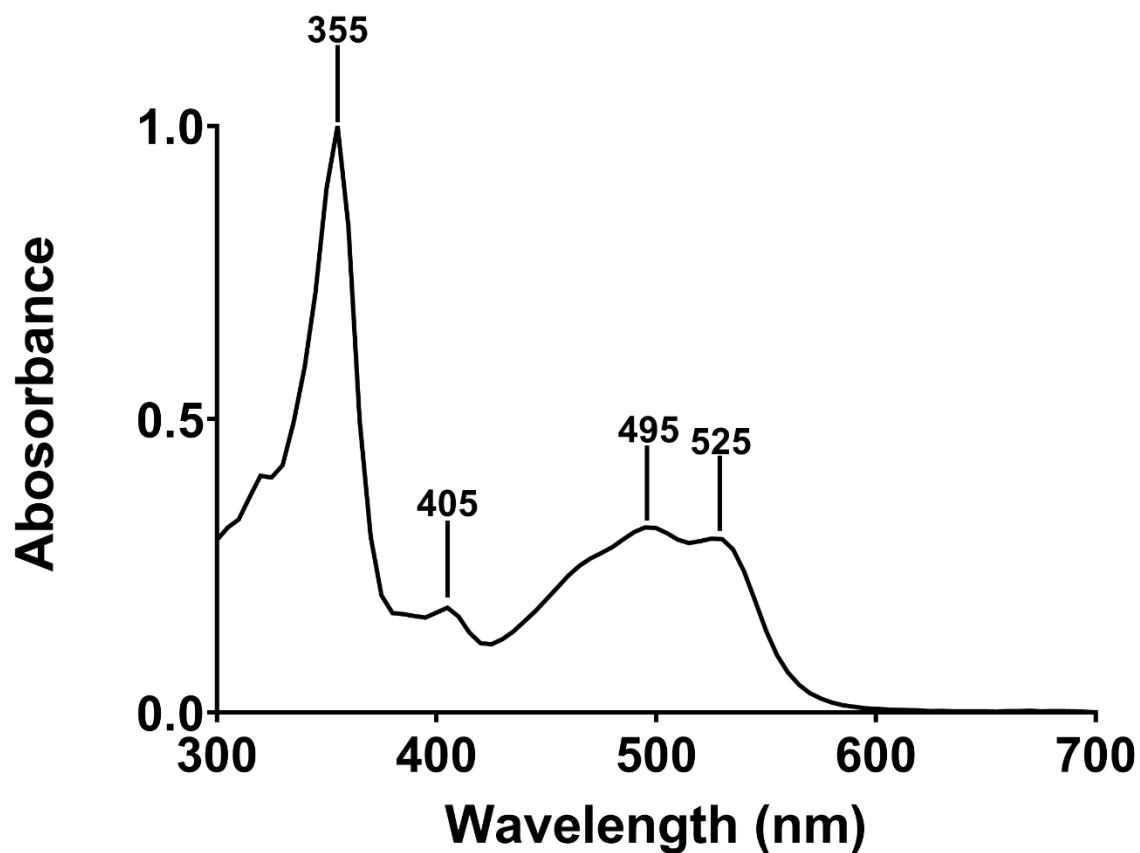


**Figure 8.** Electronic absorption spectroscopy of **4**.

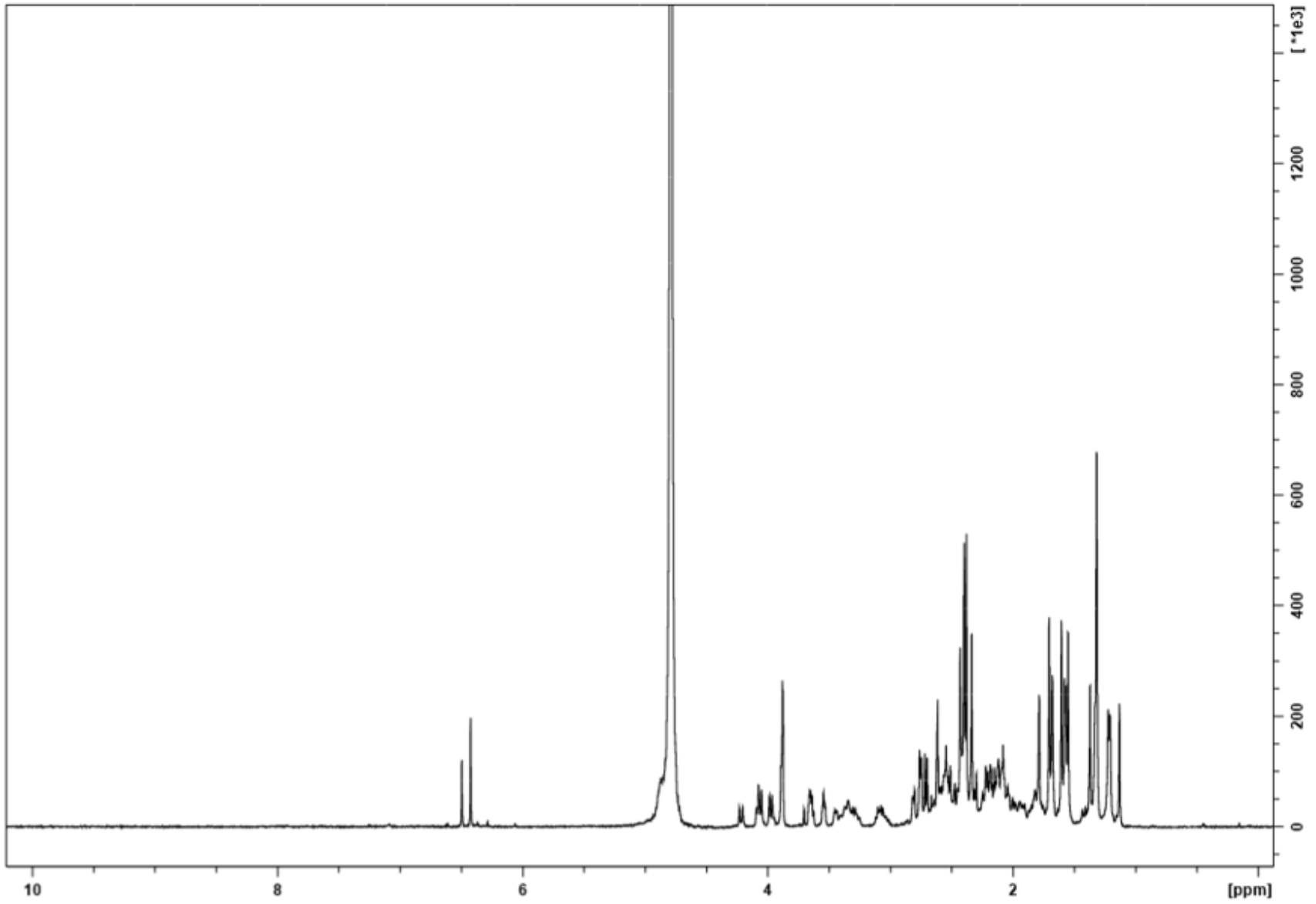


**Figure 9.**  $^1\text{H}$  NMR of **4** (400 MHz, 298K,  $\text{D}_2\text{O}$ ).



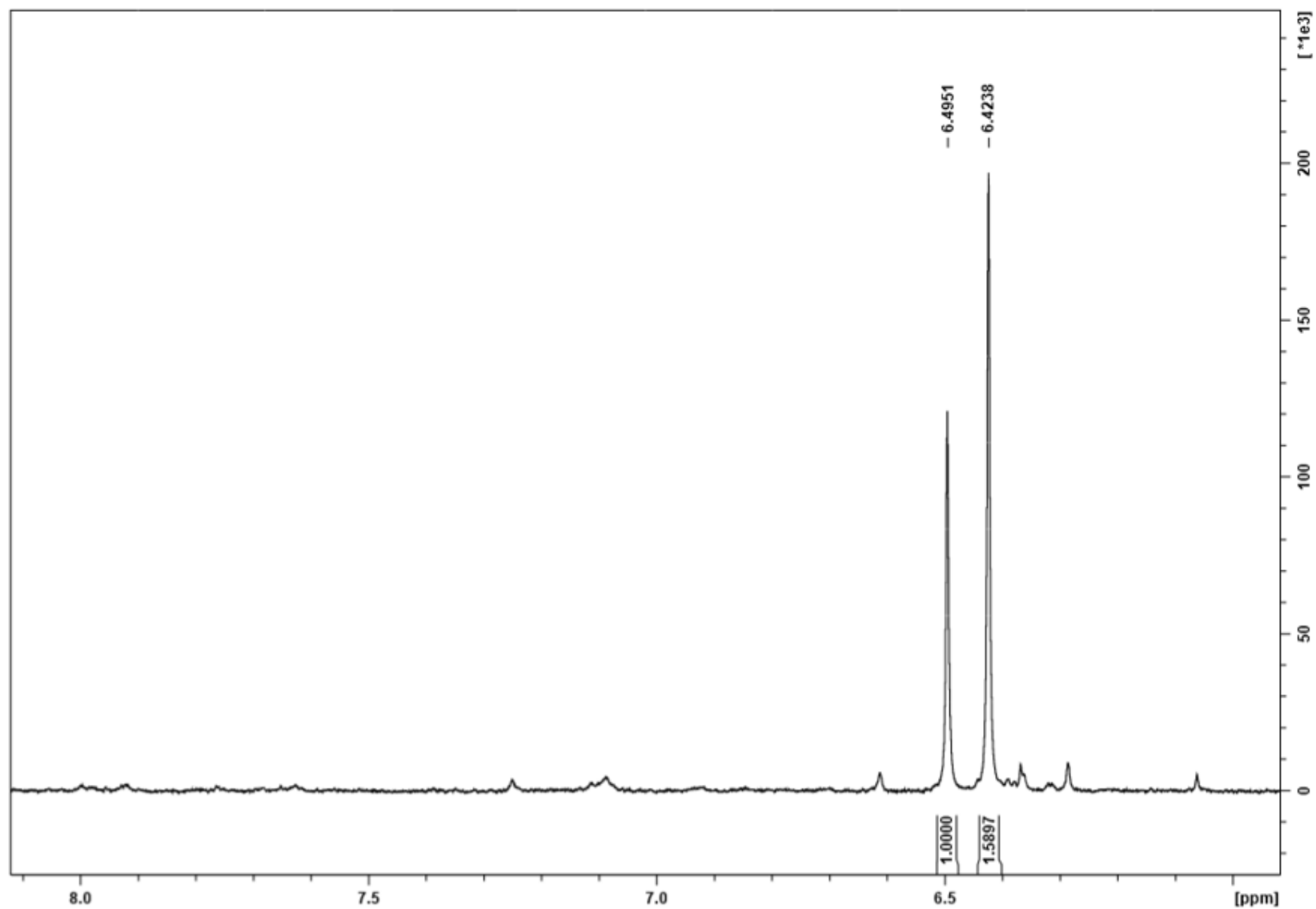


**Figure 10.**  $^1\text{H}$  NMR of **4** (400 MHz, 298K,  $\text{D}_2\text{O}$ ) (Aromatic). Characteristic signals (H19) of  $\beta$ - (6.50) and  $\alpha$ - (6.42) aquo-isomers of **4** are observed.<sup>4</sup>

### 6.6.2.2 Synthesis of Cbi-Butyne (Cbi-But) (5)

**5** was prepared by combining **2** (20.5 mg, 0.0197 mmol) with CDT (61.3 mg, 0.3740 mmol) and allowed to stir for one hour at which time 1-amino-3-butyne (32.0  $\mu$ L, 27.0 mg, 0.391 mmol) and TEA (50  $\mu$ L) were added and stirred for one hour after which point a second equivalent of 1-amino-3-butyne and TEA were added and allowed to stir for one hour to give the target compound, which was purified using RP-HPLC method A1 to produce **5** as an orange solid to 95% purity. Yield 53% (11.4 mg, 0.010 mmol). The product obtained was in the form of two different isomers with the aquo-group located on the alpha and beta positions ( $\alpha$ -cyano- $\beta$ -aqua- and  $\alpha$ -aqua- $\beta$ -cyano-).  $t_R$ : 7.4 and 7.9 min (Figure 11); ESI-MS expected  $m/z$  = 1129, observed  $m/z$  =  $[M^+ - H_2O]^+$ : 1111,  $[M^+ - H_2O + H^+]^{+2}$ : 556 (Figure 12). EAS Ext Coeff<sub>354</sub> = 19,804  $M^{-1} cm^{-1}$  (Figure 13).  $^1H$  NMR (400 MHz,  $D_2O$ ):  $\delta$  6.49 (1H, s, Ar-H,  $\beta$ -aqua isomer) 6.42 (1H, s, Ar-H,  $\alpha$ -aqua isomer) (Figure 14, 15).

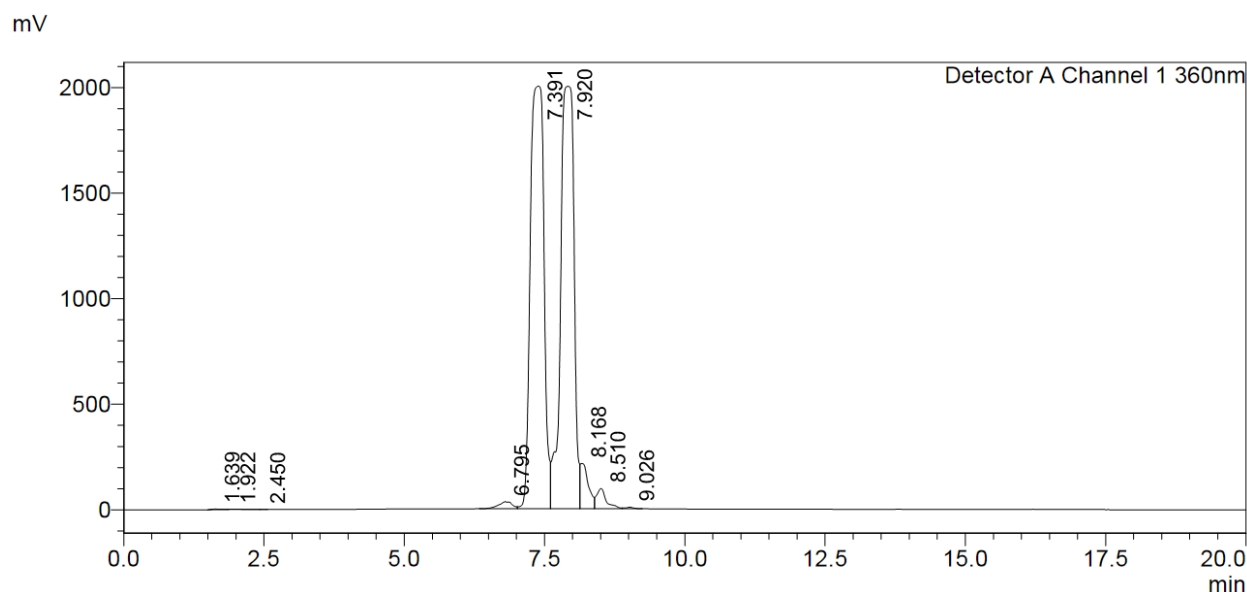


**Figure 11.** RP-HPLC trace showing the  $\alpha$ - and  $\beta$ -isomer products of **5** at 7.4 and 7.9 min.

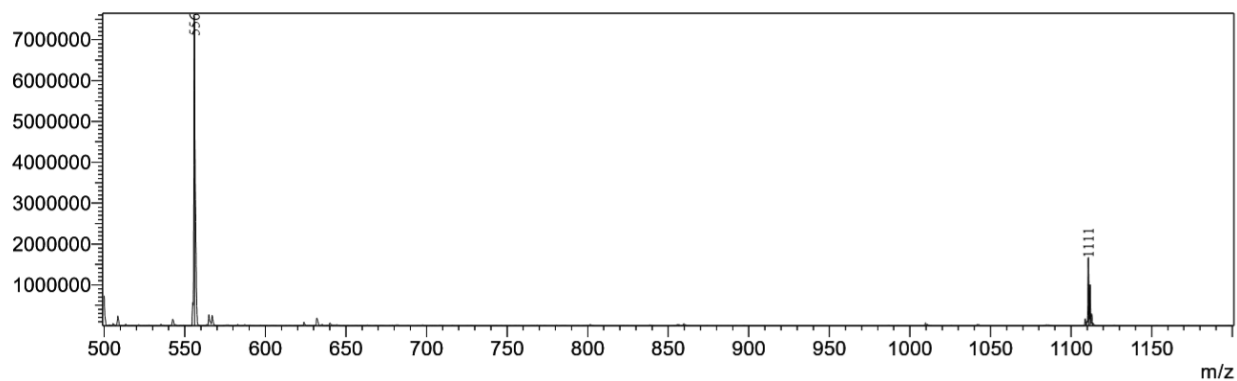


**Figure 12.** ESI-MS of **5**, expected  $m/z = 1129$ , observed  $m/z = [M+H_2O]^+1: 1111$ ,  $[M+H_2O+H^+]^+2: 556$ .

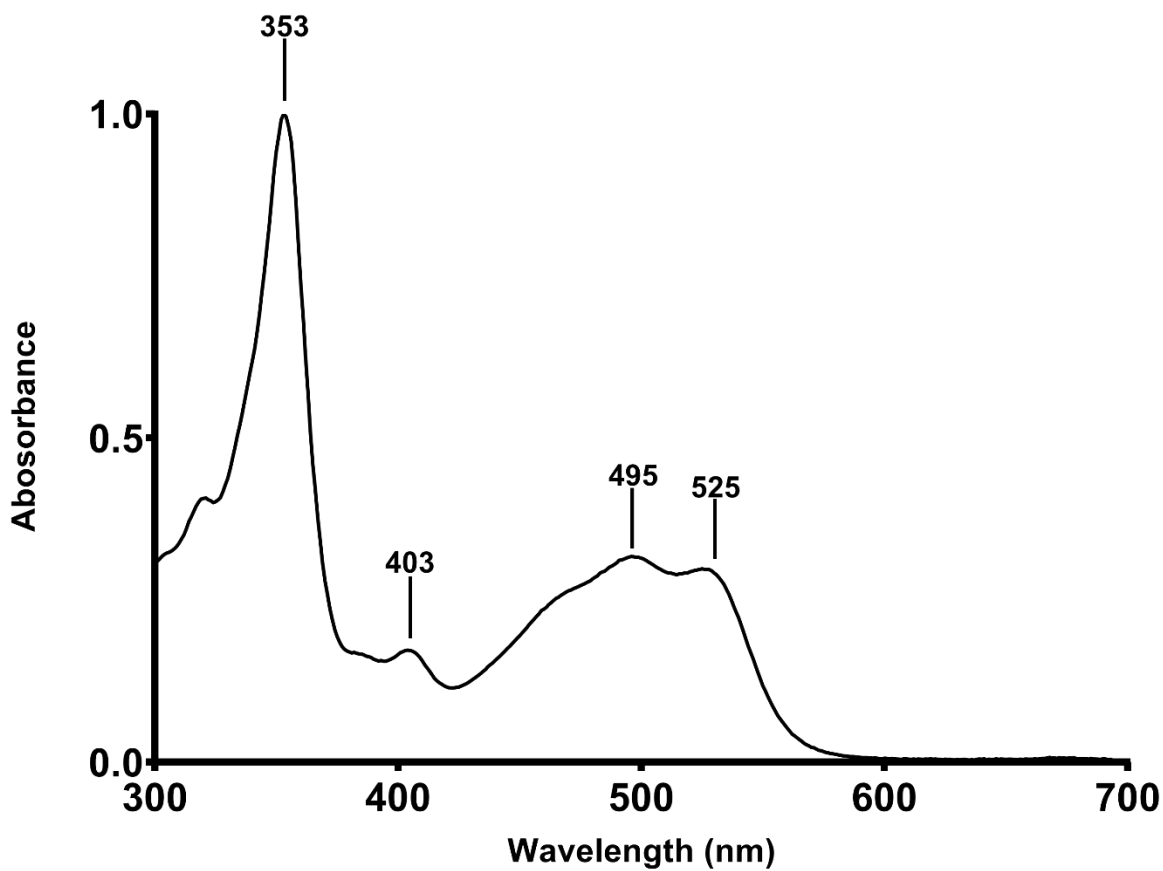


**Figure 13.** Electronic absorption spectroscopy of **5**.

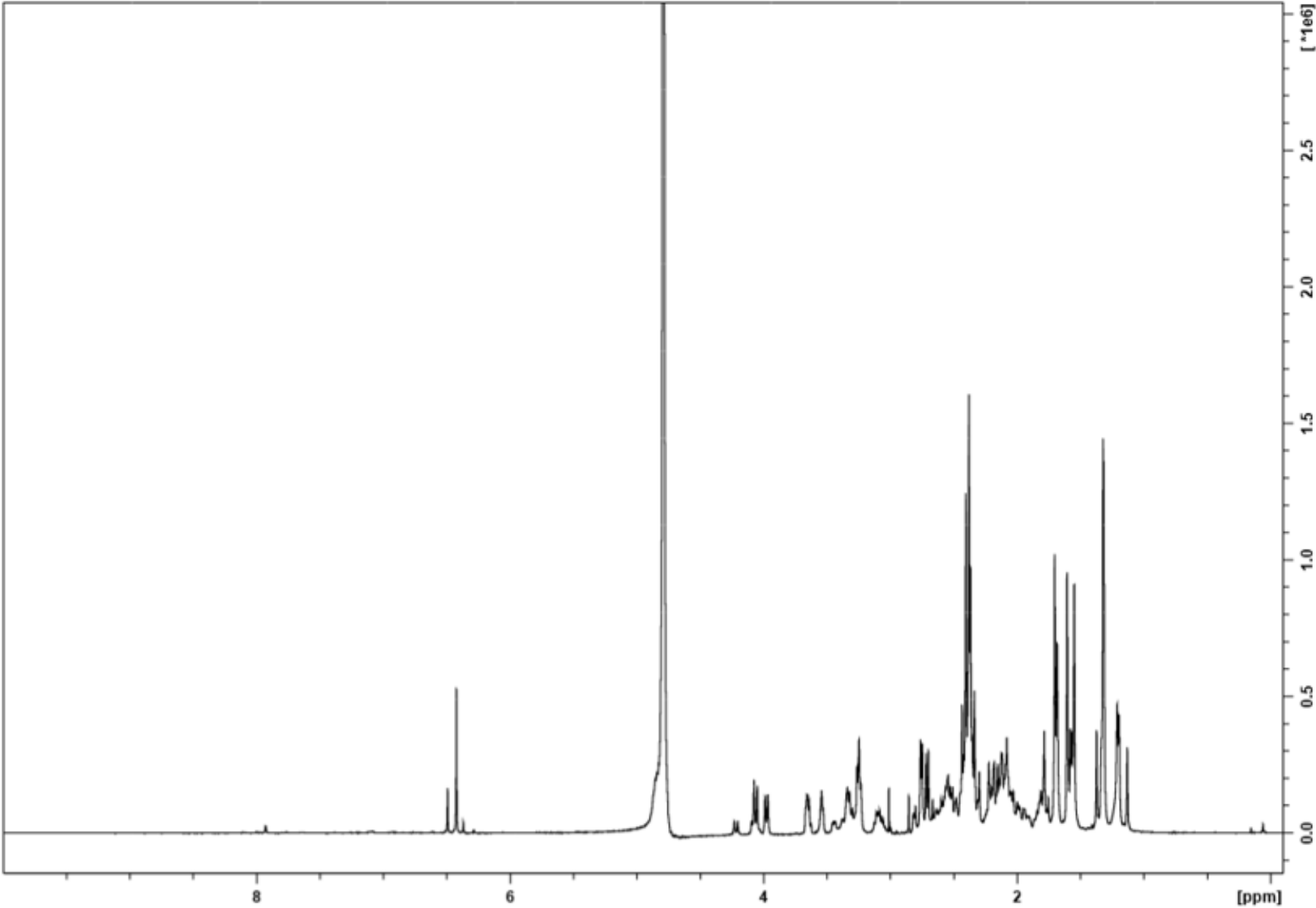
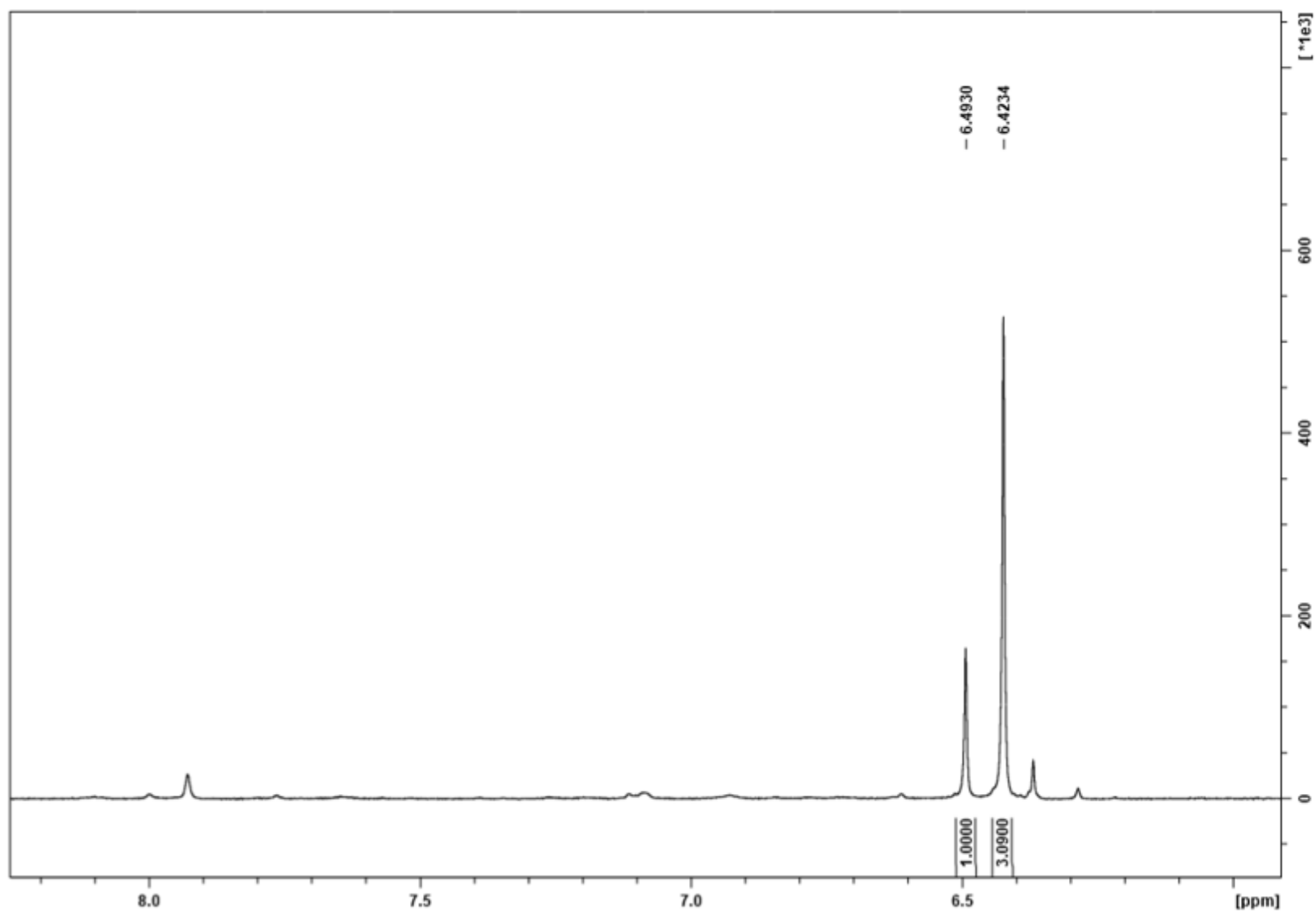


Figure 14. <sup>1</sup>H NMR of 5 (400 MHz, 298K, D<sub>2</sub>O).



**Figure 15.** <sup>1</sup>H NMR of **5** (400 MHz, 298K, D<sub>2</sub>O) (Aromatic). Characteristic signals (H19) of β-(6.49) and α- (6.42) aquo-isomers of **5** are observed.<sup>4</sup>

### 6.6.2.3 Synthesis of Cbi-Pentyne (Cbi-Pent) (6)

**6** was prepared by combining **2** (17.3 mg, 0.0166 mmol) with CDT (49.1 mg, 0.299 mmol) and allowed to stir for one hour at which time 4-pentyne-1-amine (29.0  $\mu$ L, 24.9 mg, 0.300 mmol) and TEA (50  $\mu$ L) were added and stirred for one hour after which point a second equivalent amount 4-pentyne-1-amine and TEA were added and allowed to stir for one hour to give the target compound, which was purified using RP-HPLC method A1 to produce **6** as an orange solid to 97% purity. Yield 21% (4.0 mg, 0.003 mmol). The product obtained was in the form of two different isomers with the aquo-group located on the alpha and beta positions ( $\alpha$ -cyano- $\beta$ -aqua- and  $\alpha$ -aqua- $\beta$ -cyano-).  $t_R$ : 10.4 and 11.0 min (Figure 16); ESI-MS-expected  $m/z$  = 1143, observed  $m/z$  =  $[M^+ - H_2O]^{+1}$ : 1124,  $[M^+ - H_2O + H^+]^{+2}$ : 563 (Figure 17). EAS Ext Coeff<sub>354</sub> = 15,001  $M^{-1} cm^{-1}$  (Figure 18).  $^1H$  NMR (400 MHz,  $D_2O$ ):  $\delta$  6.50 (1H, s, Ar-H,  $\beta$ -aqua isomer) 6.43 (1H, s, Ar-H,  $\alpha$ -aqua isomer) (Figure 19,20).

mV

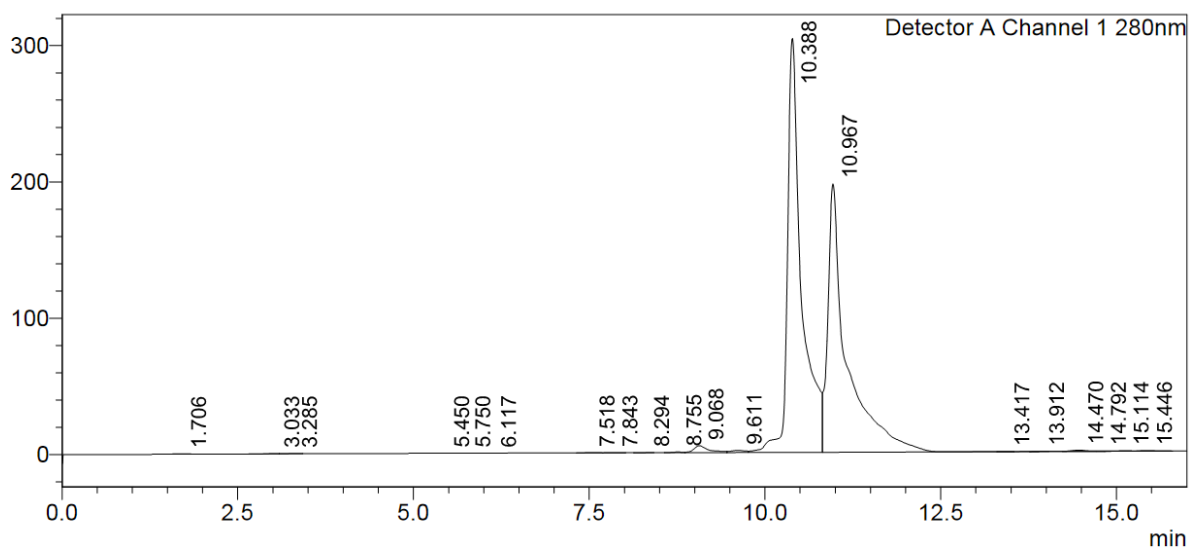


**Figure 16.** RP-HPLC trace showing the  $\alpha$ - and  $\beta$ -isomer products of **6** at 10.4 and 11.0 min.

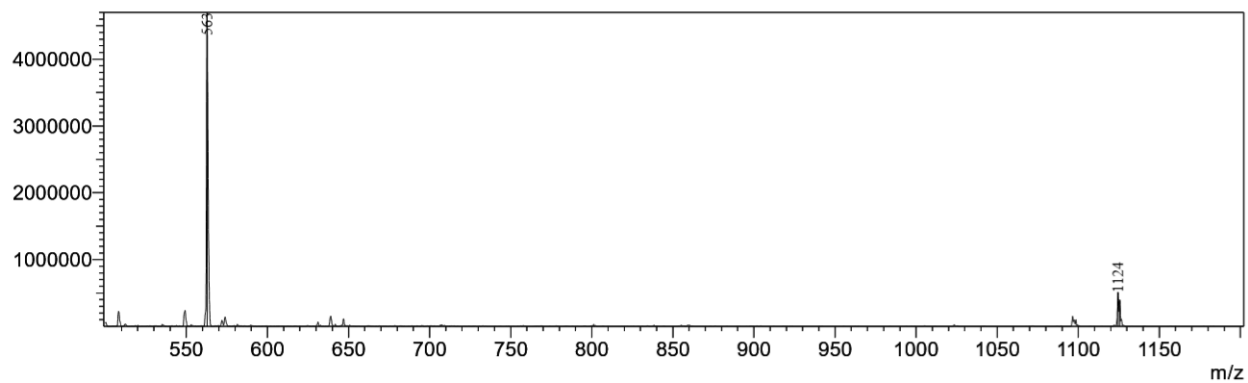


**Figure 17.** ESI-MS of **6**, expected  $m/z = 1143$ , observed  $m/z = [M^+ - H_2O]^{+1}: 1124$ ,  $[M^+ - H_2O + H^+]^{+2}: 563$ .

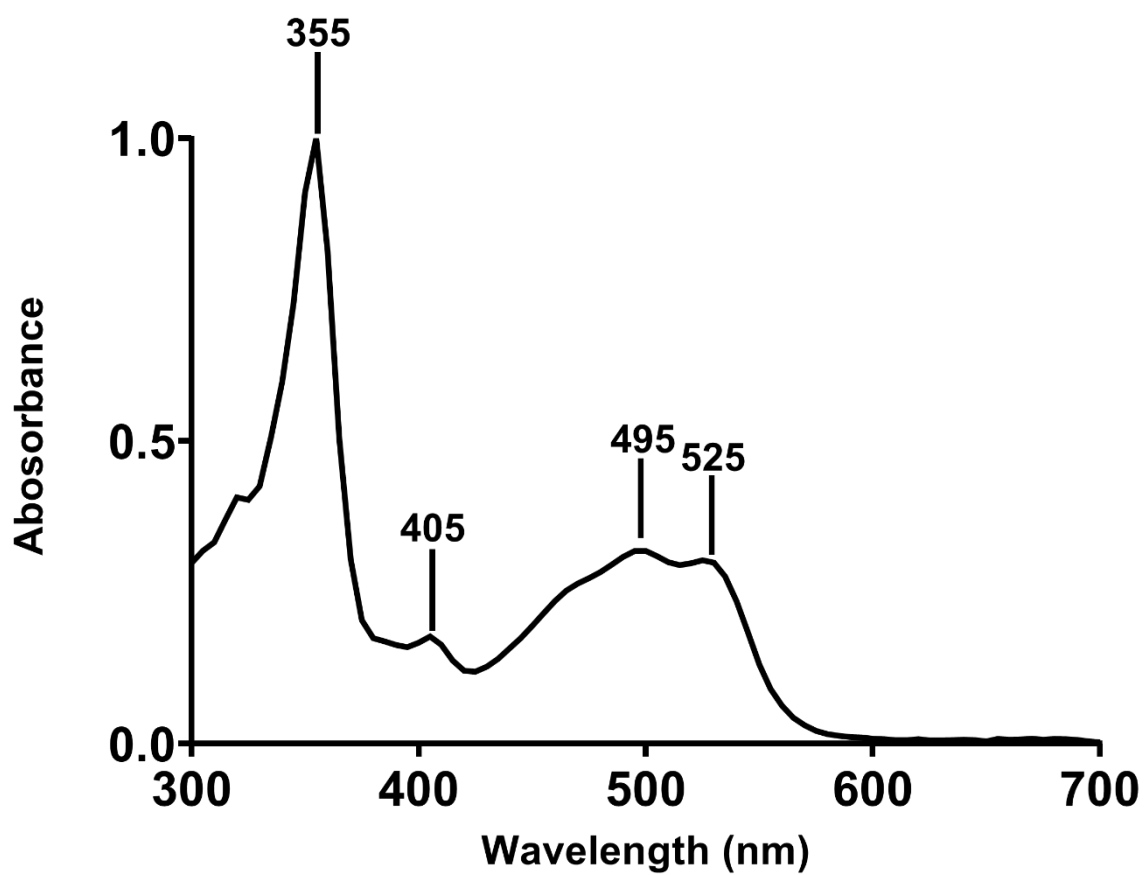


**Figure 18.** Electronic absorption spectra of **6**.

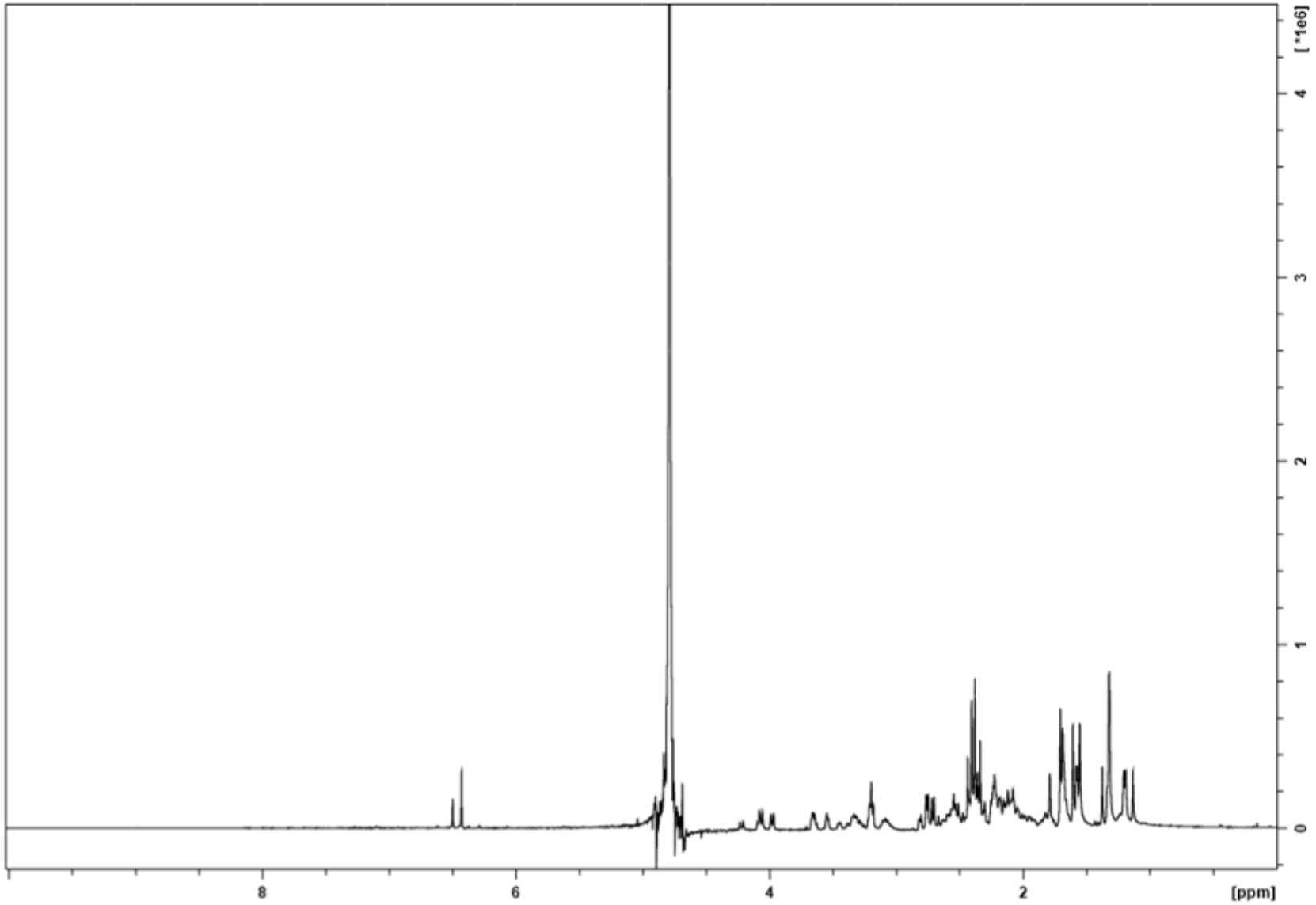


**Figure 19.**  $^1\text{H}$  NMR of **6** (400 MHz, 298K,  $\text{D}_2\text{O}$ ).



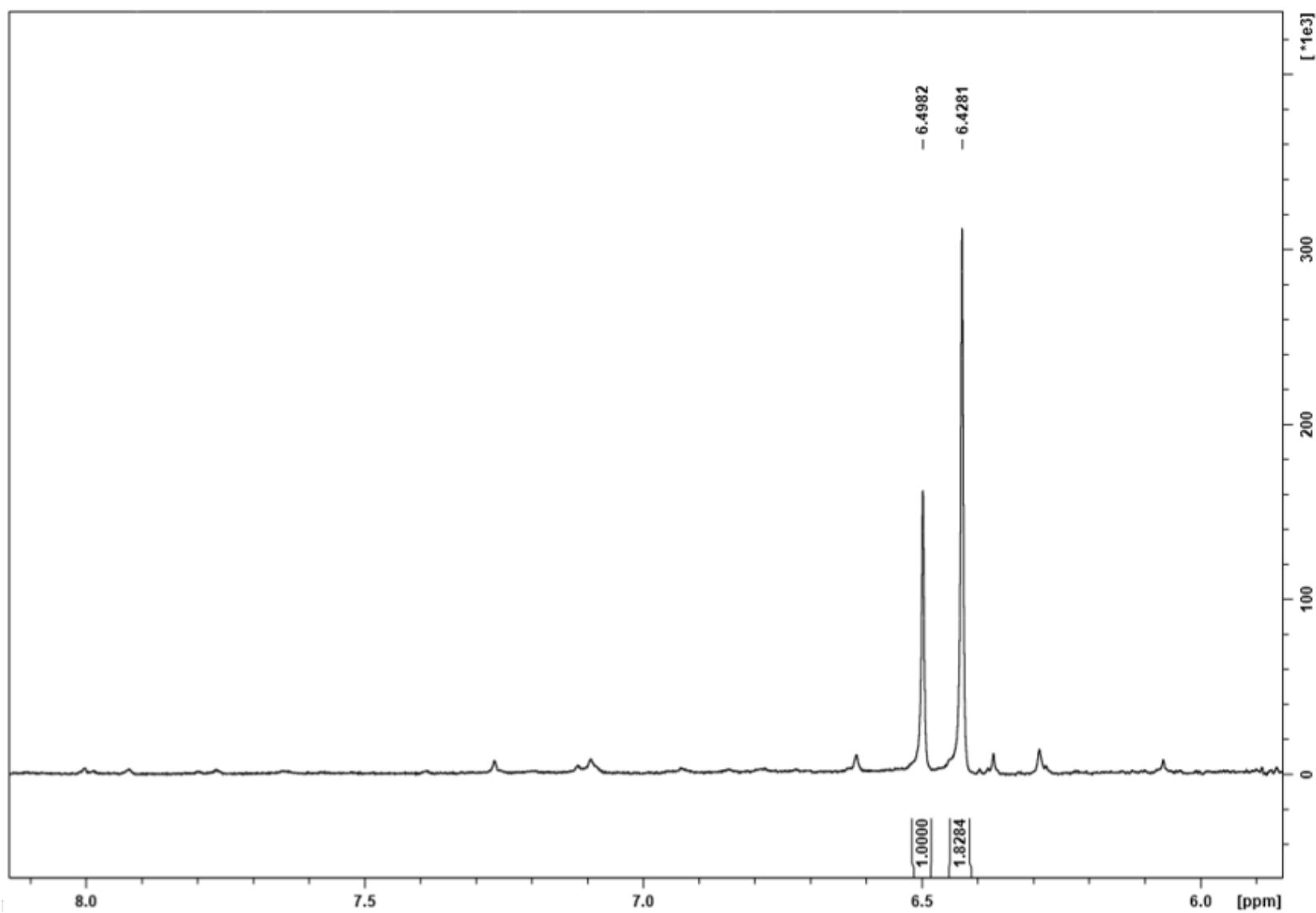


**Figure 20.**  $^1\text{H}$  NMR of **6** (400 MHz, 298K,  $\text{D}_2\text{O}$ ) (Aromatic). Characteristic signals (H19) of  $\beta$ - (6.50) and  $\alpha$ - (6.43) aquo-isomers of **6** are observed.<sup>4</sup>

#### 6.6.2.4 Synthesis of Cbi-Hexyne (Cbi-Hex) (7)

**7** was prepared by combining **2** (15.8 mg, 0.0151 mmol) with CDT (51.6 mg, 0.314 mmol) and allowed to stir for one hour at which time 5-hexyn-1-amine (36.5  $\mu$ L, 29.2 mg, 0.300 mmol) and TEA (50  $\mu$ L) were added and stirred for one hour after which point a second equivalent amount 5-hexyn-1-amine and TEA were added and allowed to stir for one hour to give the target compound, which was purified using RP-HPLC method A1 to produce **7** as an orange solid to 98% purity. Yield 35% (6.0 mg, 0.005 mmol). The product obtained was in the form of two different isomers with the aquo-group located on the alpha and beta positions ( $\alpha$ -cyano- $\beta$ -aqua- and  $\alpha$ -aqua- $\beta$ -cyano-).  $t_R$ : 11.3 and 11.8 min (Figure 21); ESI-MS-expected  $m/z$  = 1157, observed  $m/z$  =  $[M^+-H_2O]^+1$ : 1139,  $[M^+-H_2O+H^+]^{+2}$ : 570 (Figure 22). EAS Ext Coeff<sub>354</sub> = 17,982 M<sup>-1</sup> cm<sup>-1</sup> (Figure 23). <sup>1</sup>H NMR (400 MHz, D<sub>2</sub>O):  $\delta$  6.49 (1H, s, Ar-H,  $\beta$ -aqua isomer) 6.42 (1H, s, Ar-H,  $\alpha$ -aqua isomer) (Figure 24, 25).

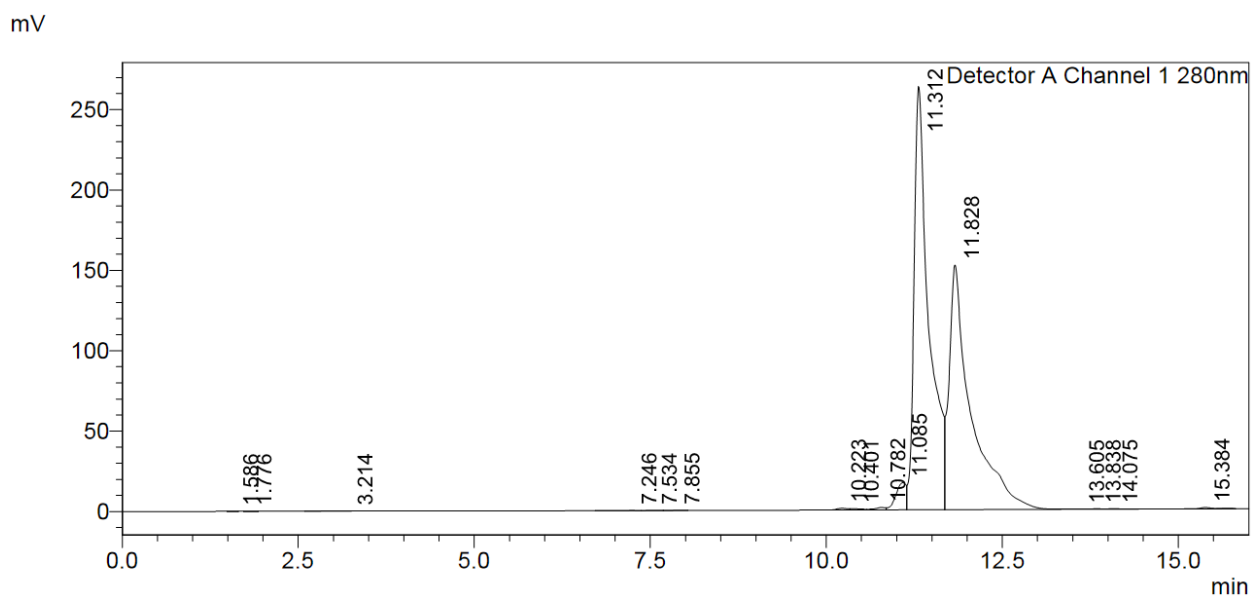


**Figure 21.** RP-HPLC trace showing the  $\alpha$ - and  $\beta$ -isomer products of **7** 11.3 and 11.8 min.

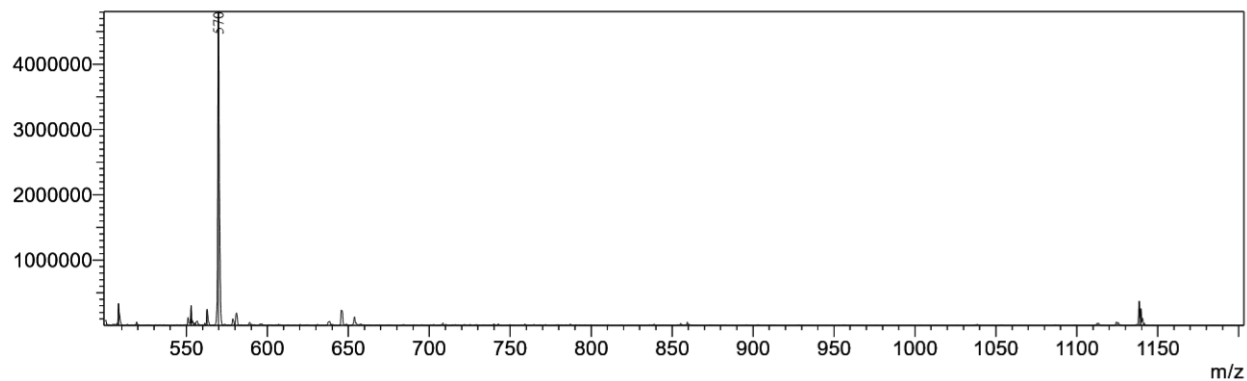


**Figure 22.** ESI-MS of **7**, expected  $m/z = 1157$ , observed  $m/z = [M^+ - H_2O]^{+1}: 1139$ ,  $[M^+ - H_2O + H^+]^{+2}: 570$ .

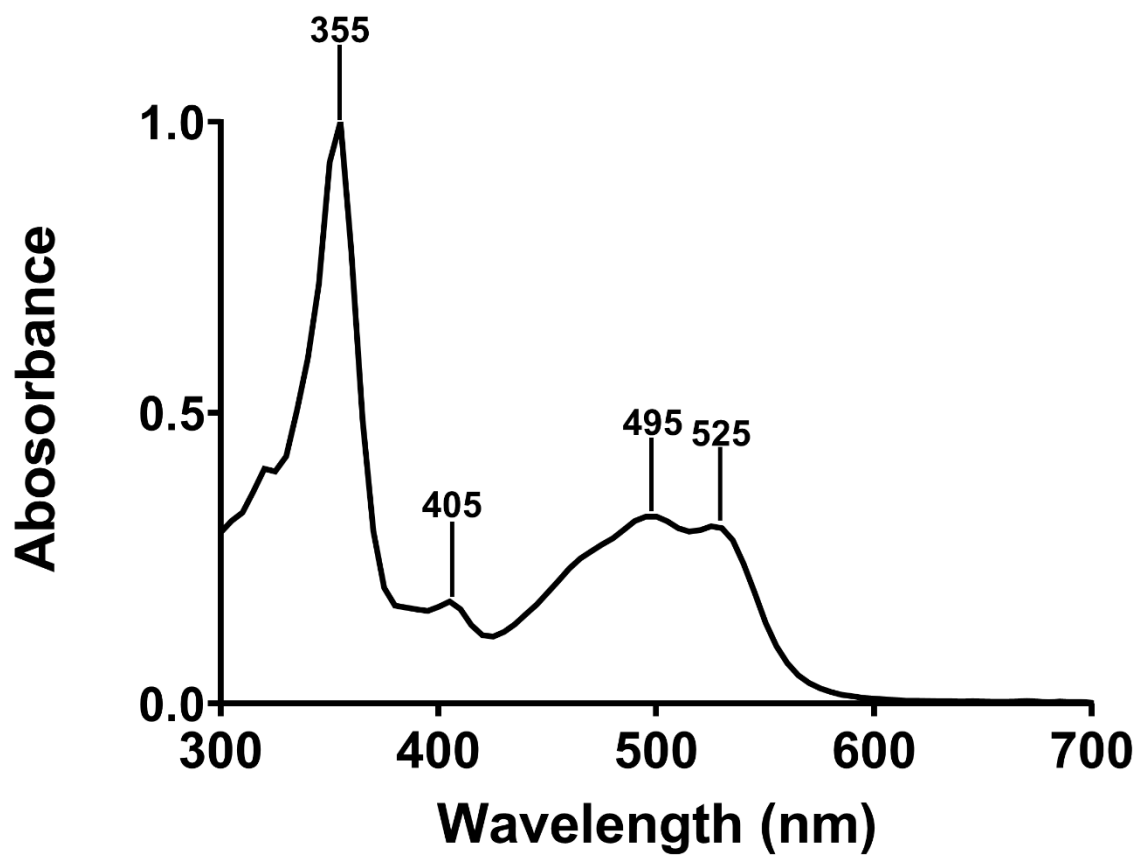


**Figure 23.** Electronic absorption spectra of **7**.

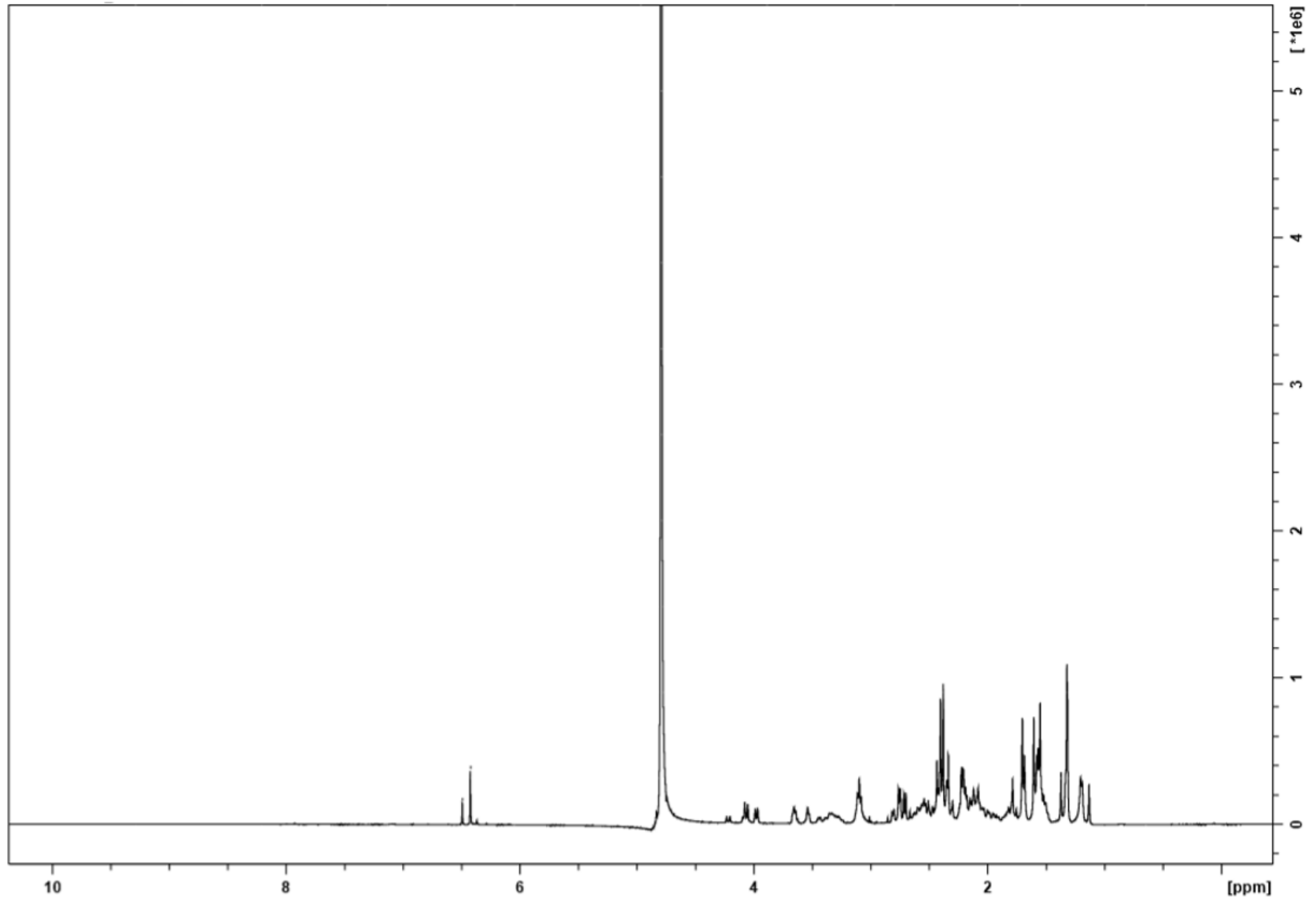


**Figure 24.**  $^1\text{H}$  NMR of **7** (400 MHz, 298K,  $\text{D}_2\text{O}$ ).

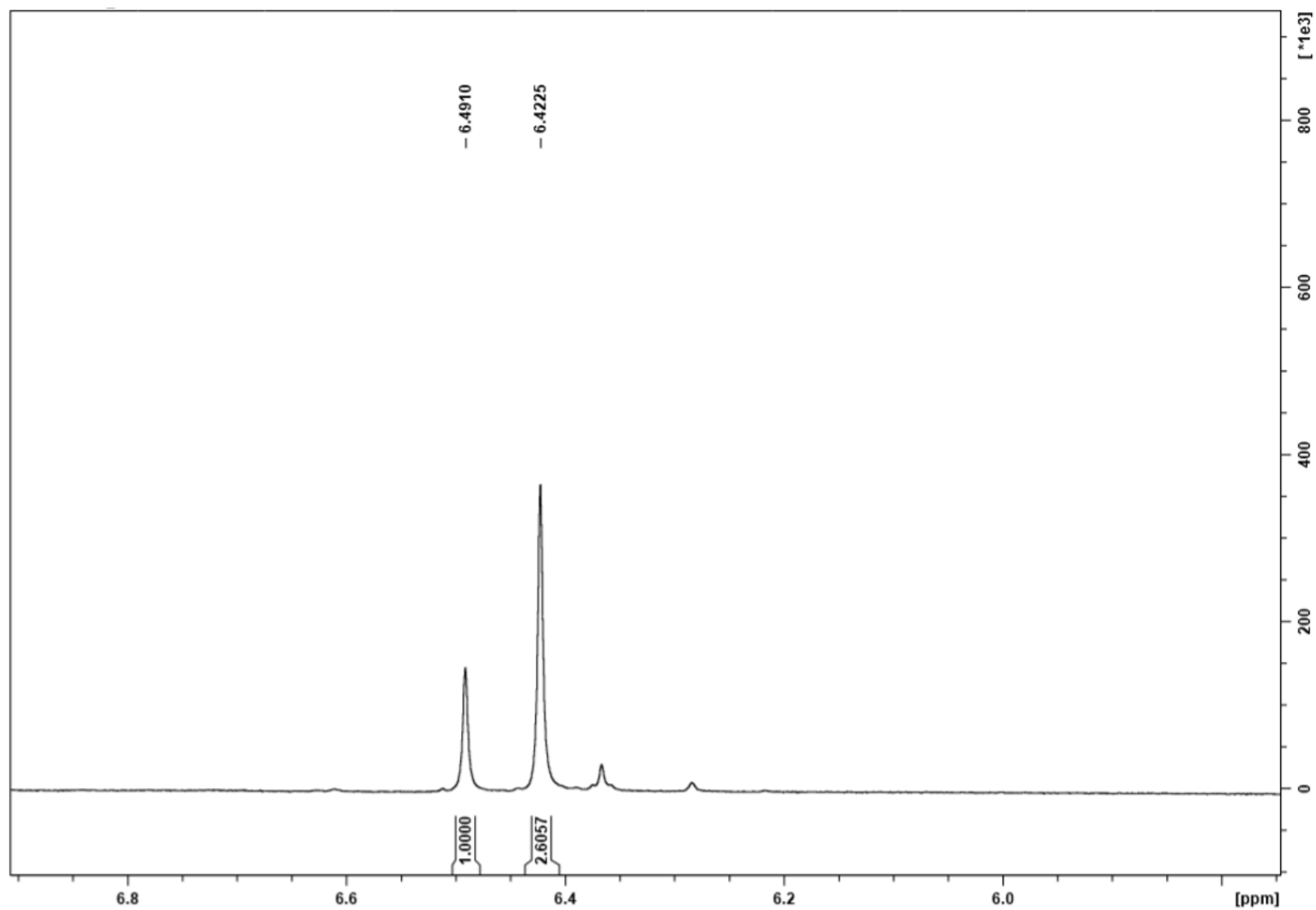


**Figure 25.**  $^1\text{H}$  NMR of **7** (400 MHz, 298K,  $\text{D}_2\text{O}$ ) (Aromatic). Characteristic signals (H19) of  $\beta$ - (6.49) and  $\alpha$ - (6.42) aquo-isomers of **7** are observed.<sup>4</sup>

### 6.6.2.5 Synthesis of Cbi-PEG2 (8)

**8** was prepared by combining **2** (19.9 mg, 0.0191 mmol) with CDT (67.1 mg, 0.409 mmol) and allowed to stir for one hour at which time propargyl-PEG2-amine (25.1  $\mu$ L, 25.4 mg, 0.177 mmol) and TEA (50  $\mu$ L) were added and stirred for one hour after which point a second equivalent amount propargyl-PEG2-amine and TEA were added and allowed to stir for one hour to give the target compound, which was purified using RP-HPLC method A1 to produce **8** as an orange solid to 98% purity. Yield 39% (8.8 mg, 0.007 mmol). The product obtained was in the form of two different isomers with the aquo-group located on the alpha and beta positions ( $\alpha$ -cyano- $\beta$ -aqua- and  $\alpha$ -aqua- $\beta$ -cyano-).  $t_R$ : 18.4 and 19.3 min (Figure 26); ESI-MS-expected  $m/z$  = 1204, observed  $m/z$  =  $[M^+-H_2O]^{+1}$ : 1185,  $[M^+-H_2O+H^+]^{+2}$ : 593 (Figure 27). EAS Ext Coeff<sub>354</sub> = 22,919  $M^{-1} cm^{-1}$  (Figure 28).  $^1H$  NMR (400 MHz,  $D_2O$ ):  $\delta$  6.50 (1H, s, Ar-H,  $\beta$ -aqua isomer) 6.43 (1H, s, Ar-H,  $\alpha$ -aqua isomer) (Figure 29, 30).

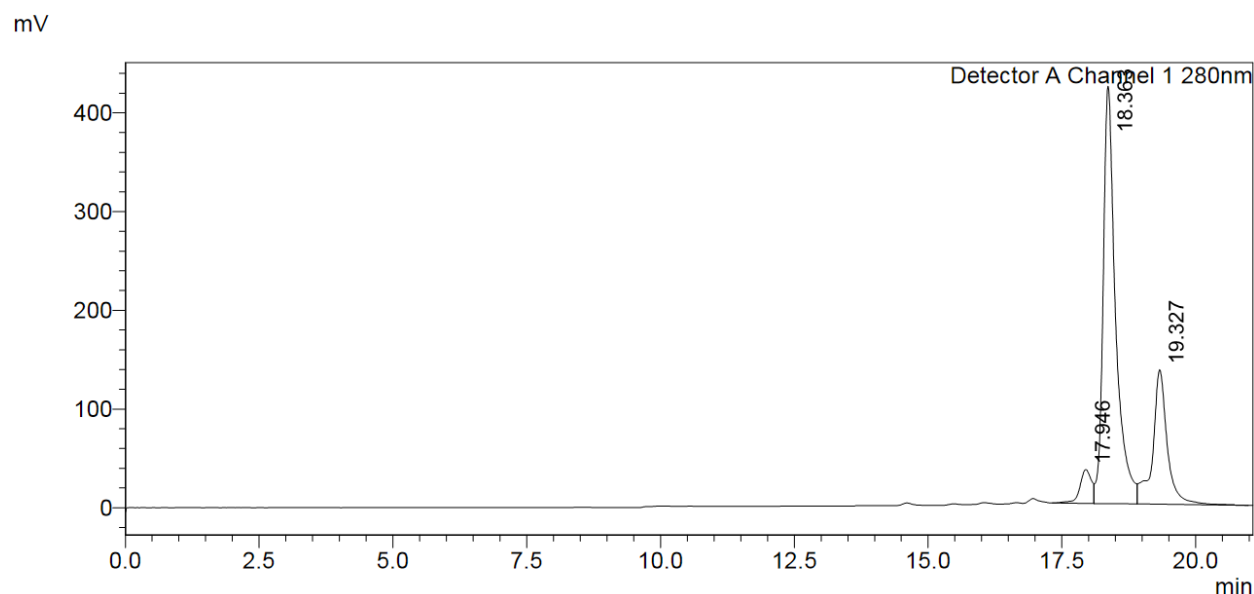


**Figure 26.** RP-HPLC trace showing the  $\alpha$ - and  $\beta$ -isomer products of **8** at 18.4 and 19.3 min.

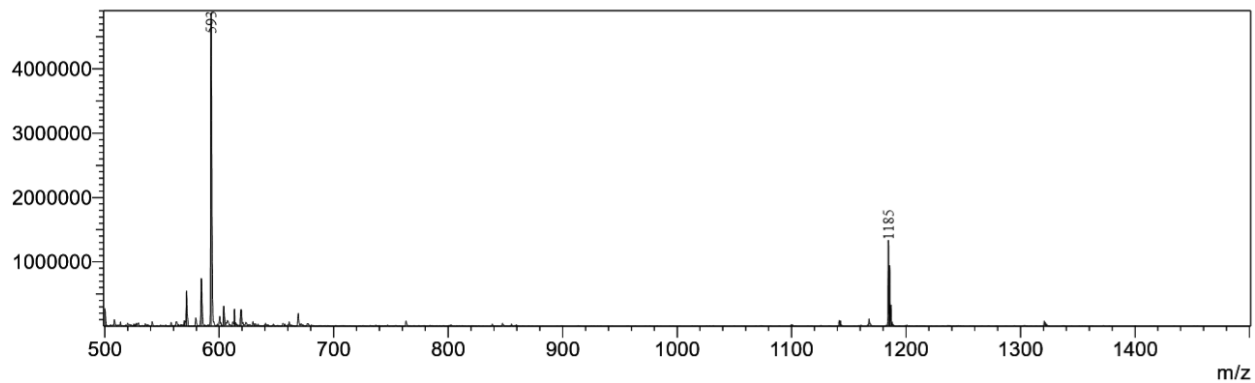


**Figure 27.** ESI-MS of **8**, expected  $m/z = 1204$ , observed  $m/z = [M^+ - H_2O]^{+1}$ : 1185,  $[M^+ - H_2O + H^+]^{+2}$ : 593.

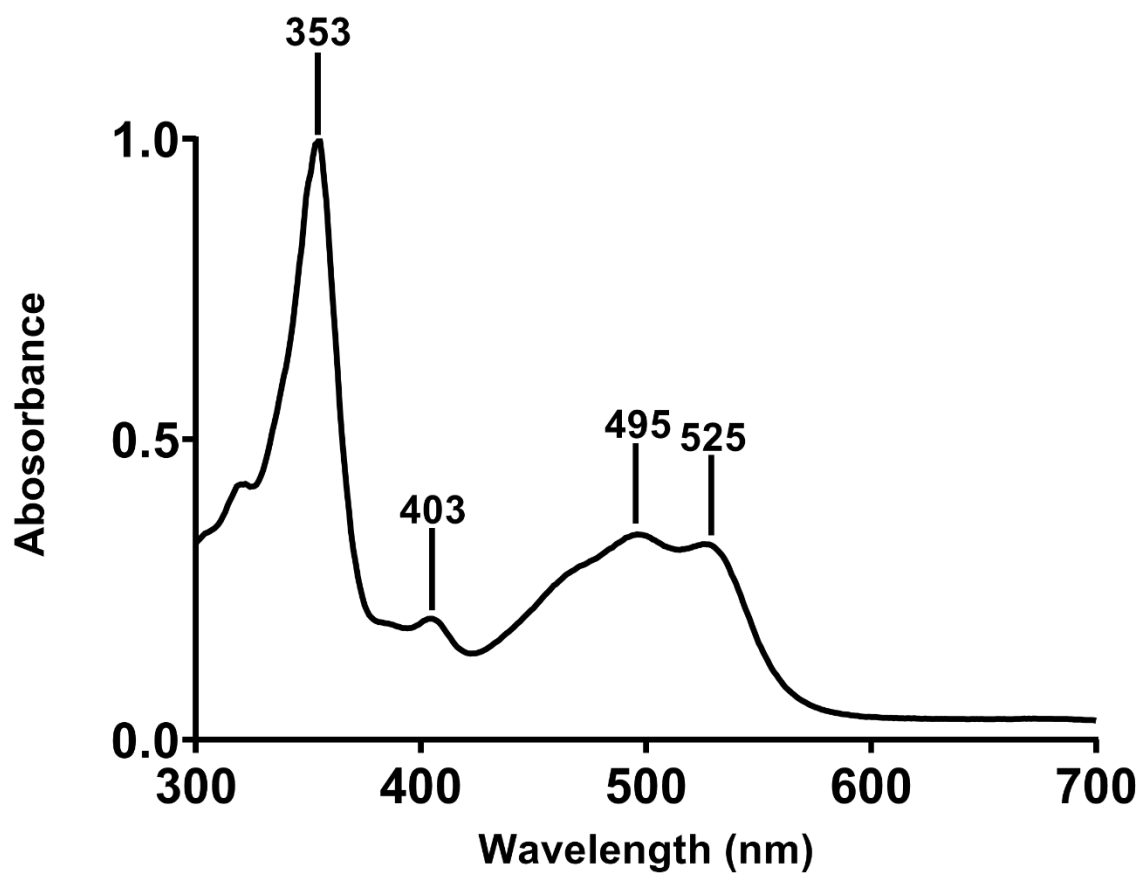


**Figure 28.** Electronic absorption spectra of **8**.

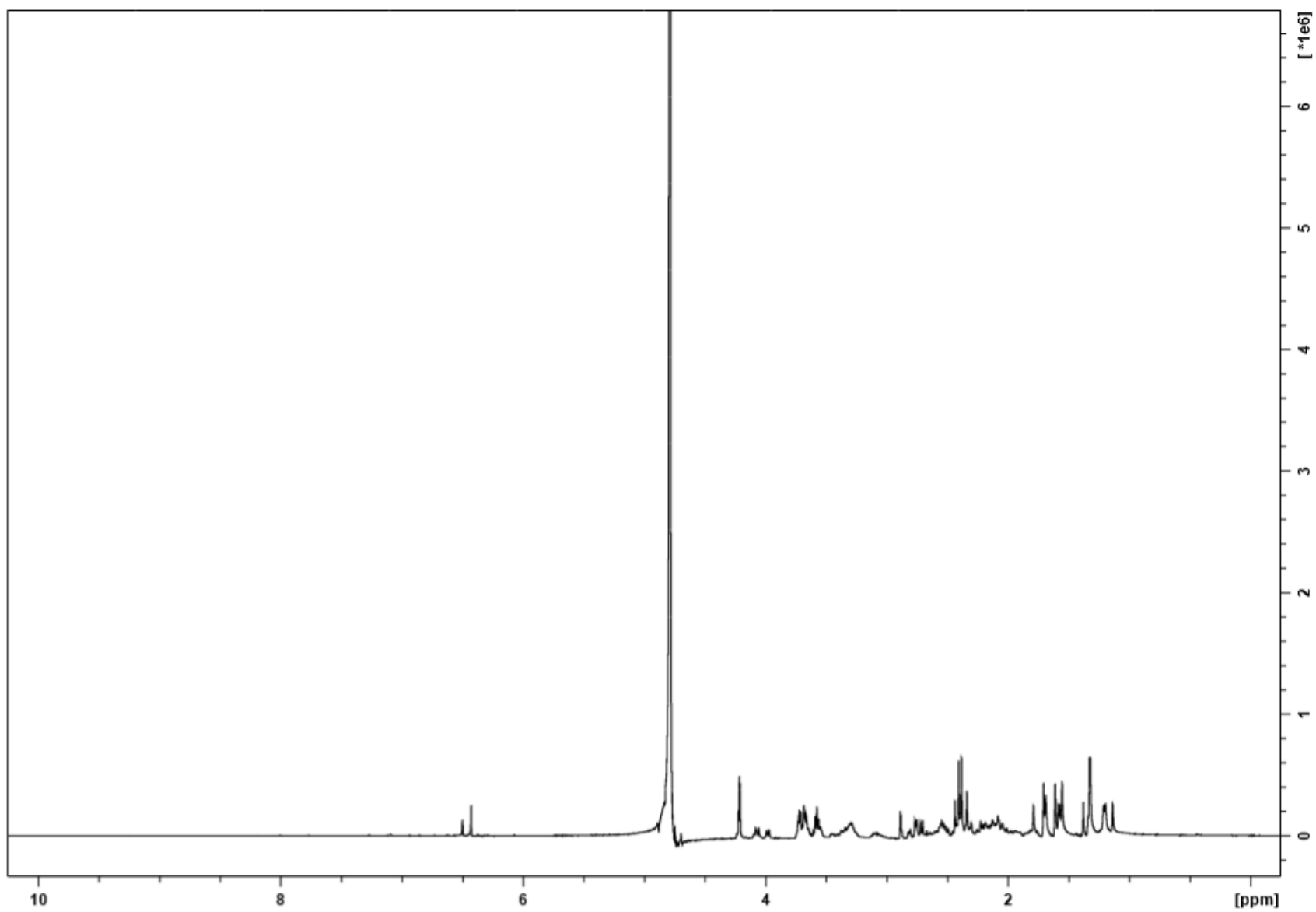
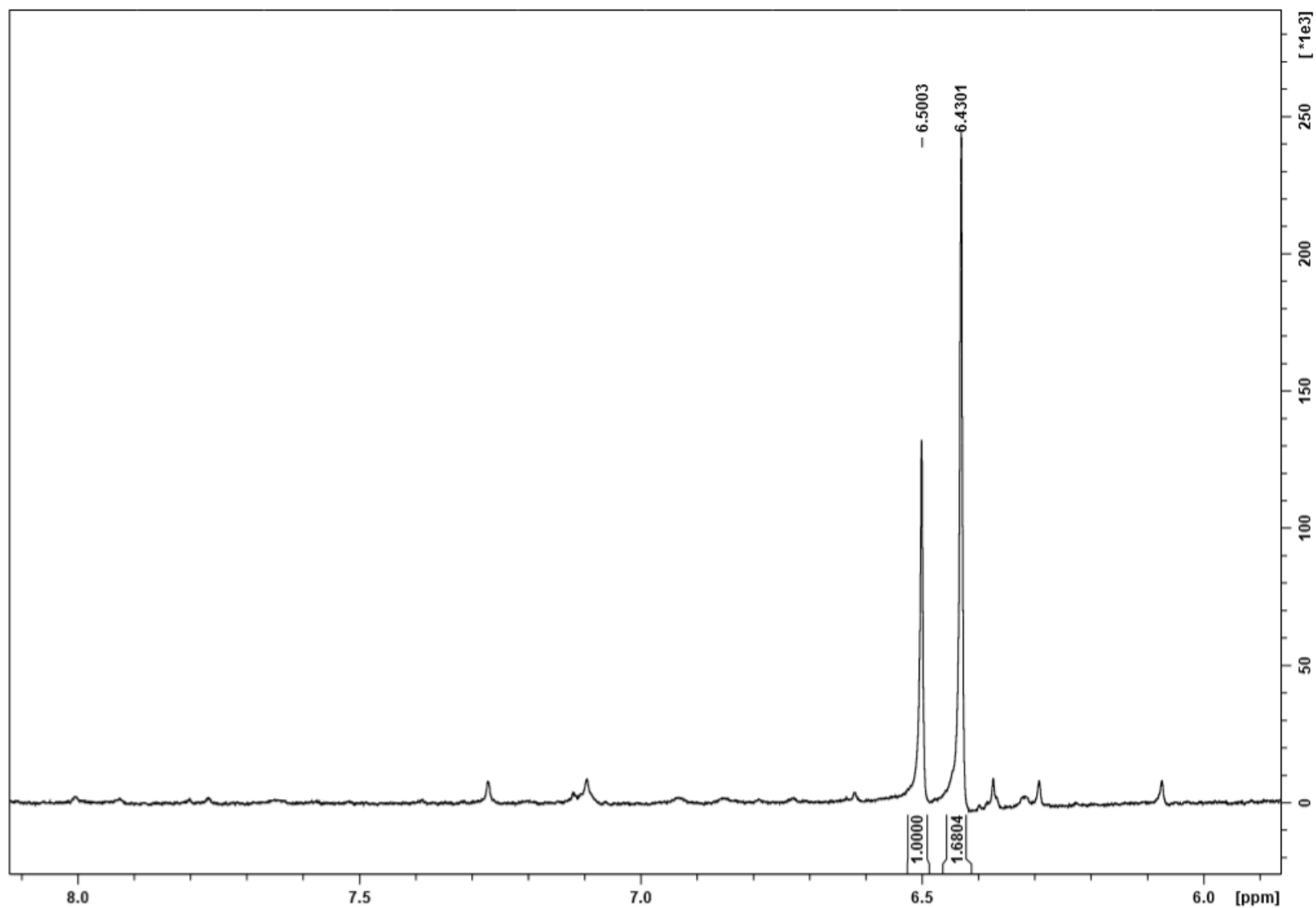


Figure 29.  $^1\text{H}$  NMR of **8** (400 MHz, 298K,  $\text{D}_2\text{O}$ ).





**Figure 30.**  $^1\text{H}$  NMR of **8** (400 MHz, 298K,  $\text{D}_2\text{O}$ ) (Aromatic). Characteristic signals (H19) of  $\beta$ - (6.50) and  $\alpha$ - (6.43) aquo-isomers of **8** are observed.<sup>4</sup>

### 6.6.2.6 Synthesis of Cbi-PEG4 (9)

**9** was prepared by combining **2** (15.5 mg, 0.0149 mmol) with CDT (51.3 mg, 0.313 mmol) and allowed to stir for one hour at which time propargyl-PEG4-amine (18.8  $\mu$ L, 19.5 mg, 0.0843 mmol) and TEA (50  $\mu$ L) were added and stirred for one hour after which point a second equivalent amount propargyl-PEG4-amine and TEA were added and allowed to stir for one hour to give the target compound which was purified using RP-HPLC method A1 to produce **9** as an orange solid to 97% purity. Yield 32% (6.1 mg, 0.005 mmol). The product obtained was in the form of two different isomers with the aquo-group located on the alpha and beta positions ( $\alpha$ -cyano- $\beta$ -aqua- and  $\alpha$ -aqua- $\beta$ -cyano-).  $t_R$ : 20.0 and 21.8 min (Figure 31); ESI-MS-expected  $m/z$  = 1292, observed  $m/z$  =  $[M^+-H_2O]^+1$ : 1273,  $[M^+-H_2O+H^+]^{+2}$ : 637 (Figure 32). EAS Ext Coeff<sub>354</sub> = 19,439  $M^{-1} cm^{-1}$  (Figure 33).  $^1H$  NMR (400 MHz,  $D_2O$ ):  $\delta$  6.50 (1H, s, Ar-H,  $\beta$ -aqua isomer) 6.43 (1H, s, Ar-H,  $\alpha$ -aqua isomer) (Figure 34, 35).

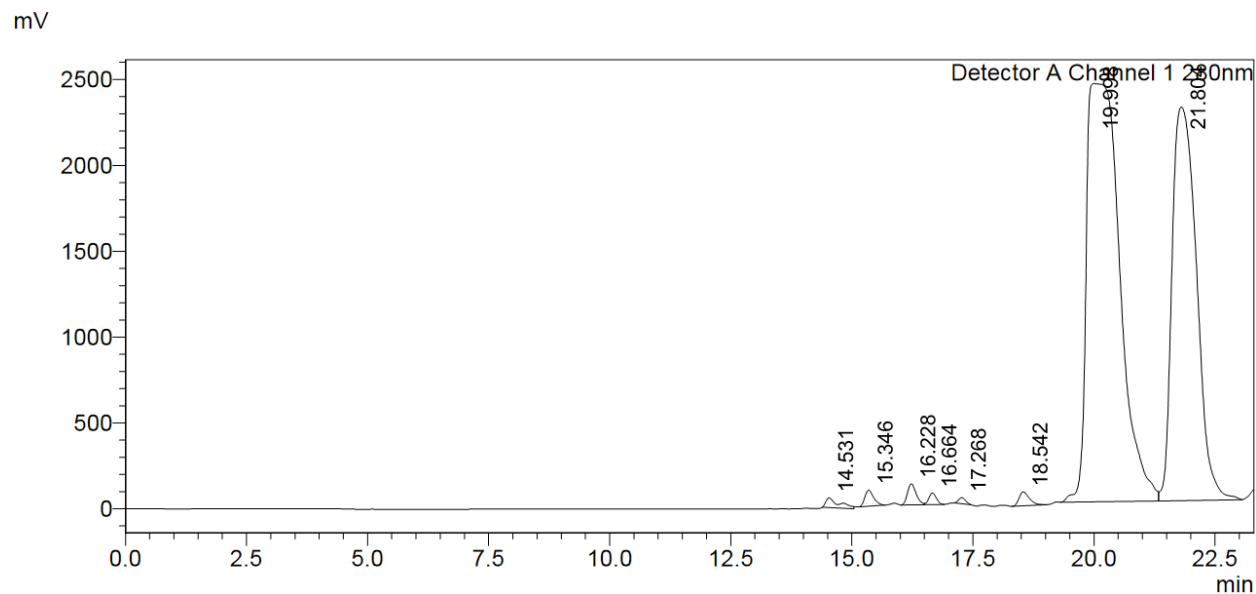


**Figure 31.** RP-HPLC trace showing the  $\alpha$ - and  $\beta$ -isomer products of **9** at 20.0 and 21.8 min.

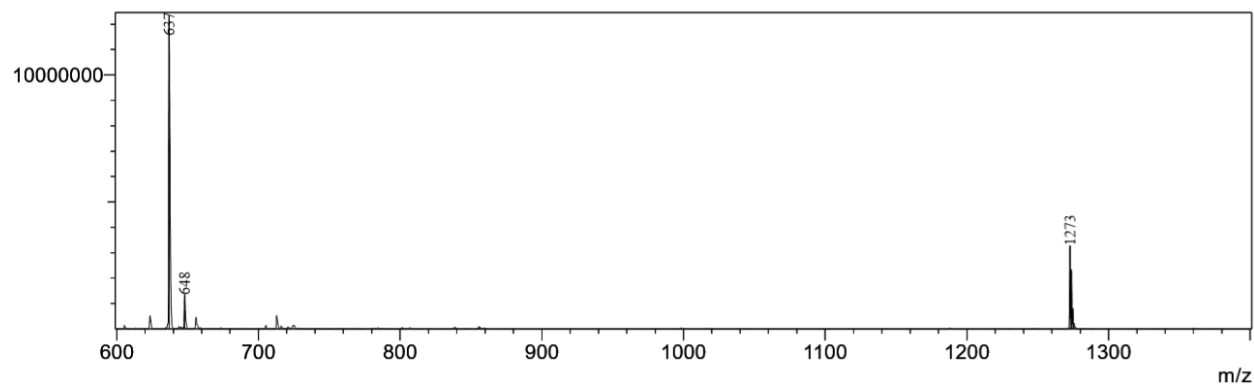


**Figure 32.** ESI-MS of **9**, expected  $m/z = 1292$ , observed  $m/z = [M^+ - H_2O]^{+1}: 1273$ ,  $[M^+ - H_2O + H^+]^{+2}: 637$ .

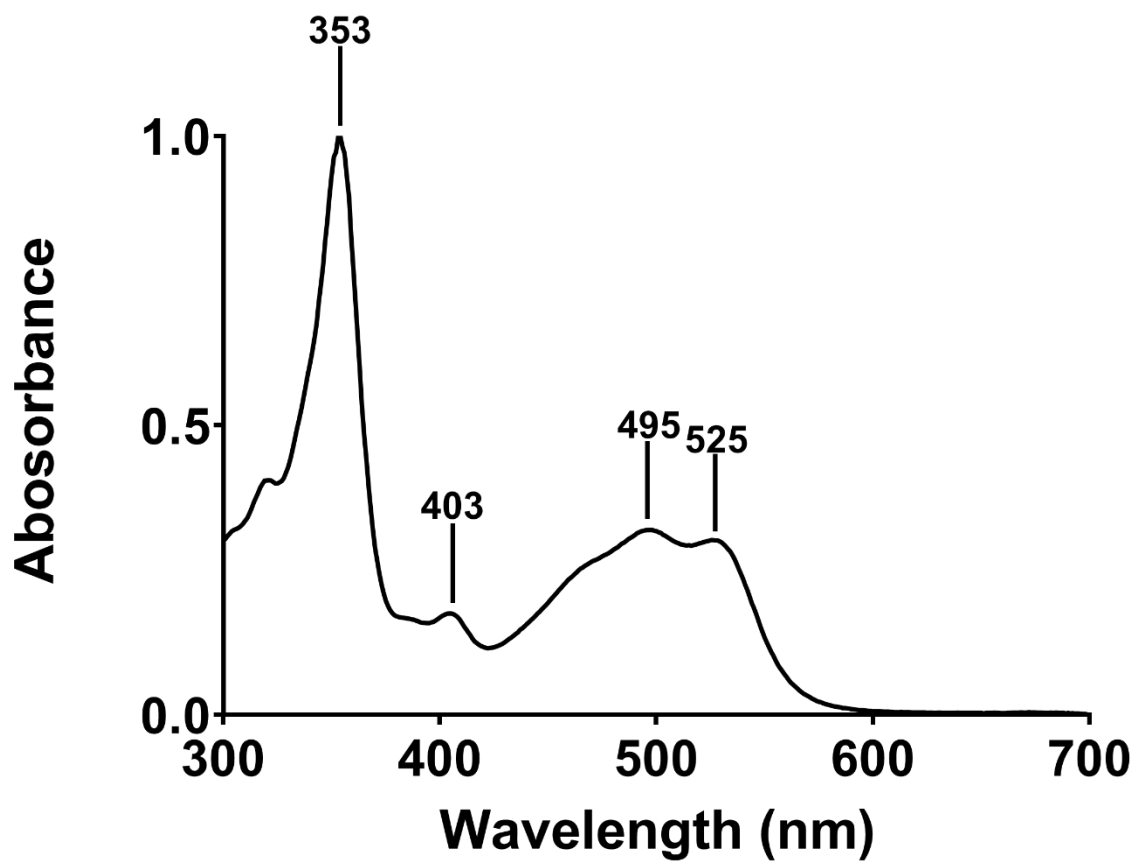


**Figure 33.** Electronic absorption spectra of **9**.

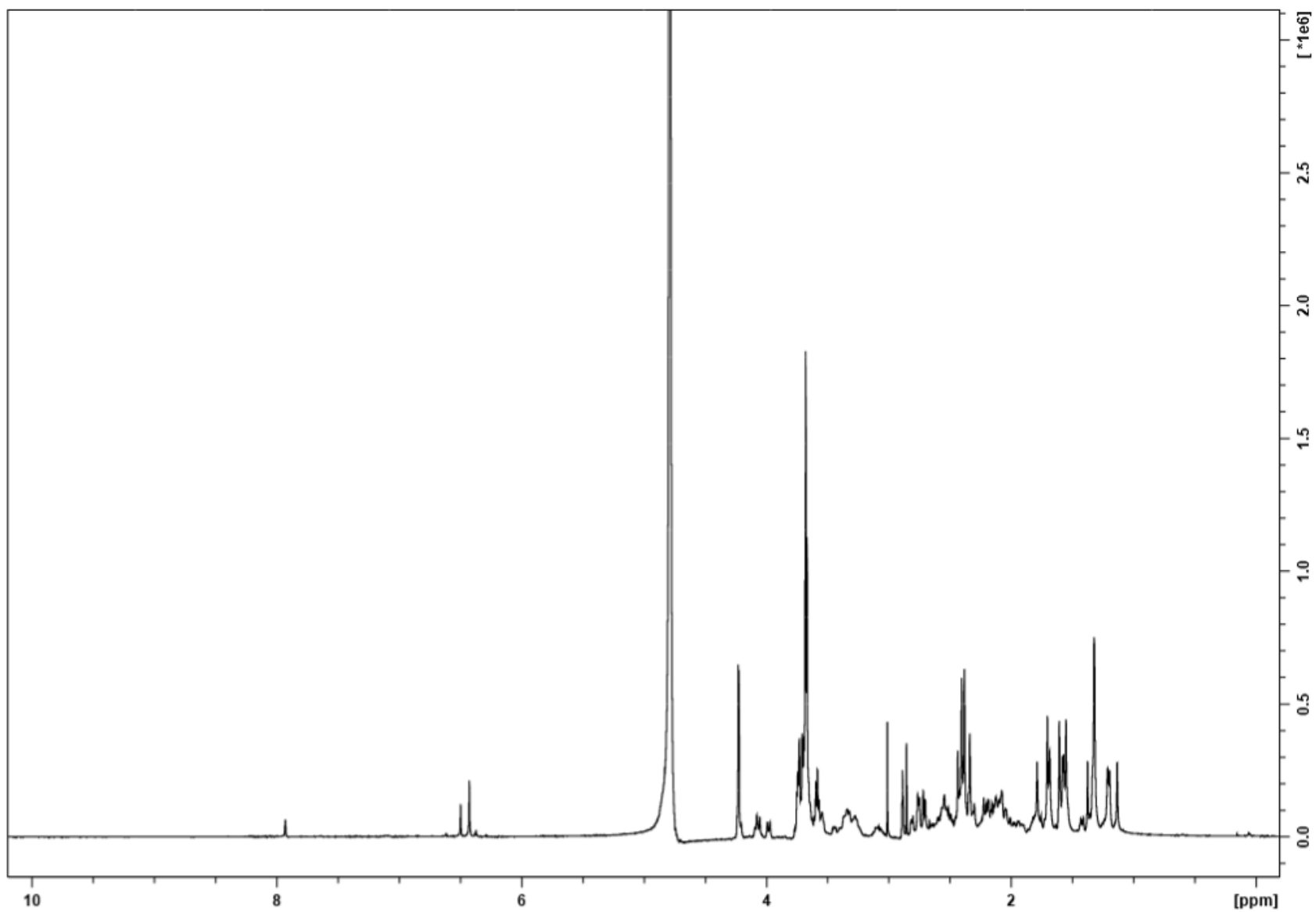


**Figure 34.**  $^1\text{H}$  NMR of **9** (400 MHz, 298K,  $\text{D}_2\text{O}$ ).

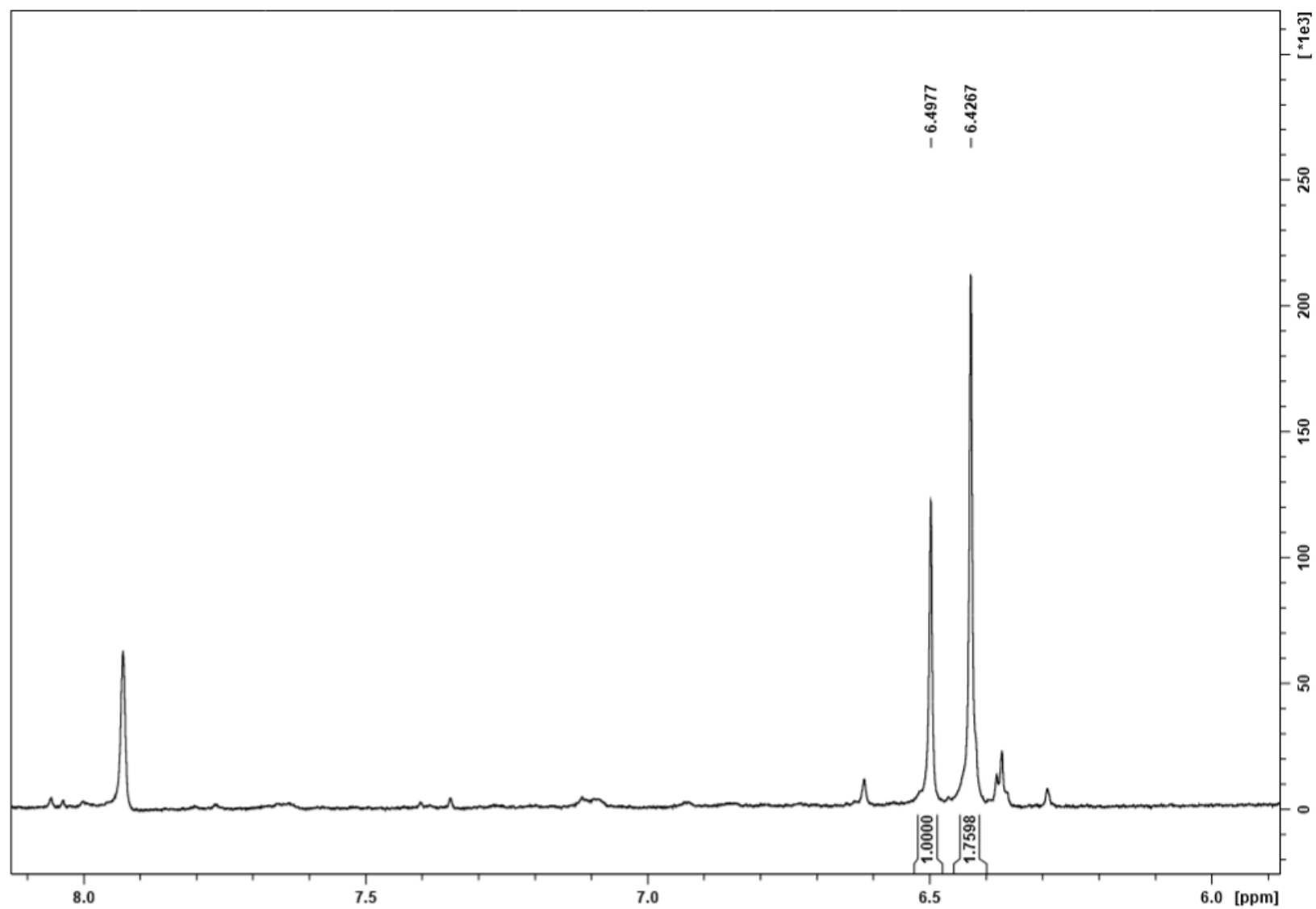


**Figure 35.**  $^1\text{H}$  NMR of **9** (400 MHz, 298K,  $\text{D}_2\text{O}$ ) (Aromatic). Characteristic signals (H19) of  $\beta$ - (6.50) and  $\alpha$ - (6.43) aquo-isomers of **9** are observed.<sup>4</sup>

### 6.6.2.7 Synthesis of Cbi-4EPMA (10)

**10** was prepared by combining **2** (14.9 mg, 0.0143 mmol) with CDT (50.1 mg, 0.305 mmol) and allowed to stir for one hour at which time (4-ethynylphenyl)methanamine (23.8 mg, 0.181 mmol) and TEA (50  $\mu$ L) were added and stirred for one hour after which point a second equivalent amount (4-ethynylphenyl)methanamine and TEA were added and allowed to stir for one hour to give the target compound, which was purified using RP-HPLC method A1 to produce **10** as an orange solid to 97% purity. Yield 10% (1.5 mg, 0.001 mmol). The product obtained was in the form of two different isomers with the aquo-group located on the alpha and beta positions ( $\alpha$ -cyano- $\beta$ -aqua- and  $\alpha$ -aqua- $\beta$ -cyano-).  $t_R$ : 12.4 and 12.8 min (Figure 36); ESI-MS-expected  $m/z$  = 1191, observed  $m/z$  =  $[M^+ - H_2O]^{+1}$ : 1173 (Figure 37). EAS Ext Coeff<sub>354</sub> = 15,886  $M^{-1} cm^{-1}$  (Figure 38).  $^1H$  NMR (400 MHz,  $D_2O$ ):  $\delta$  6.49 (1H, s, Ar-H,  $\beta$ -aqua isomer) 6.43 (1H, s, Ar-H,  $\alpha$ -aqua isomer) (Figure 39, 40).

mV

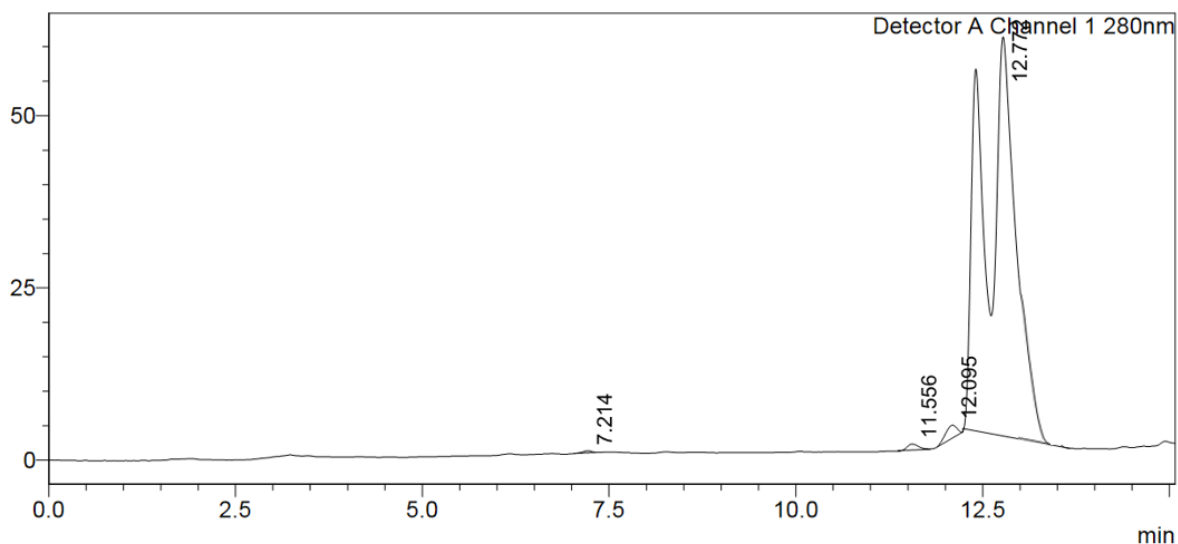


**Figure 36.** RP-HPLC trace showing the  $\alpha$ - and  $\beta$ - isomer products of **10** at 12.4 and 12.8 min.

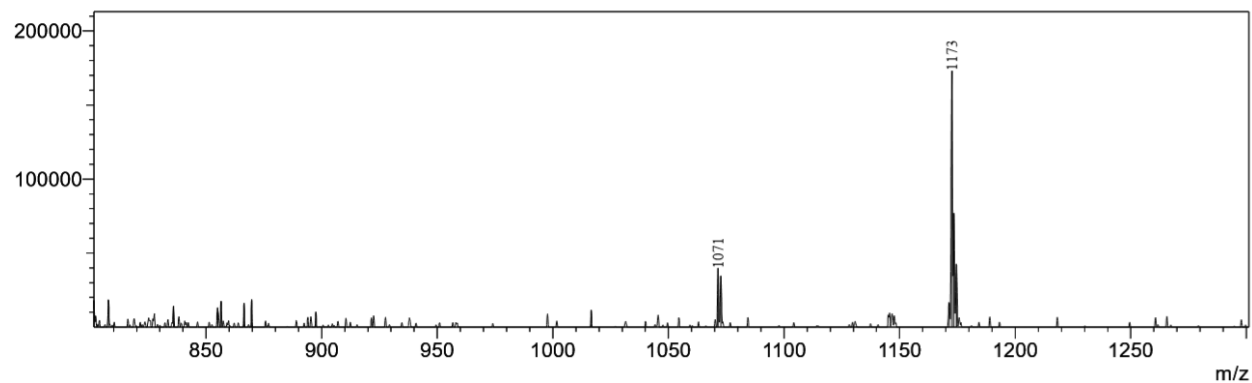


Figure 37. ESI-MS of **10**, expected  $m/z = 1191$ , observed  $m/z = [M^+ - H_2O]^{+1}$ : 1173.

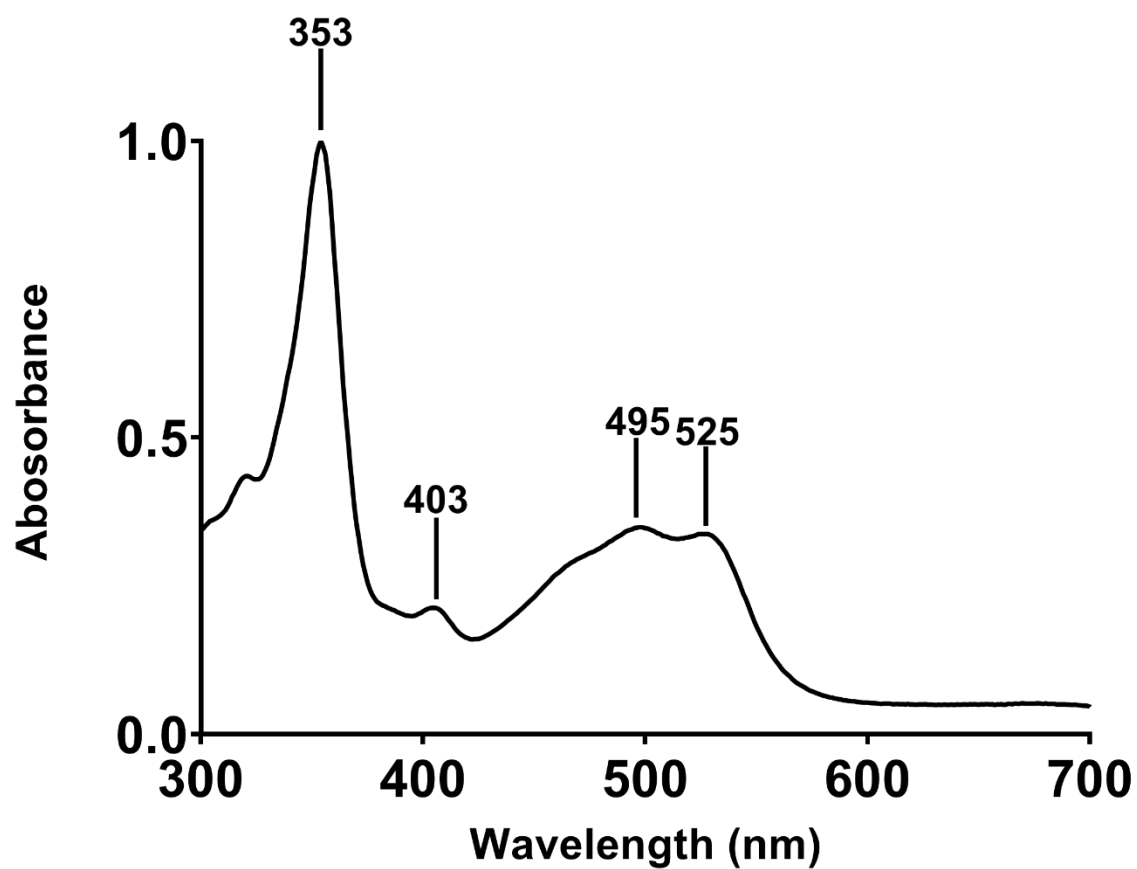


Figure 38. Electronic absorption spectra of **10**.

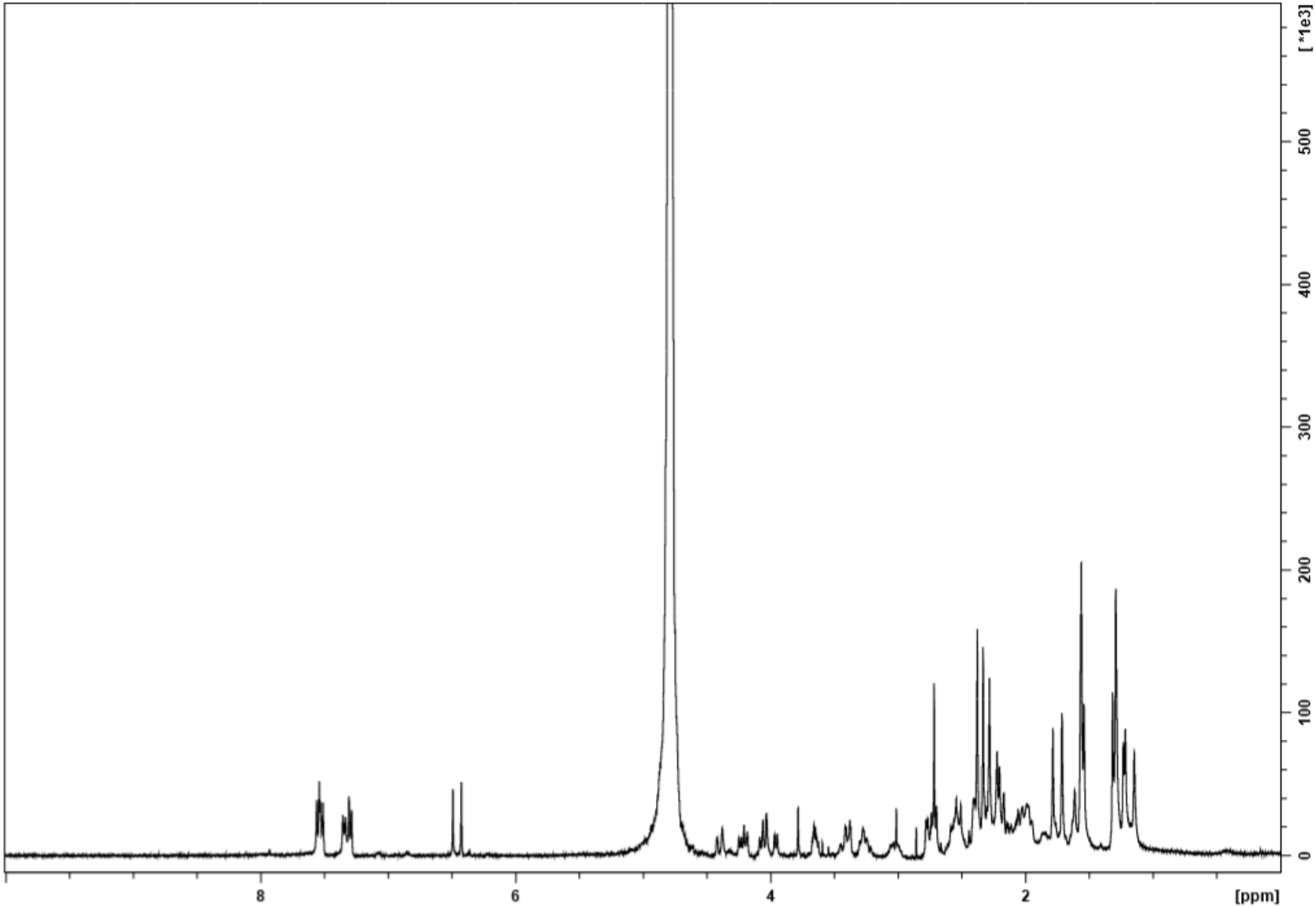
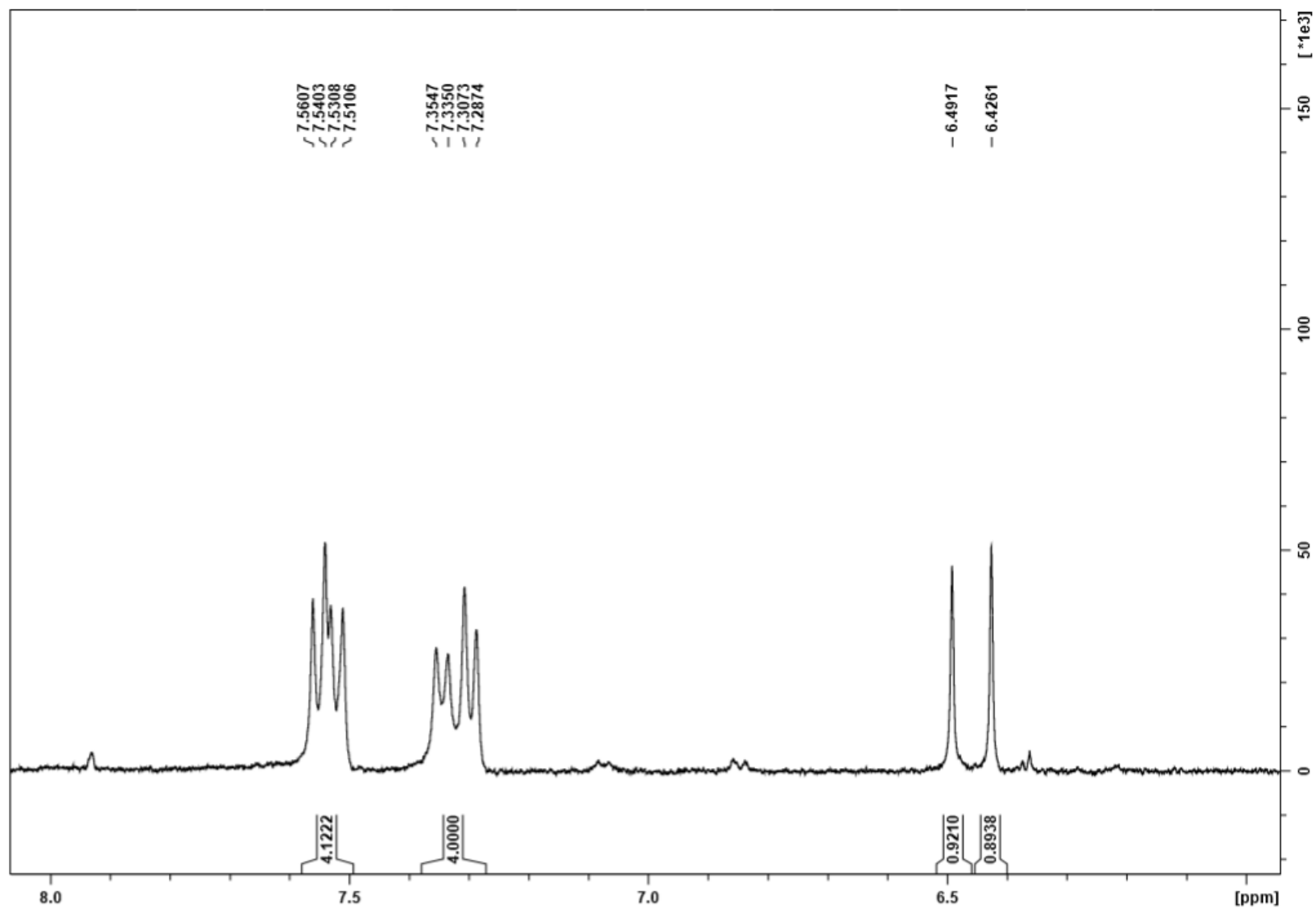


Figure 39. <sup>1</sup>H NMR of **10** (400 MHz, 298K, D<sub>2</sub>O).





**Figure 40.** <sup>1</sup>H NMR of **10** (400 MHz, 298K, D<sub>2</sub>O) (Aromatic). Characteristic Signals (H<sub>19</sub>) of  $\beta$ - (6.49) and  $\alpha$ - (6.43) aquo-isomers of **10** are observed.<sup>4</sup> Additional peak groupings between 7.56-7.51 and 7.35-7.28 are indicative of the phenyl ring linker.

### 6.6.2.8 Synthesis of Cbi-3EPMA (11)

**11** was prepared by combining **2** (15.7 mg, 0.0151 mmol) with CDT (51.1 mg, 0.311 mmol) and allowed to stir for one hour at which time (3-ethynylphenyl)methanamine (21.0  $\mu$ L, 21.2 mg, 0.162 mmol) and TEA (50  $\mu$ L) were added and stirred for one hour after which point a second equivalent amount (3-ethynylphenyl)methanamine and TEA were added and allowed to stir for one hour to give the target compound, which was purified using RP-HPLC method A1 to produce **11** as an orange solid to 97% purity. Yield 14% (2.6 mg, 0.002 mmol). The product obtained was in the form of two different isomers with the aquo-group located on the alpha and beta positions ( $\alpha$ -cyano- $\beta$ -aqua- and  $\alpha$ -aqua- $\beta$ -cyano-).  $t_R$ : 12.6 and 13.0 min (Figure 41); ESI-MS-expected  $m/z$  = 1191, observed  $m/z$  =  $[M^+ - H_2O]^{+1}$ : 1172,  $[M^+ - H_2O + H^+]^{+2}$ : 587 (Figure 42). EAS Ext Coeff<sub>354</sub> = 15,669  $M^{-1} cm^{-1}$  (Figure 43).  $^1H$  NMR (400 MHz,  $D_2O$ ):  $\delta$  6.49 (1H, s, Ar-H,  $\beta$ -aqua isomer) 6.42 (1H, s, Ar-H,  $\alpha$ -aqua isomer) (Figure 44, 45).

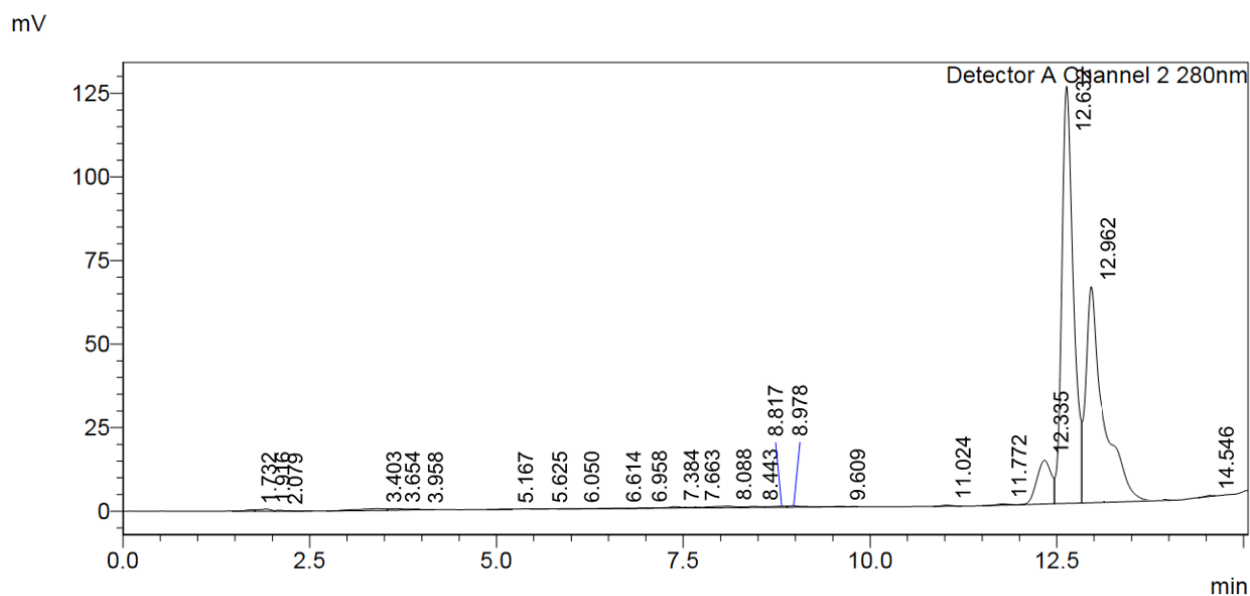


**Figure 41.** RP-HPLC trace showing the  $\alpha$ - and  $\beta$ - isomer products of **11** at 12.6 and 13.0 min.

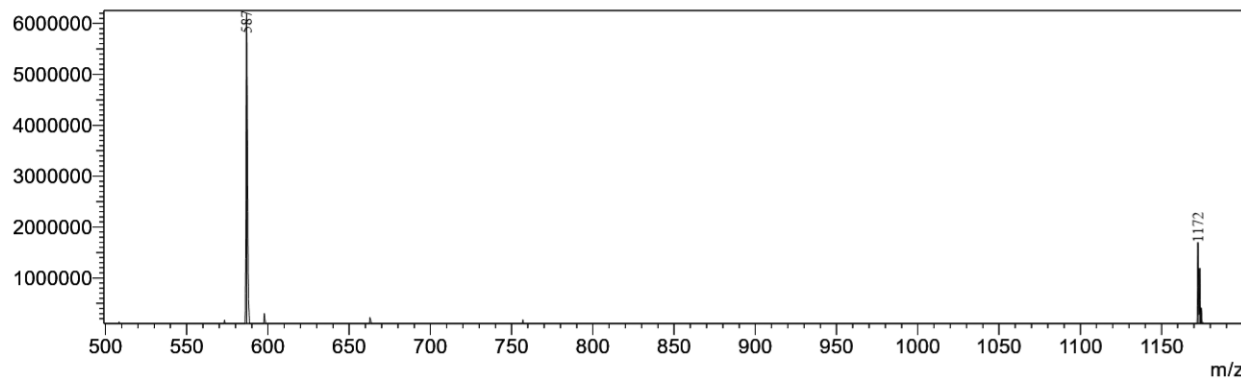


**Figure 42.** ESI-MS of **11**, expected  $m/z = 1191$ , observed  $m/z = [M^+ - H_2O]^{+1}: 1172$ ,  $[M^+ - H_2O + H^+]^{+2}: 587$ .

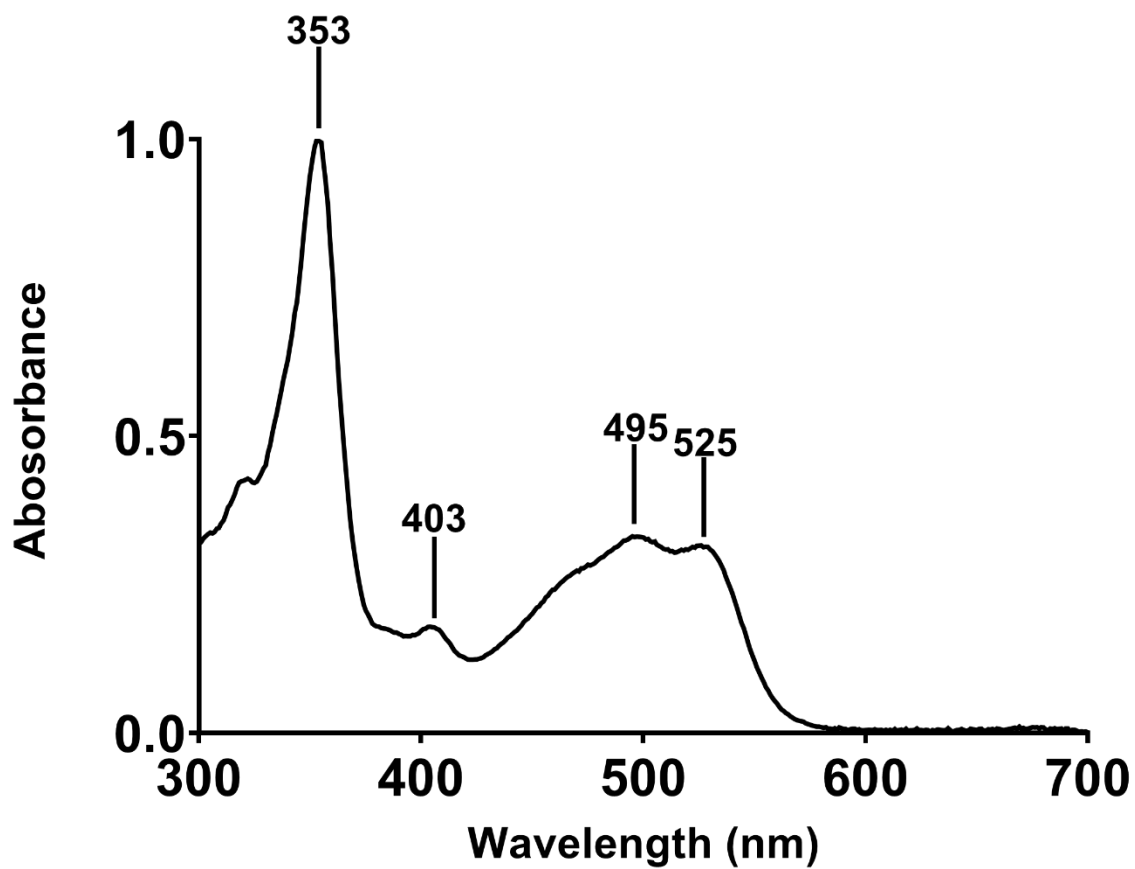


**Figure 43.** Electronic absorption spectra of **11**.

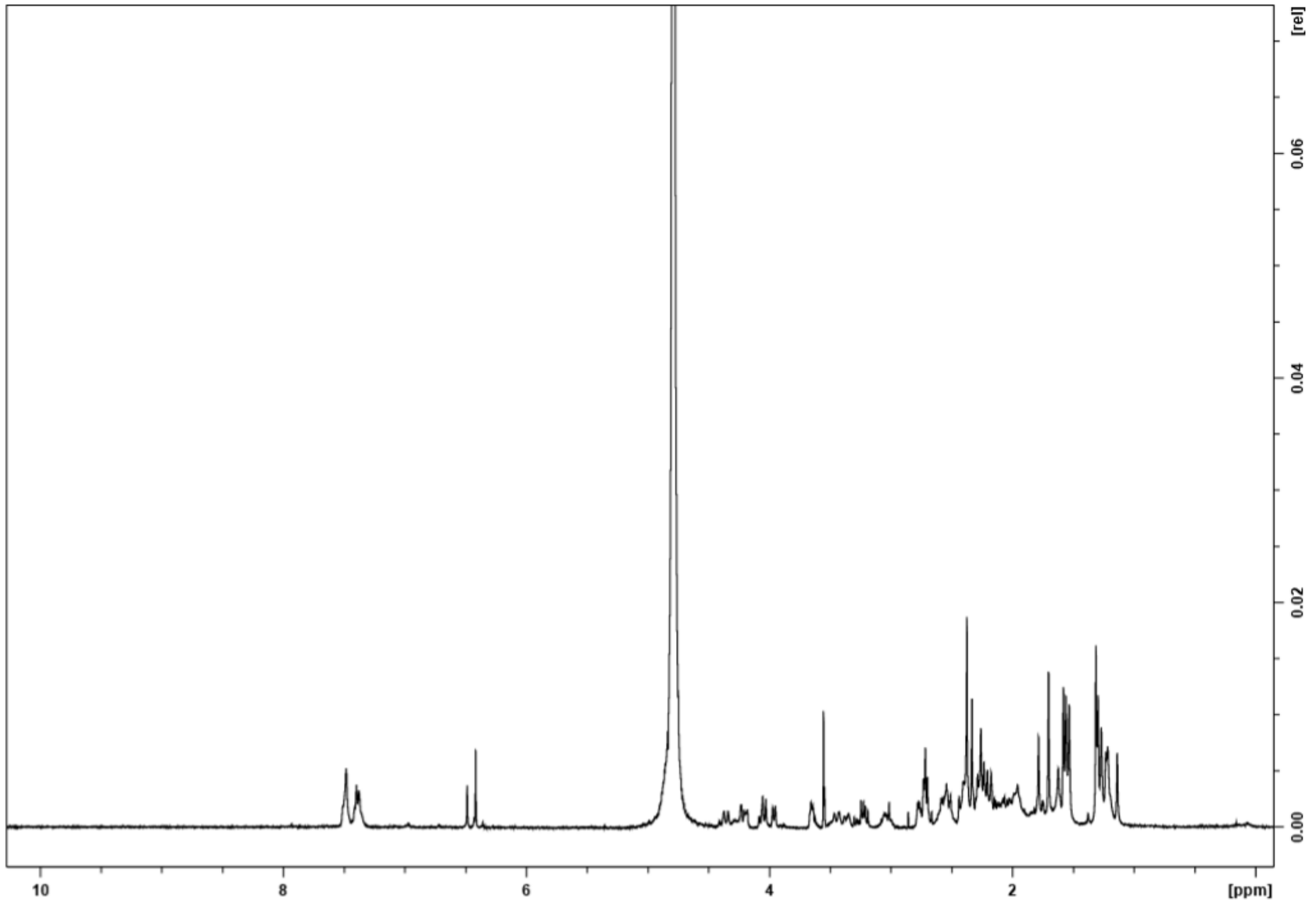


**Figure 44.**  $^1\text{H}$  NMR of **11**. (400 MHz, 298K,  $\text{D}_2\text{O}$ ).

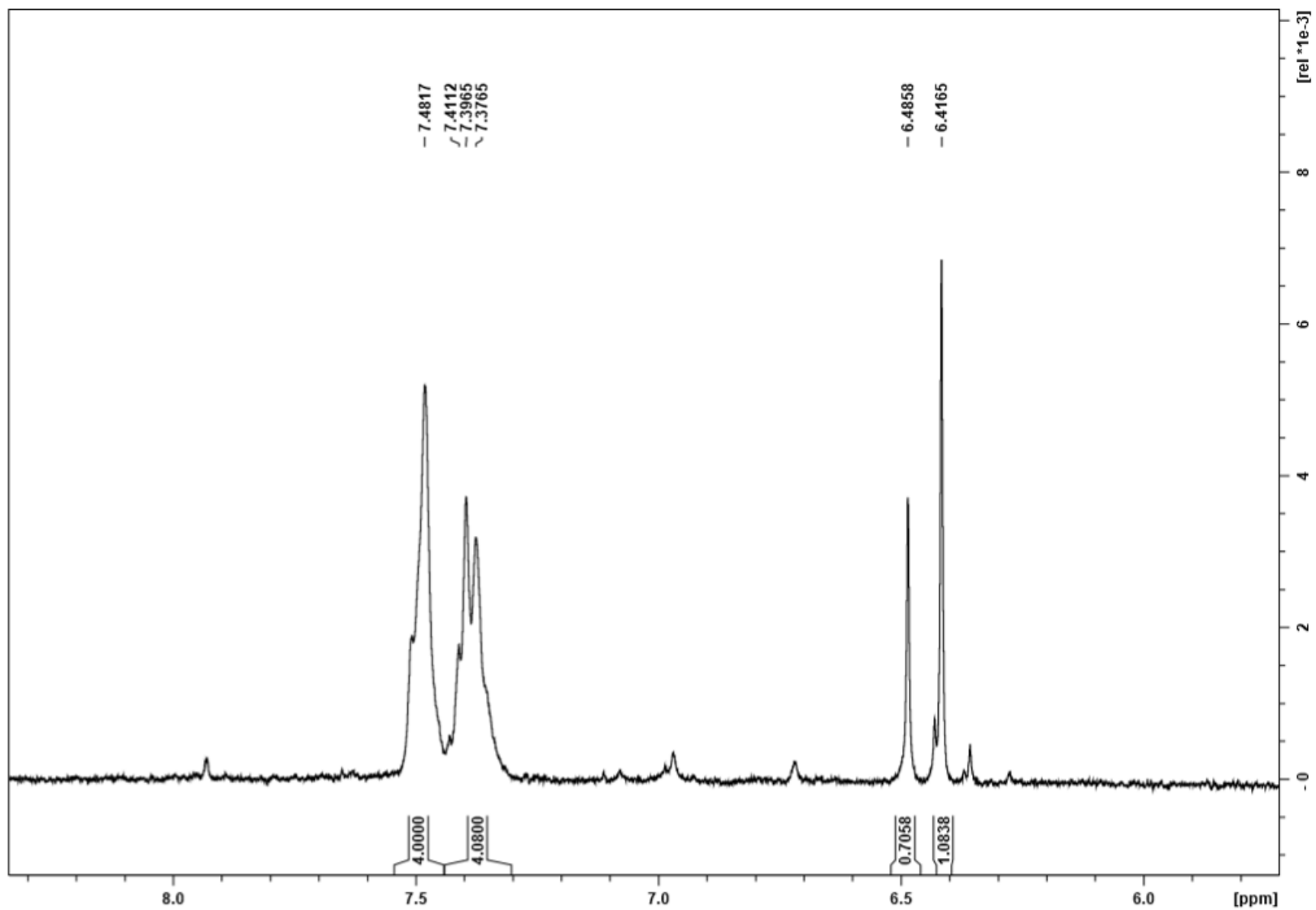


**Figure 45.**  $^1\text{H}$  NMR of **11**. (400 MHz, 298K,  $\text{D}_2\text{O}$ ) (Aromatic). Characteristic signals (H19) of  $\beta$ - (6.49) and  $\alpha$ - (6.42) aquo-isomers of **11** are observed.<sup>4</sup> Additional peak groupings between 7.48-7.37 are indicative of the phenyl ring linker.

### 6.6.2.9 Synthesis of Cbi-Pro-Ex4 (**12**)

**12** was prepared by combining **4** (1.1 mg, 0.001 mmol) with CuI (4.0 mg, 0.021 mmol), TBTA (7.5 mg, 0.014 mmol), and Ex4 (3.1 mg 0.0007 mmol) gave the target compound, which was purified using RP-HPLC method A2 to produce **12** as a red solid to 98% purity.  $t_R$ : 11.7 min (Figure 46); ESI-MS-expected  $m/z = 5327$ , observed  $m/z = [M^+ - H_2O + 2H^+]^{+3}$ : 1771,  $[M^+ - H_2O + 3H^+]^{+4}$ : 1328 (Figure 47). *In vitro* function of **10** was determined in GLP-1R stably transfected HEK-293-H188 c20 cells (Figure 48).

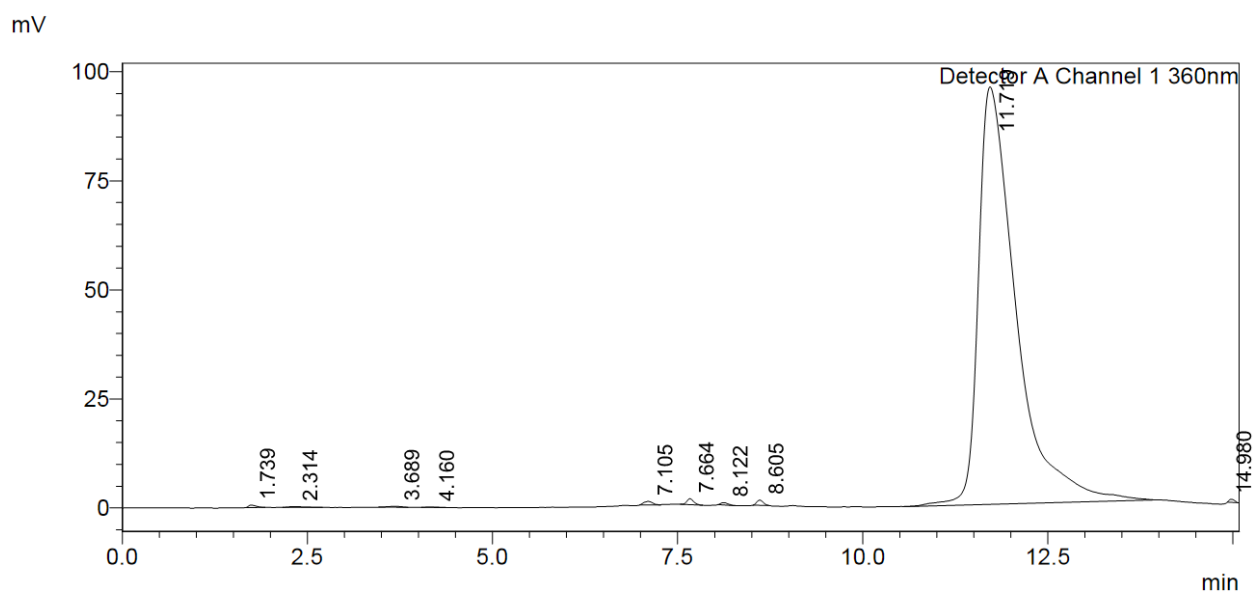


**Figure 46.** RP-HPLC trace showing product **12** at 11.7 min.

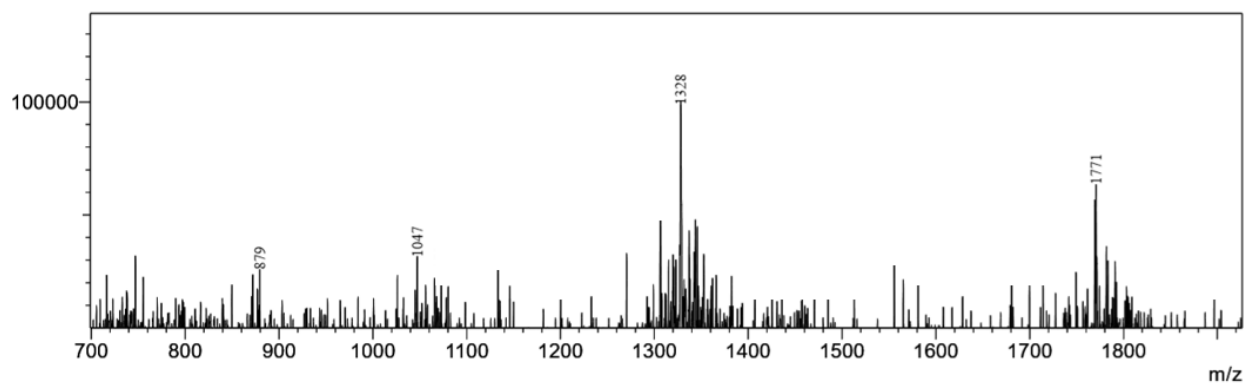


**Figure 47.** ESI-MS of **12**, expected  $m/z = 5327$ , observed  $m/z = [M^+ - H_2O + 2H^+]^{+3}$ : 1771,  $[M^+ - H_2O + 3H^+]^{+4}$ : 1328.

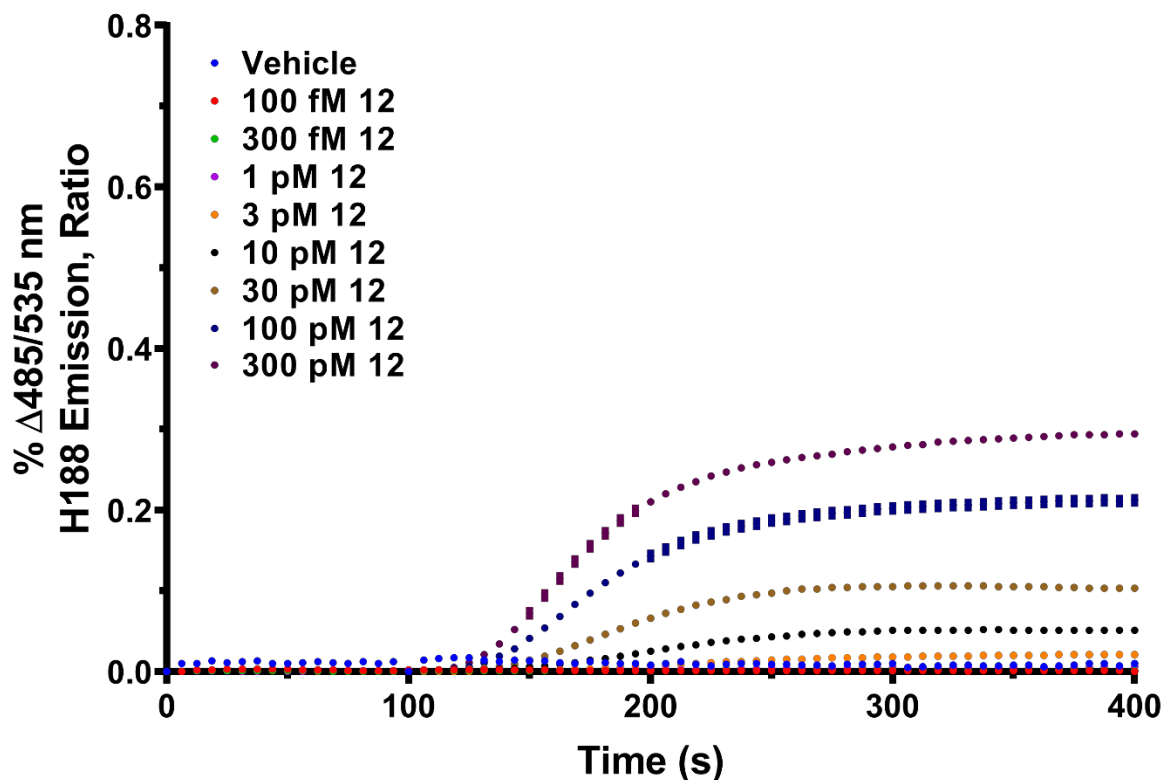


**Figure 48.** *In vitro* dose escalation study of **12** showing increase in cAMP levels in GLP-1R stably transfected HEK-293-H188 c20 cells.

#### 6.6.2.10 Synthesis of Cbi-But-Ex4 (**13**)

**13** was prepared by combining **5** (5.7 mg, 0.005 mmol) with CuI (4.2 mg, 0.022 mmol), TBTA (7.5 mg, 0.014 mmol), and Ex4 (4.2 mg 0.0010 mmol) gave the target compound, which was purified using RP-HPLC method A2 to produce **13** as a red solid to 98% purity.  $t_R$ : 12.0 min (Figure 49); ESI-MS-expected  $m/z = 5341$ , observed  $m/z = [M^+ - H_2O + 2H^+]^{+3}$ : 1775,  $[M^+ - H_2O + 3H^+ + CH_3OH]^{+4}$ : 1364,  $[M^+ - H_2O + 3H^+]^{+4}$ : 1332 (Figure 50). *In vitro* function of **13** was determined in GLP-1R stably transfected HEK-293-H188 c20 cells (Figure 51).

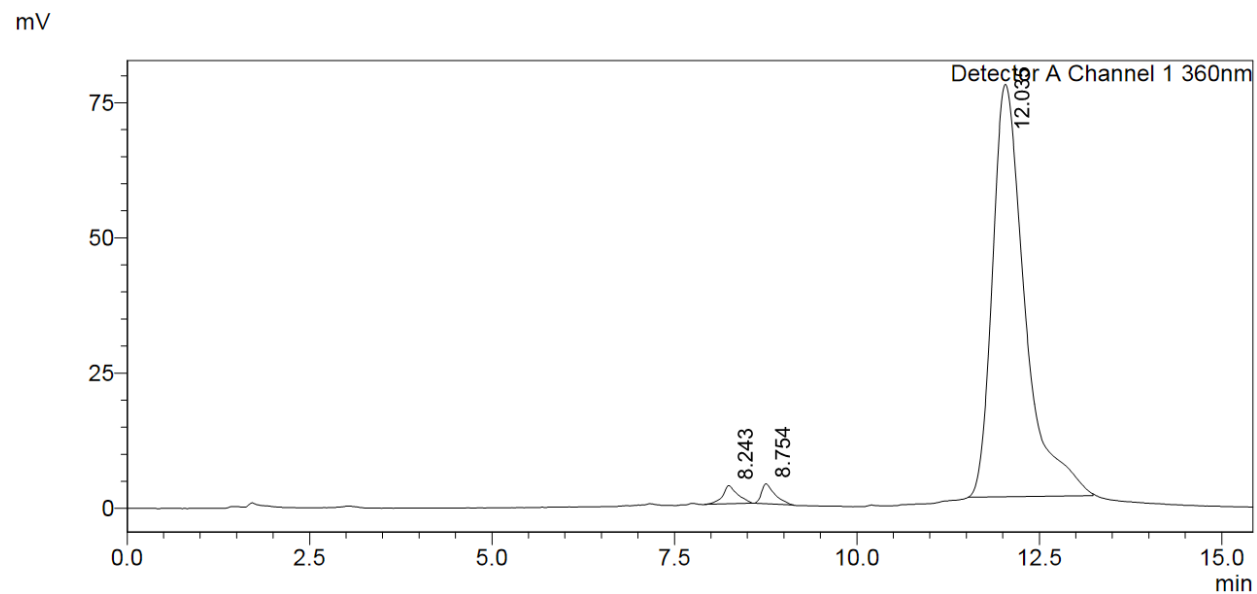


**Figure 49.** RP-HPLC trace showing product **13** at 12.0 min.

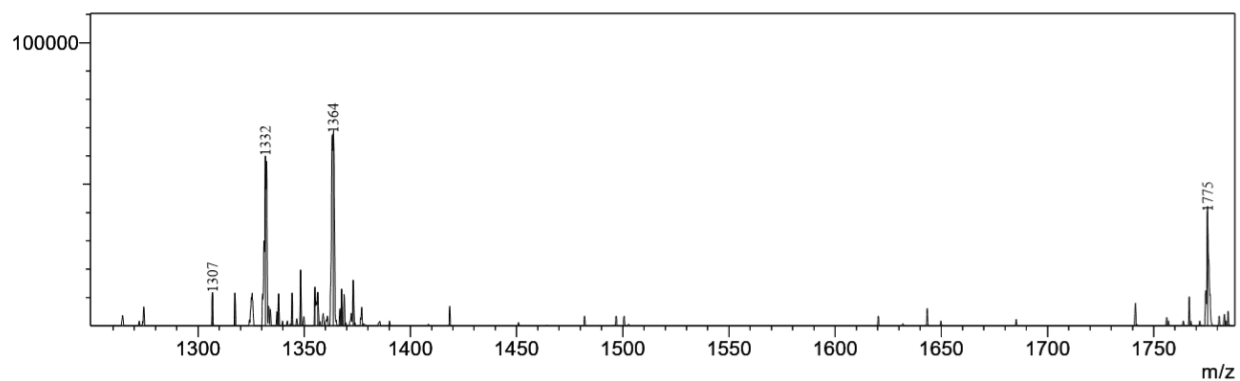


**Figure 50.** ESI-MS of **13**, expected  $m/z = 5341$ , observed  $m/z = [M^+ - H_2O + 2H^+]^{+3}$ : 1775,  $[M^+ - H_2O + 3H^+ + CH_3OH]^{+4}$ : 1364,  $[M^+ - H_2O + 3H^+]^{+4}$ : 1332.



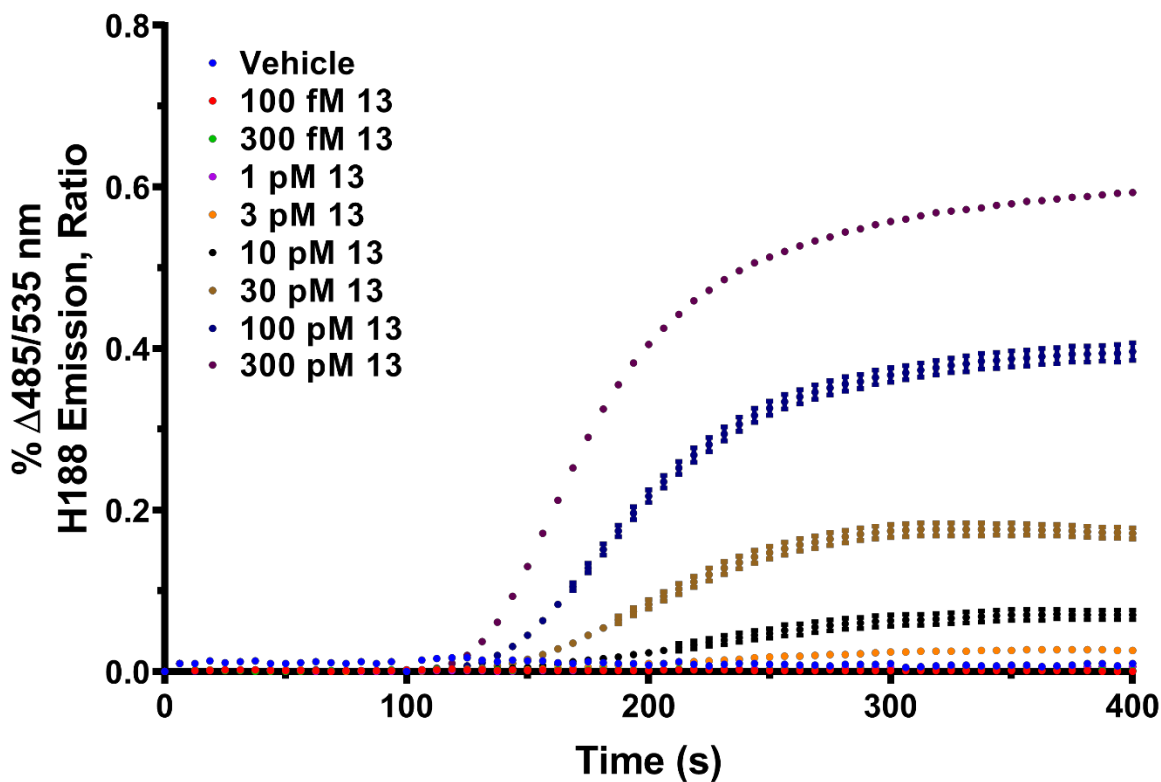


**Figure 51.** *In vitro* dose escalation study of **13** showing increase in cAMP levels in GLP-1R stably transfected HEK-293-H188 c20 cells.

#### 6.6.2.11 Synthesis of Cbi-Pent-Ex4 (**14**)

**14** was prepared by combining **6** (4.9 mg, 0.0043 mmol) with CuI (3.6 mg, 0.019 mmol), TBTA (6.2 mg, 0.012 mmol), and Ex4 (3.9 mg 0.0009 mmol) gave the target compound, which was purified using RP-HPLC method A2 to produce **14** as a red solid to 98% purity.  $t_R$ : 12.0 min (Figure 52); ESI-MS-expected  $m/z$  = 5355, observed  $m/z$  =  $[M^+ - H_2O + 2H^+]^{+3}$ : 1780,  $[M^+ - H_2O + 3H^+]^{+4}$ : 1335 (Figure 53). *In vitro* function of **15** was determined in GLP-1R stably transfected HEK-293-H188 c20 cells (Figure 54).

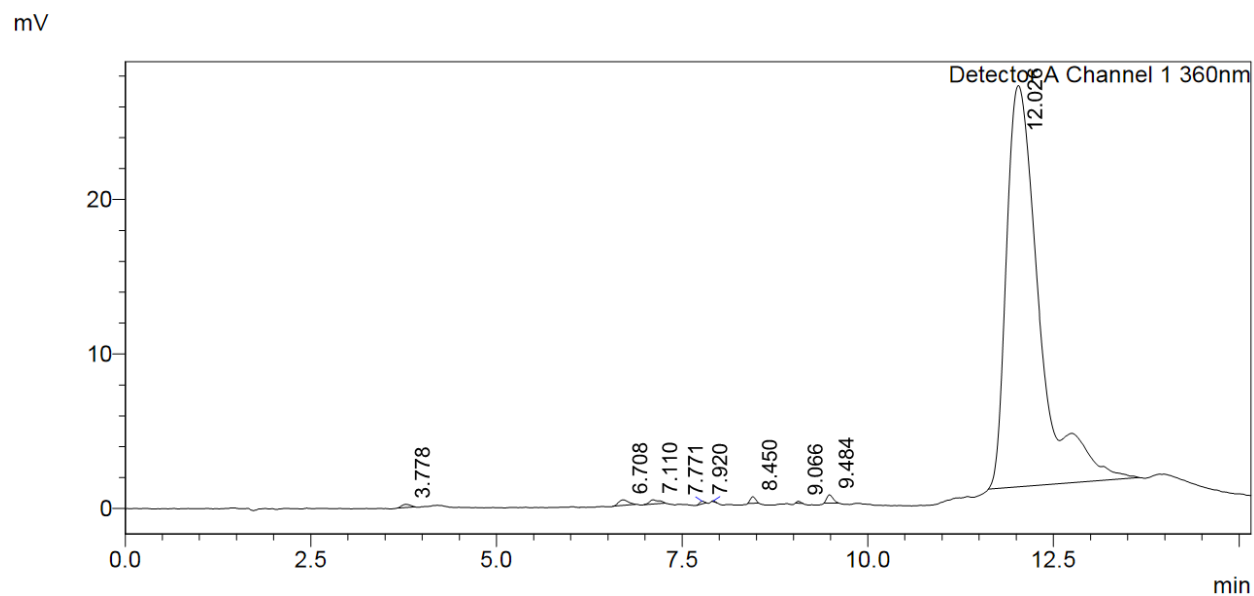


**Figure 52.** RP-HPLC trace showing product **14** at 12.0 min.

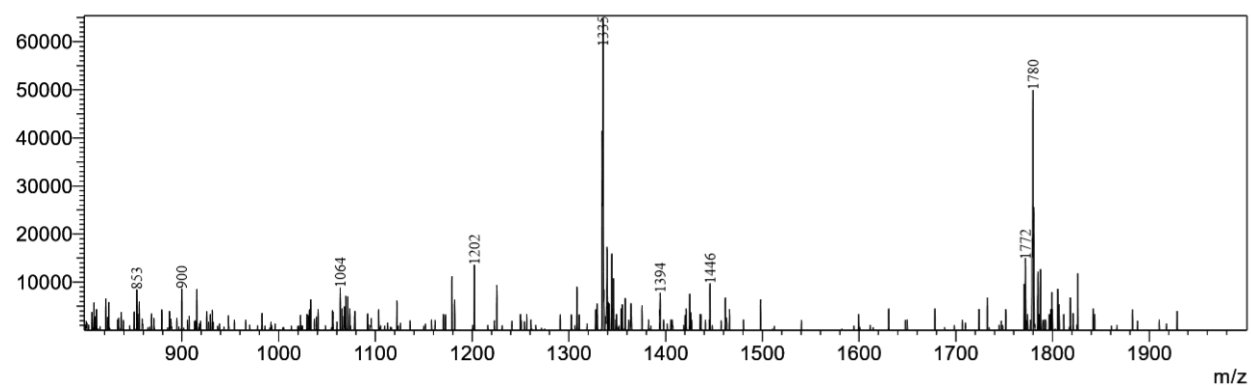


**Figure 53.** ESI-MS of **14**, expected  $m/z = 5355$ , observed  $m/z = [M^+ - H_2O + 2H^+]^{+3}$ : 1780,  $[M^+ - H_2O + 3H^+]^{+4}$ : 1335.

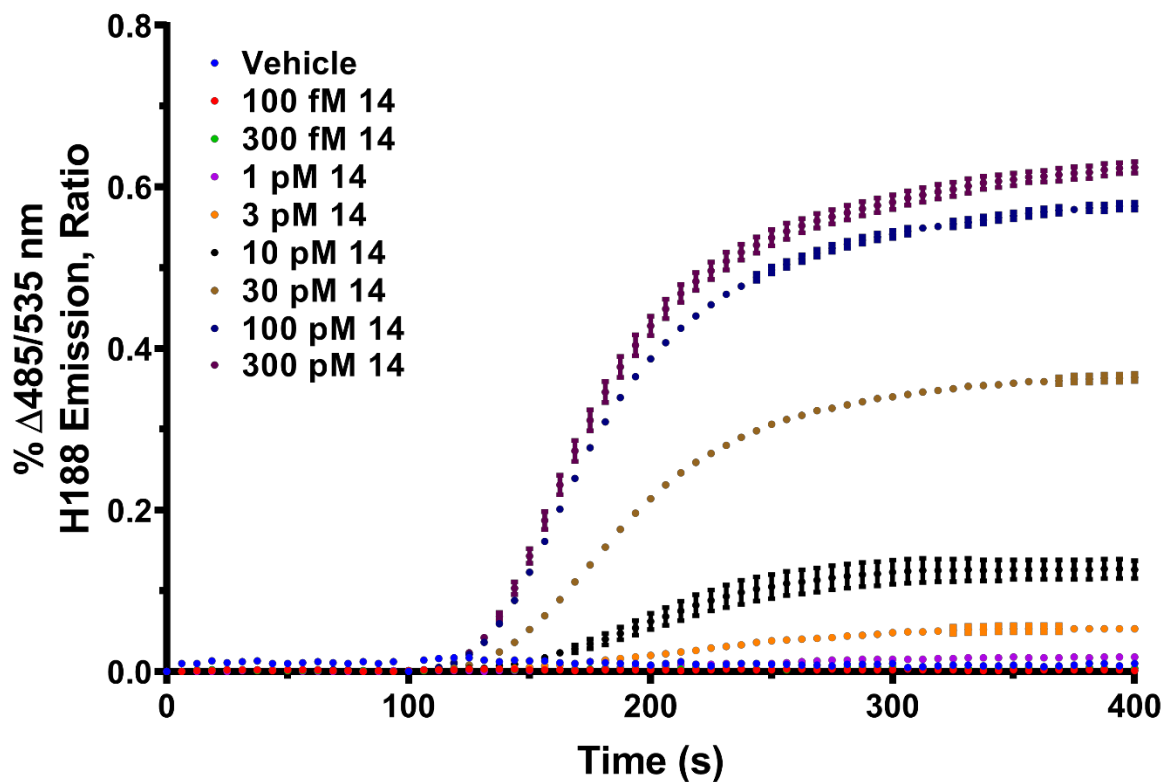


**Figure 54.** *In vitro* dose escalation study of **14** showing increase in cAMP levels in GLP-1R stably transfected HEK-293-H188 c20 cells.

#### 6.6.2.12 Synthesis of Cbi-Hex-Ex4 (**15**)

**15** was prepared by combining **7** (9.7 mg, 0.0084 mmol) with CuI (3.5 mg, 0.018 mmol), TBTA (6.6 mg, 0.012 mmol), and Ex4 (5.3 mg 0.0013 mmol) gave the target compound, which was purified using RP-HPLC method A3 to produce **15** as a red solid to 98% purity.  $t_R$ : 12.0 min (Figure 55); ESI-MS-expected  $m/z$  = 5369, observed  $m/z$  =  $[M^+ - H_2O + 2H^+]^{+3}$ : 1784,  $[M^+ - H_2O + 3H^+]^{+4}$ : 1339 (Figure 56). *In vitro* function of **22** was determined in GLP-1R stably transfected HEK-293-H188 c20 cells (Figure 57).

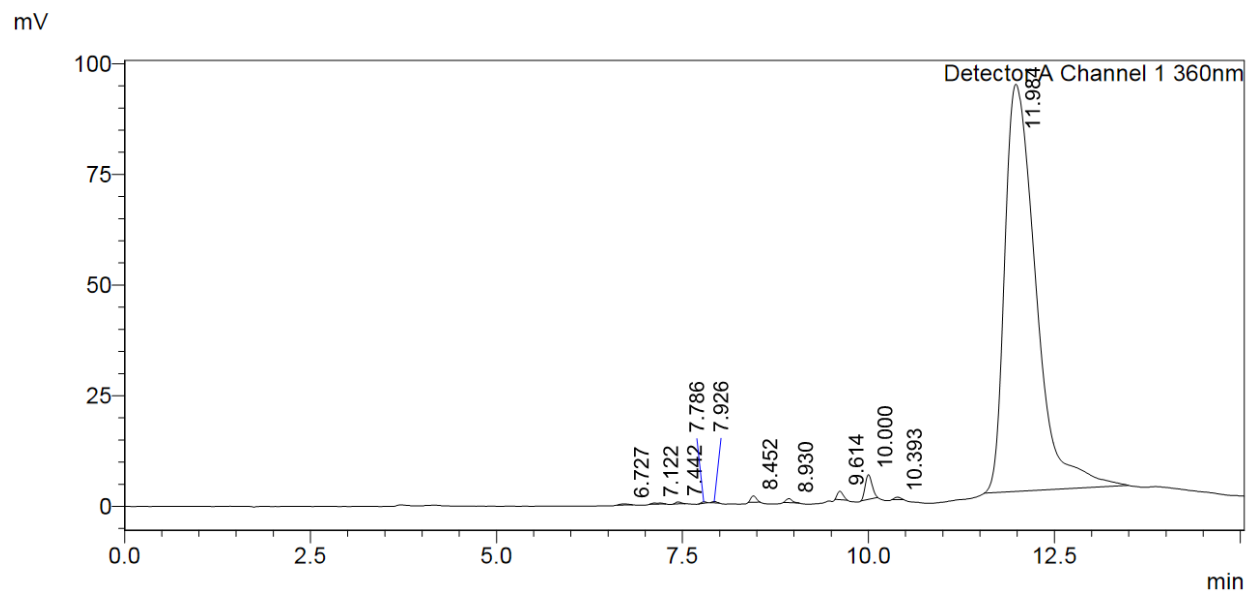


**Figure 55.** RP-HPLC trace showing product **15** at 12.0 min.

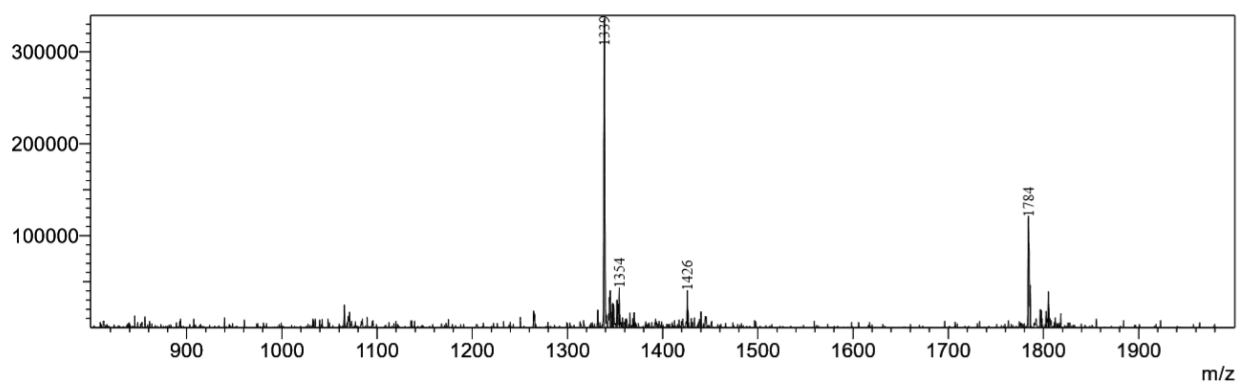


**Figure 56.** ESI-MS of **15**, expected  $m/z$  = 5369, observed  $m/z$  =  $[M^+-H_2O+2H^+]^3$ : 1784,  $[M^+-H_2O+3H^+]^4$ : 1339.

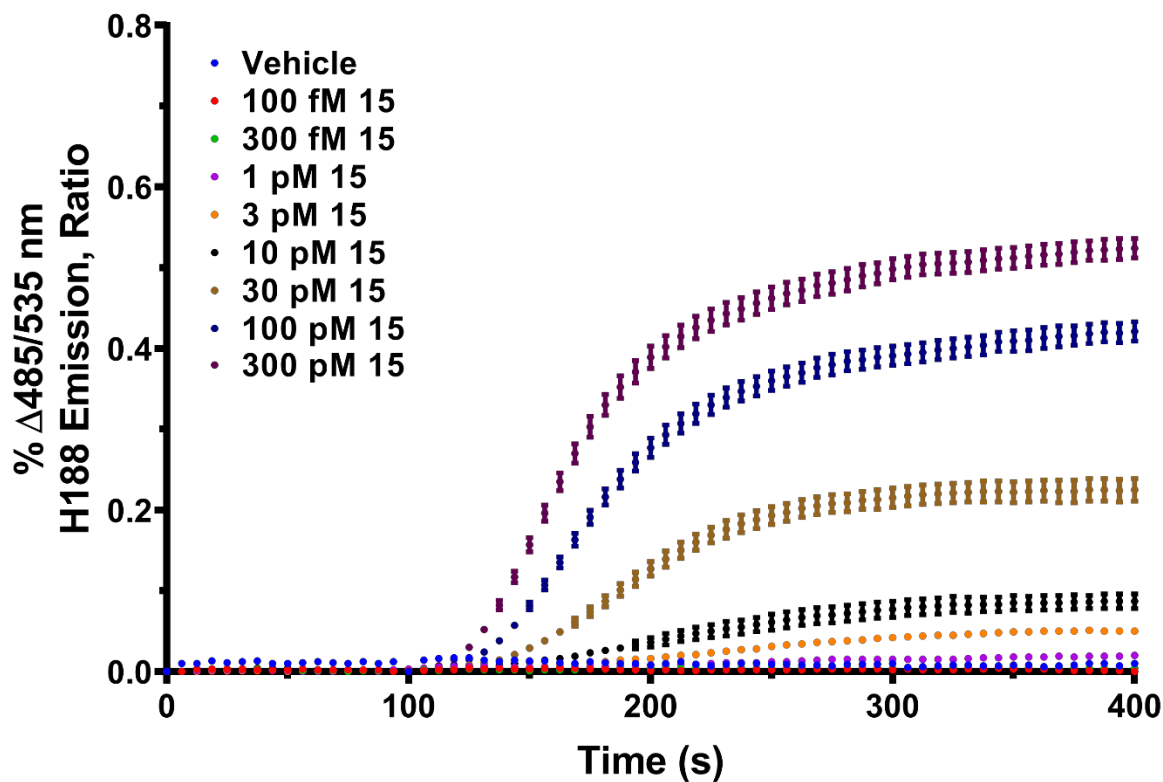


**Figure 57.** *In vitro* dose escalation study of **15** showing increase in cAMP levels in GLP-1R stably transfected HEK-293-H188 c20 cells.

#### 6.6.2.13 Synthesis of Cbi-PEG2-Ex4 (**16**)

**16** was prepared by combining **8** (2.0 mg, 0.0017 mmol) with CuI (3.6 mg, 0.019 mmol), TBTA (7.1 mg, 0.013 mmol), and Ex4 (3.0 mg 0.0007 mmol) gave the target compound, which was purified using RP-HPLC method A2 to produce **16** as a red solid to 98% purity.  $t_R$ : 11.7 min (Figure 58); ESI-MS-expected  $m/z$  = 5416, observed  $m/z$  =  $[M^+ - H_2O + 2H^+]^{+3}$ : 1800,  $[M^+ - H_2O + 3H^+]^{+4}$ : 1350 (Figure 59). *In vitro* function of **22** was determined in GLP-1R stably transfected HEK-293-H188 c20 cells (Figure 60).

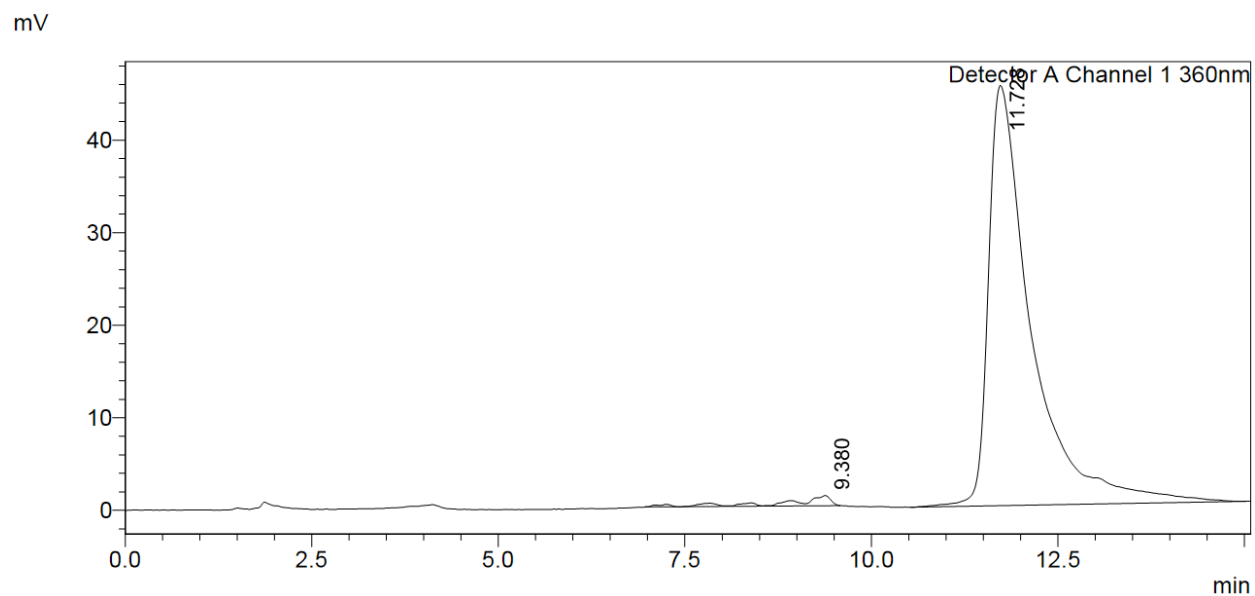


**Figure 58.** RP-HPLC trace showing product **16** at 11.7 min.

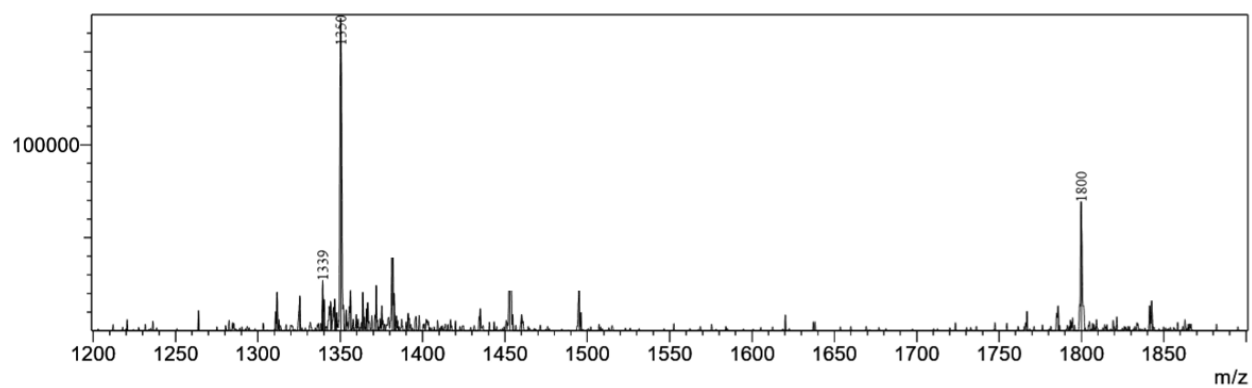


**Figure 59.** ESI-MS of **16**, expected  $m/z$  = 5416, observed  $m/z$  =  $[M^+ - H_2O + 2H^+]^{+3}$ : 1800,  $[M^+ - H_2O + 3H^+]^{+4}$ : 1350.

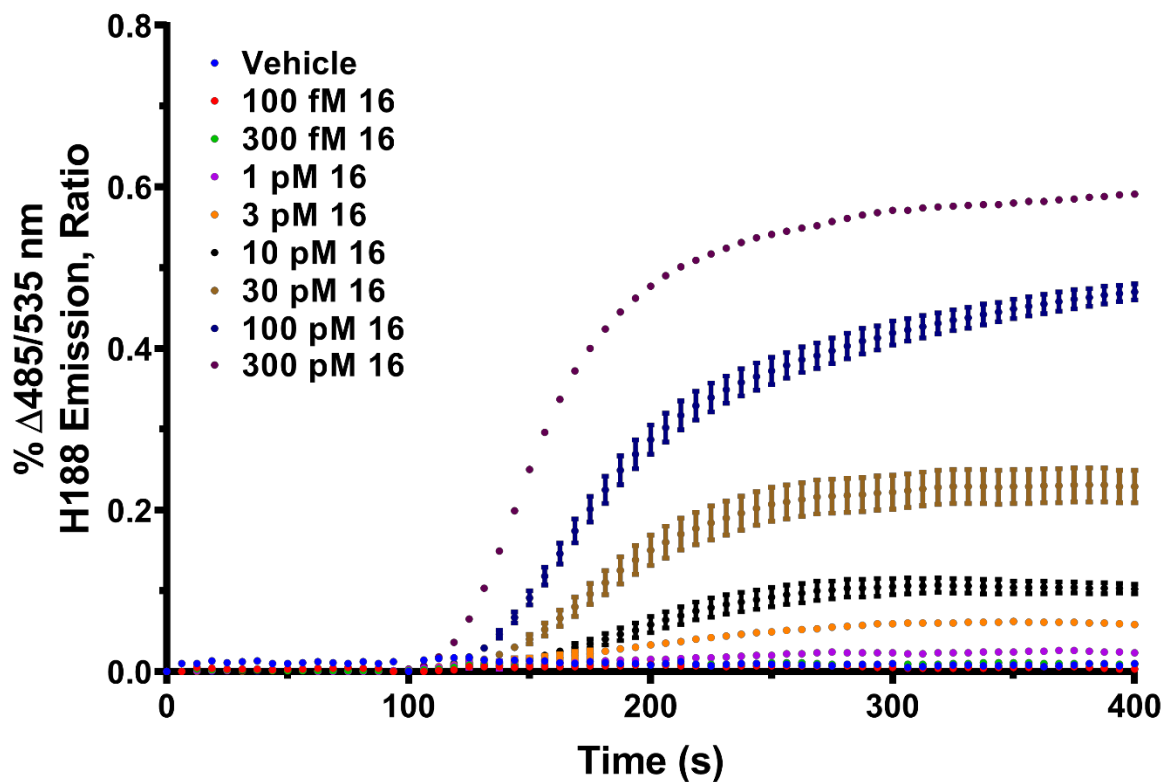


**Figure 60.** *In vitro* dose escalation study of **16** showing increase in cAMP levels in GLP-1R stably transfected HEK-293-H188 c20 cells.

#### 6.6.2.14 Synthesis of Cbi-PEG4-Ex4 (**17**)

**17** was prepared by combining **9** (3.0 mg, 0.0023 mmol) with CuI (3.4 mg, 0.018 mmol), TBTA (7.3 mg, 0.014 mmol), and Ex4 (4.1 mg 0.0010 mmol) gave the target compound, which was purified using RP-HPLC method A2 to produce **17** as a red solid to 98% purity.  $t_R$ : 12.3 min (Figure 61); ESI-MS-expected  $m/z$  = 5504, observed  $m/z$  =  $[M^+ - H_2O + 2H^+ + CH_3CN]^{+3}$ : 1870,  $[M^+ - H_2O + 3H^+ + CH_3OH]^{+4}$ : 1404,  $[M^+ - H_2O + 4H^+]^{+5}$ : 1098 (Figure 62). *In vitro* function of **22** was determined in GLP-1R stably transfected HEK-293-H188 c20 cells (Figure 63).

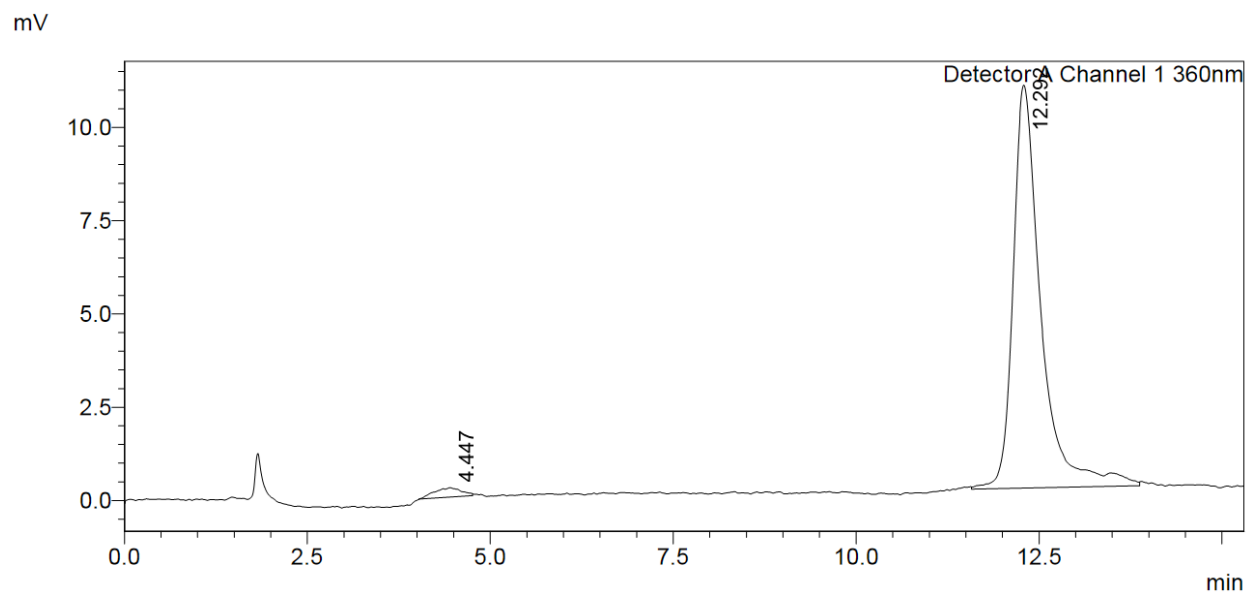


**Figure 61.** RP-HPLC trace showing product **17** at 12.3 min.

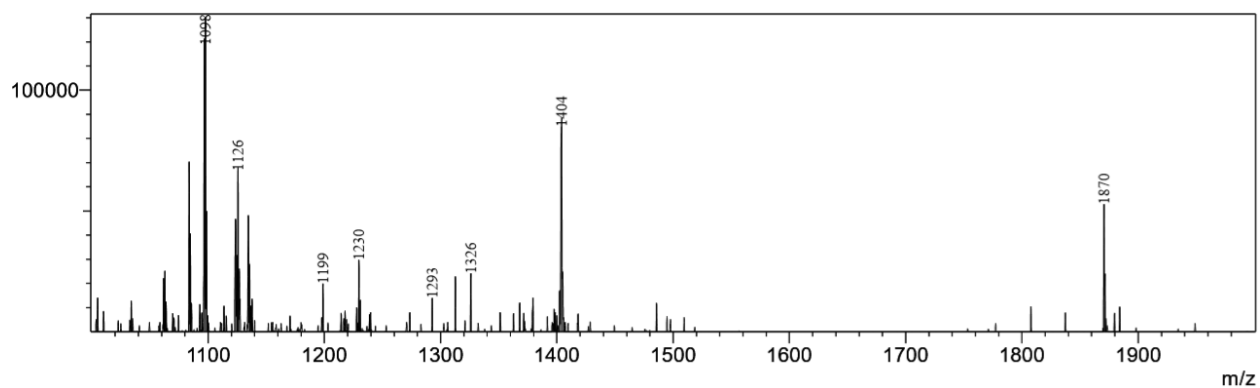


**Figure 62.** ESI-MS of **17**, expected  $m/z = 5504$ , observed  $m/z = [M^+ - H_2O + 2H^+ + CH_3CN]^{+3}$ : 1870,  $[M^+ - H_2O + 3H^+ + CH_3OH]^{+4}$ : 1404,  $[M^+ - H_2O + 4H^+]^{+5}$ : 1098.



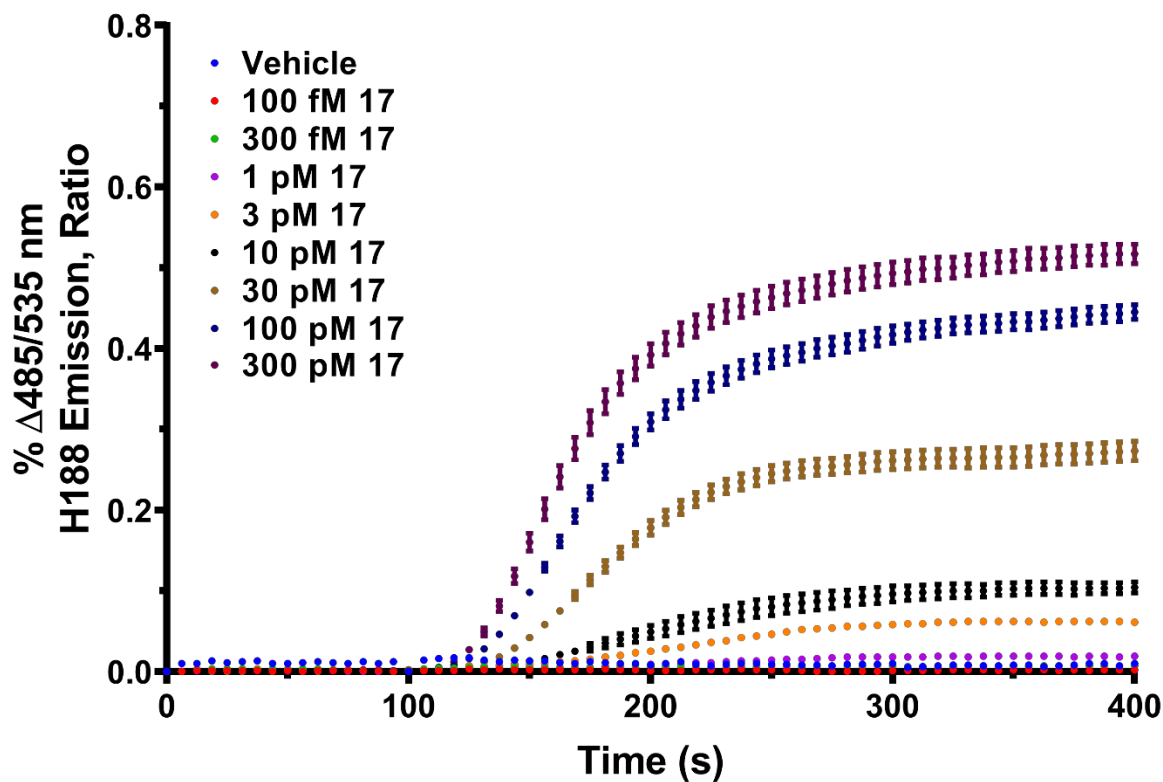


**Figure 63.** *In vitro* dose escalation study of **17** showing increase in cAMP levels in GLP-1R stably transfected HEK-293-H188 c20 cells.

#### 6.6.2.15 Synthesis of Cbi-4EPMA-Ex4 (**18**)

**18** was prepared by combining **10** (3.3 mg, 0.0028 mmol) with CuI (3.6 mg, 0.019 mmol), TBTA (7.2 mg, 0.014 mmol), and Ex4 (3.0 mg 0.0007 mmol) gave the target compound, which was purified using RP-HPLC method A2 to produce **18** as a red solid to 98% purity.  $t_R$ : 12.2 min (Figure 64); ESI-MS-expected  $m/z$  = 5403, observed  $m/z$  =  $[M^+ - H_2O + 2H^+]^{+3}$ : 1796,  $[M^+ - H_2O + 3H^+]^{+4}$ : 1347 (Figure 65). *In vitro* function of **22** was determined in GLP-1R stably transfected HEK-293-H188 c20 cells (Figure 66).

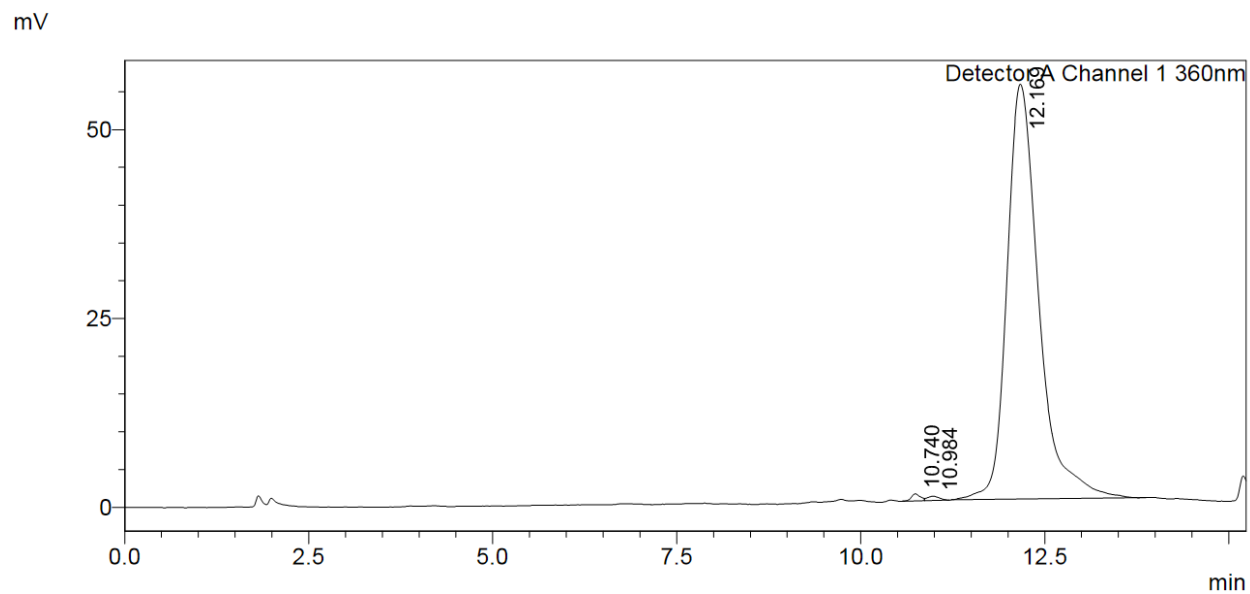


**Figure 64.** RP-HPLC trace showing product **18** at 12.2 min.

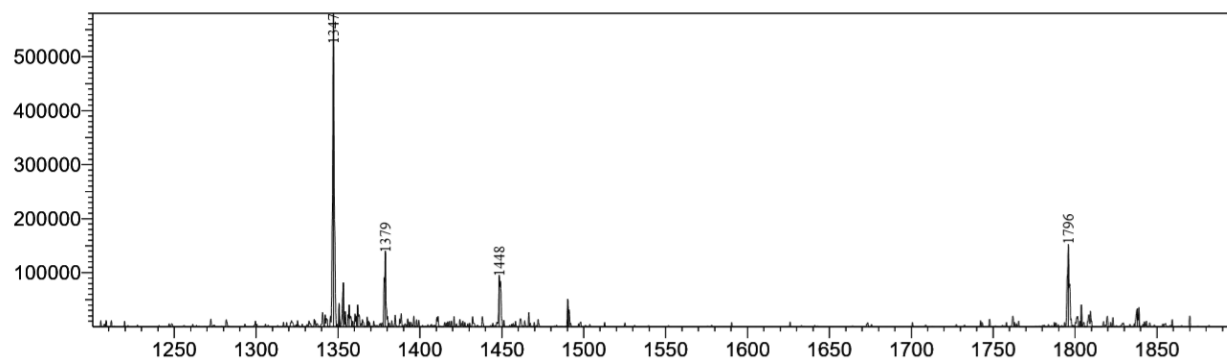


**Figure 65.** ESI-MS of **18**, expected  $m/z = 5403$ , observed  $m/z = [M^+ - H_2O + 2H^+]^{+3}$ : 1796,  $[M^+ - H_2O + CH_3OH + 3H^+]^{+4}$ : 1379,  $[M^+ - H_2O + 3H^+]^{+4}$ : 1347.

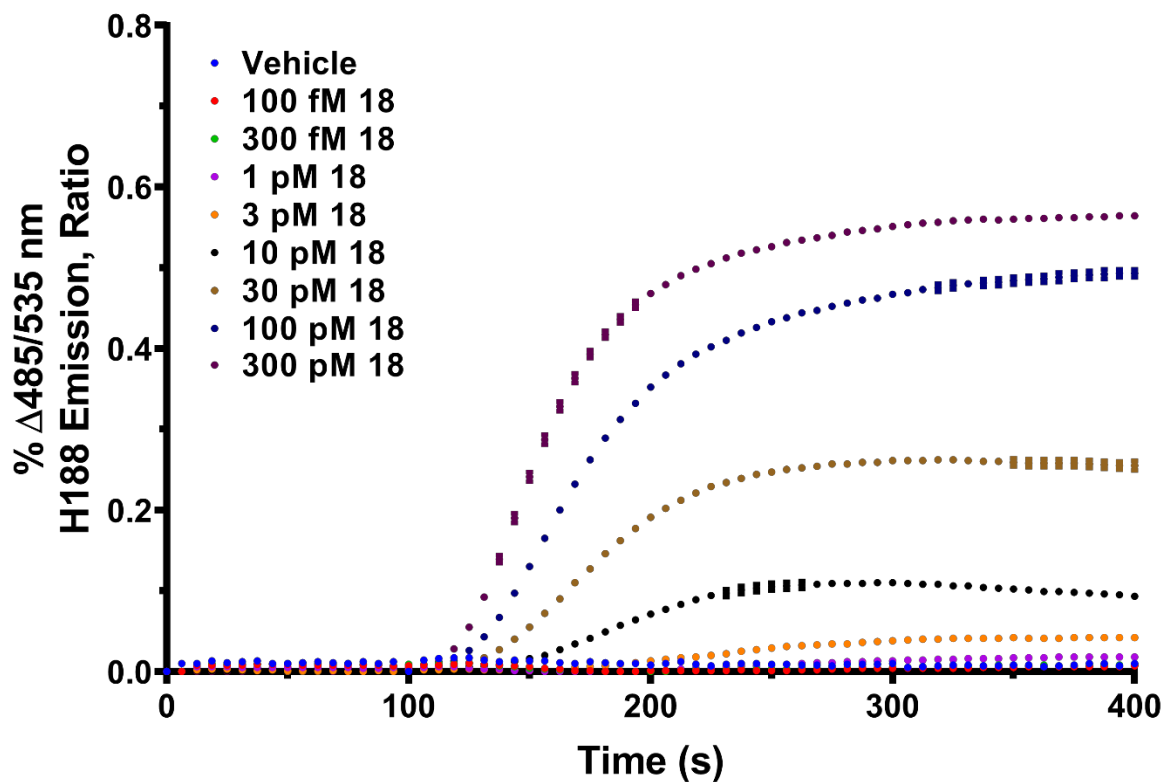


**Figure 66.** *In vitro* dose escalation study of **18** showing increase in cAMP levels in GLP-1R stably transfected HEK-293-H188 c20 cells.

#### 6.6.2.16 Synthesis of Cbi-3EPMA-Ex4 (**19**)

**19** was prepared by combining **11** (3.0 mg, 0.0025 mmol) with CuI (4.5 mg, 0.024 mmol), TBTA (7.6 mg, 0.014 mmol), and Ex4 (2.7 mg 0.0006 mmol) gave the target compound, which was purified using RP-HPLC method A2 to produce **19** as a red solid to 97% purity.  $t_R$ : 12.6 min (Figure 67); ESI-MS-expected  $m/z$  = 5403, observed  $m/z$  =  $[M^+ - H_2O + 2H^+]^{+3}$ : 1796,  $[M^+ - H_2O + 2H^+ + CH_3OH]^{+3}$ : 1379,  $[M^+ - H_2O + 3H^+]^{+4}$ : 1347 (Figure 68). *In vitro* function of **22** was determined in GLP-1R stably transfected HEK-293-H188 c20 cells (Figure 69).

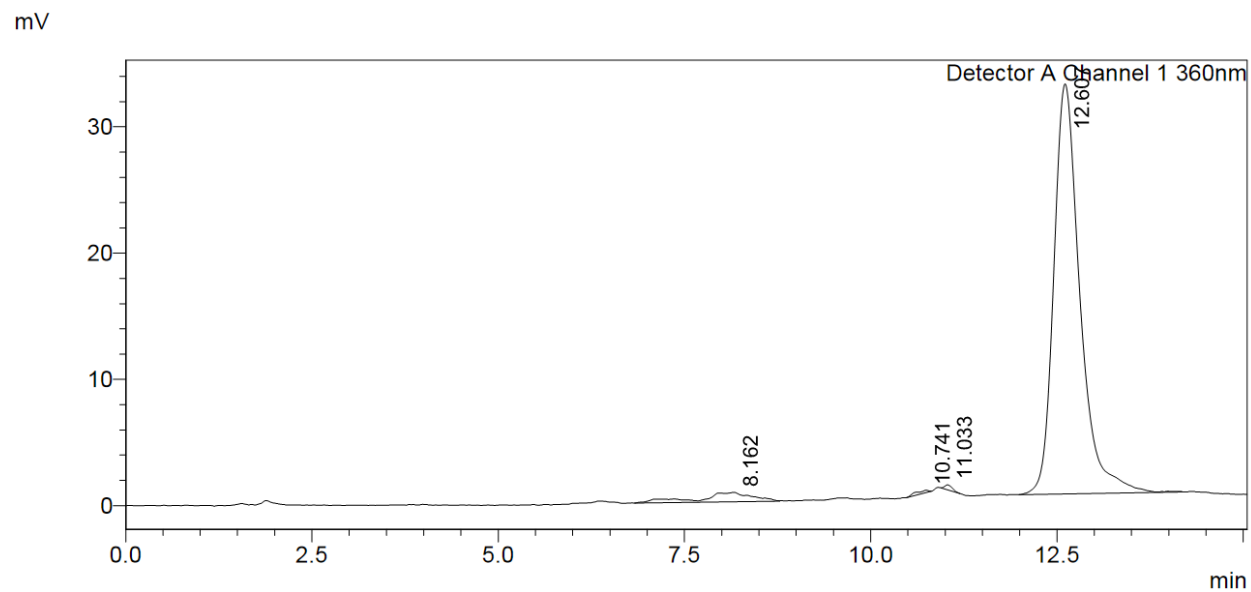


**Figure 67.** RP-HPLC trace showing product **19** at 12.6 min.

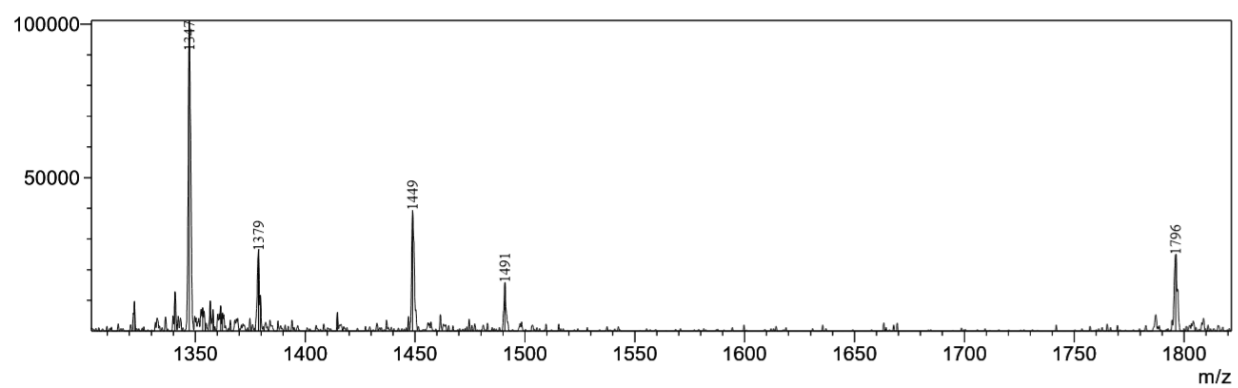


**Figure 68.** ESI-MS of **19**, expected  $m/z = 5403$ , observed  $m/z = [M^+ - H_2O + 2H^+]^{+3}$ : 1796,  $[M^+ - H_2O + CH_3OH + 3H^+]^{+4}$ : 1379,  $[M^+ - H_2O + 3H^+]^{+4}$ : 1347.

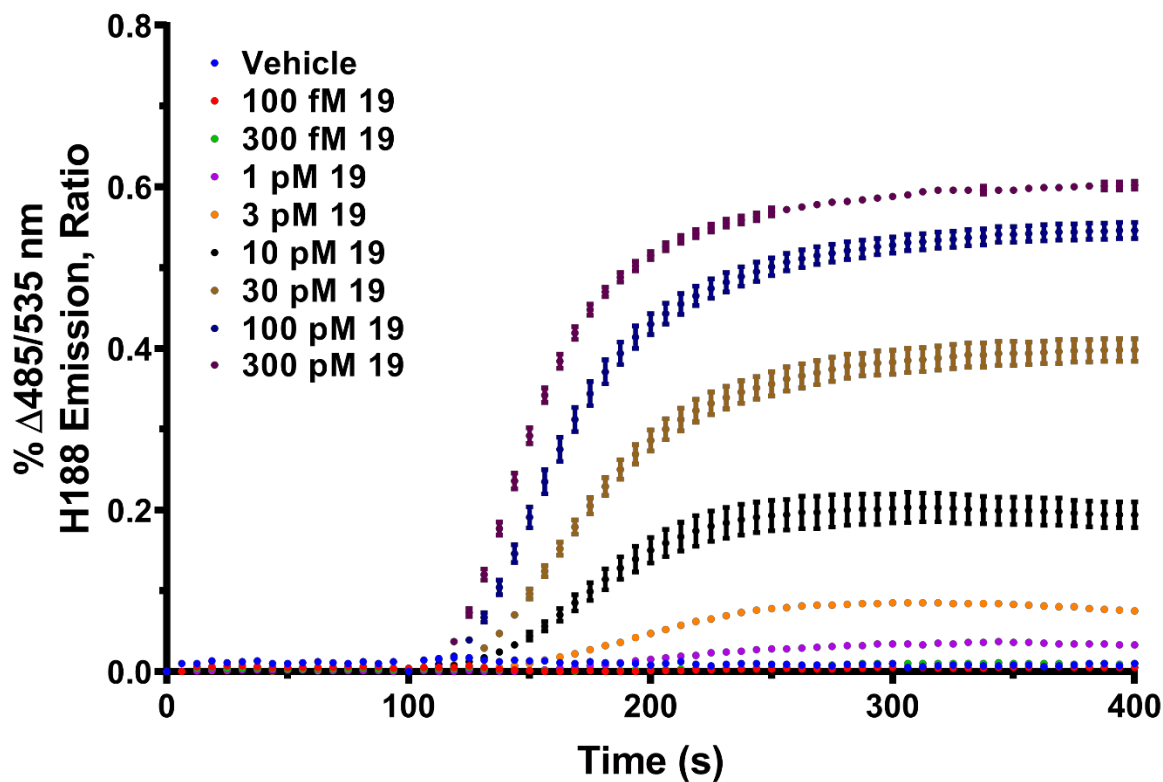


**Figure 69.** *In vitro* dose escalation study of **19** showing increase in cAMP levels in GLP-1R stably transfected HEK-293-H188 c20 cells.

#### 6.6.2.17 Synthesis of Cbi-Pro-Ex40 (**20**)

**20** was prepared by combining **4** (3.0 mg, 0.0027 mmol) with CuI (3.6 mg, 0.019 mmol), TBTA (7.0 mg, 0.013 mmol), and Ex40 (3.0 mg 0.0007 mmol) gave the target compound, which was purified using RP-HPLC method A2 to produce **20** as a red solid to 97% purity.  $t_R$ : 11.8 min (Figure 70); ESI-MS-expected  $m/z$  = 5456, observed  $m/z$  =  $[M^+ - H_2O + 2H^+]^{+3}$ : 1813,  $[M^+ - H_2O + 3H^+]^{+4}$ : 1360,  $[M^+ - H_2O + 4H^+]^{+5}$ : 1088,  $[M^+ - H_2O + 5H^+]^{+6}$ : 907,  $[M^+ - H_2O + 6H^+]^{+7}$ : 777 (Figure 71). *In vitro* function of **20** was determined in GLP-1R stably transfected HEK-293-H188 c20 cells (Figure 72).

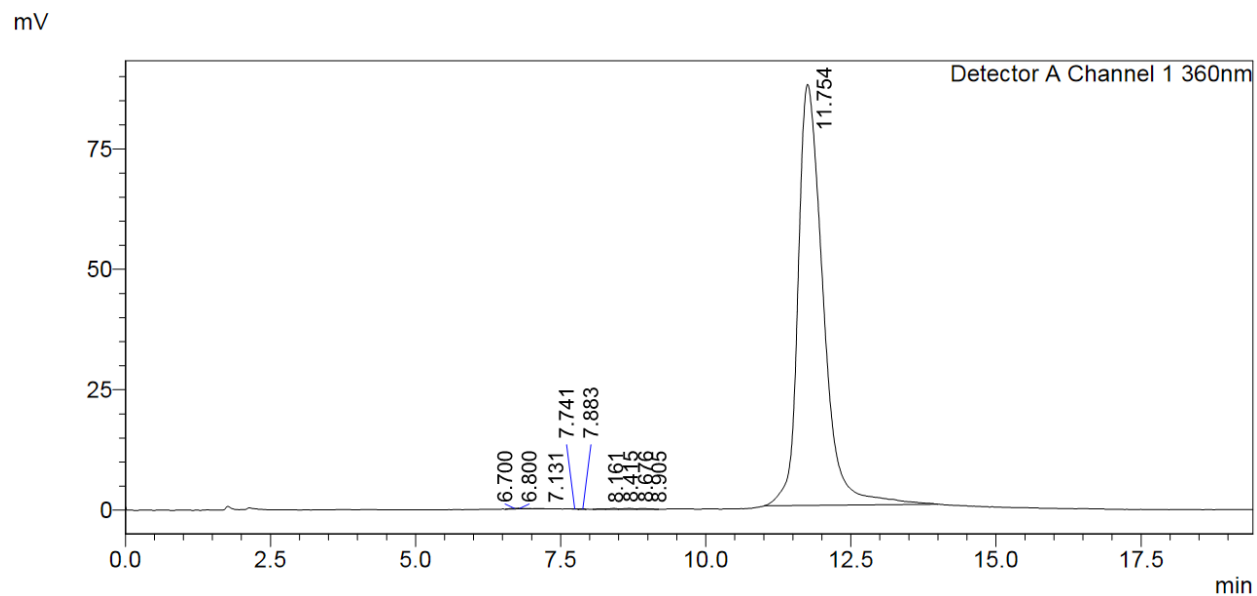


**Figure 70.** RP-HPLC trace showing product **20** at 11.8 min.

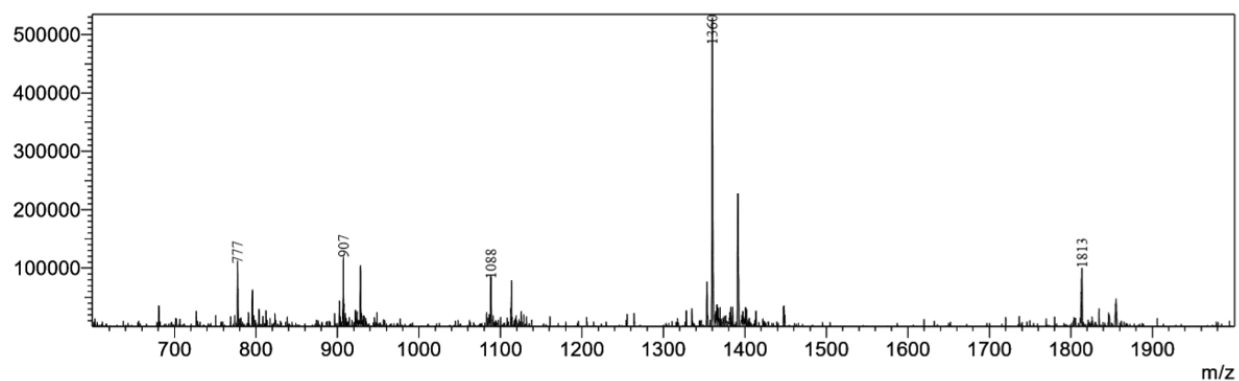


**Figure 71.** ESI-MS of **20**, expected  $m/z = 5456$ , observed  $m/z = [M^+ - H_2O + 2H^+]^{+3}$ : 1813,  $[M^+ - H_2O + 3H^+]^{+4}$ : 1360,  $[M^+ - H_2O + 4H^+]^{+5}$ : 1088,  $[M^+ - H_2O + 5H^+]^{+6}$ : 907,  $[M^+ - H_2O + 6H^+]^{+7}$ : 777.

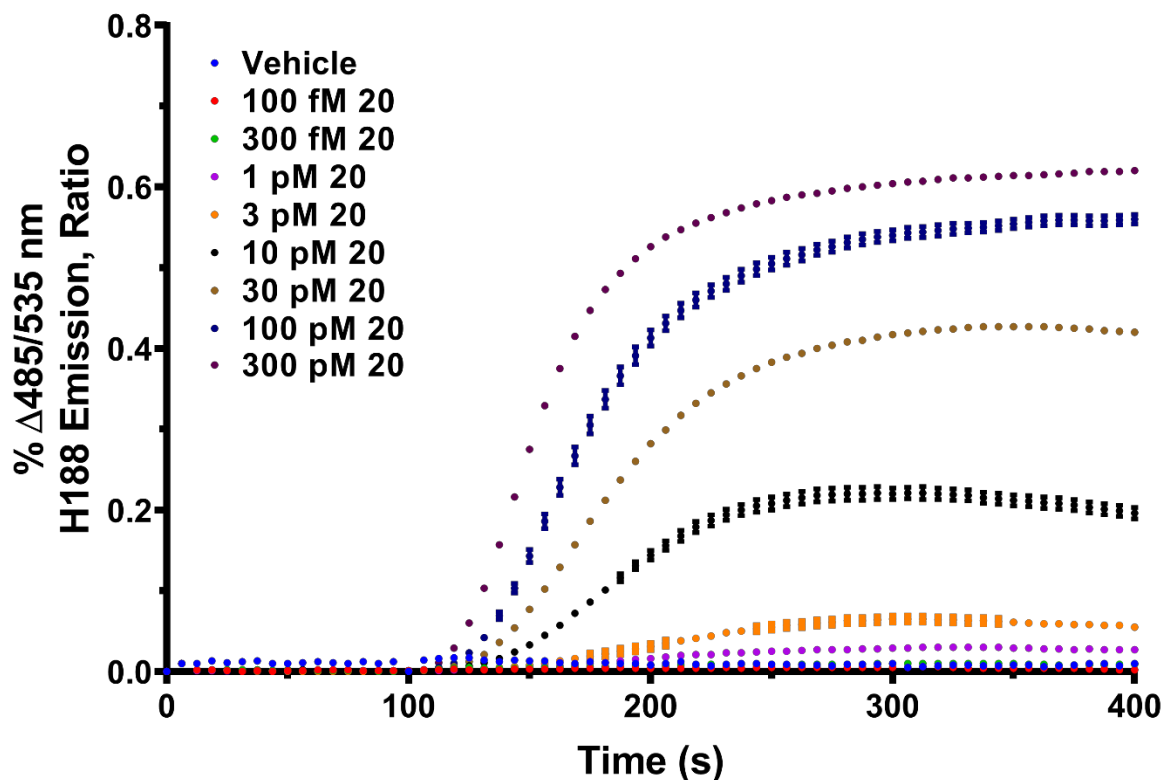


**Figure 72.** *In vitro* dose escalation study of **20** showing increase in cAMP levels in GLP-1R stably transfected HEK-293-H188 c20 cells.

#### 6.6.2.18 Synthesis of Cbi-But-Ex40 (**21**)

**21** was prepared according to the general procedure described above; combining **5** (3.4 mg, 0.0030 mmol) with CuI (4.0 mg, 0.021 mmol), TBTA (6.5 mg, 0.012 mmol), and Ex40 (3.3 mg 0.0007 mmol) gave the target compound, which was purified using RP-HPLC method A2 to produce **21** as a red solid to 97% purity.  $t_R$ : 11.7 min (Figure 73); ESI-MS-expected  $m/z$  = 5469, observed  $m/z$  =  $[M^+ - H_2O + 2H^+ + CH_3CN]^{+3}$ : 1859,  $[M^+ - H_2O + 2H^+]^{+3}$ : 1819,  $[M^+ - H_2O + 3H^+ + CH_3OH]^{+4}$ : 1395,  $[M^+ - H_2O + 3H^+]^{+4}$ : 1364,  $[M^+ - H_2O + 4H^+]^{+5}$ : 1091 (Figure 74). *In vitro* function of **21** was determined in GLP-1R stably transfected HEK-293-H188 c20 cells (Figure 75).

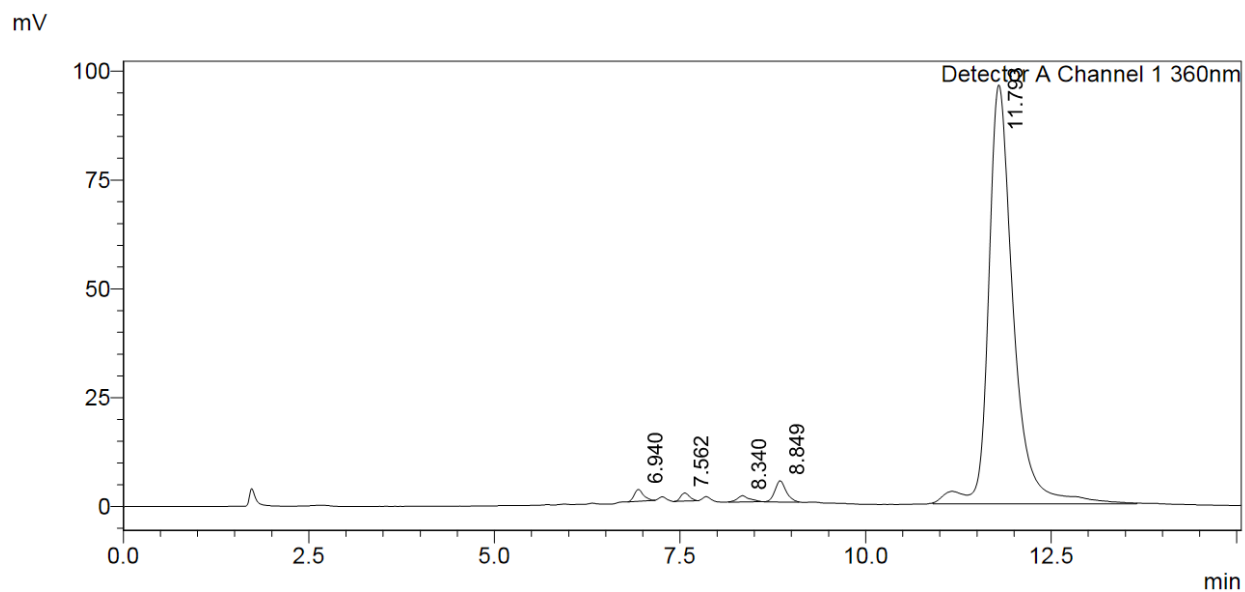


**Figure 73.** RP-HPLC trace showing product **21** at 11.8 min.

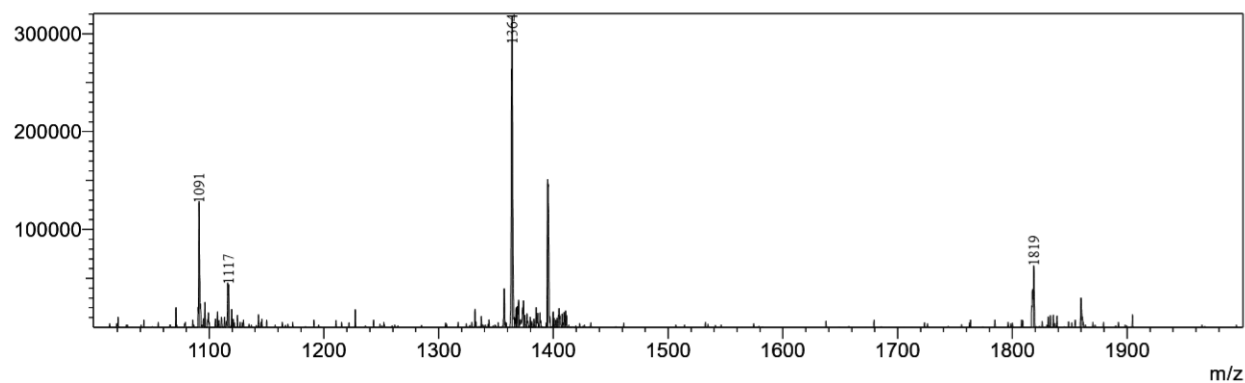


**Figure 74.** ESI-MS of **21**, expected  $m/z = 5469$ , observed  $m/z = [M^+ - H_2O + 2H^+ + CH_3CN]^{+3}: 1859$ ,  $[M^+ - H_2O + 2H^+]^{+3}: 1819$ ,  $[M^+ - H_2O + 3H^+ + CH_3OH]^{+4}: 1395$ ,  $[M^+ - H_2O + 3H^+]^{+4}: 1364$   $[M^+ - H_2O + 4H^+]^{+5}: 1091$ .



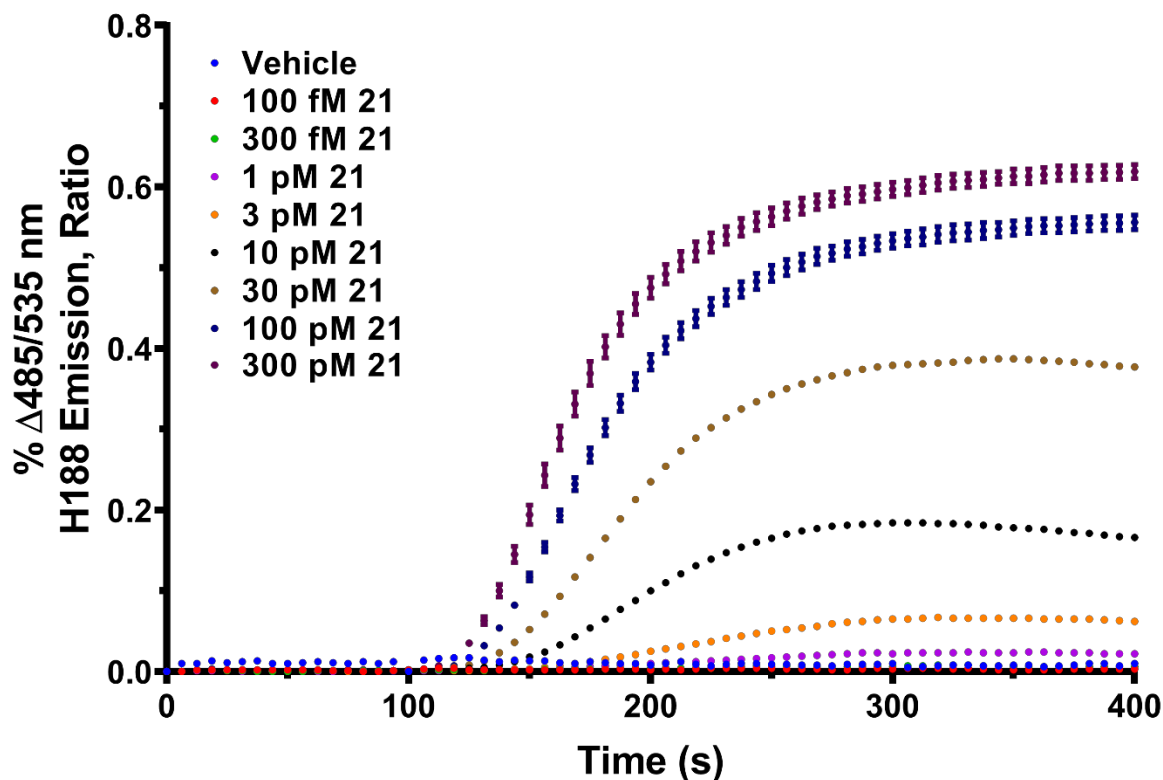


**Figure 75.** *In vitro* dose escalation study of **21** showing increase in cAMP levels in GLP-1R stably transfected HEK-293-H188 c20 cells.

#### 6.6.2.19 Synthesis of Cbi-Pent-Ex40 (**22**)

**22** was prepared by combining **6** (4.4 mg, 0.00388 mmol) with CuI (3.2 mg, 0.017 mmol), TBTA (6.5 mg, 0.012 mmol), and Ex40 (4.3 mg 0.0010 mmol) gave the target compound, which was purified using RP-HPLC method A2 to produce **22** as a red solid to 97% purity.  $t_R$ : 11.8 min (Figure 76); ESI-MS-expected  $m/z$  = 5483, observed  $m/z$  =  $[M^+ - H_2O + 2H^+]^{+3}$ : 1822,  $[M^+ - H_2O + 3H^+]^{+4}$ : 1367,  $[M^+ - H_2O + 5H^+]^{+6}$ : 912,  $[M^+ - H_2O + 6H^+]^{+7}$ : 781 (Figure 77). *In vitro* function of **22** was determined in GLP-1R stably transfected HEK-293-H188 c20 cells (Figure 78).

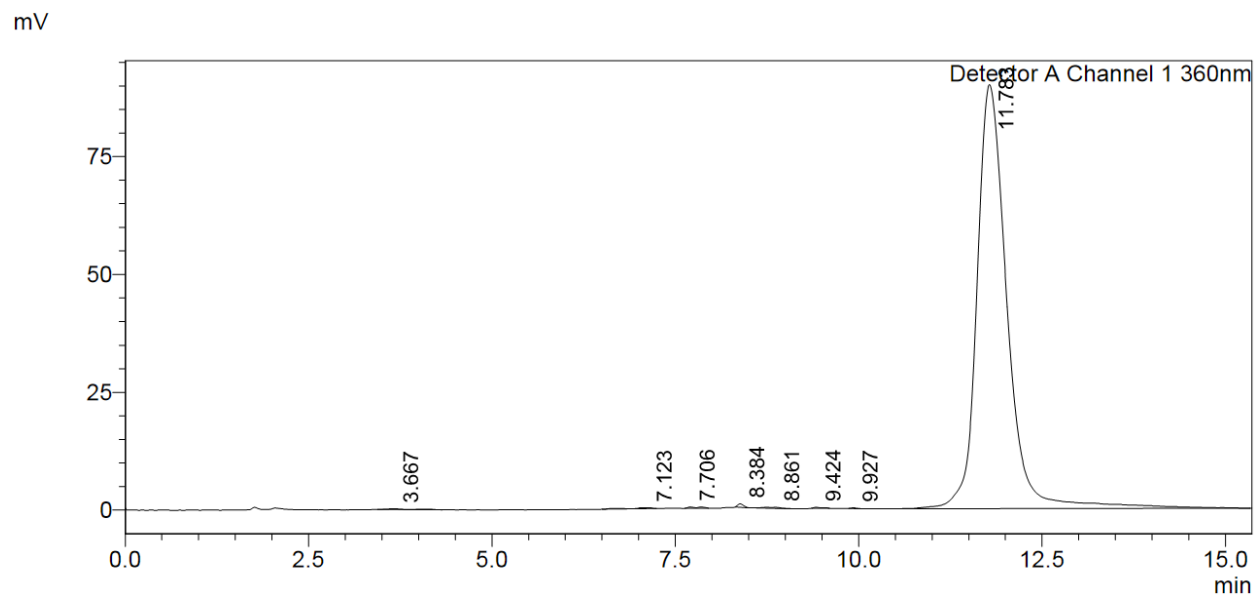


**Figure 76.** RP-HPLC trace showing product **22** at 11.8 min.

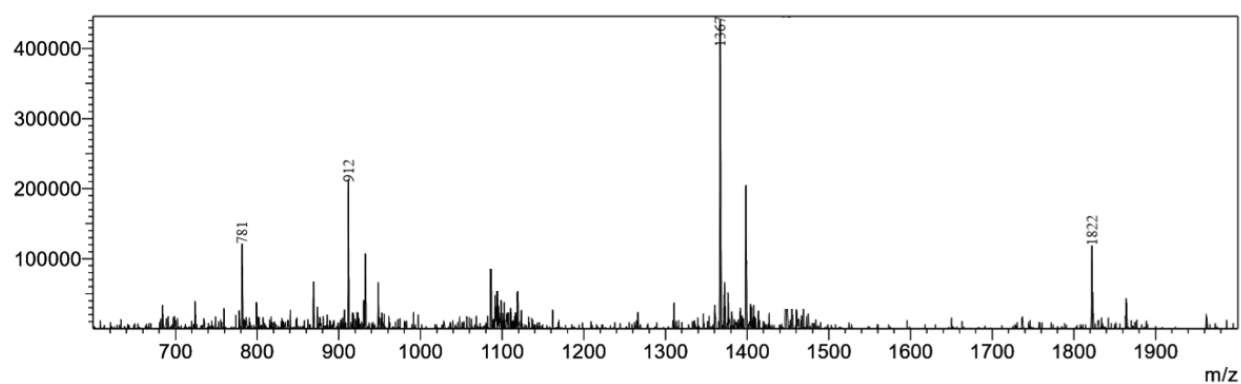


**Figure 77.** ESI-MS of **22**, expected  $m/z = 5483$ , observed  $m/z = [M^+ - H_2O + 2H^+]^{+3}$ : 1822,  $[M^+ - H_2O + 3H^+]^{+4}$ : 1367,  $[M^+ - H_2O + 5H^+]^{+6}$ : 912,  $[M^+ - H_2O + 6H^+]^{+7}$ : 781.

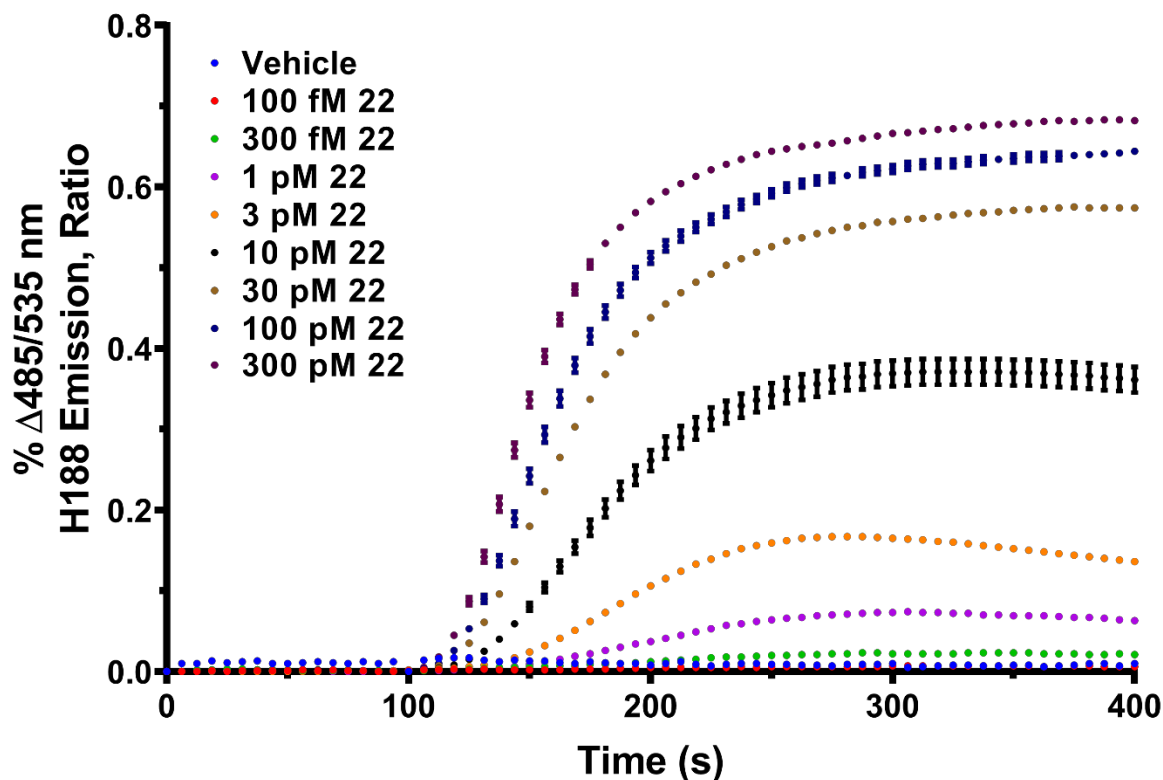


**Figure 78.** *In vitro* dose escalation study of **22** showing increase in cAMP levels in GLP-1R stably transfected HEK-293-H188 c20 cells.

#### 6.6.2.20 Synthesis of Cbi-Hex-Ex40 (**23**)

**23** was prepared according to the general procedure described above; combining **7** (2.1 mg, 0.0018 mmol) with CuI (3.6 mg, 0.019 mmol), TBTA (7.1 mg, 0.013 mmol), and Ex40 (2.6 mg, 0.0006 mmol) gave the target compound, which was purified using RP-HPLC method A2 to produce **23** as a red solid to 97% purity.  $t_R$ : 11.8 min (Figure 79); ESI-MS-expected  $m/z$  = 5497, observed  $m/z$  =  $[M^+ - H_2O + 2H^+]^{+3}$ : 1827,  $[M^+ - H_2O + 3H^+]^{+4}$ : 1371,  $[M^+ - H_2O + 5H^+]^{+6}$ : 914,  $[M^+ - H_2O + 6H^+]^{+7}$ : 784,  $[M^+ - H_2O + 7H^+]^{+8}$ : 685 (Figure 80). *In vitro* function of **23** was determined in GLP-1R stably transfected HEK-293-H188 c20 cells (Figure 81).

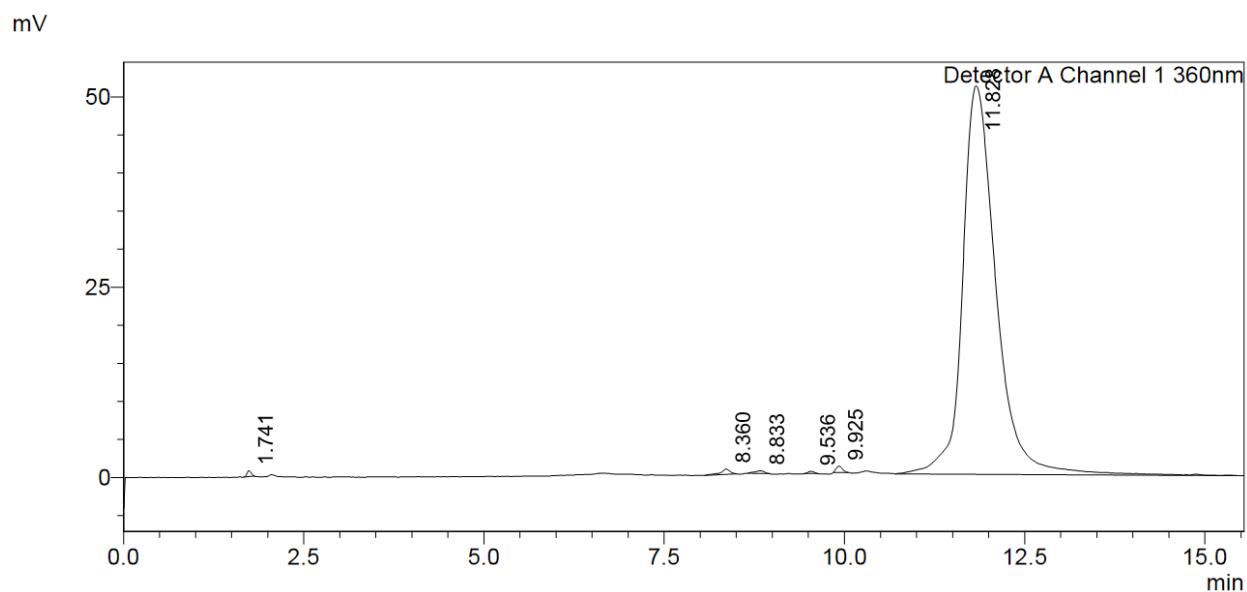


**Figure 79.** RP-HPLC trace showing product **23** at 11.8 min.

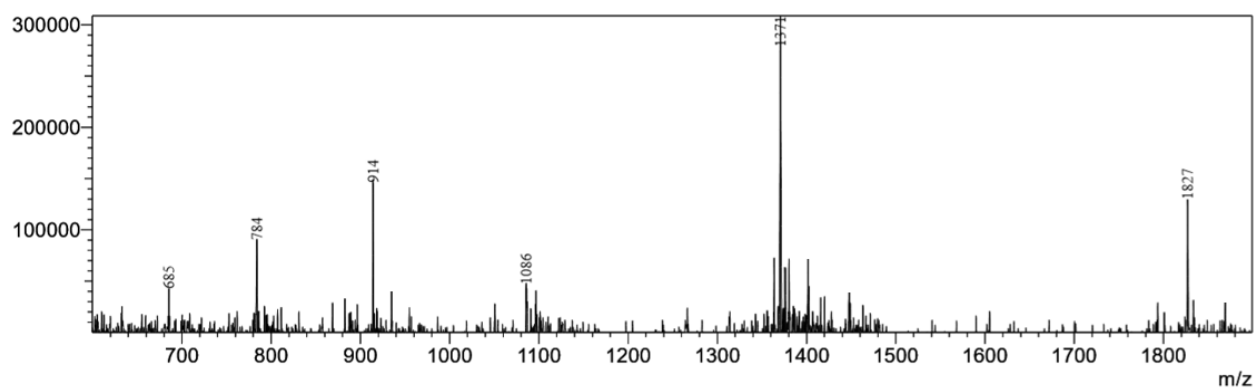


**Figure 80.** ESI-MS of **23**, expected  $m/z = 5497$ , observed  $m/z = [M^+ - H_2O + 2H^+]^{+3}$ : 1827,  $[M^+ - H_2O + 3H^+]^{+4}$ : 1371,  $[M^+ - H_2O + 5H^+]^{+6}$ : 914,  $[M^+ - H_2O + 6H^+]^{+7}$ : 784,  $[M^+ - H_2O + 7H^+]^{+8}$ : 685.

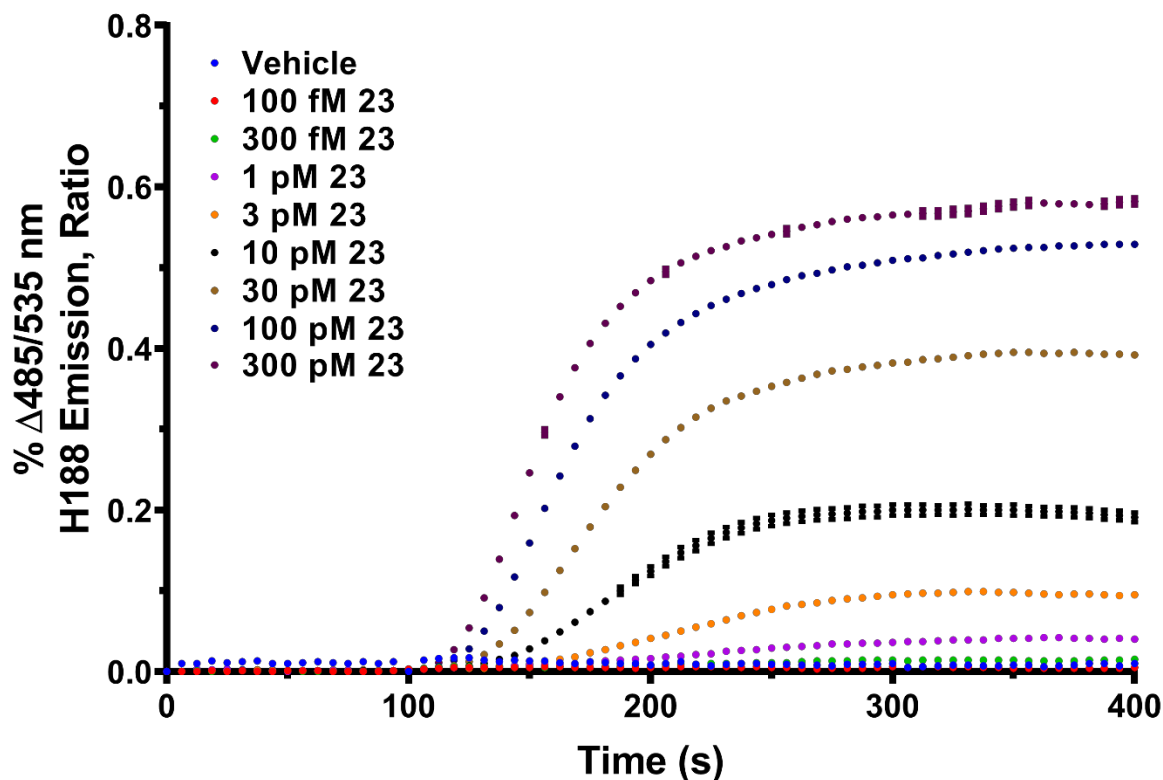


**Figure 81.** *In vitro* dose escalation study of **23** showing increase in cAMP levels in GLP-1R stably transfected HEK-293-H188 c20 cells.

#### 6.6.2.21 Synthesis of Cbi-PEG2-Ex40 (**24**)

**24** was prepared by combining **8** (2.0 mg, 0.0017 mmol) with CuI (4.1 mg, 0.022 mmol), TBTA (7.4 mg, 0.014 mmol), and Ex40 (4.0 mg 0.0009 mmol) gave the target compound, which was purified using RP-HPLC method A2 to produce **24** as a red solid to 97% purity.  $t_R$ : 11.6 min (Figure 82); ESI-MS-expected  $m/z$  = 5544, observed  $m/z$  =  $[M^+ - H_2O + 2H^+ + CH_3CN]^{+3}$ : 1884,  $[M^+ - H_2O + 3H^+ + CH_3OH]^{+4}$ : 1414,  $[M^+ - H_2O + 3H^+]^{+4}$ : 1382 (Figure 83). *In vitro* function of **24** was determined in GLP-1R stably transfected HEK-293-H188 c20 cells (Figure 84).

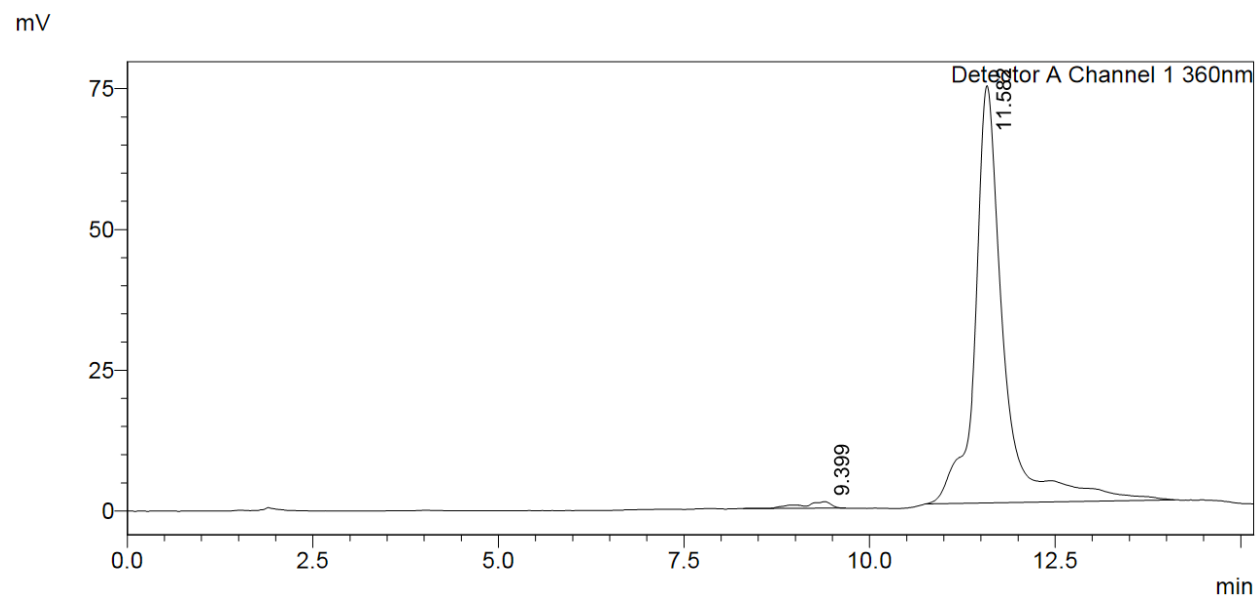


**Figure 82.** RP-HPLC trace showing product **24** at 11.6 min.

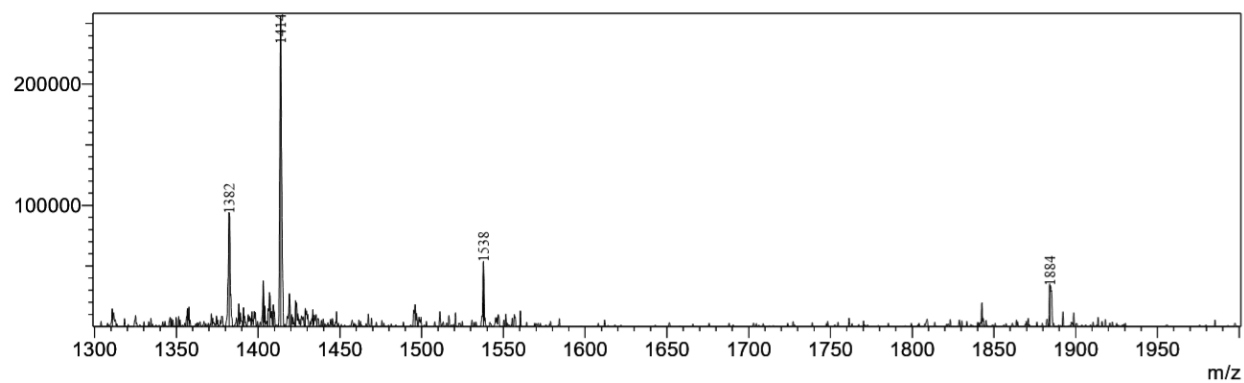


**Figure 83.** ESI-MS of **24**, expected  $m/z = 5544$ , observed  $m/z = [M^+ - H_2O + 2H^+ + CH_3CN]^{+3}: 1884$ ,  $[M^+ - H_2O + 3H^+ + CH_3OH]^{+4}: 1414$ ,  $[M^+ - H_2O + 3H^+]^{+4}: 1382$ .

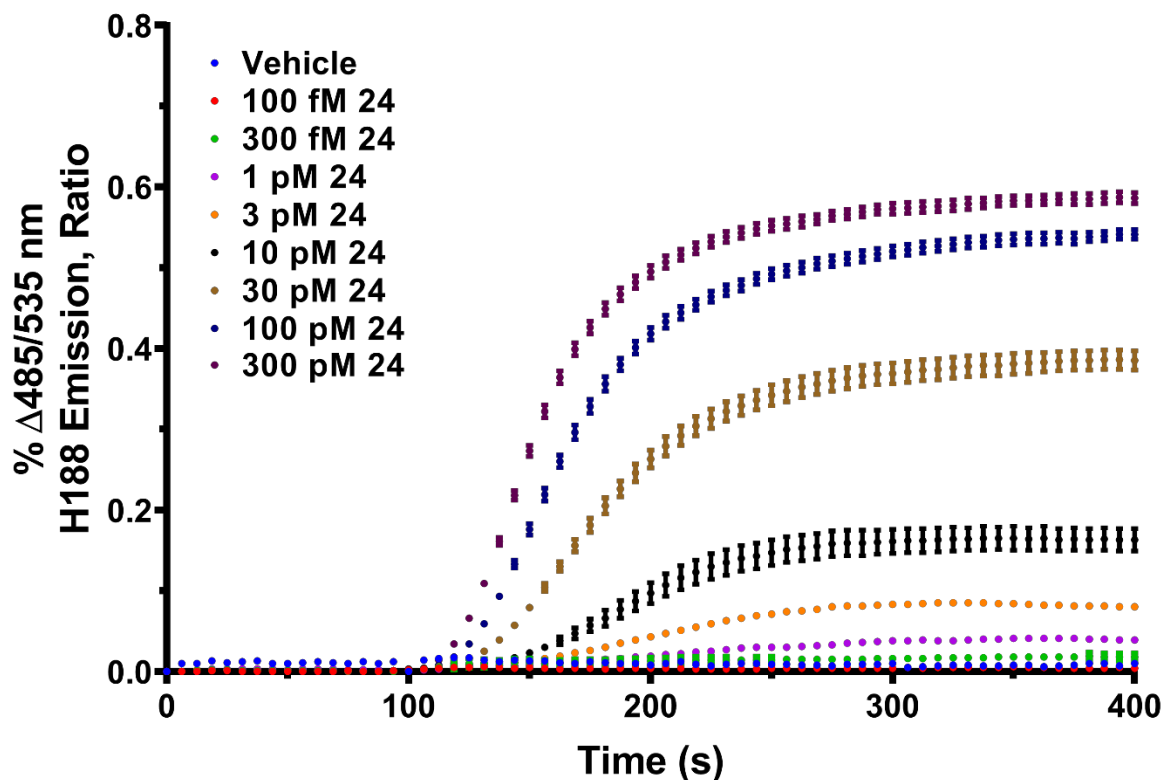


**Figure 84.** *In vitro* dose escalation study of **24** showing increase in cAMP levels in GLP-1R stably transfected HEK-293-H188 c20 cells.

#### 6.6.2.22 Synthesis of Cbi-PEG4-Ex40 (**25**)

**25** was prepared by combining **9** (3.0 mg, 0.0023 mmol) with CuI (3.3 mg, 0.017 mmol), TBTA (6.8 mg, 0.013 mmol), and Ex40 (4.1 mg 0.0009 mmol) gave the target compound, which was purified using RP-HPLC method A2 to produce **25** as a red solid to 97% purity.  $t_R$ : 12.0 min (Figure 85); ESI-MS-expected  $m/z$  = 5632, observed  $m/z$  =  $[M^+ - H_2O + 2H^+ + CH_3CN]^{+3}$ : 1914,  $[M^+ - H_2O + 3H^+ + CH_3OH]^{+4}$ : 1436 (Figure 86). *In vitro* function of **25** was determined in GLP-1R stably transfected HEK-293-H188 c20 cells (Figure 87).

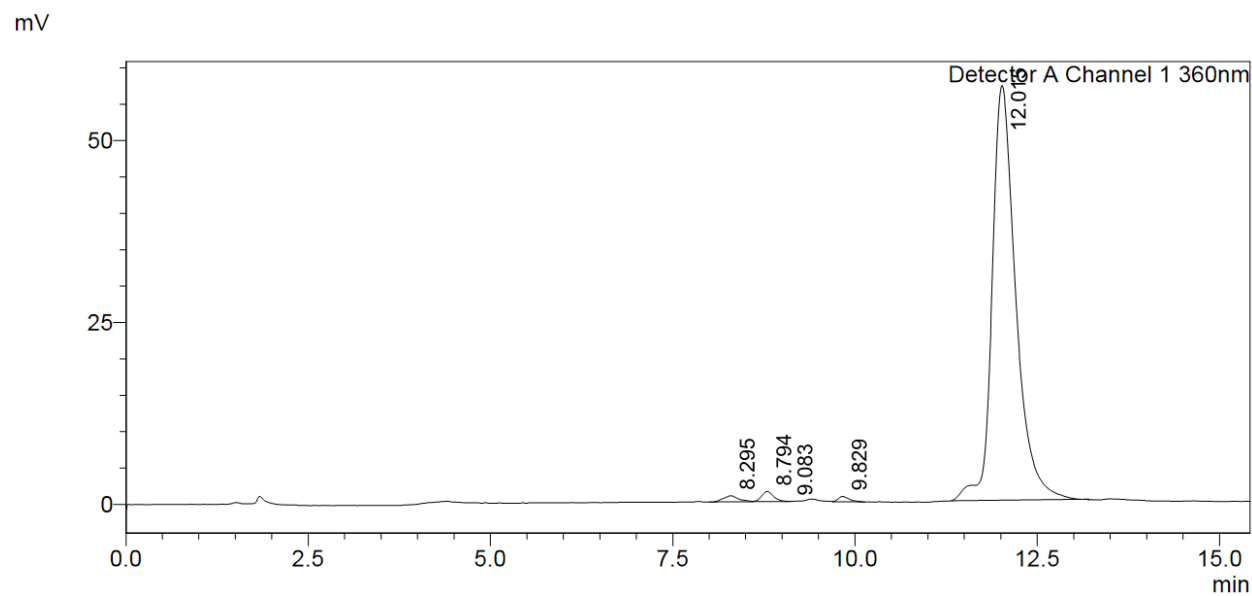


**Figure 85.** RP-HPLC trace showing product **25** at 12.0 min.

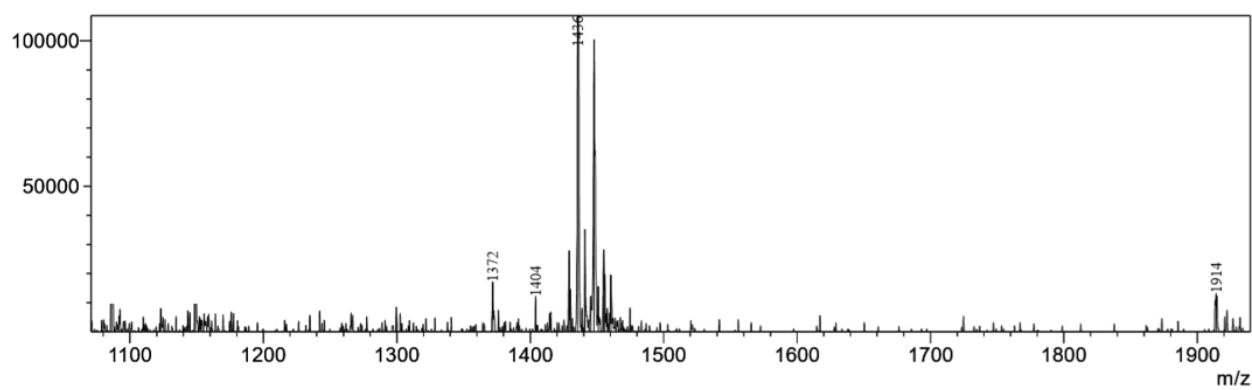


**Figure 86.** ESI-MS of **25**, expected  $m/z = 5632$ , observed  $m/z = [M^+ - H_2O + 2H^+ + CH_3CN]^{+3}$ : 1914,  $[M^+ - H_2O + 3H^+ + CH_3OH]^{+4}$ : 1436.



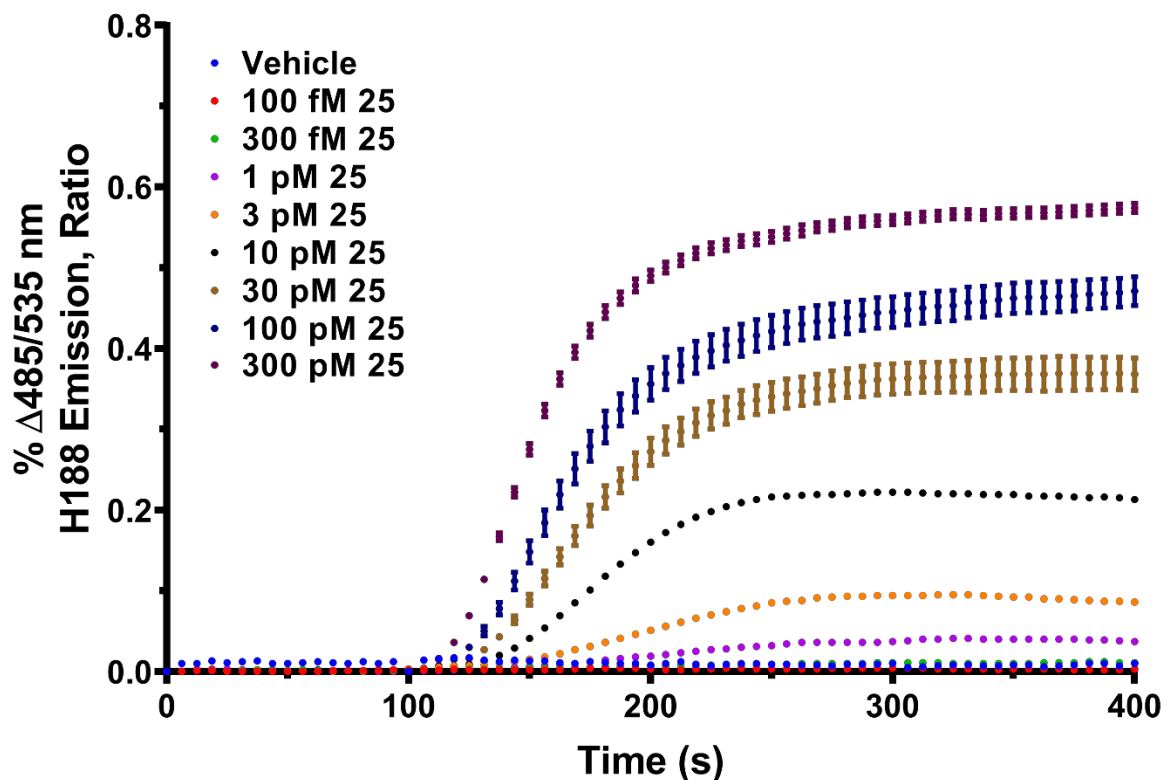


**Figure 87.** *In vitro* dose escalation study of **25** showing increase in cAMP levels in GLP-1R stably transfected HEK-293-H188 c20 cells.

#### 6.6.2.23 Synthesis of Cbi-4EPMA-Ex40 (**26**)

**26** was prepared by combining **10** (2.1 mg, 0.0018 mmol) with CuI (3.0 mg, 0.016 mmol), TBTA (6.7 mg, 0.013 mmol), and Ex40 (2.3 mg 0.0005 mmol) gave the target compound, which was purified using RP-HPLC method A2 to produce **26** as a red solid to 98% purity.  $t_R$ : 11.9 min (Figure 88); ESI-MS expected  $m/z$  = 5531, observed  $m/z$  =  $[M^+ - H_2O + 3H^+ + CH_3OH]^{+4}$ : 1411,  $[M^+ - H_2O + 3H^+]^{+4}$ : 1379,  $[M^+ - H_2O + 4H^+]^{+5}$ : 1104 (Figure 89). *In vitro* function of **26** was determined in GLP-1R stably transfected HEK-293-H188 c20 cells (Figure 90).

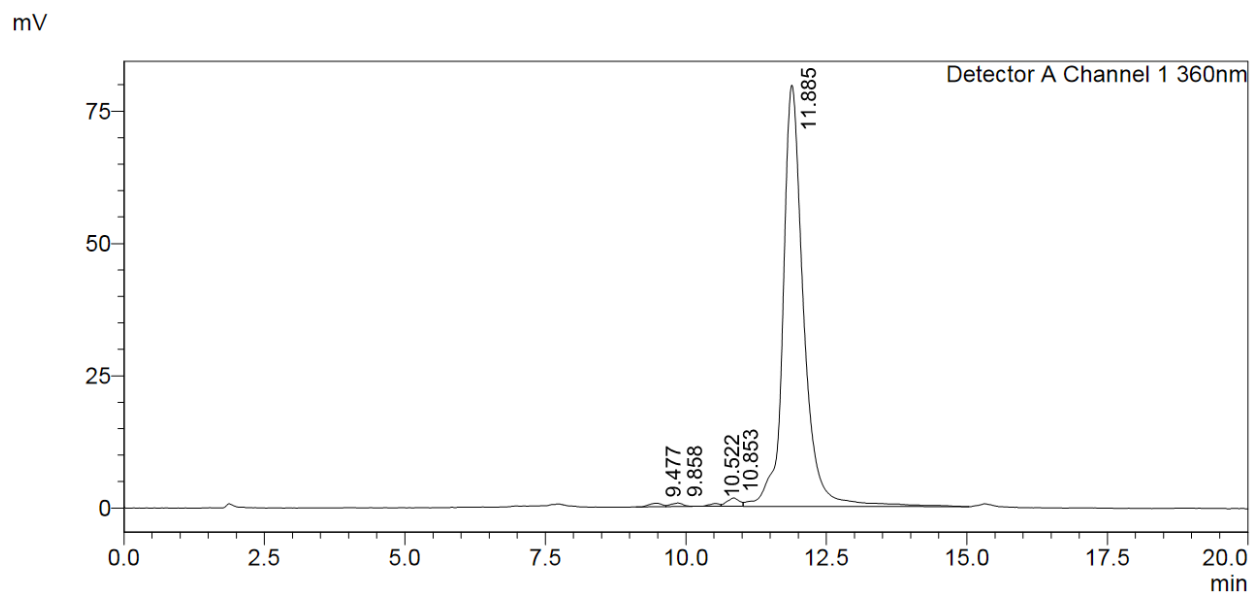


**Figure 88.** RP-HPLC trace showing product **26** at 11.9 min.

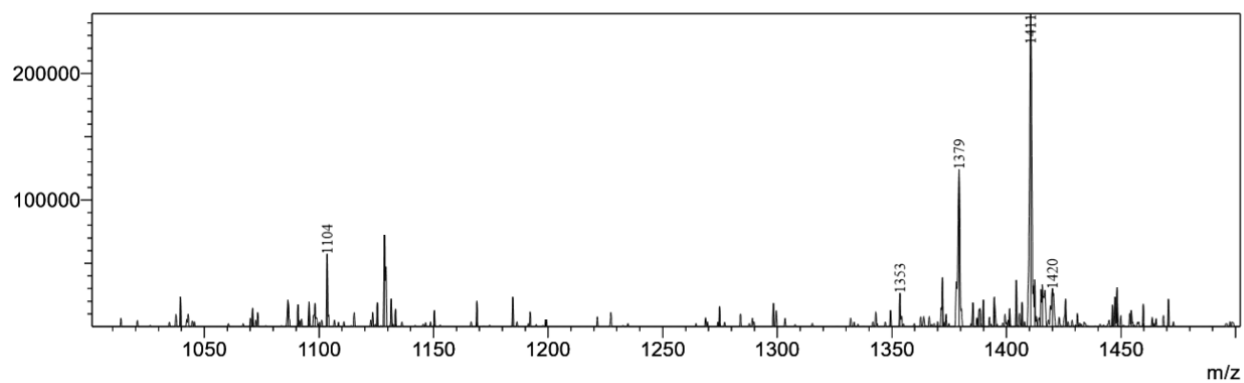


**Figure 89.** ESI-MS of **26**, expected  $m/z = 5531$ , observed  $m/z = [M^+-H_2O+CH_3OH+3H^+]^{+4}: 1411$ ,  $[M^+-H_2O+3H^+]^{+4}: 1379$ ,  $[M^+-H_2O+4H^+-CN]^{+4}: 1353$ ,  $[M^+-H_2O+4H^+]^{+5}: 1104$ .

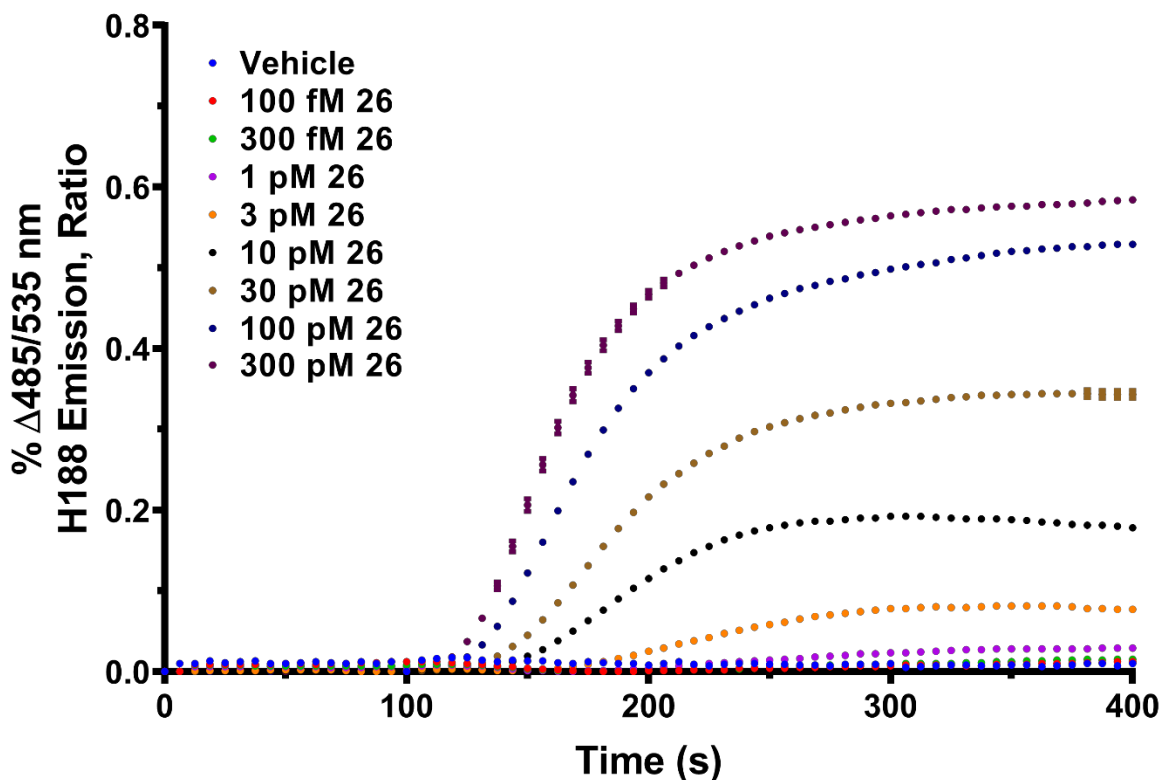


**Figure 90.** *In vitro* dose escalation study of **26** showing increase in cAMP levels in GLP-1R stably transfected HEK-293-H188 c20 cells.

#### 6.6.2.24 Synthesis of Cbi-3EPMA-Ex40 (**27**)

**27** was prepared by combining **11** (3.0 mg, 0.0025 mmol) with CuI (3.4 mg, 0.018 mmol), TBTA (7.0 mg, 0.013 mmol), and Ex40 (2.0 mg 0.0005 mmol) gave the target compound, which was purified using RP-HPLC method A2 to produce **27** as a red solid to 97% purity.  $t_R$ : 11.9 min (Figure 91); ESI-MS-expected  $m/z$  = 5531, observed  $m/z$  =  $[M^+ - H_2O + 2H^+ + CH_3CN]^{+3}$ : 1880,  $[M^+ - H_2O + 2H^+]^{+3}$ : 1838,  $[M^+ - H_2O + 3H^+ + CH_3OH]^{+4}$ : 1410,  $[M^+ - H_2O + 3H^+]^{+4}$ : 1379,  $[M^+ - H_2O + 4H^+]^{+5}$ : 1103 (Figure 92). *In vitro* function of **27** was determined in GLP-1R stably transfected HEK-293-H188 c20 cells (Figure 93).

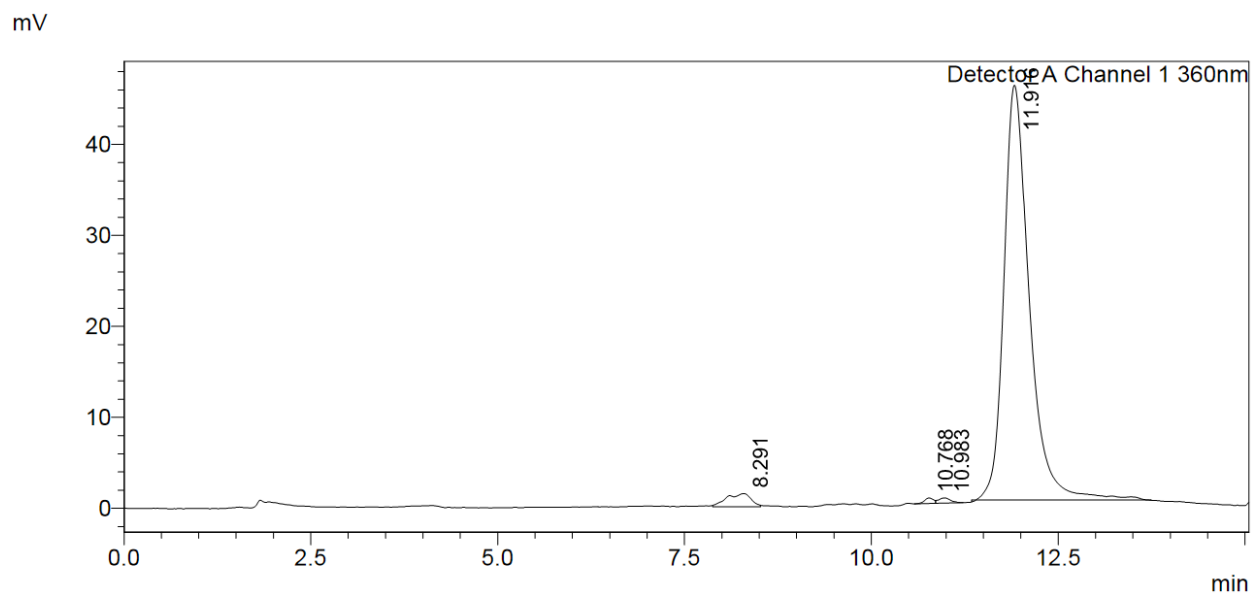


**Figure 91.** RP-HPLC trace showing product **27** at 11.9 min.

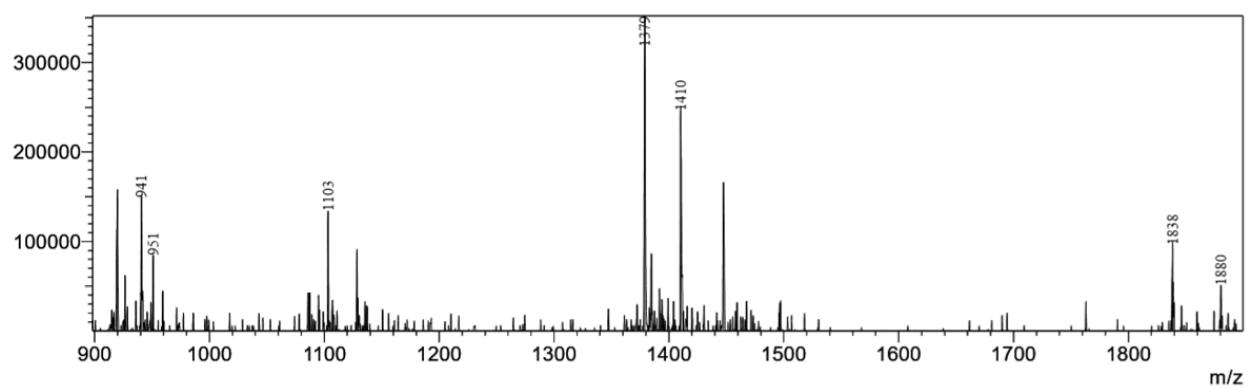


**Figure 92.** ESI-MS of **27**, expected  $m/z = 5531$ , observed  $m/z = [M^+ - H_2O + CH_3CN + 2H^+]^{+3}$ : 1880,  $[M^+ - H_2O + 2H^+]^{+3}$ : 1838,  $[M^+ - H_2O + CH_3OH + 3H^+]^{+4}$ : 1410,  $[M^+ - H_2O + 3H^+]^{+4}$ : 1379,  $[M^+ - H_2O + 4H^+]^{+5}$ : 1103.

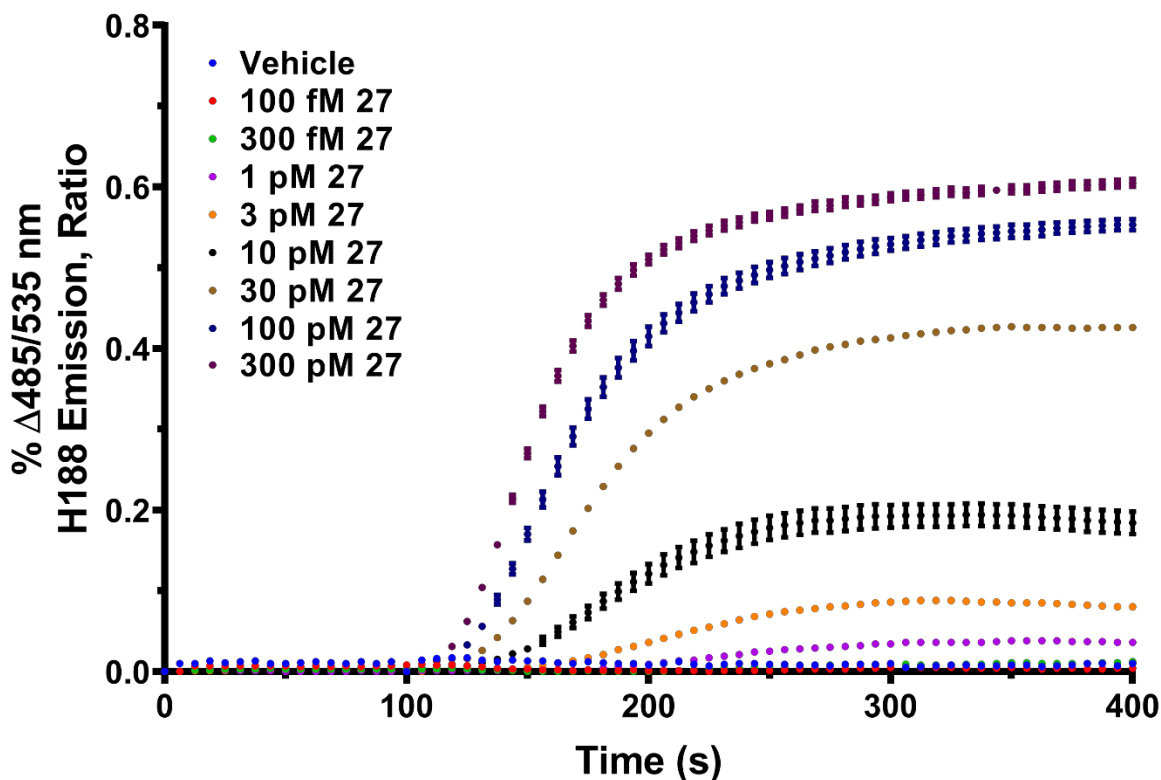


**Figure 93.** *In vitro* dose escalation study of **27** showing increase in cAMP levels in GLP-1R stably transfected HEK-293-H188 c20 cells.

### 6.6.3 Agonism ( $EC_{50}$ ) at Human GLP-1R

Agonism at the GLP-1R was monitored utilizing HEK-293 cells stably transfected with both the human GLP-1R and H188 cAMP FRET reporter cultured in DMEM with 15% FBS, 1% pen/strep and 250  $\mu\text{g}/\text{mL}$  geneticin/G-418. Cells were placed in 96-well plate in suspension at 200  $\mu\text{L}$  standard extracellular saline with 11 mM glucose and 0.1% BSA at  $\sim 60,000$  cells/well. Peptides and conjugates were injected to each well at 5x the required concentration. Agonism was determined through an increase in 485/535 nm FRET ratio, indicative of an increase in cAMP level through binding to the H188 cAMP FRET reporter.

#### **6.6.4 Competitive Binding Assay (IC<sub>50</sub>) at Human GLP-1R**

IC<sub>50</sub> values were measured in CHO-K1 cells at the human GLP-1R by Euroscreen Fast (Gosselies, Belgium) using their proprietary Taglite fluorescent competitive binding assay (Cat No. FAST0154B). Agonist tracer was GLP-1red at 4 nM with reference competitor native Ex-4. Conjugates were assayed in duplicate independent runs at nine concentrations per run ranging from 1 pM to 1 μM.

#### **6.6.5 Ex4 and Cbi-Ex4 ELISA**

Concentrations of Ex4 and Cbi-Ex4 were measured using a commercial kit purchased from Phoenix Pharmaceuticals (Exendin-4 (Heloderma suspectum) EK-070-94). The ELISA was performed according to the manufacturer's protocol with the exception of shrew blood serum that had been dosed with Cbi-Ex4. A Cbi-Ex4 standard curve was generated by matching concentrations provided by the manufacturer's standards.

#### **6.6.6 Structural Studies Using Circular Dichroism (CD)**

All CD spectra were recorded in three independent runs in 100 μL of H<sub>2</sub>O with a final concentration of 40 μM using a Jasco J-715 circular dichroism spectropolarimeter at 25 °C in a 0.1 cm path-length cuvette. The spectra were recorded from 250 to 200 nm and averaged over 6 scans with a resolution of 1.0 nm, a band width of 1.0 nm, and a response time of 4 s. The mean residue ellipticity was plotted versus wavelength using Prism GraphPad 8.

## 6.7 Experimental of Chapter 4

### 6.7.1 Determining Structure of GRASP-05 Utilizing 2D NMR

Experiments were done on the 800MHz instrument at SUNY College of Environmental Science and Forestry (ESF) with the cryoprobe at 25 and 30 °C.

To assign the peaks, the following experiments were performed:

Nuclear overhauser effect spectroscopy (NOESY) using excitation sculpting for water suppression. The spectral width in both dimensions was 12.4971 ppm centered at 4.691 ppm. Number of points acquired in the direct dimension was 2048 and 512 in the remote dimension. The relaxation delay was set to 2 seconds and the mixing time to 200 ms.

Total correlation spectroscopy (TOCSY) using excitation sculpting for water suppression and MLEV17 for the TOCSY transfer. The spectral width in both dimensions was 12.4971 ppm centered at 4.691 ppm. Number of points acquired in the direct dimension was 1024 and 512 in the remote dimension. The relaxation delay was set to 1.5 seconds and the TOCSY mixing time to 90 ms.

Correlation spectroscopy (COSY) using excitation sculpting for water suppression. The spectral width in both dimensions was 12.4971 ppm centered at 4.691 ppm. Number of points acquired in the direct dimension was 1024 and 512 in the remote dimension.

Heteronuclear single quantum coherence (HSQC) with multiplicity editing. The spectral width for the proton dimensions was 11.001 ppm centered at 4.691 ppm and for the carbon dimension 169.9983 ppm centered at 80 ppm. Number of points acquired in the direct dimension was 1024 and 512 in the remote dimension.

2D HSQC-TOCSY using DISPI2 sequence for the TOCSY transfer. The spectral width for the proton dimensions was 11.001 ppm centered at 4.691 ppm and for the carbon dimension 169.9983 ppm centered at 80 ppm. Number of points acquired in the direct dimension was 1024 and 512 in the remote dimension. The relaxation delay was set to 1.5 seconds and the TOCSY mixing time to 80 ms.

### 6.7.2 Synthesis of AF546-GRASP-05

DBCO modified AlexaFluor<sup>®</sup>564 (DBCO-AF546) (1.0 mg, 0.910 nmol) was “clicked” to GRASP-05 (3.0 mg, 0.920 nmol) by dissolving in 4:1 DMF: H<sub>2</sub>O (1200 $\mu$ L) and allowed to stir overnight at room temperature to produce AF546-GRASP-05 (GRASP-555). GRASP-555 was purified using RP-HPLC (H<sub>2</sub>O + 0.1% TFA and MeOH from 1% CH<sub>3</sub>OH/H<sub>2</sub>O + 0.1% TFA to 90% CH<sub>3</sub>OH/H<sub>2</sub>O + 0.1% TFA in 25 min) to produce GRASP-555 in 99% purity in stoichiometric yields. ESI-MS expected  $m/z$  = 4386, observed  $m/z$  = [M+2H<sup>+</sup>+Na<sup>+</sup>]<sup>+3</sup>: 1487, [M+3H]<sup>+3</sup>: 1463, [M+4H<sup>+</sup>+H<sub>2</sub>O]<sup>+4</sup>: 1116, [M+4H]<sup>+4</sup>: 1097, [M+5H]<sup>+5</sup>: 878. Successfully linkage of GRASP-05 to DBCO-AF546 resulted in an excitation-maxima shift from 554 nm to 560 nm and emission maxima shift from 570 nm to 571 nm (Figures found in Chapter 4).



### 6.7.3 Development by this author of an in-house ELISA for GDF15 Binding

#### *ELISA PROTOCOL FOR GDF15/ GRASP ANTAGONISTS*

1. Dilute the 20x EIA/ELISA Buffer (Phoenix Pharmaceuticals EK-BUF) with distilled water to a final concentration of 1x (amount may vary based on needs).

- Prior to diluting this buffer be sure no crystals are found in the sample. If crystals are found place in a warm water bath until they are completely dissolved.
- This buffer will be used to dilute or reconstitute all peptides or antibodies using during this assay.
- This buffer will also be used for washing the 96-well plate.

2. Reconstitute the recombinant human GDF-15 (R&D systems 9279-GD-50) in the 1x assay buffer to desired concentration and vortex thoroughly. Allow the solution to sit at room temperature for 30min to ensure all peptide has been completely dissolved.

- This is your standard peptide stock. Use this stock to perform a serial dilution to desired concentrations of peptide to be tested.

3. Reconstitute the primary antibody (Abcam ab206414) in the appropriate amount of 1x assay buffer to reach desired concentration. Allow the solution to sit at room temperature for 5min to ensure all the antibody has been completely dissolved.

4. Reconstitute the recombinant human GFR $\alpha$ -like His-tag receptor (R&D 9647-GR-050) in the appropriate amount of 1x assay buffer to reach desired concentration. Allow the solution to sit at room temperature for 30min to ensure all of the receptor has been completely dissolved.

5. Reconstitute the positive control (Abcam ab206414) in the appropriate amount of 1x assay buffer to reach desired concentration. All the solution to sit at room temperature for 5min to ensure all the antibody has been completely dissolved.

*To a Pierce™ Nickel Coated Plat (Clear, 96-well) (ThermoFisher Scientific 15442)*

1. Leave wells A1 and A2 empty on the plate.

- These wells will serve as your blanks.

2. Add 100uL of 1x assay buffer to wells B1 and B2.

3. To all wells except A1, A2, B1, and B2 add 100µL of recombinant human GFRα-like His-tag receptor (R&D 9647-GR-050) (0.1µg/mL).

4. Seal the 96-well plate and incubate and rock at room temperature for two hours.

5. After two hours wash the plate with 300µL of 1x assay buffer, discard the buffer, invert immunoplate, and blot dry, repeat three times.

6. To all wells except A1, A2, B1, and B2 add 100µL of recombinant human GDF-15 (R&D systems 9279-GD-50).

7. Seal the 96-well plate and incubate and rock at room temperature for one hour.

8. After one hour wash the plate with 300µL of 1x assay buffer, discard the buffer, invert immunoplate, blot dry, repeat three times.

9. To all wells except A1, A2, B1, and B2 add 100µL of Anti-GDF antibody [EPR19939] (Abcam ab206414) according to manufacturer's dilution protocol.

10. Seal the 96-well plate and incubate and rock at room temperature for one hour.

11. After one hour wash the plate with 300 $\mu$ L of 1x assay buffer, discard the buffer, invert immunoplate, blot dry, repeat three times.
12. To all wells except A1, A2, B1, and B2 add 100 $\mu$ L of Goat Anti-Rabbit IgG H&L (HRP) (Abcam ab6721) according to manufacturer's dilution protocol.
13. Seal the 96-well plate and incubate and rock at room temperature for one hour.
14. After one hour wash the plate with 300 $\mu$ L of 1x assay buffer, discard the buffer, invert immunoplate, blot dry, repeat three times.
15. To all wells except A1, A2, B1, and B2 add 100 $\mu$ L of TMB ELISA Substrate (High Sensitivity) (Abcam ab171523) according to manufacturer's protocol.
16. Seal the 96-well plate and incubate and rock at room temperature for one hour.
  - Protect from light.
17. To all wells except A1, A2, B1, and B2 add 100 $\mu$ L of 450nm Stop Solution for TMB Substrate (Abcam ab171529) according to manufacturer's protocol.
18. Load the immunoplate onto the microplate reader and measure absorbance at 450nm.

*Testing for Antagonism of GRASP*

1. Following step five in the previously listed protocol add 100 $\mu$ L of antagonist at desired concentration and allow to sit for one hour.
2. After one hour wash the plate with 300 $\mu$ L of 1x assay buffer, discard the buffer, invert immunoplate, blot dry, repeat three times.
3. Proceed to step six in the previously listed protocol.

## 6.8 Experimental-Chapter 5

### 6.8.1 Synthesis of Fluorescent Probes

#### 6.8.1.1 Synthesis of AF546-Ex4 (Rex)

DBCO modified AlexaFluor®564 (DBCO-AF546) (1.0 mg, 0.910 nmol) was “clicked” Exendin-4 (Ex4) where the twelfth residue, lysine, was substituted by an azido modified lysine (3.0 mg, 0.712 nmol) by dissolving in 4:1 DMF: H<sub>2</sub>O (1200 μL) and allowed to stir overnight at room temperature to produce AF546-Ex4 (REX). REX was purified using RP-HPLC (H<sub>2</sub>O + 0.1% TFA and MeOH from 1% CH<sub>3</sub>OH/H<sub>2</sub>O + 0.1% TFA to 90% CH<sub>3</sub>OH/H<sub>2</sub>O + 0.1% TFA in 25 min) to produce REX in 97% purity in stoichiometric yields. ESI-MS expected  $m/z = 5319$ , observed  $m/z = [M+3H]^+3$ : 1773,  $[M+4H]^+4$ : 1331. Successfully linkage of Ex4 to DBCO-AF546 resulted in an excitation-maxima shift from 554 nm to 560 nm and emission maxima shift from 570 nm to 575 nm (Figures found in Chapter 5).

#### 6.8.1.2 Synthesis of Cy5-Leptin (Cy5-Leptin)

1.0 mg of mouse recombinant leptin was dissolved in 450 μL phosphate buffer pH 7.8 and allowed to rock at room temperature. 0.2 mg of NHS-Ester-Sulfo-Cy5 (Cy5) was dissolved in 50 μL of DMSO and added to the rocking solution in 10 μL aliquots over one hour. Following the final addition of Cy5 the reaction rocked for an additional 2 hours to produce the final product, Cy5-Leptin. The reaction was always protected from light. Cy5-Leptin was purified using RP-HPLC (H<sub>2</sub>O + 0.1% TFA and MeOH from 1% CH<sub>3</sub>OH/H<sub>2</sub>O + 0.1% TFA to 90% CH<sub>3</sub>OH/H<sub>2</sub>O + 0.1% TFA in 20 min). The mass of the Cy5-Leptin was confirmed via SDS-PAGE analysis. Successfully linkage of Cy5 to Leptin resulted in an excitation-maxima shift from 646 nm to 650 nm and emission maxima shift from 662 nm to 669 nm (Figures found in Chapter 5).

### 6.8.1.3 Synthesis of AF546-Oxytocin (ROxy)

AlexaFluor®564 (DBCO-AF546) (2.0 mg, 0.002 mmol) was successfully “clicked” to an azido modified oxytocin (OTaz) (2.5mg, 0.002 mmol) where the eighth residue, leucine, was substituted by an azido modified lysine by dissolving both compounds in 4:1 DMF: H<sub>2</sub>O and allowed to stir overnight at room temperature to produce AF546-Oxy (Roxy). Roxy was purified using RP-HPLC (H<sub>2</sub>O + 0.1% TFA and MeOH from 1% CH<sub>3</sub>OH/H<sub>2</sub>O + 0.1% TFA to 90% CH<sub>3</sub>OH/H<sub>2</sub>O + 0.1% TFA in 25 min) to produce Roxy in 99% purity in stoichiometric yields. ESI-MS expected  $m/z = 2154$ , observed  $m/z = [M+H_2O+2H^+]^{+2}: 1097$ ,  $[M+2H]^{+2}: 1078$ . Successfully linkage of OTaz to DBCO-AF546 resulted in an excitation-maxima shift from 554 nm to 558 nm and emission maxima shift from 570 nm to 572 nm (Figures found in Chapter 5).

## 6.9 Experimental-Chapter 7

### 6.9.1 Synthesis of Linear Oxytocin

Linear oxytocin was synthesized by Fmoc/tBu solid-phase peptide synthesis methodology on a CEM Liberty Blue automated microwave peptide synthesizer (CEM Corporation, Matthews, NC) starting with Fmoc-Rink Amide Protide Resin (LL) and employed repetitive DIC/ Oxyma activation. The side chain protecting group scheme consisted of Asn(Trt); Gln(OtBu); Tyr(tBu); and Trp(Boc). All amino acids and activating agents were purchased from CEM Corporation (Matthews, NC). Oxytocin was cleaved from the resin and deprotected using a CEM Corporation Razor: rapid peptide cleavage system with treatment of 92.5% TFA trifluoroacetic acid (TFA) containing 2.5% TIPS, 2.5% water, 2.5% DODT. The obtained solution was precipitated with cold diethylether at centrifuged at 4000 rpm for 5 min. The diethylether supernatant was discarded and the remaining precipitate was redissolved in water and placed on a Labconco FreeZone 1

lyophilizer. The resulting peptide were analyzed and characterized by LC-MS (Shimadzu 8040). ESI-MS expected  $m/z = 1050$ , observed  $m/z = [M+H]^+$ : 1050,  $[M+2H]^{+2}$ : 525.

### 6.9.2 Cyclic Oxytocin - Disulfide Bridge Formation in Oxytocin

Cyclic oxytocin was formed through the formation of a disulfide bridge between cysteine residues found at position one and six of linear oxytocin. Linear oxytocin was dissolved in 10% DMSO in water and allowed to stir for 48 hours. The resulting solution was diluted with water and placed on a Labconco FreeZone 1 lyophilizer. Due to DMSO concentration, a 'film' on the vessel was produced following the initial lyophilization process. The film was redissolved in water and the lyophilization process was repeated to now produce a white powder. The peptide was purified by semi-preparative RP-HPLC ( $H_2O + 0.1\%$  TFA and  $CH_3CN$  from  $1\%$   $CH_3CN/H_2O + 0.1\%$  TFA to  $65\%$   $CH_3CN/H_2O + 0.1\%$  TFA in 25 min) on an Agilent ZORBAX 300SB-C8 ( $5\ \mu m$ ,  $9.4 \times 250$  mm) column. Cyclic oxytocin was analyzed and characterized by LC-MS (Shimadzu 8040). ESI-MS expected  $m/z = 1048$ , observed  $m/z = [M+H]^+$ : 1048.

### 6.9.3 Synthesis of Oxytocin Conjugates

#### 6.9.3.1 Synthesis of B12-DBCO (B12-DBCO)

B12-DBCO was prepared by combining B12 (25.0 mg, 0.018 mmol) with CDT (10.0 mg, 0.061 mmol) and allowed to stir for one hour at which time sulfo-DBCO-amine (25.0 mg, 0.059 mmol) and TEA (50  $\mu L$ ) were added and stirred overnight to give the target compound, which was purified using RP-HPLC ( $H_2O + 0.1\%$  TFA and MeOH from  $1\%$   $CH_3OH/H_2O + 0.1\%$  TFA to  $90\%$   $CH_3OH/H_2O + 0.1\%$  TFA in 25 min) to produce B12-DBCO to 92% purity in 80 % yield. ESI-MS expected  $m/z = 1808$ , observed  $m/z = [M+2H]^{+2}$ : 905 (Figures found in Chapter 7).

### 6.9.3.2 Synthesis of B12-Oxytocin (B12-Oxy)

B12-Oxy was prepared by combining B12-DBCO (12.0 mg, 0.011 mmol) with cyclic oxytocin (10.0 mg, 0.010 mmol) where the eighth residue, leucine, was substituted by an azido modified lysine (OTaz). The B12-DBCO was linked to OTaz by dissolving both compounds in 4:1 DMF: H<sub>2</sub>O and allowing to react at room temperature overnight to produce B12-Oxytocin (B12-Oxy). B12-Oxy was purified using RP-HPLC (H<sub>2</sub>O + 0.1% TFA and MeOH from 1% CH<sub>3</sub>OH/H<sub>2</sub>O + 0.1% TFA to 90% CH<sub>3</sub>OH/H<sub>2</sub>O + 0.1% TFA in 25 min) to produce B12-OXY to 99% purity in stoichiometric yields. ESI-MS expected  $m/z = 2856$ , observed  $m/z = [M+2H]^+{}^2$ : 1429,  $[M+3H]^+{}^3$ : 953 (Figures found in Chapter 7).

## 6.10 References

- (1) Klarenbeek, J.; Goedhart, J.; Van Batenburg, A.; Groenewald, D.; Jalink, K. Fourth-Generation Epac-Based FRET Sensors for CAMP Feature Exceptional Brightness, Photostability and Dynamic Range: Characterization of Dedicated Sensors for FLIM, for Ratiometry and with High Affinity. *PLoS One* **2015**, *10* (4), e0122513.
- (2) Bonaccorso, R. L.; Chepurny, O. G.; Becker-Pauly, C.; Holz, G. G.; Doyle, R. P. Enhanced Peptide Stability Against Protease Digestion Induced by Intrinsic Factor Binding of a Vitamin B12 Conjugate of Exendin-4. *Mol. Pharm.* **2015**, *12* (9), 3502–3506.
- (3) Mietlicki-Baase, E. G.; Liberini, C. G.; Workinger, J. L.; Bonaccorso, R. L.; Borner, T.; Reiner, D. J.; Koch-Laskowski, K.; McGrath, L. E.; Lhamo, R.; Stein, L. M.; De Jonghe, B. C.; Holz, G. G.; Roth, C. L.; Doyle, R. P.; Hayes, M. R. A Vitamin B12 Conjugate of Exendin-4 Improves Glucose Tolerance without Associated Nausea or Hypophagia in Rodents. *Diabetes, Obes. Metab.* **2018**, *20* (5), 1223–1234.
- (4) Zhou, K.; Zelder, F. Identification of Diastereomeric Cyano - Aqua Cobinamides with a Backbone-Modified Vitamin B12 Derivative and with <sup>1</sup>H NMR Spectroscopy. *Eur. J. Inorg. Chem.* **2011**, No. 1, 53–57.



## 7. Ongoing and Future Work

### 7.1 Building on lead candidate **22** (Chapter 3)

As shown in Chapter 3, I was able to successfully design and synthesize a glucagon-like peptide-1 (GLP-1) receptor agonist (GLP-1RA), **22**, with reduced brain penetrance, but with comparable binding, agonism, and pharmacodynamic profile to that of Exendin-4 (Ex4).<sup>1-3</sup> While *in vivo* tests were performed to investigate the function of **22**, we did not examine how conjugate site may affect the pharmacokinetic profile of this therapeutic compared to that of Ex4. Such an investigation was performed on our initial Cbi-Ex4 construct, **1**, which showed reduced plasma clearance.<sup>2</sup> This effect is predicted due to improved stability of the conjugate to proteolytic activity, a feature previously demonstrated, or reduced renal clearance.<sup>1</sup> This experiment should be replicated to further explore **22**.

To continue to improve **22** in an *in vivo* setting, further conjugation techniques may be explored. Some current long acting GLP-1RAs, including liraglutide<sup>4-7</sup> and semaglutide,<sup>4,5,7</sup> utilize lipidation to improve their pharmacokinetic profile allowing for once daily or once weekly administration, respectively.<sup>4,7</sup> Given our previous investigations into the pharmacokinetic (PK) profile of Cbi-Ex4,<sup>2</sup> it would not be capable of being delivered once weekly as a therapeutic. The successful lipidation of **22** would provide such an opportunity. Current synthetic attempts have been made to produce such a product. While previous investigations have been performed on optimal locations of lipidation,<sup>8</sup> none of these studies have looked at a system in which multiple conjugations sites would be utilized. While **22** utilizes an additional amino acid to conjugate Cbi to Ex4,<sup>3</sup> lipidation would occur on the native Ex4 sequence. To determine the optimal location of lipidation (C14, C16, C18 lipids) a structure activity relationship (SAR) experiment should be

performed aimed at maintaining function at the GLP-1R and pharmacodynamic profile while improving the therapeutics PK profile. Such a construct, with once weekly administration, would be utilized for glucoregulation without nausea and emesis in individuals suffering from additional diseases *i.e.*, cystic fibrosis.<sup>9</sup>

In addition, the effects of small amphiphilic or flexible spacers placed between the lipid and peptide backbone has proven highly important in successfully taking strong pharmacodynamic leads and adding clinically relevant PK properties. Key linkers of choice here would be the use of  $\gamma$ -Glu monomers or dimers, with or without di-PEG units initially.<sup>10</sup>

## **7.2 Prebinding of Corrinated Conjugates to Human Haptocorrin for Improved Pharmacokinetics**

The use of peptides as therapeutics offers specificity and often increased potency compared to synthetic small molecules.<sup>11</sup> However, peptides are often limited by their solubility and short half-life.<sup>12,13</sup> The short half-life of peptides is commonly attributed to the fact that they are readily degraded by enzymes *in vivo*.<sup>12,13</sup> To combat such issues amino acid substitutions or further chemical modification is often utilized.<sup>14</sup> Corrination offers additional avenues for improved PK.<sup>1-3,15-19</sup> The conjugation to corrins may be further exploited by prebinding to one of the proteins found in the B12 uptake pathway.<sup>1</sup> Previous work by Bonaccorso *et al.* showed that a B12-Ex4 conjugate prebound to intrinsic factor was protected from proteolytic degradation and maintained function in an *in vitro* assay.<sup>1</sup> Haptocorrin (HC) has a half-life of 9-11 days and offers an ideal target for selectively prebinding a corrin conjugate.<sup>20</sup> An initial attempt was made to explore this avenue, see chapter 3, which yielded a non-functional construct.<sup>2</sup> Given our newly identified conjugation site, K40 in Ex4, further investigations should be performed to determine

if conjugation site effects the ability of the peptide to be prebound to a protein.<sup>3</sup> An alternative approach would be to perform an SAR with the aim of producing an optimal prebound construct. Such a construct may not be the optimal construct while unbound to the protein but would once bound by HC. Given HC's ability to bind not only B12, but also other corrins, both B12, Cbi, and possibly other corrin constructs may be utilized.<sup>21-23</sup>

### **7.3 The Future of Corriation**

The use of corriation is little explored and to date has primarily focused on conjugates of peptides.<sup>1-3,18,19</sup> Corriation shows promise as a platform technology for conjugation to therapeutics, especially if one seeks to target the peripheral nervous system while avoiding the central nervous system. One such corrin of interest is Cbi, due to its high-water solubility (400 mg/mL),<sup>3</sup> it offers the ability to improve therapeutics limited by their physical properties, one such example is glucagon. To further maximize the potential that corriation offers, new avenues should be investigated including, conjugation to small molecules.

While the ability of corriation to impact the use of the peptide therapeutics its conjugation has application beyond protection from proteolytic degradation and solubility improvements. Peptides conjugated to both B12 and Cbi have drastically diminished CNS penetrance while maintaining function in the peripheral.<sup>2,3,18,19</sup> Such a construct makes it an ideal mechanistic tool for differentiating the function of a therapeutic at multiple activation sites. One current avenue being explored is through the conjugation of oxytocin (Oxy) to B12.

#### **7.3.1 Satiation Signaling via Vagal Oxytocin Receptors**

A body of evidence indicates that the GIT generates several post-ingestive signals capable of triggering satiation and suppression of central reward circuits. Oxy is well investigated and

recognized for its role in bonding behaviors,<sup>24</sup> but its role in energy homeostasis is much less defined.<sup>25</sup> To investigate the role oxy may play in this system a B12-Oxytocin (B12-Oxy) construct was designed to target the oxy receptor expressed in the vagal afferents.<sup>26</sup>

#### **7.3.1.1 Design, Synthesis, and Characterization of B12-Oxytocin (B12-Oxy)**

The design and synthesis of a B12-Oxy construct had to consider the fact that oxy readily binds copper metal in the “tail” portion of its structure. Thus, previously design B12 constructs that utilized copper-catalyzed alkyne-azide cycloaddition (CuAAC) could not be utilized, and a new “clickable” construct needed to be developed. I utilized a dibenzylcyclooctyne (DBCO) linker to produce B12-DBCO linker with the aim of utilizing strained promoted alkyne-azide cycloaddition (SPAAC) to produce a B12-Oxy.

#### **7.3.1.2 Synthesis of B12-DBCO Linker**

B12-Sulfo-DBCO-Amine (B12-DBCO) was synthesized by conjugating off the 5' hydroxyl group found in the ribose ring of the *f*-side chain of B12. The alcohol was activated with CDT at 40° C for 1 hour in DMSO then Sulfo-DBCO-Amine and triethylamine (TEA) was added, and the reaction was stirred overnight to give the target compound (Figure 1), which was purified using RP-HPLC (H<sub>2</sub>O + 0.1% TFA and MeOH from 1% CH<sub>3</sub>OH/H<sub>2</sub>O + 0.1% TFA to 90% CH<sub>3</sub>OH/H<sub>2</sub>O + 0.1% TFA in 25 min) to produce B12-DBCO to 92% purity in 80 % yield (Figure 2). ESI-MS expected  $m/z$  = 1808, observed  $m/z$  = [M+2H<sup>+</sup>]<sup>+2</sup>: 905 (Figure 3).



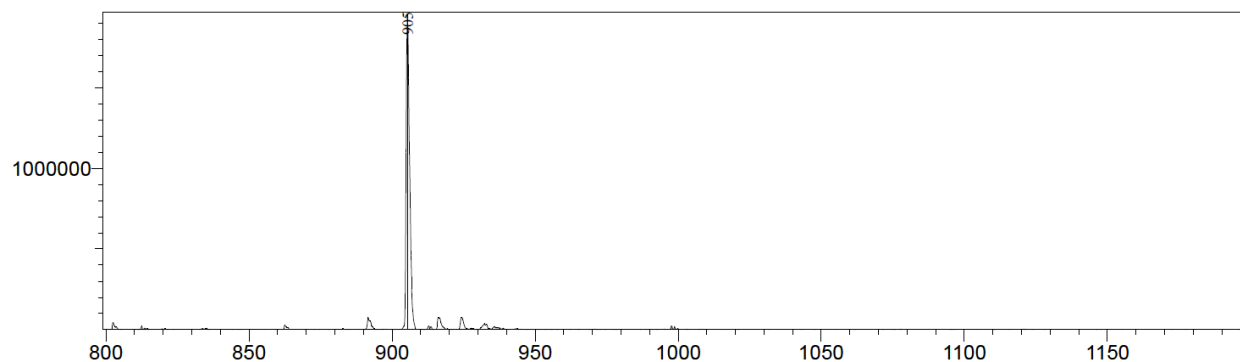


**Figure 3.** ESI-MS (Shimadzu LCMS-8040) of B12-DBCO, expected  $m/z = 1808$ , observed  $m/z = [M+2H]^{2+}: 905$ .

### 7.3.1.3 Synthesis of B12-Oxytocin (B12-Oxy)

Utilizing strained promoted alkyne-azide cycloaddition (SPAAC), B12-DBCO was successfully “clicked” to an azido modified oxytocin (OTaz) where the eighth residue, leucine, was substituted by an azido modified lysine. The B12-DBCO was linked to OTaz by dissolving both compounds in 4:1 DMF: H<sub>2</sub>O and allowing to rock at room temperature overnight to produce B12-Oxytocin (B12-Oxy) (Figure 4). B12-Oxy was purified using RP-HPLC (H<sub>2</sub>O + 0.1% TFA and MeOH from 1% CH<sub>3</sub>OH/H<sub>2</sub>O + 0.1% TFA to 90% CH<sub>3</sub>OH/H<sub>2</sub>O + 0.1% TFA in 25 min) to produce B12-OXY to 99% purity in stoichiometric yields (Figure 5). ESI-MS expected  $m/z = 2856$ , observed  $m/z = [M+2H]^{+2}: 1429$ ,  $[M+3H]^{+3}: 953$  (Figure 6).

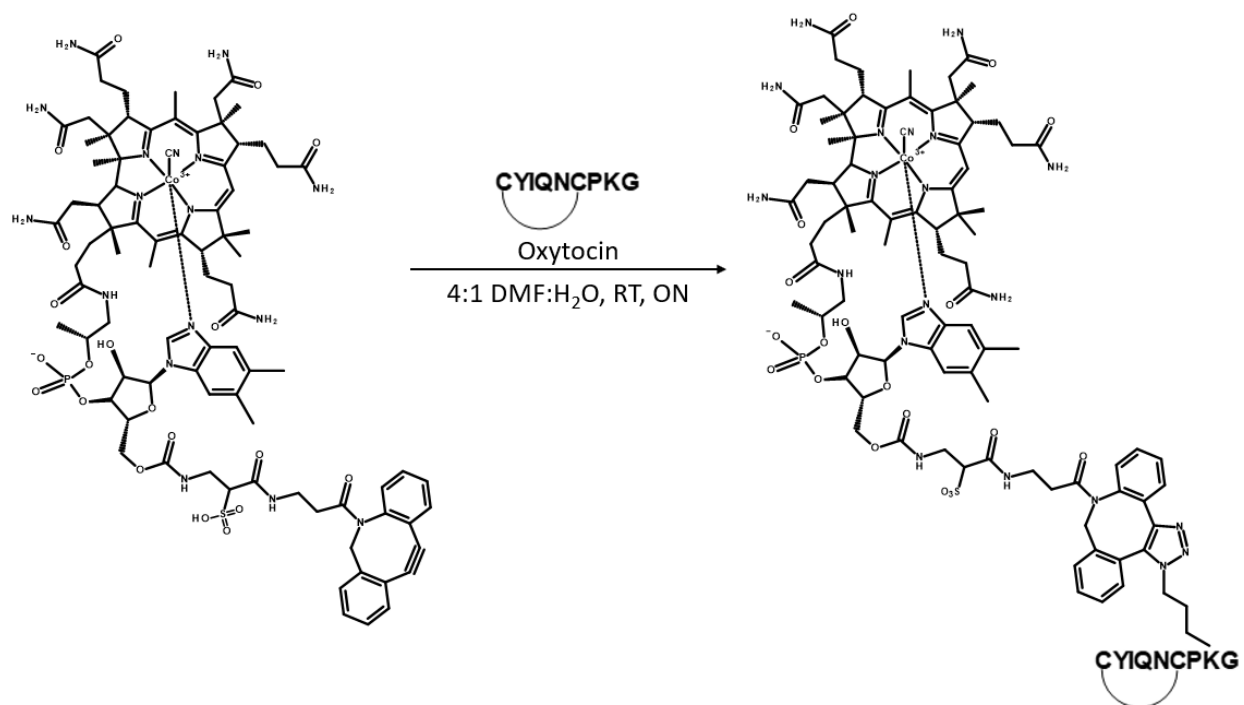


**Figure 4.** Synthetic scheme for B12-Oxy. B12-DBCO was successfully “clicked” to OTaz utilizing SPAAC.

mV

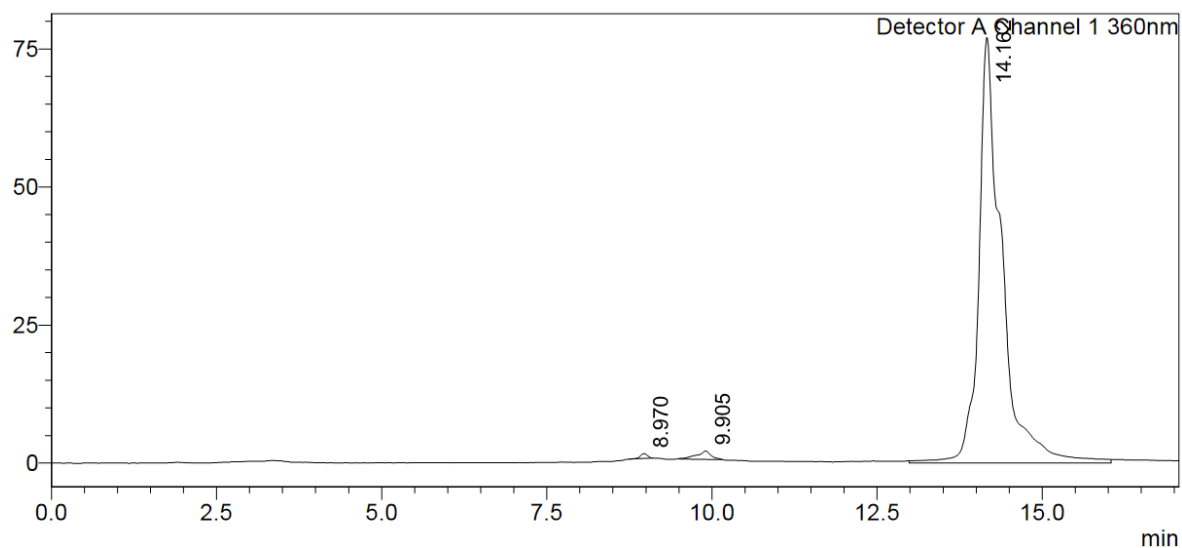


**Figure 5.** RP-HPLC Trace (Shimadzu Prominence HPLC using a C18 column (Eclipse XDB-C18 5 $\mu$ m, 4.6 x 150 mm) (RP-HPLC, from 1% CH<sub>3</sub>OH/H<sub>2</sub>O + 0.1% TFA to 90% CH<sub>3</sub>OH/H<sub>2</sub>O + 0.1% TFA in 25 min)) showing B12-Oxy product at 11.2 min. Purity 99%.

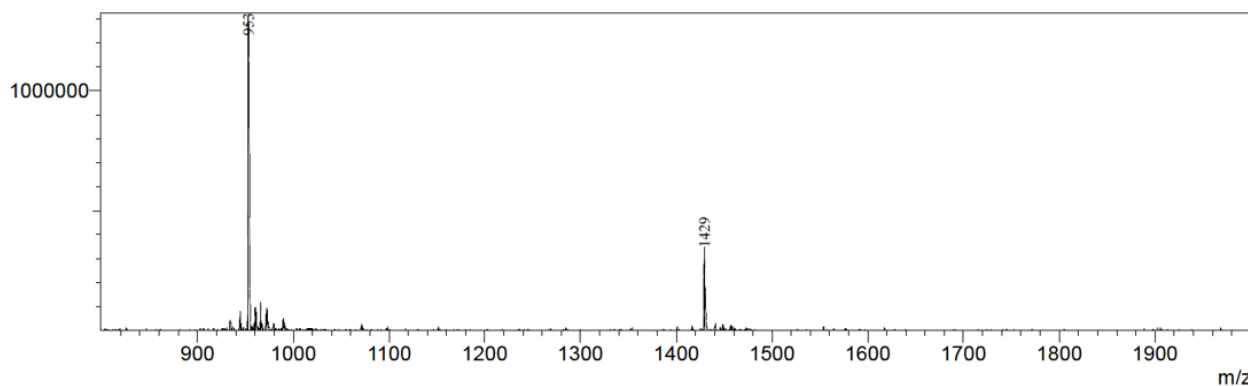


**Figure 6.** ESI-MS (Shimadzu LCMS-8040) of B12-Oxy, expected  $m/z = 2856$ , observed  $m/z = [M+2H^+]^{+2}: 1429$ ,  $[M+3H^+]^{+3}: 953$ .

#### 7.3.1.4 *In Vivo* investigations of B12-Oxy in Male and Female Rats

To date initial *in vivo* experiments have focused on examining the role peripheral oxy plays in energy homeostasis. Following intraperitoneal (IP) injection, oxytocin was found to induce a hypophagic effect both male and female rats. Female rats were more sensitive to oxy administration, 250  $\mu\text{g}/\text{kg}$ , than their male counterparts (Figure 7).

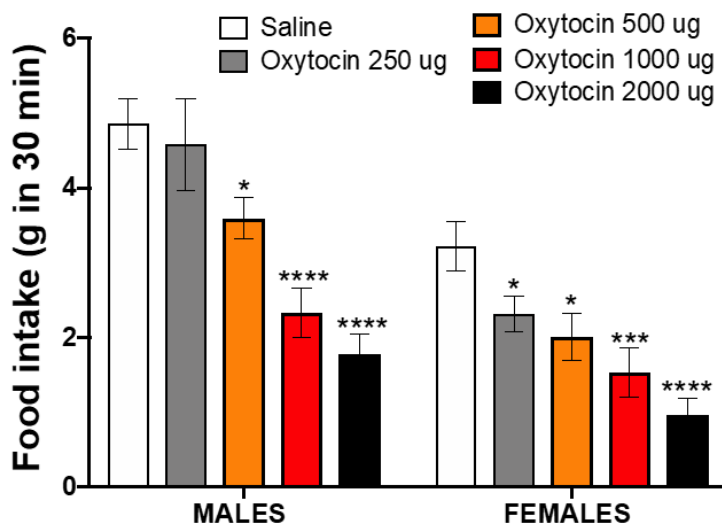


**Figure 7.** Peripherally administered, IP, oxytocin reduces food intake in male and female rats.



Following the production of B12-Oxy (Figure 4) the hypophagic effects of oxytocin and B12-oxy were examined. Following IP injection of equimolar, 0.5 mg/kg, oxy and B12-Oxy in female rats, B12-oxy was shown to reduce food intake with prolonged duration and sensitivity compared to that of unconjugated native oxy (Figure 8).

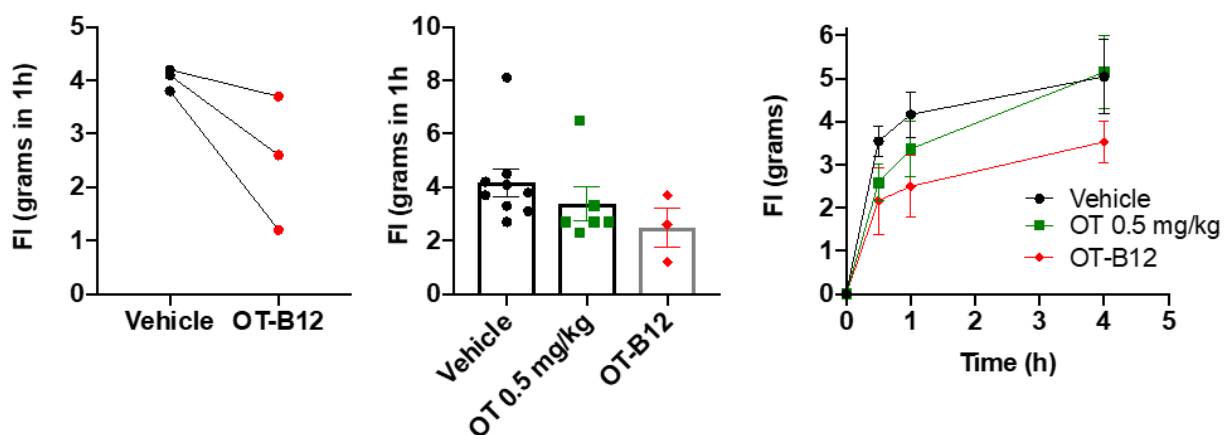


**Figure 8.** CNS penetrance is not required for the hypophagic effect of oxy. All rats receiving B12-Oxy reduced food intake compared to their intake on vehicle (saline). Equimolar dose of oxy also reduced food intake, with preliminary indication of a more potent and longer-lasting feeding behavior impact of B12-OT.

These results support the notion that CNS penetrance is not required for the hypophagic effects of oxy. This also suggests that the feeding control associated with oxy receptor (Oxy-R) agonism is specific to the receptor population found on the vagal afferents and not populations observed in the CNS.

## 7.4 References

- (1) Bonaccorso, R. L.; Chepurny, O. G.; Becker-Pauly, C.; Holz, G. G.; Doyle, R. P. Enhanced Peptide Stability Against Protease Digestion Induced by Intrinsic Factor Binding of a Vitamin B12 Conjugate of Exendin-4. *Mol. Pharm.* **2015**, *12* (9), 3502–3506.
- (2) Borner, T.; Workinger, J. L.; Tinsley, I. C.; Fortin, S. M.; Stein, L. M.; Chepurny, O. G.; Holz, G. G.; Wierzba, A. J.; Gryko, D.; Nexø, E.; Shaulson, E. D.; Bamezai, A.; Da Silva, V. A. R.; De Jonghe, B. C.; Hayes, M. R.; Doyle, R. P. Corination of a GLP-1 Receptor Agonist for Glycemic Control without Emesis. *Cell Rep.* **2020**, *31* (11), 107768.
- (3) Tinsley, I. C.; Borner, T.; Swanson, M. L.; Chepurny, O. G.; Doebley, S. A.; Kamat, V.; Sweet, I. R.; Holz, G. G.; Hayes, M. R.; De Jonghe, B. C.; Doyle, R. P. Synthesis, Optimization, and Biological Evaluation of Corinated Conjugates of the GLP-1R Agonist Exendin-4. *J. Med. Chem.* **2021**, *64*, 3479–3492.
- (4) Knudsen, L. B.; Lau, J. The Discovery and Development of Liraglutide and Semaglutide. *Front. Endocrinol. (Lausanne)*. **2019**, *10*, 155.
- (5) Madsen, K.; Knudsen, L. B.; Agersøe, H.; Nielsen, P. F.; Thøgersen, H.; Wilken, M.; Johansen, N. L. Structure-Activity and Protraction Relationship of Long-Acting Glucagon-like Peptide-1 Derivatives: Importance of Fatty Acid Length, Polarity, and Bulkiness. *J. Med. Chem.* **2007**, *50* (24), 6126–6132.
- (6) Knudsen, L. B.; Nielsen, P. F.; Huusfeldt, P. O.; Johansen, N. L.; Madsen, K.; Pedersen, F. Z.; Thøgersen, H.; Wilken, M.; Agersø, H. Potent Derivatives of Glucagon-like Peptide-1 with Pharmacokinetic Properties Suitable for Once Daily Administration. *J. Med. Chem.* **2000**, *43* (9), 1664–1669.

- (7) O'Neil, P. M.; Birkenfeld, A. L.; McGowan, B.; Mosenzon, O.; Pedersen, S. D.; Wharton, S.; Carson, C. G.; Jepsen, C. H.; Kabisch, M.; Wilding, J. P. H. Efficacy and Safety of Semaglutide Compared with Liraglutide and Placebo for Weight Loss in Patients with Obesity: A Randomised, Double-Blind, Placebo and Active Controlled, Dose-Ranging, Phase 2 Trial. *Lancet* **2018**, *392* (10148), 637–649.
- (8) Evers, A.; Haack, T.; Lorenz, M.; Bossart, M.; Elvert, R.; Henkel, B.; Stengelin, S.; Kurz, M.; Glien, M.; Dudda, A.; Lorenz, K.; Kadereit, D.; Wagner, M. Design of Novel Exendin-Based Dual Glucagon-like Peptide 1 (GLP-1)/Glucagon Receptor Agonists. *J. Med. Chem.* **2017**, *60* (10), 4293–4303.
- (9) Moheet, A.; Moran, A. CF-Related Diabetes: Containing the Metabolic Miscreant of Cystic Fibrosis. *Pediatr. Pulmonol.* **2017**, *52*, S37–S43.
- (10) Lau, J.; Bloch, P.; Schäffer, L.; Pettersson, I.; Spetzler, J.; Kofoed, J.; Madsen, K.; Knudsen, L. B.; McGuire, J.; Steensgaard, D. B.; Strauss, H. M.; Gram, D. X.; Knudsen, S. M.; Nielsen, F. S.; Thygesen, P.; Reedtz-Runge, S.; Kruse, T. Discovery of the Once-Weekly Glucagon-Like Peptide-1 (GLP-1) Analogue Semaglutide. *J. Med. Chem.* **2015**, *58* (18), 7370–7380.
- (11) Fosgerau, K.; Hoffmann, T. Peptide Therapeutics: Current Status and Future Directions. *Drug Discov. Today* **2015**, *20* (1), 122–128.
- (12) Di, L. Strategic Approaches to Optimizing Peptide ADME Properties. *AAPS J.* **2015**, *17* (1), 134–143.
- (13) Mathur, D.; Singh, S.; Mehta, A.; Agrawal, P.; Raghava, G. P. S. In Silico Approaches for Predicting the Half-Life of Natural and Modified Peptides in Blood. *PLoS One* **2018**, *13* (6), 1–10.

- (14) Mroz, P. A.; Perez-Tilve, D.; Mayer, J. P.; DiMarchi, R. D. Stereochemical Inversion as a Route to Improved Biophysical Properties of Therapeutic Peptides Exemplified by Glucagon. *Commun. Chem.* **2019**, *2*, 2.
- (15) Henry, K. E.; Elfers, C. T.; Burke, R. M.; Chepurny, O. G.; Holz, G. G.; Blevins, J. E.; Roth, C. L.; Doyle, R. P. Vitamin B12 Conjugation of Peptide-YY3-36 Decreases Food Intake Compared to Native Peptide-YY3-36 upon Subcutaneous Administration in Male Rats. *Endocrinology* **2015**, *156* (5), 1739–1749.
- (16) Clardy, S. M.; Allis, D. G.; Fairchild, T. J.; Doyle, R. P. Vitamin B12 in Drug Delivery: Breaking through the Barriers to a B12 Bioconjugate Pharmaceutical. *Expert Opin. Drug Deliv.* **2011**, *8* (1), 127–140.
- (17) Clardy-James, S.; Chepurny, O. G.; Leech, C. A.; Holz, G. G.; Doyle, R. P. Synthesis, Characterization and Pharmacodynamics of Vitamin-B12-Conjugated Glucagon-Like Peptide-1. *ChemMedChem* **2013**, *8* (4), 582–586.
- (18) Mietlicki-Baase, E. G.; Liberini, C. G.; Workinger, J. L.; Bonaccorso, R. L.; Borner, T.; Reiner, D. J.; Koch-Laskowski, K.; McGrath, L. E.; Lhamo, R.; Stein, L. M.; De Jonghe, B. C.; Holz, G. G.; Roth, C. L.; Doyle, R. P.; Hayes, M. R. A Vitamin B12 Conjugate of Exendin-4 Improves Glucose Tolerance without Associated Nausea or Hypophagia in Rodents. *Diabetes, Obes. Metab.* **2018**, *20* (5), 1223–1234.
- (19) Borner, T.; Shaulson, E. D.; Tinsley, I. C.; Stein, L. M.; Horn, C. C.; Hayes, M. R.; Doyle, R. P.; De Jonghe, B. C. A Second-Generation Glucagon-like Peptide-1 Receptor Agonist Mitigates Vomiting and Anorexia While Retaining Glucoregulatory Potency in Lean Diabetic and Emetic Mammalian Models. *Diabetes, Obes. Metab.* **2020**, *22* (10), 1729–1741.

- (20) Burger, R. L.; Schneider, R. J.; Mehlman, C. S.; Allen, R. H. Human Plasma R Type Vitamin B12 Binding Proteins. II. The Role of Transcobalamin I, Transcobalamin III, and the Normal Granulocyte Vitamin B12 Binding Protein in the Plasma Transport of Vitamin B12. *J. Biol. Chem.* **1975**, *250* (19), 7707–7713.
- (21) Gherasim, C.; Lofgren, M.; Banerjee, R. Navigating the B12 Road: Assimilation, Delivery, and Disorders of Cobalamin. *J. Biol. Chem.* **2013**, *288* (19), 13186–13193.
- (22) Jensen, H. R.; Laursen, M. F.; Lildballe, D. L.; Andersen, J. B.; Nexø, E.; Licht, T. R. Effect of the Vitamin B12-Binding Protein Haptocorrin Present in Human Milk on a Panel of Commensal and Pathogenic Bacteria. *BMC Res. Notes* **2011**, *4*, 2–7.
- (23) Samson, R. R.; Mirtle, C.; McClelland, D. B. L. Secretory IgA Does Not Enhance the Bacteriostatic Effects of Iron-Binding or Vitamin B12-Binding Proteins in Human Colostrum. *Immunology* **1979**, *38* (2), 367–36773.
- (24) Lee, H.-J.; Macbeth, A. H.; Pagani, J.; Young, W. S. Oxytocin: The Great Facilitator of Life. *Prog. Neurobiol.* **2009**, *88* (2), 127–151.
- (25) Chaves, V. E.; Tilelli, C. Q.; Brito, N. A.; Brito, M. N. Role of Oxytocin in Energy Metabolism. *Peptides* **2013**, *45*, 9–14.
- (26) Zingg, H. H.; Laporte, S. A. The Oxytocin Receptor. *Trends Endocrinol. Metab.* **2003**, *14* (5), 222–227.

## Appendix A: Publications

**Tinsley, I. C.;** Borner, T.; Swanson, M. L.; Hayes, M. R.; De Jonghe, B. C.; Cherpurny, O. G.; Holz, G. G.; Doyle, R. P. Design, Synthesis and Biological Evaluation of ‘Corrinated’ Conjugates of the GLP-1R agonist Exendin-4. *J. Med. Chem.* **2021**, 64, 3479-3492.

**Tinsley, I. C.;** Bonrer, T.; Workinger, J. L.; Fortin, S. M.; Stein, L. M.; Cherpurny, O. G.; Holz, G. G.; Wierzba, A. J.; Gryko, D.; Nexo, E.; Shaulson, E. D.; Bamezai, A.; Rodriguez Da Silva, V. A.; De Jonghe, B. C.; Hayes, M. R.; Doyle, R. P. ‘Corrination’ of a GLP-1 receptor agonist for glycemic control without emesis. *Cell Reports.* **2020**, 31 (11), 107768.

Borner, T.; Shaulson, E. D.; **Tinsley, I. C.;** Stein, L. M.; Horn, C. C.; Hayes, M. R.; Doyle, R. P.; De Jonghe, B. C. A second generation GLP-1 receptor agonist prevents vomiting and anorexia while retaining glucoregulatory potency in lean diabetic and emetic mammalian models. *Diabetes Obes. Metab.* **2020**, 22 (10), 1729-1741.

Stein, L. M.; Lhamo, R.; Cao, A.; Workinger, J.; **Tinsley, I.;** Doyle, R. P.; Grill, H. J.; Hermann, G. E.; Rogers, R. C.; Hayes, M. R. *Transl Psychiatry.* **2020**, 10 (90), 1-12.

**Tinsley, I. C.;** Borner, T.; De Jonghe, B. C.; Hayes, M. R.; Doyle, R. P. Peptide Ligands of the GDNF Family Receptor A-Like (GFRAL) Receptor. Non-provisional file date March 5<sup>th</sup>, 2020.

## Appendix B: Curriculum Vitae

# Synthesis, Optimization, and Biological Evaluation of Corrinated Conjugates of the GLP-1R Agonist Exendin-4

Ian C. Tinsley,<sup>#</sup> Tito Borner,<sup>#</sup> MacKenzie L. Swanson, Oleg G. Chepurny, Sarah A. Doebley, Varun Kamat, Ian R. Sweet, George G. Holz, Matthew R. Hayes, Bart C. De Jonghe, and Robert P. Doyle\*

Cite This: *J. Med. Chem.* 2021, 64, 3479–3492

Read Online

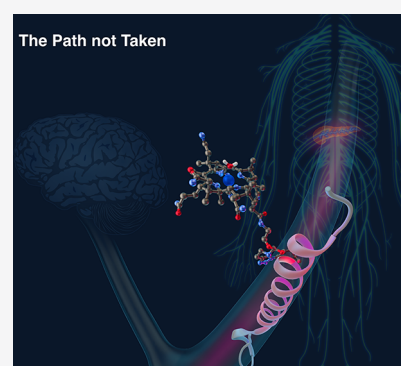
ACCESS |

Metrics & More

Article Recommendations

Supporting Information

**ABSTRACT:** Corination is the conjugation of a corrin ring containing molecule, such as vitamin B<sub>12</sub> (B12) or B12 biosynthetic precursor dicyanocobinamide (Cbi), to small molecules, peptides, or proteins with the goal of modifying pharmacology. Recently, a corrinated GLP-1R agonist (GLP-1RA) exendin-4 (Ex4) has been shown *in vivo* to have reduced penetration into the central nervous system relative to Ex4 alone, producing a glucoregulatory GLP-1RA devoid of anorexia and emesis. The study herein was designed to optimize the lead conjugate for GLP-1R agonism and binding. Two specific conjugation sites were introduced in Ex4, while also utilizing various linkers, so that it was possible to identify Cbi conjugates of Ex4 that exhibit improved binding and agonist activity at the GLP-1R. An optimized conjugate (**22**), comparable with Ex4, was successfully screened and subsequently assayed for insulin secretion in rat islets and *in vivo* in shrews for glucoregulatory and emetic behavior, relative to Ex4.



## INTRODUCTION

The dramatic rise of type 2 diabetes (T2D) and obesity as comorbidities has driven a concomitant rise in new pharmaceutical interventions to treat such disorders, either together or individually.<sup>1–7</sup> One extremely successful family of pharmaceuticals in this field has been that of glucagon-like peptide-1 receptor agonists (GLP-1RAs),<sup>8–13</sup> such as exenatide (i.e., Exendin-4; Ex4), liraglutide,<sup>14–17</sup> and semaglutide.<sup>16–18</sup> Exenatide and liraglutide confer glucoregulation in tandem with a body weight reduction of 5–6% over ~1 year,<sup>16,17</sup> while semaglutide can produce a weight loss of 10–12% over the same time period.<sup>16,17</sup> The hypophagic effects of all GLP-1RAs are however accompanied by nausea and vomiting (emesis) in upward of 25% of patients,<sup>19–25</sup> the result of penetrance and direct action of the GLP-1RA in the central nervous system (CNS), particularly in the nucleus tractus solitarius and area postrema of the hind-brain.<sup>26–29</sup> Thus, the development of a GLP-1RA that does not access the CNS would be expected then to mitigate the side effects of nausea and emesis and reduce the hypophagic effects. The reasons for removing the side effects are obvious, but less clear is the fact that there is a current unmet clinical need to broaden pharmacopoeia for certain subpopulations of T2D patients, including lean individuals, those in a state of cachexia (wasting of body tissues/chronic weight loss), or those who must avoid weight loss from other life-threatening diseases such as chronic obstructive pulmonary disease, cystic fibrosis, cancer, and HIV, among others.<sup>30–34</sup> Thus, we set out to create GLP-1RAs with reduced brain penetrance but with

retained, comparable pharmacodynamic profiles on pancreatic GLP-1R populations (Figure 1).<sup>35–39</sup> Recently, we have taken the approach of utilizing components of the vitamin B<sub>12</sub> (B12)

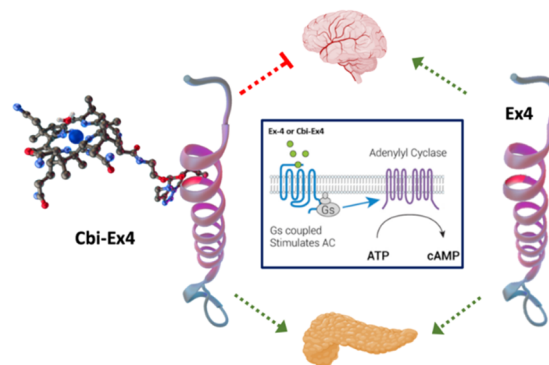


**Figure 1.** Corination of Ex4 (Cbi-Ex4) does not prevent GLP-1R agonism in the pancreas but does mitigate agonism in the CNS as tracked by emesis and anorexia.<sup>18</sup> Ex4 alone agonizes GLP-1R populations in both the pancreas and CNS.

Received: February 1, 2021

Published: March 6, 2021



Scheme 1. Synthesis of Cbi Linkers (4–11) and Cbi-Peptide Conjugates (12–27). Linkers 3A–3H are shown in Figure 2

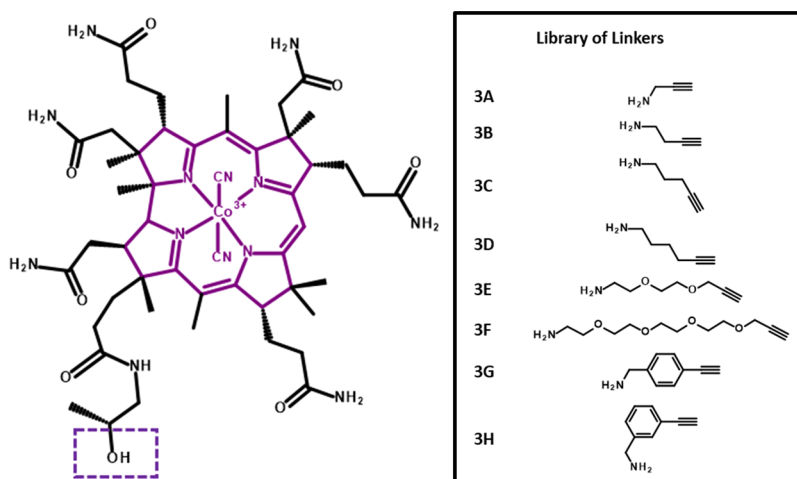
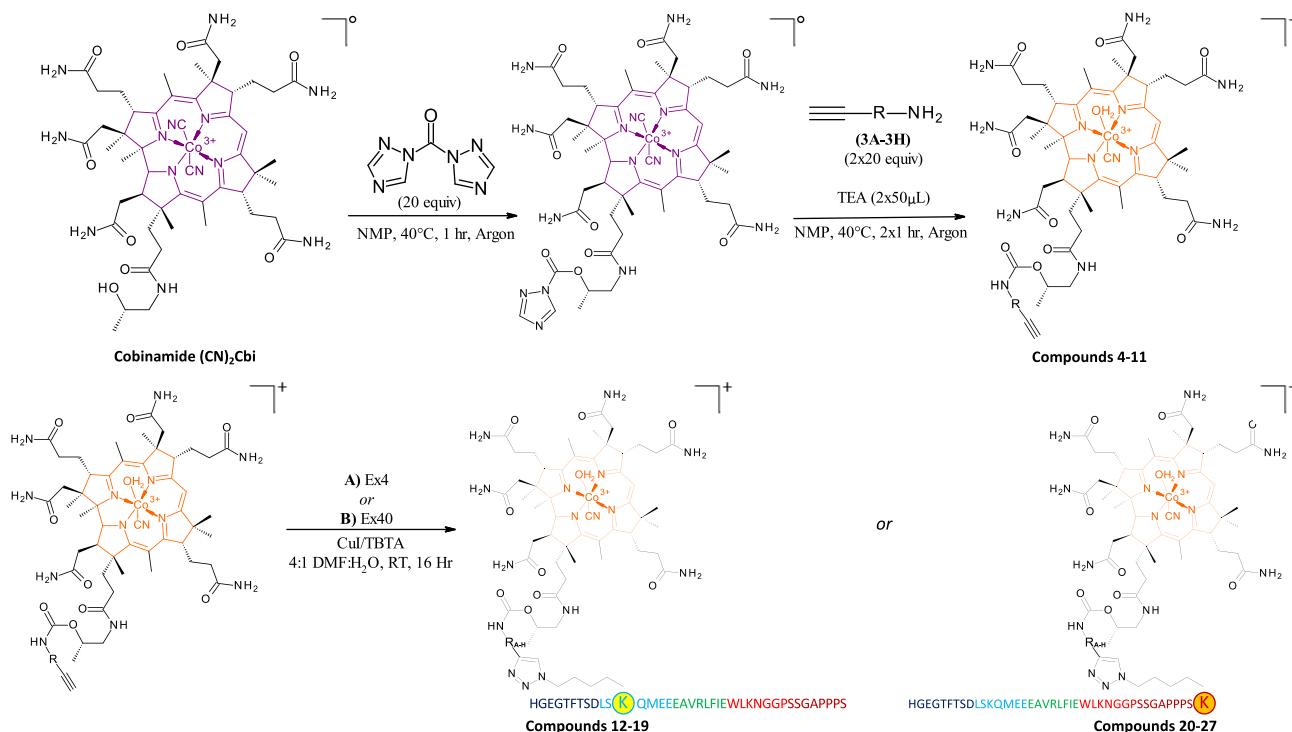


**Figure 2.** (Left) Structure of the dicyanocobinamide (CN)<sub>2</sub>Cbi starting material, a purple solid prepared via microwave chemistry from B12, with the hydroxyl group boxed used as a site of conjugation to linker series. (Right) Library of linkers used in the conjugation of Cbi to Ex4 peptides. The library of linkers chosen in this study included short hydrophobic alkane chains, amphiphilic PEG, and rigid substituted ethynyl phenyl methanamines, which were coupled to the Cbi hydroxyl group via CDT-mediated amide formation, resulting in Cbi compounds (4–11) with an available alkyne group for subsequent reaction with azido-modified Ex4 peptides via copper-mediated alkyne-azide click chemistry (Scheme 1).

dietary uptake pathway including that of the corrin ring containing B12<sup>35–38,40</sup> itself as well as B12 precursors such as dicyanocobinamide (Cbi)<sup>39</sup> in a process we have coined “corriation”. The benefits of corriation over other conjugation modes lie in the ability to specifically target select corrin binding proteins such as intrinsic factor, transcobalamin, or haptocorrin for use in targeting or to affect pharmacokinetics, modify solubility, and alter drug localization, all without having to reverse the process to allow for maintained drug function (pending suitable design). Our recent report explored the conjugation of Cbi with Ex4, to produce Cbi-Ex4 (1),<sup>39</sup> and its effects were tested *in vivo* in the musk shrew (*Suncus murinus*), a mammal capable of

emesis<sup>41,42</sup> and responsive to GLP-1R targeting therapeutics.<sup>39,43,44</sup> Our data showed that Cbi-Ex4 enhanced the glucoregulatory response following an intraperitoneal glucose tolerance test (IPGTT), without producing hypophagia, anorexia, body weight loss, and, more importantly, without emesis, all characteristics of classical Ex4-based therapies.<sup>39</sup> We hypothesized that these results are due to reduced drug penetrance into the CNS (see Figure 1).<sup>35–39</sup> This proof-of-concept corriated Ex4 (1) was, however, notably less potent an agonist for the GLP-1R than Ex4 alone (200 vs 30 pM, respectively, in the same GLP-1R FRET assay).<sup>39</sup> With that in mind, we set out to optimize 1 in terms of receptor binding and agonism for the purposes of future translation. As such,



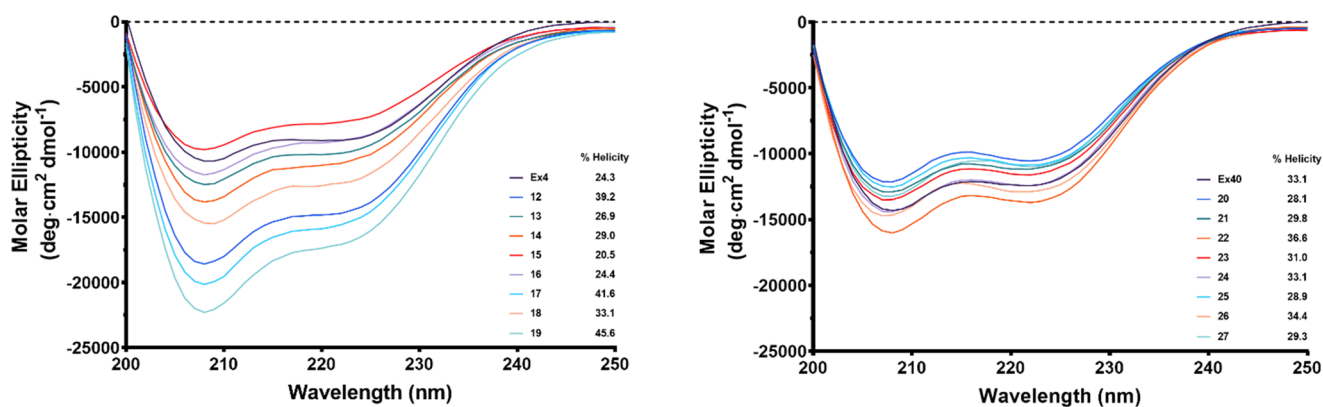


**Figure 3.** Effect of Cbi conjugation on the secondary structure of Ex4 or Ex40. CD spectra were collected with a sample concentration of 40  $\mu$ M at pH 7 between 200 and 250 nm. % helicity was measured at 222 nm.

we needed to synthesize and characterize a new library of Cbi-Ex4 conjugates. Of note here is that there is a dearth of synthetic cobinamide chemistry in the literature, mostly focusing on the novel cobinamides to treat hydrogen sulfide<sup>45,46</sup> or cyanide poisoning,<sup>47–54</sup> and even less so in terms of conjugation chemistry (an excellent exception being that from the Gryko group using Cbi-PNA);<sup>55</sup> hence, we wanted to produce Cbi-linkers that would be readily amenable to conjugation to Ex4 but indeed any targeted peptide moving forward. Here, we report a set of 16 new constructs (12–27) conjugated between Cbi and Ex4 at two positions (K12 and K40) by various linkers with a set of diverse chemical properties including hydrophobicity, amphiphilicity, and rigidity. The successful design and synthesis lead to the production of a new series of corrinated Ex4 constructs with comparable agonism and binding to unconjugated Ex4. One of these conjugates (22) displayed equipotency and binding at the GLP-1R *in vitro* and was subsequently selected for *ex vivo* screening for insulin secretion in rat islets and *in vivo* in shrews for glucoregulation, food intake, body weight, and emesis, compared to Ex4 and 1.

## RESULTS AND DISCUSSION

**Design.** Our initial report on the effects of corrination on Ex4 included evidence for glucoregulation without emesis nor a reduction in food intake.<sup>39</sup> In these subsequent studies, we have looked to optimize 1 with a focus on agonism and binding at the GLP-1R while also expanding to the little explored chemistry pertaining to the synthesis of Cbi conjugates. As such, the structure–activity data presented in these studies integrates synthesis, receptor agonism, receptor binding, *ex vivo* insulin secretion, *in vivo* glucoregulation, emetic response, and food intake to explore the role of the peptide conjugate site (Scheme 1) and/or the role of a specific set of spacers (linkers) as shown in Figure 2. In terms of the linkers, there are three subsets that were chosen to sample space across particular structural features, namely, steric, hydrophobic, and amphiphilic. The Ex4 conjugate site was restricted to K12 and a K40 residue added to the C-terminus of Ex4 (Ex40) since both sites were proven to be amenable to modification with minimal loss of function in our hands<sup>35–39</sup> and in prior literature.<sup>56–58</sup>

**Chemistry.** The Cbi linker compounds (4–11) and Ex4 conjugates of such (12–27) amounted to a library of 32 compounds. The experimental details are shown in Scheme 1, with linkers (Figure 2) indicated as R-groups. Initially, Cbi

was produced in-house via microwave-assisted reaction of B12 with sodium cyanide in EtOH as previously described.<sup>59</sup> The purple dicyanocobinamide (CN<sub>2</sub>Cbi) produced was then activated with an excess of 1,1'-carbonyl-di-(1,2,4-triazole) (CDT) in dry *N*-methyl-2-pyrrolidone (NMP) and heating at 40 °C under argon for ~10 min or until complete dissolution was observed. Upon dissolution, a specific linker (Figure 2; 3A–3H) was added in large excess (20 $\times$ ) relative to the activated CN<sub>2</sub>Cbi along with triethylamine (TEA), and the reaction was allowed to proceed for 1 h, again at 40 °C under argon with stirring. Initially, it was observed via RP-HPLC tracking on a C18 column (data not shown) that the reaction proceeded slowly, so in subsequent experiments, a second equivalent of linker (20 $\times$ ) and TEA were added at the 1 h time point and the reaction was allowed to proceed, as before, for an additional hour. Based on the additional step, yields for all Cbi-linkers were in the 30–50% range with facile purification to produce the Cbi-Linkers (4–11) with purities at, or in excess of, 97% (as tracked by RP-HPLC; see the Supporting Information). It should also be noted, and such is indicated in the color scheme used in Scheme 1 for the corrin rings, that a color change was observed upon formation of the Cbi-linkers, going from purple to orange upon purification of the Cbi-linkers in water. This color change was previously reported by Zhou and Zelder<sup>60</sup> and assigned to the formation of isomers, namely,  $\alpha$ -cyano- $\beta$ -aqua- and  $\alpha$ -aqua- $\beta$ -cyano-Cbi (as indicated in Scheme 1). This suggestion of isomer formation was supported by the HPLC traces of the linkers, which clearly showed the presence of both isomers (subsequently confirmed by nuclear magnetic resonance (NMR); Figure S7). Given the fact that such isomers were not expected to negatively affect the subsequent chemistry or biology, isomers were combined prior to peptide coupling and were characterized via NMR, electrospray ionization-mass spectrometry (ESI-MS), and electronic absorption spectroscopy (EAS).

Coupling of 4–11 with K12-azido- or K40-azido-modified Ex4 (noted throughout here simply as Ex4 or Ex40) to produce conjugates 12–27 was achieved via copper(I)-mediated alkyne-azide cycloaddition over 16 h at room temperature in a 4:1 dimethylformamide (DMF)/H<sub>2</sub>O solvent system in the presence of the tertiary amine tris((1-benzyl-4-triazolyl)methyl)amine (TBTA) to stabilize copper(I).<sup>61</sup> Yields obtained were quantitative based on the starting peptide, and all conjugates were produced to at least 97%

Table 1. EC<sub>50</sub> and IC<sub>50</sub> Values with Hill Slopes and % Helicity of Cbi Conjugates 12–27

	EC <sub>50</sub> (pM) <sup>a</sup>	EC <sub>50</sub> Hill slope <sup>b</sup>	% helicity <sup>c</sup>	IC <sub>50</sub> (nM) <sup>d</sup>	IC <sub>50</sub> Hill slope <sup>e</sup>
Ex4	12.5 ± 3.7	1.1970	24.3	5.98 ± 0.94	-1.3010
12	75.4 ± 4.1	0.9110	39.2	24.6 ± 6.3	-1.1170
13	105.6 ± 4.1	1.0100	26.9	135 ± 122.5	-0.5661
14	33.2 ± 4.4	1.4170	29.0	79.5 ± 28.8	-0.7858
15	38.9 ± 15.6	1.0470	20.5	82.7 ± 15.4	-1.6990
16	34.1 ± 9.7	0.9976	24.4	36.5 ± 16.0	-1.1770
17	36.5 ± 7.6	1.0980	41.6	45.9 ± 16.3	-1.1740
18	40.5 ± 17.1	1.3030	33.1	34.3 ± 11.9	-1.1530
19	31.2 ± 16.9	1.1130	45.6	11.6 ± 2.4	-1.1270
Ex40	10.4 ± 3.9	1.1160	33.1	7.34 ± 1.37	-0.9107
20	13.4 ± 4.2	1.1890	28.1	26.2 ± 6.3	-1.1350
21	37.8 ± 11.5	1.1830	29.8	21.4 ± 8.0	-0.8940
22	20.7 ± 8.3	1.2090	36.6	11.9 ± 2.5	-1.3970
23	10.7 ± 6.0	1.0120	31.0	27.2 ± 6.3	-1.1780
24	16.4 ± 3.1	1.1370	33.1	15.1 ± 4.1	-1.2540
25	26.0 ± 14.1	0.9817	28.9	18.5 ± 4.6	-1.0840
26	27.9 ± 4.2	0.9957	34.4	26.4 ± 8.0	-1.2370
27	23.1 ± 7.1	1.2130	29.3	24.6 ± 6.3	-1.2790

<sup>a</sup>Data represents EC<sub>50</sub> obtained using nonlinear regression analysis of data from highest FRET values obtained for each data point. Experiments were performed as three independent runs. <sup>b</sup>Data represents the Hill slope obtained using nonlinear regression analysis of data from highest FRET values obtained for each data point. Experiments were performed as three independent runs. <sup>c</sup>Data represents mean residue ellipticity  $[\theta]_{222}$  determined from the CD spectra of a 40 μM solution of peptide in H<sub>2</sub>O at RT pH 7.0. Average  $[\theta]_{222}$  values utilized to calculate percent helicity were obtained by performing the experiment in triplicate. Percent helicity was calculated using  $100 \times \frac{([\theta]_{222} / \max[\theta]_{222})}{(2.5/n)}$ , where  $n$  is the residue number. Experiments were performed as three independent runs. <sup>d</sup>Data represents IC<sub>50</sub> values obtained from competitive binding assays against red fluorescent GLP-1 using nonlinear regression analysis from highest values obtained for each data point. Experiments were performed as two independent runs. <sup>e</sup>Hill slopes were obtained using nonlinear regression analysis from highest values obtained for each data point. Results are expressed as mean ± SEM.

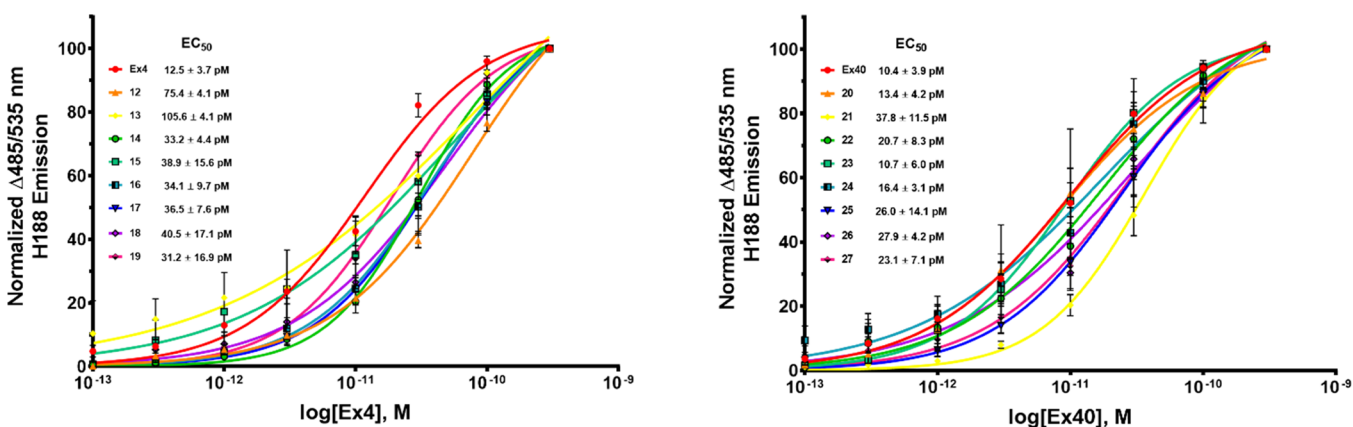


Figure 4. Conjugation of Cbi to Ex4 or Ex40 peptides maintains agonism at the GLP-1R. Nonlinear regression analysis was performed with GraphPad Prism 8. All compounds were assayed at least as triplicate independent runs. Data are shown as mean ± SEM.

purity prior to biological or *in vivo* evaluation (as tracked by RP-HPLC; shown in the Supporting Information).

**Structural Studies Using Circular Dichroism (CD).** All conjugates were investigated for the effects of corination on helicity at a concentration of 40 μM in water at pH 7.0 (Figure 3). Immediately, it was evident that there was minimal variation in percent helicity whereupon the Cbi was conjugated at the Ex4 C-terminal K40 (20–27; % helicity ranged from ~28 to 36%; Ex40 control 33.1%; Table 1). There was however a noticeable variation in the percent helicity for the conjugates (12–19) whereupon Cbi was conjugated to the K12 within the Ex4 helix (% helicity range ~20–46%; Ex4 control 24.3; Table 1). These results are consistent with the fact that conjugation at the C-terminus renders less consequence to the linker type or spacer distance

between Cbi and the peptide, given that this region is away from the helical region of Ex4 and does not interfere with the role of this region with receptor binding/agonism. The variation noted upon conjugation at the K12 residue renders the linker critical with the highest % helicity noted as 41% with the amphiphilic PEG spacer 3F (Figure 2, Table 1) and the lowest percent helicity noted with the small alkyl spacers 3B–3D (Figure 2, Table 1). No overall correlation between the structure and agonism or binding was observed upon data fitting (not shown).

**Biological Evaluation.** To determine how the conjugation site of the peptide affects its function and the role linker choice plays in the attachment of the peptide to Cbi, we sought to screen 12–27 utilizing *in vitro* assays to determine potency and binding at the GLP-1R.

**In Vitro Functional Agonism ( $EC_{50}$ ) at Human GLP-1R.** Our previously published<sup>39</sup> Cbi-Ex4 construct **1** resulted in agonism at the GLP-1R with an  $EC_{50}$  of 200 pM. The design of the newly constructed conjugates, **12–27**, aimed to increase the potency of the original construct to that comparable of unconjugated Ex4 (<30 pM). **12–27** were assessed utilizing *in vitro* screening in HEK C20 cells stably expressing the human GLP-1R and cAMP FRET reporter H188 produced in-house (see *Methods*).<sup>62,63</sup> To determine if the azido modification to lysine at position K12 (Ex4) or the addition of this residue to position 40 (Ex40) had any effect on agonism at GLP-1R, they were also screened for agonism to compare with native Ex4 (nEx4; no azido modifications), resulting in  $EC_{50}$  values of 20 pM for nEx4,  $12.5 \pm 3.7$  pM for Ex4, and  $10.4 \pm 3.9$  pM for Ex40 (Table 1). All newly synthesized compounds were functional at the GLP-1R with improved potency in all cases ( $EC_{50}$  range  $13.4 \pm 4.2$  to  $105.6 \pm 4.1$  pM) to that of our previously reported construct **1** (200 pM; Table 1 and Figure 4). In general, the Ex4 conjugates **12–20** were inferior to the Ex40 conjugates (**20–27**) and displayed greater variance, with  $EC_{50}$  values ranging from 31 to 106 pM for **12–19** compared to 13 to 38 pM for **20–27**. As with the variance observed in the folded state for **12–19**, it is likely that proximity and/or interactions of the Cbi moiety to the helix interferes with receptor binding and/or interactions necessary for agonism. Conjugations performed at the C-terminal end of the peptide would be expected to place the corrin ring away from such residues as we have shown previously with B12 conjugates of the neuropeptide PYY<sub>3–36</sub>.<sup>38</sup> One Cbi-Ex4 conjugate however (**19**), which bridged Ex4 at the K12 residue with Cbi through one of the hydrophobic, rigid linkers (3H), was shown to be equipotent to Ex4 with an  $EC_{50}$  value of  $31.2 \pm 16.9$  pM and an  $IC_{50}$  of  $11.6 \pm 2.4$  nM (compared to  $5.98 \pm 0.94$  nM for Ex4 alone; Table 1). All Ex40-based conjugates (**20–27**) were shown to be equipotent to the unconjugated peptide. Such results are consistent with the fact that addition of, and conjugation to, the K40 residue is optimal when conjugating Cbi to Ex4.

**In Vitro Competitive Binding ( $IC_{50}$ ) at Human GLP-1R.** As shown in Table 1, the presence of Cbi influences the ability of the conjugate to agonize the GLP-1R compared to that of Ex4 or Ex40. To further investigate how conjugation of Cbi affects Ex4 or Ex40, a series of competitive binding assays against GLP-1red (a red fluorescent analog of GLP-1) were conducted. nEx4 was utilized as a reference competitor with an  $IC_{50}$  value of 4.97 nM. We first aimed to determine if the azido modification to lysine at position K12 and the addition of this residue to position 40 had any effect on binding. It was found that both Ex4 and Ex40 had comparable binding to that of the reference compound with  $IC_{50}$  values of  $5.98 \pm 0.94$  and  $7.34 \pm 1.37$  nM, respectively. All conjugates had decreased binding (12–135 nM) compared to the unconjugated peptide azido-modified Ex4 (6 nM) and Ex40 (7 nM) and nEx4 controls (5 nM). When comparing the two clusters of conjugates, **20–27** showed greater binding affinity overall compared to **12–19**. The same trend was observed when agonizing the GLP-1R (Table 1) in which collectively **20–27** outperformed **12–19**. Two constructs, namely, **19** and **22**, did show promising binding with  $IC_{50}$  values of  $11.6 \pm 2.4$  and  $11.9 \pm 2.5$  nM, respectively. The increased binding observed in these two conjugates was consistent with their agonism ( $31 \pm 16.9$  and  $20.7 \pm 8.3$  pM, respectively) of the GLP-1R. Based on overall binding potent agonism, facile synthesis, and

high yield observed for **22**, especially related to those of **19**, we chose to further investigate **22** in *ex vivo* and *in vivo* experiments.

**Glucose-Stimulated Insulin Secretion (GSIS) in Rat Pancreatic Islets.** The effects of **22** on GSIS were evaluated using rat pancreatic islets (Figure 5). At 10 mM glucose, both

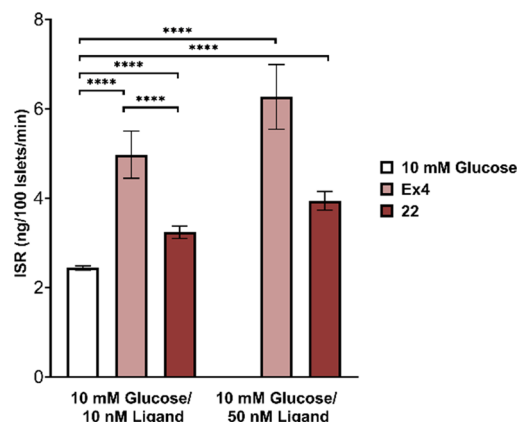


**Figure 5.** **22** increases glucose-stimulated insulin secretion in rat islets relative to glucose controls. Insulin secretion rate from static cultures of Sprague–Dawley rat islets incubated in media containing glucose (10 mM) and Ex4 (10 or 50 nM) or **22** (10 or 50 nM). Data was calculated from three independent experiments and analyzed with repeated-measurements two-way ANOVA followed by Tukey's posthoc test. Results are expressed as mean  $\pm$  SEM, \*\*\*\*  $p < 0.0001$ .

**22** and nEx4 increased GSIS in a dose-responsive manner. The effect from **22** was observed to be one-third lower than that of nEx4. To investigate whether there was a difference between Ex40 and **22**, specific to the rat GLP-1R, we assayed each for functional ( $EC_{50}$ ) agonism. We observed a slight drop-off in potency with  $EC_{50}$  values of 7.8 and 22 pM recorded for Ex40 and **22** (Figures S106–S111), respectively. nEx4 control had an  $EC_{50}$  of 48 pM at the rat GLP-1R.

**In Vivo Functional Experiments.** To functionally compare the activity of the corrinated conjugates *in vivo*, we first tested the effects of Ex4, **1** (the original proof-of-concept conjugate),<sup>39</sup> and **22** on plasma glucose levels following an IPGTT in shrews. A shrew is a mammal capable of emesis<sup>41,42</sup> with published sensitivity to GLP-1RAs<sup>39,43,44</sup> and the same serum B12 binding proteins (IF and Haptocorrin) as that found in humans<sup>39</sup> and thus was considered an ideal model for the *in vivo* studies. We observed that shrews treated with **1**, **22**, or nEx4 display similar improvements in glucose handling following glucose load compared to vehicle controls (Figure 6A). Posthoc analyses showed that all three compounds significantly suppressed blood glucose (BG) at 20 and at 40 min after glucose administration versus vehicle treatment (all  $p < 0.001$ ). Remarkably, BG values at 20 min post glucose injection in animals receiving **22** were significantly lower than those in animals treated with **1**, denoting an improved glucose tolerance/superior pharmacological efficacy ( $p < 0.01$ ). Additionally, the variation in plasma glucose concentrations, represented as area under the curves (0–60' and 0–120', respectively) for **22**, did not differ from nEx4 and were significantly lower than controls (Figure 6B,C, all  $p < 0.05$ ).

We then analyzed the effects of **1**, **22**, and Ex4 on food intake and body weight at a single, proof-of-concept, dose, in

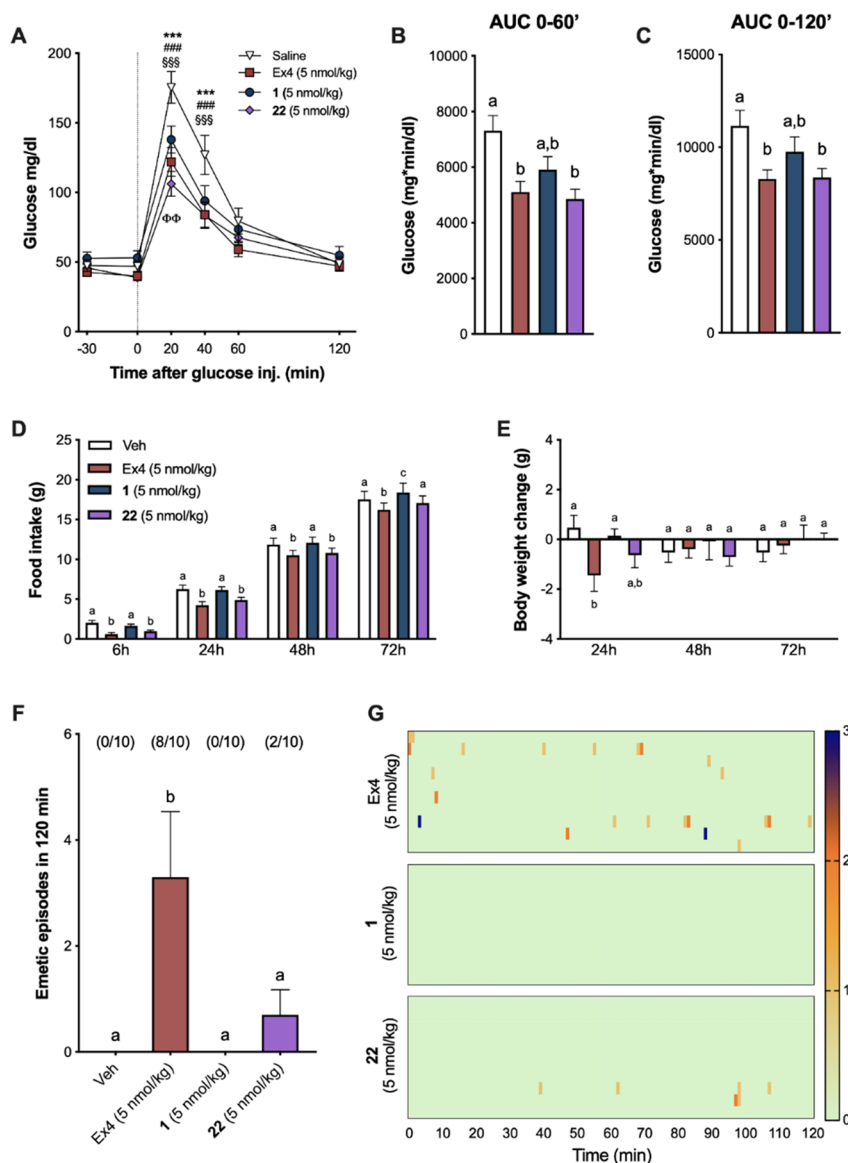


**Figure 6.** Cbi-Ex4 enhances glucose clearance without inducing emesis or body weight loss. (A) In an IPGTT, Ex4, 1, and 22 (50 nmol/kg, IP) showed similar potency in suppressing BG levels after glucose administration (2 g/kg, IP) compared to saline; vehicle vs 1: \*\*\*  $P < 0.001$ ; vehicle vs 22: ###  $P < 0.001$ ; vehicle vs Ex4: §§§  $P < 0.001$ ; 1 vs 22:  $\Phi\Phi$   $P < 0.01$  ( $n = 12$  shrews). (B) Area under the curve (AUC) analysis from 0 (i.e., post-glucose bolus) to 60 min following 1, 22, and Ex4. (C) AUC analysis from 0 to 120 min; 22 and Ex4 similarly reduced AUCs compared to vehicle ( $P < 0.05$ ). (D) Ex4 and 22 (5 nmol/kg, IP) induced anorexia at 6, 24, and 48 h (and at 72 h for Ex4 only), whereas 1 had no effect on food intake ( $n = 10$ ). (E) Ex4-induced anorexia was accompanied by significant body weight loss at 24 h. No significant changes in body weight occurred after 1 and 22 administration compared to controls. (F) The number of single emetic episodes following Ex4, 1, 22, or saline systemic administration was recorded for 120 min. The number of animals exhibiting emesis, expressed as a fraction of the total number of animals tested, is indicated above each treatment group. Ex4 induced robust emetic responses that were not observed after 1 or saline injections. 22 induced emesis in two of the animals tested; however, the number of emetic episodes was significantly lower than that of Ex4 and did not differ from animals treated with vehicle or 1 ( $n = 10$ ). (G) Heatmaps showing latency, number, and intensity of emesis following Ex4, 1, and 22 dosing for each individual animal across time. All data expressed as mean  $\pm$  SEM ( $n = 10$ ). Data in panels (A), (D), and (E) were analyzed with repeated-measurements two-way ANOVA followed by Tukey's posthoc test. Data in panels (B), (C), and (F) were analyzed with repeated-measurements one-way ANOVA followed by Tukey's posthoc test. Means with different letters are significantly different ( $P < 0.05$ ).

line with previous reports.<sup>35–37,39</sup> Ex4 administration produced anorexia in shrews at all measured time points (Figure 6D), while 1 had no impact on feeding. 22 treatment suppressed food intake similar to Ex4 at 6, 24, and 48 h. The anorectic effect of Ex4 treatment was paralleled by a significant reduction in body weight at 24 h ( $p < 0.05$ ), which was not observed following treatment with 1 or 22 (Figure 6E).

To test whether 22 treatment retained the non-emetic properties of the lead conjugate 1, indicative of an altered pharmacodynamic profile, despite its comparable potency and GLP-1R binding affinity compared to 1, and comparable to nEx4, we compared the emetogenic properties of 1, 22, and native Ex4 in shrews. Ex4 induced profound emesis in the majority of the shrews tested (Figure 6F). Indeed, 80% of the animals exhibited emesis upon administration of native Ex4 within minutes after injection ( $29 \pm 16$  min). In line with a



previous report, treatment with **1** did not cause emesis in any of the shrews tested.<sup>39</sup> Importantly, the number of single emetic episodes occurring in the 120 min window after drug administration was also significantly reduced after **22** administration compared to Ex4 and did not differ from vehicle- or **1**-treated groups. Only two animals that received **22** experienced emesis with an average latency of  $70 \pm 29$  min. The greater emetic effect observed for **22** over **1** is likely a consequence of the greater binding and agonism of **22** at the GLP-1R, an effect that is likely to be mitigated, without loss of glucoregulation, by use of lower doses of **22** (on-going work). The difference in the emetogenic profiles of the corrinated constructs versus native Ex4 is further emphasized by the graphical visualization of emetic intensity, recurrence, and latency for each individual animal across time (Figure 6G).

## CONCLUSIONS

Neuroendocrine associated pharmacological side effects such as nausea and emesis are often downplayed or dismissed, left in the shadow of the overriding target, be it glucoregulation, weight loss, *etc.* Indeed, the weight loss gleaned from GLP-1RAs, for example, has proven to be a beneficial “side effect” of T2D treatment due to the high comorbidity of T2D with obesity.<sup>64</sup> In many cases, however, such as lean T2D patients, or patients with comorbidities where nutritional status is critical (cystic fibrosis, cancer-cachexia, sarcopenia, chronic obstructive pulmonary disease, *etc.*), removal of the CNS-associated side effects would be greatly beneficial. Indeed, GLP-1RAs have proven to be life-altering, and the ability to expand their use, or increase patient compliance when using, should not be understated. Herein, we conceived 16 new Cbi-Ex4/Ex40 conjugates with the aim of designing a construct with equipotent binding and agonism of the GLP-1R to that of Ex4 with a view of maintaining activity at peripheral GLP-1R populations and mitigating such activity in CNS populations. We were able to successfully design several constructs with comparable binding and agonism at GLP-1R as Ex4, with one conjugate, **22** ( $IC_{50}$   $11.9 \pm 2.5$  nM,  $EC_{50}$   $20.7 \pm 8.3$  pM), translated into *ex vivo* and *in vivo* studies. **22** increased glucose secretion compared to vehicle controls in a glucose-dependent insulin secretion assay in rat islets. In an *in vivo* IPGTT, **22** provided glucoregulation comparable to Ex4. Critically, **22** showed a near absence of emesis and mild body weight lowering actions compared to profound emesis and body weight loss observed for nEx4.

While corrination is poorly explored, especially as it pertains to applications that seek to prevent CNS penetration while maintaining peripheral activity of a target drug, it shows considerable promise as a platform technology, moving beyond GLP-1RAs. An additional highlight of Cbi is its water solubility (400 mg/mL), akin to glucose (450 mg/mL). Use of Cbi conjugation with drugs with physical properties not suited to drug development, such as glucagon<sup>65–67</sup> for rescue of hypoglycemia, offers a great scope for exploration.

## EXPERIMENTAL SECTION

**General Considerations.** All commercial reagents and anhydrous solvents purchased were used without further purification. All reactions containing air- and/or moisture-sensitive reactants were performed under argon. Compounds were purified using a Shimadzu Prominence HPLC using a C18 column (Eclipse XDB-C18 5  $\mu$ m,  $4.6 \times 150$  mm). All compounds had purities at, or in excess of, 97% (as tracked by RP-HPLC; see the Supporting Information). Products

were analyzed for mass using a Shimadzu LCMS-8040. <sup>1</sup>H NMR and <sup>13</sup>C NMR spectra were acquired on a Bruker NMR spectrometer (Avance 400 MHz) in D<sub>2</sub>O at a D1 of 3 for all compounds. EAS was collected on a Varian Cary 50bio UV–visible spectrophotometer in a 1 mL quartz cuvette with baseline correction. CD spectra were recorded with a Jasco J-715 circular dichroism spectropolarimeter in 40  $\mu$ M H<sub>2</sub>O in a 0.1 cm quart cuvette. Data was analyzed and fit using GraphPad Prism 8.0. We established a new clone of HEK293 cells designated here as HEK293-GLP-1R-H188-C20. This clone was obtained by G418 antibiotic resistance selection after cotransfection of cells with the human GLP-1R and the cAMP FRET reporter H188. Cells were grown in a Memmert Incubator I (Schwabach, Germany) at 37 °C gassed with 5% CO<sub>2</sub> at ~95% humidity. FRET assays were conducted utilizing a Molecular Devices FlexStation 3 Multi-Mode Microplate Reader. Data was analyzed utilizing Molecular Devices SoftMax Pro v.5.4.6. Linear regression analyses were performed utilizing GraphPad Prism 8.

**Materials.** The following were purchased from Sigma Aldrich: acetonitrile (Cat # 14851), diethyl ether (Cat # 673811), ethanol (Cat # 459844), ethyl acetate (Cat # 319902), isopropyl alcohol (Cat # 34863), methanol (Cat # 34885), *n*-methyl-2-pyrrolidone (Cat # 328634), triethylamine (Cat # 8.08352), vitamin B<sub>12</sub> (Cat # V2876), sodium cyanide (Cat # 205222), 1,1'-carbonyl-di-(1,2,4-triazole) (Cat # 21863), propargylamine (Cat # P50900), 1-amino-3-butylene-1-amine (Cat # 715190), 4-pentyne-1-amine (Cat # 779407), hex-5-yne-1-amine (Cat # COM497512576), bovine serum albumin (Cat # A7030), Dulbecco's modified Eagle medium (Cat # D6429), fetal bovine serum (Cat # 12303C), G-418 disulfate salt solution (Cat # G8168), and HEPES (Cat # H0887). The following were purchased from ThermoFisher Scientific: penicillin–streptomycin (Cat # 15140122) and trypsin–EDTA (Cat # 25200072). The following were purchased from Fisher Scientific: calcium chloride dihydrate (Cat # BP510), magnesium chloride hexahydrate (Cat # BP214), potassium chloride (Cat # BP366), and sodium chloride (Cat # BP358–1). The following were purchased from BroadPharm: propargyl-PEG2-amine (Cat # BP22519) and propargyl-PEG4-amine (Cat # BP22520). The following were purchased from Enamine: (4-ethynylphenyl)methanamine (Cat # EN300–233648) and (3-ethynylphenyl)methanamine (Cat # EN300–248722). Krebs-Ringer Bicarbonate (KRB) buffer was prepared as described previously.<sup>68</sup> D-Glucose (Cat # G 5767) and nEx4 (Cat # E7144) were purchased from Sigma-Aldrich. Ex4 K12-azido and Ex40 K40-azido were produced by Genscript (Piscataway, New Jersey, United States). The rat insulin radioimmunoassay (RIA) kit was purchased from Millipore Sigma, Burlington, MA Cat no. RI-13 K. The human GLP-1R plasmid was provided by M. Beinborn, Tufts University School of Medicine to author G.G.H.<sup>62</sup> The H188 plasmid was provided by K. Jalink, Netherlands Cancer Institute to authors G.G.H. and R.P.D.<sup>63</sup>

**Methods. Synthesis of Dicyanocobinamide (Cbi) (2).** The synthesis of dicyanocobinamide (Cbi) was performed according to previously reported methods.<sup>59</sup> Briefly, to a 10 mL microwave reaction vessel containing a magnetic stir bar were added B12 (cyanocobalamin) (303.8 mg, 0.225 mmol) (see Figures S1–S6), sodium cyanide (NaCN) (36.9 mg, 0.7096 mmol), and 5 mL of EtOH, and the vessel was sealed. The reaction was heated to 120 °C for 10 min. Following completion of the microwave reaction, the remaining solution was transferred and diluted using isopropyl alcohol (iPrOH). The reaction was purified utilizing a normal-phase silica column. The reaction was eluted using 100% methanol (MeOH). The product eluted as a purple product. The isolated product was precipitated utilizing diethyl ether (Et<sub>2</sub>O) and allowed to dry producing a solid, purple product, **2** (see Figure 2), in 80% yield (187.4 mg, 0.1795 mmol). Solubility was measured to be 400 mg/mL in distilled water. **2** was purified by RP-HPLC as described for method A1, to 98%;  $t_R$ : 5.2 and 6.7 min; ESI-MS expected  $m/z$  = 1042, observed  $m/z$  =  $[M-CN]^{+1}$  1016. <sup>1</sup>H NMR (400 MHz, D<sub>2</sub>O):  $\delta$  5.90 (s, 1H), 3.95–3.87 (m, 1H), 3.85 (d,  $J$  = 8.4 Hz, 1H), 3.75 (d,  $J$  = 10.4 Hz, 1H), 3.41 (m, 1H), 3.36 (s, 5H), 3.30 (m, 2H), 3.25 (d,  $J$  = 4.7 Hz, 1H), 3.17 (dd,  $J$  = 6.8, 6.9 Hz, 1H), 2.92–2.86 (m,

1H), 2.75–2.73 (m, 2H), 2.65–2.39 (m, 7H), 2.32–2.26 (m, 15H), 2.19–2.08 (m, 5H), 2.03–1.95 (m, 1H), 1.91–1.76 (4H), 1.69 (s, 3H), 1.54 (s, 3H), 1.50 (s, 3H), 1.44 (s, 3H), 1.32 (s, 3H), 1.19 (s, 4H), 1.16 (d,  $J = 6.4$  Hz, 4H).  $^{13}\text{C}$  NMR (400 MHz,  $\text{D}_2\text{O}$ ): 178.6, 178.4, 177.9, 177.5, 177.3, 176.8, 175.1, 175.0, 172.1, 163.4, 162.9, 105.1, 103.1, 91.0, 83.1, 75.0, 66.2, 64.2, 58.8, 56.3, 55.2, 53.2, 49.2, 48.9, 46.8, 46.3, 46.1, 43.7, 42.2, 39.0, 34.9, 32.5, 32.4, 31.9, 31.7, 31.5, 30.5, 26.6, 25.7, 24.9, 23.8, 21.7, 19.4, 18.7, 18.5, 17.4, 16.5, 15.1, 14.8. See Figures S7–S11.

**General Procedure for Cobinamide Linker Coupling.** To a 5 mL round bottom flask containing a stir bar were added **2** (15.8 mg, 0.0152 mmol) and 1 mL of NMP, and the solution was allowed to stir at 40 °C under argon until the starting material was fully dissolved. To the stirring solution of **2** was added CDT (51.4 mg, 0.313 mmol, ~20 equiv.), and the solution was allowed to stir for 1 h at which time one of the **3A–3H** (see Figure 2) (19.2  $\mu\text{L}$ , 16.5 mg, 0.300 mmol, ~20 equiv.) and triethylamine (TEA) (50  $\mu\text{L}$ ) were added. Upon stirring for an additional hour, a second equivalent of linker (**3A–3H**) and TEA were added, and the solution was stirred for 1 h. The reaction was then poured into ethyl acetate (AcOEt) (50 mL) and centrifuged (5 min, 4000 rpm, RT). The crude solid was redissolved in a minimal amount of MeOH (~5 mL) and precipitated with diethyl ether ( $\text{Et}_2\text{O}$ ) and centrifuged. The crude product was redissolved in 1 mL of deionized (DI)  $\text{H}_2\text{O}$  and purified utilizing RP-HPLC as described below.

**HPLC Purification Methods.** **4–27** were purified using a Shimadzu Prominence HPLC using a C18 column (Eclipse XDB-C18 5  $\mu\text{m}$ , 4.6  $\times$  150 mm). Two differing purification methods were used: A1,  $\text{H}_2\text{O}$  + 0.1% TFA and MeOH from 1%  $\text{CH}_3\text{OH}/\text{H}_2\text{O}$  + 0.1% TFA to 90%  $\text{CH}_3\text{OH}/\text{H}_2\text{O}$  + 0.1% TFA in 25 min; A2,  $\text{H}_2\text{O}$  + 0.1% TFA and  $\text{CH}_3\text{CN}$  from 1%  $\text{CH}_3\text{CN}/\text{H}_2\text{O}$  + 0.1% TFA to 70%  $\text{CH}_3\text{CN}/\text{H}_2\text{O}$  + 0.1% TFA in 15 min.

**Cbi-Propyne (4).** **4** was prepared according to the general procedure described above, combining **2** (16.8 mg, 0.0161 mmol) with CDT (51.4 mg, 0.3000 mmol) and stirring the solution for 1 h at which time **3A** (19.2  $\mu\text{L}$ , 16.5 mg, 0.300 mmol) and TEA (50  $\mu\text{L}$ ) were added and stirred for 1 h after which point a second equivalent amount of **3A** and TEA were added and allowed to stir for 1 h to give the target compound, which was purified using RP-HPLC method A1 to produce **4** as an orange solid to 97% purity. Yield 43% (7.8 mg, 0.007 mmol). The product obtained was in the form of two different isomers with the aquo-group located on the alpha and beta positions ( $\alpha$ -cyano- $\beta$ -aqua- and  $\alpha$ -aqua- $\beta$ -cyano-).  $t_{\text{R}}$ : 8.8 and 9.5 min; ESI-MS expected  $m/z = 1115$ , observed  $m/z = [\text{M}^+ - \text{H}_2\text{O}]^{+1}$ : 1096,  $[\text{M}^+ - \text{H}_2\text{O} + \text{H}^+]^{+2}$ : 549.  $^1\text{H}$  NMR (400 MHz,  $\text{D}_2\text{O}$ ):  $\delta$  6.50 (1H, s, Ar-H,  $\beta$ -aqua isomer) 6.42 (1H, s, Ar-H,  $\alpha$ -aqua isomer). EAS Ext Coeff $_{354} = 14,500 \text{ M}^{-1} \text{ cm}^{-1}$ . See Figures S18–S22.

**Cbi-Butyne (5).** **5** was prepared according to the general procedure described above, combining **2** (20.5 mg, 0.0197 mmol) with CDT (61.3 mg, 0.3740 mmol) and stirring the solution for 1 h at which time **3B** (32.0  $\mu\text{L}$ , 27.0 mg, 0.391 mmol) and TEA (50  $\mu\text{L}$ ) were added and stirred for 1 h after which point a second equivalent of **3B** and TEA were added and allowed to stir for 1 h to give the target compound, which was purified using RP-HPLC method A1 to produce **5** as an orange solid to 95% purity. Yield 53% (11.4 mg, 0.010 mmol). The product obtained was in the form of two different isomers with the aquo-group located on the alpha and beta positions ( $\alpha$ -cyano- $\beta$ -aqua- and  $\alpha$ -aqua- $\beta$ -cyano-).  $t_{\text{R}}$ : 7.4 and 7.9 min; ESI-MS expected  $m/z = 1129$ , observed  $m/z = [\text{M}^+ - \text{H}_2\text{O}]^{+1}$ : 1111,  $[\text{M}^+ - \text{H}_2\text{O} + \text{H}^+]^{+2}$ : 556.  $^1\text{H}$  NMR (400 MHz,  $\text{D}_2\text{O}$ ):  $\delta$  6.49 (1H, s, Ar-H,  $\beta$ -aqua isomer) 6.42 (1H, s, Ar-H,  $\alpha$ -aqua isomer). EAS Ext Coeff $_{354} = 19,804 \text{ M}^{-1} \text{ cm}^{-1}$ . See Figures S29–S33.

**Cbi-Pentyne (6).** **6** was prepared according to the general procedure described above, combining **2** (17.3 mg, 0.0166 mmol) with CDT (49.1 mg, 0.299 mmol) and stirring the solution for 1 h at which time **3C** (29.0  $\mu\text{L}$ , 24.9 mg, 0.300 mmol) and TEA (50  $\mu\text{L}$ ) were added and stirred for 1 h after which point a second equivalent amount of **3C** and TEA were added and allowed to stir for 1 h to give the target compound, which was purified using RP-HPLC method A1 to produce **6** as an orange solid to 97% purity. Yield 21%

(4.0 mg, 0.003 mmol). The product obtained was in the form of two different isomers with the aquo-group located on the alpha and beta positions ( $\alpha$ -cyano- $\beta$ -aqua- and  $\alpha$ -aqua- $\beta$ -cyano-).  $t_{\text{R}}$ : 10.4 and 11.0 min; ESI-MS-expected  $m/z = 1143$ , observed  $m/z = [\text{M}^+ - \text{H}_2\text{O}]^{+1}$ : 1124,  $[\text{M}^+ - \text{H}_2\text{O} + \text{H}^+]^{+2}$ : 563.  $^1\text{H}$  NMR (400 MHz,  $\text{D}_2\text{O}$ ):  $\delta$  6.50 (1H, s, Ar-H,  $\beta$ -aqua isomer) 6.43 (1H, s, Ar-H,  $\alpha$ -aqua isomer). EAS Ext Coeff $_{354} = 15,001 \text{ M}^{-1} \text{ cm}^{-1}$ . See Figures S40–S44.

**Cbi-Hexyne (7).** **7** was prepared according to the general procedure described above, combining **2** (15.8 mg, 0.0151 mmol) with CDT (51.6 mg, 0.314 mmol) and stirring the solution for 1 h at which time **3D** (36.5  $\mu\text{L}$ , 29.2 mg, 0.300 mmol) and TEA (50  $\mu\text{L}$ ) were added and stirred for 1 h after which point a second equivalent amount of **3D** and TEA were added and allowed to stir for 1 h to give the target compound, which was purified using RP-HPLC method A1 to produce **7** as an orange solid to 98% purity. Yield 35% (6.0 mg, 0.005 mmol). The product obtained was in the form of two different isomers with the aquo-group located on the alpha and beta positions ( $\alpha$ -cyano- $\beta$ -aqua- and  $\alpha$ -aqua- $\beta$ -cyano-).  $t_{\text{R}}$ : 11.3 and 11.8 min; ESI-MS-expected  $m/z = 1157$ , observed  $m/z = [\text{M}^+ - \text{H}_2\text{O}]^{+1}$ : 1139,  $[\text{M}^+ - \text{H}_2\text{O} + \text{H}^+]^{+2}$ : 570.  $^1\text{H}$  NMR (400 MHz,  $\text{D}_2\text{O}$ ):  $\delta$  6.49 (1H, s, Ar-H,  $\beta$ -aqua isomer) 6.42 (1H, s, Ar-H,  $\alpha$ -aqua isomer). EAS Ext Coeff $_{354} = 17,982 \text{ M}^{-1} \text{ cm}^{-1}$ . See Figures S51–S55.

**Cbi-PEG2-Alkyne (8).** **8** was prepared according to the general procedure described above, combining **2** (19.9 mg, 0.0191 mmol) with CDT (67.1 mg, 0.409 mmol) and stirring the solution for 1 h at which time **3E** (25.1  $\mu\text{L}$ , 25.4 mg, 0.177 mmol) and TEA (50  $\mu\text{L}$ ) were added and stirred for 1 h after which point a second equivalent amount of **3E** and TEA were added and allowed to stir for 1 h to give the target compound, which was purified using RP-HPLC method A1 to produce **8** as an orange solid to 98% purity. Yield 39% (8.8 mg, 0.007 mmol). The product obtained was in the form of two different isomers with the aquo-group located on the alpha and beta positions ( $\alpha$ -cyano- $\beta$ -aqua- and  $\alpha$ -aqua- $\beta$ -cyano-).  $t_{\text{R}}$ : 18.4 and 19.3 min; ESI-MS-expected  $m/z = 1204$ , observed  $m/z = [\text{M}^+ - \text{H}_2\text{O}]^{+1}$ : 1185,  $[\text{M}^+ - \text{H}_2\text{O} + \text{H}^+]^{+2}$ : 593.  $^1\text{H}$  NMR (400 MHz,  $\text{D}_2\text{O}$ ):  $\delta$  6.50 (1H, s, Ar-H,  $\beta$ -aqua isomer) 6.43 (1H, s, Ar-H,  $\alpha$ -aqua isomer). EAS Ext Coeff $_{354} = 22,919 \text{ M}^{-1} \text{ cm}^{-1}$ . See Figures S62–S66.

**Cbi-PEG4-Alkyne (9).** **9** was prepared according to the general procedure described above, combining **2** (15.5 mg, 0.0149 mmol) with CDT (51.3 mg, 0.313 mmol) and stirring the solution for 1 h at which time **3F** (18.8  $\mu\text{L}$ , 19.5 mg, 0.0843 mmol) and TEA (50  $\mu\text{L}$ ) were added and stirred for 1 h after which point a second equivalent amount of **3F** and TEA were added and allowed to stir for 1 h to give the target compound, which was purified using RP-HPLC method A1 to produce **9** as an orange solid to 97% purity. Yield 32% (6.1 mg, 0.005 mmol). The product obtained was in the form of two different isomers with the aquo-group located on the alpha and beta positions ( $\alpha$ -cyano- $\beta$ -aqua- and  $\alpha$ -aqua- $\beta$ -cyano-).  $t_{\text{R}}$ : 20.0 and 21.8 min; ESI-MS-expected  $m/z = 1292$ , observed  $m/z = [\text{M}^+ - \text{H}_2\text{O}]^{+1}$ : 1273,  $[\text{M}^+ - \text{H}_2\text{O} + \text{H}^+]^{+2}$ : 637.  $^1\text{H}$  NMR (400 MHz,  $\text{D}_2\text{O}$ ):  $\delta$  6.50 (1H, s, Ar-H,  $\beta$ -aqua isomer) 6.43 (1H, s, Ar-H,  $\alpha$ -aqua isomer). EAS Ext Coeff $_{354} = 19,439 \text{ M}^{-1} \text{ cm}^{-1}$ . See Figures S73–S77.

**Cbi-4EPMA-Alkyne (10).** **10** was prepared according to the general procedure described above, combining **2** (14.9 mg, 0.0143 mmol) with CDT (50.1 mg, 0.305 mmol) and stirring the solution for 1 h at which time **3G** (23.8 mg, 0.181 mmol) and TEA (50  $\mu\text{L}$ ) were added and stirred for 1 h after which point a second equivalent amount of **3G** and TEA were added and allowed to stir for 1 h to give the target compound, which was purified using RP-HPLC method A1 to produce **10** as an orange solid to 97% purity. Yield 10% (1.5 mg, 0.001 mmol). The product obtained was in the form of two different isomers with the aquo-group located on the alpha and beta positions ( $\alpha$ -cyano- $\beta$ -aqua- and  $\alpha$ -aqua- $\beta$ -cyano-).  $t_{\text{R}}$ : 12.4 and 12.8 min; ESI-MS-expected  $m/z = 1191$ , observed  $m/z = [\text{M}^+ - \text{H}_2\text{O}]^{+1}$ : 1173.  $^1\text{H}$  NMR (400 MHz,  $\text{D}_2\text{O}$ ):  $\delta$  6.49 (1H, s, Ar-H,  $\beta$ -aqua isomer) 6.43 (1H, s, Ar-H,  $\alpha$ -aqua isomer). EAS Ext Coeff $_{354} = 15,886 \text{ M}^{-1} \text{ cm}^{-1}$ . See Figures S84–S88.

**Cbi-3EPMA-Alkyne (11).** **11** was prepared according to the general procedure described above, combining **2** (15.7 mg, 0.0151 mmol) with CDT (51.1 mg, 0.311 mmol) and stirring the solution for 1 h at



which time **3H** (21.0  $\mu\text{L}$ , 21.2 mg, 0.162 mmol) and TEA (50  $\mu\text{L}$ ) were added and stirred for 1 h after which point a second equivalent amount of **3H** and TEA were added and allowed to stir for 1 h to give the target compound, which was purified using RP-HPLC method A1 to produce **11** as an orange solid to 97% purity. Yield 14% (2.6 mg, 0.002 mmol). The product obtained was in the form of two different isomers with the aquo-group located on the alpha and beta positions ( $\alpha$ -cyano- $\beta$ -aqua- and  $\alpha$ -aqua- $\beta$ -cyano-).  $t_{\text{R}}$ : 12.6 and 13.0 min; ESI-MS-expected  $m/z = 1191$ , observed  $m/z = [\text{M}^+ - \text{H}_2\text{O}]^+1$ : 1172,  $[\text{M}^+ - \text{H}_2\text{O} + \text{H}^+]^+2$ : 587.  $^1\text{H NMR}$  (400 MHz,  $\text{D}_2\text{O}$ ):  $\delta$  6.49 (1H, s, Ar-H,  $\beta$ -aqua isomer) 6.42 (1H, s, Ar-H,  $\alpha$ -aqua isomer). EAS Ext Coef $_{354} = 15,669 \text{ M}^{-1} \text{ cm}^{-1}$ . See Figures S95–S99.

**General Procedure for Copper-Mediated Alkyne-Azide. Cyclo-addition.** To a 5 mL round bottom flask containing a stir bar, copper(I) iodide (CuI) (3.3 mg, 0.017 mmol) and TBTA (7.0 mg, 0.013 mmol) were added to 1 mL of 4:1 DMF/ $\text{H}_2\text{O}$ . The reaction mixture was allowed to stir at room temperature until a color change occurred (clear to yellowish brown) (~15 min). The solution was treated with azido-exendin-4/40 (2.0 mg, 0.0004 mmol) (see Figures S12–S17) and the corresponding Cbi-alkynes (**4–11**) (4.8 mg, 0.004 mmol) and allowed to stir overnight.

**Cbi-Pro-Ex4 (12).** **12** was prepared according to the general procedure described above; combining **4** (1.1 mg, 0.001 mmol) with CuI (4.0 mg, 0.021 mmol), TBTA (7.5 mg, 0.014 mmol), and Ex4 (3.1 mg 0.0007 mmol) gave the target compound, which was purified using RP-HPLC method A2 to produce **12** as a red solid to 98% purity.  $t_{\text{R}}$ : 11.7 min; ESI-MS-expected  $m/z = 5327$ , observed  $m/z = [\text{M}^+ - \text{H}_2\text{O} + 2\text{H}^+]^+3$ : 1771,  $[\text{M}^+ - \text{H}_2\text{O} + 3\text{H}^+]^+4$ : 1328. See Figures S23–S25.

**Cbi-But-Ex4 (13).** **13** was prepared according to the general procedure described above; combining **5** (5.7 mg, 0.005 mmol) with CuI (4.2 mg, 0.022 mmol), TBTA (7.5 mg, 0.014 mmol), and Ex4 (4.2 mg 0.0010 mmol) gave the target compound, which was purified using RP-HPLC method A2 to produce **13** as a red solid to 98% purity.  $t_{\text{R}}$ : 12.0 min; ESI-MS-expected  $m/z = 5341$ , observed  $m/z = [\text{M}^+ - \text{H}_2\text{O} + 2\text{H}^+]^+3$ : 1775,  $[\text{M}^+ - \text{H}_2\text{O} + 3\text{H}^+ + \text{CH}_3\text{OH}]^+4$ : 1364,  $[\text{M}^+ - \text{H}_2\text{O} + 3\text{H}^+]^+4$ : 1332. See Figures S34–S36.

**Cbi-Pent-Ex4 (14).** **14** was prepared according to the general procedure described above; combining **6** (4.9 mg, 0.0043 mmol) with CuI (3.6 mg, 0.019 mmol), TBTA (6.2 mg, 0.012 mmol), and Ex4 (3.9 mg 0.0009 mmol) gave the target compound, which was purified using RP-HPLC method A2 to produce **14** as a red solid to 98% purity.  $t_{\text{R}}$ : 12.0 min; ESI-MS-expected  $m/z = 5355$ , observed  $m/z = [\text{M}^+ - \text{H}_2\text{O} + 2\text{H}^+]^+3$ : 1780,  $[\text{M}^+ - \text{H}_2\text{O} + 3\text{H}^+]^+4$ : 1335. See Figures S45–S47.

**Cbi-Hex-Ex4 (15).** **15** was prepared according to the general procedure described above; combining **7** (9.7 mg, 0.0084 mmol) with CuI (3.5 mg, 0.018 mmol), TBTA (6.6 mg, 0.012 mmol), and Ex4 (5.3 mg 0.0013 mmol) gave the target compound, which was purified using RP-HPLC method A3 to produce **15** as a red solid to 98% purity.  $t_{\text{R}}$ : 12.0 min; ESI-MS-expected  $m/z = 5369$ , observed  $m/z = [\text{M}^+ - \text{H}_2\text{O} + 2\text{H}^+]^+3$ : 1784,  $[\text{M}^+ - \text{H}_2\text{O} + 3\text{H}^+]^+4$ : 1339. See Figures S56–S58.

**Cbi-PEG2-Ex4 (16).** **16** was prepared according to the general procedure described above; combining **8** (2.0 mg, 0.0017 mmol) with CuI (3.6 mg, 0.019 mmol), TBTA (7.1 mg, 0.013 mmol), and Ex4 (3.0 mg 0.0007 mmol) gave the target compound, which was purified using RP-HPLC method A2 to produce **16** as a red solid to 98% purity.  $t_{\text{R}}$ : 11.7 min; ESI-MS-expected  $m/z = 5416$ , observed  $m/z = [\text{M}^+ - \text{H}_2\text{O} + 2\text{H}^+]^+3$ : 1800,  $[\text{M}^+ - \text{H}_2\text{O} + 3\text{H}^+]^+4$ : 1350. See Figures S67–S69.

**Cbi-PEG4-Ex4 (17).** **17** was prepared according to the general procedure described above; combining **9** (3.0 mg, 0.0023 mmol) with CuI (3.4 mg, 0.018 mmol), TBTA (7.3 mg, 0.014 mmol), and Ex4 (4.1 mg 0.0010 mmol) gave the target compound, which was purified using RP-HPLC method A2 to produce **17** as a red solid to 98% purity.  $t_{\text{R}}$ : 12.3 min; ESI-MS-expected  $m/z = 5504$ , observed  $m/z = [\text{M}^+ - \text{H}_2\text{O} + 2\text{H}^+ + \text{CH}_3\text{CN}]^+3$ : 1870,  $[\text{M}^+ - \text{H}_2\text{O} + 3\text{H}^+ + \text{CH}_3\text{OH}]^+4$ : 1404,  $[\text{M}^+ - \text{H}_2\text{O} + 4\text{H}^+]^+5$ : 1098. See Figures S79–S80.

**Cbi-4EPMA-Ex4 (18).** **18** was prepared according to the general procedure described above; combining **10** (3.3 mg, 0.0028 mmol) with CuI (3.6 mg, 0.019 mmol), TBTA (7.2 mg, 0.014 mmol), and Ex4 (3.0 mg 0.0007 mmol) gave the target compound, which was purified using RP-HPLC method A2 to produce **18** as a red solid to 98% purity.  $t_{\text{R}}$ : 12.2 min; ESI-MS-expected  $m/z = 5403$ , observed  $m/z = [\text{M}^+ - \text{H}_2\text{O} + 2\text{H}^+]^+3$ : 1796,  $[\text{M}^+ - \text{H}_2\text{O} + 3\text{H}^+]^+4$ : 1347. See Figures S89–S91.

**Cbi-3EPMA-Ex4 (19).** **19** was prepared according to the general procedure described above; combining **11** (3.0 mg, 0.0025 mmol) with CuI (4.5 mg, 0.024 mmol), TBTA (7.6 mg, 0.014 mmol), and Ex4 (2.7 mg 0.0006 mmol) gave the target compound, which was purified using RP-HPLC method A2 to produce **19** as a red solid to 97% purity.  $t_{\text{R}}$ : 12.6 min; ESI-MS-expected  $m/z = 5403$ , observed  $m/z = [\text{M}^+ - \text{H}_2\text{O} + 2\text{H}^+]^+3$ : 1796,  $[\text{M}^+ - \text{H}_2\text{O} + 2\text{H}^+ + \text{CH}_3\text{OH}]^+3$ : 1379,  $[\text{M}^+ - \text{H}_2\text{O} + 3\text{H}^+]^+4$ : 1347. See Figures S100–S102.

**Cbi-Pro-Ex40 (20).** **20** was prepared according to the general procedure described above; combining **4** (3.0 mg, 0.0027 mmol) with CuI (3.6 mg, 0.019 mmol), TBTA (7.0 mg, 0.013 mmol), and Ex40 (3.0 mg 0.0007 mmol) gave the target compound, which was purified using RP-HPLC method A2 to produce **20** as a red solid to 97% purity.  $t_{\text{R}}$ : 11.8 min; ESI-MS-expected  $m/z = 5456$ , observed  $m/z = [\text{M}^+ - \text{H}_2\text{O} + 2\text{H}^+]^+3$ : 1813,  $[\text{M}^+ - \text{H}_2\text{O} + 3\text{H}^+]^+4$ : 1360,  $[\text{M}^+ - \text{H}_2\text{O} + 4\text{H}^+]^+5$ : 1088,  $[\text{M}^+ - \text{H}_2\text{O} + 5\text{H}^+]^+6$ : 907,  $[\text{M}^+ - \text{H}_2\text{O} + 6\text{H}^+]^+7$ : 777. See Figures S26–S28.

**Cbi-But-Ex40 (21).** **21** was prepared according to the general procedure described above; combining **5** (3.4 mg, 0.0030 mmol) with CuI (4.0 mg, 0.021 mmol), TBTA (6.5 mg, 0.012 mmol), and Ex40 (3.3 mg 0.0007 mmol) gave the target compound, which was purified using RP-HPLC method A2 to produce **21** as a red solid to 97% purity.  $t_{\text{R}}$ : 11.7 min; ESI-MS-expected  $m/z = 5469$ , observed  $m/z = [\text{M}^+ - \text{H}_2\text{O} + 2\text{H}^+ + \text{CH}_3\text{CN}]^+3$ : 1859,  $[\text{M}^+ - \text{H}_2\text{O} + 2\text{H}^+]^+3$ : 1819,  $[\text{M}^+ - \text{H}_2\text{O} + 3\text{H}^+ + \text{CH}_3\text{OH}]^+4$ : 1395,  $[\text{M}^+ - \text{H}_2\text{O} + 3\text{H}^+]^+4$ : 1364,  $[\text{M}^+ - \text{H}_2\text{O} + 4\text{H}^+]^+5$ : 1091. See Figures S37–S39.

**Cbi-Pent-Ex40 (22).** **22** was prepared according to the general procedure described above; combining **6** (4.4 mg, 0.00388 mmol) with CuI (3.2 mg, 0.017 mmol), TBTA (6.5 mg, 0.012 mmol), and Ex40 (4.3 mg 0.0010 mmol) gave the target compound, which was purified using RP-HPLC method A2 to produce **22** as a red solid to 97% purity.  $t_{\text{R}}$ : 11.8 min; ESI-MS-expected  $m/z = 5483$ , observed  $m/z = [\text{M}^+ - \text{H}_2\text{O} + 2\text{H}^+]^+3$ : 1822,  $[\text{M}^+ - \text{H}_2\text{O} + 3\text{H}^+]^+4$ : 1367,  $[\text{M}^+ - \text{H}_2\text{O} + 5\text{H}^+]^+6$ : 912,  $[\text{M}^+ - \text{H}_2\text{O} + 6\text{H}^+]^+7$ : 781. See Figures S48–S50.

**Cbi-Hex-Ex40 (23).** **23** was prepared according to the general procedure described above; combining **7** (2.1 mg, 0.0018 mmol) with CuI (3.6 mg, 0.019 mmol), TBTA (7.1 mg, 0.013 mmol), and Ex40 (2.6 mg 0.0006 mmol) gave the target compound, which was purified using RP-HPLC method A2 to produce **23** as a red solid to 97% purity.  $t_{\text{R}}$ : 11.8 min; ESI-MS-expected  $m/z = 5497$ , observed  $m/z = [\text{M}^+ - \text{H}_2\text{O} + 2\text{H}^+]^+3$ : 1827,  $[\text{M}^+ - \text{H}_2\text{O} + 3\text{H}^+]^+4$ : 1371,  $[\text{M}^+ - \text{H}_2\text{O} + 5\text{H}^+]^+6$ : 914,  $[\text{M}^+ - \text{H}_2\text{O} + 6\text{H}^+]^+7$ : 784,  $[\text{M}^+ - \text{H}_2\text{O} + 7\text{H}^+]^+8$ : 685. See Figures S59–S61.

**Cbi-PEG2-Ex40 (24).** **24** was prepared according to the general procedure described above; combining **8** (2.0 mg, 0.0017 mmol) with CuI (4.1 mg, 0.022 mmol), TBTA (7.4 mg, 0.014 mmol), and Ex40 (4.0 mg 0.0009 mmol) gave the target compound, which was purified using RP-HPLC method A2 to produce **24** as a red solid to 97% purity.  $t_{\text{R}}$ : 11.6 min; ESI-MS-expected  $m/z = 5544$ , observed  $m/z = [\text{M}^+ - \text{H}_2\text{O} + 2\text{H}^+ + \text{CH}_3\text{CN}]^+3$ : 1884,  $[\text{M}^+ - \text{H}_2\text{O} + 3\text{H}^+ + \text{CH}_3\text{OH}]^+4$ : 1414,  $[\text{M}^+ - \text{H}_2\text{O} + 3\text{H}^+]^+4$ : 1382. See Figures S70–S72.

**Cbi-PEG4-Ex40 (25).** **25** was prepared according to the general procedure described above; combining **9** (3.0 mg, 0.0023 mmol) with CuI (3.3 mg, 0.017 mmol), TBTA (6.8 mg, 0.013 mmol), and Ex40 (4.1 mg 0.0009 mmol) gave the target compound, which was purified using RP-HPLC method A2 to produce **25** as a red solid to 97% purity.  $t_{\text{R}}$ : 12.0 min; ESI-MS-expected  $m/z = 5632$ , observed  $m/z = [\text{M}^+ - \text{H}_2\text{O} + 2\text{H}^+ + \text{CH}_3\text{CN}]^+3$ : 1914,  $[\text{M}^+ - \text{H}_2\text{O} + 3\text{H}^+ + \text{CH}_3\text{OH}]^+4$ : 1436. See Figures S81–S83.

**Cbi-4EPMA-Ex40 (26).** **26** was prepared according to the general procedure described above; combining **10** (2.1 mg, 0.0018 mmol)

with CuI (3.0 mg, 0.016 mmol), TBTA (6.7 mg, 0.013 mmol), and Ex40 (2.3 mg 0.0005 mmol) gave the target compound, which was purified using RP-HPLC method A2 to produce **26** as a red solid to 98% purity.  $t_R$ : 11.9 min; ESI-MS-expected  $m/z = 5531$ , observed  $m/z = [M^+ - H_2O + 3H^+ + CH_3OH]^{+5}$ : 1411,  $[M^+ - H_2O + 3H^+]^{+4}$ : 1379,  $[M^+ - H_2O + 4H^+]^{+5}$ : 1104. See Figures S92–S94.

**Cbi-3EPMA-Ex4 (27)**. **27** was prepared according to the general procedure described above; combining **11** (3.0 mg, 0.0025 mmol) with CuI (3.4 mg, 0.018 mmol), TBTA (7.0 mg, 0.013 mmol), and Ex40 (2.0 mg 0.0005 mmol) gave the target compound, which was purified using RP-HPLC method A2 to produce **27** as a red solid to 97% purity.  $t_R$ : 11.9 min; ESI-MS-expected  $m/z = 5531$ , observed  $m/z = [M^+ - H_2O + 2H^+ + CH_3CN]^{+3}$ : 1880,  $[M^+ - H_2O + 2H^+]^{+3}$ : 1838,  $[M^+ - H_2O + 3H^+ + CH_3OH]^{+4}$ : 1410,  $[M^+ - H_2O + 3H^+]^{+4}$ : 1379,  $[M^+ - H_2O + 4H^+]^{+5}$ : 1103. See Figures S103–S105.

**Circular Dichroism (CD) Measurements**. All CD spectra were recorded in three independent runs in 100  $\mu$ L of H<sub>2</sub>O with a final concentration of 40  $\mu$ M using a Jasco J-715 circular dichroism spectropolarimeter at 25 °C in a 0.1 cm path-length cuvette. The spectra were recorded from 250 to 200 nm and averaged over 6 scans with a resolution of 1.0 nm, a band width of 1.0 nm, and a response time of 4 s. The mean residue ellipticity was plotted versus wavelength using Prism GraphPad 8.

**Statement on Biological Evaluations**. All Cbi-peptide conjugates were at or above 97% purity as confirmed by RP-HPLC (see the figures in the Supporting Information) prior to use in *in vitro*, in islet, or in *in vivo* experiments.

All *in vitro* and islet experiments were conducted at least in triplicate independent runs, aside from the binding experiments, which were in duplicate independent runs. *In vivo* data was analyzed with repeated-measurements one-way or two-way ANOVA followed by Tukey's posthoc test.

**Agonism ( $EC_{50}$ ) at the Human GLP-1R for 12–27**. Agonism at the GLP-1R was monitored utilizing HEK-293 cells stably transfected with both the human GLP-1R and H188 cAMP FRET reporter cultured in DMEM with 15% FBS, 1% pen/strep, and 250  $\mu$ g/mL geneticin/G-418. Cells were placed in a 96-well plate in suspension at 200  $\mu$ L of standard extracellular saline with 11 mM glucose and 0.1% BSA at ~60,000 cells/well. Peptides and conjugates were injected to each well at 5 $\times$  the required concentration. Agonism was determined through an increase in the 485/535 nm FRET ratio, indicative of an increase in the cAMP level through binding to the H188 cAMP FRET reporter.

**Agonism ( $EC_{50}$ ) at the Rat GLP-1R**. Ex4, Ex40, and **22** were screened as previously described.<sup>69</sup>

**Competitive Binding Assay ( $IC_{50}$ ) at Human GLP-1R for 12–27**.  $IC_{50}$  values were measured in CHO-K1 cells at the human GLP-1R by Euroscreen Fast (Gosselies, Belgium) using their proprietary Taglite fluorescence competitive binding assay (Cat No. FAST0154B). The agonist tracer was GLP-1red at 4 nM with reference competitor nEx-4. Conjugates were assayed in duplicate independent runs at nine concentrations per run ranging from 1 pM to 1  $\mu$ M (Figure S110).

**Statement on Animal Experiments**. All procedures conducted in rats were approved by the Institutional Care and Use Committee of the University of Washington and conducted in compliance with the U.S. federal law and institutional guidelines, which are congruent with the NIH guide for the Care and Use of Laboratory Animals.

All procedures conducted in shrews were approved by the Institutional Care and Use Committee of the University of Pennsylvania and conducted in compliance with the U.S. federal law and institutional guidelines, which are congruent with the NIH guide for the Care and Use of Laboratory Animals.

**Rat Islet Isolation and Culture**. Islets were harvested from Sprague–Dawley rats (approximately 250 g; Envigo/Harlan) anesthetized by intraperitoneal injection of pentobarbital sodium (150 mg/kg rat). Islets were prepared and purified as described.<sup>70,71</sup> Islets were then cultured for 18 h at 37 °C, gassed with 5% CO<sub>2</sub> in an incubator in an RPMI medium supplemented with 10% heat-inactivated fetal bovine serum (Invitrogen).

**Static Measurement of ISR**. ISR was determined statically as described previously.<sup>72</sup> Briefly, islets were handpicked into a Petri dish containing KRB buffer supplemented with 0.1% bovine serum albumin and 3 mM glucose and incubated at 37 °C gassed with 5% CO<sub>2</sub> for 60 min. Subsequently, islets were placed into 96-well plates containing desired amounts of glucose and agents as indicated (Figure 5) and incubated for an additional 60 min. At the end of this period, the supernatant was assayed for insulin by RIA.

**In Vivo Study Design in Shrews**. Adult male shrews ( $n = 32$ , *Suncus murinus*) weighing ~60 g were bred at the University of Pennsylvania. These animals generated in our lab were originally derived from a colony maintained at the University of Pittsburgh Cancer Institute (a Taiwanese strain derived from stock supplied by the Chinese University of Hong Kong). Shrews were single-housed in plastic cages (37.3  $\times$  23.4  $\times$  14 cm, Innovive), fed *ad libitum* with a mixture of feline (75%, Laboratory Feline Diet 5003, Lab Diet) and ferret food (25%, High Density Ferret Diet 5LI4, Lab Diet), and had *ad libitum* access to tap water except where noted. All animals were housed under a 12/12 h light/dark cycle in a temperature- and humidity-controlled environment. Shrews were habituated to single housing in their home cages and injected IP at least 1 week prior to experimentation. All experimental injections in shrews were separated by at least 72 h. Behavioral experiments were conducted in a within-subjects, Latin square design.

**Effects of Ex4, 1, and 22 on Energy Balance in Shrews**. We first evaluated in shrews the effects on food intake and body weight of doses of nEx4, **1**, and **22**. Food intake was evaluated using our custom-made feedometers, consisting of a standard plexiglass rodent housing cage (29  $\times$  19  $\times$  12.7 cm) with mounted food hoppers resting on a plexiglass cup (to account for spillage). Shrews had *ad libitum* access to powdered food through a circular (3 cm diameter) hole in the cage. Food was removed 1 h prior to the dark onset. Shortly before the dark onset, shrews ( $n = 10$ ) received IP injection of Ex4 (5 nmol/kg), **1** (5 nmol/kg), **22** (5 nmol/kg), or vehicle (1 mL/100 g BW sterile saline). Food intake was manually measured at 6, 24, and 48 h post injection. BW was measured at 0, 24, and 48 h. Treatments occurred in a within-subject, counter-balanced design and were at least 3 days apart.

**Effects of Ex4, 1, and 22 on Glucoregulation Following an IPGTT in Shrews**. The protocol for performing an IPGTT in shrews was similar to that previously described.<sup>18,51</sup> Briefly; 3 h before the dark onset, shrews ( $n = 12$ ) were food- and water-deprived. Two hours later, baseline BG levels were determined from a small drop of tail blood and measured using a standard glucometer. nEx4 (5 nmol/kg), **1** (5 nmol/kg), **22** (5 nmol/kg), or vehicle (1 mL/100 g BW sterile saline) were then administered IP. BG was measured 30 min later ( $t = 0$  min), and then each shrew received an IP bolus of glucose (2 g/kg). Subsequent BG readings were taken at 20, 40, 60, and 120 min after glucose injection. After the final BG reading, food and water were returned. IPGTT studies were carried out in a within-subject, counter-balanced design and separated by at least 72 h.

**Effects of Ex4, 1, and 22 on Emesis in Shrews**. Shrews ( $n = 10$ ) were habituated to IP injections and to clear plastic observation chambers (23.5  $\times$  15.25  $\times$  17.8 cm) for four consecutive days prior to experimentation. The animals were injected IP with nEx4, **1**, **22** (all at 5 nmol/kg), or vehicle, placed in their respective emetic cages, and then video-recorded (Vixia HF-R62, Canon) for 120 min. All recordings started within 2 min after drug administration. After 120 min, the animals were returned to their cages. Treatments were separated by 72 h. Analysis of emetic episodes was performed by an observer blinded to treatment groups. Emetic episodes were characterized by strong rhythmic abdominal contractions associated with either oral expulsion from the gastrointestinal tract (vomiting) or without the passage of materials (retching). Latency to the first emetic episode, the total number of emetic episodes, and the number of emetic episodes per minute were recorded.



## ■ ASSOCIATED CONTENT

### Supporting Information

The Supporting Information is available free of charge at <https://pubs.acs.org/doi/10.1021/acs.jmedchem.1c00185>.

RP-HPLC purity traces, electrospray ionization mass spectra,  $^1\text{H}$  and  $^{13}\text{C}$  nuclear magnetic resonance spectra, electronic absorption spectra, and in vitro dose response curves (PDF)

## ■ AUTHOR INFORMATION

### Corresponding Author

Robert P. Doyle – Department of Chemistry, Syracuse University, Syracuse, New York 13244, United States; Department of Medicine, State University of New York, Upstate Medical University, Syracuse, New York 13210, United States; [orcid.org/0000-0001-6786-5656](https://orcid.org/0000-0001-6786-5656); Email: [rpdoyle@syr.edu](mailto:rpdoyle@syr.edu)

### Authors

Ian C. Tinsley – Department of Chemistry, Syracuse University, Syracuse, New York 13244, United States  
Tito Borner – Department of Biobehavioral Health Sciences, University of Pennsylvania, School of Nursing, Philadelphia, Pennsylvania 19104, United States  
MacKenzie L. Swanson – Department of Chemistry, Syracuse University, Syracuse, New York 13244, United States  
Oleg G. Chepurny – Department of Medicine, State University of New York, Upstate Medical University, Syracuse, New York 13210, United States  
Sarah A. Doebley – Department of Biobehavioral Health Sciences, University of Pennsylvania, School of Nursing, Philadelphia, Pennsylvania 19104, United States  
Varun Kamat – Department of Medicine, University of Washington, Medicine Diabetes Institute, Seattle, Washington 98109, United States  
Ian R. Sweet – Department of Medicine, University of Washington, Medicine Diabetes Institute, Seattle, Washington 98109, United States  
George G. Holz – Department of Medicine, State University of New York, Upstate Medical University, Syracuse, New York 13210, United States  
Matthew R. Hayes – Department of Psychiatry, University of Pennsylvania, Perelman School of Medicine, Philadelphia, Pennsylvania 19104, United States  
Bart C. De Jonghe – Department of Biobehavioral Health Sciences, University of Pennsylvania, School of Nursing, Philadelphia, Pennsylvania 19104, United States

Complete contact information is available at: <https://pubs.acs.org/doi/10.1021/acs.jmedchem.1c00185>

### Author Contributions

<sup>#</sup>I.C.T. and T.B. contributed equally to the work.

### Author Contributions

The project was conceived by R.P.D. All syntheses, purification, and chemical characterizations (NMR/CD/ESMS) were performed by I.C.T. and M.L.S. All  $\text{EC}_{50}$  measurements were conducted by O.G.C. and I.C.T. Stably transfected HEK-hGLP-1R-H188 C20-cells were generated by O.G.C. Binding experiments were conducted by Euroscreen Fast (Gosselies, Belgium) using compounds synthesized by I.C.T. and M.L.S. Insulin secretion in islets was performed by I.R.S. and V.K. All *in vivo* work was designed by M.R.H.,

B.C.D.J., and T.B. and was conducted by T.B. and S.A.D. The manuscript was written mainly by I.C.T. and R.P.D., with contributions from all authors. All authors have given approval to the final version of the manuscript.

### Notes

The authors declare the following competing financial interest(s): RPD is the named inventor of a patent associated with this work, which is assigned to Syracuse University. R.P.D., I.C.T., T.B., B.C.D.J. and M.R.H. are owners of Cantius Therapeutics LLC (Lansdale, Pennsylvania, United States), which played no role in this work. MRH receives research support from Eli Lilly & Co. and Boehringer Ingelheim for projects unrelated to the current manuscript. <sup>‡</sup>M.R.H., B.C.D.J., and R.P.D. are senior authors.

## ■ ACKNOWLEDGMENTS

This work was supported in part by National Institutes of Health R15 DK097675 and CUSE pilot study awards to R.P.D., a SOURCE research support award to M.L.S., National Institutes of Health R01 DK069575 and DK122332 to G.G.H., National Institutes of Health grant DK17047 (Cell Function Analysis Core, University of Washington), National Institutes of Health R01s DK112812 to B.C.D.J., DK115762 to M.R.H. and DK128443 to B.C.D.J., M.R.H. and R.P.D., and by the Swiss National Science Foundation (SNSF P400PB\_186728) to T.B.

## ■ ABBREVIATIONS

3EPMA, (3-ethynylphenyl)methanamine; 4EPMA, (4-ethynylphenyl)methanamine; AUC, area under the curve; BG, blood glucose; BSA, bovine serum albumin; cAMP, cyclic adenosine monophosphate; Cbi, dicyanocobinamide; CD, circular dichroism; CDT, 1,1'-carbonyl-di-(1,2,4-triazole); CNS, central nervous system; DMEM, Dulbecco's modified Eagle medium; DMF, dimethylformamide; EAS, electronic absorption spectra;  $\text{EC}_{50}$ , half-maximal effective concentration; EPAC, exchange protein directly activated by cAMP; Ex4, exendin-4 with K12 azido modification; Ex40, exendin-4 with an azido-lysine added as residue 40; FBS, fetal bovine serum; FRET, Forster resonance energy transfer; GLP-1R, glucagon like peptide-1 receptor; GPCR, G-protein coupled receptor; GSIS, glucose-stimulated insulin secretion; HEK, human embryonic kidney cells;  $\text{IC}_{50}$ , half-maximal inhibitory concentration; IPGTT, intraperitoneal glucose tolerance test; ISR, insulin secretion rate; nEx4, native Exendin-4; NMP, 1-methyl-2-pyrrolidinone; NMR, nuclear magnetic resonance; PNS, peripheral nervous system; RIA, radioimmunoassay; RP-HPLC, reversed-phase high-performance liquid chromatography; SD, Sprague–Dawley rat; SEM, standard error of the mean; SES, standard extracellular saline; T2D, type 2 diabetes mellitus; BTA, tris(benzyltriazolylmethyl)amine; TEA, triethylamine;  $t_R$ , retention time

## ■ REFERENCES

- (1) Chen, L.; Magliano, D. J.; Zimmet, P. Z. The worldwide epidemiology of type 2 diabetes mellitus—present and future perspectives. *Nat. Rev. Endocrinol.* **2012**, *8*, 228–236.
- (2) Flegal, K. M.; Carroll, M. D.; Ogden, C. L.; Curtin, L. R. Prevalence and trends in obesity among US adults, 1999–2008. *JAMA* **2010**, *303*, 235–241.
- (3) Sherwin, R.; Jastreboff, A. M. Year in diabetes 2012: The diabetes tsunami. *J. Clin. Endocrinol. Metab.* **2012**, *97*, 4293–4301.

- (4) Franks, P. W.; McCarthy, M. I. Exposing the exposures responsible for type 2 diabetes and obesity. *Science* **2016**, *354*, 69–73.
- (5) Upadhyay, J.; Polyzos, S. A.; Perakakis, N.; Thakkar, B.; Paschou, S. A.; Katsiki, N.; Underwood, P.; Park, K. H.; Seufert, J.; Kang, E. S.; Sternthal, E.; Karagiannis, A.; Mantzoros, C. S. Pharmacotherapy of type 2 diabetes: An update. *Metabolism*. **2018**, *78*, 13–42.
- (6) Sadry, S. A.; Drucker, D. J. Emerging combinatorial hormone therapies for the treatment of obesity and T2DM. *Nat. Rev. Endocrinol.* **2013**, *9*, 425–433.
- (7) Drucker, D. J.; Sherman, S. I.; Bergenstal, R. M.; Buse, J. B. The safety of incretin-based therapies—review of the scientific evidence. *J. Clin. Endocrinol. Metab.* **2011**, *96*, 2027–2031.
- (8) Hayes, M. R.; Miettlicki-Baase, E. G.; Kanoski, S. E.; De Jonghe, B. C. Incretins and amylin: neuroendocrine communication between the gut, pancreas, and brain in control of food intake and blood glucose. *Annu. Rev. Nutr.* **2014**, *34*, 237–260.
- (9) Holst, J. J. The physiology of glucagon-like peptide 1. *Physiol. Rev.* **2007**, *87*, 1409–1439.
- (10) Baggio, L. L.; Drucker, D. J. Biology of incretins: GLP-1 and GIP. *Gastroenterology* **2007**, *132*, 2131–2157.
- (11) Lovshin, J. A.; Drucker, D. J. Incretin-based therapies for type 2 diabetes mellitus. *Nat. Rev. Endocrinol.* **2009**, *5*, 262–269.
- (12) Hayes, M. R.; Schmidt, H. D. GLP-1 influences food and drug reward. *Curr. Opin. Behav. Sci.* **2016**, *9*, 66–70.
- (13) Kanoski, S. E.; Hayes, M. R.; Skibicka, K. P. Glp-1 and weight loss: Unraveling the diverse neural circuitry. *Am. J. Physiol. Regul. Integr. Comp. Physiol.* **2016**, *310*, R885–R895.
- (14) Knudsen, L. B.; Bielsen, P. F.; Huusfeldt, P. O.; Johansen, N. L.; Madsen, K.; Pederson, F. Z.; Thogersen, H.; Wilken, M.; Agerso, H. Potent Derivatives of glucagon-like peptide-1 with pharmacokinetic properties suitable for once daily administration. *J. Med. Chem.* **2000**, *43*, 1664–1669.
- (15) Madsen, K.; Knudsen, L. B.; Agresoe, H.; Nielsen, P. F.; Thogersen, H.; Wilken, M.; Johansen, N. L. Structure-activity and protraction relationship of long-acting glucagon-like peptide-1 derivative: importance of fatty acid length, polarity, and bulkiness. *J. Med. Chem.* **2007**, *50*, 6126–6132.
- (16) Knudsen, L. B.; Lau, J. The discovery and development of liraglutide and semaglutide. *Front. Endocrinol.* **2019**, *10*, 155.
- (17) O’Neil, P. M.; Birkenfeld, A. L.; McGowan, B.; Mosenzon, O.; Pederson, S. D.; Wharton, S.; Carson, C. G.; Jepsen, C. H.; Kabisch, M.; Wilding, J. P. H. Efficacy and safety of semaglutide compared with liraglutide and placebo for weightloss in patients with obesity: a randomised, double-blind, placebo and active controlled, dose-ranging, phase 2 trial. *Lancet* **2018**, *392*, 637–649.
- (18) Lau, J.; Bloch, P.; Schaffer, L.; Pettersson, I.; Spetzler, J.; Kofoed, J.; Madsen, K.; Knudsen, L. B.; McGuire, J.; Steensgaard, D. B.; Strauss, H. M.; Gram, D. X.; Knudsen, S. M.; Bielsen, F. S.; Thygesen, P.; Reedt-Runge, S.; Kruse, T. Discovery of the once-weekly glucagon-like peptide-1 (GLP-1) analog semaglutide. *J. Med. Chem.* **2015**, *58*, 7370–7380.
- (19) Bergenstal, R. M.; Wysham, C.; Macconell, L.; Malloy, J.; Walsh, B.; Yan, P.; Wilhelm, K.; Malone, J.; Porter, L. E. Efficacy and safety of exenatide once weekly versus sitagliptin or pioglitazone as an adjunct to metformin for treatment of type 2 diabetes (DURATION-2): a randomised trial. *Lancet* **2010**, *376*, 431–439.
- (20) Buse, J. B.; Henry, R. R.; Han, J.; Kim, D. D.; Fineman, M. S.; Baron, A. D. Effects of exenatide (exendin-4) on glycemic control over 30 weeks in sulfonylurea-treated patients with type 2 diabetes. *Diabetes Care* **2004**, *27*, 2628–2635.
- (21) DeFronzo, R. A.; Ratner, R. E.; Han, J.; Kim, D. D.; Fineman, M. S.; Baron, A. D. Effects of exenatide (exendin-4) on glycemic control and weight over 30 weeks in metformin-treated patients with type 2 diabetes. *Diabetes Care* **2005**, *28*, 1092–1100.
- (22) Kendall, D. M.; Riddle, M. C.; Rosenstock, J.; Zhuang, D.; Kim, D. D.; Fineman, M. S.; Baron, A. D. Effects of exenatide (exendin-4) on glycemic control over 30 weeks in patients with type 2 diabetes treated with metformin and a sulfonylurea. *Diabetes Care* **2005**, *28*, 1083–1091.
- (23) John, L. E.; Kane, M. P.; Busch, R. S.; Hamilton, R. A. Expanded use of exenatide in the management of type 2 diabetes. *Diabetes Spectrum*. **2007**, *20*, 59–63.
- (24) Weinstock, R. S.; Guerci, B.; Umpierrez, G.; Nauck, M. A.; Skrivaneck, Z.; Milicevic, Z. Safety and efficacy of once-weekly dulaglutide versus sitagliptin after 2 years in metformin-treated patients with type 2 diabetes (AWARD-5): a randomized, phase III study. *Diabetes, Obes. Metab.* **2015**, *17*, 849–858.
- (25) Wang, T.; Gou, Z.; Wang, F.; Ma, M.; Zhai, S. D. Comparison of GLP-1 analogues versus sitagliptin in the management of type 2 diabetes: systematic review and meta-analysis of head-to-head studies. *PLoS One* **2014**, *9*, No. e103798.
- (26) Kanoski, S. E.; Fortin, S. M.; Arnold, M.; Grill, H. J.; Hayes, M. R. Peripheral and central GLP-1 receptor populations mediate the anorectic effects of peripherally administered GLP-1 receptor agonists, liraglutide and exendin-4. *Endocrinology* **2011**, *152*, 3103–3112.
- (27) Sisley, S.; Gutierrez-Aguilar, R.; Scott, M.; D’Alessio, D. A.; Sandoval, D. A.; Seeley, R. J. Neuronal GLP1R mediates liraglutide’s anorectic but not glucose-lowering effect. *J. Clin. Invest.* **2014**, *124*, 2456–2463.
- (28) Secher, A.; Jelsing, J.; Baquero, A. F.; Hecksher-Sorensen, J.; Cowley, M. A.; Dalboge, L. S.; Hansen, G.; Grove, K. L.; Pyke, C.; Raun, K.; Schaffer, L.; Tang-Christensen, M.; Verma, S.; Witgen, B. M.; Vrang, N.; Knudsen, L. B. The arcuate nucleus mediates GLP-1 receptor agonist liraglutide-dependent weight loss. *J. Clin. Invest.* **2014**, *124*, 4473–4488.
- (29) Kanoski, S. E.; Rupperecht, L. E.; Fortin, S. M.; De Jonghe, B. C.; Hayes, M. R. The role of nausea in food intake and body weight suppression by peripheral GLP-1 receptor agonists, exendin-4 and liraglutide. *Neuropharmacology* **2012**, *62*, 1916–1927.
- (30) Moheet, A.; Moran, A. CF-related diabetes: Containing the metabolic miscreant of cystic fibrosis. *Pediatr. Pulmonol.* **2017**, *52*, S37–S43.
- (31) Husain, N. E.; Noor, S.; Elmadhoun, W.; Almobarak, A.; Awadalla, H.; Woodward, C.; Mital, D.; Ahmed, M. Diabetes, metabolic syndrome and dyslipidemia in people living with HIV in Africa: re-emerging challenges not to be forgotten. *HIV AIDS* **2017**, *Volume 9*, 193–202.
- (32) Gallo, M.; Muscogiuri, G.; Felicetti, F.; Faggiano, A.; Trimarchi, F.; Arvat, E.; Vigneri, R.; Colao, A. Adverse glycaemic effects of cancer therapy: indications for a rational approach to cancer patients with diabetes. *Metabolism*. **2018**, *78*, 141–154.
- (33) Ho, T.-W.; Huang, C.-T.; Ruan, S.-Y.; Tsai, Y.-J.; Lai, F.; Yu, C.-J. Diabetes mellitus in patients with chronic obstructive pulmonary disease-The impact on mortality. *PLoS One* **2017**, *12*, No. e0175794.
- (34) Honors, M. A.; Kinzig, K. P. The role of insulin resistance in the development of muscle wasting during cancer cachexia. *J. Cachexia Sarcopenia Muscle*. **2012**, *3*, 5–11.
- (35) Bonaccorso, R. L.; Chepurny, O. G.; Becker-Pauly, C.; Holz, G. G.; Doyle, R. P. Enhanced peptide stability against protease digestion induced by intrinsic factor binding of a vitamin B12 conjugate of exendin-4. *Mol. Pharmaceutics* **2015**, *12*, 3502–3506.
- (36) Miettlicki-Baase, E. G.; Liberini, C. G.; Workinger, J. L.; Bonaccorso, R. L.; Borner, T.; Reiner, D. J.; Koch-Lasowski, K.; McGrath, L. E.; Lhamo, R.; Stein, L. M.; De Jonghe, B. C.; Holz, G. G.; Roth, C. L.; Doyle, R. P.; Hayes, M. R. A vitamin B12 conjugate of exendin-4 improves glucose tolerance without associated nausea or hypophagia in rodents. *Diabetes, Obes. Metab.* **2018**, *20*, 1223–1234.
- (37) Borner, T.; Shaulson, E. D.; Tinsley, I. C.; Stein, L. M.; Horn, C. C.; Hayes, M. R.; Doyle, R. P.; De Jonghe, B. C. A second-generation glucagon-like peptide-1 receptor agonist mitigates vomiting and anorexia while retaining gluco-regulatory potency in lean diabetic and emetic and mammalian models. *Diabetes, Obes. Metab.* **2020**, *22*, 1729–1741.

- (38) Henry, K. E.; Elfers, C. T.; Burke, R. M.; Chepurny, O. G.; Holz, G. G.; Blevins, J. E.; Roth, C. L.; Doyle, R. P. Vitamin B12 conjugation of peptide-YY(3-36) decreases food intake compared to native peptide-YY(3-36) upon subcutaneous administration in male rats. *Endocrinology* **2015**, *156*, 1739–1749.
- (39) Borner, T.; Workinger, J. L.; Tinsley, I. C.; Fortin, S. M.; Stein, L. M.; Chepurny, O. G.; Holz, G. G.; Wierzba, A. J.; Gryko, D.; Nexø, E.; Shaulson, E. D.; Bamezai, A.; Rodriguez Da Silva, V. A.; De Jonghe, B. C.; Hayes, M. R.; Doyle, R. P. Corination of a GLP-1 receptor agonist for glycemic control without emesis. *Cell Rep.* **2020**, *31*, 107768.
- (40) Workinger, J. L.; Kuda-Wedagedara, A. N. W.; Julin, M. M.; White, J. M.; Nexø, E.; Viola, N. T.; Doyle, R. P. Systemically administered plant recombinant holo-intrinsic factor targets the liver and is not affected by endogenous B12 levels. *Sci. Rep.* **2019**, *9*, 12269.
- (41) De Jonghe, B. C.; Lawler, M. P.; Horn, C. C.; Tordoff, M. G. Pica as an adaptive response: kaolin consumption helps rats recover from chemotherapy-induced illness. *Physiol. Behav.* **2009**, *97*, 87–90.
- (42) Ueno, S.; Matsuki, N.; Saito, H. *Suncus murinus*: a new experimental model in emesis research. *Life Sci.* **1987**, *41*, 513–518.
- (43) Chan, S. W.; Lin, G.; Yew, D. T. W.; Yeung, C. K.; Rudd, J. A. Separation of emetic and anorexic responses of exendin-4, a GLP-1 receptor agonist in *Suncus murinus* (house musk shrew). *Neuropharmacology* **2013**, *70*, 141–147.
- (44) Chan, S. W.; Lin, G.; Yew, D. T. W.; Rudd, J. A. A physiological role of glucagon-like peptide-1 receptors in the central nervous system of *Suncus murinus* (house musk shrew). *Eur. J. Pharmacol.* **2011**, *668*, 340–346.
- (45) Anantharam, P.; Whitley, E. M.; Mahama, B.; Kim, D. S.; Sarkar, S.; Santana, C.; Chan, A.; Kanthasamy, A. G.; Kanthasamy, A.; Boss, G. R.; Rumbelha, W. Cobinamide is effective for treatment of hydrogen sulfide-induced neurological sequelae in a mouse model. *Anna. N.Y. Acad. Sci.* **2017**, *1408*, 61–78.
- (46) Hendry-Hofer, T. B.; Ng, P. C.; McGrath, A. M.; Mukai, D.; Brenner, M.; Mahon, S.; Maddry, J. K.; Boss, G. R.; Bebart, V. S. Intramuscular aminotetrazole cobinamide as a treatment for inhaled hydrogen sulfide poisoning in a large swine model. *Ann. N.Y. Acad. Sci.* **2020**, *1479*, 159–167.
- (47) Ma, J.; Dasgupta, P. K.; Zelder, F. H.; Boss, G. R. Cobinamide chemistries for photometric cyanide determination. A merging zone liquid core waveguide cyanide analyzer using cyanoaquacobinamide. *Anal. Chim. Acta* **2012**, *736*, 78–84.
- (48) Männel-Croisé, C.; Probst, B.; Zelder, F. A straightforward method for the colorimetric detection of endogenous biological cyanide. *Anal. Chem.* **2009**, *81*, 9493–9498.
- (49) Brenner, M.; Mahon, S. B.; Lee, J.; Kim, J.; Mukai, D.; Goodman, S.; Kreuter, K. A.; Ahdout, R.; Mohammad, O.; Sharma, V. S.; Blackledge, W.; Boss, G. R. Comparison of cobinamide to hydroxocobalamin in reversing cyanide physiologic effects in rabbits using diffuse optical spectroscopy monitoring. *J. Biomed. Opt.* **2010**, *15*, No. 017001.
- (50) Broderick, K. E.; Potluri, P.; Zhuang, S.; Scheffler, I. E.; Sharma, V. S.; Pilz, R. B.; Boss, G. R. Cyanide detoxification by the cobalamin precursor cobinamide. *Exp. Biol. Med.* **2016**, *231*, 641–649.
- (51) Chan, A.; Jiang, J.; Fridman, A.; Guo, L. T.; Shelton, G. D.; Liu, M.-T.; Green, C.; Haushalter, K. J.; Patel, H. H.; Lee, J.; Yoon, D.; Burney, T.; Mukai, D.; Mahon, S. B.; Brenner, M.; Pilz, R. B.; Boss, G. R. Nitrocobinamide, a new cyanide antidote that can be administered by intramuscular injection. *J. Med. Chem.* **2015**, *58*, 1750–1759.
- (52) Chan, A.; Balasubramanian, M.; Blackledge, W.; Mohammad, O. M.; Alvarez, L.; Boss, G. R.; Bigby, T. D. Cobinamide is superior to other treatments in a mouse model of cyanide poisoning. *Clin. Toxicol.* **2010**, *48*, 709–717.
- (53) Lee, J.; Mahon, S. B.; Mukai, D.; Burney, T.; Katebian, B. S.; Chan, A.; Bebart, V. S.; Yoon, D.; Boss, G. R.; Brenner, M. The vitamin B12 analog cobinamide is an effective antidote for oral cyanide poisoning. *J. Med. Toxicol.* **2016**, *12*, 370–379.
- (54) Greenawald, L. A.; Snyder, J. L.; Fry, N. L.; Sailor, M. J.; Boss, G. R.; Finklea, H. O.; Bell, S. Development of a cobinamide-based end-of-service-life indicator for detection of hydrogen cyanide gas. *Sens. Actuators B Chem.* **2015**, *221*, 379–385.
- (55) Wierzba, A. J.; Maximova, K.; Wincenciuk, A.; Równicki, M.; Wojciechowska, M.; Nexø, E.; Trylska, J.; Gryko, D. Does a conjugation site affect transport of vitamin B12-peptide nucleic acid conjugates into bacterial cells. *Chem. – Eur. J.* **2018**, *24*, 18772–18778.
- (56) Evers, A.; Haack, T.; Lorenz, M.; Bossart, M.; Elvert, R.; Henkel, B.; Stengelin, S.; Kurz, M.; Glien, M.; Dudda, A.; Lorenz, K.; Kadereit, D.; Wagner, M. Design of novel exendin-based dual glucagon-like peptide 1 (GLP-1)/glucagon receptor agonists. *J. Med. Chem.* **2017**, *60*, 4293–4303.
- (57) Dai, S.; Liu, S.; Li, C.; Zhou, Z.; Wu, Z. Site-selective modification of exendin 4 with variable molecular weight dextrans by oxime-ligation chemistry for improving type 2 diabetic treatment. *Carbohydr. Polym.* **2020**, *249*, 116864.
- (58) Lee, J. G.; Ryu, J. H.; Kim, S. M.; Park, M. Y.; Kim, S. H.; Shin, Y. G.; Sohn, J. W.; Kim, H. H.; Park, Z. Y.; Seong, J. Y.; Kim, J. I. Replacement of the C-terminal Trp-cage of exendin-4 with a fatty acid improves therapeutic utility. *Biochem. Pharmacol.* **2018**, *151*, 59–68.
- (59) Ó Proinsias, K.; Karczewski, M.; Zieleniewska, A.; Gryko, D. Microwave-assisted cobinamide synthesis. *J. Org. Chem.* **2014**, *79*, 7752–7757.
- (60) Zhou, K.; Zelder, F. Identification of diastereomeric cyano-aqua cobinamides with a backbone-modified vitamin B12 derivative and with <sup>1</sup>H NMR spectroscopy. *Eur. J. Inorg. Chem.* **2011**, 53–57.
- (61) Berg, R.; Straub, B. F. Advancements in the mechanistic understanding of the copper-catalyzed azide-alkyne cycloaddition. *Beilstein J. Org. Chem.* **2013**, *9*, 2715–2750.
- (62) Tibaduiza, E. C.; Chen, C.; Beinborn, M. A Small molecule ligand of the glucagon-like peptide 1 receptor targets its amino-terminal hormone binding domain. *J. Biol. Chem.* **2001**, *276*, 37787–37793.
- (63) Klarenbeek, J.; Goedhart, J.; van Batenburg, A.; Groenewald, D.; Jalink, K. Fourth generation EPAC-based FRET sensors for cAMP feature exceptional brightness, photostability and dynamic range: characterization of dedicated sensors for FLIM, for ratiometry and with high affinity. *PLoS One* **2015**, *10*, No. e0122513.
- (64) Khaothiar, L.; McCowen, K. C.; Blackburn, G. L. Obesity and its comorbid conditions. *Clin. Cornerstone.* **1999**, *2*, 17–31.
- (65) Mroz, P. A.; Perez-Tilve, D.; Mayer, J. P.; DiMarchi, R. D. Stereochemical inversion as a route to improved biophysical properties of therapeutic peptides exemplified by glucagon. *Commun. Chem.* **2019**, *2*, 2.
- (66) Chabenne, J. R.; Mroz, P. A.; Mayer, J. P.; DiMarchi, R. D. Structural refinement of glucagon for therapeutic use. *J. Med. Chem.* **2020**, *63*, 3447–3460.
- (67) Chabenne, J. R.; DiMarchi, M. A.; Gelfanov, V. M.; DiMarchi, R. D. Optimization of the native glucagon sequence for medicinal purposes. *J. Diabetes Sci. Technol.* **2010**, *4*, 1322–1331.
- (68) Chen, W.; Lisowski, M.; Khalil, G.; Sweet, I. R.; Shen, A. Q. Microencapsulated 3-Dimensional sensor for the measurement of oxygen in single isolated pancreatic islets. *PLoS One* **2012**, *7*, No. e33070.
- (69) Milliken, B. T.; Chepurny, O. G.; Doyle, R. P.; Holz, G. G. FRET reporter assays for cAMP and calcium in a 96-well format using genetically encoded biosensors expressed in living cells. *Bio-Protoc.* **2020**, *10*, No. e3641.
- (70) Sweet, I. R.; Cook, D. L.; DeJulio, E.; Wallen, A. R.; Khalil, G.; Callis, J.; Reems, J. Regulation of ATP/ADP in pancreatic islets. *Diabetes* **2004**, *53*, 401–409.
- (71) Matsumoto, S.; Shibata, S.; Kirchhof, N.; Hiraoka, K.; Sageshima, J.; Zhang, X. W.; Gilmore, T.; Ansite, J.; Zhang, H. J.; Sutherland, D. E. R.; Hering, B. J. Immediate reversal of diabetes in

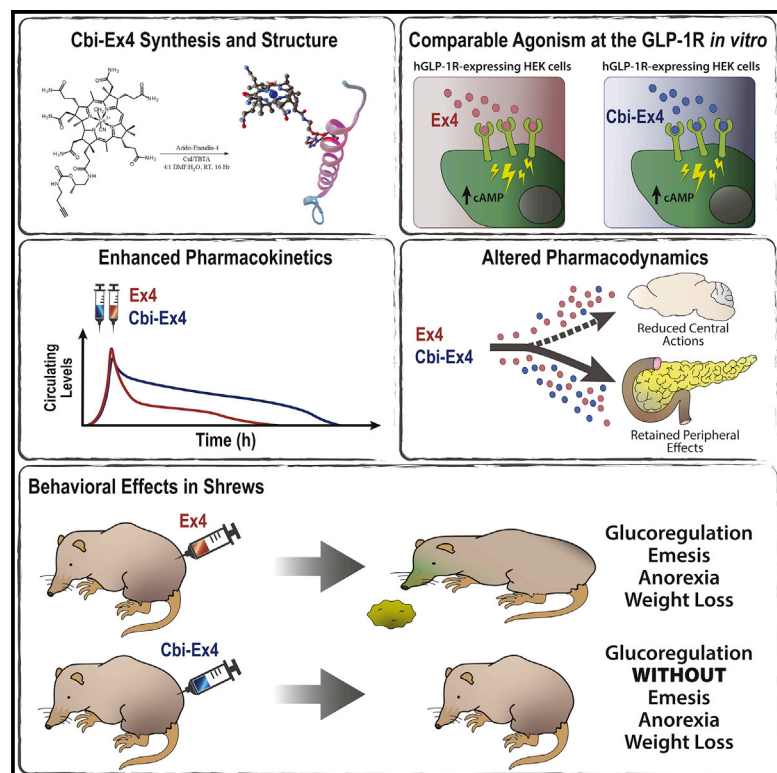


primates following intraportal transplantation of porcine islets purified on a new histidine-lactoiniate-iodixanol gradient. *Transplantation*. **1999**, *67*, S220.

(72) Jung, S.-R.; Reed, B. J.; Sweet, I. R. A highly energetic process couples calcium influx through L-type calcium channels to insulin secretion in pancreatic beta-cells. *Am. J. Physiol.* **2009**, *297*, E717–E727.

# Corrination of a GLP-1 Receptor Agonist for Glycemic Control without Emesis

## Graphical Abstract



## Authors

Tito Borner, Jayme L. Workinger, Ian C. Tinsley, ..., Bart C. De Jonghe, Matthew R. Hayes, Robert P. Doyle

## Correspondence

rpdoyle@syrr.edu

## In Brief

Borner et al. describe the creation of a conjugated GLP-1R agonist (Cbi-Ex4) with reduced brain penetrance. Cbi-Ex4 enhances glycemic control without inducing emesis or anorexia. Our preclinical findings highlight its potential therapeutic use for patients seeking improved glycemic control without the loss of appetite and emesis characteristic of current GLP-1 therapeutics.

## Highlights

- The Cbi-Ex4 conjugate retains GLP-1R agonism *in vitro* and improved half-life *in vivo*
- Cbi-Ex4 displays similar glucoregulatory properties compared to native Ex4
- Cbi-Ex4 does not induce anorexia, weight loss, or hindbrain neuronal activation
- In contrast to Ex4, Cbi-Ex4 does not cause emesis indicative of improved tolerance



## Article

# Corination of a GLP-1 Receptor Agonist for Glycemic Control without Emesis

Tito Borner,<sup>3,7</sup> Jayme L. Workinger,<sup>1,7</sup> Ian C. Tinsley,<sup>1,7</sup> Samantha M. Fortin,<sup>2</sup> Lauren M. Stein,<sup>2</sup> Oleg G. Chepurny,<sup>4</sup> George G. Holz,<sup>4</sup> Aleksandra J. Wierzbica,<sup>5</sup> Dorota Gryko,<sup>5</sup> Ebba Nexø,<sup>6</sup> Evan D. Shaulson,<sup>3</sup> Ankur Bamezai,<sup>2</sup> Valentina A. Rodriguez Da Silva,<sup>2,3</sup> Bart C. De Jonghe,<sup>3,8</sup> Matthew R. Hayes,<sup>2,3,8</sup> and Robert P. Doyle<sup>1,4,8,9,\*</sup>

<sup>1</sup>Department of Chemistry, Syracuse University, Syracuse, NY, USA

<sup>2</sup>Department of Psychiatry, Perelman School of Medicine, University of Pennsylvania, Philadelphia, PA, USA

<sup>3</sup>Department of Biobehavioral Health Sciences, School of Nursing, University of Pennsylvania, Philadelphia, PA 19104, USA

<sup>4</sup>Department of Medicine, Upstate Medical University, State University of New York, Syracuse, NY, USA

<sup>5</sup>Institute of Organic Chemistry, Polish Academy of Sciences, Warsaw, Poland

<sup>6</sup>Department of Clinical Biochemistry and Clinical Medicine, University of Aarhus, Aarhus, Denmark

<sup>7</sup>These authors contributed equally

<sup>8</sup>These authors contributed equally

<sup>9</sup>Lead Contact

\*Correspondence: [rpdoylesyr@syr.edu](mailto:rpdoylesyr@syr.edu)

<https://doi.org/10.1016/j.celrep.2020.107768>

## SUMMARY

Glucagon-like peptide-1 receptor (GLP-1R) agonists used to treat type 2 diabetes mellitus often produce nausea, vomiting, and in some patients, undesired anorexia. Notably, these behavioral effects are caused by direct central GLP-1R activation. Herein, we describe the creation of a GLP-1R agonist conjugate with modified brain penetrance that enhances GLP-1R-mediated glycemic control without inducing vomiting. Covalent attachment of the GLP-1R agonist exendin-4 (Ex4) to dicyanocobinamide (Cbi), a corrin ring containing precursor of vitamin B12, produces a “corinated” Ex4 construct (Cbi-Ex4). Data collected in the musk shrew (*Suncus murinus*), an emetic mammal, reveal beneficial effects of Cbi-Ex4 relative to Ex4, as evidenced by improvements in glycemic responses in glucose tolerance tests and a profound reduction of emetic events. Our findings highlight the potential for clinical use of Cbi-Ex4 for millions of patients seeking improved glycemic control without common side effects (e.g., emesis) characteristic of current GLP-1 therapeutics.

## INTRODUCTION

Type 2 diabetes mellitus (T2DM) management involves lifelong pharmaceutical interventions (Drucker et al., 2011; Sadry and Drucker, 2013), including those based on glucagon-like peptide-1 (GLP-1), an incretin hormone produced in the intestine and brainstem (Hayes et al., 2014; Holst, 2007). Existing US Food and Drug Administration (FDA)-approved GLP-1 receptor (GLP-1R) agonists enhance postprandial insulin secretion and reduce food intake (Hayes et al., 2014; Hayes and Schmidt, 2016; Kanoski et al., 2016). While the latter is attractive when considering GLP-1R agonists for obesity treatment, the hypophagic effects of all known GLP-1R agonists are accompanied by nausea and vomiting, which affects ~20%–50% of patients and leads to discontinuation of drug treatment in ~6%–10% and reduced dose tolerance in another ~15% of patients (Bergental et al., 2010; Buse et al., 2004; DeFronzo et al., 2005; John et al., 2007; Kendall et al., 2005). Evidence-based medical reports are now clear that nausea and emesis are the principal side effects of existing GLP-1 therapeutics (Bettge et al., 2017). Even with common approaches to mitigate side effects such as slow-dose escalation or titration, a recent report from GlaxoSmithKline concluded that patients reported GI-related is-

issues that “made me feel sick” (64.4%) and “made me throw up” (45.4%) as their major reasons for treatment discontinuation (Sikirica et al., 2017). Importantly, such adverse gastrointestinal events of GLP-1R agonists are persistent in the profile of current second-generation GLP-1R-based drugs such as dulaglutide, semaglutide, and albiglutide (Ahrén et al., 2018; Pratley et al., 2018; Wysham et al., 2014). Importantly, for some diabetic patients with comorbidities such as cancer, cystic fibrosis, HIV, or general disease-cachexia, any further weight loss and malaise are unacceptable side effects that necessitate the creation of a new class of GLP-1 therapeutic.

There is convincing evidence that a significant portion of the increase in glucose-stimulated insulin secretion following administration of current exogenous GLP-1R ligands is mediated by direct activation of GLP-1R expressed on pancreatic  $\beta$ -cells (for review, see Drucker, 2006; Hayes et al., 2010, 2014; Kanoski et al., 2016), mimicking the paracrine effects of pancreatic-derived GLP-1 that may not occur with endogenous L-cell-derived GLP-1 (Chambers et al., 2017; Lamont et al., 2012; Smith et al., 2014). In contrast, GLP-1Rs expressed in the central nervous system (CNS), in particular those in the hindbrain (Alhadeff et al., 2016; Hayes et al., 2011), mediate the food intake- and body weight-suppressive effects of GLP-1R agonists, such as



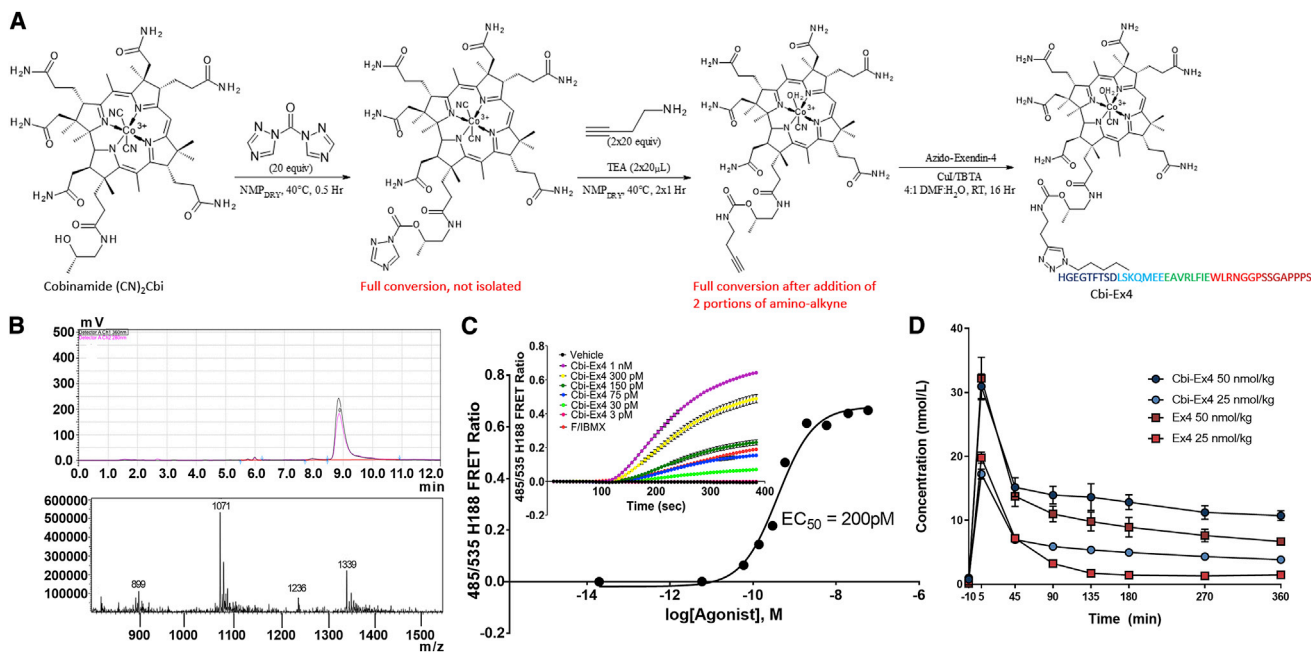


**Figure 1. Covalent Conjugation of Ex4 to Cbi Retains GLP-1R Agonism *In Vitro* and Displays Improved Half-Life *In Vivo***

(A) Synthetic scheme for Cbi-Ex4 synthesis: 1-amino-3-butynol was coupled to Cbi utilizing carbonyl ditriazole (CDT), priming the Cbi for conjugation to Ex4. Ex4 was covalently bound to the Cbi-alkyne via copper-catalyzed alkyne-azide cycloaddition.

(B) RP-HPLC of Cbi-Ex4 showing purity of  $\geq 97\%$  and liquid chromatography-mass spectrometry (LC-MS) showing 1,339 [M+4H]<sup>4+</sup> and 1,071 [M+5H]<sup>5+</sup>, consistent with the conjugate.

(C) Dose-dependent Cbi-Ex4 agonism at the human GLP-1 receptor, as monitored in FRET assays using the cAMP biosensor H188 expressed in HEK293 cells. EC<sub>50</sub> value for Cbi-Ex4 was determined to be  $200 \pm 0.09$  pM (mean  $\pm$  SEM) (Chepurny et al., 2019).

(D) Pharmacokinetic profile of two equimolar doses (25 nmol/kg and 50 nmol/kg) of Ex4 and Cbi-Ex4. Data expressed as mean  $\pm$  SEM. Full PK parameters are given in Table S2.

liraglutide and exenatide (synthetic Ex4) (Kanoski et al., 2011; Miettlicki-Baase et al., 2013; Secher et al., 2014; Sisley et al., 2014). This CNS site-of-action, and not a vagally mediated effect, is also responsible for mediating the illness-like behaviors (e.g., nausea, conditioned taste avoidance, emesis) of systemically delivered GLP-1R agonists (Kanoski et al., 2012). Thus, from a therapeutic standpoint aimed at normalizing the chronic hyperglycemia of diabetic patients, designing a GLP-1R agonist that does not penetrate readily into the CNS (or at least the hind-brain), but retains enhanced pharmacological action on  $\beta$ -cells, would theoretically provide an improved tool for glycemic control without eliciting unwanted nausea/malaise.

Taking advantage of the highly controlled transport and trafficking of vitamin B12 (B12) that occurs in mammalian physiology, together with bioconjugate technology involving peptide-based conjugation to B12 and B12 fragments, Ex4 was covalently attached to dicyanocobinamide (Cbi), a corrin-ring-containing precursor of B12, to create the compound Cbi-Ex4 (Figure 1A). The theoretical advantage of this construct was 3-fold. First, there is no known biological function of Cbi in humans and Cbi does not affect intact B12 physiology (Green et al., 2017). Second, Cbi is highly water soluble and the uptake of Cbi-Ex4 through the blood brain barrier and into the CNS would putatively be extremely low (Green et al., 2017). Indeed, evidence collected postmortem from human brain and liver

clearly demonstrated negligible amounts of B12 (11.3 pmol/g) and an  $\sim 10$ -fold lower relative concentration of corrinoid-type analogs (1.3 pmol/g; including cobinamide) in the brain, with the liver being the main site of concentration for both B12 and corrinoid analogs (total  $>600$  pmol/g) (Kanazawa and Herbert, 1983). These first two advantages of Cbi-Ex4 provide support for the third and most important hypothesized benefit—namely that Cbi-Ex4 should theoretically be a GLP-1R agonist that retains a peripheral site of action when systemically administered, providing a pancreatic-mediated mechanism for Cbi-Ex4 to improve hyperglycemia, without producing any CNS-mediated illness-like behaviors.

Cbi has been identified in humans (Hardle and Nexø, 2009), but has no influence on normal B12 homeostasis (Green et al., 2017) since it is *not* recognized by the B12 blood transporting protein transcobalamin (TC), critical for blood-brain barrier penetration and cell entry via the CD320 receptor (Green et al., 2017). Instead, Cbi is recognized in blood *only* by the B12 binding protein haptocorrin (HC). The function of circulating HC is unknown and no known specific receptor for the Cbi-HC complex has been identified (Furger et al., 2012). Indeed, congenital defects in plasma HC are asymptomatic, suggesting that HC and Cbi are not physiologically relevant in humans (Rosenblatt et al., 2001). Further, the plasma-binding capacity of HC for molecular forms of B12, including Cbi, in humans is very limited (reference

interval 90–270 pM; Gimsing and Nexø, 1989). Thus, using Cbi (in a conjugate process we coin here “corrination”) as a pharmacodynamic/pharmacokinetic modifier of a target peptide pharmaceutical, we have created an “inert” carrier in terms of affecting B12 homeostasis, but one that would have the advantage of putatively reducing/avoiding CNS permeability/localization while improving the general proteolytic survival and/or reduce clearance of the bound peptide. Unfortunately, rodents do not represent ideal models to test Cbi-Ex4 as (1) they lack the separate HC and TC proteins as found in human blood (Kuda-Wedagedara et al., 2017) and (2) they lack the emetic reflex (Horn et al., 2013). The musk shrew (*Suncus murinus*) was therefore chosen as the model system to evaluate the *in vivo* efficacy and tolerability of Cbi-Ex4, as shrews are capable of emesis (Ueno et al., 1987) and were believed, through bioinformatics, to have the same B12 binding profile in blood as humans (*vide infra*). Importantly, in the context of modeling the GLP-1 system, the shrew also shows hypoglycemia, anorexia, and emetic sensitivity to existing GLP-1R agonists (Chan et al., 2011; Chan et al., 2013).

## RESULTS AND DISCUSSION

### Covalent Conjugation of Ex4 to Cbi Retains GLP-1R Agonism *In Vitro*

Here, we present a method, with validation, for corrination of Ex4 with the Cbi compound dicyanocobinamide to produce a GLP-1R agonist, namely, Cbi-Ex4 (Figures 1A and 1B), with an half maximal effective concentration ( $EC_{50}$ ) of  $\sim 200$  pM in fluorescence resonance energy transfer (FRET) assays that monitor levels of cAMP in HEK-239 cells stably transfected with the human GLP-1R (Figure 1C). The conjugate is linked between the K12 residue of Ex4 and the terminal f-branch of Cbi. These two positions were previously reported by us (Mietlicki-Baase et al., 2018) and others (Równicki et al., 2017; Wierzbica et al., 2019) to support high-efficiency conjugation. While no spacer optimization was conducted, we utilized a spacer length that was already established by us to yield a high-potency B12-Ex4 conjugate (Clardy-James et al., 2013).

### Cbi-Ex4 Binds to Shrew HC and Displays Improved Half-Life *In Vivo*

Initially, we confirmed the presence of both HC and TC in shrew blood by performing radio- $^{57}\text{Co}$ -B12 binding assays and serum B12 protein isolation and identification (see Table S1). In addition to confirming the presence of HC (and separately TC, the profile found in humans, but not rodents [Hygum et al., 2011]), we showed that the total blood B12 binding in *S. murinus* was  $\sim 12$  nM, of which  $\sim 4.5$  nM was due to apo-HC. We also demonstrate that, as hypothesized, only HC ( $K_a$  0.45 nM Cbi-Ex4 versus 0.036 nM for Cbi), not TC ( $K_a$  for Cbi-Ex4  $> 0.2$   $\mu\text{M}$ ), binds Cbi-Ex4, and that such binding to HC was  $\sim 10$ -fold lower in affinity than for Cbi alone (see Figure S1).

Cbi-Ex4 exhibited reduced plasma clearance (as evidenced by the area under the curve [AUC] and elimination constants) relative to native Ex4 (Figure 1D; Table S2). This finding is likely due, at least in part, to improved stability of the conjugate to proteolytic activity, as we have demonstrated previously for full-vitamin-B12 conjugates (Bonaccorso et al., 2015), and/or

reduced renal clearance, both major routes of Ex4 clearance *in vivo* (Copley et al., 2006; Simonsen et al., 2006). ELISA-based pharmacokinetic studies demonstrated that Cbi-Ex4 had a reduced rate of elimination as evidenced by the elimination constants ( $K_e$ ) of  $0.034\text{ h}^{-1}$  for Cbi-Ex4 versus  $0.047\text{ h}^{-1}$  for Ex4, and reduced clearance ( $0.0044\text{ L/h}$  for Cbi-Ex4 versus  $0.0056\text{ L/h}$  for Ex4) with no significant difference in volume of distribution between either drug (see Table S2). Overall, Cbi-Ex4 provided greater drug exposure over time, as evidenced by the greater  $AUC_{0-360}$  ( $2.82\text{ mg}\cdot\text{h/L}$  for Ex4 versus  $4.55\text{ mg}\cdot\text{h/L}$  for Cbi-Ex4), all above the values reported for the  $50\text{ nmol/kg}$  dose (Figure 1D; Table S2). We noted also that the  $C_{\text{max}}$  values for both the  $25\text{ nmol/Kg}$  and  $50\text{ nmol/Kg}$  doses of Cbi-Ex4 were  $17.25$  and  $30.96\text{ nmol/L}$  (4- to 7-fold greater than the maximum apo-HC levels measured and recorded above), suggesting that the effects of corrination are due to the Cbi itself, and are not primarily dependent on binding to HC (the only known binder of Cbi) *in vivo*. At this point it is interesting to note that Herbert and Herzlich (1983) first suggested that HC may play a role in removing corrinoids from the human brain, an idea supported by subsequent work by Hansen et al. (1985), who showed HC was found in human CSF (CSF-HC) at concentrations ranging from 10 to 41 pmol/L (median 21 pmol/L; Hansen et al., 1985) with plasma/CSF ratios suggesting such HC was produced in the CNS directly. Overall, the results described herein then may be a consequence of naturally less penetrance of Cbi-Ex4 due to the presence of the highly polar Cbi group, a lack of facilitated transport into the brain for Cbi-Ex4, and/or binding by CSF-HC and subsequent removal or deactivation of Cbi-Ex4 in the CNS. In regard to the latter point, we subsequently assayed HC-Cbi-Ex4 at the GLP-1R and noted an  $EC_{50}$  of  $\sim 3$  nM, essentially rendering a physiologically irrelevant construct (see Figure S2).

### Cbi-Ex4 Enhances Glucose Clearance but Does Not Affect Feeding Behavior

Glucose-stimulated insulin secretion following administration of a GLP-1 analog is mediated principally by activation of GLP-1Rs expressed on pancreatic  $\beta$ -cells (Chambers et al., 2017; Lamont et al., 2012; Smith et al., 2014). Therefore, as a proof of concept, we first tested whether Cbi-Ex4 retains its *in vivo* ability to reduce blood glucose following an intraperitoneal (i.p.) glucose tolerance test (IPGTT) across different doses compared to equimolar doses of native Ex4. We observed that shrews treated with Cbi-Ex4 and native Ex4 display improved glucose clearance following i.p. glucose administration compared to vehicle injections (Figures 2A–2C). Furthermore, the plasma glucose clearing rate of Cbi-Ex4 did not differ from the relative equimolar dose of native Ex4 following acute administration, which is indicative of a retained glucoregulatory potency (Figures 2B–2D and S3).

Based on these observations, we then further hypothesized that Cbi-Ex4 may also retain a plasma glucose-lowering action for a longer duration compared to native Ex4. Therefore, a “delayed” IPGTT was performed, in which an i.p. glucose bolus was administered 360 min *after* drug administration to determine whether a longer time window exists for Cbi-Ex4 to facilitate glucose clearance relative to native Ex4. Results show a significant suppression in plasma glucose concentrations 6 h following



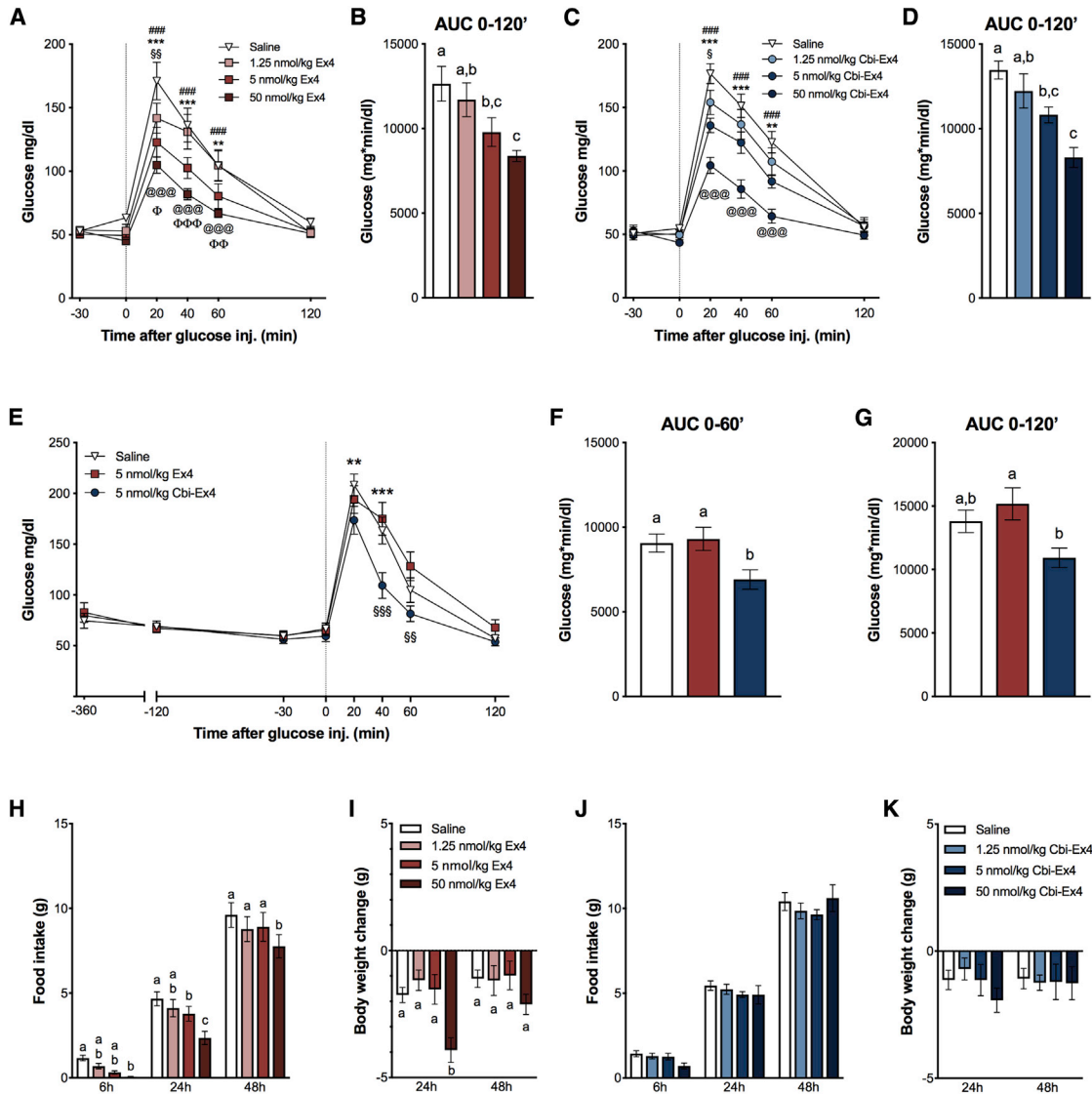


**Figure 2. Cbi-Ex4 Enhances Glucose Clearance but Does Not Affect Feeding Behavior**

(A) Ex4 (1.25, 5, and 50 nmol/kg, i.p.; i.e., ~5, 20, and 200  $\mu$ g/kg; respectively) dose-dependently suppressed blood glucose (BG) levels following glucose administration (2 g/kg, i.p.). Saline versus 5 nmol/kg Ex4:  $^{**}p < 0.01$ ,  $^{***}p < 0.001$ ; saline versus 50 nmol/kg Ex4:  $^{###}p < 0.001$ ; saline versus 1.25 nmol/kg Ex4:  $^{§§}p < 0.01$ ; 1.25 nmol/kg Ex4 versus 50 nmol/kg Ex4:  $^{@@@}p < 0.001$ ; 1.25 nmol/kg Ex4 versus 5 nmol/kg Ex4:  $^{\Phi}p < 0.05$ ,  $^{\Phi\Phi}p < 0.01$ ,  $^{\Phi\Phi\Phi}p < 0.001$ .

(B) Area under the curve (AUC) from 0 (i.e., post-glucose bolus) to 120 min after Ex4.

(C) In an IPGTT Cbi-Ex4 dose-dependently reduced BG levels comparably to equimolar doses of Ex4. Saline versus 5-nmol/kg Cbi-Ex4:  $^{**}p < 0.01$ ,  $^{***}p < 0.001$ ; saline versus 50 nmol/kg Cbi-Ex4:  $^{###}p < 0.001$ ; saline versus 1.25 nmol/kg Cbi-Ex4:  $^{\S}p < 0.05$ ; 1.25 nmol/kg Cbi-Ex4 versus 50 nmol/kg Cbi-Ex4:  $^{@@@}p < 0.001$ .

(D) AUC from 0 to 120 min following Cbi-Ex4.

(E) In a delayed glucose load IPGTT, Ex4, Cbi-Ex4 (5 nmol/kg) or vehicle were injected 6 h before glucose load. While Ex4-treatment was no longer effective in reducing BG levels, Cbi-Ex4 retained its BG lowering properties; saline versus Cbi-Ex4:  $^{**}p < 0.01$ ,  $^{***}p < 0.001$ ; Ex4 versus Cbi-Ex4:  $^{§§}p < 0.01$ ,  $^{§§§}p < 0.001$ .

(F and G) AUC analyses from 0 to 60 min and 0 to 120 min, respectively. Cbi-Ex4-treated animals had lower AUC 0-120 compared to Ex4-treated animals and a lower AUC 0-60 compared to Ex4-treated animals and controls.

(H and I) Ex4 dose-dependently induced anorexia leading to weight loss.

(J and K) Equimolar doses of Cbi-Ex4 had no effect on food intake or body weight. All data expressed as mean  $\pm$  SEM.

Data in (A), (B), (E), and (H)–(K) were analyzed with repeated-measurements two-way ANOVA followed by Tukey's *post hoc* test. Data in (B), (D), (F), and (G) were analyzed with repeated-measurements one-way ANOVA followed by Tukey's *post hoc* test. Means with different letters are significantly different ( $p < 0.05$ ).

Cbi-Ex4 administration in an IPGTT, with no effect on plasma glucose tolerance being observed after a 6h time delay of native Ex4 administration (Figures 2E–2G).

Direct activation of GLP-1R expressed in various nuclei of the CNS (including, but not limited to those of the hypothalamus and dorsal vagal complex [DVC]), contributes to the body weight and

food intake suppressive effects of exogenously administered first-generation GLP-1R agonists (Kanoski et al., 2011; Miettlicki-Baase et al., 2018; Secher et al., 2014; Sisley et al., 2014). Indeed, both liraglutide and Ex4 penetrate into the CNS and activate GLP-1R-expressing nuclei to induce hypophagia and body weight loss (Chambers et al., 2017; Kanoski et al., 2011; Miettlicki-Baase et al., 2018). In line with previous reports (Chan et al., 2013), systemic administration of native Ex4 produced a strong hypophagic response in the shrew, leading to body-weight loss in a dose-dependent fashion (Figures 2H–2I). This effect is due in part to the ability of native Ex4 to significantly increase the latency of the shrew to initiate feeding compared to vehicle injections (Figure S3). In contrast, Cbi-Ex4 did not significantly affect 24 h food intake or latency to eat, suggesting a lack of neural activation within the CNS (Figures 2J–2K).

Reduced caloric intake and body weight may be viewed as positive therapeutic outcomes in many T2DM patients prescribed existing GLP-1-based therapeutics (i.e., in those patients with accompanying obesity); however, there is a substantial number of T2DM patients that require glycemic control without weight loss. Indeed, in the Western world, 5%–15% of the patients diagnosed with T2DM have a body mass index (BMI) of 25 or lower (Centers for Disease Control and Prevention, 2004; George et al., 2015; Hartmann et al., 2017). The prevalence of T2DM in lean subjects seems to be even higher in some Asiatic countries and among American ethnic minorities (Coleman et al., 2014; Mohan et al., 1997). In addition, there are also diabetic patients suffering from life-threatening diseases or medical treatments including, but not limited to cystic fibrosis (Moheet and Moran, 2017), cancer (Gallo et al., 2018), HIV (Noubissi et al., 2018), chronic heart failure (Nasir and Aguilar, 2012), or COPD (Gläser et al., 2015). Indeed, the prevalence of T2DM in COPD patients is ~20% with an incidence for COPD of ~10% in the overall diabetic population (Caughey et al., 2010; Kerr et al., 2007; Mannino et al., 2008). Further, depending on the tumor type, between 8% and 18% of the cancer patients at the time of diagnosis also suffer from T2DM (Gallo et al., 2018; van de Poll-Franse et al., 2007), and 30%–40% of hospitalized heart-failure patients are diabetic (Echouffo-Tcheugui et al., 2016). This subgroup of T2DM patients is already at increased risk for cachexia, nausea/malaise, and unintended weight loss (von Haehling et al., 2016; von Haehling and Anker, 2014). In these T2DM patients, as well as overweight/obese T2DM patients that cannot effectively tolerate the nausea/emesis of existing GLP-1-based therapeutics, the data provided here support the hypothesis that the Cbi-Ex4 construct can improve glycemic control without producing anorexia and drug-treatment-induced malaise.

### Emetic Episodes Are Significantly Reduced Following Cbi-Ex4 Treatment Compared to Native Ex4, Indicative of Improved Tolerance

The most common side effects of all existing FDA-approved GLP-1R agonists are nausea, vomiting, and malaise, with approximately 20%–50% of T2DM patients that had been prescribed GLP-1-based medication, experiencing nausea and/or vomiting (Bergenstal et al., 2010; Buse et al., 2004; DeFronzo

et al., 2005; John et al., 2007; Kendall et al., 2005). These adverse events are surprisingly under-investigated, as they limit the widespread use, efficacy, and potential ubiquitous utility of existing GLP-1R agonists for treating metabolic disease. Notably, GLP-1-mediated malaise is not caused by GLP-1-mediated vagal afferent signaling, but is rather promoted by direct central GLP-1R activation (Kanoski et al., 2012), primarily in the brainstem. We therefore hypothesized that the conjugation of Cbi to Ex4 would modify CNS penetrance of Ex4, due to the B12-selective transport system involving TC binding (and the receptor CD320), a system that does not specifically support Cbi binding/transport in general (Miettlicki-Baase et al., 2018), and specifically not in the case of Cbi-Ex4 as measured herein (see Table S1 and Figure S1).

Ex4 dose-dependently induced emesis with the majority of the shrews experiencing emesis after 5- and 50-nmol/kg Ex4 dosing (Figure 3A). Indeed, 29% of the animals exhibited emesis upon administration of the lowest dose of native Ex4, 79% with the intermediate one, and 93% with the highest dose tested. All doses of native Ex4 triggered emesis within minutes after administration (1.25 nmol/kg Ex4:  $21 \pm 15$ ; 5 nmol/kg Ex4:  $10 \pm 5$  min; 50 nmol/kg:  $12 \pm 5$  min, Figure 3B). In contrast to the profound emesis observed after Ex4, both the prevalence and the number of emetic episodes following equimolar injections of Cbi-Ex4 were significantly reduced (5 nmol/kg Ex4 versus Cbi-Ex4:  $p = 0.005$ , 50 nmol/kg Ex4 versus Cbi-Ex4:  $p = 0.0003$ ; Figure 3C). Only one shrew experienced emesis after 1.25 nmol/kg Cbi-Ex4 (i.e., 7%), 28% after 5 nmol/kg Cbi-Ex4, and 64% after 50 nmol/kg Cbi-Ex4. In animals that displayed emesis after Cbi-Ex4 treatment, the latency was similar to native Ex4 (Figure 3D). However, the severity and occurrence of the emetic episodes was less severe, as represented by the heatmaps of Ex4 and Cbi-Ex4 depicting emetic intensity and latency for each individual animal across time (Figures 3E, 3F, and S4). These differences are particularly striking at the 5 nmol/kg dose of Cbi-Ex4, which shows a virtual absence of emetic events with the concurrence of strong glycemic effects (see also Figures S3 and S4). Thus, the conjugation of Ex4 to Cbi renders a GLP-1R agonist that, at pharmacological doses, retains glucoregulatory ability without CNS-mediated emesis.

Further support for this hypothesis is found by the near absence of c-Fos protein immunofluorescence (i.e., neuronal activation) in the DVC by Cbi-Ex4 compared to the robust c-Fos activation by native Ex4 (Figure 3G). The DVC is a set of brainstem nuclei (comprised of the nucleus tractus solitarius [NTS], area postrema [AP], and dorsal motor nucleus of the vagus) implicated in regulation of food intake and the processing of aversive stimuli and emetic events (Grill and Hayes, 2012; Hesketh, 2008; Horn, 2014; Miller and Leslie, 1994). Figures 3G and 3H show that systemic native Ex4 induces robust c-Fos expression in both the NTS and AP, whereas an equimolar dose of Cbi-Ex4 did not significantly induce greater c-Fos expression compared to vehicle injections.

### Despite Not Affecting Feeding Behavior, Albiglutide Triggers Profound Emesis

Finally, as an additional reference control, we performed a set of studies investigating the emetogenic, anorectic, and

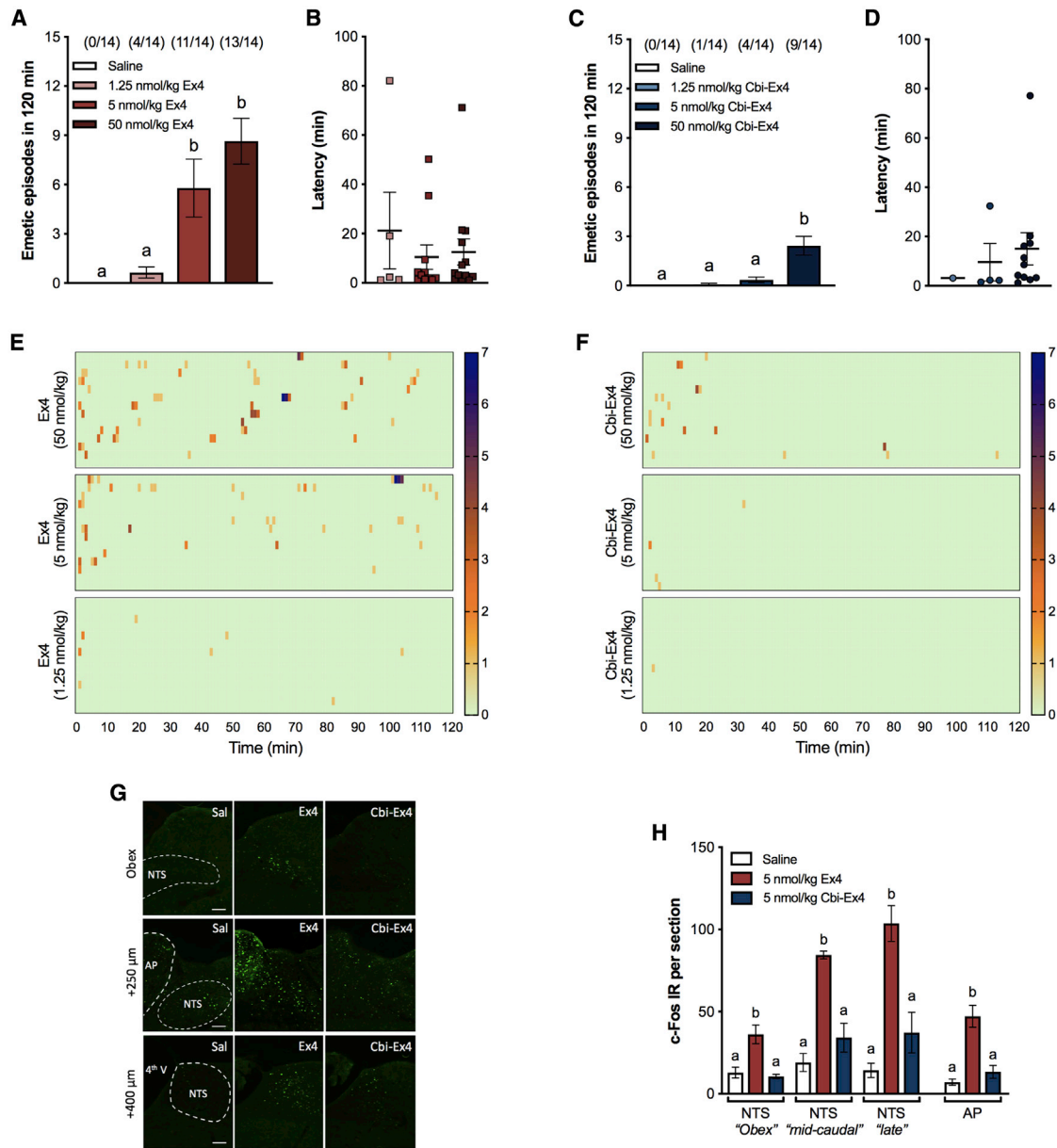


**Figure 3. Emetic Episodes Are Significantly Reduced Following Cbi-Ex4 Treatment Compared to Native Ex4, Indicative of Improved Tolerance**

(A) Ex4 (1.25, 5, and 50 nmol/kg) induced emesis during 120 min after injection in a dose-related fashion. The number of animals exhibiting emesis, expressed as a fraction of the total number of animal tested, is indicated above each treatment group.

(B) Latency to the first emetic episode of shrews that exhibited emesis after Ex4 treatment.

(C) Number of shrews experiencing emesis following Cbi-Ex4 (1.25, 5, and 50 nmol/kg) during 120 min after injection. The ratio of animals exhibiting emesis is indicated above each treatment group.

(D) Latency to the first emetic episode of shrews that experienced emesis after Cbi-Ex4 treatment.

(E and F) Heatmaps showing latency, number, and intensity of emesis following Ex4 and Cbi-Ex4 dosing for each individual animal across time.

(G) Representative immunofluorescent images showing c-Fos-positive across different NTS plane levels (0, 250, and 400 μm rostral to the obex) and in the medial part of the AP, 3 h after Ex4 (5 nmol/kg), Cbi-Ex4 (5 nmol/kg), or saline i.p. injection.

(H) Quantification of c-Fos positive neurons in the rostral, medial, and caudal NTS and medial AP. Peripheral Ex4 administration significantly increased the number of c-Fos immunoreactive cells in the AP/NTS of shrews 3 h after injection. The number of c-Fos positive cells in the AP/NTS was significantly lower in Cbi-Ex4-treated animals.

All data expressed as mean ± SEM. Means with different letters are significantly different ( $p < 0.05$ ). Data in (A) and (C) were analyzed with repeated-measurements one-way ANOVA followed by Tukey's *post hoc* test. Data in (H) with one-way ANOVA followed by Tukey's *post hoc* test. Scale bar, 100 μm (G).

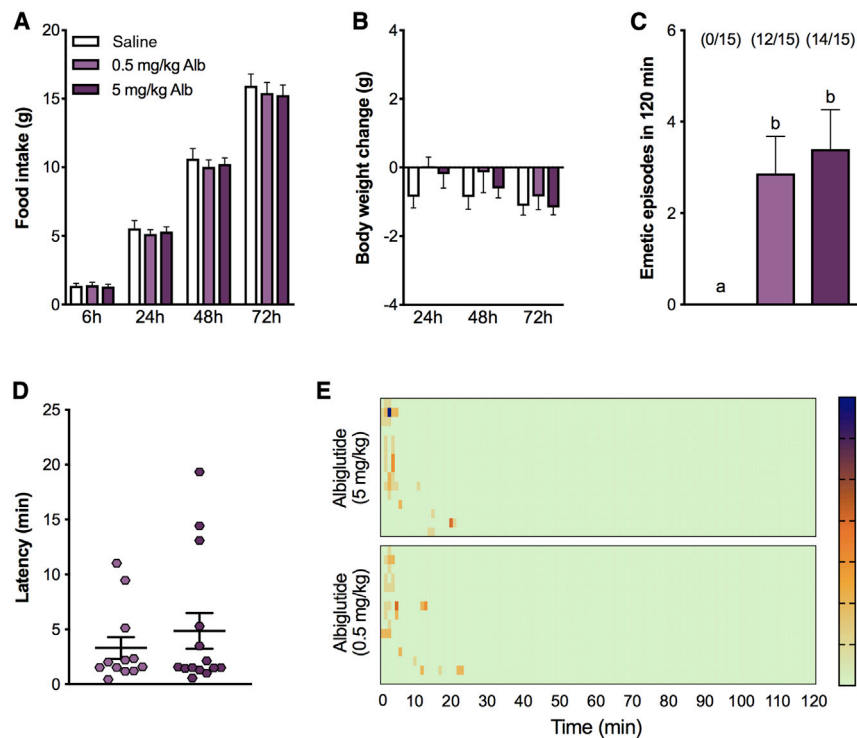


**Figure 4. Albiglutide Does Not Cause Anorexia or Body Weight Loss but It Induces Profound Emesis in the Shrew**

(A) Number of shrews experiencing emesis and the number of single emetic episodes following albiglutide (0.5 and 5 mg/kg) for 120 min after injection. (B) Latency to the first emetic episode of shrews that exhibited emesis after albiglutide treatment. (C) Heatmap showing latency, number, and intensity of emesis for each animal across time. (D) Food intake at 6, 24, 48, and 72 h post treatment. (E) Body-weight change at 24, 48, and 72 h after albiglutide or saline treatment. All data expressed as mean  $\pm$  SEM.

Data in (A) and (B) were analyzed with repeated-measurements one-way ANOVA followed by Tukey's *post hoc* test. Data in (C) and (D) were analyzed with repeated-measurements two-way ANOVA followed by Tukey's *post hoc* test.

body-weight-lowering properties of the long-acting GLP-1 analog albiglutide in our shrew model. This GLP-1-based “macromolecule,” consisting of a modified GLP-1 dimer fused to recombinant human albumin, was hypothesized to display minimal brain penetrance due to its size and provide an extended half-life of several days in humans (Rosenstock et al., 2009). Compared to short acting GLP-1 analogs (e.g., Ex4), albiglutide was reported to show reduced incidence of adverse effects (i.e., nausea and vomiting) and with attenuated body-weight-suppressing effects in humans, making it the hoped-for, pre-clinical gold standard for T2DM lean patients (Bettge et al., 2017; Dar et al., 2015; Leiter et al., 2016; Madsbad, 2016; Müller et al., 2019; Prasad-Reddy and Isaacs, 2015; Pratley et al., 2014; Rosenstock et al., 2009).

In line with the reduced anorectic effects of albiglutide previously observed in rodents and humans (Baggio et al., 2004; Pratley et al., 2014), and similarly to Cbi-Ex4, albiglutide at two doses (0.5 and 5 mg/kg) did not cause anorexia and body-weight loss (Figures 4A and 4B) in shrews. Our results demonstrate, however, that both doses of albiglutide induced profound emesis in the majority of shrews tested, albeit with a different temporal profile of emetic responses. The first emetic episode following albiglutide administration occurs within minutes after administration (Figures 4C–4E). This is in direct contrast to comparable doses of Cbi-Ex4 (5 and 0.5 mg/kg of albiglutide correspond to 68 and 6.8 nmol/kg, respectively). While c-Fos following albiglutide treatment was not evaluated in the current study, previous work in rodents demonstrates neuronal activation in nuclei expressing GLP-1Rs, including the AP/NTS following albiglutide systemic delivery (Baggio et al., 2004). Collectively, these data

and previous reports suggest that although the whole-brain penetrance may be reduced using a GLP-1R macromolecule agonist like albiglutide, there are still parts of the brain (e.g., AP/NTS) that provide an access point for albiglutide to drive significant adverse effects. Altogether, these results further strengthen the potential future clinical utility that Cbi-Ex4 could have on treating T2DM at doses that do not produce emesis.

### Limitations of Study

In summary, by exploiting a biosynthetic precursor of B12 found naturally in humans, but that is inert in the normal physiology of the vitamin, we generated a potent and metabolically stable GLP-1 receptor agonist via corination, with enhanced and prolonged peripheral glucoregulatory actions at doses that do not affect feeding and, astonishingly, is virtually devoid of emetic responses. Chronic animal studies as well as clinical trials are required to fully elucidate the long-term efficacy and tolerability of Cbi-Ex4. Given the high prevalence of obesity/overweight among T2DM patients, the lack of major effects on feeding and body weight could be considered a negative outcome of the corination technology. For these patients, “classic” GLP-1R analogs, if well tolerated, may be most favorable as weight loss contributes to improved overall health. Nevertheless, our data highlight the incredible potential of corination, exemplified herein with the development of Cbi-Ex4, as a treatment that would be most beneficial in treating lean T2DM patients, T2DM patients suffering from other comorbidities associated with an anorectic/cachectic state (cancer, COPD, and cystic fibrosis), and T2DM patients seeking glycemic control without emesis.

T2DM and cancer anorexia-cachexia syndrome show similarities in metabolic alterations (Chevalier and Farsijani, 2014; Porporato, 2016). Insulin resistance and reduced glucose tolerance in cancer patients are well-known phenomena. As early as the



1920s, glucose intolerance became a recognized metabolic alteration observed in cancer patients (Petruzzelli and Wagner, 2016). Data from tumor-bearing rodents, partially recapitulating the human clinical state, showed some beneficial effects of Ex4 treatment in attenuating muscle atrophy and in counteracting cancer-induced-insulin-signaling dysregulation (Honors and Kinzig, 2014). However, the CNS-mediated anorectic and emetic effects induced by native Ex4 represents a substantive limitation for possible applications in humans. Cbi-Ex4 could therefore represent an interesting and new GLP-1R-based approach for future investigations into the treatment of cancer-induced insulin resistance.

## STAR★METHODS

Detailed methods are provided in the online version of this paper and include the following:

- **KEY RESOURCES TABLE**
- **RESOURCE AVAILABILITY**
  - Lead Contact
  - Materials Availability
  - Data and Code Availability
- **EXPERIMENTAL MODEL AND SUBJECT DETAILS**
  - Cell lines
  - Animals and in vivo study designs
- **METHOD DETAILS**
  - Drugs
  - Cbi-alkyne synthesis and purification
  - Cbi-Ex4 synthesis and purification
  - Shrew serum total B12, total apo-TC and apo-HC binding capacities
  - HC and TC binding of Cbi-Ex4 and Ex4
  - In vitro GLP-1 binding assay
  - Jugular catheter surgery and pharmacokinetic profile of Ex4 and Cbi-Ex4 in shrews
  - Dose-response effects of Cbi-Ex4 and native Ex4 on glycemic control
  - Direct comparison of pharmacological doses of Cbi-Ex4 and Ex4 on glucoregulation during a standard and a delayed IPGTT
  - Dose-response effects of Ex4 and Cbi-Ex4 on energy balance
  - Direct comparison of pharmacological doses of Cbi-Ex4 and Ex4 on energy balance
  - Emetogenic properties of Ex4 and Cbi-Ex4
  - Direct comparison of pharmacological doses of Cbi-Ex4 and Ex4 on emesis
  - Assessment of neuronal activation in the DVC following Ex4, Cbi-Ex4 or saline treatments
  - Emetogenic properties of albiglutide
  - Effects of albiglutide on energy balance
- **QUANTIFICATION AND STATISTICAL ANALYSIS**

## SUPPLEMENTAL INFORMATION

Supplemental Information can be found online at <https://doi.org/10.1016/j.celrep.2020.107768>.

## ACKNOWLEDGMENTS

The authors gratefully acknowledge Prof. Charles C. Horn (University of Pittsburgh) for his assistance and for the supply of the shrews. This work was supported by the National Institutes of Health (grants NIH-DK-097675 to R.P.D., DK112812 to B.C.D.J., DK097675 to M.R.H., DK115762 to M.R.H., and DK069575 to G.G.H.); the Foundation for Polish Sciences (FNP TEAM POIR.04.04.00-00-4232/17-00 to D.G.); the Swiss National Science Foundation (grants SNF P2ZHP3-178114 and SNF P400PB-186728 to T.B.); and by Xeragenx, St. Louis, Missouri (to R.P.D.).

## AUTHOR CONTRIBUTIONS

R.P.D. invented the Cbi-Ex4 technology; T.B., J.L.W., B.C.D.J., M.R.H., and R.P.D. developed the study rationale and experimental designs; T.B., R.P.D., and M.R.H. drafted the manuscript, which was commented on and edited by all authors; T.B. designed and performed most of the *in vivo* experiments with T.B., B.C.D.J., and M.R.H. analyzing the *in vivo* data; J.L.W., I.C.T., and R.P.D. generated the constructs and analyzed the structural data; J.L.W., O.G.C., and I.C.T. performed the *in vitro* experiments with J.L.W., I.C.T., G.G.H., and R.P.D. analyzing the *in vitro* data; E.N. performed the binding studies on TC and HC; S.M.F., L.M.S., A.J.W., D.G., E.N., E.D.S., A.B., and V.A.R.D.S. performed experiments and/or assisted with data analysis; all authors approved the final version of the manuscript.

## DECLARATION OF INTERESTS

R.P.D. is a scientific advisory board member and received funds from Balchem Corporation, New Hampton, New York, which were not used in support of these studies. R.P.B. is the named author of a patent pursuant to this work that is owned by Syracuse University. M.R.H. and B.C.D.J. receive funding from Zealand Pharma that was not used in support of these studies. B.C.D.J. receives funding from Pfizer that was not used in support of these studies. M.R.H. receives funding from Novo Nordisk, Eli Lilly & Co. and Boehringer Ingelheim that was not used in support of these studies. All authors declare no other competing financial interests or conflicts of interest.

Received: February 20, 2019

Revised: May 10, 2019

Accepted: May 22, 2020

Published: June 16, 2020

## REFERENCES

- Ahrén, B., Atkin, S.L., Charpentier, G., Warren, M.L., Wilding, J.P.H., Birch, S., Holst, A.G., and Leiter, L.A. (2018). Semaglutide induces weight loss in subjects with type 2 diabetes regardless of baseline BMI or gastrointestinal adverse events in the SUSTAIN 1 to 5 trials. *Diabetes Obes. Metab.* **20**, 2210–2219.
- Alhadeff, A.L., Holland, R.A., Nelson, A., Grill, H.J., and De Jonghe, B.C. (2015). Glutamate receptors in the central nucleus of the amygdala mediate cisplatin-induced malaise and energy balance dysregulation through direct hindbrain projections. *J. Neurosci.* **35**, 11094–11104.
- Alhadeff, A.L., Mergler, B.D., Zimmer, D.J., Turner, C.A., Reiner, D.J., Schmidt, H.D., Grill, H.J., and Hayes, M.R. (2016). Endogenous glucagon-like peptide-1 receptor signaling in the nucleus tractus solitarius is required for food intake control. *Neuropsychopharmacology* **42**, 1471–1479.
- Baggio, L.L., Huang, Q., Brown, T.J., and Drucker, D.J. (2004). A recombinant human glucagon-like peptide (GLP)-1-albumin protein (albugon) mimics peptidergic activation of GLP-1 receptor-dependent pathways coupled with satiety, gastrointestinal motility, and glucose homeostasis. *Diabetes* **53**, 2492–2500.
- Bergental, R.M., Wysham, C., Macconell, L., Malloy, J., Walsh, B., Yan, P., Wilhelm, K., Malone, J., and Porter, L.E.; DURATION-2 Study Group (2010). Efficacy and safety of exenatide once weekly versus sitagliptin or pioglitazone as

- an adjunct to metformin for treatment of type 2 diabetes (DURATION-2): a randomised trial. *Lancet* 376, 431–439.
- Bettge, K., Kahle, M., Abd El Aziz, M.S., Meier, J.J., and Nauck, M.A. (2017). Occurrence of nausea, vomiting and diarrhoea reported as adverse events in clinical trials studying glucagon-like peptide-1 receptor agonists: A systematic analysis of published clinical trials. *Diabetes Obes. Metab.* 19, 336–347.
- Bonaccorso, R.L., Chepurny, O.G., Becker-Pauly, C., Holz, G.G., and Doyle, R.P. (2015). Enhanced peptide stability against protease digestion induced by intrinsic factor binding of a vitamin B12 conjugate of exendin-4. *Mol. Pharm.* 12, 3502–3506.
- Buse, J.B., Henry, R.R., Han, J., Kim, D.D., Fineman, M.S., and Baron, A.D.; Exenatide-113 Clinical Study Group (2004). Effects of exenatide (exendin-4) on glycemic control over 30 weeks in sulfonylurea-treated patients with type 2 diabetes. *Diabetes Care* 27, 2628–2635.
- Caughey, G.E., Roughead, E.E., Vitry, A.I., McDermott, R.A., Shakib, S., and Gilbert, A.L. (2010). Comorbidity in the elderly with diabetes: identification of areas of potential treatment conflicts. *Diabetes Res. Clin. Pract.* 87, 385–393.
- Centers for Disease Control and Prevention (CDC) (2004). Prevalence of overweight and obesity among adults with diagnosed diabetes—United States, 1988–1994 and 1999–2002. *MMWR Morb. Mortal. Wkly. Rep.* 53, 1066–1068.
- Chambers, A.P., Sorrell, J.E., Haller, A., Roelofs, K., Hutch, C.R., Kim, K.S., Gutierrez-Aguilar, R., Li, B., Drucker, D.J., D'Alessio, D.A., et al. (2017). The role of pancreatic proglucagon in glucose homeostasis in mice. *Cell Metab* 25, 927–934 e923.
- Chan, S.W., Lin, G., Yew, D.T., and Rudd, J.A. (2011). A physiological role of glucagon-like peptide-1 receptors in the central nervous system of *Suncus murinus* (house musk shrew). *Eur. J. Pharmacol.* 668, 340–346.
- Chan, S.W., Lin, G., Yew, D.T., Yeung, C.K., and Rudd, J.A. (2013). Separation of emetic and anorexic responses of exendin-4, a GLP-1 receptor agonist in *Suncus murinus* (house musk shrew). *Neuropharmacology* 70, 141–147.
- Chepurny, O.G., Bonaccorso, R.L., Leech, C.A., Wöllert, T., Langford, G.M., Schwede, F., Roth, C.L., Doyle, R.P., and Holz, G.G. (2018). Chimeric peptide EP45 as a dual agonist at GLP-1 and NPY2R receptors. *Sci. Rep.* 8, 3749.
- Chepurny, O.G., Matsoukas, M.T., Liapakis, G., Leech, C.A., Milliken, B.T., Doyle, R.P., and Holz, G.G. (2019). Nonconventional glucagon and GLP-1 receptor agonist and antagonist interplay at the GLP-1 receptor revealed in high-throughput FRET assays for cAMP. *J. Biol. Chem.* 294, 3514–3531.
- Chevalier, S., and Farsijani, S. (2014). Cancer cachexia and diabetes: similarities in metabolic alterations and possible treatment. *Appl. Physiol. Nutr. Metab.* 39, 643–653.
- Clardy-James, S., Chepurny, O.G., Leech, C.A., Holz, G.G., and Doyle, R.P. (2013). Synthesis, Characterization and Pharmacodynamics of Vitamin-B12-Conjugated Glucagon-Like Peptide-1. *ChemMedChem* 4, 582–586.
- Coleman, N.J., Miernik, J., Philipson, L., and Fogelfeld, L. (2014). Lean versus obese diabetes mellitus patients in the United States minority population. *J. Diabetes Complications* 28, 500–505.
- Copley, K., McCowen, K., Hiles, R., Nielsen, L.L., Young, A., and Parkes, D.G. (2006). Investigation of exenatide elimination and its in vivo and in vitro degradation. *Curr. Drug Metab.* 7, 367–374.
- Dar, S., Tahrani, A.A., and Piya, M.K. (2015). The role of GLP-1 receptor agonists as weight loss agents in patients with and without type 2 diabetes. *Pract. Diabetes* 32, 295–300.
- De Jonghe, B.C., and Horn, C.C. (2009). Chemotherapy agent cisplatin induces 48-h Fos expression in the brain of a vomiting species, the house musk shrew (*Suncus murinus*). *Am. J. Physiol. Regul. Integr. Comp. Physiol.* 296, R902–R911.
- DeFronzo, R.A., Ratner, R.E., Han, J., Kim, D.D., Fineman, M.S., and Baron, A.D. (2005). Effects of exenatide (exendin-4) on glycemic control and weight over 30 weeks in metformin-treated patients with type 2 diabetes. *Diabetes Care* 28, 1092–1100.
- Drucker, D.J. (2006). The biology of incretin hormones. *Cell Metab.* 3, 153–165.
- Drucker, D.J., Sherman, S.I., Bergenstal, R.M., and Buse, J.B. (2011). The safety of incretin-based therapies—review of the scientific evidence. *J. Clin. Endocrinol. Metab.* 96, 2027–2031.
- Echouffo-Tcheugui, J.B., Xu, H., DeVore, A.D., Schulte, P.J., Butler, J., Yancy, C.W., Bhatt, D.L., Hernandez, A.F., Heidenreich, P.A., and Fonarow, G.C. (2016). Temporal trends and factors associated with diabetes mellitus among patients hospitalized with heart failure: Findings from Get With The Guidelines-Heart Failure registry. *Am. Heart J.* 182, 9–20.
- Furger, E., Fedosov, S.N., Lidballe, D.L., Waibel, R., Schibli, R., Nexø, E., and Fischer, E. (2012). Comparison of recombinant human haptocorrin expressed in human embryonic kidney cells and native haptocorrin. *PLoS ONE* 7, e37421.
- Gallo, M., Muscogiuri, G., Felicetti, F., Faggiano, A., Trimarchi, F., Arvat, E., Vigneri, R., and Colao, A. (2018). Adverse glycaemic effects of cancer therapy: indications for a rational approach to cancer patients with diabetes. *Metabolism* 78, 141–154.
- George, A.M., Jacob, A.G., and Fogelfeld, L. (2015). Lean diabetes mellitus: an emerging entity in the era of obesity. *World J. Diabetes* 6, 613–620.
- Gimsing, P., and Nexø, E. (1989). Cobalamin-binding capacity of haptocorrin and transcobalamin: age-correlated reference intervals and values from patients. *Clin. Chem.* 35, 1447–1451.
- Gläser, S., Krüger, S., Merkel, M., Bramlage, P., and Herth, F.J. (2015). Chronic obstructive pulmonary disease and diabetes mellitus: a systematic review of the literature. *Respiration* 89, 253–264.
- Green, R., Allen, L.H., Björke-Monsen, A.L., Brito, A., Guéant, J.L., Miller, J.W., Molloy, A.M., Nexø, E., Stabler, S., Toh, B.H., et al. (2017). Vitamin B<sub>12</sub> deficiency. *Nat. Rev. Dis. Primers* 3, 17040.
- Grill, H.J., and Hayes, M.R. (2012). Hindbrain neurons as an essential hub in the neuroanatomically distributed control of energy balance. *Cell Metab.* 16, 296–309.
- Hansen, M., Brynskov, J., Christensen, P.A., Krintel, J.J., and Gimsing, P. (1985). Cobalamin binding proteins (haptocorrin and transcobalamin) in human cerebrospinal fluid. *Scand. J. Haematol.* 34, 209–212.
- Hardlei, T.F., and Nexø, E. (2009). A new principle for measurement of cobalamin and corrinoids, used for studies of cobalamin analogs on serum haptocorrin. *Clin. Chem.* 55, 1002–1010.
- Hartmann, B., Lanzinger, S., Bramlage, P., Groß, F., Danne, T., Wagner, S., Krakow, D., Zimmermann, A., Malcharzik, C., and Holl, R.W. (2017). Lean diabetes in middle-aged adults: a joint analysis of the German DIVE and DPV registries. *PLoS ONE* 12, e0183235.
- Hayes, M.R., and Schmidt, H.D. (2016). GLP-1 influences food and drug reward. *Curr. Opin. Behav. Sci.* 9, 66–70.
- Hayes, M.R., De Jonghe, B.C., and Kanoski, S.E. (2010). Role of the glucagon-like-peptide-1 receptor in the control of energy balance. *Physiol. Behav.* 100, 503–510.
- Hayes, M.R., Lechner, T.M., Zhao, S., Lee, G.S., Chowansky, A., Zimmer, D., De Jonghe, B.C., Kanoski, S.E., Grill, H.J., and Bence, K.K. (2011). Intracellular signals mediating the food intake-suppressive effects of hindbrain glucagon-like peptide-1 receptor activation. *Cell Metab.* 13, 320–330.
- Hayes, M.R., Miettlicki-Baase, E.G., Kanoski, S.E., and De Jonghe, B.C. (2014). Incretins and amylin: neuroendocrine communication between the gut, pancreas, and brain in control of food intake and blood glucose. *Annu. Rev. Nutr.* 34, 237–260.
- Herbert, V., and Herzlich, B. (1983). Quantitation of intrinsic factor. *Blood* 61, 819.
- Hesketh, P.J. (2008). Chemotherapy-induced nausea and vomiting. *N. Engl. J. Med.* 358, 2482–2494.
- Holst, J.J. (2007). The physiology of glucagon-like peptide 1. *Physiol. Rev.* 87, 1409–1439.
- Honors, M.A., and Kinzig, K.P. (2014). Chronic exendin-4 treatment prevents the development of cancer cachexia symptoms in male rats bearing the Yoshida sarcoma. *Horm. Cancer* 5, 33–41.

- Horn, C.C. (2014). Measuring the nausea-to-emesis continuum in non-human animals: refocusing on gastrointestinal vagal signaling. *Exp. Brain Res.* *232*, 2471–2481.
- Horn, C.C., Kimball, B.A., Wang, H., Kaus, J., Diemel, S., Nagy, A., Gathright, G.R., Yates, B.J., and Andrews, P.L. (2013). Why can't rodents vomit? A comparative behavioral, anatomical, and physiological study. *PLoS ONE* *8*, e60537.
- Hygum, K., Lildballe, D.L., Greibe, E.H., Morkbak, A.L., Poulsen, S.S., Sorensen, B.S., Petersen, T.E., and Nexø, E. (2011). Mouse transcobalamin has features resembling both human transcobalamin and haptocorrin. *PLoS ONE* *6*, e20638.
- John, L.E., Kane, M.P., Busch, R.S., and Hamilton, R.A. (2007). Expanded use of exenatide in the management of type 2 diabetes. *Diabetes Spectr.* *20*, 59–63.
- Kanazawa, S., and Herbert, V. (1983). Noncobalamin vitamin B12 analogues in human red cells, liver, and brain. *Am. J. Clin. Nutr.* *37*, 774–777.
- Kanoski, S.E., Fortin, S.M., Arnold, M., Grill, H.J., and Hayes, M.R. (2011). Peripheral and central GLP-1 receptor populations mediate the anorectic effects of peripherally administered GLP-1 receptor agonists, liraglutide and exendin-4. *Endocrinology* *152*, 3103–3112.
- Kanoski, S.E., Rupprecht, L.E., Fortin, S.M., De Jonghe, B.C., and Hayes, M.R. (2012). The role of nausea in food intake and body weight suppression by peripheral GLP-1 receptor agonists, exendin-4 and liraglutide. *Neuropharmacology* *62*, 1916–1927.
- Kanoski, S.E., Hayes, M.R., and Skibicka, K.P. (2016). GLP-1 and weight loss: unraveling the diverse neural circuitry. *Am. J. Physiol. Regul. Integr. Comp. Physiol.* *310*, R885–R895.
- Kendall, D.M., Riddle, M.C., Rosenstock, J., Zhuang, D., Kim, D.D., Fineman, M.S., and Baron, A.D. (2005). Effects of exenatide (exendin-4) on glycemic control over 30 weeks in patients with type 2 diabetes treated with metformin and a sulfonylurea. *Diabetes Care* *28*, 1083–1091.
- Kerr, E.A., Heisler, M., Krein, S.L., Kabeto, M., Langa, K.M., Weir, D., and Pilette, J.D. (2007). Beyond comorbidity counts: how do comorbidity type and severity influence diabetes patients' treatment priorities and self-management? *J. Gen. Intern. Med.* *22*, 1635–1640.
- Klarenbeek, J., Goedhart, J., van Batenburg, A., Groenewald, D., and Jalink, K. (2015). Fourth-generation epac-based FRET sensors for cAMP feature exceptional brightness, photostability and dynamic range: characterization of dedicated sensors for FLIM, for ratiometry and with high affinity. *PLoS ONE* *10*, e0122513.
- Kuda-Wedagedara, A.N.W., Workinger, J.L., Nexø, E., Doyle, R.P., and Viola-Villegas, N. (2017). <sup>89</sup>Zr-cobalamin PET tracer: synthesis, cellular uptake, and use for tumor imaging. *ACS Omega* *2*, 6314–6320.
- Lamont, B.J., Li, Y., Kwan, E., Brown, T.J., Gaisano, H., and Drucker, D.J. (2012). Pancreatic GLP-1 receptor activation is sufficient for incretin control of glucose metabolism in mice. *J. Clin. Invest.* *122*, 388–402.
- Leiter, L.A., Mallory, J.M., Wilson, T.H., and Reinhardt, R.R. (2016). Gastrointestinal safety across the albiglutide development programme. *Diabetes Obes. Metab.* *18*, 930–935.
- Madsbad, S. (2016). Review of head-to-head comparisons of glucagon-like peptide-1 receptor agonists. *Diabetes Obes. Metab.* *18*, 317–332.
- Mannino, D.M., Thorn, D., Swensen, A., and Holguin, F. (2008). Prevalence and outcomes of diabetes, hypertension and cardiovascular disease in COPD. *Eur. Respir. J.* *32*, 962–969.
- Mietlicki-Baase, E.G., Ortinski, P.I., Rupprecht, L.E., Olivos, D.R., Alhadeff, A.L., Pierce, R.C., and Hayes, M.R. (2013). The food intake-suppressive effects of glucagon-like peptide-1 receptor signaling in the ventral tegmental area are mediated by AMPA/kainate receptors. *Am. J. Physiol. Endocrinol. Metab.* *305*, E1367–E1374.
- Mietlicki-Baase, E.G., Liberini, C.G., Workinger, J.L., Bonaccorso, R.L., Borner, T., Reiner, D.J., Koch-Laskowski, K., McGrath, L.E., Lhamo, R., Stein, L.M., et al. (2018). A vitamin B12 conjugate of exendin-4 improves glucose tolerance without associated nausea or hypophagia in rodents. *Diabetes Obes. Metab.* *20*, 1223–1234.
- Miller, A.D., and Leslie, R.A. (1994). The area postrema and vomiting. *Front. Neuroendocrinol.* *15*, 301–320.
- Mohan, V., Vijayaprabha, R., Rema, M., Premalatha, G., Poongothai, S., Deepa, R., Bhatia, E., Mackay, I.R., and Zimmet, P. (1997). Clinical profile of lean NIDDM in South India. *Diabetes Res. Clin. Pract.* *38*, 101–108.
- Moheet, A., and Moran, A. (2017). CF-related diabetes: containing the metabolic miscreant of cystic fibrosis. *Pediatr. Pulmonol.* *52* (S48), S37–S43.
- Müller, T.D., Finan, B., Bloom, S.R., D'Alessio, D., Drucker, D.J., Flatt, P.R., Fritsche, A., Gribble, F., Grill, H.J., Habener, J.F., et al. (2019). Glucagon-like peptide 1 (GLP-1). *Mol. Metab.* *30*, 72–130.
- Nasir, S., and Aguilar, D. (2012). Congestive heart failure and diabetes mellitus: balancing glycemic control with heart failure improvement. *Am. J. Cardiol.* *110*, 50B–57B.
- Noubissi, E.C., Katte, J.C., and Sobngwi, E. (2018). Diabetes and HIV. *Curr. Diab. Rep.* *18*, 125.
- Petruzzelli, M., and Wagner, E.F. (2016). Mechanisms of metabolic dysfunction in cancer-associated cachexia. *Genes Dev.* *30*, 489–501.
- Porporato, P.E. (2016). Understanding cachexia as a cancer metabolism syndrome. *Oncogenesis* *5*, e200.
- Prasad-Reddy, L., and Isaacs, D. (2015). A clinical review of GLP-1 receptor agonists: efficacy and safety in diabetes and beyond. *Drugs Context* *4*, 212283.
- Pratley, R.E., Nauck, M.A., Barnett, A.H., Feinglos, M.N., Ovalle, F., Harman-Boehm, I., Ye, J., Scott, R., Johnson, S., Stewart, M., and Rosenstock, J.; HARMONY 7 study group (2014). Once-weekly albiglutide versus once-daily liraglutide in patients with type 2 diabetes inadequately controlled on oral drugs (HARMONY 7): a randomised, open-label, multicentre, non-inferiority phase 3 study. *Lancet Diabetes Endocrinol.* *2*, 289–297.
- Pratley, R.E., Aroda, V.R., Lingvay, I., Lüdemann, J., Andreassen, C., Navarria, A., and Viljoen, A.; SUSTAIN 7 Investigators (2018). Semaglutide versus dulaglutide once weekly in patients with type 2 diabetes (SUSTAIN 7): a randomised, open-label, phase 3b trial. *Lancet Diabetes Endocrinol.* *6*, 275–286.
- Rosenblatt, D.S., Fenton, W.A., Scriver, C.R., Beaudet, A.L., Valle, D., and Sly, W.S. (2001). *Inherited Disorders of Folate and Cobalamin Transport and Metabolism* (McGraw-Hill).
- Rosenstock, J., Reusch, J., Bush, M., Yang, F., and Stewart, M.; Albiglutide Study Group (2009). Potential of albiglutide, a long-acting GLP-1 receptor agonist, in type 2 diabetes: a randomized controlled trial exploring weekly, biweekly, and monthly dosing. *Diabetes Care* *32*, 1880–1886.
- Równicki, M., Wojciechowska, M., Wierzbza, A.J., Czarniecki, J., Bartosik, D., and Gryko, D. (2017). Vitamin B12 as a carrier of peptide nucleic acid (PNA) into bacterial cells. *Sci. Rep.* *7*, 7644.
- Sadry, S.A., and Drucker, D.J. (2013). Emerging combinatorial hormone therapies for the treatment of obesity and T2DM. *Nat. Rev. Endocrinol.* *9*, 425–433.
- Secher, A., Jelsing, J., Baquero, A.F., Hecksher-Sørensen, J., Cowley, M.A., Dalbøge, L.S., Hansen, G., Grove, K.L., Pyke, C., Raun, K., et al. (2014). The arcuate nucleus mediates GLP-1 receptor agonist liraglutide-dependent weight loss. *J. Clin. Invest.* *124*, 4473–4488.
- Sikirica, M.V., Martin, A.A., Wood, R., Leith, A., Piercy, J., and Higgins, V. (2017). Reasons for discontinuation of GLP1 receptor agonists: data from a real-world cross-sectional survey of physicians and their patients with type 2 diabetes. *Diabetes Metab. Syndr. Obes.* *10*, 403–412.
- Simonsen, L., Holst, J.J., and Deacon, C.F. (2006). Exendin-4, but not glucagon-like peptide-1, is cleared exclusively by glomerular filtration in anaesthetised pigs. *Diabetologia* *49*, 706–712.
- Sisley, S., Gutierrez-Aguilar, R., Scott, M., D'Alessio, D.A., Sandoval, D.A., and Seeley, R.J. (2014). Neuronal GLP1R mediates liraglutide's anorectic but not glucose-lowering effect. *J. Clin. Invest.* *124*, 2456–2463.
- Smith, E.P., An, Z., Wagner, C., Lewis, A.G., Cohen, E.B., Li, B., Mahbod, P., Sandoval, D., Perez-Tilve, D., Tamarina, N., et al. (2014). The role of  $\beta$  cell

glucagon-like peptide-1 signaling in glucose regulation and response to diabetes drugs. *Cell Metab.* **19**, 1050–1057.

Stupperich, E., and Nexø, E. (1991). Effect of the cobalt-N coordination on the cobamide recognition by the human vitamin B12 binding proteins intrinsic factor, transcobalamin and haptocorrin. *Eur. J. Biochem.* **199**, 299–303.

Ueno, S., Matsuki, N., and Saito, H. (1987). *Suncus murinus*: a new experimental model in emesis research. *Life Sci.* **41**, 513–518.

van de Poll-Franse, L.V., Houterman, S., Janssen-Heijnen, M.L., Dercksen, M.W., Coebergh, J.W., and Haak, H.R. (2007). Less aggressive treatment and worse overall survival in cancer patients with diabetes: a large population based analysis. *Int. J. Cancer* **120**, 1986–1992.

von Haehling, S., and Anker, S.D. (2014). Prevalence, incidence and clinical impact of cachexia: facts and numbers—update 2014. *J. Cachexia Sarcopenia Muscle* **5**, 261–263.

von Haehling, S., Anker, M.S., and Anker, S.D. (2016). Prevalence and clinical impact of cachexia in chronic illness in Europe, USA, and Japan: facts and numbers update 2016. *J. Cachexia Sarcopenia Muscle* **7**, 507–509.

Wierzba, A.J., Hassan, S., and Gryko, D. (2019). Synthetic Approaches toward Vitamin B12 Conjugates. *Asian Journal of Chemistry* **8**, 6–24.

Wysham, C., Blevins, T., Arakaki, R., Colon, G., Garcia, P., Atisso, C., Kuhstoss, D., and Lakshmanan, M. (2014). Efficacy and safety of dulaglutide added onto pioglitazone and metformin versus exenatide in type 2 diabetes in a randomized controlled trial (AWARD-1). *Diabetes Care* **37**, 2159–2167.



STAR★METHODS

KEY RESOURCES TABLE

REAGENT or RESOURCE	SOURCE	IDENTIFIER
<b>Antibodies</b>		
Alexa fluor 488 Donkey Anti-Rabbit 1gG (H+L)	Jackson Immuno Research	CAT# 711-545-152; RRID:AB_2313584
c-Fos 9F6 Rabbit mAb	Cell Signaling	CAT# s22505; RRID:AB_2247211
<b>Bacterial and Virus Strains</b>		
H188 adenovirus	Lab of Prof. Jeess Kalink, Division of Cell Biology, the Netherlands Cancer Institute, Amsterdam, the Netherlands.	N/A
<b>Biological Samples</b>		
Shrew brain	In house (University of Pennsylvania)	N/A
Shrew blood	In house (University of Pennsylvania)	N/A
<b>Chemicals, Peptides, and Recombinant Proteins</b>		
Exendin-4	Bachem	CAT # H-8730
Cbi-Exendin-4	This paper	N/A
Albiglutide	AdooQ Bioscience	CAT# A16823
aCSF	Harvard Apparatus	CAT# 59-7316
Vitamin B <sub>12</sub>	Sigma-Aldrich	CAT# V2876
Dicyanocobinamide	Sigma-Aldrich	CAT#C3021
1,1'-Carbonyl-di-(1,2,4-triazole)	Sigma-Aldrich	CAT# 21861
1-Amino-3-butyne	Sigma-Aldrich	CAT# 715190
Fetal Bovine Serum	Sigma-Aldrich	CAT# 12303C
Dulbecco's Modified Eagle Medium	Sigma-Aldrich	CAT# D6429
Penicillin-Streptomycin	ThermoFisher Scientific	CAT# 15140122
G-418 Disulfate Salt Solution	Sigma-Aldrich	CAT# G8168
Bovine Serum Albumin	Sigma-Aldrich	CAT# A7030
Sodium Chloride	Fisher Scientific	CAT# BP358-1
Potassium Chloride	Fisher Scientific	CAT# BP366
Magnesium Chloride Hexahydrate	Fisher Scientific	CAT# BP214
Calcium Chloride Dihydrate	Fisher Scientific	CAT# BP510
HEPES	Sigma-Aldrich	CAT# H0887
Trypsin-EDTA	ThermoFisher Scientific	CAT# 25200072
Activated Charcoal	Sigma-Aldrich	CAT#C5197
Bovine hemoglobin	Sigma Aldrich	CAT#H2500
<sup>57</sup> Co-B12	KemEnTec	N/A
0.1% Human albumin	Sigma Aldrich	CAT#A9731
<sup>22</sup> Na	GE Healthcare Europe	N/A
<b>Critical Commercial Assays</b>		
Ex4 ELISA kit	Phoenix Pharmaceuticals	EK-070-94
<b>Experimental Models: Cell Lines</b>		
HEK293 Stably Transfected with hGLP1-R	Generated in-house, SUNY, Upstate Medical University	N/A
<b>Experimental Models: Organisms/Strains</b>		
Adult male shrews ( <i>Suncus murinus</i> )	UPMC Hillman Cancer Center	N/A
<b>Software and Algorithms</b>		
GraphPad PRISM	GraphPad Software	RRID: SCR_000306
Illustrator (CS6)	Above	RRID: SCR_010279

(Continued on next page)

**Continued**

REAGENT or RESOURCE	SOURCE	IDENTIFIER
Other		
Feline diet	PMI Lab Diets	CAT# 5003
Ferret diet	PMI Lab Diets	CAT# 5L14
Silicone tubing	SAI Infusion Technologies	CAT# Sku SIL-3-25
Glucose test strips OneTouch Ultra Blue	CVS	NA

**RESOURCE AVAILABILITY**

**Lead Contact**

Further information and requests for resources and reagents should be directed to and will be fulfilled by the Lead Contact, Robert P. Doyle ([rpdoyle@syr.edu](mailto:rpdoyle@syr.edu)).

**Materials Availability**

This study generated new unique reagents. RP Doyle is the named author of a patent pursuant to this work that is owned by Syracuse University and will supply the reagent under MTA upon request.

**Data and Code Availability**

The published article includes all data generated or analyzed during this study. No code was used or generated in this study

**EXPERIMENTAL MODEL AND SUBJECT DETAILS**

**Cell lines**

HEK293 cells stably expressing the human GLP-1R at a density of 150,000 receptors/cell were obtained from Novo Nordisk A/S (Bagsvaerd, Denmark) by GGH. HEK293 cells stably expressing H188 were generated by O.G. Chepurny in the Holz laboratory (Chepurny et al., 2018). All cell cultures were maintained in Dulbecco's Modified Eagles Medium (DMEM) containing 25 mM glucose and supplemented with 10% fetal bovine serum (FBS) and 1% penicillin-streptomycin. Cell cultures equilibrated at 37 C in a humidified incubator with 5% CO<sub>2</sub> were passaged twice a week.

**Animals and in vivo study designs**

Adult male shrews (*Suncus murinus*) weighing ~50-80 g (n = 156 total), were obtained from Dr. Charles Horn, University of Pittsburgh. These animals were offspring from a colony maintained at the University of Pittsburgh Cancer Institute (a Taiwanese strain derived from stock supplied by the Chinese University of Hong Kong).

Animals were single housed in plastic cages (37.3 × 23.4 × 14 cm, Innovive) under a 12-hour:12-hour light/dark cycle in a temperature- and humidity- controlled environment. Animal were fed *ad libitum* with a mixture of feline (75%, Laboratory Feline Diet 5003, Lab Diet) and mink food (25%, High Density Ferret Diet 5L14, Lab Diet) and had *ad libitum* access to tap water except where noted.

Shrews were habituated to single housing in their home cage and IP injections at least 1 wk prior to experimentation. All animals were naive to any experimental drug and test prior to the beginning of the experiment. All experimental injections were separated by at least 72h. For most *in vivo* experiments, injections were administered using a within-subjects, Latin square design. The exceptions were the pharmacokinetic and the immunohistochemical studies, which were conducted in a between-subjects design. All procedures were approved by the Institutional Care and Use Committee of the University of Pennsylvania.

**METHOD DETAILS**

**Drugs**

CN<sub>2</sub>Cbi was purchased from Sigma-Aldrich. K12-azido modified Ex4 was produced by NeoScientific (Cambridge, USA). Cbi-conjugated exendin-4 (Cbi-Ex4) was synthesized, characterized and screened as described below. For all *in vivo* studies Cbi-Ex4, Ex4 (Bachem), and albiglutide (AdooQ Bioscience, Cat. No. A16823) were dissolved in 0.9% saline. In all studies, except in the pharmacokinetic study, Ex4 (1.25, 5 and 50 nmol/kg; i.e., ~5, 20 and 200 μg/kg; respectively), Cbi-Ex4 (equimolar dose to Ex4), and albiglutide (0.5 and 5 mg/kg) were administered intraperitoneally (IP). For the pharmacokinetic study, Ex4 (25 and 50 nmol/kg) and Cbi-Ex4 (equimolar doses to Ex4) were infused intravenously (IV) (see details below).

### Cbi-alkyne synthesis and purification

(CN)<sub>2</sub>Cbi (0.077 mmol; 80 mg; 1 equiv.) and CDT (1,1'-carbonyl-di-(1,2,4-triazole); 1.535 mmol; 252 mg, 20 equiv.) were dissolved in dry N-Methyl-2-pyrrolidone (NMP, 2.5 mL) at 40°C under an argon atmosphere. The resulting solution was stirred for 30 min at 40°C (full conversion of Cbi to Cbi-CDT adduct was achieved over this time (as established by RP-HPLC). Subsequently, the aminoalkyne (NH<sub>2</sub>-C2-alkyne, 126 μL, 20 equiv.) and triethylamine (TEA, 20 μL) were added under an argon atmosphere. The resulting solution was stirred at 40°C for 1h. After this time the conversion (monitored by RP-HPLC) was not complete, thus another portion of the aminoalkyne (126 μL, 20 equiv.) and TEA (20 μL) were added and the mixture was stirred for an additional hour at 40°C. The reaction mixture was subsequently poured into ethyl acetate (50 mL), and centrifuged (the residue being transferred with a minimal amount of MeOH into ethyl acetate). After complete precipitation, the solid was dissolved in 2 mL of MeOH and precipitated with diethyl ether (50 mL). The crude solid was dissolved in water and purified via preparative HPLC (see supplementary details for full synthetic details and characterization).

### Cbi-Ex4 synthesis and purification

To a 5mL round bottom flask containing a stir bar, copper (I) iodide (Cu(I)) (3.3 mg, 0.017 mmol), and tris[(1-benzyl-1H-1,2,3-triazol-4-yl)methyl]amine (TBTA) (7.0 mg, 0.013 mmol) was added to 500 μL of 4:1 DMF:H<sub>2</sub>O. The reaction mixture was allowed to stir at room temperature until a color change occurred (clear to yellowish brown) (~15 min). The solution was treated with K12-azido-exendin-4 (2.0 mg, 0.0004 mmol) and Cbi-alkyne (4.8 mg, 0.004 mmol) and allowed to stir overnight (Figure 1A). The product was purified using Shimadzu Prominence HPLC using a C18 column (Eclipse XDB-C18 5 μm, 4.6 × 150 mm) with H<sub>2</sub>O + 0.1% TFA and acetonitrile. *t<sub>R</sub>* (RP-HPLC, from 1% CH<sub>3</sub>CN/H<sub>2</sub>O + 0.1% to TFA to 70% % CH<sub>3</sub>CN/H<sub>2</sub>O + 0.1% to TFA in 15 min): 11.2 min. ESI-MS shows the expected *m/z* 5354, observed *m/z* = 1339 [M+4H]<sup>4+</sup>, 1071 [M+5H]<sup>5+</sup> (Figure 1B).

### Shrew serum total B12, total apo-TC and apo-HC binding capacities

Pool of shrew serum from two animals (1 and 2) as: 3 × 150 μl animal 1 + 2 mixed, 3 × 150 μl animal 1 only, 3 × 150 μl animal 2 only were assayed as previously described (Gimsing and Nexø, 1989). Briefly, total B12 was measured using serum diluted 1:5 with 0.9% NaCl on the automatic platform Advia Centaur CP Immunoassay system. Unsaturated B12 binding capacity was measured on serum diluted 1:10 employing coated charcoal to separate free and bound <sup>57</sup>Co-B12 (KemEnTec) to separate TC and HC. A sample saturated with <sup>57</sup>Co-B12 was run on a Superdex® 200 HR 10/30 column (GE Healthcare Europe) using a Dionex® ICS-3000 chromatograph (Dionex Corporation), eluted at a flow rate of 400 μL/min for approx. 70 min employing a Tris buffer (0.1 mol/L) (Sigma Aldrich), 1 mol/L NaCl (Merck), 0.5 g/L bovine albumin (Sigma Aldrich), 0.2 g/L sodium-azide (Merck), pH 8.0. The eluted fractions were counted in a Wizard Automatic Gamma Counter to monitor the elution of <sup>57</sup>Co-B12. Molecular mass markers Blue Dextran (Sigma Aldrich) and <sup>22</sup>Na (GE Healthcare Europe) were used for determination of void volume (V<sub>0</sub>), and total volume (V<sub>t</sub>).

### HC and TC binding of Cbi-Ex4 and Ex4

HC and TC binding assays were conducted as previously reported (Stupperich and Nexø, 1991). In brief, typically 50 pmol <sup>57</sup>Co-B12 (KemEnTec) was mixed with Cbi-Ex4 and the binding protein (HC or TC) was added in a concentration between 25-40 pmol/l. The total incubation volume was 0.375 ml, with 0.1 M sodium phosphate and 0.1% human albumin (Sigma-Aldrich), pH 8. The mixture was equilibrated at 4°C for 20 h. Free versus protein bound corrinoids (cyanocobalamin versus Cbi-Ex4) were separated by precipitating with hemoglobin-coated charcoal previously prepared by mixing equal volumes of a 5% aqueous suspension of activated charcoal (Sigma-Aldrich) with a 0.5% aqueous solution of bovine hemoglobin (Sigma-Aldrich). Protein-bound [<sup>57</sup>Co-B12] was then measured in a multichannel counter (Merlsgaard, DK).

### In vitro GLP-1 binding assay

Agonism at the GLP-1R of Ex4 and Cbi-Ex4, was monitored using HEK293 cells stably transfected with the human GLP-1 receptor. The cells were cultured in Dulbecco's Modified Eagle Medium (DMEM) with 10% FBS, 1% pen/strep and 250 μg/mL geneticin/g-418. HEK293 cells stably transfected with GLP-1R were seeded at ~8.5x10<sup>5</sup> cells/mL in 12 mL in DMEM in a 100 mm x 20 mm sterile tissue culture dish (TCD). Within 24h of seeding the TCD is ~80% confluent and infected with the H188 adenovirus, the most sensitive cAMP FRET reporter (Klarenbeek et al., 2015), and incubated for 20h prior to screening. Cells, now infected with the H188 adenovirus, were grown to > 95% confluency at which time they were removed from cultured media and placed in 96-well clear-bottom assay plate (Costar 3904, Corning, NY) in 200 μL/well of a standard extracellular saline (SES) solution supplemented with 11 mM glucose and 0.1% BSA. Real-time kinetic FRET assays were performed using a FlexStation 3 Multi-Mode Microplate Reader. Assays were performed at 25°C, over 400 s with subsequent stimulant injections of Ex4 and Cbi-Ex4 concentrations ranging from 3 pM to 1 nM (see Figure 1C, inset) at 100 s, with emission measurements every 6 s. To determine agonism, an increase in 485/535 nm FRET ratio was monitored indicating increase of cAMP concentration through cAMP binding to an exchange protein directly activate by cAMP (EPAC) (Klarenbeek et al., 2015).

### Jugular catheter surgery and pharmacokinetic profile of Ex4 and Cbi-Ex4 in shrews

Shrews (n = 15) were deeply anesthetized with a cocktail of ketamine, (180 mg/kg; Butler Schein), xylazine (5.4 mg/kg; Anased), and acepromazine (1.28 mg/kg; Butler Schein). Homemade silicone catheters (9 cm-long, 3Fr, ID 0.56 mm, OD 1 mm, cat. Sku SIL-3-25,

SAI Infusion Technologies) were pre-filled with bacteriostatic saline 5 IU/mL heparin solution (Butler Schein). A 3 cm-long incision in the interscapular region and a 2 cm-long incision from the right mandible toward the shoulder were made without cutting any underlying tissue. A subcutaneous route was cleared between the incision sites and the catheter was threaded over the shoulder of the animal through the cleared path and fixed to a round mesh back-mount that was implanted subcutaneously between the shoulder blades. The tissue underlying the ventral neck incision was gently dissected using forceps to expose the right jugular vein. The exposed jugular vein was stretched and tied off toward the surface of the incision and using a flat spatula. Using microsurgical scissors a partial perpendicular incision was made and microsurgical forceps were used to insert the catheter through the incision and gently inserted 1 cm (a small silicone ball of sealant glue attached to catheter used as stop guide) into the vein. Cannula placement and patency were verified by drawing up vein blood with a syringe attached to the catheter before the catheter was sealed with metal obturator. The catheter was secured to the vein by tying two sutures (4-0, silk) around the catheter above and below the silicone ball. Sutures were tied together and acrylic glue was placed over the insertion point to secure the catheter in place. Incisions were closed with simple interrupted sutures (4-0, silk) and all animals received 2 mL of warm saline and analgesic (Meloxicam, 5mg/kg, IP, Boehringer Ingelheim). To prevent infection and maintain patency, catheters were flushed daily with 0.05 mL of the antibiotic Timentin (0.93 mg/mL; Fisher) dissolved in heparinized saline solution (5 IU/mL), except for the testing days in which the catheters were flushed with heparinized saline only 30 min prior drug administration.

Three hours before dark onset, shrews were briefly anesthetized with isoflurane (Henry Schein Animal Health) and 50  $\mu$ L of blood were collected from their tail into a heparin container ( $t = -10$ ). Immediately after, each shrew received a bolus IV infusion of either Ex4 (100 and 200  $\mu$ g/kg [i.e., 25, 50 nmol/kg; respectively]), or equimolar doses Cbi-Ex4. Subsequent blood collection occurred at 5, 45, 90, 135, 180, 270 and 360 min post IV infusion. Plasma was obtained by spinning blood at 6000 g for 6 min and subsequently stored at  $-80^{\circ}\text{C}$ . Concentrations of Ex4 and Cbi-Ex4 were measured using a commercial kit purchased from Phoenix Pharmaceuticals (Exendin-4 (*Heloderma suspectum*) EK-070-94). The ELISA was performed according to the manufacturer's protocol with the exception of shrew blood serum that had been dosed with Cbi-Ex4. A Cbi-Ex4 standard curve was generated by matching concentrations provided by the manufacturer's standards.

#### Dose-response effects of Cbi-Ex4 and native Ex4 on glycemic control

The protocol for performing an intraperitoneal glucose tolerance test (IPGTT) in shrews was similar to that previously used in rodents (Mietlicki-Baase et al., 2018). Two hours before dark onset, shrews were food- and water- deprived. Three hours later, baseline blood glucose levels were determined from a small drop of tail blood and measured using a standard glucometer (AccuCheck). Immediately following, each shrew ( $n = 10$ ) received IP injection of Ex4 (1.25, 5 or 50 nmol/kg) or vehicle (1 mL/100 g BW sterile saline). BG was measured 30 minutes later ( $t = 0$  min), then each shrew received an IP bolus of glucose (2 g/kg). Subsequent BG readings were taken at 20, 40, 60 and 120 min after glucose injection. After the final BG reading, food and water were returned. IPGTT studies were carried out in a within-subject, counter-balanced design and separated by 7 days. In another cohort of animals ( $n = 11$ ), the same paradigm was applied but each shrew received IP injection of Cbi-Ex4 (1.25, 5 or 50 nmol/kg) or vehicle instead.

#### Direct comparison of pharmacological doses of Cbi-Ex4 and Ex4 on glucoregulation during a standard and a delayed IPGTT

In shrews ( $n = 14$ ) a standard IPGTT was performed as described above. In this experiment each shrew received IP injection of Ex4 (5 nmol/kg), Cbi-Ex4 (5 nmol/kg) or vehicle in a within-subject, counter-balanced design. Each treatment was separated by 72h.

For the delayed glucose load IPGTT, food (6h pre-IPGTT) and water (4h prior to testing) were removed in a separate cohort of animals ( $n = 13$ ). A baseline BG reading ( $t = -360$  min) was performed immediately followed by an IP injection of Ex4 (5 nmol/kg), Cbi-Ex4 (5 nmol/kg) or vehicle. BG was measured 3h ( $t = -120$  min), 5.30h ( $t = -30$  min) and 6h ( $t = 0$  min) later and each shrew received IP injection of glucose (2 g/kg). Subsequent BG readings were taken at 20, 40, 60 and 120 min after glucose injection. After the final BG reading, food and water were returned. Each IPGTT round was 72h apart.

#### Dose-response effects of Ex4 and Cbi-Ex4 on energy balance

We first evaluated in two separate group of shrews the effects on food intake and body weight of different doses of native Ex4 and Cbi-Ex4; respectively. Food was removed one hour prior to dark onset. Shortly before dark onset the first group of shrews ( $n = 9$ ) received IP injection of Ex4 (1.25, 5 or 50 nmol/kg), or vehicle. In a second group of shrews ( $n = 10$ ), IP injections of Cbi-Ex4 (1.25, 5 or 50 nmol/kg) or vehicle were performed. Shrews had *ad libitum* access to powdered food through a circular (3 cm diameter) hole in the cage. Food intake was evaluated using our custom-made feedometers, consisting of a standard plexiglass rodent housing cage (29  $\times$  19  $\times$  12.7 cm) with mounted food hoppers resting on a plexiglass cup (to account for spillage). Food intake was manually measured at 6, 24 and 48h post injection. Body weight was taken at 0, 24 and 48h. Treatments occurred in a within-subject, counter-balanced design and were 7 days apart.

#### Direct comparison of pharmacological doses of Cbi-Ex4 and Ex4 on energy balance

We then compare the effects of Ex4 (5 nmol/kg), Cbi-Ex4 (5 nmol/kg) or vehicle in the same animals ( $n = 8$ ) using in a within-subject, counter-balanced design. Food was removed one hour prior to dark onset. In this experiment, food intake was evaluated using our custom-made automated feedometers, in which the food hoppers were attached to a load-cell. The amount of powdered food

consumed was measured every 10 s to the nearest 0.1 g (Arduino 1.8.8). Data obtained from the feedometer were processed and converted by computer software (Processing 3.4 and Microsoft Excel) to determine food ingestion every 10 s. Total food intake curves were cumulated for 3, 6 and 24h. Latency to eat (defined as time required before the onset of a meal exceeding 0.25 g) was also measured and analyzed. Treatments occurred 72h apart.

### Emetogenic properties of Ex4 and Cbi-Ex4

Shrews (n = 14) were habituated to IP injections and to clear plastic observation chambers (23.5 × 15.25 × 17.8 cm) for two consecutive days prior to experimentation. The animals were injected IP with Ex4 (1.25, 5 or 50 nmol/kg), or vehicle, then video-recorded (Vixia HF-R62, Canon) for 120 minutes. After 120 min, the animals were returned to their cages. In a second group of shrews (n = 14), IP injections of Cbi-Ex4 (1.25, 5 or 50 nmol/kg) or vehicle were performed. Treatments were separated by 7 days. Analysis of emetic episodes were measured by an observer blinded to treatment groups. Emetic episodes were characterized by strong rhythmic abdominal contractions associated with either oral expulsion from the gastrointestinal tract (i.e., vomiting) or without the passage of materials (i.e., retching). Latency to the first emetic episode, total number of emetic episodes and number of emetic episodes per minute were quantified.

### Direct comparison of pharmacological doses of Cbi-Ex4 and Ex4 on emesis

Shrews (n = 8) were habituated to the experimental conditions as described above. The animals were injected IP with Ex4 (5 nmol/kg), Cbi-Ex4 (5 nmol/kg) or vehicle, then video-recorded (Vixia HF-R62, Canon) for 120 minutes. After 120 min, the animals were returned to their cages. Treatments were separated by 72 h. Analysis of emetic episodes were measured by an observer blinded to treatment groups. Emetic episodes as well as emetic bouts (defined as series of one or more emetic episodes that occurred within one minute from each other) were evaluated. Latency to the first emetic episode, total number of emetic episodes, number of emetic episodes per minute and total emetic bouts were also quantified.

### Assessment of neuronal activation in the DVC following Ex4, Cbi-Ex4 or saline treatments

Body weight-matched shrews (n = 13) received IP injection of Ex4 (5 nmol/kg, n = 3), Cbi-Ex4 (5 nmol/kg, n = 6) or vehicle (n = 4) just prior to dark onset. Food was removed to avoid feeding-related changes in c-Fos expression between groups. Three hours later, shrews were deeply anesthetized with IP triple cocktail of ketamine, xylazine and acepromazine (180 mg/kg, 5.4 mg/kg and 1.28 mg/kg; respectively) and transcardially perfused with 0.1M PBS (Boston Bioproducts), followed by 4% PFA (in 0.1M PBS, pH 7.4, Boston Bioproducts). Brains were removed and post fixed in 4% PFA for 48h and then stored in 25% sucrose for two days. Brains were subsequently frozen in cold hexane and stored at  $-20^{\circ}\text{C}$  until further processing. Thirty micrometer-thick frozen coronal sections containing the DVC were cut in a cryomicrotome (CM3050S, Leica Microsystem), collected and stored in cryoprotectant (30% sucrose, 30% ethylene glycol, 1% polyvinyl-pyrrolidone-40, in 0.1M PBS) at  $-20^{\circ}\text{C}$  until further processing. IHC was conducted according to previously described procedure (Alhadeff et al., 2015). Briefly, free-floating sections were washed with 0.1M PBS (3x8min), incubated in 0.1M PBS containing 0.3% Triton X-100 (PBST) and 5% normal donkey serum (NDS) for 1h, followed by an overnight incubation with rabbit anti-Fos antibody (1:1000 in PBST; s2250; Cell Signaling.). After washing (3x8min) with 0.1M PBS sections were incubated with the secondary antibody donkey anti-rabbit Alexa Fluor 488 (1:500 in 5% NDS PBST; Jackson Immuno Research Laboratories,) for 2h at room temperature. After final washing (3x8min in 0.1M PBS) the sections were mounted onto glass slides (Superfrost Plus, VWR) and coverslipped with Fluorogel (Electron Microscopy Sciences). c-Fos positive neurons spanning the DVC were visualized (20x; Nikon 80i, NIS Elements AR 3.0) and quantified (FIJI software) using fluorescence microscopy. A total of 4 DVC sections per animal were used to quantify the number of c-Fos labeled cells in the AP and NTS at the level of the obex, caudal medial DVC (200 and 250  $\mu\text{m}$  rostral to the obex, and medial DVC (400  $\mu\text{m}$  rostral to the obex), similarly as previously described (De Jonghe and Horn, 2009) by an experimenter blinded to the treatment.

### Emetogenic properties of albiglutide

Shrews (n = 15) were habituated to the experimental conditions (see above). The animals were injected IP with albiglutide (0.5 or 5 mg/kg) or vehicle, and video-recorded for 120 minutes. Treatments were carried out in a within-subject, counter-balanced design and separated by 7 days. Latency to the first emetic episode, total number of emetic episodes, number of emetic episodes per minute and total emetic bouts were quantified.

### Effects of albiglutide on energy balance

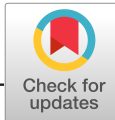
The effects of albiglutide on food intake and body weight were analyzed similarly as described above. Shrews (n = 10) were injected with albiglutide (0.5 or 5 mg/kg) or vehicle. Food intake was measured manually at 6, 24 and 48h post injection. Body weight was taken at 0, 24, 48, and 72h. Treatments occurred in a within-subject, counter-balanced design and were 7 days apart.

### QUANTIFICATION AND STATISTICAL ANALYSIS

All data were expressed as mean  $\pm$  SEM. For behavioral studies, data were analyzed by a repeated-measures One-Way ANOVA or Two-Way ANOVA, followed by Tukey's post hoc test. For all statistical tests, a p value less than 0.05 was considered significant.

Information on replicates and significance is reported in the figure legends. In the pharmacokinetic study, area under curves (AUCs) were calculated from –10 to 360 or 1440 min using the trapezoidal method, and analyzed using One-Way ANOVA followed by Tukey's post hoc test. BG levels were analyzed using Repeated-measurements Two-Way ANOVA followed by Tukey's post hoc test. AUCs were calculated from 0 to 60 and 0 to 120 min; respectively, using the trapezoidal method. Resulting AUCs were analyzed using Repeated-measurements One-Way ANOVA followed by Tukey's post hoc test. Total number of emetic episodes and emetic bouts were analyzed using Repeated-measurements One-Way ANOVA followed by Tukey's post hoc test. Student's t test was used to analyze emetic episodes between two equimolar doses. Comparisons between different proportions of shrews experiencing emesis under the different treatment conditions (i.e., occurrence) were made using the Fisher's exact test. Data obtained from the feedometer were analyzed with Repeated-measurements One-Way ANOVA followed by Tukey's post hoc test. For IHC, statistical comparisons were performed using One-way ANOVA followed by Tukey's post hoc test. All data were analyzed using Prism GraphPad 8.





## ORIGINAL ARTICLE

WILEY

# A second-generation glucagon-like peptide-1 receptor agonist mitigates vomiting and anorexia while retaining glucoregulatory potency in lean diabetic and emetic mammalian models

Tito Borner PhD<sup>1</sup> | Evan D. Shaulson BS<sup>1</sup> | Ian C. Tinsley BS<sup>2</sup> |  
Lauren M. Stein PhD<sup>3</sup> | Charles C. Horn PhD<sup>4,5,6</sup> | Matthew R. Hayes PhD<sup>1,3</sup>   
Robert P. Doyle PhD<sup>2,7</sup> | Bart C. De Jonghe PhD<sup>1</sup>

<sup>1</sup>Department of Biobehavioral Health Sciences, School of Nursing, University of Pennsylvania, Philadelphia, Pennsylvania

<sup>2</sup>Department of Chemistry, Syracuse University, Syracuse, New York

<sup>3</sup>Department of Psychiatry, Perelman School of Medicine, University of Pennsylvania, Philadelphia, Pennsylvania

<sup>4</sup>Department of Medicine, University of Pittsburgh School of Medicine, Pittsburgh, Pennsylvania

<sup>5</sup>UPMC Hillman Cancer Center, University of Pittsburgh School of Medicine, Pittsburgh, Pennsylvania

<sup>6</sup>Center for Neuroscience, University of Pittsburgh, Pittsburgh, Pennsylvania

<sup>7</sup>Department of Medicine, Upstate Medical University, State University of New York, Syracuse, New York

## Correspondence

Bart C. De Jonghe, Department of Biobehavioral Health Sciences, School of Nursing, University of Pennsylvania, 125 South 31st Street, Philadelphia, PA 19104.

Email: bartd@nursing.upenn.edu

## Funding information

This work was supported by National Institutes of Health-DK-112812 (B.C.D.), NIH-DK-097675 (R.P.D.), NIH-DK-115762 (M.R.H.), SNF P2ZHP3\_178114, P400PB\_186728 (T.B.) and NIH-CA-201962 (C.C.H.)

## Abstract

**Aim:** To develop a conjugate of vitamin B12 bound to the glucagon-like peptide-1 receptor (GLP-1R) agonist exendin-4 (Ex4) that shows reduced penetrance into the central nervous system while maintaining peripheral glucoregulatory function.

**Methods:** We evaluated whether a vitamin B12 conjugate of Ex4 (B12-Ex4) improves glucose tolerance without inducing anorexia in Goto-Kakizaki (GK) rats, a lean type 2 diabetes model of an understudied but medically compromised population of patients requiring the glucoregulatory effects of GLP-1R agonists without anorexia. We also utilized the musk shrew (*Suncus murinus*), a mammalian model capable of emesis, to test B12-Ex4 on glycaemic profile, feeding and emesis.

**Results:** In both models, native Ex4 and B12-Ex4 equivalently blunted the rise in blood glucose levels during a glucose tolerance test. In both GK rats and shrews, acute Ex4 administration decreased food intake, leading to weight loss; by contrast, equimolar administration of B12-Ex4 had no effect on feeding and body weight. There was a near absence of emesis in shrews given systemic B12-Ex4, in contrast to reliable emesis produced by Ex4. When administered centrally, both B12-Ex4 and Ex4 induced similar potency of emesis, suggesting that brain penetrance of B12-Ex4 is required for induction of emesis.

**Conclusions:** These findings highlight the potential therapeutic value of B12-Ex4 as a novel treatment for type 2 diabetes devoid of weight loss and with reduced adverse effects and better tolerance, but similar glucoregulation to current GLP-1R agonists.

## KEYWORDS

animal pharmacology, antidiabetic drug

## 1 | INTRODUCTION

Nausea and vomiting are omnipresent side effects of human diseases and pharmacotherapies that have spawned significant drug discovery efforts to combat their many causes.<sup>1</sup> Glucagon-like peptide-1 receptor (GLP-1R)-based therapies for the treatment of type 2 diabetes (T2D), such as Exendin-4 (Ex4) and liraglutide, are no exception,<sup>2</sup> causing nausea and vomiting in ~25% to 50% of patients prescribed these drugs.<sup>3–7</sup>

We have recently reported that a vitamin B12 conjugate of Ex4 (hereafter called 'B12-Ex4')<sup>8,9</sup> shows retention of glucoregulation comparable with native Ex4 without producing Ex4-associated anorexia and conditioned taste avoidance in lean, healthy rats. Furthermore, B12-Ex4 co-localized with insulin-containing  $\beta$ -cells within the pancreas, while brain penetrance of fluorescently tagged B12-Ex4 was not detected within the hypothalamus, nor the area postrema (AP), nor the nucleus tractus solitarius (NTS) of the hindbrain. These results corroborated that the incretin action on the pancreas<sup>10–12</sup> and hypoglycaemic effects of Ex4 remained intact when bound to B12, while central sites of Ex4 action controlling energy homeostasis and nausea/malaise (e.g. the brainstem AP and NTS, as well as hypothalamic nuclei)<sup>13–15</sup> were putatively not agonized following B12-Ex4 treatment. The B12-Ex4 construct may be of considerable clinical utility given the potential for retained glycaemic control in combination with improved tolerability and associated patient compliance through a mechanism of action that simultaneously limits central nervous system (CNS) penetrance and retains peripheral (i.e. pancreatic) pharmacodynamics.

Weight loss is considered desirable for the majority of patients with T2D considered overweight or obese, as they may benefit from improvements in insulin signalling and overall health with concomitant adipose tissue loss.<sup>16,17</sup> However, patients with T2D who also suffer from comorbidities associated with cachexia (e.g. cancer,<sup>18</sup> cystic fibrosis,<sup>19</sup> HIV,<sup>20</sup> chronic obstructive pulmonary disease<sup>21</sup> and sarcopenia<sup>22</sup>), would also benefit from use of the front-line treatments for T2D in the form of GLP-1R agonists, without affecting their body weight. In addition, ~10% of patients with T2D, such as those potentially with polygenic/inherited T2D, are not overweight/obese,<sup>23</sup> and weight loss below normal weight status is undesirable. To this end, given our previous work in healthy, lean rats, where we showed comparable glycaemic control without anorexia/weight loss following acute B12-Ex4 treatment compared with native Ex4, we employ the use of the Goto-Kakizaki (GK) rat, a model of spontaneous insulin resistance and T2D.<sup>24</sup> These animals develop T2D early in life and maintain a lean phenotype (see Ostenson and Efendic<sup>25</sup> for a discussion/review), making this strain ideal to model T2D without concomitant obesity.

The musk shrew (*Suncus murinus*) is a well-established model of emesis<sup>26</sup> and feeding behaviour<sup>27</sup> and is suitable for examination of the GLP-1 system as this species exhibits glucoregulatory, hypophagic and emetic responsivity following administration of current Food and Drug Administration-approved GLP-1R agonists.<sup>14,15</sup> Here, we employ behavioural, immunohistochemical and pharmacological analyses to examine the effects of B12-Ex4 versus Ex4 administration on glycaemic control, emesis and feeding behaviour in shrews.

We report both the preservation of hypoglycaemic responses and superior tolerance of B12-Ex4 over native Ex4 in musk shrews and the GK rat. B12-Ex4 shows substantially decreased effects on emesis compared with the native drug, while maintaining an incretin profile of glucoregulatory effects with no change in energy balance in shrews. These data support the potential clinical utility of B12-Ex4 in lean patients, where anorexia and weight loss are undesirable outcomes of T2D management and/or where dose scheduling of GLP-1R agonists is of major concern for patient compliance because of considerations of extensive episodes of nausea and vomiting.

## 2 | METHODS

### 2.1 | Drugs

B12-Ex4 was synthesized, characterized and screened as previously described.<sup>8</sup> For all systemic administrations, B12-Ex4 and Ex4 (Bachem, USA) were dissolved in 0.9% saline and administered intraperitoneally (IP). B12-Ex4 and Ex4 were dissolved in artificial cerebrospinal fluid (aCSF) for intracerebroventricular (ICV) delivery. Liraglutide (Sigma-Aldrich) was dissolved in PBS and injected IP. Fluorophore-labelled B12-Ex4 (Cy5-B12-Ex4) was synthesized as previously described.<sup>9</sup>

### 2.2 | Animals

Experimentally naive adult male shrews (n = 81) weighing ~70–80 g used in this study were offspring from a colony maintained at the University of Pittsburgh Cancer Institute (a Taiwanese strain derived from stock supplied by the Chinese University of Hong Kong). At ~2 months of age, the animals were moved to the University of Pennsylvania, where all studies presented here were conducted.

Shrews were single-housed in plastic cages (37.3 × 23.4 × 14 cm, Innovive), fed *ad libitum* with a mixture of feline (75%, Laboratory Feline Diet 5003, Lab Diet) and ferret food (25%, High Density Ferret Diet 5L14, Lab Diet) and had *ad libitum* access to tap water except where noted. Experimentally naive adult male GK rats (n = 21, Taconic) weighing ~350 g upon arrival were individually housed in hanging wire mesh cages. Rats were fed *ad libitum* with a chow diet (NIH-31 M Diet, Taconic) and had *ad libitum* access to tap water, except where noted. All animals were housed under a 12-hour/12-hour light/dark cycle in a temperature- and humidity-controlled environment. All procedures were approved by the Institutional Care and Use Committee of the University of Pennsylvania.

### 2.3 | In vivo study design

Shrews and GK rats were habituated to single housing in their home cages and IP injections at least 1 week prior to experimentation. All



experimental injections in shrews were separated by at least 72 hours. Experimental testing in GK rats was conducted every 7 days. In vivo experiments used a within-subjects, Latin-square design, except for immunohistochemical studies, which were conducted between subjects.

## 2.4 | Stereotaxic surgery in shrews

The surgical procedure was similar to that previously described.<sup>14</sup> Shrews ( $n = 8$ ) were deeply anaesthetized with a triple cocktail of KAX (ketamine [180 mg/kg; Butler Animal Health Supply], acepromazine [1.28 mg/kg; Butler Animal Health Supply] and xylazine [5.4 mg/kg; Anased]) and placed into a stereotaxic frame equipped with custom-made ear bars (Kopf Instruments). An incision was made, the temporalis muscles on either side of the sagittal crest were displaced, and the area was cleaned of connective tissue. A hole was made according to the following coordinates: 8.2 mm rostral to lambda and 0.9 mm lateral to the midline. A 26-gauge stainless steel guide cannula (C315G/SPC, PlasticOne) was lowered 1.2 mm below the surface of the dura (2 mm above the lateral ventricle) and cemented to the skull using two screws. After surgery, animals received 2 mL of warm saline and analgesia (Meloxicam, 5 mg/kg, IP, Boehringer Ingelheim). Shrews were allowed 7 days of recovery before the beginning of the experiment. During drug administration, the guide cannula was fitted with a 33-gauge injection cannula (C315I/SPC, PlasticOne) that extended 2 mm beyond the tip of the guide cannula. At the end of the experiments, 1  $\mu$ L of Evans Blue dye was injected ICV following termination of the animals with IP KAX. Brains were immediately removed and frozen in cold hexane on dry ice. Coronal sections were performed to confirm the site of injection. Only those animals with blue staining in the ventricles were included in the analysis.

## 2.5 | Effects of Ex4 and B12-Ex4 on glycaemic control in shrews

The protocol for performing an intraperitoneal glucose tolerance test (IPGTT) in shrews was similar to that previously used in mice.<sup>9</sup> One hour before dark onset, shrews ( $n = 13$ ) were food- and water-deprived. Four hours later ( $t = -30$  minutes), baseline blood glucose (BG) levels were determined from a small drop of tail blood and measured using a standard glucometer (AccuCheck). Immediately following this blood sample, each shrew received an IP injection of 5 nmol/kg Ex4 (i.e.  $\sim 200$   $\mu$ g/kg), 5 nmol/kg B12-Ex4 or vehicle (sterile saline, 1 mL/100 g body weight). BG was measured 30 minutes later ( $t = 0$  minutes), then each shrew received an IP bolus of glucose (2 g/kg). Subsequent BG readings were taken at 20, 40, 60 and 120 minutes after glucose injection. After the final BG reading, food and water were returned. The dose selection of Ex4 was based on the literature and pilot experiments showing reliable BG suppression following glucose challenge in shrews.<sup>15</sup> Intraperitoneal delivery was

chosen as the route of glucose administration because of the emetogenic properties of Ex4, which could produce expulsion of glucose delivered to the gastrointestinal tract and confound interpretation of results because of the potential variability of intestinal glucose absorption.

To evaluate the effects of Ex4 and B12-Ex4 on baseline BG without subsequent glucose administration, Ex4, B12-Ex4 or vehicle was administered in a separate cohort of animals ( $n = 5$ ). Shrews were food- and water-deprived as described above. Four hours later ( $t = -30$  minutes), baseline BG levels were determined, and each shrew received an IP injection of 5 nmol/kg Ex4, 5 nmol/kg B12-Ex4 or vehicle (1 mL/100 g BW sterile saline). BG was measured 30 minutes later ( $t = 0$  minutes), followed by an IP saline injection (1 mL/100 g BW). Subsequent BG readings were taken at 20, 40, 60 and 120 minutes after glucose injection. After the final BG reading, food and water were returned.

## 2.6 | Effects of Ex4 and B12-Ex4 on energy balance in shrews

Shrews ( $n = 14$ ) were adapted to powdered food for 5 days and habituated to IP injections for 2 days prior to experimentation. In one cohort ( $n = 8$ ), shortly before dark onset, shrews received an IP injection of 5 nmol/kg Ex4, 5 nmol/kg B12-Ex4 or vehicle. In another subgroup of animals ( $n = 6$ ), 50 nmol/kg Ex4 (i.e.  $\sim 200$   $\mu$ g/kg), 50 nmol/kg B12-Ex4 or vehicle was injected. Food intake was evaluated using our custom-made automated feedometers,<sup>28</sup> which consisted of a standard plexiglass rodent housing cage (29  $\times$  19  $\times$  12.7 cm) with mounted food hoppers resting on a plexiglass cup (to account for spillage) attached to a load-cell. Shrews had *ad libitum* access to powdered food through a circular (3 cm diameter) hole in the cage. Food weights were measured every 10 seconds to the nearest 0.1 g (Arduino 1.8.8). Data obtained from the feedometer were processed and converted by computer software (Processing 3.4 and Microsoft Excel) to determine food ingestion each 10 seconds. Total food intake curves were cumulated for 3, 6 and 24 hours.

## 2.7 | Emetogenic properties of systemic Ex4 and B12-Ex4

Shrews ( $n = 24$ ) were habituated to IP injections and to clear plastic observation chambers (23.5  $\times$  15.25  $\times$  17.8 cm) for 2 consecutive days prior to experimentation. In one group ( $n = 16$ ), the animals were injected IP with 5 nmol/kg Ex4, 5 nmol/kg B12-Ex4 or vehicle, then video-recorded (Vixia HF-R62, Canon) for 90 minutes; the camera was positioned at a slight angle above the chamber. After 90 minutes, the animals were returned to their cages. In a second cohort ( $n = 8$ ), the animals received supra-pharmacological doses of 50 nmol/kg Ex4, B12-Ex4 or vehicle, and were then video-recorded as described. Analysis of emetic episodes was carried out by an observer blinded to treatment groups. Emetic episodes were

characterized by strong rhythmic abdominal contractions associated with either oral expulsion from the gastrointestinal tract (i.e. vomiting) or without the passage of materials (i.e. retching movements). An emetic bout was defined as a series of one or more emetic episodes that occurred within 1 minute of each other. Latency to the first emetic episode, total number of emetic episodes and the number of emetic episodes per minute, as well as emetic bouts, were calculated.

## 2.8 | Emetogenic properties of centrally administered Ex4 and B12-Ex4

Lateral ventricle cannulated shrews ( $n = 8$ ) were habituated to observation chambers for 2 days prior to experimentation, as in peripheral administration experiments. Ex4 (0.24 nmol, i.e. 1  $\mu\text{g}$ ), 0.24 nmol B12-Ex4 or vehicle (aCSF) was infused ICV (total volume 1  $\mu\text{L}$ ). Shrews were then video-recorded for 120 minutes. After

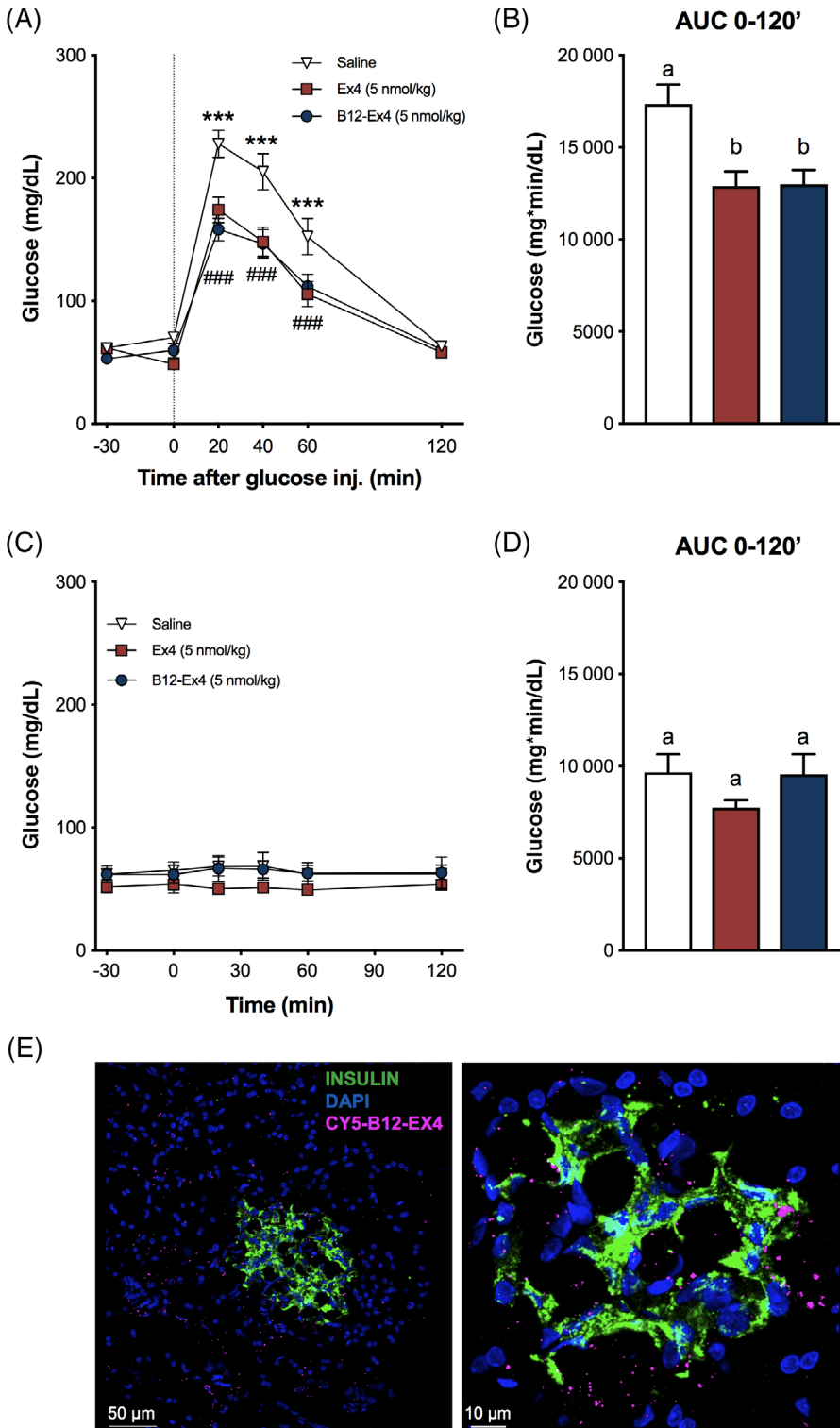


**FIGURE 1** Systemically delivered B12-Ex4 enhances glucose clearance during an intraperitoneal glucose tolerance test (IPGTT) and co-localizes with insulin in pancreatic  $\beta$ -cells in shrews. (A) In an IPGTT, Ex4 (5 nmol/kg, i.e.  $\sim 20 \mu\text{g}/\text{kg}$ ) and B12-Ex4 (5 nmol/kg) showed a similar potency in suppressing blood glucose (BG) levels after intraperitoneal (IP) glucose administration (2 g/kg, IP) compared with saline; saline versus B12-Ex4: \*\*\*  $P < .001$ ; saline versus Ex4: ###  $P < .001$ . (B) Area under the curve (AUC) analysis from 0 (i.e. postglucose bolus) to 120 minutes; B12-Ex4 and Ex4 similarly reduced AUCs compared with saline. (C, D) To investigate the effects of B12-Ex4 and Ex4 on baseline glucose homeostasis, the same doses of Ex4, B12-Ex4 or saline were administered without subsequent glucose administration. Ex4 and B12-Ex4 treatments were no longer effective in reducing BG levels and had no effect on AUC. (E) Systemically injected fluorophore-labelled B12-Ex4 (Cy5-B12-Ex4, 5 nmol/kg) co-localized with insulin in shrew pancreatic tissue supporting the hypothesis that B12-Ex4 acts at the pancreas to improve glycaemic control. All data are expressed as mean  $\pm$  SEM. Data in (A) and (C) were analysed with repeated measurements two-way ANOVA followed by Tukey's post hoc test. Data in (B) and (D) were analysed with repeated measurements one-way ANOVA followed by Tukey's post hoc test. Means with different letters are significantly different ( $P < .05$ ). In (A, B),  $n = 13$ , within subject; in (C-D),  $n = 5$ , within subject

120 minutes, the animals were returned to their cages. Each treatment was 72 hours apart. Analysis of emetic episodes was performed as described above.

## 2.9 | Assessment of neuronal activation in the dorsal vagal complex following Ex4, B12-Ex4 or saline treatments in shrews

Body weight-matched shrews ( $n = 13$ ) received an IP injection of 5 nmol/kg Ex4, 5 nmol/kg B12-Ex4 or vehicle, just prior to dark onset. Food was removed to avoid feeding-related changes in c-Fos expression between groups. Three hours later, shrews were deeply anaesthetized with an IP triple cocktail of KAX and transcardially perfused with phosphate buffered saline (PBS, 0.1 M, pH 7.4; Boston Bioproducts), followed by 4% paraformaldehyde (PFA) in PBS. Brains were removed and postfixed in 4% PFA for 48 hours and then stored in 30% sucrose for 2 days. Brains were subsequently frozen in cold

hexane and stored at  $-20^{\circ}\text{C}$  until further processing. Thirty micrometre-thick frozen coronal sections containing the dorsal vagal complex (DVC) were cut in a cryomicrotome (CM3050S, Leica Microsystems), then collected and stored in cryoprotectant (30% sucrose, 30% ethylene glycol, 1% polyvinyl-pyrrolidone-40, in PBS) at  $-20^{\circ}\text{C}$  until further processing. Immunohistochemistry was conducted according to a previously described procedure.<sup>29</sup> Briefly, free-floating sections were washed with PBS ( $3 \times 8$  minutes), incubated in PBS containing 0.3% Triton X-100 (PBST) and 5% normal donkey serum (NDS) for 1 hour, followed by an overnight incubation with rabbit anti-Fos antibody (1:1000 in PBST; s2250; Cell Signaling). After washing ( $3 \times 8$  minutes) with PBS, sections were incubated with the secondary antibody donkey anti-rabbit Alexa Fluor 555 (1:500 in 5% NDS PBST; Jackson Immuno Research Laboratories) for 2 hours at room temperature. After final washing ( $3 \times 8$  minutes in 0.1 M PBS) the sections were mounted onto glass slides (Superfrost Plus, VWR) and coverslipped with Fluorogel (Electron Microscopy Sciences). A total of three DVC sections per

### Doses: 5 nmol/kg

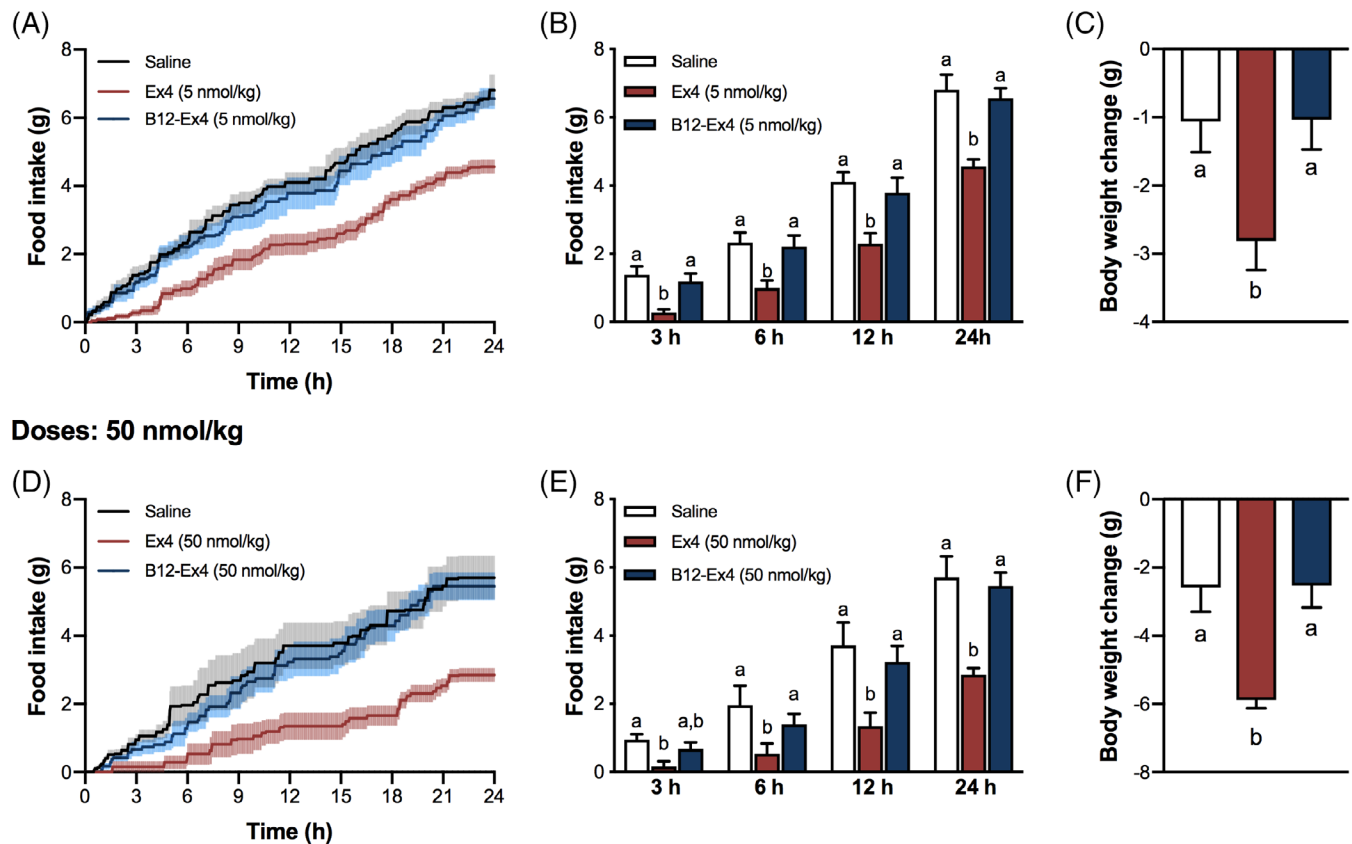


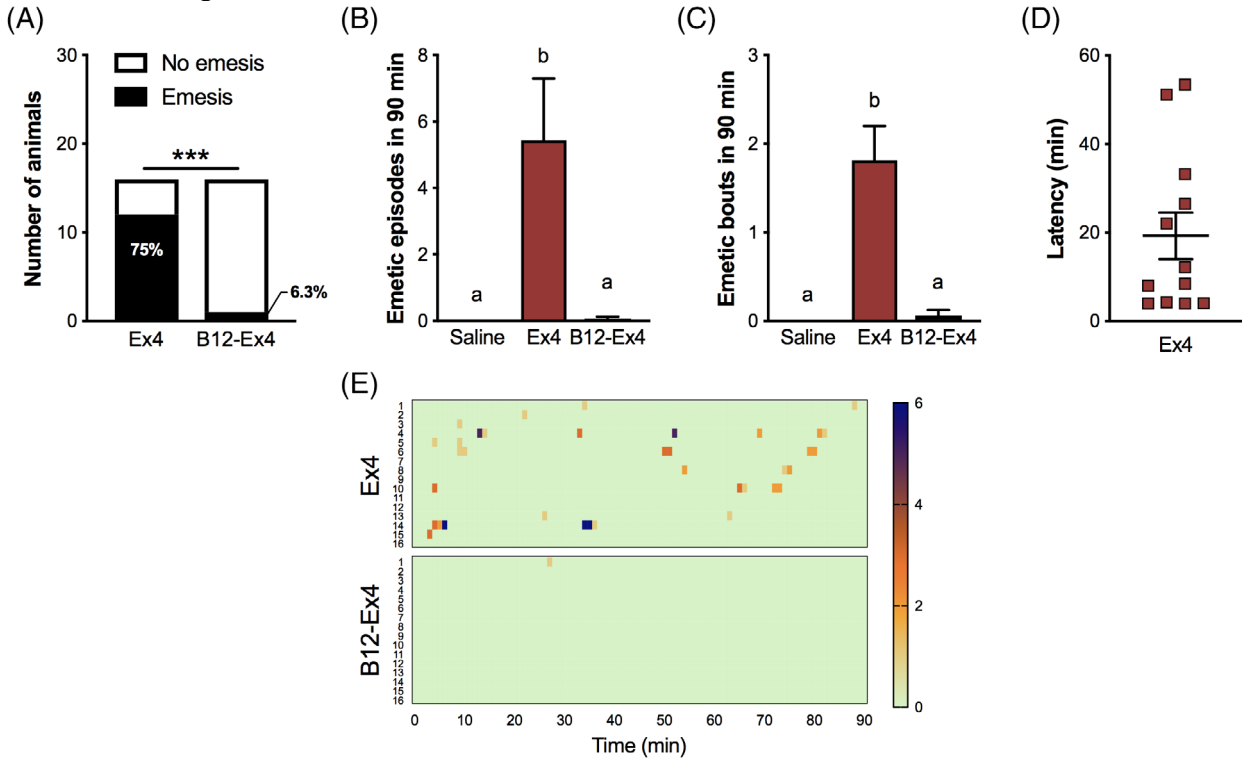
**FIGURE 2** Pharmacological and supra-pharmacological doses of B12-Ex4 do not affect feeding and body weight in shrews. (A, B) Ex4 (5 nmol/kg) suppressed feeding at 3, 6, 12 and 24 hours, whereas equimolar doses of B12-Ex4 had no effect on food intake. (C) Ex4-induced anorexia was accompanied by body weight loss. No significant changes in body weight were observed after B12-Ex4 administration compared with controls. (D, E) Ex4 (50 nmol/kg, i.e.  $\sim 200 \mu\text{g}/\text{kg}$ ) suppressed eating at all measured time points. By strict contrast, supra-pharmacological equimolar doses of B12-Ex4 did not show any effects. (F) While severe body weight loss occurred following supra-pharmacological doses of Ex4, no significant changes occurred in the B12-Ex4-treated animals. All data are expressed as mean  $\pm$  SEM. Data were analysed with repeated measurements one-way ANOVA followed by Tukey's post hoc test. Means with different letters are significantly different ( $P < .05$ ). In (A-C),  $n = 8$ , within subject; in (D-F),  $n = 6$ , within subject

animal were used to quantify the number of c-Fos-labelled cells in the AP and NTS of the DVC (~200-250 µm rostral to the obex). c-Fos-positive neurons were visualized and quantified manually in a blind fashion using fluorescence microscopy (20x; Nikon 80i, NIS Elements AR 3.0).

### 2.10 | Evaluation of B12-Ex4 presence/penetrance in the pancreas

Shrews (n = 4) received an IP injection of 5 nmol/kg Cy5-B12-Ex4 and were transcardially perfused 3 hours later as described above.

**Doses: 5 nmol/kg**



**Doses: 50 nmol/kg**

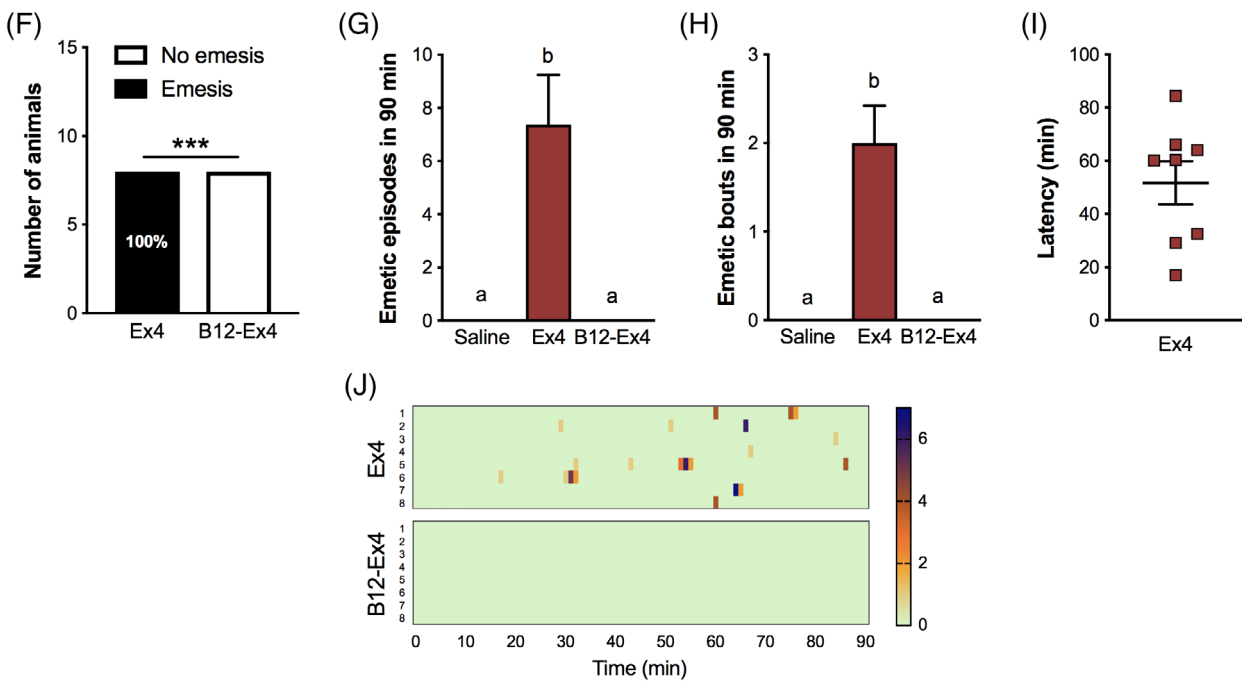


**FIGURE 3** Legend on next page.

Pancreases were immediately dissected. Thirty micrometre-thick frozen sagittal sections were processed via immunohistochemistry for insulin and coverslipped with 4',6-diamidino-2-phenylindole mounting medium as previously described.<sup>9</sup> Sections were visualized with confocal microscopy (Leica SP5 X) using the 488 and 594 laser lines with 10x and 20x objectives. All images were collected sequentially to avoid contamination of signals from other fluorophores.

## 2.11 | Effects of B12-Ex4, Ex4 and liraglutide on glycaemic control, insulin profile and energy balance in GK rats

GK rats ( $n = 21$ ) were adapted to insertion of a gavage for 1 week before the beginning of the experiment. On the test day, animals were food deprived 2 hours before dark onset and, just after onset of the dark phase, water was also removed from the cage. Three hours later, a small drop of blood was collected from the tail tip and analysed for BG level using a standard glucometer (AccuCheck). Immediately after this baseline BG reading ( $t = -60$  minutes), each rat received an IP injection of 5 nmol/kg Ex4, 5 nmol/kg B12-Ex4, liraglutide (100  $\mu\text{g}/\text{kg}$ ) or vehicle (1 mL/kg sterile saline). Doses of drugs were selected based on previous reports<sup>9,30,31</sup> and pilot studies conducted in GK rats. BG was measured 60 minutes later ( $t = 0$  minutes) and each rat received an oral gavage of glucose (1 g/kg). Subsequent BG readings were taken at 20, 40, 60, 120 and 180 minutes after glucose gavage. After the final BG reading, food and water were returned.

## 2.12 | Statistical analyses

All data were expressed as mean  $\pm$  SEM. For behavioural studies, data were analysed by a repeated measures one- or two-way ANOVA, followed by Tukey's post hoc tests. For all statistical tests, a  $P$ -value of less than 0.05 was considered significant. Data were analysed using Prism GraphPad 8.0. BG levels measured during the oral glucose tolerance tests (OGTTs) and IPGTTs were analysed using a repeated

measures two-way ANOVA followed by Tukey's post hoc test. Each area under the curve (AUC) was calculated from 0 to 120 minutes using the trapezoidal method. The resulting AUCs were analysed using a repeated measures one-way ANOVA followed by Tukey's post hoc test. The total numbers of emetic episodes and emetic bouts were analysed using a repeated measures one-way ANOVA followed by Tukey's post hoc test. Data obtained from the feedometer were analysed with repeated measures one-way ANOVA followed by Tukey's post hoc test. For the immunohistological study, statistical comparisons were performed using a one-way ANOVA followed by Tukey's post hoc test.

## 3 | RESULTS

### 3.1 | Study 1: systemically delivered B12-Ex4 enhances glucose clearance relative to Ex4 and co-localizes with insulin in pancreatic $\beta$ -cells in the shrew

We first tested whether B12-Ex4 reduces BG following an IPGTT in shrews. We observed that shrews treated with equimolar B12-Ex4 and native Ex4 display similar improvements in glucose clearance following glucose load compared with saline controls (Treatment  $\times$  Time interaction  $F_{[10, 140]} = 5.522$ ;  $P < .0001$ , Figure 1A). Post hoc analyses showed that both compounds significantly suppressed BG at 20, 40 and 60 minutes after glucose administration compared with saline treatment (all  $P < .001$ ). Furthermore, the AUC for B12-Ex4 did not differ from native Ex4 following glucose administration (Treatment effect  $F_{(2, 28)} = 7.218$ ;  $P < .003$ , Cbi-Ex4 vs. Ex4;  $P > .05$ , Figure 1B). Additionally, we administered Ex4, B12-Ex4 or saline without subsequent glucose injection and observed that both Ex4 and B12-Ex4 did not produce basal BG change (Treatment  $\times$  Time interaction  $F_{[10, 60]} = 0.1682$ ;  $P > .05$ ) or impact the glucose AUC (Treatment effect  $F_{(2, 8)} = 1.652$ ;  $P > .05$ , Figure 1C,D). To assess whether B12-Ex4 is taken up by insulin-producing cells in the pancreas, shrews were injected IP with a fluorescently labelled version of B12-Ex4 (Cy5-B12-Ex4, 5 nmol/kg) and sacrificed 3 hours after delivery.

**FIGURE 3** Emesis in shrews is significantly reduced following B12-Ex4 treatment compared with native Ex4, denoting improved tolerance across different doses. (A) The percentage of shrews experiencing emesis was significantly different between Ex4 (5 nmol/kg) and equimolar B12-Ex4 (\*\* $P < .001$ ). None of the animals experienced emesis following saline administration (data not shown). (B) The number of single emetic episodes following Ex4 (5 nmol/kg), equimolar B12-Ex4 or saline systemic administration was recorded for 90 minutes. Ex4 induced robust emetic responses that were not observed after B12-Ex4 or saline injections. (C) The number of emetic bouts was also lower after B12-Ex4 treatment compared with Ex4 and it did not differ from saline controls. (D) Latency to the first emetic episode in Ex4 animals that exhibited emesis. (E) Heatmap showing the emetic latency and intensity, as well as the number of emetic episodes induced by Ex4 or B12-Ex4 for each animal across time. A similar experiment was conducted with supra-pharmacological doses of Ex4 and B12-Ex4. Astonishingly, no emesis occurred after B12-Ex4 administration. (F) The percentage of shrews experiencing emesis was completely reversed between Ex4 (50 nmol/kg, i.e.  $\sim 200 \mu\text{g}/\text{kg}$ ) and equimolar B12-Ex4 (\*\* $P < .001$ ). No animal experienced emesis following saline injection (data not shown). (G, H) The number of emetic episodes and bouts following Ex4 (50 nmol/kg), equimolar B12-Ex4 or saline administration was analysed over 90 minutes. Also, at this dosage Ex4 induced robust emetic responses. (I) Latency to the first emetic episode in Ex4 shrews that exhibited emesis. (J) Heatmap showing the emetic latency and intensity, as well as the number of emetic episodes for each animal across time. All data are expressed as mean  $\pm$  SEM. Data in (A, F) were analysed with Fisher's exact test. Data in (B, C, G, H) were analysed with repeated measurements one-way ANOVA followed by Tukey's post hoc test. In (A-C),  $n = 16$ , within-subject; in (F-H),  $n = 8$ , within subject. Means with different letters are significantly different ( $P < .05$ )



Results show that upon systemic administration, Cy5-B12-Ex4 co-localized with insulin in pancreatic  $\beta$ -cells (Figure 1E).

### 3.2 | Study 2: B12-Ex4 does not alter food intake or body weight, contrary to administration of Ex4, which does reduce food intake and leads to body weight loss in the shrew

Shrews received an IP injection of Ex4 (5 nmol/kg), B12-Ex4 (5 nmol/kg) or saline, to test whether B12-Ex4 administration alters food intake or body weight in this species. In line with previous reports,<sup>14</sup> systemic administration of Ex4 produced hypophagia in shrews at all measured time points (all  $P < .05$ , Treatment  $\times$  Time

interaction  $F_{(6, 42)} = 4.097$ ;  $P < .003$ , Figure 2A,B) and body weight loss 24 hours after injection (all  $P < .05$ , Treatment effect  $F_{(2, 14)} = 6.9$ ;  $P < .01$ , Figure 2C). By contrast, no significant effects on food intake (all  $P > .05$ , Figure 2A,B) or body weight ( $P > .05$ , Figure 2C) were observed following B12-Ex4 treatment. In a second experiment, shrews were injected IP with a supra-pharmacological dose of Ex4 (50 nmol/kg, i.e.  $\sim 200 \mu\text{g}/\text{kg}$ ), B12-Ex4 (50 nmol/kg) or saline. Ex4 induced anorexia at all measured time points (all  $P < .05$ , Treatment  $\times$  Time interaction  $F_{(6, 30)} = 6.894$ ;  $P < .001$ , Figure 2D,E), and 24 hours body weight loss ( $P < .05$ , Treatment effect  $F_{(2, 10)} = 12.94$ ;  $P < .002$ , Figure 2F). By contrast, administration of equimolar doses of B12-Ex4 did not induce hypophagia (Figure 2D,E) or body weight loss compared with saline-treated animals (Figure 2F).

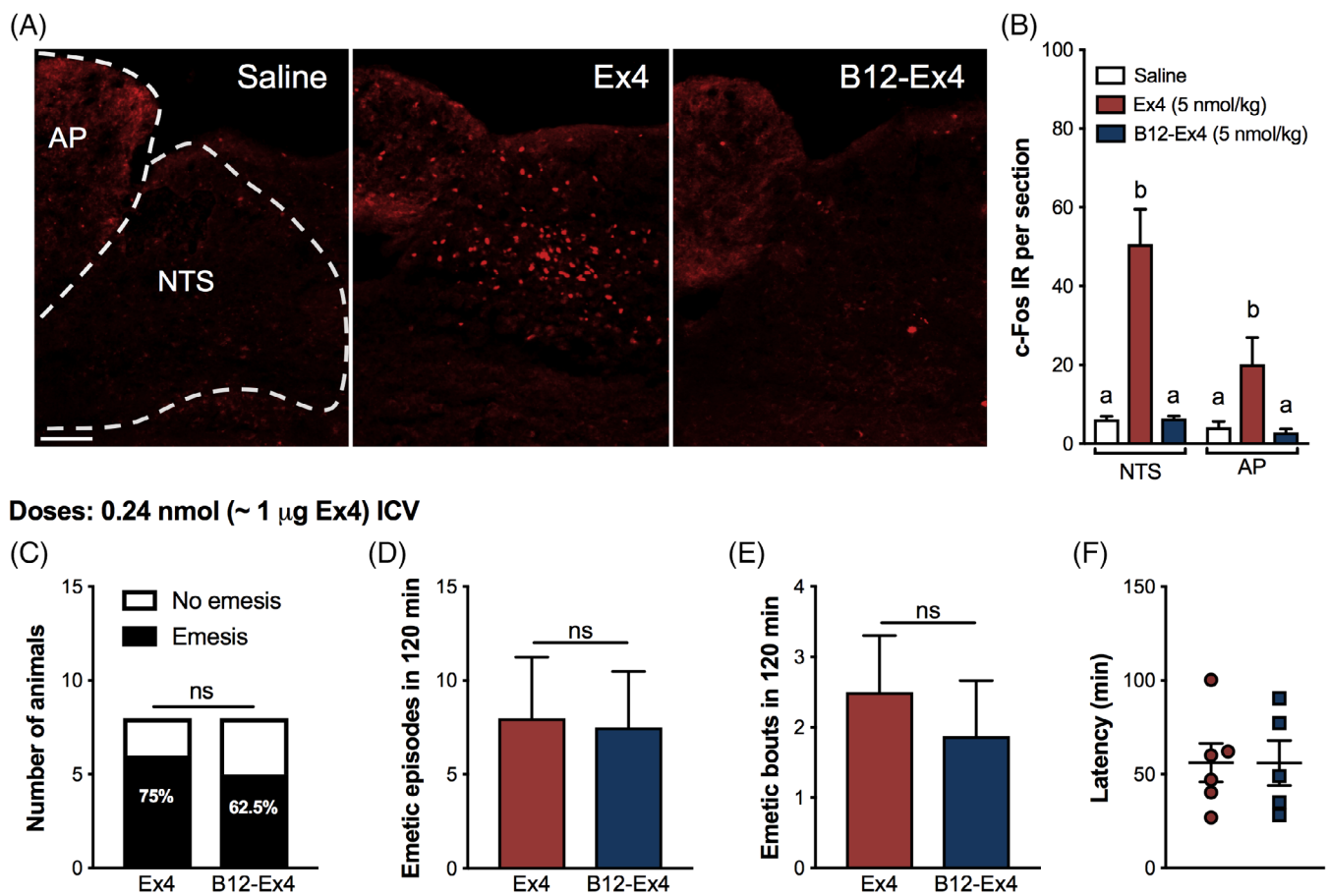


**FIGURE 4** Systemic administered B12-Ex4 does not activate the area postrema (AP) or the nucleus tractus solitarius (NTS) in shrews but it causes emesis when administered centrally. (A) Representative immunostainings of the AP/NTS region showing the c-Fos response following saline ( $n = 4$ ), Ex4 (5 nmol/kg,  $n = 4$ ) and equimolar B12-Ex4 ( $n = 5$ ) systemic treatment. (B) Peripheral Ex4 administration significantly increased the number of c-Fos immunoreactive (IR) cells in the AP/NTS of shrews 3 hours after injection. The number of c-Fos-positive cells in the AP/NTS was significantly lower in B12-Ex4-treated animals and it did not differ from saline-treated shrews. (C) Ex4 (0.24 nmol, i.e.  $1 \mu\text{g}$ ), equimolar B12-Ex4 or vehicle was infused into the lateral ventricle. The percentage of shrews showing emesis was similar between Ex4 and B12-Ex4. (D, E) The number of single emetic episodes or bouts following Ex4, B12-Ex4 or saline was recorded for 120 minutes. Both Ex4 and B12-Ex4 induced comparable emetic responses, while none of the animals experienced emesis following vehicle delivery (data not shown). (F) Latency to the first emetic episode in Ex4- and B12-Ex4-treated animals that exhibited emesis did not differ. Data in (B) were analysed with one-way ANOVA followed by Tukey post hoc test. Means with different letters are significantly different from each other ( $P < .05$ ). In (C) the analysis was performed with Fisher's exact test. Data in (D-F) were analysed with Student t-test ( $n = 8$ , within subject). Values are expressed as mean  $\pm$  SEM. Scale bar 100  $\mu\text{m}$

### 3.3 | Study 3: B12-Ex4 treatment produces only slight emesis compared with the potent emetic effects of Ex4

Ex4 (5 nmol/kg) induced emesis in the majority of the shrews tested (Figure 3A). By contrast, only one shrew experienced emesis after equimolar B12-Ex4 administration ( $P < .001$ ). The number of single emetic episodes (Treatment effect  $F_{(2, 30)} = 9.368$ ;  $P < .002$ , Figure 3B) and emetic bouts (Treatment effect  $F_{(2, 30)} = 20.5$ ;  $P < .0001$ , Figure 3C) in the 90 minutes window after drug administration were also significantly reduced after B12-Ex4 compared with Ex4 and did not differ from the control condition. Ex4 triggered emesis with an average latency of  $19 \pm 5$  minutes (Figure 3D). A heatmap representation of the Ex4 and B12-Ex4 effects on emetic intensity and latency for each individual animal across time can be seen in Figure 3E.

Next, we tested supra-pharmacological doses of Ex4 and B12-Ex4 and observed that Ex4 induced profound emesis, reflected by both the number and severity of emetic episodes, in 100% (i.e. 8/8,  $P < .001$ ) of the shrews tested, while an equimolar dose of B12-Ex4 did not induce emesis in shrews (Treatment effect on single emetic episodes  $F_{(2, 14)} = 15.39$ ;  $P < .0003$ , and Treatment effect on emetic bouts  $F_{(2, 14)} = 20.4$ ;  $P < .0001$ , Figure 3G,H). The average latency to first emetic episode induced by Ex4 was  $52 \pm 8$  minutes (Figure 3I). The emetic profiles of each animal following B12-Ex4 or Ex4 administration are represented in Figure 3J.

### 3.4 | Study 4: systemically administered B12-Ex4 does not induce c-Fos in the AP or the NTS, while central administration of B12-Ex4 and Ex4 similarly produce emesis

Ex4, but not B12-Ex4, induced c-Fos immunofluorescence compared with saline-treated controls within the NTS (Treatment effect  $F_{(2, 10)} = 28.82$ ;  $P < .0001$ ) and AP (Treatment effect  $F_{(2, 10)} = 6.62$ ;  $P < .02$ , Figure 4A,B). ICV administration of Ex4 (0.24 nmol) and B12-Ex4 (0.24 nmol) induced emesis with similar emetogenic profiles. We observed no difference in the percentage of shrews experiencing emesis following central B12-Ex4 or Ex4 administration (Figure 4C). Furthermore, the number of single emetic episodes (Figure 4D), the number of emetic bouts (Figure 4E), as well as the latency to the first emetic response (Figure 4F), were not statistically different between B12-Ex4 and Ex4. ICV administration of aCSF did not induce any emesis in shrews (data not shown).

### 3.5 | Study 5: B12-Ex4 enhances glucose clearance during an OGTT without inducing anorexia and body weight loss in the GK rat

We tested the effects of Ex4, B12-Ex4 and liraglutide on oral glucose tolerance, food intake and body weight in GK rats. Similar to the effects of liraglutide (100  $\mu\text{g}/\text{kg}$ ), B12-Ex4 reduced the glucose level following an OGTT compared with saline at 20 and 40 minutes after

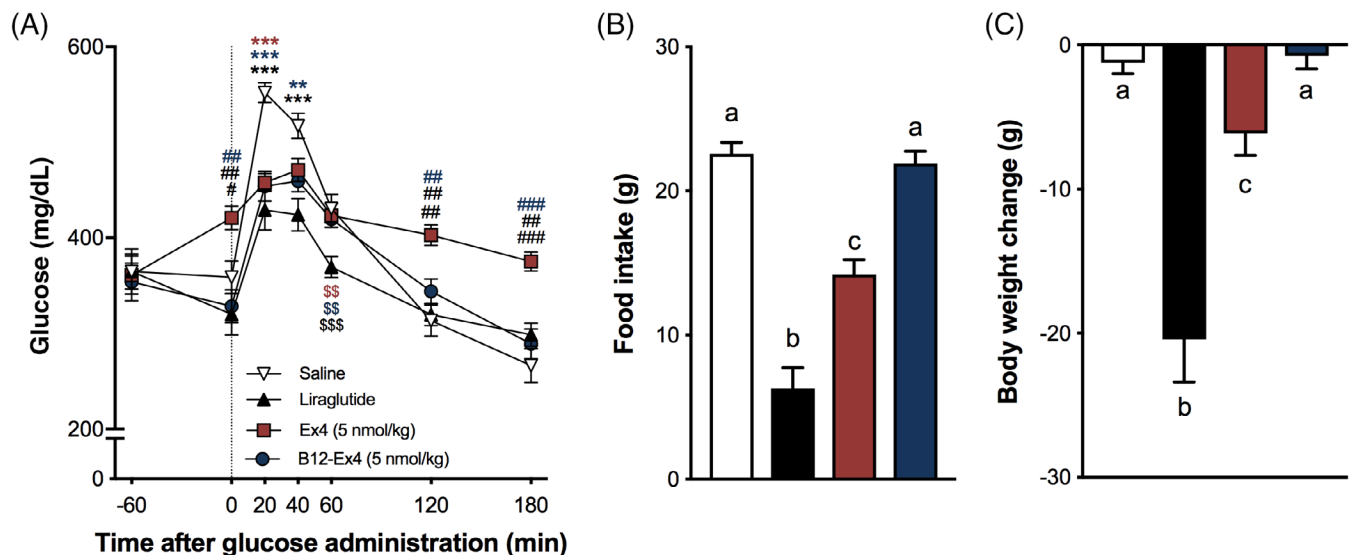


**FIGURE 5** B12-Ex4 enhances glucose clearance during an oral glucose tolerance test (OGTT) without inducing anorexia and body weight loss in the Goto-Kakizaki lean diabetic rat model. (A) In an OGTT, liraglutide (100  $\mu\text{g}/\text{kg}$ , i.e. 26.6 nmol/kg) and 5 nmol/kg B12-Ex4 suppressed blood glucose levels after intraperitoneal (IP) glucose administration (1 g/kg, PO) compared with 5 nmol/kg Ex4 (i.e.  $\sim 20 \mu\text{g}/\text{kg}$ ) and saline. \* saline versus others; #: Ex4 versus others; \$: liraglutide versus others. \*, #, \$:  $P < .05$ ; \*\*, ##, \$\$:  $P < .01$ ; \*\*\*, ###, \$\$\$:  $P < .001$ . (B) Liraglutide and Ex4 induced a strong anorectic effect, which was not observed after B12-Ex4 treatment. (C) Hypophagia was accompanied by body weight loss in liraglutide- and Ex4-treated animals, while no significant body weight change was observed following B12-Ex4. Data were analysed with repeated measure two-way ANOVA (A) or one-way ANOVA (B, C) followed by Tukey post hoc test;  $n = 21$ , within subject. All data are expressed as mean  $\pm$  SEM. Means with different letters are significantly different from each other ( $P < .05$ )

glucose load, and to native Ex4 (5 nmol/kg) at 120 and 180 minutes after glucose load (all  $P < .01$ , Treatment  $\times$  Time interaction  $F_{[18, 360]} = 11.92$ ;  $P < .0001$ , Figure 5A). However, while both liraglutide and native Ex4 suppressed 24 hours food intake leading to 24 hours body weight loss (all  $P < .05$ ), no hypohagic or body weight suppressive effects were observed after B12-Ex4 administration in this lean diabetic model (Treatment effect on food  $F_{(3, 60)} = 95.41$ ;  $P < .0001$ , and Treatment effect on body weight  $F_{(3, 60)} = 28.21$ ;  $P < .0001$ , Figure 5B,C).

## 4 | DISCUSSION

Existing GLP-1-based pharmacotherapies are excellent glucoregulatory drugs for treating hyperglycaemia in the majority of patients with T2D despite reported nausea and vomiting. These phenomena, however, are gaining notoriety as overlooked major side effects in many patients, which reduce patient compliance and make current GLP-1R agonists 'suboptimal'.<sup>3-7,32,33</sup> Designing and testing second-generation GLP-1-based drugs aimed at improving patient tolerance while preserving or enhancing glucoregulatory control therefore provides clear clinical value. Here, we report that a B12-Ex4 conjugate previously shown to exert comparable glycaemic control with limited anorexia and nausea-like effects compared with native Ex4 in rats<sup>9</sup> produced comparable glycaemic control, and better tolerance, in an emetic mammalian species and in a lean polygenetic rat model of T2D.

In line with previous reports in lean, non-diabetic rats and shrews,<sup>9,14,30,31</sup> both native Ex4 doses (5 and 50 nmol/kg) tested here induced anorexia and body weight loss over 24 hours in shrews. By contrast, no such effects occurred after B12-Ex4 treatments, even at supra-pharmacological doses (i.e. 50 nmol/kg). The lack of short-term effects on feeding was unexpected given reports of a role of vagal afferent signalling in the mediation of the early-phase anorexia induced by both GLP-1 and native Ex4 in rats.<sup>34,35</sup> Our previous report also observed this effect in lean, healthy rats treated with the highest dose of B12-Ex4.<sup>9</sup> This incongruity, however, could be explained by broad species differences in metabolism between rats and shrews, rather than by the direct action of the drug.

Furthermore, B12-Ex4 administration resulted in a near complete absence of emesis compared with potent emetic effects of Ex4 in the shrew. In fact, we observed that  $\sim 10$ -fold the threshold concentration necessary for glucoregulation did not cause emesis with B12-Ex4, while all animals tested with this dose of Ex4 experienced emesis. Together, these findings show that it is possible to both physiologically and pharmacologically separate the emetic potential of GLP-1R agonists like Ex4 from their glucoregulatory role, and that a wide range of B12-Ex4 doses produce limited anorectic or emetic side effects. These data suggest that a B12-Ex4 conjugate could improve T2D medication adherence compared with existing GLP-1 mimetic drugs. This is particularly relevant given the pleiotropic nature of GLP-1, with a myriad of effects, mainly beneficial, which render GLP-1 analogues as one of the best current treatments for T2D.

Indeed, alternative therapies approved for the treatment of T2D (e.g. dipeptidyl peptidase-4 inhibitors, metformin and sodium-glucose co-transporter-2 inhibitors) do not achieve the same overall positive outcome on glucose handling compared with GLP-1R agonists. Importantly, these alternative strategies also lead to modest but significant body weight reductions.<sup>36,37</sup>

Preventing access to CNS GLP-1Rs is the probable explanation for the lack of B12-Ex4-induced emesis in the shrew. Our immunohistological evidence supports this notion as we observed sparse c-Fos activation following systemic B12-Ex4 administration in the AP and NTS, two hindbrain nuclei known to mediate feeding behaviour and emesis,<sup>13,38-41</sup> while native Ex4 produced robust activation of these nuclei. To provide functional evidence that B12 conjugation itself does not impact the emetic nature of Ex4, we centrally administered B12-Ex4 directly into the lateral ventricle of the shrew, which produced a comparable emetic profile with that of native Ex4 (e.g. the number of emetic episodes, latency to vomit, and the proportion of treated animals experiencing emesis). These data suggest that when centrally delivered, and thus bypassing the blood-brain barrier, B12-Ex4 is a stimulus that can produce an emetic profile consistent with Ex4 alone.

To speculate how conjugation to B12 reduces CNS penetrance of Ex4, increased polarity may be an important variable rather than the increased molecular size alone, given that GLP-1R agonists with greater molecular masses, such as liraglutide, have been shown to penetrate into the hindbrain and to stimulate direct GLP-1R activation.<sup>30,42,43</sup> It is also possible that the binding of B12-Ex4 to the B12 carrier proteins transcobalamin (TC) or haptocorrin (HC) in serum, previously confirmed for this construct,<sup>9</sup> further reduces brain penetrance because its size (now  $>60$  kDa) either actively transports the conjugate to systemic targets (via TC), maintains the conjugate in serum (via HC), or protects the conjugate from proteolytic degradation (via TC or HC),<sup>8</sup> as is typical for dietary B12 alone.<sup>44</sup> As noted, however, the shrew has both TC and HC, unlike rodents, which have only TC. In comparison with studies performed for B12-Ex4 in rodents,<sup>9</sup> we see comparable pharmacodynamics (in terms of illness behaviours and glucoregulation), suggesting that the presence of both TC and HC is not specifically necessary for the conjugate. It may be that the benefits of conjugation lie solely with the B12 molecule itself, or simply through the effects of binding to any B12 binding protein in terms of protection and/or mitigation of hindbrain access. Our data suggest that it is the unique structure of B12-Ex4, rather than simply mass, which drives its unique pharmacodynamic profile and underlying properties.

Pancreatic  $\beta$ -cells expressing the GLP-1R represent the probable cellular substrate mediating the hypoglycaemic effects of B12-Ex4 in shrews. Our proof of concept (via microscopy) shows that a fluorescently tagged B12-Ex4 conjugate (Cy5-B12-Ex4) co-localizes with insulin in the shrew pancreatic  $\beta$ -cells. By employing fluorescently tagged Ex4 in combination with Cy5-B12-Ex4, further investigations are warranted to examine the binding specificity of B12-Ex4 in the pancreas. Nevertheless, the current data support our previous work in rodents<sup>9</sup> and strengthen the notion that the incretin effect occurring



after GLP-1 analogue administration is mediated by direct activation of GLP-1Rs expressed on pancreatic  $\beta$ -cells, mimicking the paracrine actions of pancreatic-derived GLP-1.<sup>10–12</sup>

It is also possible that GLP-1Rs expressed in other peripheral tissues may be engaged by B12-Ex4 and thus contribute to its beneficial effects on glucose homeostasis. For instance, it has been shown that low doses of Ex4 that mimic endogenous GLP-1 release can modulate glycaemia and gastric emptying via vagal afferent signalling.<sup>35</sup> Further, GLP-1Rs are also abundantly expressed on enteric neurons, and emerging evidence suggests a role of the enteric nervous system in the mediation of effects induced by GLP-1 analogues.<sup>45–48</sup> Whether B12-Ex4 acts on GLP-1Rs expressed in the periphery beyond the pancreas, possibly within the peripheral and enteric nervous system, and to what degree these hypothetical actions contribute to the observed augmented glucoregulation, requires further investigation.

We also report that B12-Ex4 improves glucose clearance relative to Ex4 in a lean, polygenetic model of T2D, the GK rat. Similar to liraglutide, B12-Ex4 does not produce the transient stress-induced hyperglycaemic response in the GK rat commonly observed from Ex4 across rat models (lean, obese or GK),<sup>49,50</sup> a phenomenon tied to the high CNS penetrance of Ex4. Consistent with the lack of a CNS stress-mediated hyperglycaemia reported for Ex4,<sup>49,50</sup> B12-Ex4 did not produce the documented CNS-dependent outcomes of anorexia and body weight loss in this lean model of T2D.

In summary, the data presented here in shrews and GK rats support our hypothesis that limiting or blocking Ex4 entry into the brain dramatically reduces the side effects of the Ex4 drug (i.e. prevents anorexia and emesis), while maintaining the glucoregulatory efficacy of the compound. The overall outcomes of this work highlight the translational potential of B12-Ex4-based pharmacotherapies for use in lean T2D patients where weight loss is an undesirable outcome, although chronic studies are needed to elucidate the efficacy, tolerability and pharmacodynamics of B12-Ex4 in long-term treatment. Albeit small, there is the possibility that B12-Ex4 chronic exposure would interfere with normal B12 physiology, potentially reducing the amount of dietary B12 available in the body.<sup>51</sup> Further, while we do not predict tachyphylaxis, the extent to which the observed positive effects will be maintained requires future empirical testing. Nonetheless, the current data underlie the potential use of B12-Ex4 for patients with T2D who either do not tolerate current GLP-1 agonists or suffer from co-morbidities associated with an anorectic/cachectic state, for which the body weight-suppressing effects of a standard GLP-1R agonist are an unwanted side effect, with the loss of nausea/emesis an additional benefit.

## ACKNOWLEDGMENTS

The authors would like to thank Sam Fortin and Rinzin Lhamo for technical assistance. This work was supported by NIH-DK-112812 (B.C.D.), NIH-DK-097675 (R.P.D.), NIH-DK-115762 (M.R.H.), SNF P2ZHP3\_178114, P400PB\_186728 (T.B.) and NIH-CA-201962 (C.C.H.).

## CONFLICTS OF INTEREST

BCD receives research funding from Eli Lilly & Co. and Pfizer, Inc. and provided remunerated consultancy services for Pfizer Inc. not supporting these studies. RPD is a scientific advisory board member and received funds from Xeragenx LLC (St. Louis, NY) and Balchem, New Hampton, New York, which were not used in support of these studies. MRH receives research funding from Zealand Pharma, Novo Nordisk, Eli Lilly & Co. and Boehringer Ingelheim that was not used in support of these studies. RPD is an inventor of the patents associated with this work. The other authors have no competing interests to declare.

## AUTHOR CONTRIBUTIONS

BCDJ, TB, RPD, and MRH conceived the project. BCDJ, TB and MRH conceptualized the hypotheses and designed the experiments. RPD and ICT designed and synthesized the compounds. TB, ICT, EDS and LMS conducted experiments and collected data. TB, BCDJ, RPD and MRH analyzed the data. TB, BCDJ, RPD and MRH wrote the manuscript. All authors edited the manuscript. BCDJ and RPD are guarantors for this work.

## ORCID

Matthew R. Hayes  <https://orcid.org/0000-0001-9782-6551>

Robert P. Doyle  <https://orcid.org/0000-0001-6786-5656>

Bart C. De Jonghe  <https://orcid.org/0000-0002-6980-5355>

## REFERENCES

1. Sanger GJ, Andrews PLR. A history of drug discovery for treatment of nausea and vomiting and the implications for future research. *Front Pharmacol.* 2018;9:913.
2. Htike ZZ, Zaccardi F, Papamargaritis D, Webb DR, Khunti K, Davies MJ. Efficacy and safety of glucagon-like peptide-1 receptor agonists in type 2 diabetes: a systematic review and mixed-treatment comparison analysis. *Diabetes Obes Metab.* 2017;19(4): 524–536.
3. Bergenstal RM, Wysham C, Macconell L, et al. Efficacy and safety of exenatide once weekly versus sitagliptin or pioglitazone as an adjunct to metformin for treatment of type 2 diabetes (DURATION-2): a randomised trial. *Lancet.* 2010;376(9739):431–439.
4. Buse JB, Henry RR, Han J, Kim DD, Fineman MS, Baron AD. Effects of exenatide (exendin-4) on glycemic control over 30 weeks in sulfonylurea-treated patients with type 2 diabetes. *Diabetes Care.* 2004;27(11):2628–2635.
5. DeFronzo RA, Ratner RE, Han J, Kim DD, Fineman MS, Baron AD. Effects of exenatide (exendin-4) on glycemic control and weight over 30 weeks in metformin-treated patients with type 2 diabetes. *Diabetes Care.* 2005;28(5):1092–1100.
6. John LE, Kane MP, Busch RS, Hamilton RA. Expanded use of exenatide in the management of type 2 diabetes. *Diabetes Spectr.* 2007;20:59–63.
7. Kendall DM, Riddle MC, Rosenstock J, et al. Effects of exenatide (exendin-4) on glycemic control over 30 weeks in patients with type 2 diabetes treated with metformin and a sulfonylurea. *Diabetes Care.* 2005;28(5):1083–1091.
8. Bonaccorso RL, Chepurny OG, Becker-Pauly C, Holz GG, Doyle RP. Enhanced peptide stability against protease digestion induced by intrinsic factor binding of a vitamin B12 conjugate of exendin-4. *Mol Pharm.* 2015;12(9):3502–3506.

9. Miettlicki-Baase EG, Liberini CG, Workinger JL, et al. A vitamin B12 conjugate of exendin-4 improves glucose tolerance without associated nausea or hypophagia in rodents. *Diabetes Obes Metab*. 2018;20(5):1223-1234.
10. Lamont BJ, Li YZ, Kwan E, Brown TJ, Gaisano H, Drucker DJ. Pancreatic GLP-1 receptor activation is sufficient for incretin control of glucose metabolism in mice. *J Clin Invest*. 2012;122(1):388-402.
11. Smith EP, An Z, Wagner C, et al. The role of beta cell glucagon-like peptide-1 signaling in glucose regulation and response to diabetes drugs. *Cell Metab*. 2014;19(6):1050-1057.
12. Chambers AP, Sorrell JE, Haller A, et al. The role of pancreatic proglucagon in glucose homeostasis in mice. *Cell Metab*. 2017;25(4):927-934.
13. Kanoski SE, Rupprecht LE, Fortin SM, De Jonghe BC, Hayes MR. The role of nausea in food intake and body weight suppression by peripheral GLP-1 receptor agonists, exendin-4 and liraglutide. *Neuropharmacology*. 2012;62(5-6):1916-1927.
14. Chan SW, Lin G, Yew DT, Yeung CK, Rudd JA. Separation of emetic and anorexic responses of exendin-4, a GLP-1 receptor agonist in *Suncus murinus* (house musk shrew). *Neuropharmacology*. 2013;70:141-147.
15. Chan SW, Lin G, Yew DT, Rudd JA. A physiological role of glucagon-like peptide-1 receptors in the central nervous system of *Suncus murinus* (house musk shrew). *Eur J Pharmacol*. 2011;668(1-2):340-346.
16. Andersen A, Lund A, Knop FK, Vilsboll T. Glucagon-like peptide 1 in health and disease. *Nat Rev Endocrinol*. 2018;14(7):390-403.
17. Bray GA, Fruhbeck G, Ryan DH, Wilding JP. Management of obesity. *Lancet*. 2016;387(10031):1947-1956.
18. Gallo M, Muscogiuri G, Felicetti F, et al. Adverse glycaemic effects of cancer therapy: indications for a rational approach to cancer patients with diabetes. *Metabolism*. 2018;78:141-154.
19. Moheet A, Moran A. CF-related diabetes: containing the metabolic miscreant of cystic fibrosis. *Pediatr Pulmonol*. 2017;52:S37-S43.
20. Noubissi EC, Katte JC, Sobngwi E. Diabetes and HIV. *Curr Diab Rep*. 2018;18(11):125.
21. Glaser S, Kruger S, Merkel M, Bramlage P, Herth FJ. Chronic obstructive pulmonary disease and diabetes mellitus: a systematic review of the literature. *Respiration*. 2015;89(3):253-264.
22. Mesinovic J, Zengin A, De Courten B, Ebeling PR, Scott D. Sarcopenia and type 2 diabetes mellitus: a bidirectional relationship. *Diabetes Metab Syndr Obes*. 2019;12:1057-1072.
23. Caspard H, Jabbour S, Hammar N, Fenici P, Sheehan JJ, Kosiborod M. Recent trends in the prevalence of type 2 diabetes and the association with abdominal obesity lead to growing health disparities in the USA: an analysis of the NHANES surveys from 1999 to 2014. *Diabetes Obes Metab*. 2018;20(3):667-671.
24. Goto Y, Kakizaki M, Masaki N. Production of spontaneous diabetic rats by repetition of selective breeding. *Tohoku J Exp Med*. 1976;119(1):85-90.
25. Ostenson CG, Efendic S. Islet gene expression and function in type 2 diabetes; studies in the Goto-Kakizaki rat and humans. *Diabetes Obes Metab*. 2007;9((Suppl 2)):180-186.
26. Ueno S, Matsuki N, Saito H. *Suncus murinus*: a new experimental model in emesis research. *Life Sci*. 1987;41(4):513-518.
27. Andrews PL, Friedman MI, Liu YL, Smith JE, Sims DW. Potential energetic implications of emesis in the house musk shrew (*Suncus murinus*). *Physiol Behav*. 2005;84(4):519-524.
28. Nasir S, Aguilar D. Congestive heart failure and diabetes mellitus: balancing glycemic control with heart failure improvement. *Am J Cardiol*. 2012;110(9 Suppl):50B-57B.
29. Borner T, Shaulson ED, Ghidewon MY, et al. GDF15 induces anorexia through nausea and emesis. *Cell Metab*. 2020.31(2):351-362.
30. Kanoski SE, Fortin SM, Arnold M, Grill HJ, Hayes MR. Peripheral and central GLP-1 receptor populations mediate the anorectic effects of peripherally administered GLP-1 receptor agonists, liraglutide and exendin-4. *Endocrinology*. 2011;152(8):3103-3112.
31. Hayes MR, Kanoski SE, Alhadeff AL, Grill HJ. Comparative effects of the long-acting GLP-1 receptor ligands, liraglutide and exendin-4, on food intake and body weight suppression in rats. *Obesity*. 2011;19(7):1342-1349.
32. Zhao P, Liang YL, Belousoff MJ, et al. Activation of the GLP-1 receptor by a non-peptidic agonist. *Nature*. 2020;577(7790):432-436.
33. Aroda VR, Rosenstock J, Terauchi Y, et al. PIONEER 1: randomized clinical trial of the efficacy and safety of oral semaglutide monotherapy in comparison with placebo in patients with type 2 diabetes. *Diabetes Care*. 2019;42(9):1724-1732.
34. Labouesse MA, Stadlbauer U, Weber E, Arnold M, Langhans W, Pacheco-Lopez G. Vagal afferents mediate early satiation and prevent flavour avoidance learning in response to intraperitoneally infused exendin-4. *J Neuroendocrinol*. 2012;24(12):1505-1516.
35. Krieger JP, Arnold M, Pettersen KG, Lossel P, Langhans W, Lee SJ. Knockdown of GLP-1 receptors in vagal afferents affects normal food intake and glycemia. *Diabetes*. 2016;65(1):34-43.
36. Brunton S. GLP-1 receptor agonists vs. DPP-4 inhibitors for type 2 diabetes: is one approach more successful or preferable than the other? *Int J Clin Pract*. 2014;68(5):557-567.
37. Liu J, Hu Y, Xu Y, Jia Y, Miao L, Wang G. Comparison of exenatide and metformin monotherapy in overweight/obese patients with newly diagnosed type 2 diabetes. *Int J Endocrinol*. 2017;2017:9401606.
38. Hornby PJ. Central neurocircuitry associated with emesis. *Am J Med*. 2001;111((Suppl 8A)):106S-112S.
39. Miller AD, Leslie RA. The area postrema and vomiting. *Front Neuroendocrinol*. 1994;15(4):301-320.
40. Grill HJ, Hayes MR. The nucleus tractus solitarius: a portal for visceral afferent signal processing, energy status assessment and integration of their combined effects on food intake. *Int J Obes*. 2009;33((Suppl 1)):S11-S15.
41. Price CJ, Hoyda TD, Ferguson AV. The area postrema: a brain monitor and integrator of systemic autonomic state. *Neuroscientist*. 2008;14(2):182-194.
42. Sisley S, Gutierrez-Aguilar R, Scott M, D'Alessio DA, Sandova DA, Seeley RJ. Neuronal GLP1R mediates liraglutide's anorectic but not glucose-lowering effect. *J Clin Invest*. 2014;124(6):2456-2463.
43. Secher A, Jelsing J, Baquero AF, et al. The arcuate nucleus mediates GLP-1 receptor agonist liraglutide-dependent weight loss. *J Clin Invest*. 2014;124(10):4473-4488.
44. Green R, Allen LH, Bjorke-Monsen AL, et al. Vitamin B12 deficiency. *Nat Rev Dis Primers*. 2017;3:17040.
45. Richards P, Parker HE, Adriaenssens AE, et al. Identification and characterization of GLP-1 receptor-expressing cells using a new transgenic mouse model. *Diabetes*. 2014;63(4):1224-1233.
46. Varin EM, Mulvihill EE, Baggio LL, et al. Distinct neural sites of GLP-1R expression mediate physiological versus pharmacological control of incretin action. *Cell Rep*. 2019;27(11):3371-3384.
47. Drucker DJ. Mechanisms of action and therapeutic application of glucagon-like peptide-1. *Cell Metab*. 2018;27(4):740-756.
48. Washington MC, Raboin SJ, Thompson W, Larsen CJ, Sayegh AI. Exenatide reduces food intake and activates the enteric nervous system of the gastrointestinal tract and the dorsal vagal complex of the hind-brain in the rat by a GLP-1 receptor. *Brain Res*. 2010;1344:124-133.
49. Gao W, Jusko WJ. Pharmacokinetic and pharmacodynamic modeling of exendin-4 in type 2 diabetic Goto-Kakizaki rats. *J Pharmacol Exp Ther*. 2011;336(3):881-890.

50. Perez-Tilve D, Gonzalez-Matias L, Aulinger BA, et al. Exendin-4 increases blood glucose levels acutely in rats by activation of the sympathetic nervous system. *Am J Physiol Endocrinol Metab.* 2010;298(5): E1088-E1096.
51. Lildballe DL, Mutti E, Birn H, Nexø E. Maximal load of the vitamin B12 transport system: a study on mice treated for four weeks with high-dose vitamin B12 or cobinamide. *PLoS One.* 2012;7(10): e46657.

**How to cite this article:** Borner T, Shaulson ED, Tinsley IC, et al. A second-generation glucagon-like peptide-1 receptor agonist mitigates vomiting and anorexia while retaining glucoregulatory potency in lean diabetic and emetic mammalian models. *Diabetes Obes Metab.* 2020;22: 1729–1741. <https://doi.org/10.1111/dom.14089>

ARTICLE

Open Access

# Dorsal vagal complex and hypothalamic glia differentially respond to leptin and energy balance dysregulation

Lauren M. Stein<sup>1</sup>, Rinzin Lhamo<sup>1</sup>, Anh Cao<sup>1</sup>, Jayme Worker<sup>2</sup>, Ian Tinsley<sup>2</sup>, Robert P. Doyle<sup>2</sup>, Harvey J. Grill<sup>3</sup>, Gerlinda E. Hermann<sup>4</sup>, Richard C. Rogers<sup>4</sup> and Matthew R. Hayes<sup>1</sup>

## Abstract

Previous studies identify a role for hypothalamic glia in energy balance regulation; however, a narrow hypothalamic focus provides an incomplete understanding of how glia throughout the brain respond to and regulate energy homeostasis. We examined the responses of glia in the dorsal vagal complex (DVC) to the adipokine leptin and high fat diet-induced obesity. DVC astrocytes functionally express the leptin receptor; *in vivo* pharmacological studies suggest that DVC astrocytes partly mediate the anorectic effects of leptin in lean but not diet-induced obese rats. *Ex vivo* calcium imaging indicated that these changes were related to a lower proportion of leptin-responsive cells in the DVC of obese versus lean animals. Finally, we investigated DVC microglia and astroglia responses to leptin and energy balance dysregulation *in vivo*: obesity decreased DVC astrogliosis, whereas the absence of leptin signaling in Zucker rats was associated with extensive astrogliosis in the DVC and decreased hypothalamic micro- and astrogliosis. These data uncover a novel functional heterogeneity of astrocytes in different brain nuclei of relevance to leptin signaling and energy balance regulation.

## Introduction

The development of efficacious weight management therapies to treat obesity requires a broader understanding of the underlying biological basis of obesity. Current knowledge regarding the neural circuitry that regulates energy balance is limited, due in part to an incomplete characterization of the participation of non-neuronal cells such as glia. There are four known types of glia cells found within the central nervous system (CNS); astrocytes, oligodendrocytes, microglia, and ependymal cells. These glia cells represent an important potential target for the treatment of obesity and obesity-related disorders. Astrocytes are the most abundant glia cell type in the mammalian CNS<sup>1</sup>. Rather than acting as passive

supporters of neuronal function, modern neuroscience widely acknowledges the dependence of neurons on astrocytes for synaptic efficiency and neuronal excitability (reviewed in ref. <sup>2</sup>). Astrocytes participate in numerous CNS functions including assisting in the transport of circulating factors across the blood-brain barrier<sup>3,4</sup>, regulation of synaptic glutamate levels<sup>5</sup> and the release of gliotransmitters<sup>6</sup> that participate in neurotransmission (reviewed in ref. <sup>2</sup>). Despite our growing appreciation of this bidirectional communication between astrocytes and neurons<sup>7</sup>, the specific, and likely heterogeneous, role of astrocytes in energy balance regulation is understudied.

To date, much of our knowledge about the roles of glia in the control of food intake and body weight regulation comes from seminal work in the hypothalamus. Indeed, hypothalamic astrocytes detect and transport nutrients<sup>8–10</sup>, aid in the development and plasticity of metabolic circuitry<sup>11,12</sup> and respond to an array of neuropeptides and metabolic hormones such as the adipokine hormone

Correspondence: Matthew R. Hayes ([hayesmr@penmedicine.upenn.edu](mailto:hayesmr@penmedicine.upenn.edu))

<sup>1</sup>Department of Psychiatry, University of Pennsylvania School of Medicine, Philadelphia, PA, USA

<sup>2</sup>Department of Chemistry, Syracuse University, Syracuse, NY, USA

Full list of author information is available at the end of the article

© The Author(s) 2020



**Open Access** This article is licensed under a Creative Commons Attribution 4.0 International License, which permits use, sharing, adaptation, distribution and reproduction in any medium or format, as long as you give appropriate credit to the original author(s) and the source, provide a link to the Creative Commons license, and indicate if changes were made. The images or other third party material in this article are included in the article's Creative Commons license, unless indicated otherwise in a credit line to the material. If material is not included in the article's Creative Commons license and your intended use is not permitted by statutory regulation or exceeds the permitted use, you will need to obtain permission directly from the copyright holder. To view a copy of this license, visit <http://creativecommons.org/licenses/by/4.0/>.

leptin<sup>13–15</sup>. Some research hypothesizes that, as the resident immunocompetent cells of the brain<sup>16</sup>, microglia partially drive obesity-associated “neuroinflammation”. This hypothesis is supported by the observed association between the activation and proliferation of glia cells (defined as gliosis) in the hypothalamus and obesity-induced hypothalamic inflammatory cytokines (often overstated as “neuroinflammation”)<sup>17–20</sup>. Moreover, in rats susceptible to diet-induced obesity, there is significant hypothalamic inflammation<sup>21</sup> and glia-mediated synaptic reorganization favoring orexigenic signaling<sup>22</sup>. Several studies further ascribe obesity-associated inflammation in the hypothalamus to alternations in leptin signaling at its cognate receptor (LepR). Indeed, leptin-deficient Ob/Ob mice exhibit profound hypothalamic gliosis when maintained on a high-fat diet<sup>23,24</sup>. The interactions of high-fat diet, leptin signaling, and neuroinflammation described in the medial hypothalamus and its relevance to energy balance regulation are largely uninvestigated in other key nuclei. Given that the neural control of energy balance is not restricted to the hypothalamic subnuclei, but rather is distributed throughout the brain<sup>25,26</sup>, an investigation of the role of glia in extra-hypothalamic nuclei governing energy balance may provide insight into the central dysregulation of diet-induced obesity, as well as the relationship between leptin and astrogliosis.

Looking beyond the hypothalamus, the dorsal vagal complex (DVC) of the caudal brainstem represents another CNS node in the detection, integration, and processing of numerous metabolic and endocrine signals, including leptin<sup>27–29</sup>. The DVC is comprised of the nucleus tractus solitarius (NTS), area postrema (AP), and dorsal motor nucleus of the vagus. Leptin receptor signaling in the DVC suppresses food intake and most notably potentiates the intake suppressive effects of within-meal gastrointestinally derived satiation signals (e.g., gastric distension and cholecystokinin)<sup>28,30–34</sup>. Despite a clear role for the DVC in energy homeostasis, very few studies characterize the specific cellular phenotypes that express LepR in the DVC. Evidence of LepR expression on NTS astrocytes<sup>35</sup> led to the current hypothesis investigated here, that DVC glia are a prime cellular target for central leptin signaling. We investigated the expression of LepR on astrocytes in the DVC and assessed the role of DVC astrocytes in mediating the anorectic effects of leptin. Moreover, we examine the influence of obesity and perturbations in leptin signaling on the glia landscape in both the DVC and hypothalamus.

## Materials and methods

### Animals

Male Sprague Dawley rats (250–265 g, Charles River (UPenn) or Envigo (PBRC)) were maintained on either standard chow (Purina Rodent Chow 5001; Ralston

Purina Company, St. Louis, Missouri) or a 60% high-fat diet (HFD; Rodent Diet D12492; Research Diets, New Brunswick, New Jersey) with ad libitum access to tap water. Zucker diabetic fatty rats (ZDF; Charles River) were maintained on a standard chow diet. Animals were single-housed in hanging wire cages in a temperature- and humidity-controlled environment on a reverse 12h:12h light-dark cycle. All behavioral experiments were carried out in a counter-balanced, within-subjects design, no randomization required. All experimental procedures were conducted with the approval of the University of Pennsylvania and Pennington Biomedical Research Center Institutional Animal Care and Use Committees.

### Stereotaxic surgeries

Rats were anesthetized with an intramuscular injection of ketamine (90 mg/kg; Butler Schein), xylazine (2.7 mg/kg; Midwest Veterinary Supply), and acepromazine (0.64 mg/kg; Midwest Veterinary Supply). Using stereotaxic surgery, rats were implanted with an indwelling cannula (26-gauge; Plastics One) directed at the 4th cerebroventricle (4V; coordinates: on midline, 2.5 mm anterior to the occipital suture and 7.2 mm ventral to the skull<sup>36</sup>). Postoperative analgesia (2 mg/kg meloxicam) was administered subcutaneously for 2 days, and animals were allowed to recover for one week. Proper placement and cannula patency were verified before behavioral testing via 5-thio-D-glucose (210 µg)-induced hyperglycemia as previously described<sup>37</sup>; only animals that passed verification were tested.

### Synthesis and administration of Cy5-labeled leptin

Recombinant mouse leptin (2.0 mg; NHPP) was dissolved in 500 µL of 50 mM phosphate buffer (pH 7.4) and gently rocked in non-stick Eppendorf tubes (Thermo Scientific, Cat no. 3451). A quantity of 0.2 mg sulfo-cyanine 5 NHS ester (Lumiprobe, Cat no. 23320) was dissolved in 50 µL DMSO and then added to the pre-dissolved leptin in 10-µL aliquots over 1 h. The reaction was stirred at ambient temperature overnight then purified using a Shimadzu Prominence HPLC with a C18 column (Eclipse XDB-C18 5µm, 4.6 x 150 mm) and a gradient of [1% CH<sub>3</sub>CN/H<sub>2</sub>O + 0.1% to TFA] to [70% CH<sub>3</sub>CN/H<sub>2</sub>O + 0.1% to TFA] over 15 min. The product was obtained with a  $\sim T_R$  of 10 min at 98% purity, lyophilized, and stored at  $-20^\circ\text{C}$ . Electronic absorption spectra were obtained on a Varian Cary 50 Bio spectrophotometer in a 2 mL quartz cuvette between 500–800 nm in aqueous acetonitrile. An absorption maximum was identified at 651 nm. Fluorescence spectra were obtained on an Agilent Cary Eclipse Fluorescence Spectrophotometer in a 2 mL cuvette between 500–800 nm in aqueous acetonitrile. The instrument was used in fluorescence mode with the excitation slit at 5 nm and emission slit at 5 nm. Excitation occurred at 651 nm



with an emission maximum at 669 nm. SDS-PAGE was performed using an Invitrogen Mini-cell GEL Surelock Cell Module with 12% tris-glycine gel in SDS running buffer. Protein masses were identified using the Precision Plus Protein Kaleidoscope pre-stained protein standard (BioRad, Cat no. 1610375) (Supplementary Fig. 1). A standard chow-fed male rat with an indwelling 4V cannula received a single icv injection of 4.5 ng (3  $\mu$ L at 1.5 ng/mL) fluorescently labeled leptin (Cy5-Lep) dissolved in 0.1 M PBS, pH 7.4. An hour later, the rat was anesthetized, transcardially perfused, and harvested for brain removal and IHC processing as described below. Images acquired with Leica SP5 X confocal microscope using 63x oil-immersion objective with 405, 488, 647 laser lines. Image z-stacks were collected with a step size of 1  $\mu$ m and processed using Imaris 8.1.2 software (Bitplane).

#### Fluorescent in situ hybridization of astrocytic LepR

For verification of the leptin receptor on rat DVC astrocytes, a single animal ( $n = 1$ ) was anesthetized for rapid removal of the brain and flash frozen in isopentane over dry ice. The brain was sectioned on a cryostat at 18  $\mu$ m thickness, slide mounted, and stored at  $-80^{\circ}\text{C}$ . Fluorescent in situ hybridization (FISH) was performed using the RNAscope Multiplex Fluorescent Reagent kit v2 (Cat no. 323100; ACDBio, Hayward, CA) per manufacturer instructions. Detection was carried out using probes designed by ACDBio for LepR mRNA (Rn-LepR-C1, Cat no. 415951), the astrocyte-specific marker Aldh1L1 (Rn-Aldh1L1-C2, Cat no. 459821-C2), and the neuronal marker RbFox3 (Rn-RbFox3-C3, Cat no. 436351-C3). Following a series of amplification steps, sections were mounted with DAPI-containing mounting media (Fluorogel; Fischer Scientific). Sections were visualized with a Leica SP5 X confocal microscope with a 40x objective. Image z-stacks were collected with a step size of 1  $\mu$ m. Collected z-stack images were processed using Imaris 8.1.2 software (Bitplane).

#### Live cell $\text{Ca}^{+2}$ imaging of neurons and astrocytes in NTS slice preparations

Male Sprague Dawley rats (290–420 g; chow  $n = 4$ , HFD  $n = 3$ ) were deeply anesthetized with urethane (1.5 g/kg, intraperitoneal; ethyl carbamate, Sigma; this anesthetic was selected because it readily washes out of ex vivo slices<sup>38</sup>) and placed in a stereotaxic frame. Using aseptic technique, 4 unilateral injections (40 nL each) of 0.4% Cal520 (AAT Bioquest), 0.3% sulforhodamine 101 (SR101; Sigma Chemical) and 10% pluronic-DMSO (F-127, Invitrogen) in normal Krebs solution were administered into the medial NTS. After 60 min, rats were decapitated, and the brainstem was quickly harvested. Pre-labeled brainstems were cut into 300- $\mu$ m coronal sections using a vibrating microtome (Leica VT1200) and submerged in

cold ( $\sim 4^{\circ}\text{C}$ ) carboxygenated (95%  $\text{O}_2$ ; 5%  $\text{CO}_2$ ) cutting solution. NTS slices were placed in normal Krebs' solution and bubbled with 95%  $\text{O}_2$ /5%  $\text{CO}_2$  at a constant temperature of  $29^{\circ}\text{C}$ . Sections were allowed equilibrate for 1 h prior to imaging<sup>39</sup>.

Live cell calcium imaging of pre-labeled neurons and astrocytes was performed as previously described<sup>39–41</sup>. Cal-520/SR101 pre-labeled slices were transferred to a custom imaging chamber<sup>42</sup>. Immunohistochemical confirmation of SR101 specificity to astrocytes in the DVC was previously reported<sup>43</sup>. The recording chamber was continuously perfused at a rate of 2.5 mL/min with normal Krebs' (or containing 100ng/mL leptin) solution at a constant temperature of  $33^{\circ}\text{C}$ . Hindbrain slices were viewed with a Zeiss Axioskop 2 fixed stage microscope equipped with normal epifluorescence optics, a Yokogawa CSU21 laser confocal scan head, and a Hamamatsu ORCA-ER camera. Pre-labeled cells of interest were selected visually with epifluorescence optics and subsequently confocal images were captured with the ORCA-ER camera at the rate of 1 frame per second.

Once in the recording chamber, hindbrain slices were perfused with normal Krebs' solution for a minimum of 10 min. Dual exposure images (i.e., 488 nm and 591 nm) were collected just prior to each experimental trial in order to confirm the cell types being recorded. All slices were then challenged with a cocktail of 100  $\mu$ M ATP and 500  $\mu$ M glutamate to determine which cells in the field were viable<sup>39,44</sup>. Viability was defined as a minimum increase in fluorescence of 7% in response to the ATP/glutamate challenge<sup>45</sup>. Next, slices were exposed to Krebs' solution plus 100 ng/mL leptin for 30 s. Changes in intracellular calcium concentrations in response to leptin stimuli within Cal-520 pre-labeled NST astrocytes and neurons were recorded simultaneously using the 488-nm laser line to excite the Cal-520. Increases in intracellular calcium concentrations were identified as an increase in fluorescence and interpreted to represent increased cellular activity. During experimental trials, time-lapse images of mixed fields of NTS astrocytes and neurons were monitored for responses to the leptin challenge. Time-lapse laser confocal images of changes in intracellular calcium levels of both astrocytes and neurons were captured with the ORCA-ER at a rate of 1 frame per second.

#### Behavioral experiments

Rats were maintained on either standard chow ( $n = 10$ ) or a high-fat diet for 2 weeks ( $n = 7$ ). All animals were implanted with a cannula directed at the 4th ventricle (4V) to allow for intracerebroventricular (icv) administration. The recovery period was 1 week, during which time placement of the cannula was verified with a hyperglycemic response to 5-TG<sup>46,47</sup>. Food hoppers were removed, and animals were weighed approximately 1 h

before dark onset. Thirty min before dark onset, animals received 4V icv vehicle (0.1 M PBS) or 50 nmol fluorocitrate pretreatment (Sigma Aldrich<sup>40,48–50</sup>) followed by vehicle (0.1 M NaHCO<sub>3</sub>) or 5 µg/mL leptin (NHPP<sup>51</sup>). Fluorocitrate is a well-established pharmacologic agent used to transiently inhibit the Krebs's cycle in an astrocyte-specific manner<sup>48,50,52–54</sup>. The selected dose of 50nmol fluorocitrate is established to be astrocyte-specific<sup>40,48</sup>. At dark onset, food hoppers were replaced and cumulative food intake was recorded at 1, 3, 6, and 24 h. Body weights were recorded at 0 and 24 h after injection. Experimental injections were separated by a 72 h washout period.

### Immunohistochemical analysis of gliosis

Rats were placed on either a standard chow ( $n = 6$ ) or a high-fat diet ( $n = 6$ ) for 8 weeks. Food intake and body weights were recorded every 48 h. After the 8-week period, anesthetized animals were transcardially perfused with 0.1 M sodium phosphate buffer (PBS; pH 7.4) followed by 4% paraformaldehyde (4% PFA) in 0.1 M PBS, pH 7.4. Brains were removed and stored in 4% PFA overnight at 4 °C, then transferred to a 20% sucrose solution in 0.1 M PBS. Brains were flash frozen in hexane over dry ice. Subsequently, the DVC and hypothalamus were sectioned coronally at 30 µm. Free-floating serial sections were processed for immunohistochemical detection of glia fibrillary acidic protein (GFAP; astrocyte activation marker<sup>18,55</sup>) and ionized calcium binding adaptor molecule 1 (Iba1; microglia marker<sup>56</sup>) as follows. Sections were washed 3 times for 5 min each in 0.1 M PBS, incubated in 10 mM sodium citrate buffer solution (Sigma Aldrich) for 30 min at 90 °C, then washed an additional 3 times in 0.1 M PBS containing 0.2% Triton-X (Sigma Aldrich). Next, sections were incubated in 5% normal donkey serum (NDS; Jackson ImmunoResearch) and 0.2% Triton-X in 0.1 M PBS for 1 h at RT, then incubated overnight at 4 °C in an antibody mixture of 1:1000 chicken anti-GFAP (Millipore, Cat no. AB5541) and 1:500 rabbit anti-Iba1 (Wako; Cat no. 019-19741) in blocking buffer. Following wash steps, sections were incubated for 2 h in secondary antibody mixture of 1:500 donkey anti-chicken Alexa 594 (Jackson ImmunoResearch) and 1:500 donkey anti-rabbit Alexa 488 (Jackson ImmunoResearch). Sections were mounted to Superfrost Plus slides (Fisher Scientific) with Fluorogel DAPI-containing mounting media (Fischer Scientific). Images were acquired using a Keyence BZ-X800 fluorescent microscope under a 20x or 40x objective as 1-µm z-stack images. Z-stack images were compressed using standard full focus and background subtraction. During image capture and analysis, investigator was blinded regarding corresponding diet cohort. Quantification was done using FIJI software. The integrated density of GFAP immunoreactivity was determined after default thresholding of

images<sup>57</sup>. Microglia density was determined using the MorphoLibJ plugin<sup>58</sup>.

### Statistics

All data are represented as the mean ± standard error of the mean. Power analysis was conducted prior to carrying out experiments using an alpha of 0.05 and 80% power. Comparisons in qPCR studies were made using a 1-way analysis of variance (ANOVA) with Dunnet post hoc tests. For live calcium imaging, significance was determined by one-way ANOVA with Bonferroni t-tests. Comparisons of percentage of responsive cells were performed using Fisher's exact test. For behavioral comparisons of food intake and body weight, we applied a repeated measure 3- or 2-way ANOVA, respectively, with Neuman-Keuls post hoc analyses. Statistical significance was set at  $p < 0.05$ . Statistical outliers were identified using the ROUT method ( $Q = 0.5\%$ ) and excluded from analysis.

### Results

#### DVC astrocytes express the leptin receptor

The expression of the leptin receptor on hypothalamic astrocytes is well established in rats and mice<sup>14,15,35,59</sup>. To complement, we performed immunohistochemistry to confirm LepR expression on DVC astrocytes in the rat. Following 4<sup>th</sup> intracerebroventricle (4V) injection of fluorescently labeled leptin (4.5 ng Cy5-Lep), we observed co-localization with DVC astrocytes (GFAP; green; Fig. 1a), predominately at the subpostrema, the border of the AP and NTS. The presence of LepR expression on rat DVC astrocytes was detected by FISH using RNA-scope. LepR mRNA expression (yellow) was observed on both neurons (magenta) and astrocytes (cyan) within the subpostrema and medial NTS (Fig. 1b; Supplementary Video 1).

#### High fat diet-induced obesity reduces the percentage of both DVC astrocytes and neurons showing leptin-induced Ca<sup>+2</sup> signaling in ex vivo brainstem slice preparations

To better characterize the role of DVC astrocytes in energy homeostasis, we next investigated leptin-induced intracellular Ca<sup>+2</sup> responses in DVC neurons and astrocytes in ex vivo brainstem slice preparations (Fig. 2). In addition, we examined whether leptin-induced responses were altered by dietary status and obesity (i.e., comparison of Ca<sup>+2</sup> signaling in the DVC of lean rats maintained on a standard chow or obese rats maintained on a 60% high-fat diet). Imaging experiments on the pre-labeled hindbrain slices from chow-maintained rats ( $n = 4$ ) yielded 61 viable neurons and 35 viable astrocytes; high fat diet-maintained rats ( $n = 3$ ) yielded 37 viable neurons and 24 viable astrocytes.

Both neurons and astrocytes from lean animals produced live cell Ca<sup>+2</sup> flux (i.e., increases in cytoplasmic

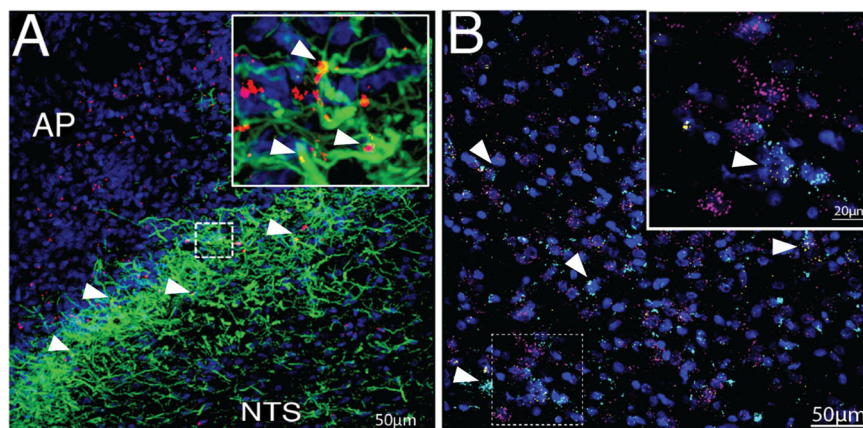


**Fig. 1 Immunohistochemical and FISH validation of leptin binding and LEP-R expression on DVC astrocytes.** **a** Immunohistochemical visualization of Cy5-Lep (4V icv 4.5 ng; red) colocalized to DVC astrocytes (GFAP; green), DAPI in blue; 63x image (inset: 2x optical zoom). **b** FISH visualization of the lateral NTS (at the level of the AP) of LEP-Rb (yellow) expression on DVC astrocytes (ALDH1L1; cyan) and neurons (RbFox3; magenta). Counterstain with DAPI (blue); 40x image (inset: 3.4x optical zoom with gaussian filter). See Supplementary Video 1 for 3D rotational image of area outlined by the dotted box.

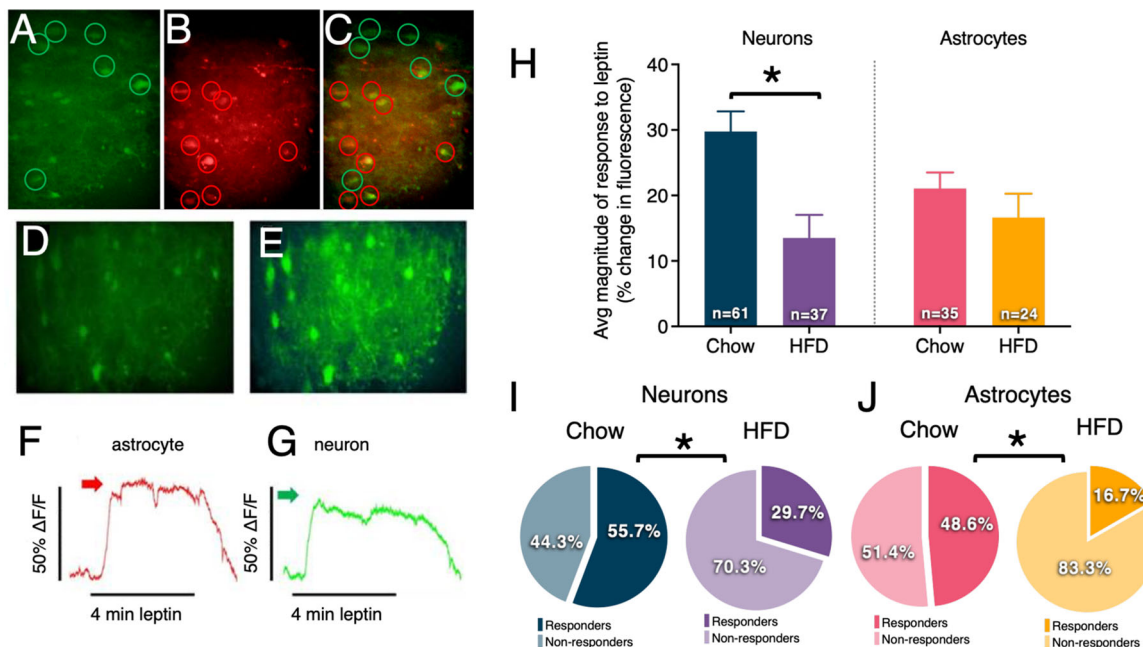


**Fig. 2 Leptin-induced  $Ca^{+2}$  flux in DVC neurons and astrocytes vary by dietary status.** Live cell calcium recordings in DVC brain slices in astrocytes and neurons simultaneously. **a** Cells pre-labeled with Ca520 (calcium sensitive dye; taken up by both neurons and astrocytes) encircled in green. **b** Cells pre-labeled with SR101 (astrocyte-specific dye) are identified as astrocytes and encircled in red. **c** Yellow localization confirms that the calcium-sensitive dye is localized within astrocytes and distinguishable from neurons (green circle). **d** Total field of view (showing both neurons and astrocytes) at “rest” (i.e., baseline) and the same field of view shown in **e** at period of peak response leptin perfusion (see Supplementary Video 2 and 3). **f** Response to leptin perfusion of individual astrocyte marked by red arrow in **g** Response to leptin perfusion of individual neuron marked by green arrow in panel. Changes in fluorescence were measured in brain slices prepared from lean rats ( $n = 4$ ) and rats exposed to a high-fat diet ( $n = 3$ ) following bath leptin exposure (100ng/mL). **h** Magnitude of the leptin response was attenuated in neurons but not astrocytes of obese compared to lean animals. Obese animals had lower proportions of leptin-responsive (**i**) neurons and (**j**) astrocytes compared to lean animals. Changes in magnitude are represented as the mean  $\pm$  standard error of the mean and were analyzed with a 2-way ANOVA and Bonferroni post hoc tests;  $*p < 0.05$ . Percentages of leptin-responsive cells were analyzed using Fisher’s exact test;  $*p < 0.05$ . See Supplementary Video 2 and Supplementary Video 3.



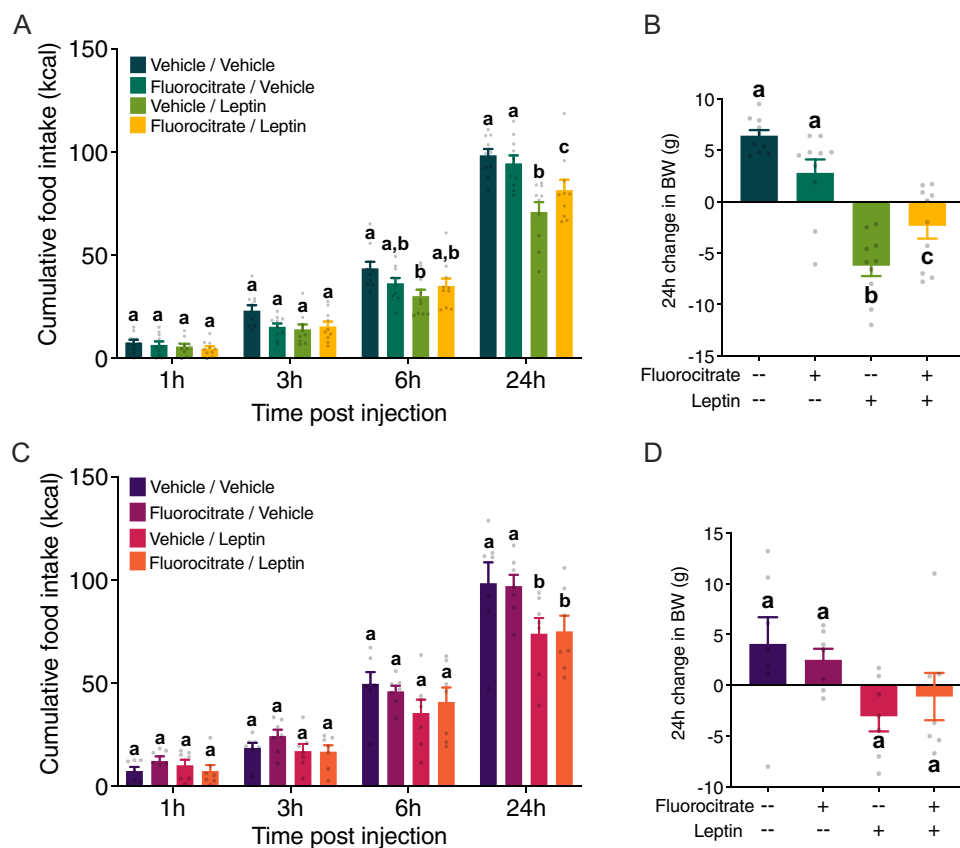


**Fig. 3 DVC astrocytes partly mediate the anorectic effects of leptin in lean but not obese rats.** Changes in cumulative food intake (**a, c**) and 24-h body weight (**b, d**) were recorded following 4V icv pretreatment with 50 nmol fluorocitrate and subsequent treatment with 5  $\mu$ g/mL leptin in rats maintained on either standard chow ( $n = 10$ ; **a, b**) or a high-fat diet ( $n = 7$ ; **c, d**). Data were analyzed using a 3-way (**a, c**) or 2-way (**b, d**) repeated measures ANOVA. Lowercase letters indicate significant differences ( $p < 0.05$ ) within each time point (**a, c**) for food intake and at 24 h (**b, d**) for body weight according to Neuman-Keuls post hoc analyses.

$\text{Ca}^{+2}$ ) in response to bath application of 100ng/mL leptin (Fig. 2h). High-fat diet maintenance attenuated DVC neuron  $\text{Ca}^{+2}$  response without affecting astrocyte responses ( $F_{3,62} = 4.072$ ;  $p = 0.01$ ). Further, animals exposed to a high-fat diet had a significant reduction in the percentage of leptin-responsive neurons and astrocytes compared to lean animals (Fig. 2i, j). In astrocytes, this suggests a potential alteration in functional expression of LepR rather than changes in leptin responsiveness at the cellular level. Representative videos show a mixed neuro-astrocytic field of live calcium imaging following leptin administration in chow (Supplementary Video 2) and HFD (Supplementary Video 3) maintained rats.

#### DVC astrocytes partly mediate the anorectic effects of leptin in lean but not obese rats

A well-established pharmacologic approach was used to assess the contribution of DVC astrocytes in mediating the intake and body weight suppressive effects of leptin. Food intake (Fig. 3a, c) and consequent body weight

change (Fig. 3b, d) were measured in rats following 4V administration of 50 nmol fluorocitrate, an astrocyte-specific Krebs cycle inhibitor<sup>48,52–54</sup>, and 5  $\mu$ g/mL leptin<sup>51</sup>. At the time of experimental treatment, animals fed a high-fat diet weighed significantly more than chow-maintained animals (Supplementary Fig. 2). While there appears to be a slight trend, fluorocitrate treatment alone did not significantly affect food intake or body weight change in either group. In lean rats, pretreatment with fluorocitrate modestly attenuated the food intake inhibitory effects of leptin on 24-h food intake (fluorocitrate  $\times$  leptin interaction:  $F_{1,9} = 7.678$ ,  $p = 0.022$ ; fluorocitrate  $\times$  leptin  $\times$  time interaction:  $F_{3,27} = 2.677$ ;  $p = 0.067$ ; Fig. 3a) and body weight gain (fluorocitrate  $\times$  leptin interaction:  $F_{1,9} = 11.19$ ;  $p = 0.009$ ; Fig. 3b). Conversely, leptin administration in early onset obese rats exerted a modest hypophagic effect at 24hr (fluorocitrate  $\times$  leptin interaction:  $F_{1,6} = 21.61$ ;  $p = 0.009$ ;  $F_{3,18} = 0.899$ ,  $p = 0.46$ ; Fig. 3c) and did not alter 24h body weight change (fluorocitrate  $\times$  leptin interaction:  $F_{1,6} = 1.348$ ,  $p = 0.29$ ; Fig. 3d).

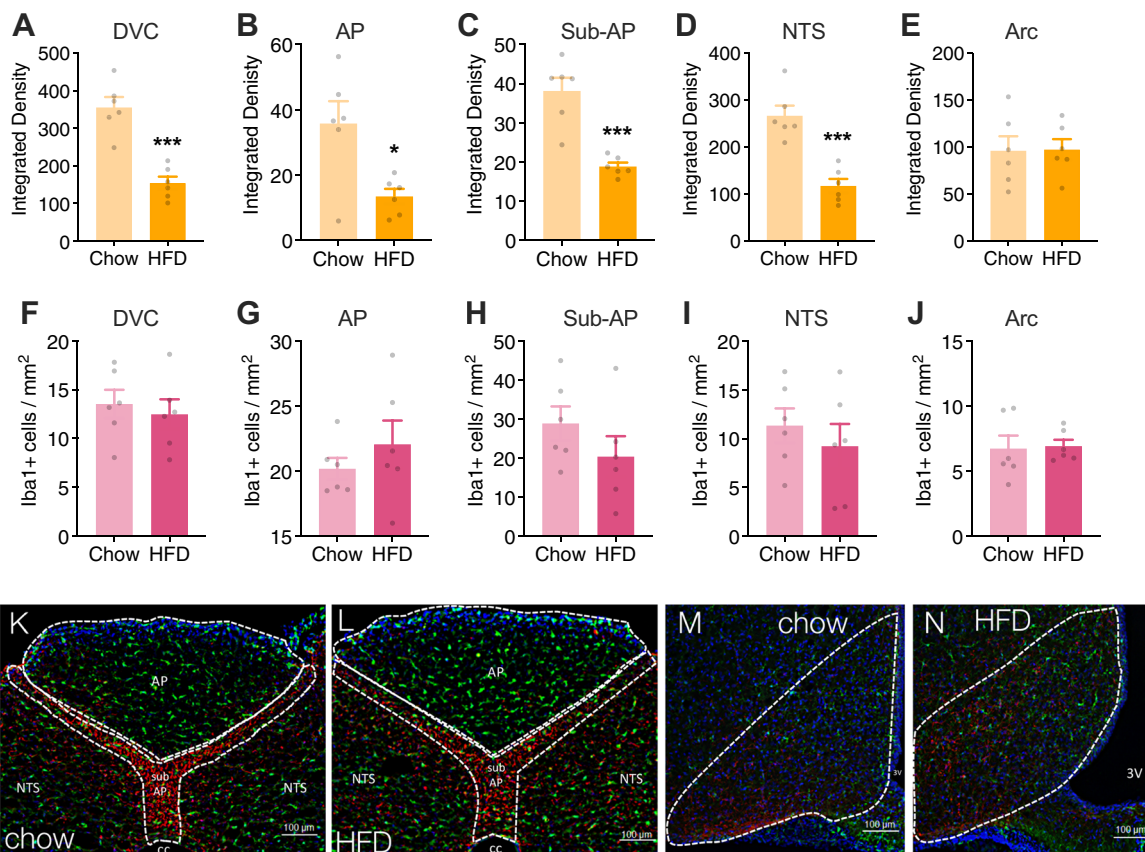


**Fig. 4 A high-fat diet alters gliosis in the brainstem but not the hypothalamus.** Astroglial and microglial infiltration determined by the degree of GFAP immunoreactivity (a–e) and density of Iba1 positive cells (f–j), respectively. HFD significantly decreased GFAP immunoreactivity but did not affect microglial density. Diet had no influence on the glial landscape of the arcuate nucleus. Representative images (20 $\times$ ) of the DVC of lean (k) and obese rats (l) and of the hypothalamus of lean (m) and obese rats (n). Images were quantified in ImageJ and analyzed using unpaired *t*-tests; \**p* < 0.05, \*\**p* < 0.01, \*\*\**p* < 0.001 compared to the lean group (*n* = 6 per group). AP, area postrema; NTS, nucleus tractus solitarius; sub-AP, sub-area postrema; cc, central canal; 3V, third ventricle.

#### Maintenance on a high-fat diet decreases DVC astrocyte activation

Maintenance on a high-fat diet is associated with increased glia activation and proliferation in the hypothalamus<sup>17,18,23</sup>, such that the degree of astroglial activation may predict metabolic outcomes<sup>60</sup>. Given the observation that a high-fat diet was associated with fewer leptin-responsive neurons and astrocytes in the DVC (Fig. 2) and an attenuated hindbrain leptin response in vivo (Fig. 3), we next investigated maladaptive changes in the neuro-glia landscape of the DVC in response to obesity and, within the same rats, compared these changes to those observed in the arcuate nucleus of the hypothalamus. Rats that were fed either standard chow or a high-fat diet for eight weeks were sacrificed for immunohistochemical analysis of astrocyte activation (measured by GFAP integrated density<sup>18,55</sup>) and microglia infiltration (measured by density of Iba1+ cells<sup>56</sup>) in the whole DVC and individual nuclei including the AP, sub-AP, NTS, as well as the arcuate nucleus of the hypothalamus. Rats fed

a high-fat diet had significantly lower GFAP integrated density in the entire DVC (Fig. 4a) as well as in all distinct nuclei of the DVC (Fig. 4b–d) compared to animals fed standard chow. There was no effect of diet on microglia density in the DVC (Fig. 4f–i). There was no detectable effect of a high-fat diet on gliosis within the arcuate nucleus (Fig. 4e, j).

#### Loss of LepR signaling promotes astroglial activation in the DVC

Zucker diabetic fatty rats (ZDF) have a mutation within the leptin receptor that prevents downstream signaling following leptin binding<sup>61,62</sup>. This form of leptin receptor deficiency results in obesity, hyperphagia, and hyperglycemia (Supplementary Fig. 3). Obesity due to deficient leptin receptor signaling in these ZDF rats was associated with significantly higher astroglial activation in the DVC (Fig. 5a–d) but a marked reduction in density of GFAP-positive cells in the arcuate nucleus compared to wild-type control rats (Fig. 5e). Microglia density was significantly lower in the arcuate nucleus of ZDF rats

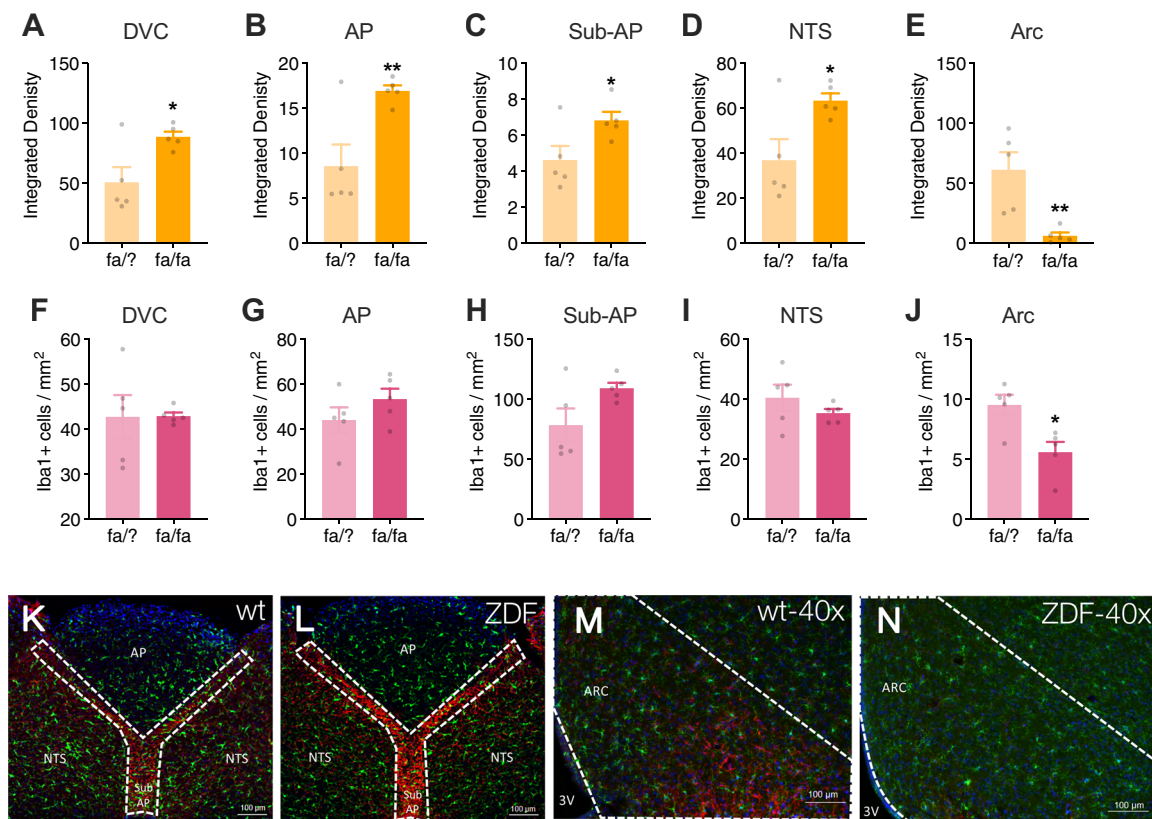


**Fig. 5 Zucker diabetic fatty rats (ZDF) exhibit heightened astroglial density in the DVC and attenuated gliosis in the arcuate nucleus compared to wild type (WT) rats.** Astroglial density was determined by quantifying the integrated density of GFAP immunoreactivity within distinct regions of the DVC. ZDF rats had significantly higher GFAP integrated density in the DVC (a), AP (b), sub-AP (c), and NTS (d) compared to WT rats. There was no difference in microglial density in the DVC between ZDF and WT rats (f–i). Conversely, there was a significant reduction in both GFAP integrated density (e) and microglial density (j) in the arcuate nucleus of ZDF vs. WT rats. Representative images at 20x magnification of WT (k) and ZDF (l) dorsal vagal complex and 40x magnification of WT (m) and ZDF (n) arcuate nucleus. Images were quantified in ImageJ and analyzed using unpaired *t*-tests; \**p* < 0.05, \*\**p* < 0.01 compared to the WT group (*n* = 5 per genotype). AP, area postrema; NTS, nucleus tractus solitarius; sub-AP, sub-area postrema; cc, central canal; 3V, third ventricle; Arc, arcuate nucleus.

compared to wild-type rats (Fig. 5j). In contrast, no alteration in microglia density was observed in the DVC of ZDF rats compared to control rats (Fig. 5f–i).

The neurobiological control of energy balance involves a vast, interconnected network of neuronal crosstalk that continually senses and responds to an organism's metabolic status<sup>25,26</sup>. Recent work has highlighted a role of glia in energy balance, but our limited knowledge regarding glia-neuron interplay in brain regions beyond the arcuate hypothalamus necessitates further exploration<sup>48</sup>. Here, we examined the contribution of caudal brainstem DVC astrocytes to the effects of leptin on food intake, as well as the effects of diet on glia cell density and activation in the DVC. Similar to previous characterizations of hypothalamic astrocytes<sup>13,14,63</sup>, an important main finding of our research was the discovery that DVC astrocytes are an additional site for leptin receptor expression and activation. The IHC and in situ observations combined with ex vivo live cell recordings of astrocytes demonstrate

functional LepR receptors on rodent DVC astrocytes. Astrocyte-specific inhibition revealed a functionally relevant role of hindbrain astrocytes in mediating the effects of leptin administered into the 4<sup>th</sup> ventricle. The current data also points to the DVC astrocytes as a site of leptin dysfunction in obesity. Calcium imaging revealed that animals fed a high-fat diet also exhibited a reduction in the proportion of leptin-responsive neurons and astrocytes in the DVC compared to lean animals. Exposure to a high-fat diet elicited the selective *reduction* of astroglial density in the DVC, in contrast with previous studies of the hypothalamus<sup>17–19</sup>, and no effect on arcuate hypothalamic astrocytes. Further, the absence of leptin signaling in Zucker diabetic fatty rats was associated with enhanced astroglial density in the DVC and decreased hypothalamic astroglial density. These data in no way suggest that the DVC astrocytes are the only cellular substrate for leptin signaling or obesity-induced leptin resistance. Instead, our data highlight the DVC as a critical and overlooked CNS

cellular site-of-action that may be targeted for restoring leptin signaling in obesity.

The role of hypothalamic astrocyte LepR signaling in energy homeostasis is well established in previous studies: knockdown of LepR in the hypothalamus leads to alterations in neural circuitry and attenuates leptin-induced anorexia in mice<sup>15,14,64</sup>. Yet, the significance of astrocytic LepR expression in the DVC is unknown. For this reason, we performed a series of pharmacologic experiments to estimate the involvement of the DVC astrocytes in the effects of leptin on food intake. We observed effects of 4V leptin on overnight food intake and subsequent weight gain in lean animals and further found that these effects were modestly attenuated by pretreatment with 4V fluorocitrate, an astrocyte-specific inhibitor of cellular respiration<sup>48,50,52,53</sup>. Albeit not significant, there appeared to be a slight inhibitory trend of fluorocitrate alone on food intake. As astrocytes and neurons comprise the tripartite synapse in which surrounding glia cells form intimate association with pre- and post-synaptic membranes<sup>7,65,66</sup>, it is plausible that a transient non-specific inhibition of astrocytes with fluorocitrate potentially elicits a modulation of vagal-NTS signaling to transiently decrease food intake. Interestingly, the attenuating effect of 4V fluorocitrate was absent in rats fed a high-fat diet. As the duration of HFD exposure does not correspond with a full manifestation of leptin resistance<sup>67,68</sup>, these data indicate a surprising, albeit limited role for hindbrain astrocytes in leptin responsiveness in obesity, and moreover, suggest that a loss of leptin responsiveness in hindbrain astrocytes represents part of the maladaptive neuroregulatory response to obesity in rodents. This idea is consistent with numerous reports describing a causal association between HFD and hypothalamic leptin resistance<sup>11,17–19,21</sup>. Our calcium imaging results support this statement, in which exposure to a high-fat diet significantly reduced the proportion of leptin-responsive astrocytes and neurons and decreased the magnitude of neuronal (but not astrocytic) responses to leptin in the DVC. While we speculate this may be a result of maladaptive changes to LepR functional expression, one cannot rule out the potential for alternative LepR signaling cascades within astrocytes. Indeed, Yasumoto et al. provide evidence of preference toward leptin-mediated increases in extracellular receptor kinase (ERK) expression as opposed to the classical increase in phosphorylation of STAT3<sup>69</sup>. Therefore, in order to provide mechanistic insight into leptin action on astrocytes and the effect of diet on astrocytic LepR signaling is required.

Astrocytes serve as the predominant regulator of synaptic glutamate (reviewed in ref. <sup>70</sup>) Given that vagal afferent transmission of all satiation signaling from the GI tract is glutamatergic, it is intriguing to consider what

effect leptin-astrocyte signaling would have on modulating vagal-to-NTS glutamatergic signaling. Leptin administration into the lateral ventricle results in a significant decrease in astrocyte specific glutamate transporters, GLT1 and GLAST, in the hypothalamus<sup>63</sup>. Thus, in the lean state, the well documented ability of DVC leptin signaling to suppress food intake via enhancement of GI-derived satiation signals<sup>31,71–73</sup>, may actually involve a leptin-mediated astrocyte specific suppression in astrocyte glutamate re-uptake transporters and subsequent augmentation of vagal glutamatergic transmission. A logical extension of this hypothesis would therefore follow that in the HFD-induced obese state, leptin's ability to downregulate these astrocyte glutamate transporters would be blunted, consistent with our observed decrease in astrocyte Ca<sup>++</sup> responsivity to leptin in HFD NTS slice preparations. It is clear that further investigations are warranted to assess the evolving role of DVC astrocytes in mediating leptin signaling and modulation of vagal-to-NTS glutamatergic transmission.

Another major finding of the current data, when considered in the context of pre-existing literature on the hypothalamus, was the remarkable divergence in the responses of DVC and hypothalamic glia cells to obesity. Since microglia serve as the resident immunocompetent cells of the central nervous system<sup>74</sup> and previously shown to be responsive to high fat diet and obesity, we measured the effects of HFD and absence of leptin signaling on microglia density. Exposure to a high fat diet alone did not result in changes to microglia density in either the DVC or hypothalamus. Future characterization of microglia state, i.e., resting vs. activated, is required to determine whether diet and/or leptin increase the number of activated microglia.

Taken together, these findings support the hypothesis that DVC astrocytes contribute to energy balance regulation and constitute a component of the maladaptive changes that occur in response to diet-induced obesity. Moreover, our results suggest that astrocytes in the DVC may be particularly susceptible to the loss of leptin signaling.

Finally, we performed an in-detail characterization of gliosis in the DVC and hypothalamus of the same rats in order to better characterize the interplay of DVC astroglia and leptin signaling in response to a high-fat diet. Our observation that fluorocitrate attenuated leptin responses in lean but not obese animals indicated the possibility of corresponding astrocytic changes at the level of the brainstem. To test this hypothesis, we quantified gliosis (astrocytic and microglia) in specific areas of the DVC and hypothalamus in lean rats, rats exposed to a high-fat diet, and ZDF rats. Both HFD-induced obesity and ZDF rats serve as models of obesity; both are hyperphagic, hyperglycemic and increased adiposity. The Zucker diabetic fatty rat (ZDF) is an inbred sub-strain of



the obese Zucker fatty rat, with a missense mutation in the LepR gene resulting in non-functional leptin signaling<sup>62</sup>. ZDF rats exhibiting early hyperglycemia, especially when maintained on a high fat diet. The HFD-induced obese model serves more clinical relevance as most forms of human obesity are due to polygenic alterations and environmental factors. Chronic exposure to a HFD not only results in an obese phenotype but is accompanied by the gradual development of leptin resistance. Studies in both humans and rodents revealed that at the level of the hypothalamus there is significant gliosis as a result of HFD exposure. Utilization of these two models begins to disentangle driving forces of obesity-induced gliosis and in turn, how gliosis contributes to the development and maintenance of obesity. Apart from the finding of an overall decrease in GFAP (but not Iba1) density in the DVC nuclei of animals exposed to a high-fat vs. standard diet, we did not observe any diet-induced changes in gliosis in the arcuate nucleus of the hypothalamus, a key target of leptin in energy homeostasis<sup>25,26</sup>. Our result is inconsistent with previous rodent (often murine) studies describing an association between a high-fat diet, increased gliosis in the hypothalamus, and the etiological development of obesity<sup>17–19</sup>. One possible explanation for this discrepancy is that the vast majority of these aforementioned studies were carried out in mice and therefore the HFD-induced gliosis, or lack of, may be species-dependent. Collectively, published studies reveal that gliosis occurs dynamically across time and does not persist throughout the entire duration of HFD exposure<sup>17,19,22,75,76</sup>. Future time-course analyses are required to fully assess HFD-induced gliosis in the hypothalamus and DVC. Nonetheless, we also observed that ZDF rats maintained on a standard diet exhibited an increase in astrogliosis in the DVC in tandem with attenuated microgliosis in the arcuate nucleus of the hypothalamus. These collective findings, although in stark contrast to previous literature, uncover a novel divergence in the leptin responses and function of glia between the DVC and hypothalamus. Whereas leptin appears to act on glia to enhance neurotransmission in the hypothalamus, leptin action in the DVC may serve to decrease neuronal output in a manner that facilitates the appetite suppressant activity of leptin. In the absence or complete dysregulation of LepR signaling, the excitatory output from the hypothalamus and inhibition of output from the DVC are lost, resulting in a loss of leptin-associated inhibitory control of food intake and weight gain.

The present study had several limitations. One caveat is that HFD-induced obese rats are hyperglycemic but not diabetic, whereas the ZDF animals display a full type II diabetic phenotype, raising the possibility that hyperglycemia and insulin resistance may contribute to the observed effect on astrocytes. Our immunohistochemical analyses of

gliosis does not provide a refined characterization of the effects of diet on glia cells. Future analyses on the diet-induced effects on gliogenesis, morphological changes to glia processes, glia activation, and associations with neuronal synapses are required. Second, we relied on historic literature examining the hypothalamic leptin-astrocyte interplay<sup>11,13–15</sup>. It is entirely possible that each of the previous reports may have some specific methodological limitations in the IHC quantifications performed.

Regardless of these limitations, the current data strongly suggest that the field would benefit from broadening our understanding of divergent astrocyte responses in different brain nuclei to obesity and alterations in leptin signaling if we are to understand fully the role that astrocytes are playing in energy balance regulation.

In conclusion, LepR is functionally expressed on astrocytes of the DVC and exert a different functional role in the DVC than it does in the hypothalamus. Unlike hypothalamic astrocytes, DVC astrocytes may be particularly vulnerable to the absence of leptin signaling. Future efforts should focus on elucidation of the neural pathways supported by the divergent functional roles of DVC vs. hypothalamic glia, as well as examine the contribution of leptin-astrocyte signaling in other CNS nuclei of relevance to energy balance control. Collectively, current findings uncover a novel role for DVC astrocytes in mediating the actions of leptin.

#### Acknowledgements

We thank David Reiner, Lauren McGrath, Kieran Koch-Laskowski, Rosa Leon, Claudia Liberini, Jack Chen, Alexis Corini, Misgana Ghidewon, Joanna Krawczyk, Celina Nhan, Nina Juntreal, Tyler Ling, Abigail Reed, and Michael Hagan for valuable technical assistance. We thank Ashley Symons for reviewing the manuscript and providing valuable feedback. We thank James Peters, Tito Borner, Samantha Fortin, and Heath Schmidt for valuable discussions. This work was supported by the National Institute of Health Grants DK115762 (MRH), DK118818 (LMS) and DK021397 (HJG/MRH). LMS received funding from The Obesity Society, Early Career Research Fellowship. MRH receives funding from Zealand Pharma, Novo Nordisk, Eli Lilly & Co. and Boehringer Ingelheim that was not used in support of these studies. HJG receives funding from Pfizer that was not used in support of these studies. RPD is a scientific advisory board member and received funds from Xeragenx LLC (St. Louis, NY) and Balchem, New Hampton, New York, that were not used in support of these studies.

#### Author details

<sup>1</sup>Department of Psychiatry, University of Pennsylvania School of Medicine, Philadelphia, PA, USA. <sup>2</sup>Department of Chemistry, Syracuse University, Syracuse, NY, USA. <sup>3</sup>Institute of Diabetes, Obesity and Metabolism and Department of Psychology, University of Pennsylvania, Philadelphia, PA, USA. <sup>4</sup>Department of Autonomic Neuroscience, Pennington Biomedical Research Center, Baton Rouge, LA, USA

#### Author contributions

L.M.S. conceptualized experimental hypotheses, designed research studies, conducted experiments, acquired and analyzed data, and wrote/revised the manuscript. M.R.H. conceptualized experimental hypotheses, designed research studies, analyzed data, and wrote/revised the manuscript. R.L. and A.C. conducted experiments, acquired and analyzed data. J.W., I.T., and R.P.D. synthesized conjugated peptide, reviewed and revised the manuscript. H.J.G. conceptualized experimental hypotheses and revised the manuscript. G.E.H. and R.C.R. designed and conducted experiments, acquired and analyzed data, and wrote/revised the manuscript.

**Conflict of interest**

The authors declare that they have no conflict of interest.

**Publisher's note**

Springer Nature remains neutral with regard to jurisdictional claims in published maps and institutional affiliations.

**Supplementary Information** accompanies this paper at (<https://doi.org/10.1038/s41398-020-0767-0>).

Received: 9 October 2019 Revised: 18 February 2020 Accepted: 25 February 2020

Published online: 09 March 2020

**References**

1. Kettenmann H. & Ransom B. R. The concept of neuroglia: a historical perspective. *Neuroglia*, 1–16 (2004) <https://doi.org/10.1093/acprof:oso/9780195152227.003.0001>.
2. Barres, B. A. The mystery and magic of glia: a perspective on their roles in health and disease. *Neuron* **60**, 430–440 (2008).
3. Abbott, J. N. Astrocyte-endothelial interactions and blood-brain barrier permeability. *J. Anat.* **200**, 629–638 (2002).
4. Marty, N. et al. Regulation of glucagon secretion by glucose transporter type 2 (glut2) and astrocyte-dependent glucose sensors. *J. Clin. Invest.* **115**, 3545–3553 (2005).
5. Rothstein, J. D. et al. Knockout of glutamate transporters reveals a major role for astroglial transport in excitotoxicity and clearance of glutamate. *Neuron* **16**, 675–686 (1996).
6. Harada, K., Kamiya, T. & Tsuboi, T. Gliotransmitter release from astrocytes: functional, developmental, and pathological implications in the brain. *Front Neurosci.* **9**, 499 (2016).
7. Araque, A., Parpura, V., Sanzgiri, R. & Haydon, P. Tripartite synapses: glia, the unacknowledged partner. *Trends Neurosci.* **22**, 208–215 (1999).
8. Chari, M. et al. Glucose transporter-1 in the hypothalamic glial cells mediates glucose sensing to regulate glucose production in vivo. *Diabetes* **60**, 1901–1906 (2011).
9. Emery, M., Tarussio, D., Bady, I. & Binnert, C. Regulation of glucagon secretion by glucose transporter type 2 (glut2) and astrocyte-dependent glucose sensors. *J. Clin. Invest.* **115**, 3545–3553 (2005).
10. Allard, C. et al. Hypothalamic astroglial connexins are required for brain glucose sensing-induced insulin secretion. *J. Cereb. Blood Flow Metab.* **34**, 339–346 (2013).
11. Chowen, J. A. et al. The role of astrocytes in the hypothalamic response and adaptation to metabolic signals. *Prog. Neurobiol.* **144**, 68–87 (2016).
12. Pannasch, U. et al. Astroglial networks scale synaptic activity and plasticity. *Proc. Natl Acad. Sci. USA* **108**, 8467–8472 (2011).
13. García-Cáceres, C. et al. Differential acute and chronic effects of leptin on hypothalamic astrocyte morphology and synaptic protein levels. *Endocrinology* **152**, 1809–1818 (2011).
14. Kim, J. et al. Leptin signaling in astrocytes regulates hypothalamic neuronal circuits and feeding. *Nat. Neurosci.* **17**, 908–910 (2014).
15. Pan, W. et al. Astrocyte leptin receptor (ObR) and leptin transport in adult-onset obese mice. *Endocrinology* **149**, 2798–2806 (2008).
16. Shrikant, P. & Benveniste, E. The central nervous system as an immunocompetent organ: role of glial cells in antigen presentation. *J. Immunol.* **157**, 1819–1822 (1996).
17. Berkseth, K. E. et al. Hypothalamic gliosis associated with high-fat diet feeding is reversible in mice: a combined immunohistochemical and magnetic resonance imaging study. *Endocrinology* **155**, 2858–2867 (2014).
18. Thaler, J. P. et al. Obesity is associated with hypothalamic injury in rodents and humans. *J. Clin. Invest.* **122**, 778–778 (2012).
19. Dorfman, M. D. & Thaler, J. P. Hypothalamic inflammation and gliosis in obesity. *Curr. Opin. Endocrinol. Diabetes Obes.* **22**, 325–330 (2015).
20. Myers, M. G., Leibel, R. L., Seeley, R. J. & Schwartz, M. W. Obesity and leptin resistance: distinguishing cause from effect. *Trends Endocrinol. Metab.* **21**, 643–651 (2010).
21. Wang, X. et al. Increased hypothalamic inflammation associated with the susceptibility to obesity in rats exposed to high-fat diet. *Exp. Diabetes Res.* **2012**, 847246 (2012).
22. Horvath, T. L. et al. Synaptic input organization of the melanocortin system predicts diet-induced hypothalamic reactive gliosis and obesity. *Proc. Natl Acad. Sci. USA* **107**, 14875–14880 (2010).
23. Gao, Y. et al. Hormones and diet, but not body weight, control hypothalamic microglial activity. *Glia* **62**, 17–25 (2014).
24. Koch, C. et al. High-fat diet induces leptin resistance in leptin-deficient mice. *J. Neuroendocrinol.* **26**, 58–67 (2014).
25. Grill, H. J. Distributed neural control of energy balance: contributions from hindbrain and hypothalamus. *Obesity* **14**, 2165–2215 (2006).
26. Berthoud, H. Homeostatic and non-homeostatic pathways involved in the control of food intake and energy balance. *Obesity* **14**, 1975–2005 (2006).
27. Hayes, M. R., Skibicka, K. P. & Grill, H. J. Caudal brainstem processing is sufficient for behavioral, sympathetic, and parasympathetic responses driven by peripheral and hindbrain glucagon-like-peptide-1 receptor stimulation. *Endocrinology* **149**, 4059–4068 (2008).
28. Grill, H. J. et al. Evidence that the caudal brainstem is a target for the inhibitory effect of leptin on food intake. *Endocrinology* **143**, 239–246 (2002).
29. Blouet, C. & Schwartz, G. J. Brainstem nutrient sensing in the nucleus of the solitary tract inhibits feeding. *Cell Metab.* **16**, 579–587 (2012).
30. Matson, C. A., Wiater, M. F., Kuijper, J. L. & Weigle, D. S. Synergy between leptin and cholecystokinin (CCK) to control daily caloric intake. *Peptides* **18**, 1275–1278 (1997).
31. Huo, L., Maeng, L., Bjorbaek, C. & Grill, H. J. Leptin and the control of food intake: neurons in the nucleus of the solitary tract are activated by both gastric distension and leptin. *Endocrinology* **148**, 2189–2197 (2007).
32. Schwartz, G. J. & Moran, T. H. Leptin and neuropeptide y have opposing modulatory effects on nucleus of the solitary tract neurophysiological responses to gastric loads: implications for the control of food intake. *Endocrinology* **143**, 3779–3784 (2002).
33. Kanoski, S. E., Alhadeff, A. L., Fortin, S. M., Gilbert, J. R. & Grill, H. J. Leptin signaling in the medial nucleus tractus solitarius reduces food seeking and willingness to work for food. *Neuropsychopharmacol.* **39**, 605–613 (2013).
34. Zhao, S., Kanoski, S., Yan, J., Grill, H. & Hayes, M. Hindbrain leptin and glucagon-like-peptide-1 receptor signaling interact to suppress food intake in an additive manner. *Int. J. Obes.* **36**, 1522–1528 (2012).
35. Dallaporta, M. et al. Expression of leptin receptor by glial cells of the nucleus tractus solitarius: possible involvement in energy homeostasis. *J. Neuroendocrinol.* **21**, 57–67 (2009).
36. Paxinos, G. & Watson, C. (5th eds) *The rat brain in stereotaxic coordinates* (Academic Press, London, 2005).
37. Ritter, R. C., Slusser, P. G. & Stone, S. Glucoreceptors controlling feeding and blood glucose: location in the hindbrain. *Science* **213**, 451–452 (1981).
38. Hara, K. & Harris, A. R. The anesthetic mechanism of urethane: the effects on neurotransmitter-gated ion channels. *Anesthesia Analgesia.* **94**, 313 (2002).
39. Vance, K. & Rogers, R. PAR1-activated astrocytes in the nucleus of the solitary tract stimulate adjacent neurons via NMDA receptors. *J. Neurosci.* **35**, 776–785 (2015).
40. Reiner, D. J. et al. Astrocytes regulate GLP-1 receptor-mediated effects on energy balance. *J. Neurosci.* **36**, 3531–3540 (2016).
41. Hermann, G., Meter, V. M., Rood, J. & Rogers, R. Proteinase-activated receptors in the nucleus of the solitary tract: evidence for glial-neural interactions in autonomic control of the stomach. *J. Neurosci.* **29**, 9292–9300 (2009).
42. Rogers, R. C. & Hermann, G. E. Tumor necrosis factor activation of vagal afferent terminal calcium is blocked by cannabinoids. *J. Neurosci.* **32**, 5237–5241 (2012).
43. McDougal, D. H., Hermann, G. E. & Rogers, R. C. Vagal afferent stimulation activates astrocytes in the nucleus of the solitary tract via AMPA Receptors: Evidence of an atypical neural-glia interaction in the brainstem. *J. Neurosci.* **31**, 14037–14045 (2011).
44. Rogers, R. C., McDougal, D. H., Ritter, S., Qualls-Creekmore, E. & Hermann, G. E. Response of catecholaminergic neurons in the mouse hindbrain to glucoprivic stimuli is astrocyte dependent. *Am. J. Physiol. Regul. Integr. Comp. Physiol.* **315**, R153–R164 (2018).
45. McDougal, D. H., Viard, E., Hermann, G. E. & Rogers, R. C. Astrocytes in the hindbrain detect glucoprivation and regulate gastric motility. *Auton. Neurosci.* **175**, 61–69 (2013).
46. Ritter, S., Dinh, T. T. & Zhang, Y. Localization of hindbrain glucoreceptive sites controlling food intake and blood glucose. *Brain Res.* **856**, 37–47 (2000).

47. Ritter, R. & Slusser, P. 5-Thio-D-glucose causes increased feeding and hyperglycemia in the rat. *Am. J. Physiol.* **238**, E141–E144 (1980).
48. Swanson, R. & Graham, S. Fluorocitrate and fluoroacetate effects on astrocyte metabolism in vitro. *Brain Res.* **664**, 94–100 (1994).
49. Hermann, G. E., Viard, E. & Rogers, R. C. Hindbrain glucoprivation effects on gastric vagal reflex circuits and gastric motility in the rat are suppressed by the astrocyte inhibitor fluorocitrate. *J. Neurosci.* **34**, 10488–10496 (2014).
50. Fonnum, F., Johnsen, A. & Hassel, B. Use of fluorocitrate and fluoroacetate in the study of brain metabolism. *Glia* **21**, 106–113 (1997).
51. Hayes, M. R., Skibicka, K. P., Bence, K. K. & Grill, H. J. Dorsal hindbrain 5'-adenosine monophosphate-activated protein kinase as an intracellular mediator of energy balance. *Endocrinology* **150**, 2175 (2009). 2182.
52. Clarke, D. Fluoroacetate and fluorocitrate: mechanism of action. *Neurochem. Res.* **16**, 1055–1058 (1991).
53. Brand, Evans, S., Mendes-Mourão, J. & Chappell, J. Fluorocitrate inhibition of aconitate hydratase and the tricarboxylate carrier of rat liver mitochondria. *Biochem J.* **134**, 217–224 (1973).
54. Paulsen, R., Contestabile, A. & Villani, L. An in vivo model for studying function of brain tissue temporarily devoid of glial cell metabolism: the use of fluorocitrate. *J. Neurochem.* **48**, 1377–1385 (1987).
55. Eng, L. F. & Ghirnikar, R. S. GFAP and astrogliosis. *Brain Pathol.* **4**, 229–237 (1994).
56. Bennett, M. L. et al. New tools for studying microglia in the mouse and human CNS. *Proc. Natl Acad. Sci. USA* **113**, E1738–E1746 (2016).
57. Healy, S., McMahon, J., Owens, P., Dockery, P. & Fitzgerald, U. Threshold-based segmentation of fluorescent and chromogenic images of microglia, astrocytes and oligodendrocytes in FJI. *J. Neurosci. Methods* **295**, 87–103 (2018).
58. Davis, B. M., Salinas-Navarro, M., Cordeiro, F. M., Moons, L. & Groef, L. Characterizing microglia activation: a spatial statistics approach to maximize information extraction. *Sci. Rep.* **7**, 1576 (2017).
59. Hsueh, H., Pan, W., Barnes, M. J. & Kastin, A. J. Leptin receptor mRNA in rat brain astrocytes. *Peptides* **30**, 2275–2280 (2009).
60. Valdearcos, M. et al. Microglial inflammatory signaling orchestrates the hypothalamic immune response to dietary excess and mediates obesity susceptibility. *Cell Metab.* **26**, 185–197.e3 (2017).
61. Shiota, M. & Printz, R. L. Animal models in diabetes research. *Methods Mol. Biol.* **933**, 103–123 (2012).
62. Clark, J. B., Palmer, C. J. & Shaw, W. N. The diabetic Zucker fatty rat. *Proc. Soc. Exp. Biol. Med.* **173**, 68–75 (1983).
63. Fuente-Martín, E. et al. Leptin regulates glutamate and glucose transporters in hypothalamic astrocytes. *J. Clin. Invest.* **122**, 3900–3913 (2012).
64. Jayaram, B. et al. Astrocytic leptin-receptor knockout mice show partial rescue of leptin resistance in diet-induced obesity. *J. Appl. Physiol.* **114**, 734–741 (2013).
65. Halassa, M. M. & Haydon, P. G. Integrated brain circuits: astrocytic networks modulate neuronal activity and behavior. *Annu. Rev. Physiol.* **72**, 335 (2010). 355.
66. Haber, M., Zhou, L. & Murai, K. K. Cooperative astrocyte and dendritic spine dynamics at hippocampal excitatory synapses. *J. Neurosci.* **26**, 8881–8891 (2006).
67. Levin, B. E. Reduced central leptin sensitivity in rats with diet-induced obesity. *Am. J. Physiol. Regul. Integr. Comp. Physiol.* **283**, R941–R948 (2002).
68. Fam, B. C. et al. Modulation of central leptin sensitivity and energy balance in a rat model of diet-induced obesity. *Diabetes Obes. Metab.* **9**, 840–852 (2007).
69. Yasumoto, Y., Miyazaki, H., Ogata, M., Kagawa, Y. & Yamamoto, Y. Glial fatty acid-binding protein 7 (FABP7) regulates neuronal leptin sensitivity in the hypothalamic arcuate nucleus. *Mol. Neurobiol.* **55**, 9016–9028 (2018).
70. Sofroniew, M. V. & Vinters, H. V. Astrocytes: biology and pathology. *Acta Neuropathol.* **119**, 7–35 (2010).
71. Hayes, M. R. et al. Endogenous leptin signaling in the caudal nucleus tractus solitarius and area postrema is required for energy balance regulation. *Cell Metab.* **23**, 744 (2016).
72. Kanoski, S. E. et al. Endogenous leptin receptor signaling in the medial nucleus tractus solitarius affects meal size and potentiates intestinal satiation signals. *Am. J. Physiol. Endocrinol. Metab.* **303**, E496–E503 (2012).
73. Emond, M., Ladenheim, E., Schwartz, G. & Moran, T. Leptin amplifies the feeding inhibition and neural activation arising from a gastric nutrient preload. *Physiol. Behav.* **72**, 123128 (2001).
74. Streit, W. Microglia as neuroprotective, immunocompetent cells of the CNS. *Glia* **40**, 133–139 (2002).
75. Vaughn, A. C. et al. Energy-dense diet triggers changes in gut microbiota, reorganization of gut-brain vagal communication and increases body fat accumulation. *Acta Neurobiol. Exp.* **77**, 18–30 (2017).
76. Baufeld, C., Osterloh, A., Prokop, S., Miller, K. R. & Heppner, F. L. High-fat diet-induced brain region-specific phenotypic spectrum of CNS resident microglia. *Acta Neuropathol.* **132**, 361–375 (2016).



(51) International Patent Classification:

A61K 38/10 (2006.01) C07K 7/06 (2006.01)  
C07K 7/08 (2006.01) A61K 38/08 (2019.01)

(21) International Application Number:

PCT/US2020/0 16844

(22) International Filing Date:

05 February 2020 (05.02.2020)

(25) Filing Language:

English

(26) Publication Language:

English

(30) Priority Data:

62/801,391 05 February 2019 (05.02.2019) US

(71) Applicants: **THE TRUSTEES OF THE UNIVERSITY OF PENNSYLVANIA** [US/US]; 3600 Civic Center Boulevard, 9th Floor, Philadelphia, Pennsylvania 19104 (US). **SYRACUSE UNIVERSITY** [US/US]; 224 Lyman Flail, Syracuse, New York 13244 (US).

(72) Inventors: **HAYES, Matthew Robert**; 3013 Fisher Road, Lansdale, Pennsylvania 19446 (US). **DE JONGHE, Bart C.**; 3502 Scotts Lane, Philadelphia, Pennsylvania 19129 (US). **BORNER, Tito**; 1806 Spruce Street, Apt. 3R,

Philadelphia, Pennsylvania 19103 (US). **DOYLE, Robert**; 4495 Red Spruce Lane, Manlius, New York 13104 (US). **TINSLEY, Ian**; 136 Northrup Boulevard, Syracuse, New York 13209 (US).

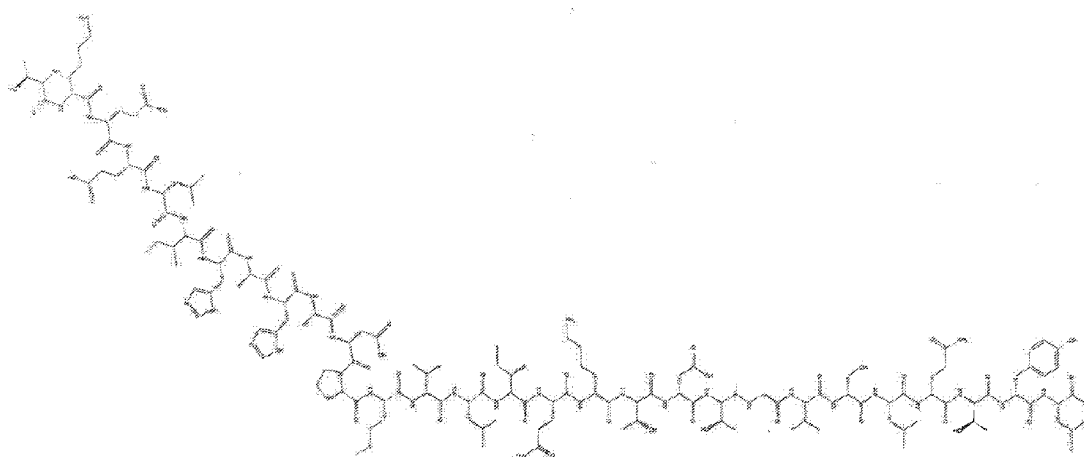
(74) Agent: **DOYLE, Kathryn** et al.; Saul Ewing Arnstein & Lehr, Centre Square West, 1500 Market Street, 38th Floor, Philadelphia, Pennsylvania 19102 (US).

(81) Designated States (unless otherwise indicated, for every kind of national protection available): AE, AG, AL, AM, AO, AT, AU, AZ, BA, BB, BG, BH, BN, BR, BW, BY, BZ, CA, CH, CL, CN, CO, CR, CU, CZ, DE, DJ, DK, DM, DO, DZ, EC, EE, EG, ES, FI, GB, GD, GE, GH, GM, GT, HN, HR, HU, ID, IL, IN, IR, IS, JO, JP, KE, KG, KH, KN, KP, KR, KW, KZ, LA, LC, LK, LR, LS, LU, LY, MA, MD, ME, MG, MK, MN, MW, MX, MY, MZ, NA, NG, NI, NO, NZ, OM, PA, PE, PG, PH, PL, PT, QA, RO, RS, RU, RW, SA, SC, SD, SE, SG, SK, SL, ST, SV, SY, TH, TJ, TM, TN, TR, TT, TZ, UA, UG, US, UZ, VC, VN, WS, ZA, ZM, ZW.

(84) Designated States (unless otherwise indicated, for every kind of regional protection available): ARIPO (BW, GH, GM, KE, LR, LS, MW, MZ, NA, RW, SD, SL, ST, SZ, TZ, UG, ZM, ZW), Eurasian (AM, AZ, BY, KG, KZ, RU, TJ,

(54) Title: PEPTIDE LIGANDS OF THE GDNF FAMILY RECEPTOR A-LKE (GFRAL) RECEPTOR

G PANTOS



Thr-Lys-Glu-Glu-Leu-Ile-His-Ala-His-Ala-Asp-Pro-Met-Val-Leu-Ile-Gln-Lys-Thr-Asp-Thr-Gly-Val-Ser-Leu-Gln-Thr-Tyr-Asp

FIG. 1

(57) Abstract: The present invention relates to engineered peptides and to methods of making engineered peptides. The present invention also relates to methods of treatment comprising administration of the engineered peptides to a subject in need thereof.





TM), European (AL, AT, BE, BG, CH, CY, CZ, DE, DK, EE, ES, FI, FR, GB, GR, HR, HU, IE, IS, IT, LT, LU, LV, MC, MK, MT, NL, NO, PL, PT, RO, RS, SE, SI, SK, SM, TR), OAPI (BF, BJ, CF, CG, CI, CM, GA, GN, GQ, GW, KM, ML, MR, NE, SN, TD, TG).

**Declarations under Rule 4.17:**

- *of inventorship (Rule 4.17(iv))*

**Published:**

- *with international search report (Art. 21(3))*
- *before the expiration of the time limit for amending the claims and to be republished in the event of receipt of amendments (Rule 48.2(h))*
- *with sequence listing part of description (Rule 5.2(a))*

## TITLE OF THE INVENTION

PEPTIDE LIGANDS OF THE GDNF FAMILY RECEPTOR A-LIKE (GFRAL)  
RECEPTOR

5

## CROSS-REFERENCE TO RELATED APPLICATIONS

The present application claims priority under 35 U.S.C. § 119(e) to U.S. Provisional Patent Application No. 62/801,391, filed February 5, 2019, which is incorporated herein by reference in its entirety.

10

## BACKGROUND OF THE INVENTION

Long-term weight management and regulation of normal ingestive behavior in patients suffering from chronic diseases are serious problems without sufficient therapeutic treatments. Cachexia, nausea and chronic emesis from chemotherapy, cancer, chronic diseases and morning sickness are all difficult to manage and can be extremely debilitating and can compromise an individual's quality-of-life. Nausea and emesis can also set the upper tolerable dose of a therapeutic due to patient intolerance, thus potentially limiting drug efficacy. Accordingly, there is a need for an approach that can modulate the anorectic / nausea / emesis response to cancer, metabolic diseases and therapeutic treatments of various diseases. There is also a need for treatments for diseases or conditions that result in unhealthy increases or decreases in body weight, including but not limited to obesity and anorexia nervosa. As energy balance regulation also includes autonomic control of sympathetic and parasympathetic neural functions that affect various physiological responses, it is conceivable that systems regulating the aversive aspects of illness behavior can also be targeted in contrast to influence motivated and maladaptive motivated behaviors, such as substance abuse. To this end, given the need for treatments for sexual dysfunction there is a possibility to target a biological system that can also influence sexual behaviors and actions.

20

25

The present invention addresses the aforementioned unmet needs.

30

## SUMMARY OF THE INVENTION

In one aspect, the invention provides an engineered peptide comprising any one of the amino acid sequences of SEQ ID NOs: 1-10.

In another aspect, the invention provides a polynucleotide encoding the engineered peptide of the invention.

In yet another aspect the invention provides a pharmaceutical composition comprising the engineered peptide of the invention.

In yet another aspect, the invention provides a method of treating a disease or a condition in a subject in need thereof, composing the step of administering the engineered peptide of the invention to the subject.

In yet another aspect, the invention provides a method of promoting weight gain in a subject in need thereof by administering the engineered peptide of the invention to the subject.

In yet another aspect, the invention provides a method of promoting weight loss in a subject in need thereof by administering the engineered peptide of the invention to the subject.

In certain embodiments, at least one of the amino acids of the peptide is a modified amino acid.

In certain embodiments, the engineered peptide is an antagonist of a GDNF family receptor alpha-like (GFRAL) receptor.

In certain embodiments, the amino acid sequence of the engineered peptide comprises SEQ ID NO: 5.

In certain embodiments, the engineered peptide is an agonist of a GFRAL receptor.

In certain embodiments, the amino acid sequence of the engineered peptide comprises SEQ ID NO: 1.

In certain embodiments, the engineered peptide is linked to a vitamin B12 compound, a lipid or a fluorophore. In certain embodiments, the vitamin B12 compound, the lipid, or the fluorophore is linked to the peptide directly or via a linker. In certain embodiments, the vitamin B12 compound, the lipid, or the fluorophore is directly linked to any amino acid of the peptide. In certain embodiments, the vitamin B12 compound, the lipid or the fluorophore is directly linked to any modified amino acid of the peptide. In certain embodiments, the engineered peptide further comprises a metal ion bound to the peptide.

In certain embodiments, the metal ion is a  $Zn^{2+}$  ion or a  $Ca^{2+}$  ion.

In certain embodiments, the disease or the condition is nausea, emesis, cachexia, unintentional weight loss, loss of appetite, pica, anorexia or illness-like behaviors.

In certain embodiments, the disease or the condition is obesity or body weight regulation.

In certain embodiments, the disease or the condition is sexual dysfunction.

In certain embodiments, the engineered peptide is administered in a dosage of 1 pmole/kg to 100 mmoles/kg.

In certain embodiments, the engineered peptide is administered acutely or chronically over the course of multiple hours or days.

5

#### BRIEF DESCRIPTION OF THE DRAWINGS

The following detailed description of selected embodiments of the invention will be better understood when read in conjunction with the appended drawings. For the purpose of illustrating the invention, selected embodiments are shown in the drawings. It should be understood, however, that the invention is not limited to the precise arrangements and instrumentalities of the embodiments shown in the drawings.

FIG. 1 illustrates the peptide GFANT05. The sequence shown is that of GFANT05, wherein the GFANT05 peptide of SEQ ID NO: 5 has a wild-type lysine (K) in position K2.

FIG. 2A shows the method of production GFANT05 peptide conjugated with palmitic acid, wherein the GFANT05 peptide of SEQ ID NO: 5 has a modified lysine (K azido) in position K2. The GFANT05 peptide is linked to 16:0 PE at the K2 residue.

FIG. 2B shows the results of electrospray mass spectrometry on the GFANT05 conjugated synthesis product.

FIG. 3A shows a <sup>1</sup>H NMR structure of GFANT05, which reveals a broad spread of peaks consistent with a folded state for this peptide. FIG. 3B displays the 2D spectra COSY NMR structure of the GFANT05 peptide. FIG. 3C shows the 2D spectra TOCSY NMR structure of the GFANT05 peptide. Both FIGs. 3B and 3C suggest that the structure of GFANT05 contains at least one alpha helix.

FIG. 4 shows the results of an ELISA binding assay measuring the affinity of Recombinant human GDF-15 (rhGDF15) for its receptor.

FIG. 5A is a graph of a food intake study performed to evaluate the efficacy of unconjugated GFANT05 peptide (TK\*EELIHAHADPMVLIQKTDGTV SLQTYD; SEQ ID NO: 5, wherein K\* is K azido) to reduce nausea. FIG. 5B shows a graph of a kaolin intake study performed to evaluate the efficacy of unconjugated GFANT05 peptide in reducing nausea.

FIG. 6 is a graph confirming GFRAL receptor antagonist binding to the GFRAL receptor. A Cy5-conjugate of GFRAL receptor antagonist was synthesized and exposed to the human GFRAL receptor *in vitro* and tracked for binding using an anti-Cy5 antibody.

FIG. 7 is a graph confirming Zinc binding to GFRAL receptor antagonist at the HAHAD region (residues H7-P12) as observed by chemical shifts in 2D NMR.

FIG. 8 is a graph illustrating the results from *in vitro* PK study of GFRAL receptor antagonist in rat microsomes. The half-life was calculated to be: 104.43 min. Reaction velocity (V) was calculated to be 511uL/lmg. Intrinsic clearance (Cl-int) was determined to be 339 uL/min/mg protein.

FIG. 9 is an image showing GFANT05 peptide technology co-localizing with the GFRAL receptor in the brainstem (a major source of illness behaviors in disease and/or disease treatments). This technology provides a new route to treat cachexia and chemotherapy induced nausea/vomiting by uniquely blocking the GDF15-GFRAL signaling in the brainstem

## DETAILED DESCRIPTION

### Definitions

Unless defined otherwise, all technical and scientific terms used herein have the same meaning as commonly understood by one of ordinary skill in the art to which the invention pertains. Although any methods and materials similar or equivalent to those described herein can be used in the practice for testing of the present invention, the preferred materials and methods are described herein. In describing and claiming the present invention, the following terminology will be used.

It is also to be understood that the terminology used herein is for the purpose of describing particular embodiments only and is not intended to be limiting.

The articles “a” and “an” are used herein to refer to one or to more than one (*i.e.*, to at least one) of the grammatical object of the article. By way of example, “an element” means one element or more than one element.

“About” as used herein when referring to a measurable value such as an amount, a temporal duration, and the like, is meant to encompass variations of  $\pm 20\%$  or  $\pm 10\%$ , more preferably  $\pm 5\%$ , even more preferably  $\pm 1\%$ , and still more preferably  $\pm 0.1\%$  from the specified value, as such variations are appropriate to perform the disclosed methods.

As used herein, the term “conservative sequence modifications” is intended to refer to amino acid modifications that do not significantly affect or alter the binding characteristics of the peptide containing the amino acid sequence. Such conservative modifications include amino acid substitutions, additions and deletions and use of similar structured non-canonical amino acids or D-isomers of any of the canonical amino acids and/or non-canonical amino acids.

Modifications can be introduced into a peptide of the invention by standard techniques known in the art, such as solid-phase peptide synthesis, site-directed mutagenesis and PCR-mediated mutagenesis. Conservative amino acid substitutions are ones in which the amino acid residue is replaced with an amino acid residue having a similar side chain. Families of amino acid residues having similar side chains have been defined in the art. These families include amino acids with basic side chains (e.g., lysine, arginine, histidine), acidic side chains (e.g., aspartic acid, glutamic acid), uncharged polar side chains (e.g., glycine, asparagine, glutamine, serine, threonine, tyrosine, cysteine, tryptophan), nonpolar side chains (e.g., alanine, valine, leucine, isoleucine, proline, phenylalanine, methionine), beta-branched side chains (e.g., threonine, valine, isoleucine) and aromatic side chains (e.g., tyrosine, phenylalanine, tryptophan, histidine). Non-canonical examples include azido-lysine, methyl-alanine.

A “disease” is a state of health of a subject wherein the subject cannot maintain homeostasis, and wherein if the disease is not ameliorated then the subject’s health continues to deteriorate. In contrast, a “disorder” in a subject is a state of health in which the subject is able to maintain homeostasis, but in which the subject’s state of health is less favorable than it would be in the absence of the disorder. Left untreated, a disorder does not necessarily cause a further decrease in the subject’s state of health.

“Effective amount” or “therapeutically effective amount” are used interchangeably herein, and refer to an amount of a compound, formulation, material, or composition, as described herein effective to achieve a particular biological result or provides a therapeutic or prophylactic benefit. Such results may include, but are not limited to, anti-tumor activity as determined by any means suitable in the art.

“Encoding” refers to the inherent property of specific sequences of nucleotides in a polynucleotide, such as a gene, a cDNA, or an mRNA, to serve as templates for synthesis of other polymers and macromolecules in biological processes having either a defined sequence of nucleotides (*i.e.*, rRNA, tRNA and mRNA) or a defined sequence of amino acids and the biological properties resulting therefrom. Thus, a gene encodes a protein if transcription and translation of mRNA corresponding to that gene produces the protein in a cell or other biological system. Both the coding strand, the nucleotide sequence of which is identical to the mRNA sequence and is usually provided in sequence listings, and the non-coding strand, used as the template for transcription of a gene or cDNA, can be referred to as encoding the protein or other product of that gene or cDNA.

As used herein “endogenous” refers to any material from or produced inside an organism, cell, tissue or system.

As used herein, the term “exogenous” refers to any material introduced from or produced outside an organism, cell, tissue or system.

5 The term “expression” as used herein is defined as the transcription and/or translation of a particular nucleotide sequence driven by its promoter.

“Expression vector” refers to a vector comprising a recombinant polynucleotide comprising expression control sequences operatively linked to a nucleotide sequence to be expressed. An expression vector comprises sufficient cis-acting elements for expression;  
10 other elements for expression can be supplied by the host cell or in an in vitro expression system. Expression vectors include all those known in the art, such as cosmids, plasmids (e.g, naked or contained in liposomes) and viruses (e.g, sendai viruses, lentiviruses, retroviruses, adenoviruses, and adeno-associated viruses) that incorporate the recombinant polynucleotide.

15 “Homologous” as used herein, refers to the subunit sequence identity between two polymeric molecules, e.g., between two nucleic acid molecules, such as, two DNA molecules or two RNA molecules, or between two polypeptide molecules. When a subunit position in both of the two molecules is occupied by the same monomeric subunit; e.g, if a position in each of two DNA molecules is occupied by adenine, then they are homologous at that  
20 position. The homology between two sequences is a direct function of the number of matching or homologous positions; e.g, if half (e.g, five positions in a polymer ten subunits in length) of the positions in two sequences are homologous, the two sequences are 50% homologous; if 90% of the positions (e.g, 9 of 10), are matched or homologous, the two sequences are 90% homologous.

25 “Humanized” forms of non-human (e.g., murine) antibodies are chimeric immunoglobulins, immunoglobulin chains or fragments thereof (such as Fv, Fab, Fab', F(ab')<sub>2</sub> or other antigen-binding subsequences of antibodies) which contain minimal sequence derived from non-human immunoglobulin. For the most part, humanized antibodies are human immunoglobulins (recipient antibody) in which residues from a  
30 complementary-determining region (CDR) of the recipient are replaced by residues from a CDR of a non-human species (donor antibody) such as mouse, rat or rabbit having the desired specificity, affinity, and capacity. In some instances, Fv framework region (FR) residues of the human immunoglobulin are replaced by corresponding non-human residues. Furthermore, humanized antibodies can comprise residues which are found neither in the

recipient antibody nor in the imported CDR or framework sequences. These modifications are made to further refine and optimize antibody performance. In general, the humanized antibody will comprise substantially all of at least one, and typically two, variable domains, in which all or substantially all of the CDR regions correspond to those of a non-human immunoglobulin and all or substantially all of the FR regions are those of a human immunoglobulin sequence. The humanized antibody optimally also will comprise at least a portion of an immunoglobulin constant region (Fc), typically that of a human immunoglobulin. For further details, see Jones et al, Nature, 321: 522-525, 1986; Reichmann et al., Nature, 332: 323-329, 1988; Presta, Curr. Op. Struct. Biol., 2: 593-596, 1992.

“Fully human” refers to an immunoglobulin, such as an antibody, where the whole molecule is of human origin or consists of an amino acid sequence identical to a human form of the antibody.

“Identity” as used herein refers to the subunit sequence identity between two polymeric molecules particularly between two amino acid molecules, such as, between two polypeptide molecules. When two amino acid sequences have the same residues at the same positions; *e.g.* if a position in each of two polypeptide molecules is occupied by an Arginine, then they are identical at that position. The identity or extent to which two amino acid sequences have the same residues at the same positions in an alignment is often expressed as a percentage. The identity between two amino acid sequences is a direct function of the number of matching or identical positions; *e.g.*, if half (*e.g.* five positions in a polymer ten amino acids in length) of the positions in two sequences are identical, the two sequences are 50% identical; if 90% of the positions (*e.g.* 9 of 10), are matched or identical, the two amino acids sequences are 90% identical.

The term “immune response” as used herein is defined as a cellular response to an antigen that occurs when lymphocytes identify antigenic molecules as foreign and induce the formation of antibodies and/or activate lymphocytes to remove the antigen.

As used herein, an “instructional material” includes a publication, a recording, a diagram, or any other medium of expression which can be used to communicate the usefulness of the compositions and methods of the invention. The instructional material of the kit of the invention may, for example, be affixed to a container which contains the nucleic acid, peptide, and/or composition of the invention or be shipped together with a container which contains the nucleic acid, peptide, and/or composition. Alternatively, the instructional



material may be shipped separately from the container with the intention that the instructional material and the compound be used cooperatively by the recipient.

“Isolated” means altered or removed from the natural state. For example, a nucleic acid or a peptide naturally present in a living animal is not “isolated,” but the same nucleic acid or peptide partially or completely separated from the coexisting materials of its natural state is “isolated.” An isolated nucleic acid or protein can exist in substantially purified form, or can exist in a non-native environment such as, for example, a host cell.

A “lentivirus” as used herein refers to a genus of the Retroviridae family. Lentiviruses are unique among the retroviruses in being able to infect non-dividing cells; they can deliver a significant amount of genetic information into the DNA of the host cell, so they are one of the most efficient methods of a gene delivery vector. HIV, SIV, and FIV are all examples of lentiviruses. Vectors derived from lentiviruses offer the means to achieve significant levels of gene transfer in vivo.

By the term “modified” as used herein, is meant a changed state or structure of a molecule or cell of the invention. Molecules may be modified in many ways, including chemically, structurally, and functionally. Cells may be modified through the introduction of nucleic acids.

By the term “modulating,” as used herein, is meant mediating a detectable increase or decrease in the level of a response in a subject compared with the level of a response in the subject in the absence of a treatment or compound, and/or compared with the level of a response in an otherwise identical but untreated subject. The term encompasses perturbing and/or affecting a native signal or response thereby mediating a beneficial therapeutic response in a subject, preferably, a human.

In the context of the present invention, the following abbreviations for the commonly occurring nucleic acid bases are used. “A” refers to adenosine, “C” refers to cytosine, “G” refers to guanosine, “T” refers to thymidine, and “U” refers to uridine.

Unless otherwise specified, a “nucleotide sequence encoding an amino acid sequence” includes all nucleotide sequences that are degenerate versions of each other and that encode the same amino acid sequence. The phrase nucleotide sequence that encodes a protein or an RNA may also include introns to the extent that the nucleotide sequence encoding the protein may in some version contain an intron(s).

The term “operably linked” refers to functional linkage between a regulatory sequence and a heterologous nucleic acid sequence resulting in expression of the latter. For example, a first nucleic acid sequence is operably linked with a second nucleic acid sequence

when the first nucleic acid sequence is placed in a functional relationship with the second nucleic acid sequence. For instance, a promoter is operably linked to a coding sequence if the promoter affects the transcription or expression of the coding sequence. Generally, operably linked DNA sequences are contiguous and, where necessary to join two protein coding regions, in the same reading frame.

The term “overexpressed” tumor antigen or “overexpression” of a tumor antigen is intended to indicate an abnormal level of expression of a tumor antigen in a cell from a disease area like a solid tumor within a specific tissue or organ of the patient relative to the level of expression in a normal cell from that tissue or organ. Patients having solid tumors or a hematological malignancy characterized by overexpression of the tumor antigen can be determined by standard assays known in the art.

“Parenteral” administration of an immunogenic composition includes, *e.g.*, subcutaneous (s.c.), intravenous (i.v.), intramuscular (i.m.), or intrastemal injection, or infusion techniques.

The term “polynucleotide” as used herein is defined as a chain of nucleotides. Furthermore, nucleic acids are polymers of nucleotides. Thus, nucleic acids and polynucleotides as used herein are interchangeable. One skilled in the art has the general knowledge that nucleic acids are polynucleotides, which can be hydrolyzed into the monomeric “nucleotides.” The monomeric nucleotides can be hydrolyzed into nucleosides. As used herein polynucleotides include, but are not limited to, all nucleic acid sequences which are obtained by any means available in the art, including, without limitation, recombinant means, *i.e.*, the cloning of nucleic acid sequences from a recombinant library or a cell genome, using ordinary cloning technology and PCR<sup>TM</sup>, and the like, and by synthetic means.

As used herein, the terms “peptide,” “polypeptide,” and “protein” are used interchangeably, and refer to a compound comprised of amino acid residues covalently linked by peptide bonds. A protein or peptide must contain at least two amino acids, and no limitation is placed on the maximum number of amino acids that can comprise a protein’s or peptide’s sequence. Polypeptides include any peptide or protein comprising two or more amino acids joined to each other by peptide bonds. As used herein, the term refers to both short chains, which also commonly are referred to in the art as peptides, oligopeptides and oligomers, for example, and to longer chains, which generally are referred to in the art as proteins, of which there are many types. “Polypeptides” include, for example, biologically active fragments, substantially homologous polypeptides, oligopeptides, homodimers,

heterodimers, variants of polypeptides, modified polypeptides, derivatives, analogs, fusion proteins, among others. The polypeptides include natural peptides, recombinant peptides, synthetic peptides, or a combination thereof.

The term “promoter” as used herein is defined as a DNA sequence recognized by the synthetic machinery of the cell, or introduced synthetic machinery, required to initiate the specific transcription of a polynucleotide sequence.

As used herein, the term “promoter/regulatory sequence” means a nucleic acid sequence which is required for expression of a gene product operably linked to the promoter/regulatory sequence. In some instances, this sequence may be the core promoter sequence and in other instances, this sequence may also include an enhancer sequence and other regulatory elements which are required for expression of the gene product. The promoter/regulatory sequence may, for example, be one which expresses the gene product in a tissue specific manner.

A “constitutive” promoter is a nucleotide sequence which, when operably linked with a polynucleotide which encodes or specifies a gene product, causes the gene product to be produced in a cell under most or all physiological conditions of the cell.

An “inducible” promoter is a nucleotide sequence which, when operably linked with a polynucleotide which encodes or specifies a gene product, causes the gene product to be produced in a cell substantially only when an inducer which corresponds to the promoter is present in the cell.

A “tissue-specific” promoter is a nucleotide sequence which, when operably linked with a polynucleotide encodes or specified by a gene, causes the gene product to be produced in a cell substantially only if the cell is a cell of the tissue type corresponding to the promoter.

A “Sendai virus” refers to a genus of the Paramyxoviridae family. Sendai viruses are negative, single stranded RNA viruses that do not integrate into the host genome or alter the genetic information of the host cell. Sendai viruses have an exceptionally broad host range and are not pathogenic to humans. Used as a recombinant viral vector, Sendai viruses are capable of transient but strong gene expression.

A “signal transduction pathway” refers to the biochemical relationship between a variety of signal transduction molecules that play a role in the transmission of a signal from one portion of a cell to another portion of a cell. The phrase “cell surface receptor” includes molecules and complexes of molecules capable of receiving a signal and transmitting signal across the plasma membrane of a cell.

The term “subject” is intended to include living organisms in which an immune response can be elicited (e.g., mammals). A “subject” or “patient,” as used therein, may be a human or non-human mammal. Non-human mammals include, for example, livestock and pets, such as ovine, bovine, porcine, canine, feline, and murine mammals. Preferably, the subject is human.

As used herein, “substantially purified” refers to being essentially free of other components. For example, a substantially purified polypeptide is a polypeptide which has been separated from other components with which it is normally associated in its naturally occurring state.

The term “therapeutic” as used herein means a treatment and/or prophylaxis. A therapeutic effect is obtained by suppression, remission, or eradication of a disease state.

The term “transfected” or “transformed” or “transduced” as used herein refers to a process by which exogenous nucleic acid is transferred or introduced into the host cell. A “transfected” or “transformed” or “transduced” cell is one which has been transfected, transformed or transduced with exogenous nucleic acid. The cell includes the primary subject cell and its progeny.

To “treat” a disease as the term is used herein, means to reduce the frequency or severity of at least one sign or symptom of a disease or disorder experienced by a subject.

The phrase “under transcriptional control” or “operatively linked” as used herein means that the promoter is in the correct location and orientation in relation to a polynucleotide to control the initiation of transcription by RNA polymerase and expression of the polynucleotide.

A “vector” is a composition of matter which comprises an isolated nucleic acid and which can be used to deliver the isolated nucleic acid to the interior of a cell. Numerous vectors are known in the art including, but not limited to, linear polynucleotides, polynucleotides associated with ionic or amphiphilic compounds, plasmids, and viruses. Thus, the term “vector” includes an autonomously replicating plasmid or a virus. The term should also be construed to include non-plasmid and non-viral compounds which facilitate transfer of nucleic acid into cells, such as, for example, polylysine compounds, liposomes, and the like. Examples of viral vectors include, but are not limited to, Sendai viral vectors, adenoviral vectors, adeno-associated virus vectors, retroviral vectors, lentiviral vectors, and the like.

As used herein, the term “genetic construct” refers to the DNA or RNA molecules that comprise a nucleotide sequence which encodes protein. The coding sequence includes

initiation and termination signals operably linked to regulatory elements including a promoter and polyadenylation signal capable of directing expression in the cells of the individual to whom the nucleic acid molecule is administered.

Ranges: throughout this disclosure, various aspects of the invention can be presented in a range format. It should be understood that the description in range format is merely for convenience and brevity and should not be construed as an inflexible limitation on the scope of the invention. Accordingly, the description of a range should be considered to have specifically disclosed all the possible subranges as well as individual numerical values within that range. For example, description of a range such as from 1 to 6 should be considered to have specifically disclosed subranges such as from 1 to 3, from 1 to 4, from 1 to 5, from 2 to 4, from 2 to 6, from 3 to 6 etc., as well as individual numbers within that range, for example, 1, 2, 2.7, 3, 4, 5, 5.3, and 6. This applies regardless of the breadth of the range.

### Description

#### 15 Peptide Ligands of the GFRAL-RET Receptor

The present invention relates to ligands for the glial cell-derived neurotrophic factor (GDNF) family receptor  $\alpha$ -like (GFRAL)-RET (a receptor tyrosine kinase) receptor complex and, more specifically, to non-naturally occurring peptides specially designed to encourage or block the action of the native ligand growth and differentiation factor 15 (GDF15, also known as Macrophage inhibitory cytokine I (MIC-1). Importantly, the GFRAL-RET receptor complex is localized in the brainstem, specifically the nuclei of the dorsal vagal complex (including the area postrema, nucleus tractus solitarius and dorsal motor nucleus of the vagus). As the area postrema lies outside of the blood brain barrier - this implicates the GFRAL-RET receptor complex accessible to a peripheral-derived ligand action.

25 GDF15 is a transforming growth factor- $\beta$  (TGF- $\beta$ ) superfamily protein. More specifically, it has been proposed that this protein belongs to the subgroup of glial-cell-derived neurotrophic factors (GDNFs). GDNF ligands include glial-cell-derived neurotrophic factor (GDNF), neurturin (NTN), artemin (ART), and persephm (PSP). These family ligands signal through GDNF receptor alpha (GFRa<sup>^</sup>), respectively. Some cross talk occurs between the GDNF ligands and their receptors, but GDF15 is unable to activate any of the GFRa's. As discussed above, GDF15 is the native ligand for GFRAL-RET receptor complex.

The invention comprises the design of a series of non-naturally occurring peptides that can act as agonists or antagonists of the GFRAL receptor. The peptides that act as agonists may be used for the control of weight gain, for the control of obesity, or to treat

sexual dysfunction. The peptides that act as antagonists may be used for treating unwanted anorexia, cachexia or for controlling nausea, emesis, gastrointestinal distress, gastroparesis, or other illness-like behaviors, including but not limited to the reduction of nausea, e.g. nausea associated with the use of chemotherapy drugs or nausea associated with cancer, morning sickness, or chronic illness.

In some embodiments, the peptides may act to control energy balance regulation. In some embodiments, the peptides regulate energy intake. In further embodiments, the peptides regulate energy expenditure (e.g. regulation of cardiac rate or locomotive activity). In some embodiments, the peptides regulate sleep and circadian rhythm.

The peptides may be conjugated to a vitamin B12 compound for preventing brain penetration, particularly the hypothalamus, and target peripheral sites of action only.

Provided herein are engineered peptides. The amino acid sequences for selected peptides is shown in Table 1.

Provided is an engineered peptide comprising any one of the amino acid sequences of SEQ ID NOs: 1-10. In some embodiments, at least one of the amino acids of the peptide is a modified amino acid.

In some embodiments, the engineered peptide is an antagonist of a GDNF family receptor alpha-like (GFRAL) receptor. In further embodiments, the antagonist comprises the amino acid sequence of SEQ ID NO: 5. Without wishing to be bound by theory, the GFRAL-RET receptor antagonist of the invention may be a competitive inhibitor, a non-competitive inhibitor and/or an allosteric inhibitor.

In some embodiments, the engineered peptide is an agonist of a GFRAL receptor. In further embodiments, the agonist comprises the amino acid sequence of SEQ ID NO: 1.

In some embodiments, the engineered peptide is linked to a vitamin B12 or precursor compound, or a polymer, or lipid or a fluorophore. In some embodiments, the vitamin B12 compound is cyanocobalamin, or aquocobalamin, or hydroxocobalamin, or methylcobalamin, or adenosylcobalamin. In some embodiments, the vitamin B12 precursor compound is dicyanocobinamide. In some embodiments, the lipid is Caprylic acid (C8), or Capric acid (C10), or Lauric acid (C12), or Myristic acid (C14), or Palmitic acid (C16) or Stearic acid (C18). In some embodiments, the fluorophore is Cy5, or Cy3, or Alexa555, or Alexa488. In some embodiments, the lipid is 16:0 PE. In further embodiments, the vitamin B12 compound, the lipid or the fluorophore is linked to the peptide directly or via a linker. In some embodiments, the linker is propargyl amine, or butargyl amine, or ethylene diamine, or polyethylene glycol. In yet further embodiments, the vitamin B12 compound, the lipid or the

fluorophore is directly linked to any amino acid of the peptide. In some embodiments, the vitamin B12 compound, the lipid or the fluorophore is directly linked to any modified amino acid of the peptide. Also provided is the engineered peptide of any one of the previous embodiments, further comprising a metal ion bound to the peptide. In some embodiments, the metal ion is a  $Zn^{2+}$  ion or a  $Ca^{2+}$  ion.

Provided is a polynucleotide encoding the engineered peptide of any one of the previous embodiments.

Also provided is a pharmaceutical composition comprising the engineered peptide of any one of the previous embodiments.

Provided is a method of treating a disease in a subject in need thereof, comprising the step of administering the engineered peptide of any one of the previous embodiments. In some embodiments, the engineered peptide is an antagonist of a GFRAL-RET receptor. In some embodiments, the disease/illness treated is nausea, cachexia, pica, loss of appetite or anorexia nervosa. In further embodiments, the engineered peptide is administered systemically (e.g. subcutaneous or intravenous) in a dosage of 1 pmole/kg to 100 mmoles/kg, e.g., 10 pmoles/kg to 90 mmoles/kg, 20 pmoles/kg to 80 mmoles/kg, 30 pmoles/kg to 70 mmoles/kg, 40 pmoles/kg to 60 mmoles/kg, 50 pmoles/kg to 50 mmoles/kg, 60 pmoles/kg to 40 mmoles/kg, 70 pmoles/kg to 30 mmoles/kg, 80 pmoles/kg to 20 mmoles/kg, 90 pmoles/kg to 10 mmoles/kg, 100 pmoles/kg to 1 mmole/kg. In some embodiments the engineered peptide is administered acutely from 1 min or chronically over the course multiple hours / days, up to once per week. In yet further embodiments, the engineered peptide is administered acutely or chronically over the course of 1min to 1, 2, 3, 4, 5, 6, 7, 8, 9,10, 11, 12, 13, 14, 15, 16, 17, 18, 19, 20, 21, 22, 23, 24, or more hours. In yet further embodiments, the engineered peptide is administered over the course of 1, 2, 3, 4, 5, 6, 7, or more days. In yet further embodiments, the engineered peptide is administered once per week.

In some embodiments, the engineered peptide is an agonist of a GFRAL-RET receptor. In some embodiments, the disease or condition is obesity or body weight regulation. In further embodiments, the engineered peptide is administered in a dosage of 1 pmole/kg to 100 mmoles/kg, e.g., 10 pmoles/kg to 90 mmoles/kg, 20 pmoles/kg to 80 mmoles/kg, 30 pmoles/kg to 70 mmoles/kg, 40 pmoles/kg to 60 mmoles/kg, 50 pmoles/kg to 50 mmoles/kg, 60 pmoles/kg to 40 mmoles/kg, 70 pmoles/kg to 30 mmoles/kg, 80 pmoles/kg to 20 mmoles/kg, 90 pmoles/kg to 10 mmoles/kg, 100 pmoles/kg to 1 mmole/kg. In yet further embodiments, the engineered peptide is administered systemically (e.g. subcutaneous). In some embodiments the engineered peptide is administered acutely from 1 min or chronically

over the course multiple hours / days, up to once per week. In yet further embodiments, the engineered peptide is administered acutely or chronically over the course of 1 min to 1, 2, 3, 4, 5, 6, 7, 8, 9,10, 11, 12, 13, 14, 15, 16, 17, 18, 19, 20, 21, 22, 23, 24, or more hours. In yet further embodiments, the engineered peptide is administered over the course of 1, 2, 3, 4, 5, 6, 7, or more days. In yet further embodiments, the engineered peptide is administered once per week

In some embodiments, the disease is sexual dysfunction. In further embodiments, the engineered peptide is administered in a dosage from 1pmole/kg to 100mmoles/kg, e.g., 10 pmoles/kg to 90 mmoles/kg, 20 pmoles/kg to 80 mmoles/kg, 30 pmoles/kg to 70 mmoles/kg, 40 pmoles/kg to 60 mmoles/kg, 50 pmoles/kg to 50 mmoles/kg, 60 pmoles/kg to 40 mmoles/kg, 70 pmoles/kg to 30 mmoles/kg, 80 pmoles/kg to 20 mmoles/kg, 90 pmoles/kg to 10 mmoles/kg, 100 pmoles/kg to 1 mmole/kg. In yet further embodiments, the engineered peptide is administered systemically (e.g. subcutaneous). In some embodiments the engineered peptide is administered acutely from 1 min or chronically over the course multiple hours / days, up to once per week. In yet further embodiments, the engineered peptide is administered acutely or chronically over the course of 1min to 1, 2, 3, 4, 5, 6, 7, 8, 9,10, 11, 12, 13, 14, 15, 16, 17, 18, 19, 20, 21, 22, 23, 24, or more hours. In yet further embodiments, the engineered peptide is administered over the course of 1, 2, 3, 4, 5, 6, 7, or more days. In yet further embodiments, the engineered peptide is administered once per week

Provided is a method of promoting weight gain in a subject in need thereof, comprising the step of administering the engineered peptide of any one of the previous embodiments. In some embodiments, the engineered peptide is an agonist of a GFRAL receptor administered in a dosage of 1 pmole/kg to 100 mmoles/kg, e.g., 10 pmoles/kg to 90 mmoles/kg, 20 pmoles/kg to 80 mmoles/kg, 30 pmoles/kg to 70 mmoles/kg, 40 pmoles/kg to 60 mmoles/kg, 50 pmoles/kg to 50 mmoles/kg, 60 pmoles/kg to 40 mmoles/kg, 70 pmoles/kg to 30 mmoles/kg, 80 pmoles/kg to 20 mmoles/kg, 90 pmoles/kg to 10 mmoles/kg, 100 pmoles/kg to 1 mmole/kg. In yet further embodiments, the engineered peptide is administered systemically (e.g. subcutaneous). In some embodiments the engineered peptide is administered acutely from 1 min or chronically over the course multiple hours / days, up to once per week. In yet further embodiments, the engineered peptide is administered acutely or chronically over the course of 1min to 1, 2, 3, 4, 5, 6, 7, 8, 9,10, 11, 12, 13, 14, 15, 16, 17, 18, 19, 20, 21, 22, 23, 24, or more hours. In yet further embodiments, the engineered peptide is administered over the course of 1, 2, 3, 4, 5, 6, 7, or more days. In yet further embodiments, the engineered peptide is administered once per week



Provided is a method of promoting weight loss in a subject in need thereof, comprising the step of administering the engineered peptide of any one of the previous embodiments. In some embodiments, the engineered peptide is an antagonist of a GFRAL receptor. In further embodiments, the engineered peptide is administered in a dosage of 1 pmole/kg to 100 mmoles/kg, e.g., 10 pmoles/kg to 90 mmoles/kg, 20 pmoles/kg to 80 mmoles/kg, 30 pmoles/kg to 70 mmoles/kg, 40 pmoles/kg to 60 mmoles/kg, 50 pmoles/kg to 50 mmoles/kg, 60 pmoles/kg to 40 mmoles/kg, 70 pmoles/kg to 30 mmoles/kg, 80 pmoles/kg to 20 mmoles/kg, 90 pmoles/kg to 10 mmoles/kg, 100 pmoles/kg to 1 mmole/kg. In yet further embodiments, the engineered peptide is administered systemically (i.e. subcutaneous). In some embodiments the engineered peptide is administered acutely from 1 min or chronically over the course multiple hours / days, up to once per week. In yet further embodiments, the engineered peptide is administered acutely or chronically over the course of 1min to 1, 2, 3, 4, 5, 6, 7, 8, 9,10, 11, 12, 13, 14, 15, 16, 17, 18, 19, 20, 21, 22, 23, 24, or more hours. In yet further embodiments, the engineered peptide is administered over the course of 1, 2, 3, 4, 5, 6, 7, or more days. In yet further embodiments, the engineered peptide is administered once per week

The practice of the present invention employs, unless otherwise indicated, conventional techniques of molecular biology (including recombinant techniques), microbiology, cell biology, biochemistry and immunology, which are well within the purview of the skilled artisan. Such techniques are explained fully in the literature, such as, “Molecular Cloning: A Laboratory Manual”, fourth edition (Sambrook, 2012); “Oligonucleotide Synthesis” (Gait, 1984); “Culture of Animal Cells” (Freshney, 2010); “Methods in Enzymology” “Handbook of Experimental Immunology” (Weir, 1997); “Gene Transfer Vectors for Mammalian Cells” (Miller and Calos, 1987); “Short Protocols in Molecular Biology” (Ausubel, 2002); “Polymerase Chain Reaction: Principles, Applications and Troubleshooting”, (Babar, 2011); “Current Protocols in Immunology” (Coligan, 2002). These techniques are applicable to the production of the polynucleotides and polypeptides of the invention, and, as such, may be considered in making and practicing the invention. The engineered cytokines of the invention were codon optimized so as to enhance their ability to modulate the immune response in a mammal into which they are introduced. The invention includes sequences that are homologous to the sequences disclosed herein. Sequence homology for nucleotides and amino acids may be determined using FASTA, BLAST and Gapped BLAST (Altschul et al, Nuc. Acids Res., 1997, 25, 3389, which is incorporated herein by reference in its entirety) and PAUP\* 4.0b10 software (D. L. Swofford, Sinauer

Associates, Massachusetts). "Percentage of similarity" is calculated using PAUP\* 4.0M0 software (D. L. Swofford, Sinauer Associates, Massachusetts). The average similarity of the consensus sequence is calculated compared to all sequences in the phylogenic tree.

Briefly, the BLAST algorithm, which stands for Basic Local Alignment Search Tool is suitable for determining sequence similarity (Altschul et al., J. Mol. Biol., 1990, 215, 403-410, which is incorporated herein by reference in its entirety). Software for performing BLAST analyses is publicly available through the National Center for Biotechnology Information. This algorithm involves first identifying high scoring sequence pair (HSPs) by identifying short words of length W in the query sequence that either match or satisfy some positive-valued threshold score T when aligned with a word of the same length in a database sequence. T is referred to as the neighborhood word score threshold (Altschul et al, supra). These initial neighborhood word hits act as seeds for initiating searches to find HSPs containing them. The word hits are extended in both directions along each sequence for as far as the cumulative alignment score can be increased. Extension for the word hits in each direction are halted when: 1) the cumulative alignment score falls off by the quantity X from its maximum achieved value; 2) the cumulative score goes to zero or below, due to the accumulation of one or more negative-scoring residue alignments; or 3) the end of either sequence is reached. The Blast algorithm parameters W, T and X determine the sensitivity and speed of the alignment. The Blast program uses as defaults a word length (W) of 11, the BLOSUM62 scoring matrix (see Henikoff et al, Proc. Natl. Acad. Sci. USA, 1992, 89, 10915-10919, which is incorporated herein by reference in its entirety) alignments (B) of 50, expectation (E) of 10, M=5, N=4, and a comparison of both strands. The BLAST algorithm (Karlin et al, Proc. Natl. Acad. Sci. USA, 1993, 90, 5873-5787, which is incorporated herein by reference in its entirety) and Gapped BLAST perform a statistical analysis of the similarity between two sequences. One measure of similarity provided by the BLAST algorithm is the smallest sum probability (P(N)), which provides an indication of the probability by which a match between two nucleotide sequences would occur by chance. For example, a nucleic acid is considered similar to another if the smallest sum probability in comparison of the test nucleic acid to the other nucleic acid is less than about 1, preferably less than about 0.1, more preferably less than about 0.01, and most preferably less than about 0.001.

When taken up by a cell, the genetic construct(s) may remain present in the cell as a functioning extrachromosomal molecule and/or integrate into the cell's chromosomal DNA. DNA may be introduced into cells where it remains as separate genetic material in the form of a plasmid or plasmids. Alternatively, linear DNA that can integrate into the chromosome

may be introduced into the cell. When introducing DNA into the cell, reagents that promote DNA integration into chromosomes may be added. DNA sequences that are useful to promote integration may also be included in the DNA molecule. Alternatively, RNA may be administered to the cell. It is also contemplated to provide the genetic construct as a linear  
5 minichromosome including a centromere, telomeres and an origin of replication. Gene constructs may remain part of the genetic material in attenuated live microorganisms or recombinant microbial vectors which live in cells. Gene constructs may be part of genomes of recombinant viral vaccines where the genetic material either integrates into the chromosome of the cell or remains extrachromosomal. Genetic constructs include regulatory  
10 elements necessary for gene expression of a nucleic acid molecule. The elements include: a promoter, an initiation codon, a stop codon, and a polyadenylation signal. In addition, enhancers are often required for gene expression of the sequence that encodes the peptide. It is necessary that these elements be operably linked to the sequence that encodes the desired proteins and that the regulatory elements are operably in the individual to whom they are  
15 administered.

Initiation codons and stop codon are generally considered to be part of a nucleotide sequence that encodes the desired protein. However, it is necessary that these elements are functional in the individual to whom the gene construct is administered. The initiation and termination codons must be in frame with the coding sequence.

20 Promoters and polyadenylation signals used must be functional within the cells of the individual.

Examples of promoters useful to practice the present invention, especially in the production of a genetic vaccine for humans, include but are not limited to promoters from Simian Virus 40 (SV40), Mouse Mammary Tumor Virus (MMTV) promoter, Human  
25 Immunodeficiency Virus (MV) such as the HIV Long Terminal Repeat (LTR) promoter, Moloney virus, ALV, Cytomegalovirus (CMV) such as the CMV immediate early promoter, Epstein Barr Virus (EBV), Rous Sarcoma Virus (RSV) as well as promoters from human genes such as human Actin, human Myosin, human Hemoglobin, human muscle creatine and human metallothionein.

30 Examples of polyadenylation signals useful to practice the present invention, especially in the production of a genetic vaccine for humans, include but are not limited to SV40 polyadenylation signals and LTR polyadenylation signals. In particular, the SV40 polyadenylation signal that is in pCEP4 plasmid (Invitrogen, San Diego Calif.), referred to as the SV40 polyadenylation signal, is used.

In addition to the regulatory elements required for DNA expression, other elements may also be included in the DNA molecule. Such additional elements include enhancers. The enhancer may be selected from the group including but not limited to: human Actin, human Myosin, human Hemoglobin, human muscle creatine and viral enhancers such as those from  
5 CMV, RSV and EBV.

Genetic constructs can be provided with mammalian origin of replication in order to maintain the construct extrachromosomally and produce multiple copies of the construct in the cell. Plasmids pVAX1, pCEP4 and pREP4 from Invitrogen (San Diego, Calif.) contain the Epstein Barr virus origin of replication and nuclear antigen EBNA-1 coding region which  
10 produces high copy episomal replication without integration. In order to maximize peptide production, regulatory sequences may be selected which are well suited for gene expression in the cells the construct is administered into. Moreover, codons may be selected which are most efficiently transcribed in the cell. One having ordinary skill in the art can produce DNA constructs that are functional in the cells. In some embodiments for which protein is used,  
15 i.e., the engineered peptides of the invention, for example, one having ordinary skill in the art can, using well known techniques, produce and isolate peptides of the invention using well known techniques. In some embodiments for which protein is used, for example, one having ordinary skill in the art can, using well known techniques, inserts DNA molecules that encode a protein of the invention into a commercially available expression vector for use in well-  
20 known expression systems. For example, the commercially available plasmid pSE420 (Invitrogen, San Diego, Calif.) may be used for production of protein in *E. coli*. The commercially available plasmid pYES2 (Invitrogen, San Diego, Calif.) may, for example, be used for production in *S. cerevisiae* strains of yeast. The commercially available MAXBAC.TM. complete baculovirus expression system (Invitrogen, San Diego, Calif.) may,  
25 for example, be used for production in insect cells. The commercially available plasmid pcDNA I or pcDNA3 (Invitrogen, San Diego, Calif.) may, for example, be used for production in mammalian cells such as Chinese Hamster Ovary cells. One having ordinary skill in the art can use these commercial expression vectors and systems or others to produce protein by routine techniques and readily available starting materials. (See e.g., Sambrook et  
30 al., *Molecular Cloning*, Third Ed. Cold Spring Harbor Press (2001) which is incorporated herein by reference.) Thus, the desired peptides can be prepared in both prokaryotic and eukaryotic systems, resulting in a spectrum of processed forms of the peptide.

One having ordinary skill in the art may use other commercially available expression vectors and systems or produce vectors using well known methods and readily available

starting materials. Expression systems containing the requisite control sequences, such as promoters and polyadenylation signals, and preferably enhancers are readily available and known in the art for a variety of hosts. See e.g., Sambrook et al, Molecular Cloning Third Ed. Cold Spring Harbor Press (2001). Genetic constructs include the protein coding sequence operably linked to a promoter that is functional in the cell line into which the constructs are transfected. Examples of constitutive promoters include promoters from cytomegalovirus or SV40. Examples of inducible promoters include mouse mammary leukemia virus or metallothionein promoters. Those having ordinary skill in the art can readily produce genetic constructs useful for transfecting with cells with DNA that encodes protein of the invention from readily available starting materials. The expression vector including the DNA that encodes the peptide is used to transform the compatible host which is then cultured and maintained under conditions wherein expression of the foreign DNA takes place.

The protein produced is recovered from the culture, either by lysing the cells or from the culture medium as appropriate and known to those in the art. One having ordinary skill in the art can, using well known techniques, isolate peptide that is produced using such expression systems. The methods of purifying protein from natural sources using antibodies which specifically bind to a specific peptide as described above may be equally applied to purifying peptide produced by recombinant DNA methodology.

In addition to producing peptides by recombinant techniques, automated peptide synthesizers may also be employed to produce isolated, essentially pure peptide. Such techniques are well known to those having ordinary skill in the art and are useful if derivatives which have substitutions not provided for in DNA-encoded protein production.

The polynucleotides encoding the engineered peptides of the invention may be delivered using any of several well-known technologies including DNA injection (also referred to as DNA vaccination), recombinant vectors such as recombinant adenovims, recombinant adenovirus associated vims and recombinant vaccinia vims.

Routes of administration include, but are not limited to, intramuscular, intranasally, intraperitoneal, intradermal, subcutaneous, intravenous, intraarterially, intraocularly and oral as well as topically, transdermally, by inhalation or suppository or to mucosal tissue such as by lavage to vaginal, rectal, urethral, buccal and sublingual tissue. Preferred routes of administration include intramuscular, intraperitoneal, intradermal and subcutaneous injection. Genetic constmcts may be administered by means including, but not limited to, electroporation methods and devices, traditional syringes, needleless injection devices, or "microprojectile bombardment gone guns".

Pharmaceutical Compositions and Dosing Regimens

Administration of the compositions of the invention is typically parenteral, by subcutaneous, intravenous, intramuscular, or intraperitoneal injection, or by infusion or by any other acceptable systemic method. In a preferred embodiment, administration is by  
5 subcutaneous injection. In another preferred embodiment, administration is by intravenous infusion, which may typically take place over a time course of about 1 to 5 hours. In addition, there are a variety of oral delivery methods for administration of therapeutic peptides, and these can be applied to the therapeutic peptides of this invention.

Often, treatment dosages are titrated upward from a low level to optimize safety and  
10 efficacy. Generally, daily dosages will fall within a range of about 0.01 to 20 mg peptide per kilogram of body weight. Typically, the dosage range will be from about 0.1 to 5 mg peptide per kilogram of body weight. Various modifications or derivatives of the peptides, such as addition of polyethylene glycol chains (PEGylation), lipidation or linkage to a vitamin B12 compound, may be made to influence their pharmacokinetic and/or pharmacodynamic  
15 properties.

To administer the peptide by other than parenteral administration, it may be necessary to coat the peptide with, or co-administer the peptide with, a material to prevent its inactivation. For example, peptide may be administered in an incomplete adjuvant, co-  
20 administered with enzyme inhibitors or in liposomes. Enzyme inhibitors include pancreatic trypsin inhibitor, diisopropylfluorophosphate (DEP) and trasylol. Liposomes include water-in-oil-in-water CGF emulsions as well as conventional liposomes (Strejan *et al.*, 1984, *J. Neuroimmunol.* 7:27).

Although the compositions of the invention can be administered in simple solution, they are more typically used in combination with other materials such as carriers, preferably  
25 pharmaceutically acceptable carriers. Useful pharmaceutically acceptable carriers can be any compatible, non-toxic substance suitable for delivering the compositions of the invention to a patient. Sterile water, alcohol, fats, waxes, and inert solids may be included in a carrier. Pharmaceutically acceptable adjuvants (buffering agents, dispersing agents) may also be incorporated into the pharmaceutical composition. Generally, compositions useful for  
30 parenteral administration of such drugs are well known; *e.g.*, *Remington's Pharmaceutical Science*, 17th Ed. (Mack Publishing Company, Easton, Pa., 1990). Alternatively, compositions of the invention may be introduced into a patient's body by implantable drug delivery systems (Urquhart *et al.*, 1984, *Ann. Rev. Pharmacol. Toxicol.* 24:199).

Therapeutic formulations may be administered in many conventional dosage formulations. Formulations typically comprise at least one active ingredient, together with one or more pharmaceutically acceptable carriers. Formulations may include those suitable for oral, rectal, nasal, or parenteral (including subcutaneous, intramuscular, intravenous and intradermal) administration.

The formulations may conveniently be presented in unit dosage form and may be prepared by any methods well known in the art of pharmacy. *See, e.g., Gilman et al. (eds.) (1990), The Pharmacological Bases of Therapeutics, 8th Ed., Pergamon Press; and Remington's Pharmaceutical Sciences, supra, Easton, Pa.; Avis et al. (eds.) (1993) Pharmaceutical Dosage Forms: Parenteral Medications, Dekker, N.Y.; Lieberman et al. (eds.) (1990) Pharmaceutical Dosage Forms: Tablets, Dekker, N.Y.; and Lieberman et al. (eds.) (1990), Pharmaceutical Dosage Forms: Disperse Systems, Dekker, N.Y.*

The pharmaceutical compositions according to the present invention are formulated according to the mode of administration to be used. In cases where pharmaceutical compositions are injectable pharmaceutical compositions, they are sterile, pyrogen free and particulate free. An isotonic formulation is preferably used. Generally, additives for isotonicity can include sodium chloride, dextrose, mannitol, sorbitol and lactose. In some cases, isotonic solutions such as phosphate buffered saline are preferred. Stabilizers include gelatin and albumin. In some embodiments, a vasoconstriction agent is added to the formulation.

In additional embodiments, the present invention contemplates administration of the peptides by gene therapy methods, e.g., administration of an isolated nucleic acid encoding a peptide of interest. The peptides of the present invention have been well-characterized, both as to the nucleic acid sequences encoding the peptides and the resultant amino acid sequences of the peptides. Engineering of such isolated nucleic acids by recombinant DNA methods is well within the ability of one skilled in the art. Codon optimization, for purposes of maximizing recombinant protein yields in particular cell backgrounds, is also well within the ability of one skilled in the art. Administration of an isolated nucleic acid encoding the fusion protein is encompassed by the expression "administering a therapeutically effective amount of a fusion protein of the invention." Gene therapy methods are well known in the art. *See, e.g., WO96/07321* which discloses the use of gene therapy methods to generate intracellular antibodies. Gene therapy methods have also been successfully demonstrated in human patients. *See, e.g., Baumgartner et al, 1998, Circulation 97: 12, 1114-1123, and more recently, Fatham, 2007, "A gene therapy approach to treatment of autoimmune diseases,"*

*Immun. Res.* 18:15-26; and U.S. Pat. No. 7,378,089, both incorporated herein by reference. See also Bainbridge *et al.*, 2008, "Effect of gene therapy on visual function in Leber's congenital Amaurosis," *N Engl Med* 358:2231-2239; and Maguire *et al.*, 2008, "Safety and efficacy of gene transfer for Leber's congenital Amaurosis," *N Engl JMed* 358:2240-8.

5 There are two major approaches for introducing a nucleic acid encoding the peptide (optionally contained in a vector) into a patient's cells: *in vivo* and *ex vivo*. For *in vivo* delivery, the nucleic acid is injected directly into the patient, usually at the site where the peptide is required. For *ex vivo* treatment, the patient's cells are removed, the nucleic acid is introduced into these isolated cells and the modified cells are administered to the patient  
10 either directly or, for example, encapsulated within porous membranes which are implanted into the patient (*see, e.g.* U.S. Pat. Nos. 4,892,538 and 5,283,187). There are a variety of techniques available for introducing nucleic acids into viable cells. The techniques vary depending upon whether the nucleic acid is transferred into cultured cells *in vitro*, or *in vivo* in the cells of the intended host. Techniques suitable for the transfer of nucleic acid into  
15 mammalian cells *in vitro* include the use of liposomes, electroporation, microinjection, cell fusion, DEAE-dextran, the calcium phosphate precipitation method, etc. Commonly used vectors for *ex vivo* delivery of the gene are retroviral and lentiviral vectors.

Preferred *in vivo* nucleic acid transfer techniques include transfection with viral vectors such as adenovirus, Herpes simplex I virus, adeno-associated virus), lipid-based  
20 systems (useful lipids for lipid-mediated transfer of the gene are DOTMA, DOPE and DC-Chol, for example), naked DNA, and transposon-based expression systems. For review of the currently known gene marking and gene therapy protocols see Anderson *et al.*, *Science* 256:808-813 (1992). See also WO 93/25673 and the references cited therein.

"Gene therapy" includes both conventional gene therapy where a lasting effect is  
25 achieved by a single treatment, and the administration of gene therapeutic agents, which involves the one time or repeated administration of a therapeutically effective DNA or mRNA. Oligonucleotides can be modified to enhance their uptake, e.g. by substituting their negatively charged phosphodiester groups by uncharged groups. Peptides of the present invention can be delivered using gene therapy methods, for example locally in tumor beds,  
30 intrathecally, or systemically (e.g., via vectors that selectively target specific tissue types, for example, tissue-specific adeno-associated viral vectors). In some embodiments, primary cells (such as lymphocytes or stem cells) from the individual can be transfected *ex vivo* with a gene encoding any of the fusion proteins of the present invention, and then returning the transfected cells to the individual's body.



“Treating” or “treatment” refers to therapeutic treatment, wherein the object is to prevent or slow down (lessen) the targeted pathologic condition or disorder. A subject is successfully “treated” if: after receiving a therapeutic amount of a peptide of the invention according to the methods of the present invention, the subject shows observable and/or measurable reduction in or absence of one or more signs and symptoms of the particular disease. Reduction of the signs or symptoms of a disease may also be felt by the patient. Treatment can achieve a complete response, defined as disappearance of all signs of cancer, or a partial response, wherein the size of the tumor is decreased, preferably by more than 50%, more preferably by 75%. A patient is also considered treated if the patient experiences a stabilization of disease. These parameters for assessing successful treatment and improvement in the disease are readily measurable by routine procedures familiar to a physician of appropriate skill in the art.

Design of peptides

15

Table 1

SEQ ID NO:	Peptide Name	Peptide Sequence
1	GFANT01	EDDVSFQK*LDDNVRHYHLRK
2	GFANT02	DDDLSFQK*LDDNVYYHLLRK
3	GFANT03	K*LDDNVYYHLLRK
4	GFANT04	K*PMVLIQKTDGTGVSLSQTYD
5	GFANT05	TK*EELIHAHADPMVLIQKTDGTGVSLSQTYD
6	GFANT06	VLSPREVQHAHADPMVLIQKTDGTGVSLSQTYD
7	GFANT07	VLSPREVQHAHADPMVLI
8	GFANT08	VITPREVQHAHADPMILIQKTDSGISIQSYE
9	GFANT09	VITPREVQHAHADPMILI
10	GFANT10	TKEELIHAHADPMILIQKTDSGISIQSYE

*\*Lysines marked with an asterisk (K\*) may be wildtype (K) or azido (K(Ns)), or otherwise modified*

20

In some embodiments, at least one of the amino acids of the peptide is a modified amino acid. In some embodiments, the peptide wherein at least one of its amino acids is a modified amino acid is an agonist of a GFRAL receptor. In further embodiments, the peptide wherein at least one of its amino acids is a modified amino acid is an antagonist of a GFRAL receptor.

25

The practice of the invention is illustrated by the following non-limiting examples. The invention should not be construed to be limited solely to the compositions and methods

described herein, but should be construed to include other compositions and methods as well. One of skill in the art will know that other compositions and methods are available to perform the procedures described herein.

The practice of the present invention employs, unless otherwise indicated, conventional techniques of molecular biology (including recombinant techniques), microbiology, cell biology, biochemistry and immunology, which are well within the purview of the skilled artisan. Such techniques are explained fully in the literature, such as, “Molecular Cloning: A Laboratory Manual”, fourth edition (Sambrook, 2012); “Oligonucleotide Synthesis” (Gait, 1984); “Culture of Animal Cells” (Freshney, 2010); “Methods in Enzymology” “Handbook of Experimental Immunology” (Weir, 1997); “Gene Transfer Vectors for Mammalian Cells” (Miller and Calos, 1987); “Short Protocols in Molecular Biology” (Ausubel, 2002); “Polymerase Chain Reaction: Principles, Applications and Troubleshooting”, (Babar, 2011); “Current Protocols in Immunology” (Coligan, 2002). These techniques are applicable to the production of the polynucleotides and polypeptides of the invention, and, as such, may be considered in making and practicing the invention. Particularly useful techniques for particular embodiments will be discussed in the sections that follow.

## EXPERIMENTAL EXAMPLES

The invention is further described in detail by reference to the following experimental examples. These examples are provided for the purposes of illustration only and are not intended to be limiting unless otherwise specified. Thus, the invention should in no way be construed as being limited to the following examples, but rather, should be construed to encompass any and all variations which become evident as a result of the teaching provided herein.

Without further description, it is believed that one of ordinary skill in the art can, using the preceding description and the following illustrating examples, make and utilize the compounds of the present invention and practice the claimed methods. The following working examples therefore specifically point out the preferred embodiments of the present invention, and are not to be construed as limiting in any way the remainder of the disclosure.

### *Example 1-Peptide Design and Conjugation of GFANT05 with or without Palmitic Acid.*

Putative agonistic and antagonistic peptide ligands of the GFRAL receptor were predicted using *in silico* analysis of known peptide ligands that bind across the GDF family

(Table 1). In some of the peptides of Table 1 (GFANT05-GFANT10), addition of a metal (e.g.  $\text{Ca}^{2+}$  or  $\text{Zn}^{2+}$ ) binding motif (HAHAD) was introduced to incorporate possible secondary structure changes to the peptide and/or to facilitate interaction with the receptor. In some embodiments, the peptides have additional residues from human GDF15 known to interact with the GFRAL receptor. In addition, specific residues were modified in order to help increase noncovalent interactions and modify hydrophilicity of the peptide, as suggested by modeling

Five peptides from Table 1 (GFANT01-GFANT05, SEQ. ID NOs 1-5, wherein the  $\text{K}^*$  in each peptide is Lysine( $\text{N}_3$ )) were synthesized. The peptides are capable of being conjugated to a lipid. GFANT05 was incubated with palmitic acid overnight at room temperature to produce GFANT conjugated to palmitic acid (FIG. 2A). The resulting molecule was subjected to electrospray mass spectrometry to confirm proper production of the GFANT05 product.

$^1\text{H}$  NMR analysis of the GFANT05 peptide alone revealed a broad spectrum of peaks consistent with a folded state (FIG. 3A). Further 2D NMR analysis revealed that the GFANT05 peptide consisted of at least one alpha helix (FIG. 3B-3C).

#### *Example 2-ELISA Assay*

To validate binding of the synthesized peptides to the GFRAL receptor, an ELISA assay was developed to determine the binding affinity of the peptides for their receptor. The primary antibody (Abeam ab206414) was diluted to 1  $\mu\text{g}/\text{mL}$ . The secondary antibody was diluted by placing 5  $\mu\text{L}$  into 10 mL assay buffer. GDF15 was run at concentrations of 100 ng/mL to 0.005 ng/mL. The recombinant human GFRa-like His-tag receptor (R&D 9647-GR-050) was added to the Pierce™ nickel coated plate (ThermoFisher Scientific 15442) at 0.1  $\mu\text{g}/\text{mL}$  in a total volume of 100  $\mu\text{L}$ . The  $\text{K}_\text{D}$  was determined to be 1.03 ng/mL, consistent with published values, thus demonstrating that the ELISA is functional (FIG. 4A). These data reveal a novel ELISA assay that can be utilized to test the ability of the artificial peptides to bind GFRAL.

#### *Example 3-Nausea / Malaise (i.e. illness-like behaviors) Studies in Rats*

Five potential ligands (GFANT01-GFANT05, SEQ. ID NOs: 1-5, wherein the  $\text{K}^*$  in each peptide is Lysine( $\text{N}_3$ )) were synthesized. The effects of each of the novel ligands were tested for their ability to alter nausea in rats over the course of 24 hours. Although

GFANT01-GFANT05 were tested, only GFANT05 was found to have a significant effect on nausea / illness-like behaviors in rats. Animals were given either MIC-1 (30 pmol), the endogenous ligand of GFRAL that suppresses appetites, GFANT05 (300 pmol), or a combination of both and their food intake was monitored for up to 24 hrs (FIG. 5A). While there was little difference in food consumption between control and treated groups early, at 24 hrs post-administration, animals given GFANT05 alone ate the same amount of food as untreated control animals. Further, the addition of GFANT05 to shrew that also received MIC-1 did not increase overall food consumption over MIC-1 (FIG. 5A). In addition, kaolin intake, a reliable measure of nausea in rats, was reduced in animals receiving GFANT05 compared to vehicle alone and that of a known nausea-inducing compound (MIC-1) (FIG. 5B). Taken together, these data suggest that GFANT05 is an antagonistic compound that promotes food consumption and decreases nausea in animals. Analysis of emetic episodes were measured by an observer blinded to treatment groups.

#### 15 *Example 4-Ejaculation Studies in Rats*

Administration of GFANT01 to rats was found to result in spontaneous ejaculation in male rats. MIC-1 was found to have the same effect on male rats. Rats were video recorded for 3h and the number of spontaneous ejaculations were analyzed by an observer blinded to treatment groups. Without wishing to be bound by theory, GFANT01 may be an agonist of the GFRAL receptor.

#### Other Embodiments

The recitation of a listing of elements in any definition of a variable herein includes definitions of that variable as any single element or combination (or subcombination) of listed elements. The recitation of an embodiment herein includes that embodiment as any single embodiment or in combination with any other embodiment or portions thereof.

The disclosures of each and every patent, patent application, and publication cited herein are hereby incorporated herein by reference in their entirety. While this invention has been disclosed with reference to specific embodiments, it is apparent that other embodiments and variations of this invention may be devised by others skilled in the art without departing from the true spirit and scope of the invention. The appended claims are intended to be construed to include all such embodiments and equivalent variations.

## CLAIMS

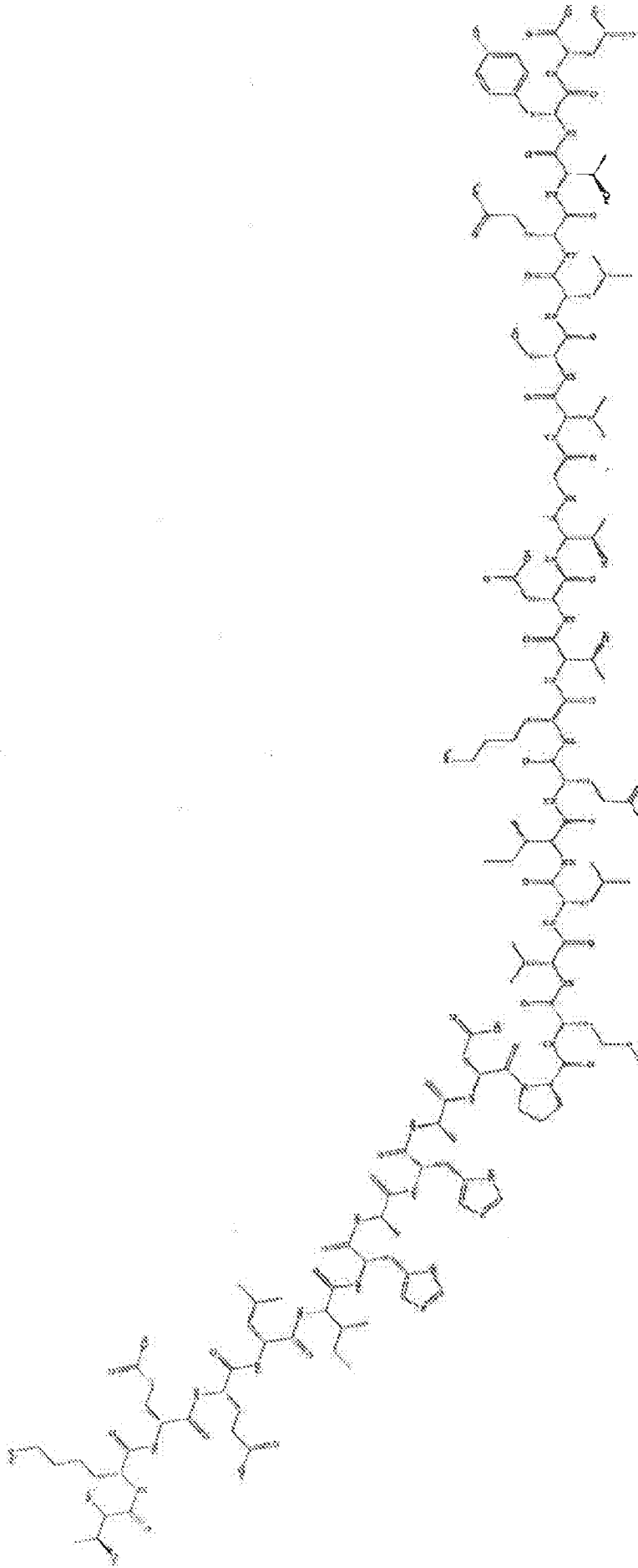
What is claimed is:

1. An engineered peptide comprising any one of the amino acid sequences of SEQ ID NOs: 1-10.
2. The engineered peptide of claim 1, wherein at least one of the amino acids of the peptide is a modified amino acid.
3. The engineered peptide of claim 1, wherein the engineered peptide is an antagonist of a GDNF family receptor alpha-like (GFRAL) receptor.
4. The engineered peptide of claim 3, wherein the amino acid sequence of the engineered peptide comprises the amino acid sequence of SEQ ID NO: 5.
5. The engineered peptide of claim 1, wherein the engineered peptide is an agonist of a GFRAL receptor.
6. The engineered peptide of claim 5, wherein the amino acid sequence of the engineered peptide comprises the amino acid sequence of SEQ ID NO: 1.
7. The engineered peptide of claim 1, wherein the engineered peptide is linked to a vitamin B12 compound, a lipid or a fluorophore.
8. The engineered peptide of claim 7, wherein the vitamin B12 compound, the lipid, or the fluorophore is linked to the peptide directly or via a linker.
9. The engineered peptide of claim 8, wherein the vitamin B12 compound, the lipid, or the fluorophore is directly linked to any amino acid of the peptide.
10. The engineered peptide of claim 8, wherein the vitamin B12 compound, the lipid or the fluorophore is directly linked to any modified amino acid of the peptide.

11. The engineered peptide of any one of claims 1-10, further comprising a metal ion bound to the peptide.
12. The engineered peptide of claim 11, wherein the metal ion is a  $Zn^{2+}$  ion or a  $Ca^{2+}$  ion.
13. A polynucleotide encoding the engineered peptide of any one of claims 1-12.
14. A pharmaceutical composition comprising the engineered peptide of any one of claims 1-12.
15. A method of treating a disease or a condition in a subject in need thereof, the method comprising administering the engineered peptide of claim 3 to the subject.
16. The method of claim 15, wherein the disease or the condition is nausea, emesis, cachexia, unintentional weight loss, loss of appetite, pica, anorexia or illness-like behaviors.
17. The method of claim 15, wherein the engineered peptide is administered in a dosage of 1 pmole/kg to 100 mmoles/kg.
18. The method of claim 15, wherein the engineered peptide is administered acutely or chronically over the course multiple hours or days.
19. A method of treating a disease or a condition in a subject in need thereof, comprising administering the engineered peptide of claim 5 to the subject.
20. The method of claim 19, wherein the disease or the condition is obesity or body weight regulation.
21. The method of claim 20, wherein the engineered peptide is administered in a dosage of 1 pmole/kg to 100 mmoles/kg.
22. The method of claim 20, wherein the engineered peptide is administered acutely or chronically over the course multiple hours or days.

23. The method of claim 19, wherein the disease or the condition is sexual dysfunction.
24. The method of claim 23, wherein the engineered peptide is administered in a dosage of 1 pmole/kg to 100 mmoles/kg.
25. The method of claim 23, wherein the engineered peptide is administered acutely or chronically over the course multiple hours or days.
26. A method of promoting weight gain in a subject in need thereof, the method comprising administering the engineered peptide of claim 3 to the subject.
27. The method of claim 26, wherein the engineered peptide is administered in a dosage of 1 pmole/kg to 100 mmoles/kg.
28. The method of claim 26, wherein the engineered peptide is administered acutely or chronically over the course multiple hours or days.
29. A method of promoting weight loss in a subject in need thereof, comprising administering the engineered peptide of claim 5 to the subject.
30. The method of claim 29, wherein the engineered peptide is administered in a dosage of 1 pmole/kg to 100 mmoles/kg.
31. The method of claim 29, wherein the engineered peptide is administered acutely or chronically over the course of multiple hours or days.

# GFANT05



Thr-Lys-Glu-Glu-Leu-Ile-His-Ala-His-Ala-Asp-Pro-Met-Val-Leu-Ile-Gln-Lys-Thr-Asp-Thr-Gly-Val-Ser-Leu-Gln-Thr-Tyr-Asp

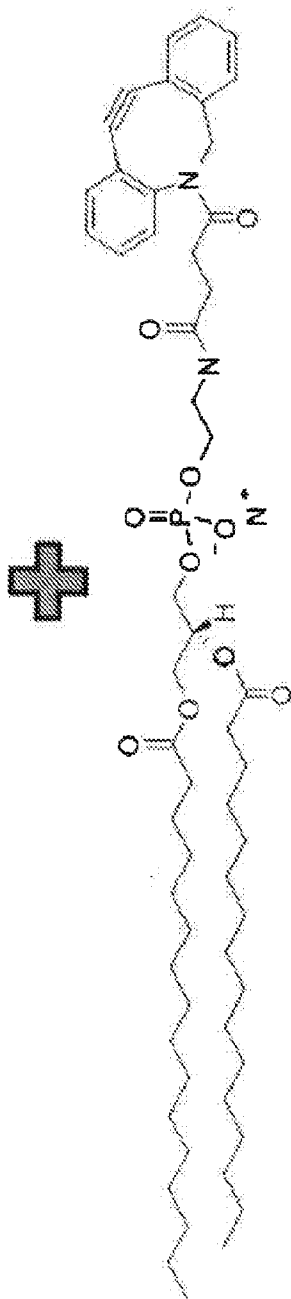
FIG. 1



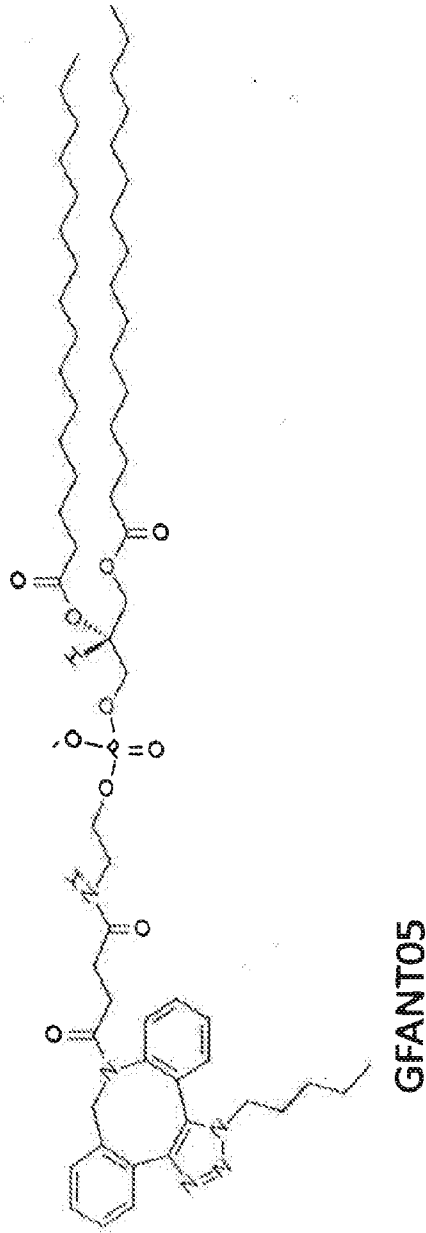
GFANT05: TK(azido)EELIHAAHADPMVLIQKTDTGVSLSQTYD  
(SEQ ID NO:5)

Theoretical MW: 3280.62  
Observed MW: 3279.64

Chemical Formula:  $C_{56}H_{90}N_3O_{10}P$   
Exact Mass: 995.636  
Molecular Weight: 996.321

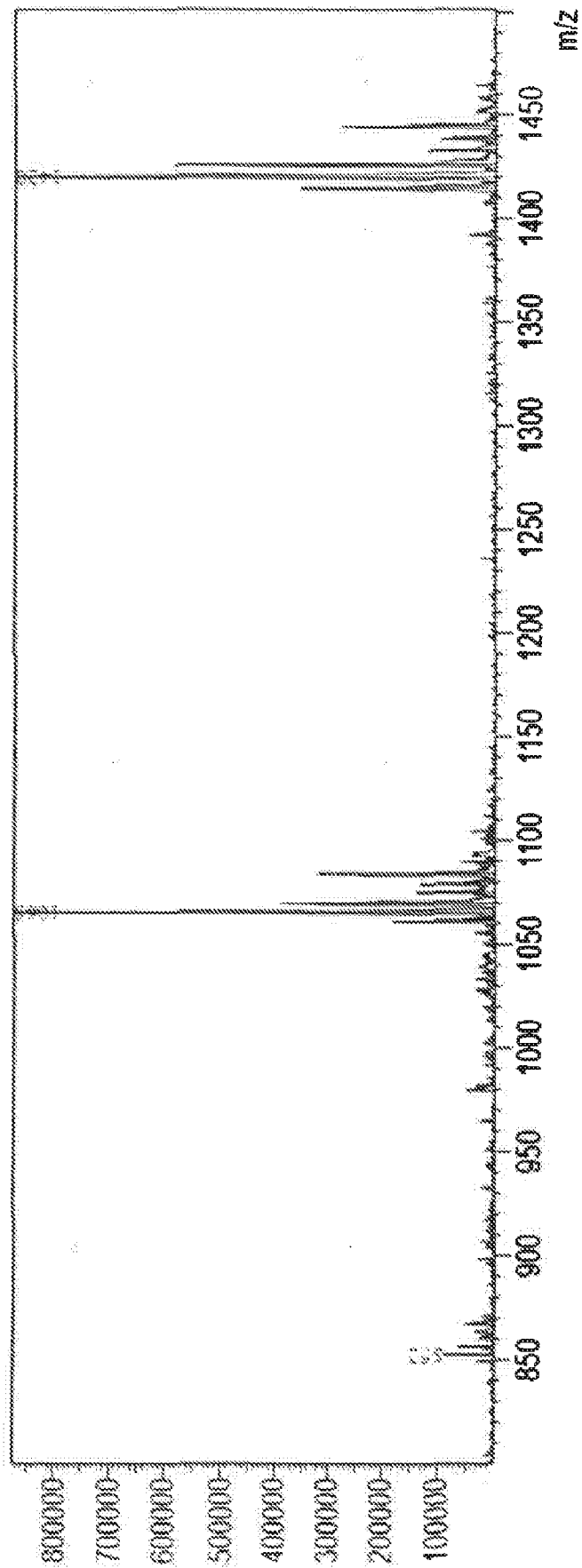


9:1 DMF:H<sub>2</sub>O  
Overnight, RT



GFANT05 is linked to 16:0 PE  
at the K2 residue  
Molecular Weight : 4257.94

FIG. 2A



ESI-MS of GFANT05 - 16:0 PE, expected m/z  
4257.94,  
observed m/z = 1420[M+3H]<sup>+3</sup>, 1065[M+4H]<sup>+4</sup>,  
852 [M+5H]<sup>+5</sup>  
Shimadzu LCMS-8040

FIG. 2B

# 1D $^1\text{H}$ NMR

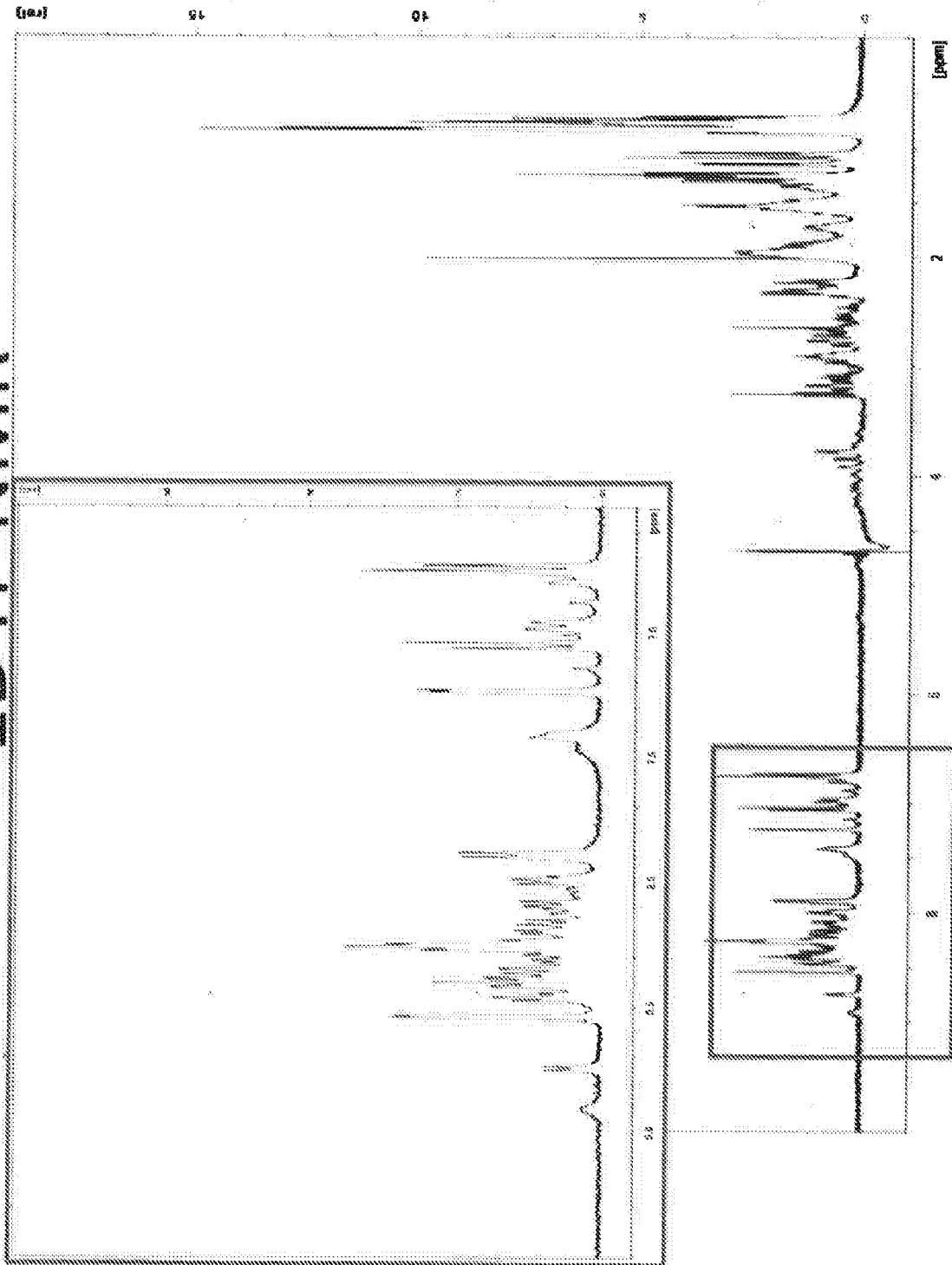


FIG. 3A

# COSY NMR

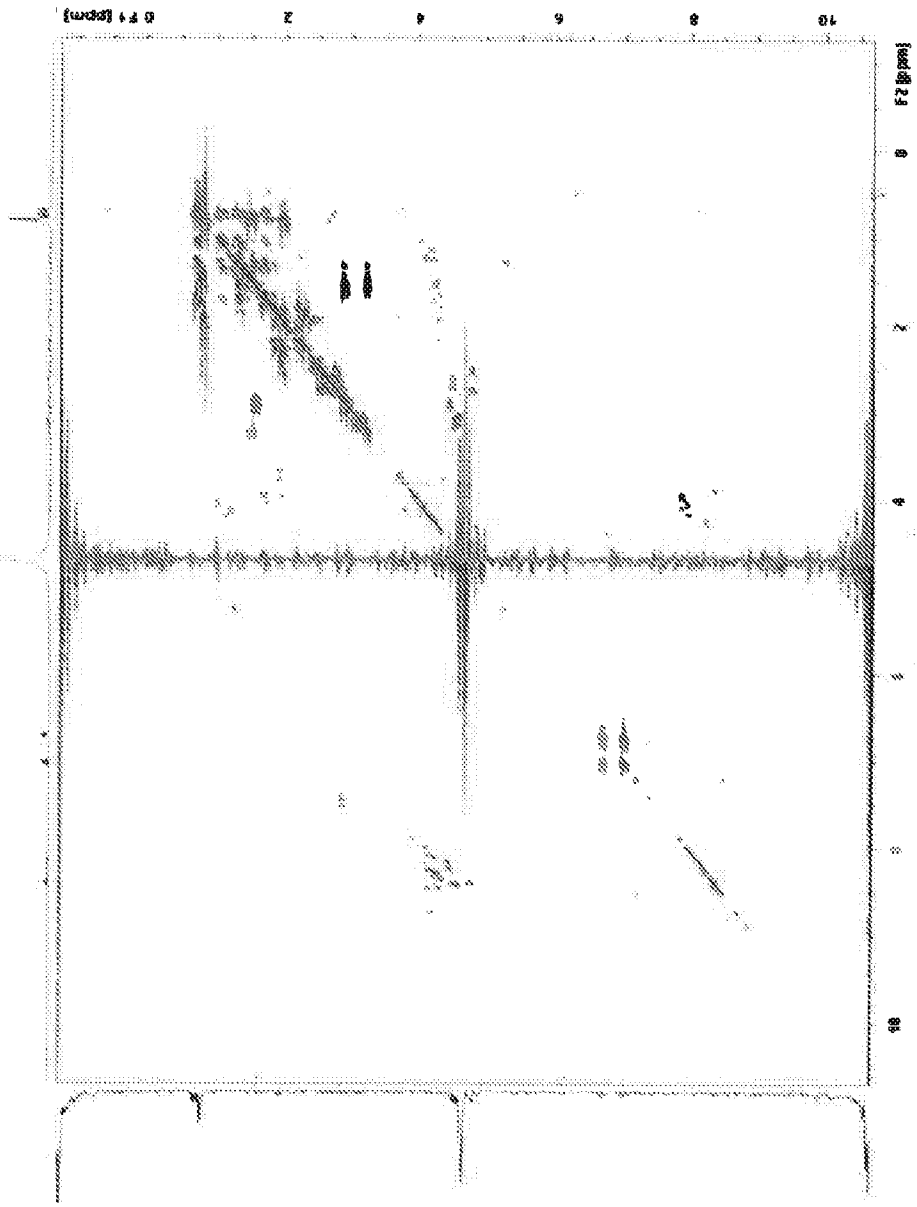


FIG. 3B

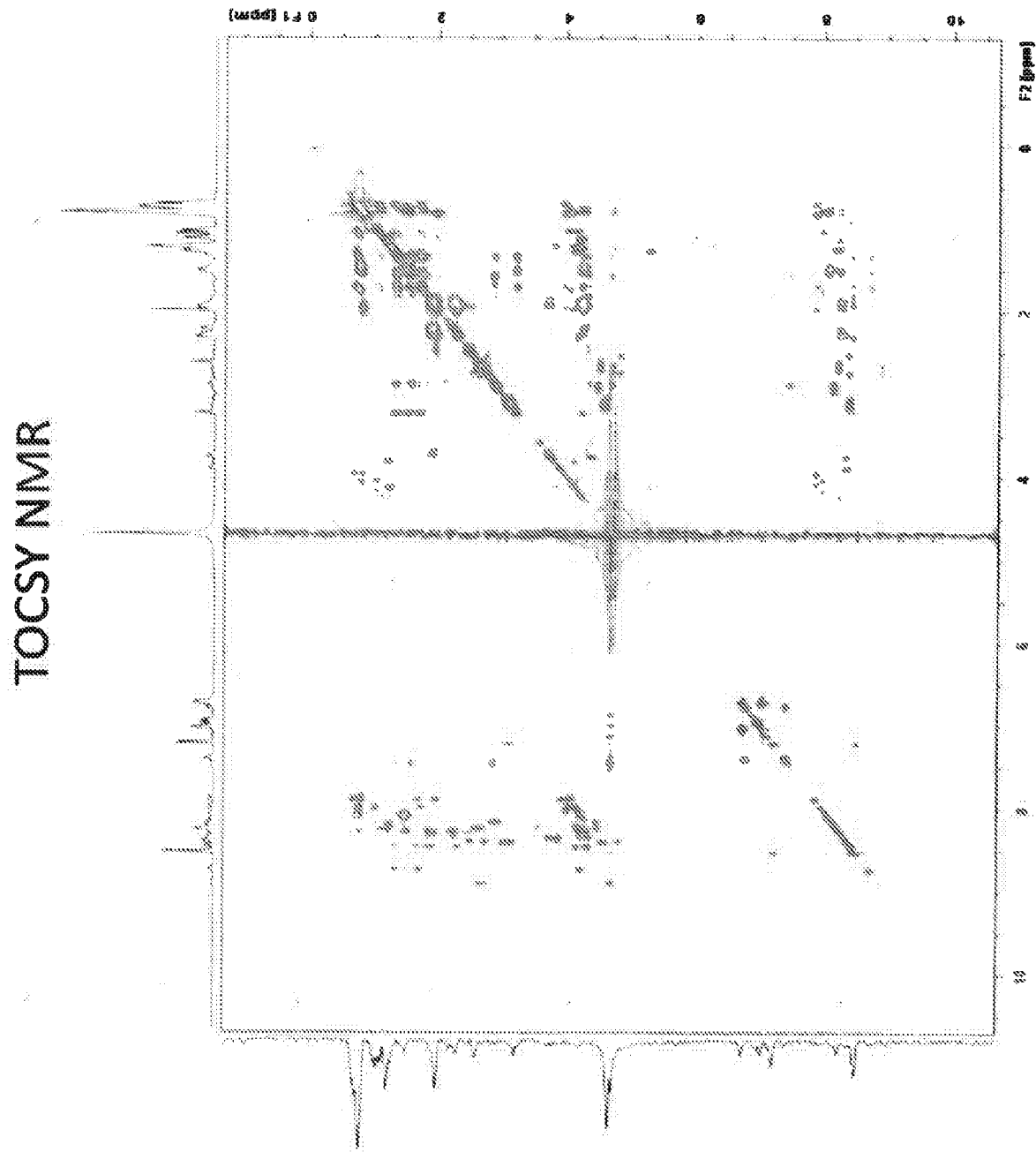


FIG. 3C

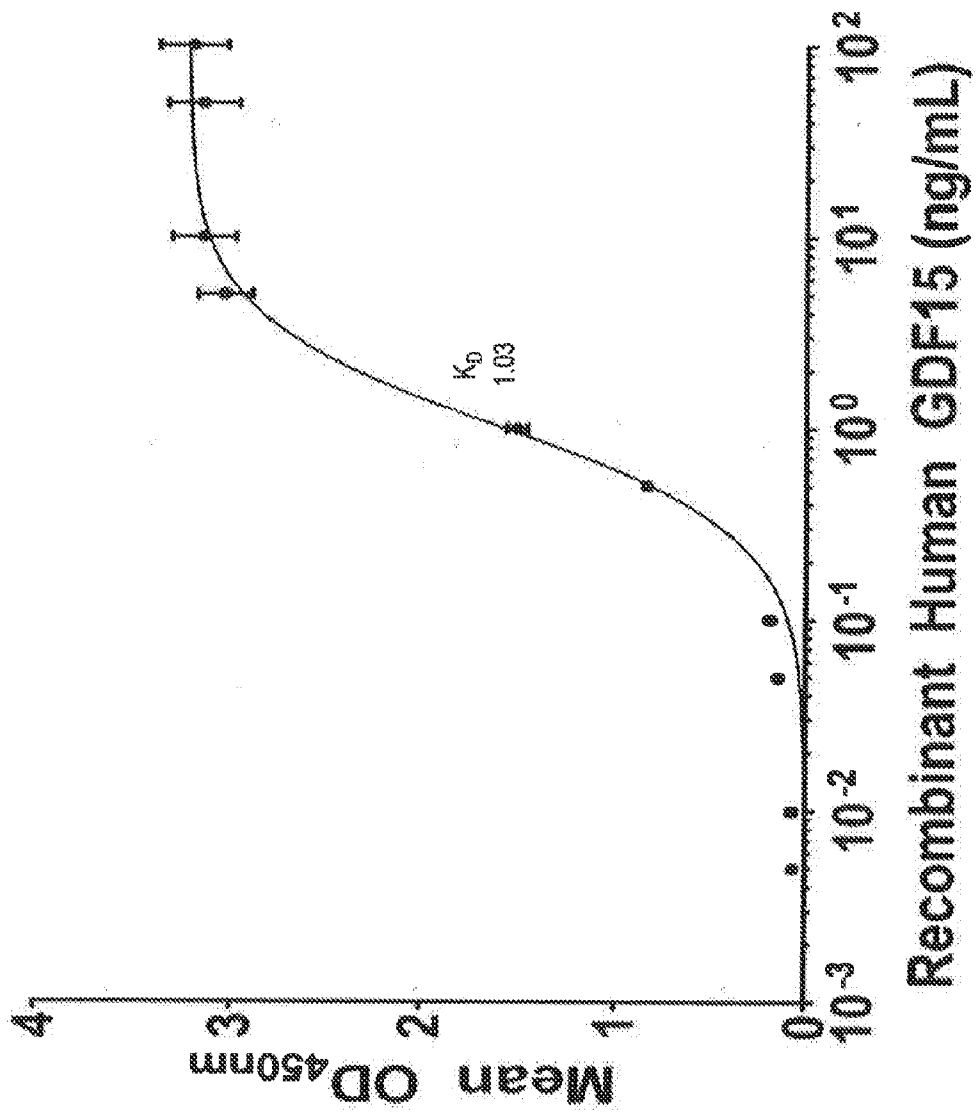


FIG. 4

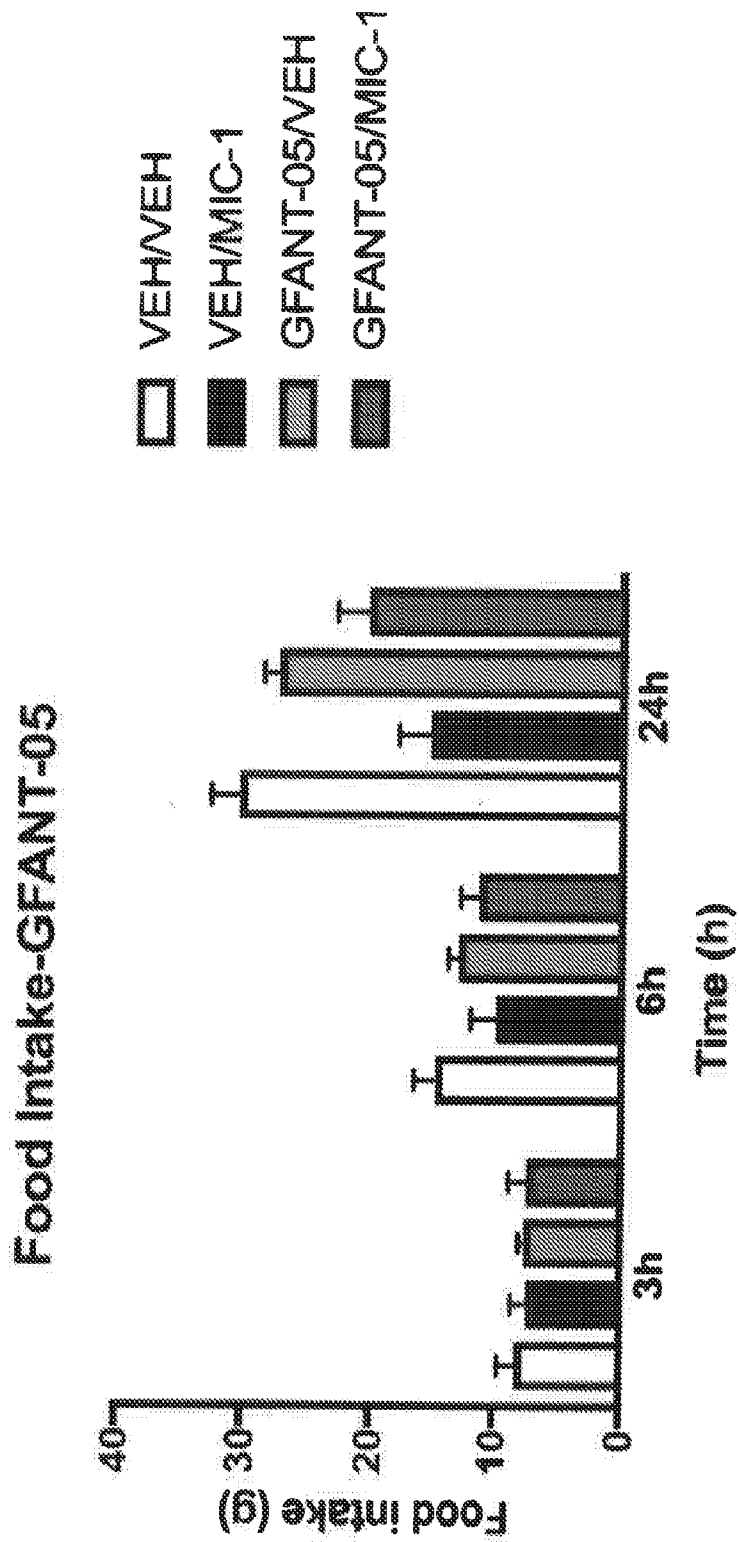


FIG. 5A

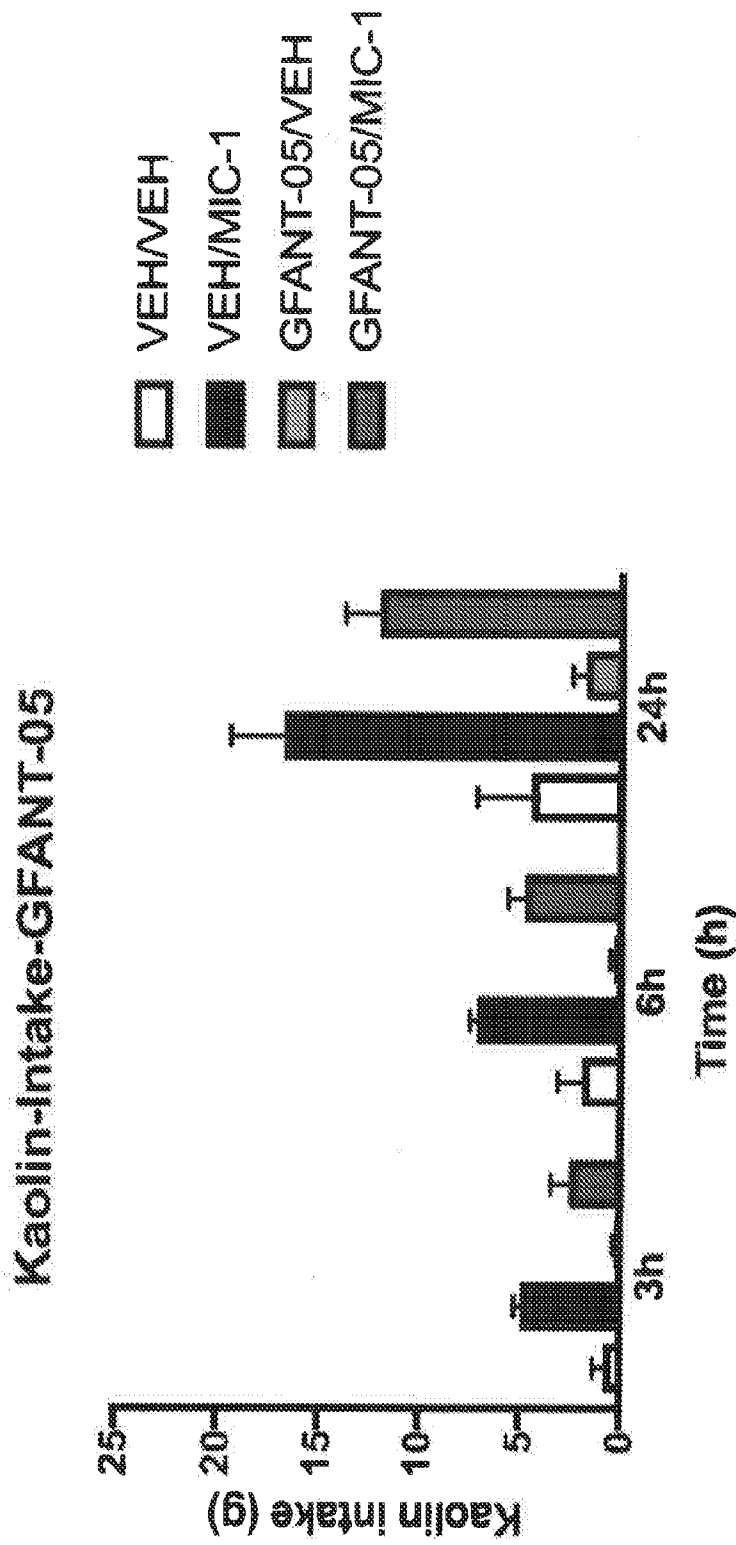


FIG. 5B



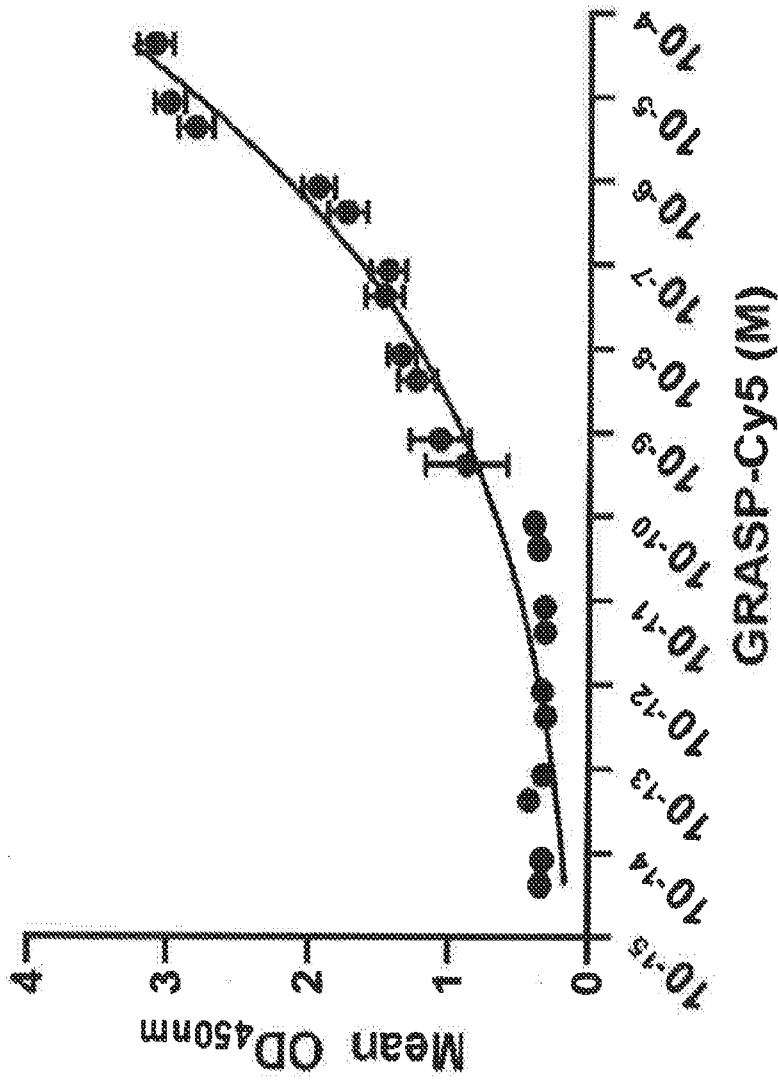


FIG. 6

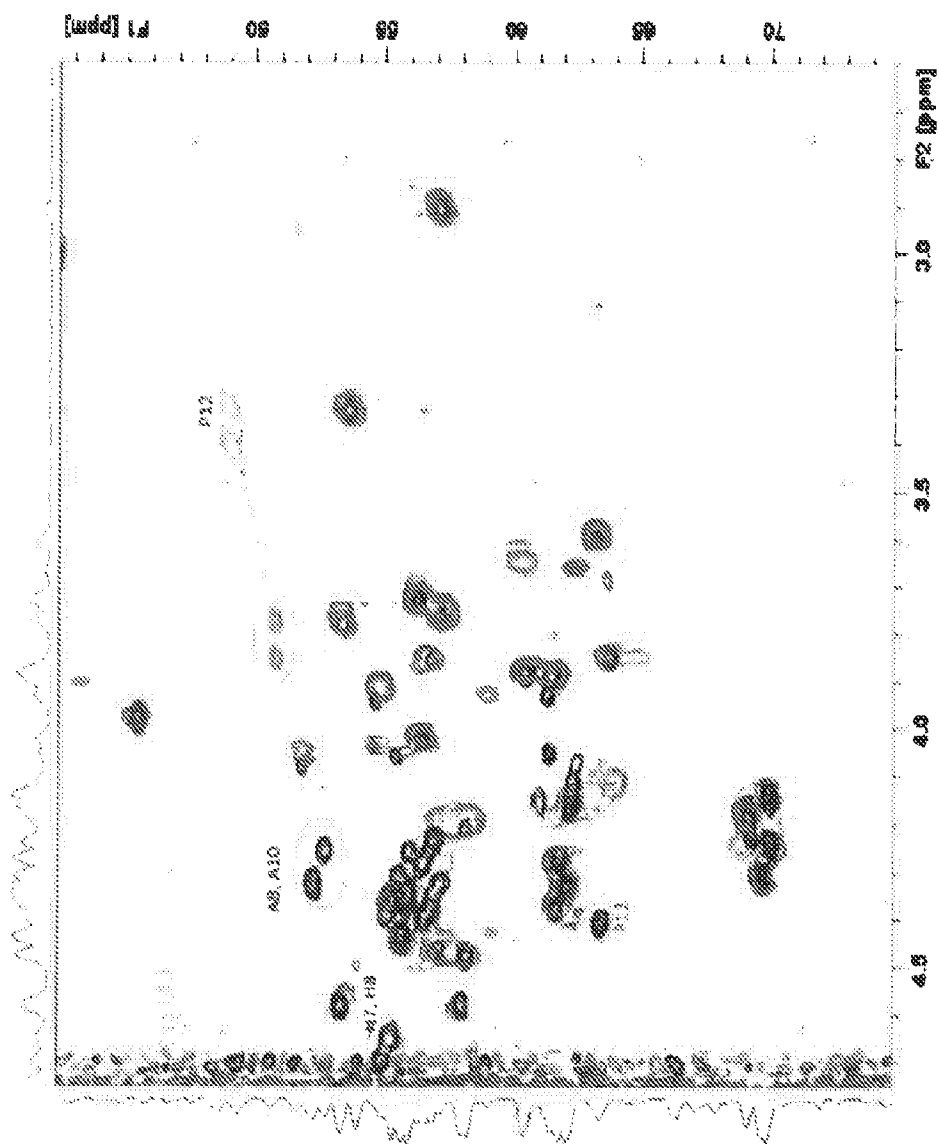


FIG. 7

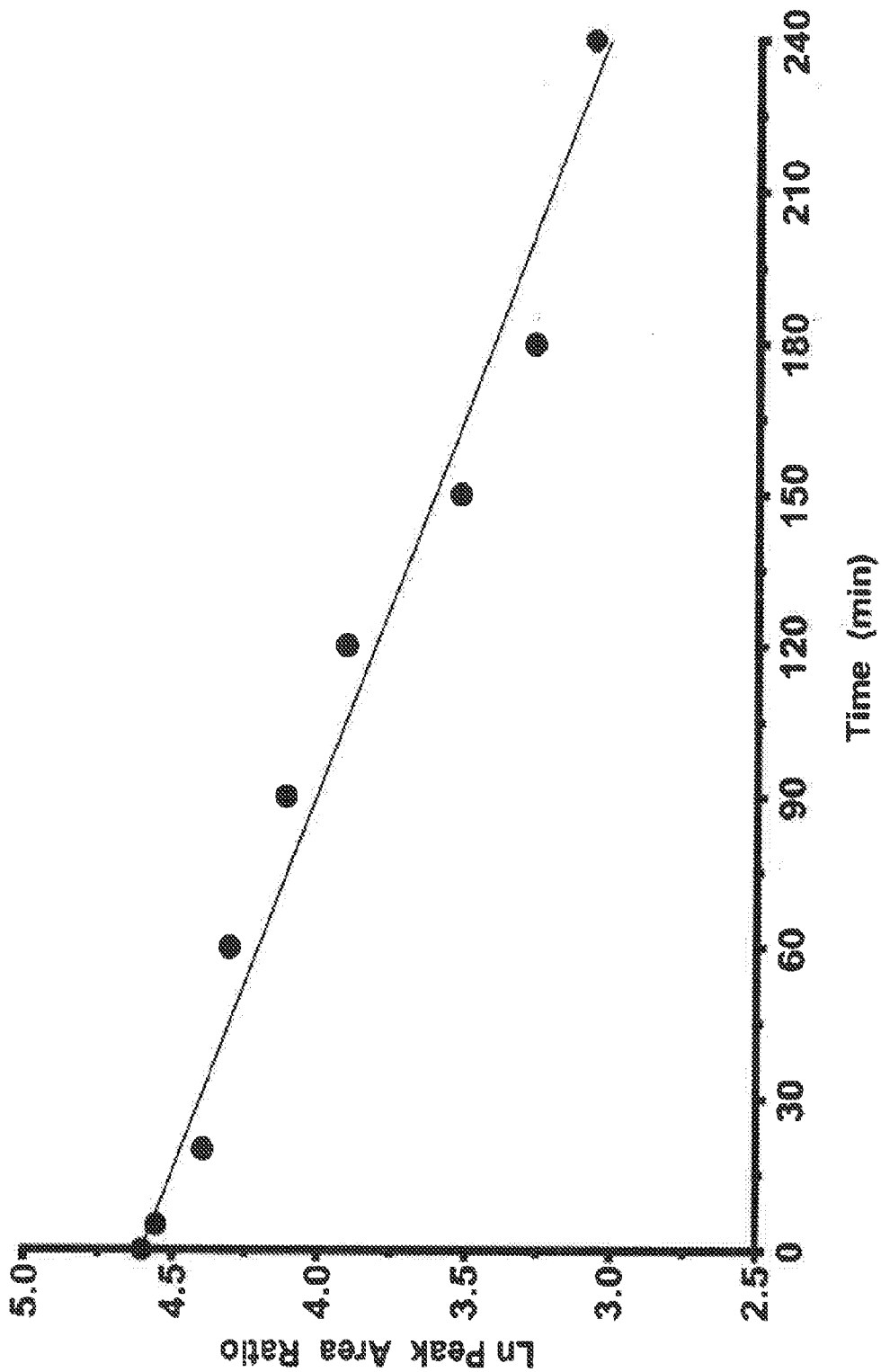


FIG. 8

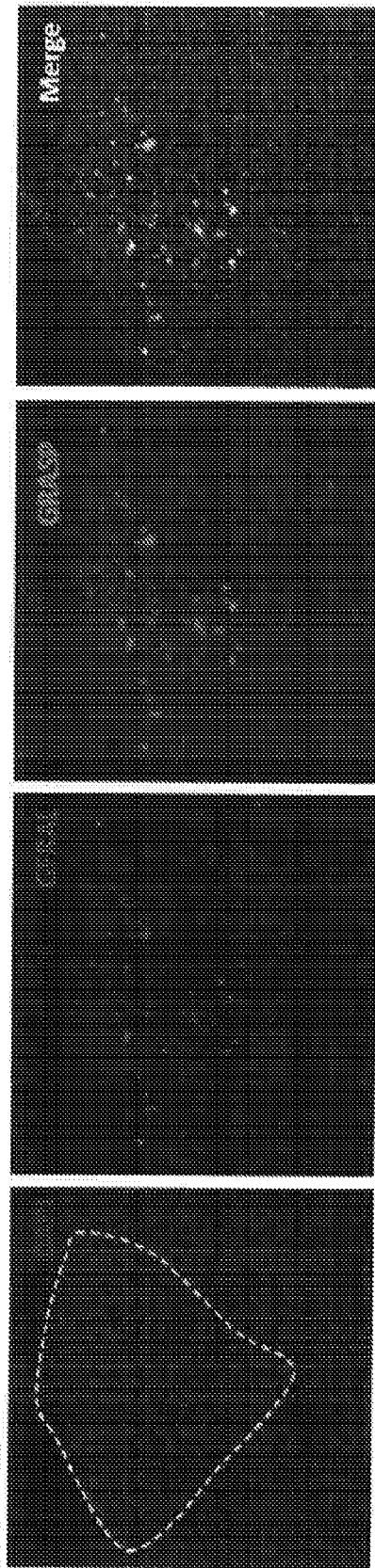


FIG. 9

## INTERNATIONAL SEARCH REPORT

International application No.

PCT/US 20/16844

**Box No. II Observations where certain claims were found unsearchable (Continuation of item 2 of first sheet)**

This international search report has not been established in respect of certain claims under Article 17(2)(a) for the following reasons:

1.  Claims Nos.:  
because they relate to subject matter not required to be searched by this Authority, namely:
  
2.  Claims Nos.:  
because they relate to parts of the international application that do not comply with the prescribed requirements to such an extent that no meaningful international search can be carried out, specifically:
  
3.  Claims Nos.: 13-14  
because they are dependent claims and are not drafted in accordance with the second and third sentences of Rule 6.4(a).

**Box No. III Observations where unity of invention is lacking (Continuation of item 3 of first sheet)**

This International Searching Authority found multiple inventions in this international application, as follows:  
This application contains the following inventions or groups of inventions which are not so linked as to form a single general inventive concept under PCT Rule 13.1. In order for all inventions to be searched, the appropriate additional search fees must be paid.

Groups I+: Claims 1-12, drawn to an engineered peptide that binds to a GDNF family receptor alpha-like (GFRAL) receptor. The composition will be searched to the extent that the engineered peptide encompasses the amino acid sequences of SEQ ID NO: 1. It is believed that claims 1-3, 5-12 encompass this first named invention, and thus these claims will be searched without fee to the extent that they encompass SEQ ID NO: 1. Additional engineered peptide(s) will be searched upon the payment of additional fees. Applicants must specify the claims that encompass any additionally elected engineered peptide(s). Applicants must further indicate, if applicable, the claims which encompass the first named invention, if different than what was indicated above for this group. Failure to clearly identify how any paid additional invention fees are to be applied to the "+" group(s) will result in only the first claimed invention to be searched. An exemplary election would be an engineered peptide encompasses the amino acid sequences of SEQ ID NO: 5 (Claims 1-5, 7-12).

\*\*\*\*\*Continued in Supplemental Box\*\*\*\*\*

1.  As all required additional search fees were timely paid by the applicant, this international search report covers all searchable claims.
2.  As all searchable claims could be searched without effort justifying additional fees, this Authority did not invite payment of additional fees.
3.  As only some of the required additional search fees were timely paid by the applicant, this international search report covers only those claims for which fees were paid, specifically claims Nos.:
  
4.  No required additional search fees were timely paid by the applicant. Consequently, this international search report is restricted to the invention first mentioned in the claims; it is covered by claims Nos.:  
1-3, 5-12 limited to SEQ ID NO: 1.

**Remark on Protest**

- The additional search fees were accompanied by the applicant's protest and, where applicable, the payment of a protest fee.
- The additional search fees were accompanied by the applicant's protest but the applicable protest fee was not paid within the time limit specified in the invitation.
- No protest accompanied the payment of additional search fees.

## INTERNATIONAL SEARCH REPORT

International application No.

PCT/US 20/16844

## A. CLASSIFICATION OF SUBJECT MATTER

IPC - A61K 38/10, C07K 7/08, C07K 7/06, A61K 38/08 (2020.01)

CPC - C07K 7/08, A61K 38/00, A61K 38/10, C07K 7/06

According to International Patent Classification (IPC) or to both national classification and IPC

## B. FIELDS SEARCHED

Minimum documentation searched (classification system followed by classification symbols)

See Search History document

Documentation searched other than minimum documentation to the extent that such documents are included in the fields searched

See Search History document

Electronic data base consulted during the international search (name of data base and, where practicable, search terms used)

See Search History document

## C. DOCUMENTS CONSIDERED TO BE RELEVANT

Category*	Citation of document, with indication, where appropriate, of the relevant passages	Relevant to claim No.
A	US 2013/0115212 A1 (NYKJAER et al.) 09 May 2013 (09.05.2013); para [0020], [0067], [0071]	1-3, 5-12
A	UniProt Submission A0A1A7XEK4_9TELE, Glial Cell derived neurotrophic factor a, [Online], October 5, 2016, [retrieved on 2020-05-13]. Retrieved from: <a href="https://www.uniprot.org/uniprot/A0A1A7XEK4">https://www.uniprot.org/uniprot/A0A1A7XEK4</a> ; whole doc.	1-3, 5-12

 Further documents are listed in the continuation of Box C. See patent family annex.

\* Special categories of cited documents:

"A" document defining the general state of the art which is not considered to be of particular relevance

"D" document cited by the applicant in the international application

"E" earlier application or patent but published on or after the international filing date

"L" document which may throw doubts on priority claim(s) or which is cited to establish the publication date of another citation or other special reason (as specified)

"O" document referring to an oral disclosure, use, exhibition or other means

"P" document published prior to the international filing date but later than the priority date claimed

"T" later document published after the international filing date or priority date and not in conflict with the application but cited to understand the principle or theory underlying the invention

"X" document of particular relevance; the claimed invention cannot be considered novel or cannot be considered to involve an inventive step when the document is taken alone

"Y" document of particular relevance; the claimed invention cannot be considered to involve an inventive step when the document is combined with one or more other such documents, such combination being obvious to a person skilled in the art

"&amp;" document member of the same patent family

Date of the actual completion of the international search

13 May 2020

Date of mailing of the international search report

26 JUN 2020

Name and mailing address of the ISA/US

Mail Stop PCT, Attn: ISA/US, Commissioner for Patents  
P.O. Box 1450, Alexandria, Virginia 22313-1450

Facsimile No. 571-273-8300

Authorized officer

Lee Young

Telephone No. PCT Helpdesk: 571-272-4300

**INTERNATIONAL SEARCH REPORT**  
Information on patent family members

International application No.

PCT/US 20/16844

Continuation of Box NO. III Observations where unity of invention is lacking:

Group II: claims 15-31, drawn to a method of treating a disease or a condition in a subject in need thereof, the method comprising administering an engineered peptide.

The inventions listed as Groups I+ and II do not relate to a single general inventive concept under PCT Rule 13.1 because, under PCT Rule 13.2, they lack the same or corresponding special technical features for the following reasons:

Groups I+ include the special technical feature of a composition which differs from the special technical feature of a method, as disclosed by Group II.

No technical features are shared between the amino acid sequences of Groups I+ and, accordingly, these groups lack unity a priori.

Additionally, even if Groups I+ were considered to share the technical features of including: an engineered peptide that binds to GFRAL, wherein the engineered peptide is an antagonist or agonist of GFRAL, these shared technical features are previously disclosed by US 2013/0115212 A1 by Nykjaer et al. (hereinafter "Nykjaer").

Nykjaer teaches (instant claims 1, 3, 5) an engineered peptide that binds to GFRAL, wherein the engineered peptide is an antagonist or agonist of GFRAL (para [0020] "In particular the present invention relates to a method, wherein the agent used to modulate the interaction between the SorLA and GDNF-family ligand receptors is selected from proteins, peptides, antibodies or small organic compounds."; [0067] "Specifically, an agonist or antagonist against SorLA or the GDNF-family ligand receptors (GFRalpha 1-4) may be binding to their extracellular domain, e.g. the domain that mediates the specific binding between SorLA and the GDNF family ligand receptors (e.g. as given in SEQ ID NO 5 or 7). Agents directed able to modulate the interaction between the SorLA and the GDNF-family ligand receptors may include soluble fragments of the SorLA or GDNF-family ligand receptors, antibodies directed to each of the receptors, natural binding partners such as GDNF or Neurotensin, or synthetic small organic compounds".).

As said technical features were known in the art at the time of the invention, these cannot be considered special technical features that would otherwise unify the groups.

Groups I+ and II therefore lack unity under PCT Rule 13 because they do not share a same or corresponding special technical feature.

Item 4 (continued):

Claims 13-14 are improper multiple dependent claims because they are dependent claims and are not drafted in accordance with the second and third sentences of Rule 6.4(a).

ictinsle@syr.edu, itins2@gmail.com  
136 Northrup Boulevard, Syracuse, NY, 13209  
(217) 891-8922

---

**EDUCATION:**

Syracuse University, Syracuse, New York Doctor of Philosophy in Chemistry	8/2017 – 5/2021
Eastern Illinois University, Charleston, Illinois Master of Science in Chemistry	8/2015 – 5/2017
University of Illinois at Springfield, Springfield, Bachelor of Science in Chemistry and Biology Minor: Women and Gender Studies	8/2008 – 5/2015

---

**RESEARCH:**

Syracuse University Chemistry Department, Syracuse, New York Medicinal Chemistry Graduate Researcher (Advisor: Dr. Robert P. Doyle) <u>Outcomes:</u> SAR studies on ‘corrinated’ conjugates of the GLP-1 receptor agonist Exendin-4. -Design, synthesis and purification of a library of cobinamide gut hormone derivatives. -Design and microwave assisted synthesis (CEM Liberty Blue) of peptides. -Characterization of new peptides and conjugates by MS, EAS, CD, 1- and 2-D NMR, ELISA/Western blot. - <i>In vitro</i> screening of conjugates utilizing stably transfected HEK293 cell line. - In vivo PD/PK screening in rats and musk shrews.	9/2017 – 5/2021
EIU Chemistry Department, Charleston, Illinois Organic Chemistry Research Assistant (Advisor: Dr. Kraig A Wheeler) <u>Outcomes:</u> Structural Boundaries of Molecular Topology to Quasiracemate Formation. -Utilized hot stage thermomicroscopy to determine molecular recognition patterns. -Solved structures from single X-ray crystallographic data. -Utilized melt to perform nuclear magnetic resonance and powder X-ray diffraction studies.	1/2016 – 5/2017
University of Illinois at Springfield, Springfield, Illinois Undergraduate Research Student (Advisor: Dr. Stephen R. Johnson) <u>Outcomes:</u> Performed a proteomic investigations of the phospholipase A2 enzyme in the South African Predacious Ant <i>Platythyrea lamellosa</i> - Isolated venom fractions using SDS-Page followed by trypsin digestion. - Assessment via high performance liquid chromatography-tandem mass spectrometry - Confirmation of the presence of Am PLA2 - Contained different primary structure and activity than purified PLA2 of <i>Apis mellifera</i>	Summer 2012

**PUBLICATIONS**

**Tinsley, I. C.;** Borner, T.; Swanson, M. L.; Hayes, M. R.; De Jonghe, B. C.; Chepurney, O. G.; Holz, G. G.; Doyle, R. P. Design, Synthesis and Biological Evaluation of ‘Corrinated’ Conjugates of the GLP-1R agonist Exendin-4. *J. Med. Chem.* **2021**, 64, 3479-3492.

**Tinsley, I. C.;** Bonrer, T.; Workinger, J. L.; Fortin, S. M.; Stein, L. M.; Cherpurny, O. G.; Holz, G. G.; Wierzba, A. J.; Gryko, D.; Nexo, E.; Shaulson, E. D.; Bamezai, A.; Rodriguez Da Silva, V. A.; De Jonghe, B. C.; Hayes, M. R.; Doyle, R. P. ‘Corrination’ of a GLP-1 receptor agonist for glycemic control without emesis. *Cell Reports.* **2020**, 31 (11), 107768.

Borner, T.; Shaulson, E. D.; **Tinsley, I. C.;** Stein, L. M.; Horn, C. C.; Hayes, M. R.; Doyle, R. P.; De Jonghe, B. C. A second generation GLP-1 receptor agonist prevents vomiting and anorexia while retaining glucoregulatory potency in lean diabetic and emetic mammalian models. *Diabetes Obes. Metab.* **2020**, 22 (10), 1729-1741.

Stein, L. M.; Lhamo, R.; Cao, A.; Workinger, J.; **Tinsley, I.** Doyle, R. P.; Grill, H. J.; Hermann, G. E.; Rogers, R. C.; Hayes, M. R. *Transl Psychiatry.* **2020**, 10 (90), 1-12.

**Tinsley, I. C.;** Spaniol, J. M.; Wheeler, K. A. *Chem. Comm.* **2017**, 53 (33), 4601–4604.



## PATENTS

- **Tinsley, I. C.**; Borner, T.; De Jonghe, B. C.; Hayes, M. R.; Doyle, R. P. Peptide Ligands of the GDNF Family Receptor A-Like (GFRAL) Receptor. Non-provisional file date March 5<sup>th</sup>, 2020.
  - Optioned to Cantius Therapeutics, a spin-out company formed between Syracuse University and PENN.

## PRESENTATIONS

- Leptin Induced Satiety and the Contribution of Brainstem Astrocytes, Experimental Biology 2019, Orlando Florida, 4/6-9/2019. Stein, L.; Lhamo, R.; **Tinsley, I.**; Doyle, R.; Hayes, M.R.
- Corination of a GLP-1 Receptor Agonist for Glycemic Control Without Emesis, Stevenson Biomaterials Lecture Series, Syracuse, New York, 3/1/2019. **Tinsley, I. C.**; Borner, T.; Workinger, J. L.; Fortin, S. M.; Stein, L. M.; Chepurny, O. G.; Holz, G. G.; Wierzba, A. J.; Gryko, D.; Nexo, E.; Shaulson, E. D.; De Jonghe, B. C.; Hayes, M. R.; Doyle, R.P.
- Exendin-4 Conjugated to Vitamin B12 Improves Glucose Tolerance in Shrews and Lean Diabetic Rats Without Inducing Vomiting or Hypophagia, Keystone Symposia on Molecular and Cellular Biology, Banff, Alberta, Canada, 2/10-14/2019. **Tinsley, I. C.**; Borner, T.; Shaulson, E. D.; Stein, L. M.; Workinger, J. L.; Hayes, M. R.; De Jonghe, B. C.; Doyle, R.P.
- Leptin Induced Satiety and the Contribution of Brainstem Astrocytes, Keystone Symposia on Molecular and Cellular Biology, Banff, Alberta, Canada, 2/10-14/2019. Stein, L.; Lhamo, R.; **Tinsley, I.**; Doyle, R.; Hayes, M.
- Prescribed Molecular Recognition Profiles Via Shape Mimicry, 255<sup>th</sup> American Chemical Society National Meeting, New Orleans, Louisiana, 3/18-22/2018. Wheeler, K. A.; Cantrell, L. S.; Pinter, E. N.; **Tinsley, I. C.**; Wagner, B. L.
- Molecular Recognition Boundaries of Diarylamide Quasiracemates, 253<sup>rd</sup> American Chemical Society National Meeting, San Francisco, California, 4/2-6/2017. **Tinsley, I. C.**; Wagner, B. L.; Wheeler, K. A.
- Molecular Recognition Boundaries of Diarylamide Quasiracemates, EIU Student Research and Creative Activity Day, Charleston, Illinois, 3/31/2017. **Tinsley, I. C.**; Wagner, B. L.; Wheeler, K. A.
- Molecular Shape Directed Crystalline Quasiracemates, Eastern Illinois University: Chemistry Research Celebration, Charleston, Illinois, 11/1/2016. **Tinsley, I. C.**; Wheeler, K. A.
- Molecular Shape Directed Crystalline Quasiracemates, 66<sup>th</sup> Annual American Crystallographic Association Meeting, Denver, Colorado, 7/22-26/2016. **Tinsley, Ian C.**; Wheeler, K. A.
- Proteomic Investigation of a Phospholipase A2 from the Venom of the South African Predacious Ant *Platythya lamellosa*, 2013 University of Illinois at Springfield StARS-Student Art & Research Symposium, Springfield, Illinois, 4/12/2013. **Tinsley, Ian C.**; Johnson, Stephen R.

## AWARDS

2017 Distinguished Graduate Student in Chemistry, Eastern Illinois University  
2016 Graduate School Research/Creativity Award, Eastern Illinois University  
2016 Williams Travel Grant, Eastern Illinois University  
2016 Travel Grant, American Crystallographic Association

---

## INSTITUTIONAL SERVICE

Academic Services for Eastern Illinois University Athletics Department	2016-2017
-Assisted student-athlete mentoring program and peer tutoring in chemistry and biology	
Eastern Illinois University Graduate Student Advisory Council (GSAC)	2016-2017
-Student representative for the chemistry department	
-Helped in developing and implementing policies related to graduate student body	
- "Ranes Outstanding Graduate Faculty Mentor Award" committee member.	
-Panelist "Making a Successful Transition from Undergraduate to Graduate Education," Eastern Illinois University Enrollment Management Conference, Charleston, Illinois, 2-8-2017.	

---

## WORK HISTORY

Syracuse University Research Assistant	8/2018 – 5/2021
Syracuse University Graduate Assistant	8/2017 – 5/2018
Eastern Illinois University Graduate Assistant	1/2017 – 5/2017
Eastern Illinois University Research Assistant	8/2015 – 1/2017

---

**REFERENCES**

Dr. Robert Doyle, Syracuse University, Department of Chemistry (315)-443-2925, rpdoyle@syr.edu

Dr. George Holz, Upstate Medical University, Department of Pharmacology (315)-464-9841, holzg@upstate.edu

Dr. Matthew Hayes, University of Pennsylvania, Department of Psychiatry, (215)-573-6070, hayesmr@mail.med.upenn.edu

Dr. Kraig Wheeler, Whitworth University, Department of Chemistry, (509)-777-3643, kraigwheeler@whitworth.edu